Surface Water Quality Modelling Considering Riparian Wetlands

by

Robert Wayne Jenkinson

A thesis
presented to the University of Waterloo
in fulfilment of the
thesis requirement for the degree of
Doctor of Philosophy
in
Civil Engineering

Waterloo, Ontario, Canada, 2009

I hereby declare that I am the sole author of this thesis. This is a true copy of the thesis, including any required final revisions, as accepted by my examiners.
I understand that my thesis may be made electronically available to the public.

R. W. Jenkinson

Abstract

Riparian wetlands are believed to play an important role in mitigating non-point source pollution, acting as physical and biochemical buffers between diffuse pollution sources and receiving waters. Many studies examined riparian wetlands at the field scale, but there is a dearth of research at the watershed scale, particularly in the region of Southern Ontario, where agricultural land use predominates.

This study examined the impacts of riparian wetlands on surface water quality at the watershed scale. A field study was conducted on two sub-watersheds at the northern headwaters of the Canagagigue Creek within the Grand River Watershed in Southern Ontario. The two watersheds were similar in area and land use but with differing riparian wetland extent adjacent to the sub-watershed main channels. A two-year study was conducted examining the hydrology, hydraulics, water quality and nutrient fluxes from the two sub-basins. Water quality data were obtained at the outlet of each sub-basin during base-flow conditions and during 16 rainfall and snow melt runoff events. The hydrology was simulated using the WatFlood model and the water quality (nitrate and total suspended solids) was simulated using an enhanced WatFlood/AGNPS model that was modified to account for continuous simulation, in-stream contaminant fate/transport and riparian wetland influences.

The hydraulics and hydrological characteristics of the two basins were distinct. The basin without riparian wetland protection ("West Basin") exhibited ephemeral tendencies, going dry for several months in the summer, whereas the basin with extensive riparian wetland protection ("East Basin") showed a persistent base-flow throughout the year with a consistently more rapid hydrological response. This study showed higher nutrient concentrations including nitrate, total nitrogen (TN), and total phosphorus (TP) in the West basin than the East basin, attributed to the lack of riparian wetland protection in the West sub-basin. Total Suspended Solids (TSS) concentration were higher in the east sub-basin than the west sub-basin attributed to differences in sediment grain size distributions and differences in local stream bed slope. Constituent loading estimates from the two sub-basins were conducted on an event-basis and on an average monthly load basis. This study showed that during events most constituents (Nitrate, TP, and TSS) were discharged in greater quantities from the East sub-basin than the West sub-basin for both rainfall and snowmelt events. Event-based TN loading was also higher for the East sub-basin but the difference was not statistically significant. Monthly average loading was significantly higher in the East sub-basin than the West sub-basin for Nitrate, TN and TSS. Monthly average loading

was higher in the East basin than the West basin for TP as well, but the difference was not statistically significant. In spite of the generally higher nutrient concentrations in the West sub-basin, the east sub-basin exhibits higher loads due to the differing hydrological conditions in that basin. The persistent stream flow in the East basin continuously transports nutrients of a lower concentration than the West, but the consistent flow dominates the loading calculations resulting in a greater constituent mass transported.

The modelling of sediment and nitrogen loading was conducted over the study period. Sediment modelling results showed that the dominant process in the model was in-channel transport with the calibrated model showing very little sensitivity to overland transport parameters and riparian wetland retention. The ability to hydrologically model the basin accurately dictated the performance of the sediment transport model. Nitrogen modelling results demonstrated an ability to generally simulate the nitrogen profiles trends during storm events. However, the WatFlood groundwater storage model provided limitations in terms matching the nutrient concentration variability observed in the measured data. The processes that dominated model performance were fertilizer loading and nitrogen mineralization coefficients, with the riparian wetlands playing a small role in nitrogen removal in the calibrated model.

Acknowledgments

I offer many sincere thanks to my supervisors, Profs. Nick Kouwen and Wayne Parker, for their steadfast support as I found my own (albeit circuitous) path. Although their supervisory approaches and areas of specialization were quite different, together they provided me a perfect balance of expertise and support to help me get the most out of my research and myself. I will always be grateful for their guidance and their friendship.

I gladly thank the remaining members of my doctoral committee for their helpful advice: Prof. Dave Rudolph, Prof. Ric Soulis and especially Prof. Bill Annable for encouraging me to operate outside my comfort zone.

I am forever grateful for the skill and assistance offered by the remarkable Civil Engineering Water Resources technicians, Mark Sobon, Bruce Stickney and especially the indefatigable Terry Ridgway. They made possible what I had imagined impossible.

For their assistance with various aspects of my research I would like to thank Dr. Alain Peitriniro, Prof. Bryan Tolson, Angela McLean, Marian Saavedra, Nero Nalliah, and Quinn Thompson. For support in providing data and equipment I would like to sincerely thank Mark Anderson and Dwight Boyd of the Grand River Conservation Authority. I would also like to thank Prof. Bill Lennox for his numerical modelling advice and his thorough review of my chapters on contaminant transport modelling.

For their friendship and emotional support through my graduate studies I would like to thank my dear friends Erica Tursan d'Espaignet, Erika Klyszejko, Frank Segleneiks, Frédéric Bosché, and Katie McGuane, my sister Leigh Jenkinson and my parents Bob and Marsha Jenkinson.

Contents

List of Figures **xiv**

List of Tables **xxii**

1 Introduction **1**

1.1 Research Objectives 4

1.2 Research Plan and Document Structure 5

1.2.1 Literature Review, References and Glossary 5

1.2.2 Study Site Selection 5

1.2.3 Hydraulic and Hydrological Characterization, Monitoring and Modelling 6

1.2.4 Water Quality Monitoring and Analysis 8

1.2.5 Water Quality Modelling 8

2 Literature Review **10**

2.1 Non-Point Source Pollution in Agricultural Systems 10

2.1.1 NPS Pollution in Southern Ontario 12

2.2 Agricultural NPS Transport and Fate Mechanisms 13

2.2.1 Sediment Transport 13

2.2.2 Nitrogen Fate and Transport 14

2.2.3 Tile Drains 16

2.3 Riparian Wetland Studies 17

2.3.1 Field Scale Studies 17

2.3.2 Regional/Watershed Scale Studies 19
2.3.3 Water Quality Modelling considering NPS Pollution and Riparian Wetlands 21
2.4 The WatFlood Model and NPS Pollution Modelling 23
2.5 Chapter Summary 25

3 Study Site **26**
3.1 Physiography and Soils 31
3.2 Riparian Wetlands 31
3.3 Land Use and Anthropogenic Influences 34
3.4 Tile Drainage 39
3.5 Chapter Summary 42

4 Hydrometric Data Collection and Analysis **44**
4.1 Introduction 44
4.2 Data Collection and Storage Approach 45
4.3 Stage Measurement Locations 45
4.4 Stage-Discharge Rating Curves 46
4.5 Anthropogenic Flow Sources - Alma Research Station 49
4.6 Flow Distribution Curves 50
4.7 Precipitation Data 50
4.8 Air Temperature Data 53
4.9 Snow Surveys 53
4.10 Streamflow and Dam Discharge Data 56
4.11 Sub-Basin Hydrological Response 56
4.12 Chapter Summary 58

5 Hydrological Simulation **60**
5.1 Introduction 60
5.2 Hydrological Modelling Approach 61
5.2.1 The WatFlood Hydrological Model and the GRU Concept 62

5.3 Watershed Model Set-up 63
5.3.1 Watershed and Drainage Network Delineation 63
5.3.2 River Classes 65
5.3.3 Land-Use / Land-Class Data 68
5.3.4 Precipitation Data 69
5.3.5 Snow Course Data and Distribution 70
5.3.6 Stream Flow Data 70
5.4 Hydrological Model Calibration 71
5.4.1 Calibration Parameters and Procedure 71
5.4.2 Model Validation 74
5.4.3 Performance of Sub-Basins 80
5.5 Hydrological Analysis for Water Quality 83
5.5.1 Wetland Storage 83
5.6 Discussion 87

6 Water Quality Sampling Methods and Results 89
6.1 Introduction 89
6.2 Sample Collection 91
6.3 Analytical Methods 92
6.3.1 Turbidity, Electrical Conductivity and pH 92
6.3.2 Total Phosphorus 93
6.3.3 Total Nitrogen 93
6.3.4 Nitrate (Colourmetric) 94
6.3.5 Anions and Cations 94
6.4 Sampling Programs 96
6.5 Investigative Sampling Program 96
6.6 Intensive Sampling Program 101
6.6.1 Storm Events 101
6.7 Intensive Sampling Program Results 104
6.7.1 Analyte Correlations 104
6.7.2 Data Interpolation and Flux Calculations 106

6.7.3 Water Quality Patterns . . . 108
6.7.4 Event-Based Load Analysis . . . 115
6.7.5 Average Monthly Load Analysis . . . 116
6.8 Discussion . . . 119

7 Water Quality Sub-Model Development 122
7.1 Introduction . . . 122
7.2 In-Channel Contaminant Transport . . . 123
7.2.1 WatFlood Channel Routing Model Structure . . . 125
7.2.2 WatFlood Contaminant Transport Model . . . 127
7.2.3 Storage Routing Contaminant-Transport Limitations . . . 128
7.2.4 Enhancements to WatFlood In-Channel Contaminant Transport . . . 129
7.2.5 Extensible Contaminant Transport Model Structure . . . 132
7.2.6 Modular Input File Structure and WatFlood Integration . . . 132
7.2.7 Sub-Grid Discretization . . . 133
7.2.8 Contaminant Transport Algorithm Selection . . . 133
7.2.9 Evaluation of Contaminant Transport Schemes . . . 137
7.2.10 Integration with WatFlood . . . 140
7.2.11 Reservoir Considerations . . . 147
7.2.12 Performance Benchmarking . . . 147
7.3 Riparian Contaminant Transport . . . 150
7.4 In-Stream Water Quality Modelling . . . 154
7.5 Reactive Transport Calculations . . . 156
7.6 Suspended Sediment Transport Calculations . . . 158
7.6.1 Solute Decay Equations . . . 161
7.7 Riparian Wetland - Channel Constituent Load Partitioning . . . 163
7.8 Riparian Wetland Suspended Sediment Processes . . . 165
7.9 Riparian Wetland Nitrate Processes . . . 171
7.9.1 Water Temperature Estimation . . . 172
7.9.2 Illustrative Riparian Nitrogen Process Simulation in the WatFlood Model . . . 173

7.10 Land Surface Process Modification 173
7.10.1 WatFlood Sub-Surface Storage and Transport 175
7.10.2 WatFlood/AGNPS Nitrogen Model Summary 177
7.10.3 Nitrogen Pool Modelling Approach 178
7.10.4 AGNPS Nitrogen Mobility 179
7.10.5 Crop Nitrogen Uptake 180
7.10.6 Fertilizer Application 183
7.10.7 Fertilizer Mineralization and Nitrification 184
7.10.8 Estimation of Soil Temperature 187
7.10.9 Illustrative Nitrogen Process Simulation in the WatFlood Model . . 190
7.10.10 Omitted Nitrogen Processes 191
7.11 Discussion 193

8 Water Quality Modelling Results **197**
8.1 Introduction 197
8.2 Sediment Transport Modelling 197
8.2.1 Parameter Estimation 198
8.2.2 Calibration Procedure 200
8.2.3 Validation Results 205
8.2.4 Model Sensitivity 210
8.2.5 Snow Ablation Adjustment 216
8.3 Nitrate Transport Modelling 221
8.3.1 WatFlood/AGNPS Model and Parameter Estimation 221
8.3.2 Crop Nitrogen Uptake Estimates 223
8.3.3 Nitrogen Loading Estimates 224
8.3.4 Nitrogen from Rainfall 228
8.3.5 Nitrogen Mineralization and Nitrification Rates 229
8.3.6 Riparian Wetland Nitrate Removal 230
8.3.7 Calibration Procedure 230
8.3.8 Model Performance 231
8.3.9 Nitrate Model Sensitivity 242

8.3.10 Riparian Wetland Contribution to Nitrate Removal 243
8.3.11 Groundwater Consideration in Nitrate Modelling with WatFlood . . 247
8.4 Discussion 249

9 Conclusions and Recommendations 252
9.1 Recommendations 254
9.1.1 Larger Modelling Domain 254
9.1.2 Extended Study Period 254
9.1.3 Hydrology of Small, Ephemeral Basins 254
9.1.4 Riparian Wetland Hydrology 255
9.1.5 Mixing in incised and well-formed channels 255
9.1.6 Examination of other nitrogen fate processes 255
9.1.7 Recommendations for Water Quality Model Improvement 256

References 256

Glossary 277

Nomenclature 280

Appendices 286

A Hydraulic Measurements 286
A.1 Summary 286
A.2 Flow Measurement Installations 286
A.3 Survey Information 287
A.4 Stage Calibration 293
A.5 Discharge Measurements 293
A.6 Flow Centroid Calculations 296
A.7 Flow-Discharge Rating Curve Development 296
A.7.1 Extrapolation of Rating Curves using HEC-RAS 296

A.7.2 Estimation of Manning's n Values 300

B Hydrological Data Collection and Analysis **305**

B.1 Introduction 305

B.2 WatFlood Model Set-up 305

B.3 Data Quality Assurance 307

B.4 Precipitation Data 308

B.4.1 University of Waterloo Weather Station Precipitation 308

B.4.2 Study Gauge Validation 308

B.4.3 Precipitation Quantity Assessment 309

B.4.4 Rainfall Event Timing Assurance 314

B.4.5 King City RADAR Data 315

B.5 Streamflow and Dam Discharge Data 315

B.6 Streamflow Modelling Results 315

B.7 WatFlood Calibration and Results 322

B.7.1 WatFlood Parameter File 327

B.7.2 WatFlood MAP File 329

C Sampling Methods **336**

C.1 Introduction 336

C.2 Quality Assurance / Quality Control Graphs 336

C.3 Method Detection Limits 337

C.3.1 Total Phosphorus MDL 339

C.3.2 Total Nitrogen MDL 339

C.3.3 Ion Chromatograph MDL 340

D Water Quality Model Development **343**

D.1 Introduction 343

D.2 Contaminant Transport Model Development 343

D.2.1 Sub-Grid Storage Routing Algorithm 343

D.2.2 QUICKEST Scheme 345

D.2.3 Holly-Preissmann / Crank-Nicholson Split-Operator Scheme 351
D.2.4 Contaminant Transport Model Performance Evaluation 357
D.3 In-Channel Sediment Transport Performance Evaluation 374
D.3.1 SOLROUTE Test Framework 374
D.4 In-Channel First-Order Decay Process Evaluation 377
D.4.1 WatFlood Unit Test 377
D.5 OMAFRA Fertilizer Loading Algorithm 382
D.6 Water Quality Model Sensitivity 383
D.6.1 Sediment Model Sensitivity 385
D.6.2 Nitrate Model Sensitivity 390
D.7 Water Quality Parameter File (WQP) 395
D.8 Riparian Wetland Definition File (RIP) 395
D.9 Sediment Definition File (SED) 396

List of Figures

3.1 Location of the Study Site within the Grand River Watershed 27
3.2 Location of Study Site 29
3.3 Canagagigue Creek and Study Site Elevation Contour Map 30
3.4 Canagagigue Creek Physiography Map 32
3.5 Canagagigue Creek Soils Map 33
3.6 Canagagigue Creek Wetlands 35
3.7 Canagagigue Creek Land Use / Land Cover (GRCA) 37
3.8 Canagagigue Creek LULC Proportions (GRCA) 38
3.9 Canagagigue Creek Land Use / Land Cover (OMAFRA) 40
3.10 Canagagigue Creek LULC Proportions (OMAFRA) 41
3.11 Tile Drain Location - West Basin without Riparian Wetlands 42
3.12 Tile Drain Location - East Basin with Riparian Wetlands 43

4.1 Map of Flow Measurement Stations and Cross Sections 47
4.2 Calculated Rating Curves Using HEC-RAS 48
4.3 Flow Distribution Curves by Reading Count and Flow Volume 51
4.4 Rain Gauge Network 54
4.5 Snow Survey Locations 55
4.6 GRCA Streamflow Measurement Locations 57
4.7 Hydrograph Centroid Lag - a) Hydrograph Lag as a function of rainfall intensity and b) Histogram of Hydrograph Lag difference between sub-basins (West-East) 59

5.1 Bankfull - Drainage Area for Natural and Incised Channels with Fitted Relationships . . . 66
5.2 Bankfull Area for Incised Channels (a) and Natural Channels (b) . . . 67
5.3 WatFlood model performance - 2006 . . . 76
5.4 Event Peak Flow (a) and Runoff Volume (b) Comparison - Floradale Stream Flow Station . . . 78
5.5 Event Peak Flow and Runoff Volume Relative Error - Floradale Stream Flow Station . . . 79
5.6 Hydrograph timing for wet antecedent condition event - Event 08 . . . 81
5.7 Hydrograph timing for dry antecedent condition event - Event 10 . . . 82
5.8 Event Peak Flow (a) and Runoff Volume (b) Comparison - East Sub-Basin 84
5.9 Event Peak Flow (a) and Runoff Volume (b) Comparison - West Sub-Basin 85
5.10 Wetland Storage Pattern - 2002 . . . 86

6.1 Investigative Sampling Program - Water Quality Sampling Locations . . . 98
6.2 Investigative Sampling Program - Concentration Box Plot by Riparian Protection . . . 100
6.3 Intensive Sampling Program - Water Quality Sampling Locations . . . 102
6.4 Nitrate - Total Nitrogen Regression relationships for the East (a) and West (b) Study Basins . . . 105
6.5 TSS - Turbidity Correlation . . . 105
6.6 TSS - TP Correlation . . . 107
6.7 Probability fequency of daily average concentrations within the East and West Basins for NO_3^- (a), total nitrogen (b), total phosphorus (c) and total suspended solids (d) . . . 110
6.8 TSS and NO_3^-Time Series - Low-flow event - 1 June 2006 . . . 113
6.9 TSS and NO_3^-Time Series - Snow melt event - 22 March 2007 . . . 114
6.10 Event-Based Total Mass Flux Comparison in East and West basins for (a) Nitrate , (b) Total Nitrogen, (c) Total Phosphorus and (d) Total Suspended Solids . . . 117
6.11 Monthly nutrient loading estimates and average monthly stream flow . . . 120

7.1 Storage Routing A-D Model - Grid Size Dependence 130
7.2 WatFlood Solute Routing Integration 131
7.3 Water Quality Model Input File Structure and WatFlood Integration . . 134
7.4 WATFLOOD Grid and Sub-Grid Elements 134
7.5 Sub-Grid Element Routing Network 135
7.6 WatFlood- Solroute Integration Flow-Chart 141
7.7 QUICKEST Model in WatFlood - Breakthrough profiles with varied grid element resolutions 143
7.8 QUICKEST Model in WatFlood - Mass conservation with varied sub-grid element resolutions 144
7.9 Storage Routing Model in WatFlood - Breakthrough profiles with varied grid element resolutions 145
7.10 Storage routing in WatFlood - Mass conservation with varied sub-grid element resolutions 146
7.11 Algorithm Performace Based on Grid Resolution 149
7.12 Riparian Sub-Grid Elements Schematic 150
7.13 Riparian-Channel Diffusion Computational Area 152
7.14 Riparian-Channel Exchange Test 153
7.15 Riparian Wetland Cover Calculation - Sample WatFlood Grid 164
7.16 Riparian Width Calculation Schematic 166
7.17 Illustrative Simulation of Riparian Loading to a Wetland in a WatFlood Grid - a) Flow from wetland to channel, b) riparian wetland nitrogen loading and fate, and c) riparian nitrate removal or denitrification rate 174
7.18 WatFlood Storage Zones Schematic 176
7.19 Nitrogen Uptake Profile - Corn 182
7.20 Soil Temperature Estimation Profiles a) 1999 Calibration b) 2000 Validation 188
7.21 Soil Temperature Estimation Calibration - University of Waterloo Weather Station 189

7.22 Nitrogen process results in a WatFlood grid for an illustrative multi-year simulation a) soil temperature, b) upper zone nitrogen species, c) lower zone nitrogen species 192

8.1 Measured and Simulated TSS Concentration Comparison for Calibration Period - a) East Sub-basin and b) West Sub-basin 204
8.2 Sediment Concentrations - Model Calibration and Validation for a) East Sub-Basin and b) West Sub-Basin 208
8.3 Sediment Model - Event Load Comparison for a) East Sub-Basin and b) West Sub-Basin 209
8.4 Monthly Sediment Load - Measured vs. Simulated - East Sub-Basin 211
8.5 Monthly Sediment Load - Measured vs. Simulated - West Sub-Basin 212
8.6 Monthly Measured and Modelled TSS Loading Comparison - a) East Sub-Basin and b) West Sub-basin 213
8.7 Monthly Sediment Load with Adjusted Snow Pack - Measured vs. Simulated - East Sub-Basin 218
8.8 Monthly Sediment Load with Adjusted Snow Pack - Measured vs. Simulated - West Sub-Basin 219
8.9 Monthly Measured and Modelled TSS Loading Comparison with Adjusted Snow Pack - a) East Sub-Basin and b) West Sub-basin 220
8.10 Measured and Simulated Nitrate Concentration Comparison - a) East Sub-basin and b) West Sub-basin 232
8.11 Nitrate Event load comparision for a) East sub-basin and b) West sub-basin 234
8.12 Monthly Nitrate Load - Measured vs. Simulated - West Sub-Basin 236
8.13 Monthly Nitrate Load - Measured vs. Simulated - East Sub-Basin 237
8.14 Nitrate Monthly Load Comparison - a) East Sub-Basin and b) West Sub-Basin 238
8.15 Measured and Simulated Nitrate Concentration Profile - Event 2, East sub-basin 239
8.16 Measured and Simulated Nitrate Concentration Profile - Event 12, East sub-basin 240

8.17 Measured and Simulated Nitrate Concentration Profile - Event 6 (Snowmelt), East sub-basin 241
8.18 Riparian Contribution to Nitrate Removal - Cumulative Nitrate Loading, East Sub-Basin 244
8.19 Instantaneous Residence Times for Riparian Wetland and Lower Zone storage 246

A.1 Stage Measurement Installation Schematic 288
A.2 Float Installation - East Sub-Basin (26-Sep-2005) 289
A.3 Float Installation - West Sub-Basin (14-Apr-2005) 289
A.4 Map of Study Site - Topographic Survey Data 290
A.5 Level Stream Cross-Section Measurement Locations 291
A.6 Bank-Full Area vs. Drainage Area 292
A.7 Stage vs. Logger Voltage Relationship – 2005, 2006 and 2007 Seasons . . . 294
A.8 Canagagigue Creek - West Sub-Basin, Velocity Profile (23-Mar-2007) . . . 297
A.9 Flow Centroid Calculation - East Sub-Basin 298
A.10 Flow Centroid Calculation - West Sub-Basin 298
A.11 Stage-Discharge Relationships 299
A.12 HEC-RAS Manning's n Calibration - West Sub-Basin 303
A.13 HEC-RAS Manning's n Calibration - East Sub-Basin 304

B.1 Canagagigue Creek Grid Areas (FRAC) 306
B.2 UW Tipping Bucket and GeoNor Gauge Comparison 309
B.3 Study Site Rain Gauge Validation - 2005 310
B.4 GRCA Rainfall 2000 310
B.5 GRCA Rainfall 2001 311
B.6 GRCA Rainfall 2002 311
B.7 GRCA Rainfall 2003 312
B.8 GRCA Rainfall 2004 312
B.9 GRCA Rainfall 2005 313
B.10 Monthly Cumulative Precipitation Source Timing Comparison 314
B.11 Hydrologic Modeling - GRCA Stream Gauges - 2000 316

B.12 Hydrologic Modeling - GRCA Stream Gauges - 2001 317
B.13 Hydrologic Modeling - GRCA Stream Gauges - 2002 318
B.14 Hydrologic Modeling - GRCA Stream Gauges - 2003 319
B.15 Hydrologic Modeling - GRCA Stream Gauges - 2004 320
B.16 Hydrologic Modeling - GRCA Stream Gauges - 2005 321
B.17 Model Validation - Nash-Sutcliffe and Relative Volume Error 323
B.18 Daily Runoff Comparison - 2005 (No Snow melt) 324
B.19 Daily Runoff Comparison - 2006 (No Snow melt) 325
B.20 Daily Runoff Comparison - 2007 (No Snow melt) 326

C.1 Ion Chromatograph - Conductivity Detector - Nitrate QA 337
C.2 HACH Spectrophotometer - Total Phosphorus QA 338
C.3 HACH Spectrophotometer - Total Nitrogen QA 338

D.1 QUICKEST Control Volume and Control Volume Interface Index Key . . . 346
D.2 QUICKEST Downstream Boundary Condition Schematic 351
D.3 Routing Profile Comparison - Point Constituent Addition of 200 at X=200m, Cr=0.75, Pe=12.5, Timestep = 15sec, Number of timesteps=80 359
D.4 Mass Conservation Comparison - Point Constituent Addition of 200 at X=200m, Cr=0.75, Pe=12.5, Timestep = 15sec 360
D.5 Profile Error - HPCN and QUICKEST Routines - Point Constituent Addition of 200 at X=200m, Cr=0.75, Pe=12.5, Timestep = 15sec 361
D.6 Routing Profile Comparison - Step Constituent Addition of 200 from 125m - 2075m, Cr=0.75, Pe=∞, Timestep = 15sec 363
D.7 Mass Conservation Comparison - Step Constituent Addition of 200 from 125m - 2075m, Cr=0.75, Pe=∞, Timestep = 15sec 364
D.8 Profile Error - HPCN and QUICKEST Routines - Step Constituent Addition of 200 from 125m - 2075m, Cr=0.75, Pe=∞, Timestep = 15sec 365
D.9 Grid-to-Grid Profile Progression - Square Wave, C=1, α=0 367
D.10 Grid-to-Grid Profile Error Comparison - Square Wave, C=1, α=0, t=6000 368
D.11 Grid-to-Grid Mass Conservation - Square Wave, C=1, α=0 369

D.12 Grid-to-Grid Profile Progression - Instantaneous Point Addition, C=0.75, Pe=12.5 371
D.13 Grid-to-Grid Profile at Grid Boundary - Instantaneous Point Addition, C=0.75, Pe=12.5, t=3600 372
D.14 Grid-to-Grid Profile Relative Error - Instantaneous Point Addition, C=0.75, Pe=12.5, t=3600 373
D.15 Grid-to-Grid Mass Conservation - Instantaneous Point Addition, C=0.75, Pe=12.5 375
D.16 Sediment Resuspension Test Case in SOLROUTE Framework - a) Resuspension Profile Comparison with Analytical Solution b) Relative Error by Time Step 376
D.17 First Order Decay - Test Framework - Point addition at x=1000 m, C=0.75, λ=0.0075, Pe=12.5 - a) Profiles at t=1200 s, t=3600 s and t=6000 s, b) comparison with analytical solution at t=3600 s c) Profile Error comparison at t=3600 s 378
D.18 Grid-to-Grid Mass Conservation - First Order Decay - Test Framework - Point addition at x=1000, C=0.75, Pe=12.5, λ=0.0075 379
D.19 QUICKEST Model in WatFlood with 1st-order decay (K=0.0005 sec^{-1} - Mass conservation with varied sub-grid element resolutions as compared to the analytical solution (a) and the total error in the system (b) 381
D.20 Fertilizer Loading Algorithm 382
D.21 Sediment Model Parameter Sensitivity - NOLS and NASH absolute sensitivity based on 5% parameter perturbation 386
D.22 Sediment Model Parameter Sensitivity - Total solids loading sensitivity by sub-basin based on 5% parameter perturbation 387
D.23 Hydrologic Model Parameter Sensitivity - Sediment model NOLS and NASH absolute sensitivity based on 5% parameter perturbation 388
D.24 Hydrologic Model Parameter Sensitivity - NOLS and NASH absolute sensitivity based on 5% parameter perturbation 389

D.25 Nitrate Model Sensitivity - Model performance absolute sensitivity by objective function based on 5% parameter perturbation 391
D.26 Nitrate Model Sensitivity - Nitrate loading sensitivity by sub-basin based on 5% parameter perturbation (Jan 2005 – May 2007) 392
D.27 Hydrologic Model Sensitivity - Model performance absolute sensitivity by nitrate objective function based on 5% parameter perturbation 393
D.28 Hydrologic Model Sensitivity - Nitrate loading sensitivity by sub-basin based on 5% parameter perturbation (Jan 2005 – May 2007) 394

List of Tables

3.1 Drainage areas and land use as percentage of basin area for the study sub-basins within the Canagagigue Creek watershed 39

4.1 Total Precipitation by Captured Event and Rain Gauge Location 56

5.1 OMAFRA LULC to WatFlood Land Class Mapping 69
5.2 Annual Non-Snowmelt Nash-Sutcliffe and Runoff Volume Differences in Calibrated Model 77

6.1 Investigative Sampling Program - Sampling Dates 97
6.2 Investigative Sampling Program - Sampling Location Grouping 99
6.3 Investigative Sampling Program - Population Mann-Whitney Test Statistics 101
6.4 Captured Runoff Events - Sampling Periods 103
6.5 TSS Regression Model Parameters 109
6.6 Alma Research Station Effluent Water Quality 112
6.7 Event Loading Signed-Rank Test Summary 116
6.8 Average monthly nutrient and sediment load for study period 118
6.9 Percentage load contribution of snowmelt months (March 2006, March 2007) to total estimated load over study period 119

7.1 Contaminant Transport Routine Performance - Simulation Time by Routine and sub-grid resolution (seconds) 148

8.1 Sediment Modelling Parameters 198

8.2 Sediment Objective Function Weighting Parameters 202
8.3 Calibrated Sediment Parameters 203
8.4 Sediment Calibration Period Objective Function Values 204
8.5 Sediment Validation Period Objective Function Values 206
8.6 Nitrate Sub-Model Parameters 222
8.7 Crop Nitrogen Annual Removal Rates 223
8.8 Crop Nitrogen Annual Uptake 224
8.9 Previous Crop Nitrogen 224
8.10 Regional Manure Application Estimates - Adapted from Scott (2006) . . . 226
8.11 Nitrate Parameters Optimized 231
8.12 Nitrate Model Calibration Statistics 233
8.13 Nitrate Model Validation Statistics 233

A.1 Manning's n Estimates 302
A.2 Calibrated Manning's n Values 303

B.1 Canagagigue Creek Sub-Basin Drainage Areas 307
B.2 Calibration Results 322

C.1 Total Phosphorus - MDL 339
C.2 Total Nitrogen - MDL 340
C.3 IC - Anion Method Deteciton Limits 341
C.4 IC - Cation Method Deteciton Limits 342

D.1 WatFlood Hydrologic Parameter List 384

Chapter 1

Introduction

The importance of maintaining a high quality of surface and groundwaters is recognized by government agencies around the world. Through anthropogenic influences the quality of surface waters have been shown to have degraded and numerous human activities have been shown to have deleterious effects. Agricultural land use activities are of particular concern. The application of fertilizers and animal manures to fields to enhance crop yields, livestock grazing and tillage of soil can have direct negative impacts on nutrient, pathogen and sediment contributions to receiving waters. Agricultural practises can be particularly problematic primarily due to their ubiquity and the difficulty in mitigating and quantify the associated negative impacts due to the distributed nature of the contaminant sources. Diffuse pollution, or a pollution source that does does not impact the environment from a discrete point, is defined as Non-Point Source (NPS) pollution (US-EPA, 2005). Non-point sources of pollution include rural activities such as farming, mining and forestry operations as well as urban activities and developments. As stewards of the environment, scientists, engineers and government authorities are challenged to accurately assess and quantify the mechanisms for the delivery of those contaminants into receiving watersheds, and because of their diffuse nature NPS pollution is more difficult to mitigate once applied and its transport is controlled by weather effects and hydrological processes over large areas.

In order to mitigate non-point source pollution impacts in agricultural watersheds, research has lead to the implementation of Best Management Practises or Beneficial Man-

agement Practises (BMP). These BMPs include modified tilling or no-tilling practises in farmers fields, the implementation of buffer zones and strategic fertilizer application techniques and are designed to mitigate the impact of the land use activity on the quality of the receiving waters. Steps have been taken by governments around the world to attempt to mitigate the impacts of non-point source pollution, particularly from agricultural activity by mandating the implementation of or adherence to BMPs. In the USA, the Clean Water Act was amended in 1987 to include a mandate requiring states implement programs for the control of non-point source pollution, including runoff from agricultural areas, urban areas, forestry, mining and construction sites. More locally to Waterloo, Ontario the Grand River Conservation Authority (GRCA) has a policy aimed at the protection of wetlands, in part due to the water quality benefits (GRCA, 2003c). The Ontario Ministry of Agriculture, Food and Rural Affairs (OMAFRA) also publishes many guides on appropriate BMPs for farmers (OMAFRA, 2003; OMAFRA, 2008a). The goals of each group is the same: to take the best scientific understanding to reduce pollution loads to receiving waters while balancing the needs of the agricultural industry.

Role of Riparian Wetlands

Riparian wetlands as a BMP have been identified as a potential solution to NPS pollution concerns in some areas. Riparian wetlands are seen as a buffer zone capable of intercepting and either storing or chemically transforming the pollutants from upland contributing areas and thereby protecting receiving waters (US-EPA, 2005). Many studies have been conducted at the field scale to assess the impacts of riparian wetlands on sediment and nutrient removal and results have indicated that generally the impact and influence of riparian wetlands is dictated largely by hydrology and flow path where retention time in the riparian wetland plays an important role in its treatment efficacy (Whigham et al., 1988; Hill, 1996; Phillips, 1996). Some results of the benefits due to riparian wetlands on receiving-water quality are varied; in some cases clear benefits to receiving waters have been shown (Lowrence et al., 1983; Peterjohn and Correll, 1984; Cey et al., 1999), in others the benefits are not clear (Whigham et al., 1988; Phillips, 1996).

Predictive Modelling

In addition to the field studies of the hydrological and water quality impacts of riparian wetlands on a watershed, having a computational model or modelling framework would be advantageous for watershed planning with regard to BMP design and maintenance.

Field studies conduced in the 1980's and 1990's were followed by model development and the implementation of process discoveries into mathematical predictive models. Much recent work has been done in the development of physically-based distributed hydrological models, due to the rapid improvement in computer technology and data acquisition techniques. Models such as WATFLOOD (Kouwen, 1988), MESH (Pietroniro et al., 2006a), and the European Hydrological System (SHE) (Abbott et al., 1986) have been developed for and to include data from a variety of distributed sources, including land cover data from remote sensing, RADAR precipitation data, etc. An extension of these advancements in hydrological modelling has been the development of hydrological water quality models that operate at a similar scale. Some of the more popular models of this type include the Agricultural Non-Point Source (AGNPS) model (Young et al., 1989) and the Soil-Water Assessment Tool (SWAT) (Arnold and Fohrer, 2005). SWAT in particular has shown much activity in recent years with the recent inclusion of the SWAT routines in the US-EPA BASINS project (US-EPA, 2001). With an emphasis on water, quality SWAT also includes some sub-routines to allow for BMP modelling to assist in the simulation and quantification of their effects on a basin scale.

The WATFLOOD model in particular was designed to be an operational model at larger scales and is a popular hydrological model employed in Canada (Singh and Frevert, 2006). With an established hydrological performance record, the WATFLOOD model has been recently enhanced for the simulation of water quality constituents within the WATFLOOD framework (Leon, 1999; Dorner et al., 2006) and isotopic isotope transport (Stadnyk et al., 2005). Additionally WATFLOOD is one of the few watershed models to contain a hydraulically coupled riparian wetland storage model in its routing routine (Kouwen, 2005).

1.1 Research Objectives

The ultimate research objective was to develop, validate and incorporate a stream water quality model into the WatFlood modelling framework that accounts for the presence of riparian wetlands. This model will build on the existing NPS pollution model developed by Leon et al. (2001) and Dorner et al. (2006). Additionally, the research took advantage of the relatively recent addition of a riparian wetland hydrologic sub-model included in the WatFlood. The region of interest was the Grand River watershed in southern Ontario, a region heavily impacted with agricultural activity, but with some riparian wetlands remaining. The Grand river has be extensively modelled using the WatFlood model.

In addition to the development of the water quality sub-model that simulates in-stream water quality and riparian zone interactions, one of the necessary tasks is the acquisition of data to provide a validation dataset for the model. Richards (2002) and Inamdar et al. (2006) among others have identified the importance of event-based sampling in characterizing contaminant fluxes in watersheds and event-based monitoring has been identified as an important approach to determining the physical transport mechanisms within a watershed. Nutrient and sediment loadings are naturally higher during periods of high flow and it becomes important to characterize the fluxes during an event to determine total loadings (Inamdar et al., 2006; Macrae, 2003). Infrequent, low-flow sampling may not characterize the rapid changes in analyte concentration with changes in the position along the hydrograph and flow rate. These observations were of particular interest when acquiring a dataset for this research.

The research objectives can be summarized as follows:

1. Assess the influence of riparian zones on water quality patterns at a sub-watershed scale through data collection from monitored basins;

2. Provide a hydrological and water quality dataset for the assessment of the influence riparian wetlands in the southern Ontario region;

3. Develop a water quality sub-model to improve in-stream water quality modelling with special consideration of riparian zones;

4. Assess the WatFlood hydrological modelling framework as a platform for NPS pollution transport simulations; and

5. Characterize influence of riparian zones using modelling tools.

1.2 Research Plan and Document Structure

This research project included the following steps:

1. Literature review;

2. Selection of study site;

3. Hydraulic and hydrological characterization, monitoring and modelling;

4. Water quality monitoring and analysis; and

5. Water quality modelling.

Each of the above tasks is outlined briefly below to provide a summary description of the research approach. Details of the methods and results are presented in subsequent chapters in this document.

1.2.1 Literature Review, References and Glossary

A literature review of relevant research and scientific principles is presented in Chapter 2. A list of references is presented on page 257. Acronyms, file names, and other terms used frequently in this document are collected in a glossary presented on page 277. A list of mathematical symbols used in this document is presented on page 280.

1.2.2 Study Site Selection

A hydrologic and water quality dataset was required to assess the influence of riparian wetland protection on the stream corridors receiving waters at the sub-watershed scale.

This dataset was also required to assess the hydroloic and water quality models that were developed to simulate the influence of riparian wetlands. Some available datasets were investigated including that of the South Tobacco Creek experimental watershed in Manitoba (AAFC, 2002) and the water quality sampling data for the Grand River watershed provided by the Ontario Ministry of the Environment (Cooke, 2006). However, the datasets did not have a clear isolation of the riparian wetland influences at sampling locations, were complicated by reservoirs and other control structures, or the sampling protocols were not of a high enough frequency to include the effects of storm or snow melt events.

A study site was established in the Canagagigue Creek watershed, a sub-basin of the Grand River Watershed in Southern Ontario. The northern headwaters of the Canagagigue Creek are heavily impacted by agricultural activity, have no reservoirs or control structures and have sub-basins with distinctly different riparian wetland cover. Additionally, the GRCA has extensive real-time monitoring of the watershed for meteorological data and stream flow, and several recent hydrological modelling studies have been conducted on the Canagagigue Creek. After some investigative sampling the study site was selected and metered hydrologically, and water quality sampling was conducted.

The selected site included two adjacent sub-basins with similar land use and physiographic characteristics, but with differing degrees of riparian wetland protection on the main corridor. The basins were adjoining with the basin to the West having virtually no riparian wetland protection along the main stream corridor. The basin to the East had approximately 46% of its main stream corridor protected by 10m or more of riparian wetland. The basins were labelled "West" and "East" respectively. Each sub-basin had a drainage area of approximately 11 km^2 and each was dominated by agricultural land use activity.

Details of the study site are presented in Chapter 3.

1.2.3 Hydraulic and Hydrological Characterization, Monitoring and Modelling

After the site was selected, the outlets of the sub-basins were metered in order to determine the stage-discharge relationships and flow rates from the East and West sub-basins. Flow

measurements were taken using velocity-area and dilution gauging methods. Topographic surveys were conducted near the confluence of the east and west basins for the development of a hydraulic model (HEC-RAS) to assist in the extrapolation of the stage-discharge rating curves beyond measured flows, and river cross sections were taken at locations throughout the sub-basins to record bank-full levels. Water level information was collected continuously during non-winter seasons to determine flow rates for hydrological analysis and the calculation of contaminant fluxes. Winter water quality samples and flow measurements were not collected due to freeze-up. Water-level and flow information was collected from March 2005 to August 2007. Additionally, the GRCA operates a number of flow measurement stations within the Canagague Creek downstream from the study site and provisional data was available from January 2000 for Floradale, Elmira and a stream gauge below Elmira.

Precipitation data was acquired from two rain gauges installed as a part of this study, as well as the rain gauge network maintained by the GRCA. The GRCA maintains one rain gauge within the Canagagigue Creek and a number of gauges around the Canagagigue Creek in adjoining watersheds. Precipitation data was also available from the University of Waterloo Weather Station. Radar precipitation estimates were collected from the King City Radar station as 5cm Doppler RADAR CAPPI 1 hour cumulative rainfall measurements. Air Temperature data was available from the GRCA and from the University of Waterloo Weather Station. Snow surveys were conducted as a part of this study and snow surveys were available from the Ontario Ministry of Natural Resources (MNR) from 2003 onward.

The precipitation, meteorological and snow survey data were used with the stream flow data to develop a hydrological model for the Canagagigue Creek for hydrological assessment as it relates to water quality within the study sub-basins. The WatFlood hydrologic model was employed in modelling the hydrology of the study basin and the Canagagigue Creek. WatFlood was identified as an appropriate choice as it includes a coupled riparian wetland component for hydrological modelling and physically-based flood routing.

Details on the collection and analysis of the hydrologic and meteorological data are described in Chapter 4.

Details of the hydrological modelling are presented in Chapter 5.

1.2.4 Water Quality Monitoring and Analysis

In order to assess the impacts of land use and riparian protection on the water quality in the upper Canagagigue Creek, two separate sampling and analysis procedures were implemented. Prior to the selection of a study site some investigative water quality sampling was conducted within the upper Canagagigue watershed. Manually collected samples were analysed for solids and nutrient components during varied hydrological conditions.

During an intensive sampling program, samples were collected at high frequency on an event-basis and additional manually collected samples were obtained during low flow periods. Combined with flow data, analyte flux calculations were produced. The two sub-basins were compared based on their total analyte fluxes as well as their analyte time-series profiles. Constituent loading estimates for the two sub basins were determined based on interpolation techniques.

Details of the water quality sampling, analysis and data interpretation can be found in Chapter 6.

1.2.5 Water Quality Modelling

A preliminary water quality sub-model was developed for the WatFlood modelling framework by Leon et al. (2001). Although extremely useful and validated as a water quality predictor in a number of studies (Leon et al., 2004; Leon, 1999; Dorner et al., 2006) this model showed four primary deficiencies for this study which are discussed in Chapter 7:

1. The contaminant routing routine was subject to excessive numerical dispersion and lack of mass conservation under certain conditions;
2. No capability for sourcing contaminants from in-stream processes;
3. No capability for continuous (multi-event) water quality modelling; and
4. No consideration of hydrological or water quality impacts due to riparian wetlands.

The existing water quality model was modified to ameliorate each of these identified issues. An improved in-stream contaminant transport model was developed using more advanced and mass conservative routines. Additionally, the water quality modelling at the land surface was modified to allow for continuous simulation required for nutrient load modelling in agricultural models including crop uptake and fertilizer mineralization and transport into deep groundwater.

The modelling efforts in this regard are described in Chapters 7 and 8.

Chapter 2

Literature Review

Water quality concerns at the watershed scale and the associated impacts of wetlands and riparian buffers require a multi-disciplinary approach to analysis. This section examines some of the research in the literature that examines the various constituent components of this type of study. The areas reviewed are: the science of riparian wetlands and buffer ecosystems, wetland models; watershed scale hydrological models and water quality models; and field-scale water quality models considering riparian buffers.

2.1 Non-Point Source Pollution in Agricultural Systems

Non-Point Source (NPS) pollution or diffuse pollution are pollution sources to receiving waters without clearly identifiable locations of discharge. Point sources are more easily defined and, by contrast, have an identifiable location where pollution is discharged to receiving waters and can include waste water discharge locations, sewer outflows, runoff from a solid waste disposal site, etc. Point sources are often regulated by local environmental authorities in terms of pollution discharge quantities, and by virtue of discharging from a single location, developing engineering solutions for pollution retention and treatment are generally more easily accomplished. NPS or diffuse source pollution is most easily

identified as *not* being form a point source and includes polluted runoff from agricultural fields, polluted rainfall such as acid rain, and runoff from urban areas, among others. NPS pollution sources provide engineering and regulatory challenges because the quantity and timing of pollution discharge to the receiving waters is driven by meteorological and hydrological processes, the sources themselves are difficult or impossible to identify because of their distributed nature, and the quantity of pollution can be affected by a number of factors including physiographic conditions and land use practises. The mitigation of NPS pollution necessarily requires remedial action over a larger geographical area rather than a single discharge point making traditional engineering solutions for water treatment untenable, and instead requiring regulations that control land use activities regionally.

Considering the distributed nature of NPS pollution, and the role of hydrology as a delivery mechanism, the quality of the receiving waters of a watershed will necessarily be affected by the type of land use activities present within it. For the USA and Canada dramatic increases in pollution levels in receiving waters have resulted from a rapid conversion to intensive agriculture in the 1950s (Novotny and Olem, 1994). It is generally accepted that NPS pollution has a direct influence on the quality of receiving waters, particularly in the case of agricultural activities (Lowrance et al., 1984b,a; Cirmo and McDonnell, 1997). It has been understood for many years that one of the primary causes of eutrophication in lakes in the United States is the over-application of fertilizer in agricultural systems (Chapra and Robertson, 1977; Carpenter et al., 1998) and similar results have been seen around the world (Oenema et al., 2005). The over-applications of fertilizers in agricultural systems with well drained soils can result in groundwater contamination by nitrate which can cause methemoglobinemia in infants (Kapoor and Viraraghavan, 1997). Additionally, nigrogenous fertilizers in high concentrations have been shown to have serious ecological consequences and can have a deleterious affect on amphibians, affecting larvae mobility, causing mutations or mortality (Blaustein and Kiesecker, 2002). Nitrate contamination of groundwater due to agricultural activity is a global problem (Spalding, 1993) and the degree of nitrate contamination of groundwater has recently shown patterns of increase in the USA with the USGS showing markedly higher concentrations of nitrate in sampled wells as part of the National Water Quality Assessment Program (Rupert, 2008).

Sediment loading in rivers is also an environmental concern. Sediment derived from erosion of agricultural fields has been recognized as a contributor of pollution to river systems in southern Ontario and the Great Lakes (Wall et al., 1982) and can adversely influence fish spawning grounds (Cordone and Kelley, 1961). Phosphorus tends to be less soluble and the largest portion of phosphorus tends to be transported with eroded soil during storms and runoff events (USGS, 1999) and represent a significant contributor to receiving water eutrophication.

2.1.1 NPS Pollution in Southern Ontario

Non point source pollution has been a perennial problem within in Southern Ontario, with the a high percentage of land use devoted to intensive agricultural activity. The Great Lakes Pollution from Land Use Activities (PLUARG) study was a major research effort conducted from 1973 to 1978 involving the International Joint Commission (IJC) designed to determine the origins of pollutions contributing to the Great Lakes. The study concluded that land runoff was a major source of pollution to the great lakes and that phosphorus and sediment loadings in particular were considered particularly problematic and recommended a reduction of NPS loadings in the region (PLUARG, 1978).

Problems in the region persist to this day. The Grand River Conservation Authority (GRCA) produced a recent report outlining the health of the Grand River as pertaining to surface water quality. The report was produced by using data collected by the GRCA as well as the Ontario Ministry of the Environment (MOE) as part of Ontario's Provincial Water Quality Monitoring Network (PWQMN) for the years 2000 to 2004 (Cooke, 2006). Data presented showed that the Grand River watershed had persistent water quality issues particularly with regard to sediment and nutrient concentrations. The sub-watersheds in the central portion of the Grand River, including the Canagagigue Creek, were shown to be the most heavily impacted. The Canagagigue Creek in particular showed high contributions of nitrate and total phosphorus. In the Grand River watershed, suspended sediment, along with total phosphorus which is highly correlated to sediment loading, is the most serious contaminant loading issue in the watershed (Cooke, 2006). Cooke (2006) highlighted limitations in the water quality sampling protocol employed as too few samples

were collected a year per sampling location (8) and the samples were not collected during high-flow conditions, necessarily limiting the ability to estimate hydrologic variation in concentrations and constituent fluxes and the estimates of the fluxes, particularly for sediment loading, may be much higher than estimated in this report. The region does not only suffer from surface water contamination but also that of groundwater. Groundwater nitrate contamination was determined during well surveys showing pervasive and significant nitrate contamination of groundwater sources in the region (Goss et al., 1998).

2.2 Agricultural NPS Transport and Fate Mechanisms

In order to predict and understand the nature of NPS pollution in agricultural watersheds it is important to understand the sources and fates of of the pollution constituents. In this study modelling efforts focused on sediment and nitrogen transport. In this section some principles of the source and transport of each are reviewed.

2.2.1 Sediment Transport

Sediment is conveyed to receiving water through erosive processes driven primarily by water flow and only in regions with almost no rainfall can wind forces be expected to be the most significant erosive agent (Leopold et al., 1992). Erosion can be loosely classified into various types, which are characterized by the nature of the hydraulic conveyance: sheet and rill erosion; gully erosion; and stream or floodplain scour (Foster, 1982; Novotny and Olem, 1994). These processes are not truly distinct, but represent a continuum of sediment conveyance scenarios based on topography and flow fields, and distinctions are made by imprecise definitions of rill and gully sizes. Hydrologically, erosive processes are often segmented into just two distinct types, upland and in-stream erosion, as this segmentation matches cleanly the segmentation between overland and in-stream hydrological transport (Novotny and Olem, 1994).

Fundamentally, sediment transport is regulated by a force balance between shear stresses acting on soil particles by flowing water and the forces that keep a particle in place at the surface. The shear stress is dictated by the hydraulic conditions of the flow field, with

higher velocities and deeper flows applying greater shear stresses to particles at the soil surface. Soil or sediment particles resist transport by their density and particle size, adhesion to other soil particles, protection from erosion by vegetation (Novotny and Olem, 1994).

Sediment is classified into two types (Leopold et al., 1992):

- *bedload*, where sedimentis of a larger size remains near the bed and is generally supported by the bed, or;
- *washload*, where the sediment is of a smaller size, remains in suspension due to turbulence in flow and can be transported great distances before settling.

Leopold et al. (1992) suggested that in humid areas the majority of total sediment delivered from watersheds is fine sediment or washload, the character of which is strongly correlated to local geology.

2.2.2 Nitrogen Fate and Transport

Nitrogen is an essential nutrient in all living organisms, required for amino acid and protein development, nucleic acids and other biologically necessary molecules. All nitrogen is ultimately sourced from the atmosphere as nitrogen gas, which is biologically unavailable, and finds its way to the biosphere through *nitrogen fixation*. Nitrogen fixation can occur biologically whereby specialist organisms can covert atmospheric nitrogen to ammonia (NH_3) or ammonium (NH_4^+). Some plants including legumes, are nitrogen fixing crops and are often included in crop rotations to replenish nitrogen in soil (Jaffe, 1992). Nitrogen can also be fixed by industrial process or by lightning activity which combines nitrogen with oxygen under high temperatures to produce nitric oxide, nitrogen dioxide or nitric acid (Jaffe, 1992).

Organic nitrogen, that is nitrogen stored in complex organic molecules including protein, nucleic acids, urea, etc., can be converted to inorganic nitrogen in a process called *mineralization*. The process has can also be identified by a more limited term, *ammonification* which is the specific production of ammonia from organic nitrogen (Tate, 1995).

Mineralization is driven by microbial activity and the rates of mineralization depend on a host of biochemical and environmental variables, including the nature of the organic nitrogen, temperature, pH, soil moisture, soil characteristics, among others (Stanford and Smith, 1972; Campbell et al., 1984; Das et al., 1995; Eghball et al., 2002). Nitrogen *immobilization* is the reverse process of nitrogen mineralization and represents the assimilation of nitrate or ammonia into bacterial biomass (Tate, 1995). Nitrogen can also be immobilized through ammonia fixation to clay or organic matter, and chemical reactions that result in the polemerization of amino acids (Novotny and Olem, 1994). The competing mineralization and immobilization processes are often combined in modelling and measurement practise to provide a *net mineralization* (Campbell et al., 1988; Van Kessel and Reeves, 2002).

Ammonia nitrogen can be assimilated by organisms for the production of biomass, but may also be changed to nitrate (NO_3^-) nitrogen through bacterial activity called *nitrification*. Nitrification is a two-stage oxidation process necessarily requiring available oxygen, the rate of which is affected by other biological limiting factors including temperature, pH, soil moisture and substrate availability (Tate, 1995). The nitrification of ammonia is usually a much more rapid process in soils than organic nitrogen mineralization making the production of nitrate nitrogen from organic nitrogen mineralization rate-limited (Tate, 1995).

It is known that plants are able to sorb inorganic nitrogen and will reduce available ammonium and nitrate/nitrite pools in the root zone via ammonia and nitrate assimilation (Jaffe, 1992; Tate, 1995). This has been the typical conceptual model in plant nitrogen uptake but recent research has shown that plants are able to assimilate more complex nitrogen molecules, especially under low nitrogen conditions (Schimel and Bennett, 2004).

Under anoxic conditions nitrate may be converted to gaseous nitrogen forms by *denitrification* by denitrifiying bacteria. Dentrification usually occurs in subsoils of low permeability that are saturated for an extended period and requires available carbon as an energy source as denitrifing bacteria are heterotopic (Novotny and Olem, 1994). Wetlands and permanently saturated groundwater soils, and hyporheic zones in streams have are identified as potential locations for possible dentrification (Duff and Triska, 1990; Novotny

and Olem, 1994; Kadlec and Knight, 1996). Because of the reliance on a saturated zone for denitrification, the capacity of a denitrifying area to remove soluble nitrate will depend on the hydraulic residence time, as well as reaction rate kinetics and available oxygen.

In soil, nitrogen can be transported from the soil matrix by leaching with moving groundwater. Nitrate and nitrite nitrogen are negatively charged ions and are highly mobile and conduct readily with groundwater flow. Ammonium ions possess a positive charge tending to attract and affix them to colloidal and organic soils resulting in a reduced mobility within soils (Jaffe, 1992).

2.2.3 Tile Drains

Areas that have poorly drained soils, low relief can be slow to drain naturally hindering their use in agricultural activity. The introduction of artificial drainage or tile drainage can facilitate drainage in an otherwise poorly drained field and allow for the development of agricultural activity on that field or a longer growing season. The Grand River watershed once had extensive wetland cover, but much of these wetlands were drained over recent centuries to facilitate agricultural development in the area (GRCA, 2003c). Tile drainage facilitates the rapid movement of near-surface groundwater to receiving waters, and consequently can have significant impacts with regard to nutrient transport. Macrae (2003) performed a study at Strawberry Creek, Ontario that illustrated the importance of high-frequency event based sampling to adequately characterize contaminant dynamics in a small watershed and that occasional base-flow sampling was inadequate to characterize loading in the basin. Macrae et al. (2007) identified that tile drains can be of particular importance when examining total phosphorus loading and can account for 43% of total phosphorus export within the study sub-basin and that fertilizer practices had an impact on the character and quantity of phosphorus loading, with manure resulting in greater TP exports. Rudolph and Parkin (1998) found that the presence of tile drains tended to reduce the degree of nitrate recharge to the groundwater and directly into the surface water drains. Uusitalo et al. (2001) studied solids concentrations in surface flow and tile drains and found that the drain TSS concentrations were not statistically different from surface runoff concentrations in 91 paired water quality samples from two clayey drained

fields in Finland, showing that tile drains can be a contributor to suspended sediment concentrations in the receiving channel.

2.3 Riparian Wetland Studies

A riparian wetland of a river, stream or other body of water is the land adjacent to the body of water that is, at least periodically, influenced by flooding and a high water table (Mitsch and Gosselink, 1993). It has long been recognized that riparian wetlands play important functional roles in fluvial ecosystems, including stream stabilization, the filtering of sediments and nutrients, flood wave attenuation and the provision of fish habitat (Gilliam, 1994; Mitsch and Gosselink, 2000; Bullock, 2003).

Regarding non-point source (NPS) pollution reduction, riparian zones and riparian wetlands have been identified as playing a role in water quality improvement including removing pollutants such as sediment, nitrogen, phosphorus and heavy metals by buffering receiving waters from the effects of pollutants or preventing entry into receiving waters (US-EPA, 2005). As riparian zones represent boundaries or interfaces between the upstream hill slopes and the receiving streams themselves they should represent an important final barrier between upland nitrogen sources and receiving waters (Cirmo and McDonnell, 1997). Studies reviewed here have tended to be either of the field scale, or of a more regional or watershed scale. They are so divided in this section.

2.3.1 Field Scale Studies

Riparian zones have been found to be effective sediment filters through physical processes and nutrient sinks through biological processes of plant uptake and denitrification (Lowrence et al., 1983; Peterjohn and Correll, 1984; Hill, 1990; Cey et al., 1999). In a field study Karr and Gorman (1975) observed in a study of Black Creek, Indiana, that riparian forests could effectively act as a sink for sediment during most storm events with a 20% reduction in suspended sediment concentration, however during very large flow events sediments could be exported from the riparian forests. Gilliam (1994) identified riparian wetlands as “tremendously effective” at trapping sediments in his manuscript reviewing

riparian wetland efficacy in removing NPS pollution. Cooper et al. (1987) examined the sediment trapping efficacy in two coastal plain watersheds and estimated a 84 to 90% retention of sediment from cultivated fields by the riparian areas. Hill and Waddington (1993) employed conservative isotopic signatures and nitrate/ammonia data within a wetland during a storm event. Ammonia concentrations were found to be unrelated to discharge and it was intimated that biological uptake was a cause.

Gale et al. (1993) performed field scale studies on constructed and natural wetlands for nitrogen removal. Nitrogen removal showed first order decay rate constants that varied from 0.086 to 0.214 (1/day) for the wetland soils examined. The mineral soils seemed to perform better at overall nitrogen removal than organic soils. Nitrification followed by denitrification seemed to be the dominant process for removal. High levels of nitrogen were being removed (80% +), but the retention times were very high (on the order of 20 days).

Cey et al. (1999) examined the effects of riparian zones on nitrate concentrations in a near-stream agricultural field. Sharp reductions in the concentrations of nitrate were observed at the boundary between the agricultural field and the riparian zone. The study showed denitrification as the primary nitrogen removal mechanism. The study also showed higher levels of groundwater recharge in the riparian zone, which forced contaminants down into groundwater.

The flow paths through wetland or riparian buffer strips have been identified as very important (Devito et al., 2000). With complex flow paths and deep confining layers the hydraulics of the system may direct flow beneath or around the benthic layers of the wetland reducing retention times and providing limited contact with DOC and limited opportunity for denitrification.

Riparian wetlands have also been shown to act as net contributers of NPS pollution under adverse hydrological or pollutant loading conditions (Whigham et al., 1988). Heavily stressed wetlands can deliver increased sediment and nutrient loads and hence can act as a source of pollution rather than a pollution sink. Brinson (1988) highlighted the importance of a holistic approach in nutrient loading considering the long-term loading of pollution to the wetland and the consequent effects on water quality mitigation as a stressed wetland can become a net exporter of pollution. Whigham et al. (1988) concluded riparian wetlands

located near the headwater were more effective at intercepting NPS pollution than riparian wetlands further downstream as a larger percentage of stream water passes through the wetlands. Phillips (1996) reviewed the efficacy of riparian wetlands to act as water quality filters and found that riparian wetlands can reduce or treat pollution but their performance will be predicated on a number of hydrological conditions, including water storage capacity, slope, roughness, and hydraulic conductivity.

Phillips (1996) also examined factors that affected riparian effectiveness in the mitigation of non-point source pollution including nitrates and sediment by comparing residence times using a comparative semi-empirical model at the Tar River basin in North Carolina. The authors identified the local slope of the riparian zone as being one of the most important factors and it more than any other factor provided an indication of the degree of surface runoff which had the greatest effect on residence time. Estimates of required width were made, but were not based on variations in antecedent conditions or hydrological state.

Lowrence et al. (1983) examined the nutrient balance for a riparian zone on a coastal watershed in Tifton, Georgia. The study examined the bulk nutrient budget for the riparian zone over a year. The authors predicted removal of nitrogen and phosphorus within the riparian zone and also predicted an order-of-magnitude increase in nutrient loading if the riparian zone were to be removed. The authors also discussed the influence of artificial drainage and the expectation for nitrate nitrogen to be higher in receiving waters with tile-drains present.

2.3.2 Regional/Watershed Scale Studies

Many studies have been conducted in Canada investigating the physical and biogeochemical processes in wetlands. A large number of field scale analyses have been conducted to determine the local behaviour of wetlands. Some researches have indicated that a better understanding of the behaviour of agricultural and urban pollutants is needed for the protection of wetlands and environmental considerations as a whole and that the understanding of the hydraulics and hydrology and hydrogeochemistry of the system is an important step (Kennedy and Mayer, 2002).

Mitsch and Gosselink (2000) examined the importance of evaluating wetlands at an appropriate scale. They proposed that the integrated effects of wetlands are best evaluated over the largest possible area. The "ease of calculation" naturally decreases with increased scale but the importance of the wetland systems will increase with scale. The authors also cite an abundance-efficacy evaluation system applied to wetlands, which was tied to their utility in water quality improvement and flood mitigation. When wetlands are abundant, their specific value (value per unit area) is relatively low. Their specific value increases as they become scarcer and their functions become more valuable. However, if the system becomes overstressed their efficacy in mitigating flood and improving water quality will start to reduce making the preservation of the systems less compelling. Assessing the efficacy of a wetland, and hence it's value is based on the hydrogeomorphic position of the wetland - which is defined as the degree the wetland is open to hydrologic and biological fluxes with other systems. Gosselink and Mitch site several beneficial impacts a wetland can have at the watershed scale, including flood attenuation. To quote from the authors directly:

> "Thus, the value to man of a forested wetland varies. If it lies along a river it probably has a greater functional role in stream water quality and downstream flooding than if it is isolated from the stream."

Gosselink and Mitch cite values associated with wetlands including sediment retention, flood control, nitrogen and phosphorus retention. Assessments were made as to the overall requirement for wetlands in a watershed for water quality improvement. Generally, 1% to 5% was required for water quality improvement but as much as 15% was required for phosphorus retention, and 3.4% to 8.8% for nitrate retention.

Sliva and Dudley Williams (2001) examined relationships between land use and water quality parameters from a MOE database for 3 sub-watersheds near Toronto, Ontario. The influence of buffer zones on these water quality data was analyzed. The authors found that in the statistical analysis that land use had a greater effect on the water quality than the buffer zones themselves, bust explained that their secondary database, which consisted of monthly grab samples, might not be adequate for a thorough understanding of the influence of riparian zones and that more temporal and geographic precision was recommended.

In an attempt to look at the effects of the presence of wetlands above the field scale Spaling (1995) examined the region of Peel, Ontario using an integral Geographic Information System (GIS) approach. Data showed that the drainage of the wetlands for agricultural activity produced an increase in nitrate concentration in the surface water. This change was explained by the adoption of new preferential pathways for nitrate to travel to the receiving streams.

Some more recent research has questioned some of the best practises implemented. Shuman (2005) showed that introduction of riparian buffers had no nitrate or sediment improvements for the Octoraro Creek in Maryland. The lack of effectiveness was explained by the time required for BMPs such as riparian buffers to become effective and is expected to take several years for the benefits to be realized, although regional guidelines expect nutrient loading reductions in the range of 31 to 45%.

2.3.3 Water Quality Modelling considering NPS Pollution and Riparian Wetlands

Many modelling efforts have been conducted to attempt to elucidate the hydrologic effects and water quality impacts of riparian wetlands, with varying degrees of complexity. Dortch (1995) produced a modelling approach for the examination of pollutant removal capability of wetlands. The resultant model, PREWET, simulated wetland treatment or mitigation of total suspended solids (TSS), nitrogen, phosphorus, BOD and total coliform bacteria. The model's hydraulic approach was to assume complete mixing in the model with a completely stirred tank reactor (CSTR) approach and hydraulic retention times (volumes) being input empirically or from dye studies on the wetland in question. TSS was removed by a simple settling velocity approach with total removal being a function of the settling velocity and the mean depth of the wetland. First order decay was employed for nitrogen removal with denitrification considered. Phosphorus fate was modelled considered using a soluble-sorbed partitioning relationship within the water column and the sediment. If the P concentrations were low a simple first order settling was assumed for reduction of P in the wetland. The PREWET model was designed for long-term steady state modelling and does not account for any effects resulting from seasonal variation.

Alvord and Kadlec (1996) developed a similar model to Dortch (1995), that involved a reactor mixing model considering a static internal dispersion for the analysis of retardation of pesticides in a standard treatment wetland. The model was applied to 3 treatment wetlands with average hydraulic residence time of 7 to 51 days. This model too is believed to have limited applicability to riparian zones, but showed reasonable success in capturing the complexity of wetland operations in a model.

Crumpton (2001) used first order, temperature dependant nitrate removal kinetics to simulate nitrate removal within wetlands for the Walnut Creek Watershed, Iowa, USA. The author examined several wetland restoration scenarios and found that based on simulations reductions could be expected but depended very much on the location of the restored wetlands and the degree of nitrate runoff the wetlands intercepted. Crumpton concluded that a watershed perspective is required if water quality benefits due to riparian wetlands are to be realized.

Inamdar et al. (1999a,b) developed a field scale riparian wetland model for the evaluation of nutrient and sediment attenuation called the Riparian Ecosystem Management Model (REMM), a detailed and highly parameterized field-scale model. REMM considers nitrogen and phosphorus sources entering buffer ecosystems through precipitation, surface and subsurface flow and adsorbed onto sediment entering via surface flow. The fate of the nutrient constituents is determined by hydrological, geochemical, microbial and plant uptake processes. The nitrogen model contains 4 species (nitrate, ammonium, active organic and stable organic). As organic carbon decays, nitrogen is released in proportion to the established C:N ratio of the carbon pool in question with nitrogen being added to the ammonium pool stochiometrically. Nitrification is calculated with a first order relationship with corrections for temperature, moisture and pH. The denitrification model process describes the rate of denitrification as a function of the degree of oxygenation in the environment, temperature, NO_3^-concentrations and carbon concentrations in the soil. REMM also includes a carbon cycle as the presence of carbon is required for denitrification to occur. Carbon is sourced from a decaying surface pile (humus). The detritus formed from decaying plant material is pooled into various components based on the lignin:C ratio.

A recent study by Liu et al. (2008) involved the introduction of a riparian wetland sub-

model into the SWAT modelling framework to predict changes in hydrology and sediment loading. Simulations predicted a 19% reduction in sediment loading in a riparian protected zone considering the presence of riparian zones in the watershed and employed the GRCA and MOE study data as a validating dataset. However, without event-based data these reported benefits during runoff events remain unvalidated.

Das et al. (2008) performed a study similar to that conducted by Liu et al. (2008), examining the sediment loading concentrations in the Canagagigue Creek at the Floradale GRCA measurement station, but using the AnnAGNPS model. The authors of this study overcame the lack of sediment data by using sediment data collected from 1974 - 1984, relating it to collected streamflow during that period and using a sediment-streamflow rating curve against more recent streamflow. The authors found some difficulties with the model in a Canadian context, particularly with regard to snow melt and event timing during snowmelt events. The daily time step of the model was also found to be problematic in determining accurate hydrograph timing on a watershed of so small a size. The authors suggested adjustments to RUSLE and SCS curve number parameters. Riparian wetlands, although predominant in areas within the watershed, were not explicitly considered.

2.4 The WatFlood Model and NPS Pollution Modelling

The WatFlood hydrological model represents a suite of hydrological programs used for hydrological modelling at the watershed scale (Kouwen, 1988, 2005). WatFlood was the first model to use the Grouped Response Unit (GRU) approach, separating land cover into a number of land classes with unique hydrologic responses and parameterizing the model accordingly (Kouwen et al., 1993). Numerous studies have shown the effectiveness of the model in regions across Canada and other parts of the world (Cranmer et al., 2001; Kouwen et al., 2005; Pietroniro et al., 2006b; Toth et al., 2006). The WatFlood model has been regularly expanded and improved upon with research findings at the University of Waterloo Hydrology Lab being regularly incorporated. For example, McKillop (1997) developed a headwater wetland model consisting of a hydrologic model coupled with a

hydraulic routing model. Model simulations showed good agreement with data collected at a headwater swamp within the Treeswater River in Southern Ontario, and showed sensitivity to wetland saturation levels. This model was adapted for and integrated into the WATFLOOD hydrologic model to account for riparian wetlands along the stream corridor (Kouwen, 2005).

The WATFLOOD model has been expanded upon recently to include a water quality sub-model via the introduction of various AGNPS subroutines by Leon (1999). The WATFLOOD/AGNPS model included routines for sediment and nutrient application to receiving waters from agricultural fields and was applied successfully to the Duffins Creek Watershed near Toronto, Ontario (Leon et al., 2001, 2004). The integrated model showed the ability to simulate both nitrate and solids loading in this watershed. The sediment transport model employed in the WATFLOOD/AGNPS model was first proposed by Hartley (1987a,b). The Hartley model differs from the perhaps more traditional universal soil loss equation model in that it is more physically based and based on the Shields transport criteria. The Hartley model considers soil detachment by runoff shear and rainfall intensity to calculate a maximum sediment yield. The total sediment transported is a minimum value of the transport capacity and maximum sediment yield.

The nutrient model is adapted from the AGNPS model (Young et al., 1989). The runoff and infiltration flow components are determined from the WATFLOOD hydrological model. The soluble nutrient components are conducted with the flow in these instances. The adsorbed or insoluble component are transported with the sediment transport model, which as described above is an adaptation of the Hartley field sedimentation transport model. The in-stream processes incorporated in the model generally follow a mixing cell model. Mixing cells are, by design, the size of the WATFLOOD model grid. Consequently, transported constituents tended to experience rapid breakthrough as a flood is routed through the watershed. Sediment, nitrogen species and phosphorus species all incorporate calibrated decay functions, which do not necessarily consider the travel time through a grid cell – that is, contaminants were modelled employing a first-order decay with a decay constant that is effectively a function of the time step employed. The in-channel transport issues with the model are acknowledged by the original author and were sited for future

research (Leon, 1999).

The WatFlood/AGNPS model was subsequently enhanced to include a pathogen transport subroutine by Dorner et al. (2006) which built upon the sediment transport routines to simulate pathogen fate at a watershed scale. The model was applied to the Canagagigue Creek in Southern Ontario and the study results simulated highest microbial concentrations when overland flow was predicted. The study also suggested that microbial concentrations could be associated with in-channel sediment resuspension, which was not accounted for in the existing model.

2.5 Chapter Summary

Non-point source pollutions has a significant impact on receiving water quality in Southern Ontario. The Grand River in particular is heavily impacted by nutrient and sediment loading from non-point sources. Mitigation of the impacts of NPS pollution requires the adoption of best management practises (BMPs) in an attempt to intercept pollutants including nutrients and sediment.

In field-scale studies riparian wetlands have shown some success at intercepting NPS pollution. However, studies have shown mixed results depending on a number of factors, including the location of the wetlands, the character of the wetlands biologically and geologically, and the hydrology of the system. The benefits riparian wetlands offer at the watershed scale require elucidation.

To evaluate the real benefits of riparian wetlands watershed-scale assessments are identified as important. Additionally, the hydrology and hydrological drivers in riparian wetlands remains an important and salient factor in all riparian wetland studies, regardless of scale. Although many studies have been conducted at the field scale, a need to deterministically assess and model the impacts of riparian zones at the watershed scale with a thorough hydrological approach is not well represented in the literature.

Chapter 3

Study Site

A study site was selected to provide hydraulic, hydrological and water quality data to assess the influence of riparian zone protection on stream corridors receiving waters at the sub-watershed scale.

The Canagagigue Creek was selected because of its proximity to the University of Waterloo in Kitchener-Waterloo and the identification of some land use characteristics within the watershed that allowed for an assessment of the influence of riparian protection on sub-basin of the watershed. The Canagagigue Creek is a sub-watershed of the Grand River, located in Southern Ontario, Canada approximately 100 km west of the City of Toronto, and 30 km north of Kitchener-Waterloo (see Figure 3.1). The Canagagigue Creek has a drainage area of approximately 130 km^2. The watershed consists generally of mild slopes and poorly drained soils. Historically the watershed consisted largely of wetlands, and consequently approximately 60% of the watershed area is tile-drained to facilitate agricultural activity (Region of Waterloo, 2004). The Canagagigue Creek has an average annual precipitation of approximately 900 mm with approximately 18% of precipitation falling as snow in a year (Environment Canada, 2007).

The selected study site consisted of two sub-basins at the north-east end of the Canagagigue Creek and were named "East" and "West" based on their relative positions as shown in Figure 3.2. These sub-basins are adjoining and are upstream from any large control structures, reservoirs or urban environments. These two sub-basins were selected

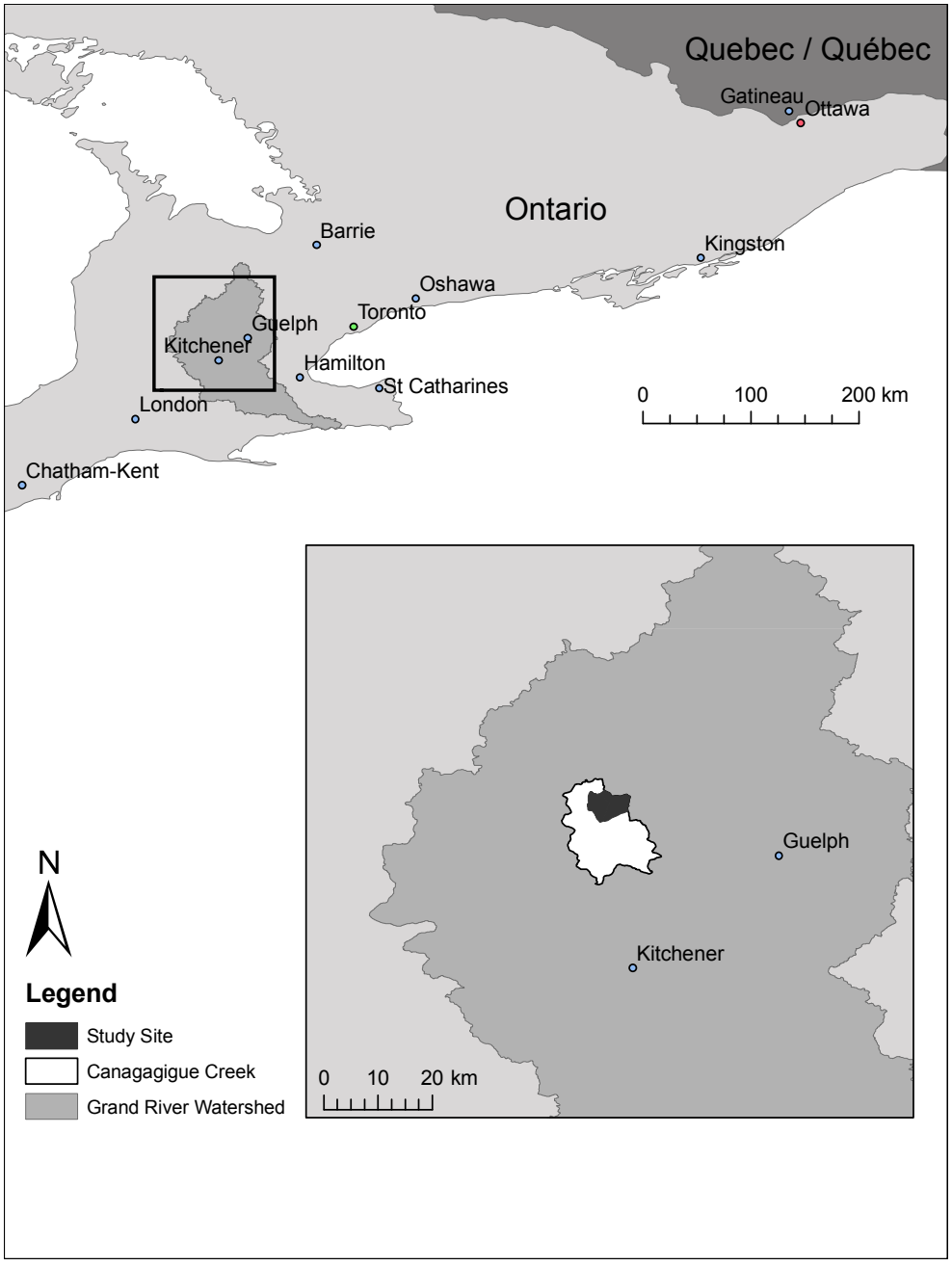

Figure 3.1: Location of the Study Site within the Grand River Watershed

primarily because they showed similar land use, but with very different riparian characteristics – the West sub-basin having incised, artificial channels with no riparian protection and the East sub-basin having natural channels with extensive riparian protection (as described in Section 3.2). Of interest is that the Canagagigue Creek watershed and the study sites cross municipal boundaries, which lead to discontinuities in available data, particularly soil surveys.

The confluence of the two study sub-watersheds is approximately 200 m upstream of a bridge on Sandy Hills Drive, just north-east of Floradale, Ontario, east of Regional Road 21. The river geometry is rather different for each of the sub-watersheds. The West sub-watershed exhibits a fair degree of natural meander on the approach to the confluence, but upstream the watercourse has been modified to follow the contours of the agricultural field boundaries in the area. The east sub-watershed exhibits a much straighter and more uniform channel approaching the confluence and as it has a good degree of natural riparian wetland, does not appear to have been actively modified by the local farmers. The east basin maintained flow all year due to groundwater contributions at the headwater as well as anthropogenic sources at the Alma Research Station[1]. The west sub-basin was ephemeral, with flow starting after snow melt and tending to stop in late July or early August and resuming only with large rainfall events.

Togographically the Canagagigue Creek shows mild slopes as shown in the contour map in Figure 3.3, however, some high local slopes are shown at the headwaters of the East sub-basin near on either side of the channel. These topographic features are explained by the physiography of the region with the low topology following a historic spillway an increase in slope at the transition to a kame moraine at the east end of the watershed as discussed in Section 3.1.

[1]Sections 4.5 and 6.7.3 provide the details of hydraulic and water quality contributions of the Alma Station, respectively

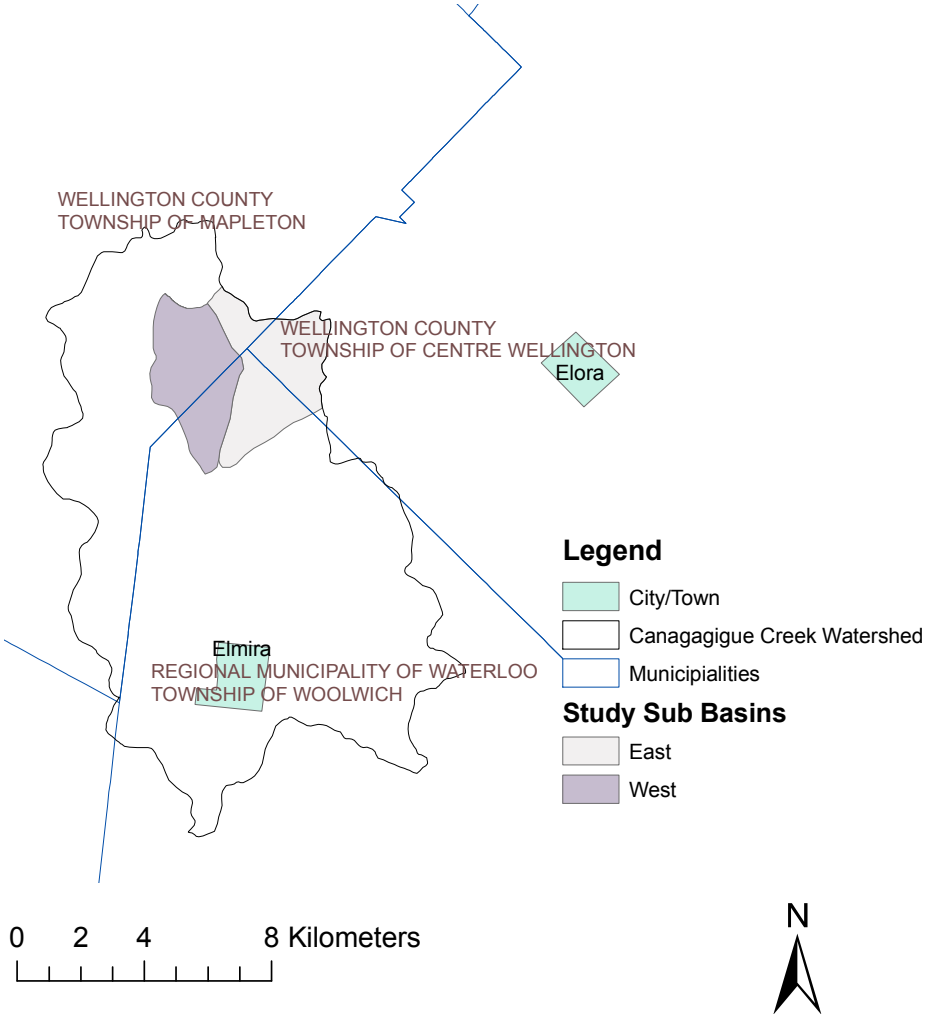

Figure 3.2: Location of Study Site

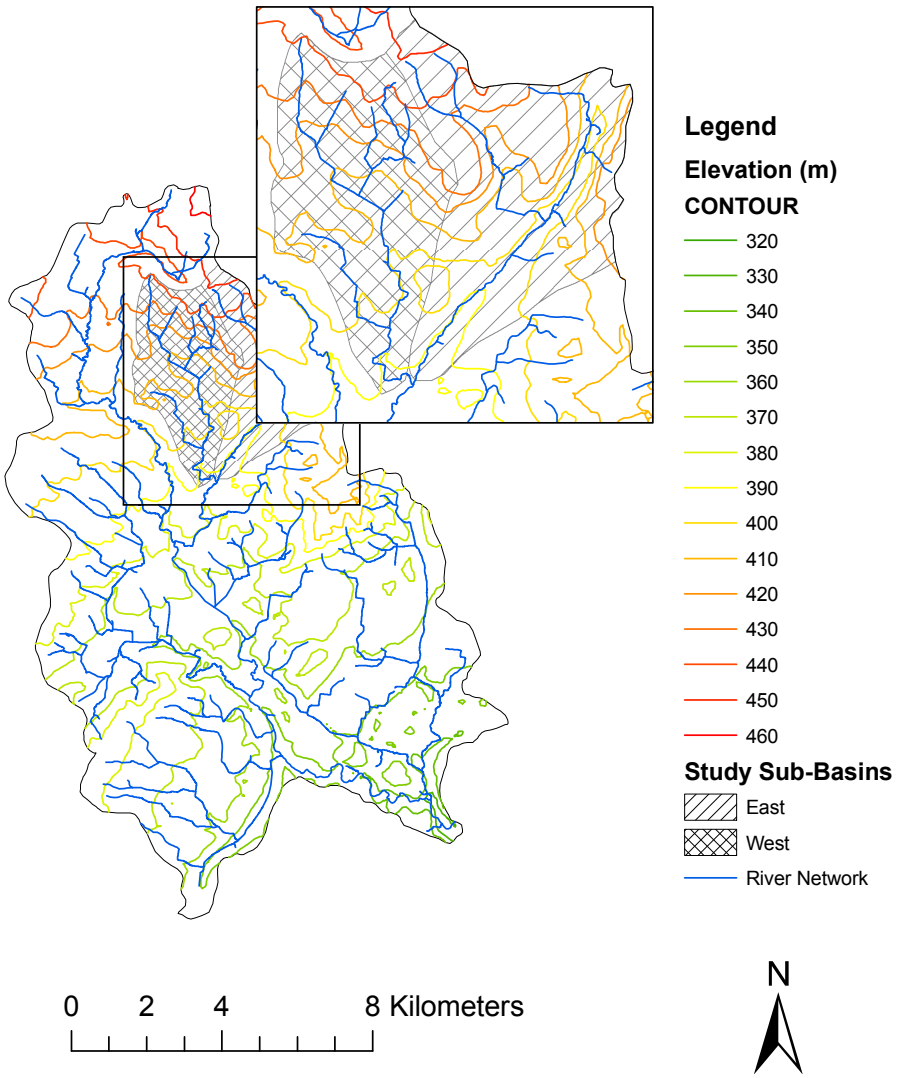

Figure 3.3: Canagagigue Creek and Study Site Elevation Contour Map

3.1 Physiography and Soils

The headwaters of the Canagagigue Creek are predominately in a low-relief till plain, characterised by poorly drained sandy silt clays with swampy depression in low-lying areas. Original vegetation of better drained areas would include hardwoods such as maple, beech and some birch, with swamps, and poorly drained depressions containing elm, ash, cedar and tamarack (Chapman and Putnam, 1984).

In the region of the study site there exist distinct physiographic characteristics even between sub-watersheds. The West sub-basin is characterised by level till plain without drumlins. The East sub-basin shows a predominance of till plain without drumlins but with evidence of a spillway along the length of the main channel and a small portion of kame moraine at the north east corner of the sub-basin. Physiographic data is presented for the Canagagigue creek in Figure 3.4.

The soils in the Canagagigue Creek are predominantly loams and silt loams throughout the watershed. Figure 3.5 presents the predominant soil types as presented by the digitized Canadian Soil Information Service (CANSIS) soil surveys (AAFC, 2000). The watershed crosses a municipal boundary, with the northern portion within Wellington County and the southern portion within the Waterloo County. Consequently, the soil surveys conducted in each county were independent resulting in discontinuities along the county boundaries.

The study site sub basins show similar soil character to the Canagagigue Creek watershed as a whole with the soil dominated by loam and silt loam. However the east basin shows some gravel loam along the main channel stream bed with some organic soil classifications near the stream corridor and headwater.

3.2 Riparian Wetlands

The northern region of the Canagagigue Creek contains a relatively large quantity of wetlands, specifically at tributary headwaters. Figure 3.6 illustrates the locations of identified wetland areas by the Ontario Ministry of Natural Resources MNR and published in the Natural Resources and Values Information System (NRVIS) database (MNR, 2002).

The differences between the East and West basin can be seen in Figure 3.6. From

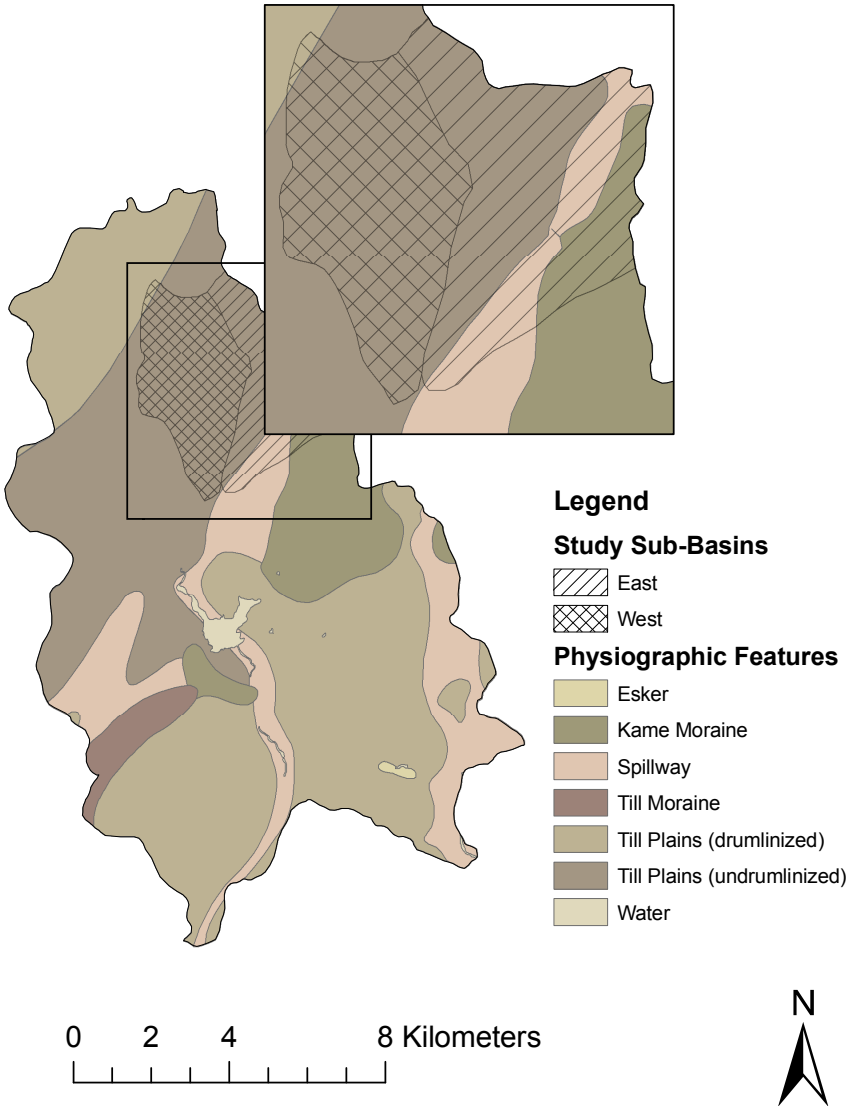

Figure 3.4: Canagagigue Creek Physiography Map

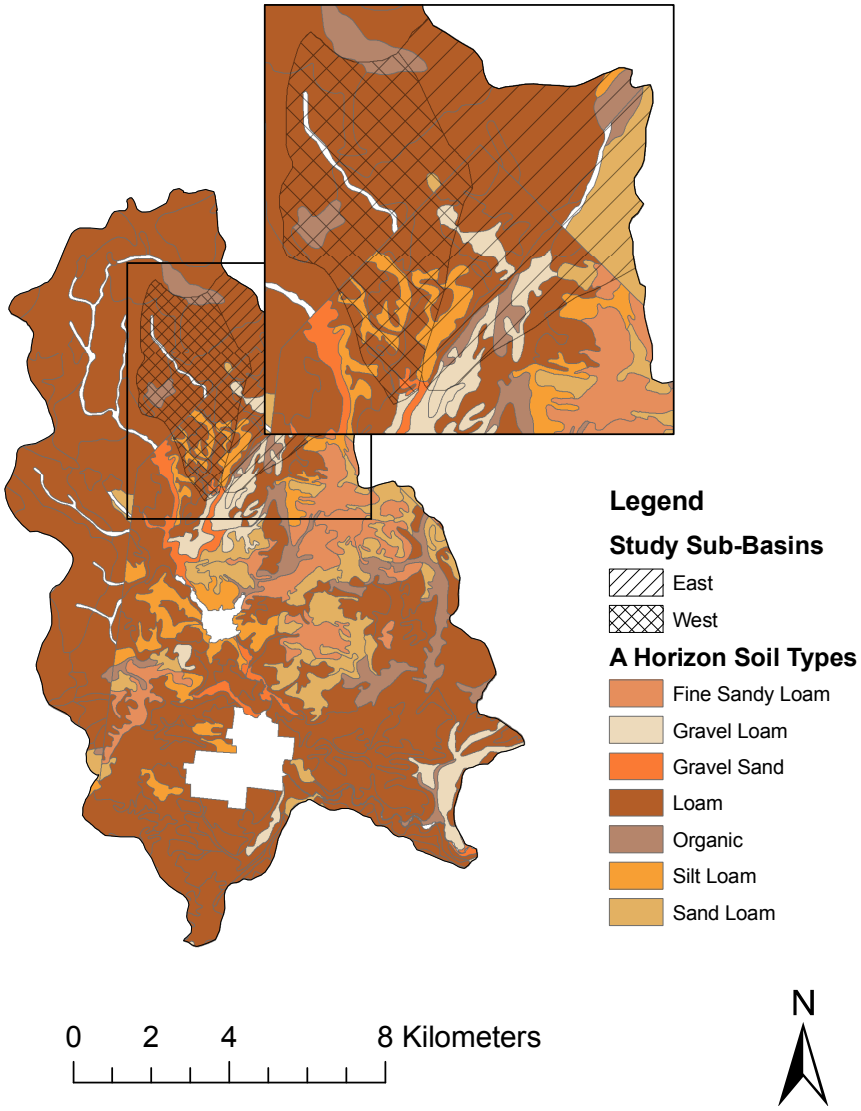

Figure 3.5: Canagagigue Creek Soils Map

analysis of the Geographic Information System (GIS) data from NRVIS and additional aerial photographic data from the GRCA it has been calculated that in the West detectable riparian wetlands protect basin 2% of the coastal length. The East basin has approximately 46% of its coastal length protected by riparian zones. In this calculation a riparian wetland was considered present if 10 m of identified riparian wetland was detected between the stream course and the closest agricultural field. The decision to use 10 m as the definition of riparian cover was somewhat arbitrary but based on published research and government recommendations. The Ontario Nutrient Management Act (NMA) recommends a 3 m buffer width (Government of Ontario, 2002). However, an US-EPA summary report of riparian zone effectiveness at removing nitrate cited recommendations from 7 to 100 m (Mayer et al., 2005). This same study cited 10 m as having an average effective nitrate removal rate of approximately 65% and riparian zones greater than 10 m were unlikely to act as a source of nitrate. The 10 m limit was chosen as a conservative demarcation point to likely produce some effective removal of nitrate with much of the riparian wetland width in the sub-basin being much larger than 10 m.

The presence of the riparian wetlands along the main corridor of the East sub-basin and absence within the West sub-basin can be explained in part by the geological history and topographical differences between the two sub-basins. The main channel of the east sub-basin is a glacial spill way (see Figure 3.4) and consequently the channel in the East sub-basin is well established with a flood plain. The West sub-basin appears to have a main channel that is more recently developed that was likely enlarged by local farmers to promote drainage in the sub-basin. Additionally the west sub-basin shows a much higher average elevation along the channels in West sub-basin than the East sub-basin (see Figure 3.3). The East sub-basin would be expected to have more persistent wet conditions considering those topographical differences.

3.3 Land Use and Anthropogenic Influences

Land Use / Land Cover (LULC) information for the Canagagigue creek was provided by the GRCA. The land use data map from the GRCA is presented in Figure 3.7. The

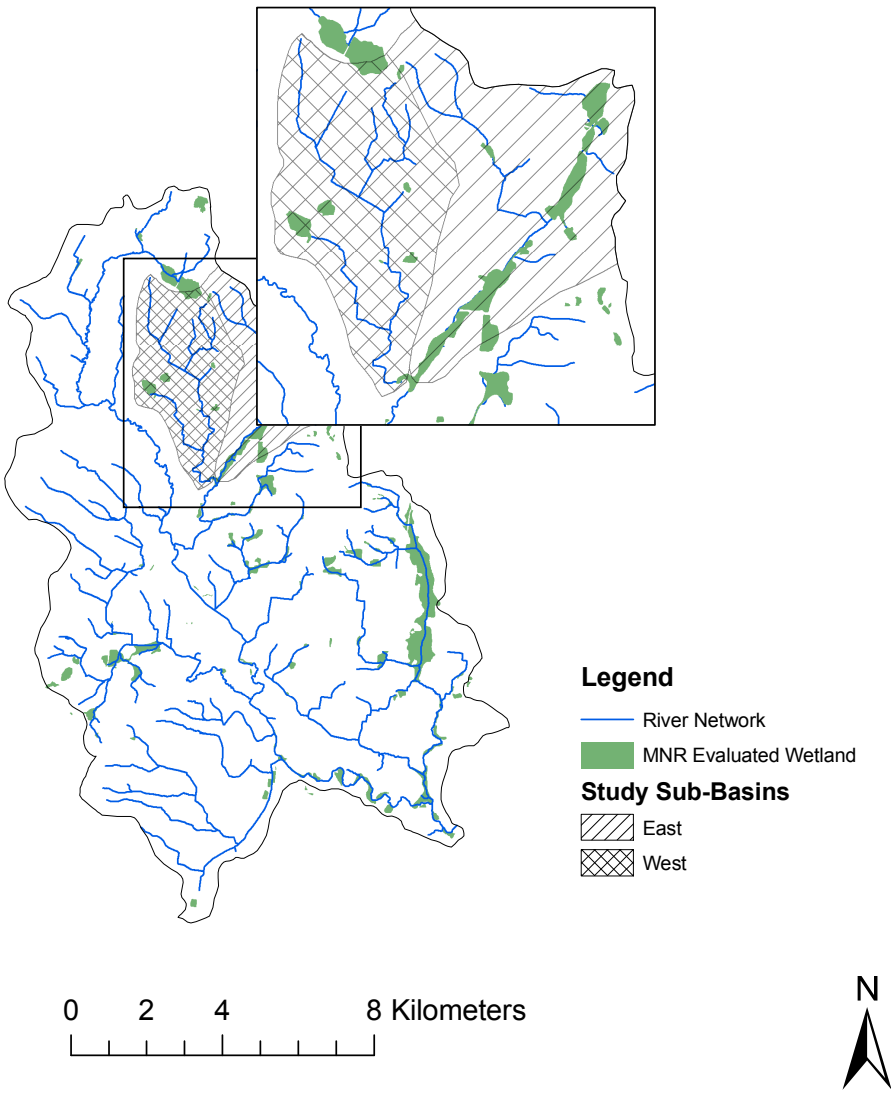

Figure 3.6: Canagagigue Creek Wetlands

Canagagigue Creek watershed land use is dominated by agricultural activities including crop, forage, and pasture land. There is a small portion of forested area identified in this survey near riparian zones and as woodlots that follow concession lines and are referenced as deciduous (D), coniferous (C) or mixed (M) stands. Notably, the Woolwich dam and reservoir are located at the centre of the watershed, downstream of the study site sub basins. Two urban or built-up centres are identified in the town of Elmira and the lower end of the watershed, and Floradale at the north-west edge of the Woolwich reservoir. Again, these two urban centres are downstream of the study sub-basins. A histogram of the LULC proportional areas of the Canagagigue Creek is shown in Figure 3.8. Here it can be seen that crops, forage and bare ground dominate the watershed, with smaller contributions from forested, pasture and small grains land classes.

OMAFRA has also published a LULC map which focuses on the crop-types and agricultural associated with a particular parcel of land as identified in 1990. This land use map for the Canagagigue Creek is identified in Figure 3.9. Of notice in this LULC map is the differences in classification as defined by the GRCA and OMAFRA. Forested areas in the GRCA map are classed as Woodlots in the OMAFRA map. The areas identified as bare by the GRCA are generally classified as "Mixed System" or other cropping system with no bare land class being identified by OMAFRA. A histogram of the LULC proportional areas for the OMAFRA survey of the Canagagigue Creek is shown in Figure 3.8. Various agricultural systems dominate the watershed area with woodlots and built-up land uses contributing to a lesser degree.

The comparison of these two land use maps illustrates the difficulty and subjectivity inherent in classifying land use. Truthing land use observations made from photographic surveys of the study site in the course of this study has shown that the identification of "bare" land use made by the GRCA is over-estimated and most of the areas identified as "bare", at least within the study basins, were observed to have some agricultural activity associated with them. The OMAFRA land use classification were observed to be more appropriate and accurate when allowing for the crop rotation on fields that takes place from season to season. To account for the riparian wetlands, the wetland delineation data provided by MNR was superimposed over the OMAFRA land class map, overriding the

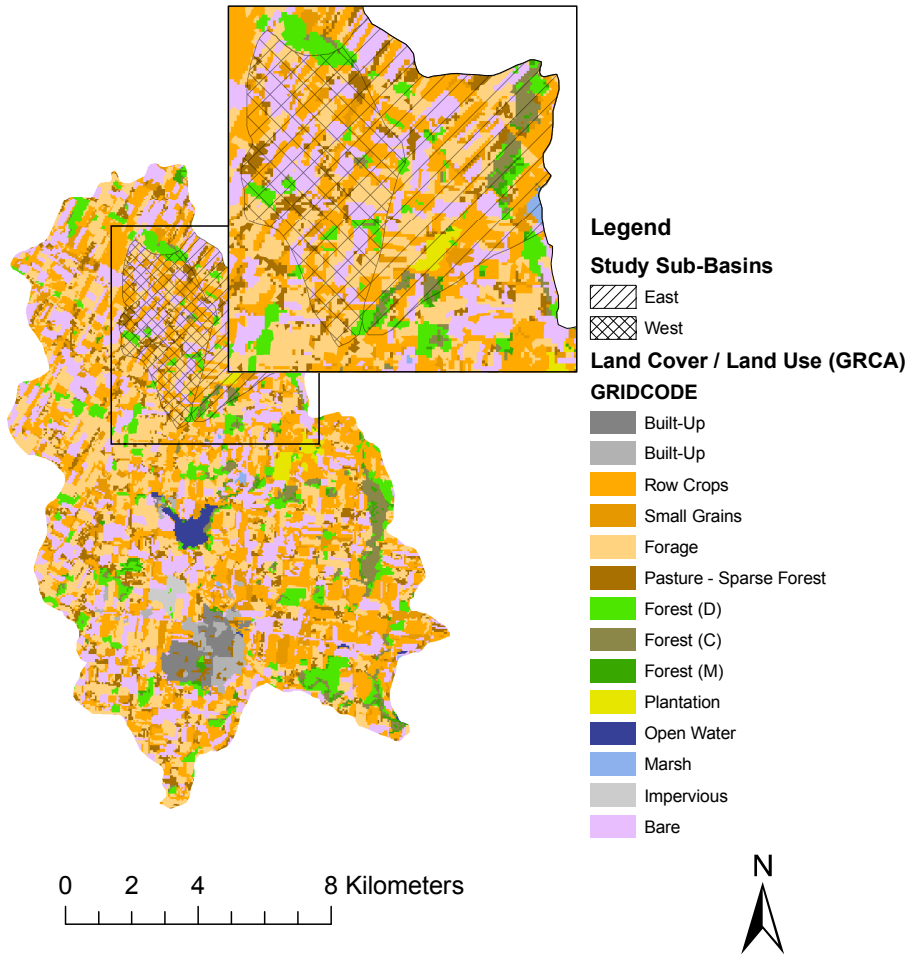

Figure 3.7: Canagagigue Creek Land Use / Land Cover (GRCA)

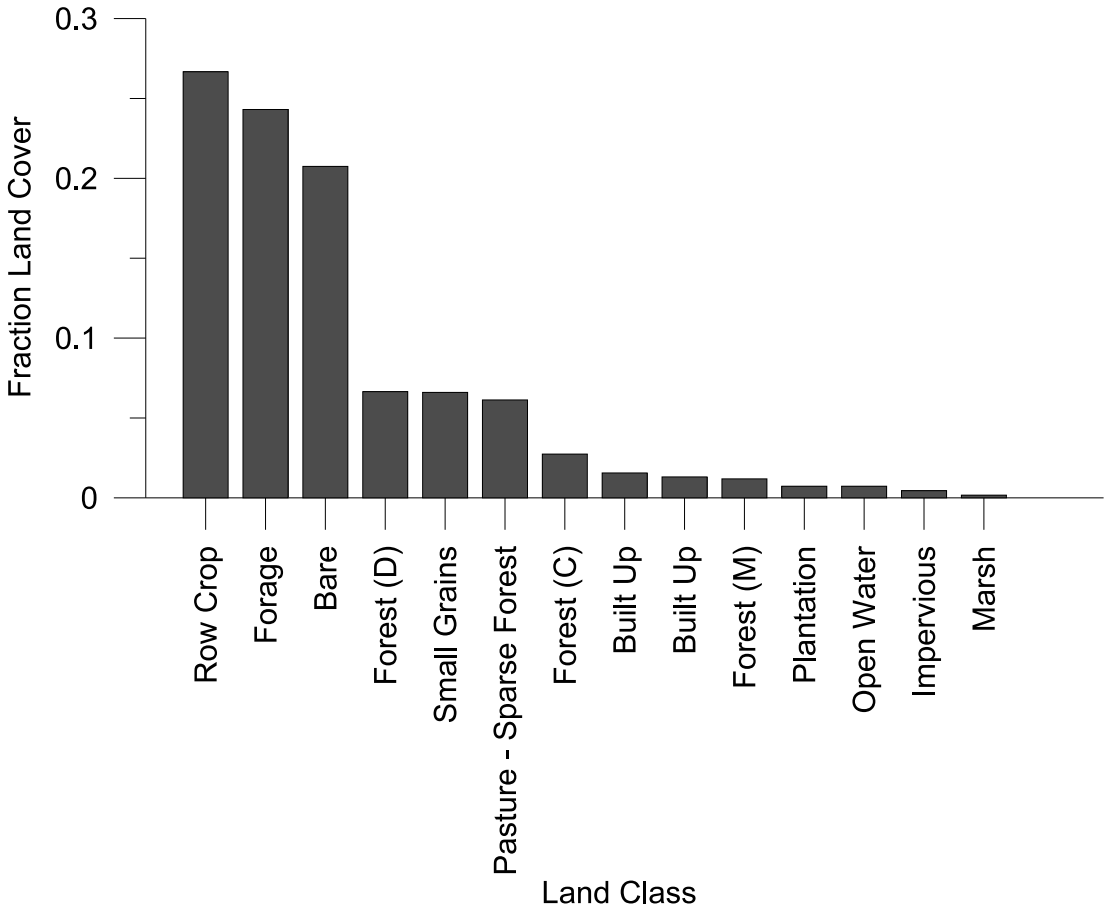

Figure 3.8: Canagagigue Creek LULC Proportions (GRCA)

OMAFRA classification.

Photographic surveys were conducted within the sub-basin to determine the actual crop percentages in the study sub-basins. Results are tabulated in Table 3.1. In this table the corp activity is determined from photographic surveys conducted during 2006. It can be seen that corn dominated along with wheat and soybean cropping. The difference between the east and west sub-basins with respect to wetland cover is also evidenced in Table 3.1

3.4 Tile Drainage

The Canagagigue Creek is extensively tile-drained. Tile-drainage maps of the region were acquired from OMAFRA outlining which fields were tile-drained in the study site. The hard-copy tile drain maps dated 1983 to 1992 and showed approximately 60% of all fields in the Canagagigue Creek are tile drained, the contribution of tile drains to the hydrology and water quality of the watershed is considered significant. It is also believed that the approximate number for tile-drain contribution is likely conservative, as some undrained fields likely had tile drains added to them in the intervening years.

For the study sites the positioning of the tile drains was observed by walking the stream corridors. In the west basin and areas where no riparian wetlands were present the tile drains tended to discharge very low into the stream, often being completely submerged. Figure 3.11 shows the positioning of a tile drain (indicated with a circle) in the West sub-basin and it can be seen the drain connects directly with the channel. Figure 3.12 shows the location of a tile drain from a farmers field contributing to a riparian wetland. The tile drain outlet in this picture (indicated with a circle) is protected by a pile of cobbles and

Watershed	**Area**	**Land Use**						
		Crop Agricultural				**Woodlot**	**Wetland**	**Other**
	(ha)	**Wheat**	**Soybean**	**Corn**	**Other**			
East	1 150	17%	18%	39%	6%	4%	15%	1%
West	1 050	26%	22%	38%	2%	3%	5%	4%

Table 3.1: Drainage areas and land use as percentage of basin area for the study sub-basins within the Canagagigue Creek watershed

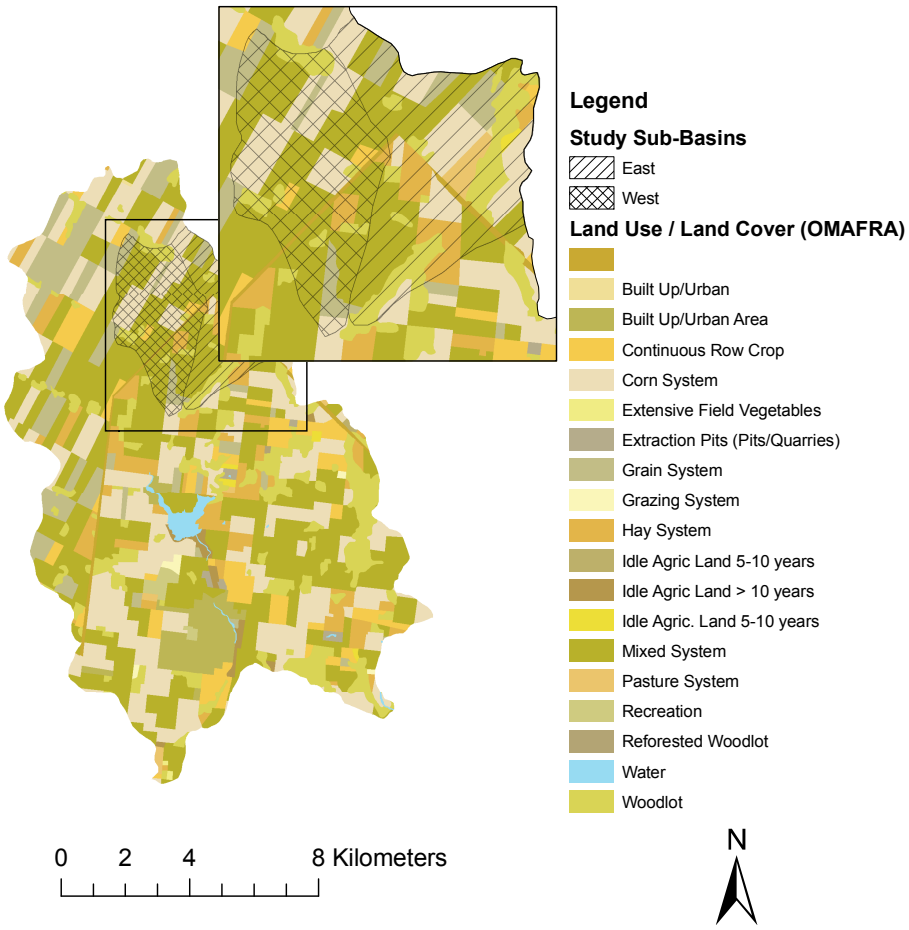

Figure 3.9: Canagagigue Creek Land Use / Land Cover (OMAFRA)

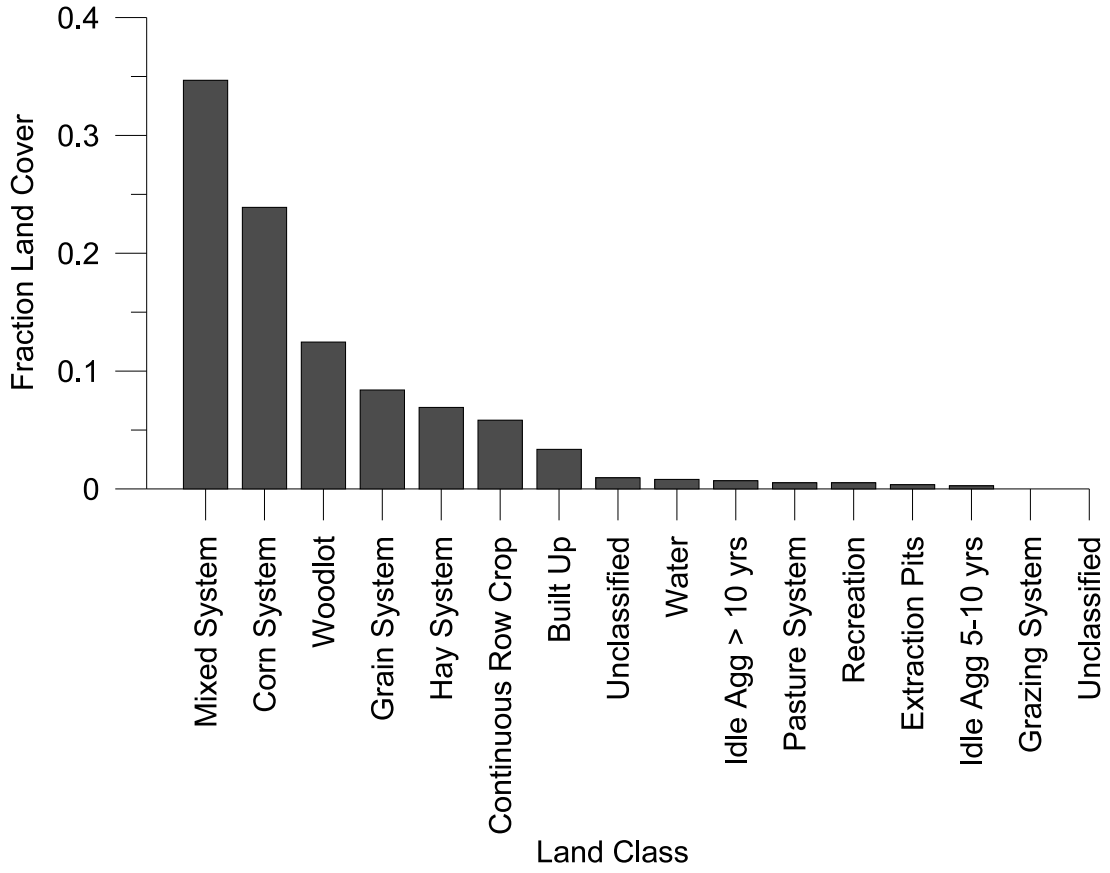

Figure 3.10: Canagagigue Creek LULC Proportions (OMAFRA)

contributes to the riparian zone, not the channel itself. These two scenarios are typical of the drainage observed in the two sub basins.

Figure 3.11: Tile Drain Location - West Basin without Riparian Wetlands

3.5 Chapter Summary

In this chapter the location of the study site was outlined and the justification for the selection of the two study sub-basins articulated. The sub-basins have very similar features, including drainage area, land use and soil types but with a significantly different degree of riparian wetland cover along the main channel corridors. There is heavy agricultural land-use in the area and, due to the low relief poorly drained soils, much of it is tile-drained. The presence of tile drains differs between the two sub basins in that the basins without riparian cover tends to have the drains discharging directly to the channel, whereas the basin with riparian wetland cover tends to have the drains stop at the extent of the field at the boundary with the riparian wetlands.

Figure 3.12: Tile Drain Location - East Basin with Riparian Wetlands

Chapter 4

Hydrometric Data Collection and Analysis

4.1 Introduction

This chapter outlines the acquisition and analysis of hydrometric data in and around the study site. These data included precipitation and flow for the two study sub basins, but also included temperature, RADAR, snow survey data. Precipitation and flow data were required as inputs and calibration data for the hydrological modelling of the watersheds and the flow data was also required for flux calculations in conjunction with the water quality sampling. In order to determine the outlet flow rates from the two sub-watersheds, a detailed study of the hydraulics of the site near the outflows was conducted. The hydraulic assessment consisted of detailed topographic surveys of the area, continuous measurement of water stage at each sub-watershed outlet, calibration of the stage measurement loggers, flow measurement using the velocity-area and tracer dilution methods, and development of rating curves using the measured stage and discharge as well as the calibration of a HEC-RAS model for each sub-basin. Precipitation data was acquired from installed rain gauges as well as those available from the GRCA.

4.2 Data Collection and Storage Approach

Due to the large quantity of data collected for this study, both as hydrometric and water quality data, a data storage approach had to be developed. A highly normalized relational database management system (RDBMS) was employed to store all collected data. This system facilitated the import of water quality data, rainfall and flow data, etc. The RDBMS solution and associated software code was named the Field Sampling Asset Management (FSAM) database. This package greatly improved data acquisition, quality control techniques and output for model input (WatFlood) and statistical analysis packages (SPSS®). WatFlood is a data-intensive hydrological model and the need to centrally store and manage the hydrological, meteorological and water quality data became immediately evident, even in a small study such as this one. Indeed, Singh and Frevert (2006) recently sited hydrological model integration with RDBMS and GIS systems as a necessary technological step as distributed models begin to process more data from more diverse and varied sources.

4.3 Stage Measurement Locations

Locations were chosen in each sub-basin to measure stage using stilling wells and float-counterweight data loggers. Each location was chosen based on accessibility, distance upstream from the confluence and location within the stream. The location of the West basin stilling well in particular was carefully selected as the meandering channel in the area showed evidence of meander cut-off in areas. Care was taken to install the stilling well in a stable location upstream of the cut-off activity. The stilling well locations are shown in Figure 4.1. The west sub basin had a stilling well installed at location "West-53" and the East sub-basin had a stilling well installed at location "East-94"[1]. The differences in stream meander between the East and West channels is clearly evident in Figure 4.1, explaining the greater distance of the West stilling well upstream of the channel confluence. The cross sections employed for velocity-area discharge measurements are also shown in Figure 4.1.

[1]The index numbers "53" and "94" refer to data-logger identification codes.

The details of the equipment used and the stilling wells are described in Appendix A.

4.4 Stage-Discharge Rating Curves

In order to convert the continuous stage data to flow data for analysis and modelling rating curves relating the measured stage elevation to the discharge in each of the sub-basin outlets were developed. Flow measurements were made using the velocity-area method and compared to measured stage values. The rating curve was developed with the assistance of a HEC-RAS model and survey data of the two sub-basins from the flow measurement point past the confluence to the nearest control structure, a bridge several hundred meters downstream. The HEC-RAS model was calibrated to measured values through the adjustment of roughness parameters and the resulting rating curves were employed in converting stage data to equivalent flow data. The complete procedure for the development of the rating curve is presented in Appendix A.

It was observed that the summer season had a markedly different rating curve than the winter season, particularly for the west basin. This was primarily due to development of weeds on both stream beds. As a result, two rating curves were created, one for each season. The winter rating curves (December to July) and the summer rating curve (June to November) were applied to the stage discharge relationships. June was considered the most appropriate cut-off period for the rating curves, particularly considering the months of June, July and August represent the lowest flow conditions in the west sub-basin. During these months, the west sub-basin was generally dry and only relatively large events produced a flowing condition at the west basin.

Figure 4.2 shows the calculated rating curves using the optimized HEC-RAS model. The rating curves used for the summer and winter periods for both the west and east sub-basin channels are shown.

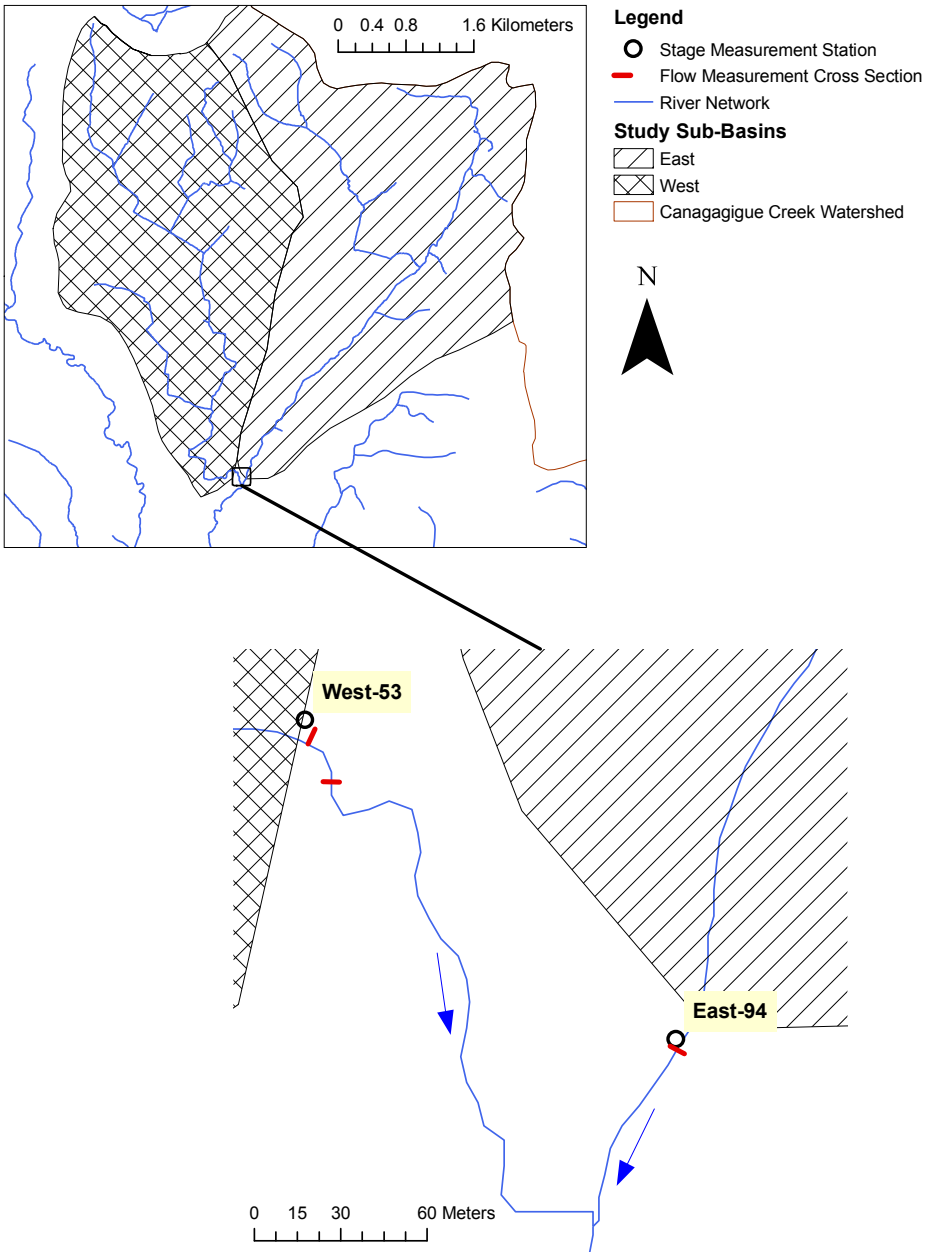

Figure 4.1: Map of Flow Measurement Stations and Cross Sections

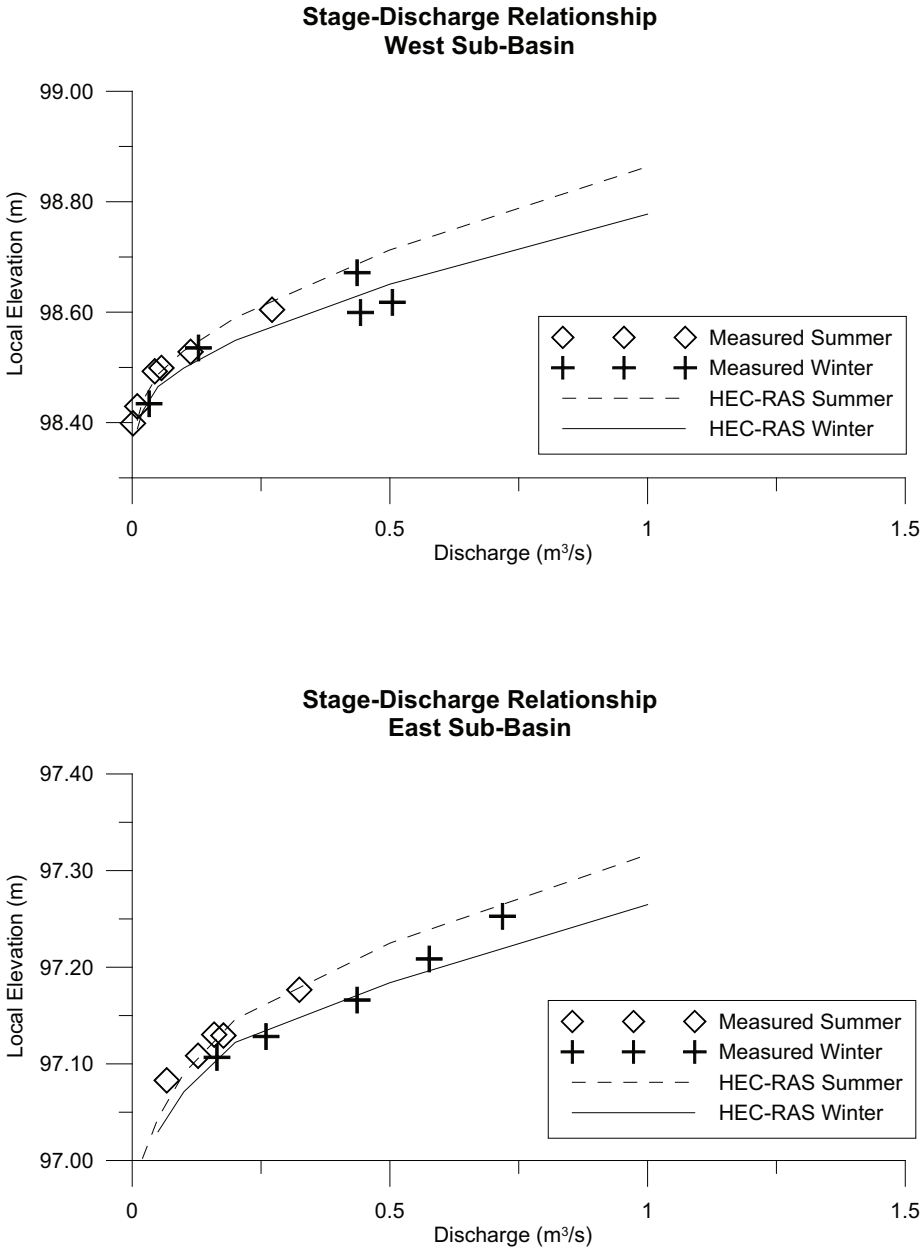

Figure 4.2: Calculated Rating Curves Using HEC-RAS

4.5 Anthropogenic Flow Sources - Alma Research Station

The Alma research station at the north end of the East basin acts a research-based fish hatchery. This research station pumps water from a local well and discharges into the Canagagigue Creek at the north end of the east sub-basin, the location of which can be seen in Figure 4.4. Water is chemically stabilized through a treatment and lagoon system before being discharged into the receiving waters. No flow records were available from the Alma research station, however the discharge from the stabilization lagoon was controlled through a sharp-crested rectangular weir 50 inches across. The depth of the pool near the weir was estimated using a yard stick at approximately 0.60 m. Eight measurements of the water level above the weir was taken during regular visits during the 2006 season along with water quality samples.

A sharp-crested weir equation was employed to determine the approximate flow contribution from the research station (Vennard and Street, 1976)

$$Q = C_w \frac{2}{3} \sqrt{2g} H^{2/3} \tag{4.1}$$

where Q is the total flow rate, H is the depth of water above the weir bottom. C_w is the weir discharge coefficient and can be estimated by

$$C_w = 0.605 + 0.08 \frac{H}{P} + \frac{1}{1000H} \tag{4.2}$$

where P is the distance from the base of the weir to the bottom of the channel and H and P must be specified in meters. Employing (4.1) and (4.2) the average flow rate was estimated at 38 L/s with the lowest measurement of 34 L/s and the highest being estimated at 56 L/s although this highest estimate showed some backwater effects due to interference due to debris in the weir. This contribution represents on average approximately one-third of the base flow quantity of the East sub-basin, with the minimum recorded base flow at the outlet of the east sub-basin being approximately 0.1 m^3/s. These values are approximately in line with flow estimates made at the Alma research station where about half of the base-flow

was assumed (Michael Burke, Manager Alma Research Station, personal communication).

The Alma research station is the only potential point-source addition of stream flow and pollutants to the study site and it was important to estimate the contributions to both the hydrology and the water quality in the East study sub-basin.

4.6 Flow Distribution Curves

The degree of extrapolation of the rating curves can be compared to the flow distribution curves (FDC) for each of the sub-basins. The FDC for each sub-basin is shown in Figure 4.3. It can be seen that less than 2% of the total readings were in excess of the maximum flow measurement for the east sub-basin ($0.8\ m^3/s$) and less than 3% of the total readings were in excess of the maximum flow measurement for the west sub-basin ($1.2\ m^3/s$). Also shown in this plot is the contribution of the East sub-basin with the average base flow due to the Alma research station removed. Although this shows a somewhat adjusted FDC the flow in the East basin remained perennial even with this adjustment.

When considering total volume, flow extrapolation from the rating curve becomes more significant. The FDC as a fraction of total volume for all readings is shown in Figure 4.3 in the bottom half of the figure. In terms of total volume the readings outside the measured rating curve account for 17% and 26% for the east and west sub-basins respectively. These FDC curves also illustrate the very different hydrological state of the two watersheds with the West sub-basin having a very low discharge ($< 0.1\ m^3/s$) for almost half of the readings taken, whereas the East sub-basin shows at least $0.1\ m^3/s$ for all readings. Adjustments to this figure due to the extra flow due to the Alma research station show only a small effect on the distribution curve for the east sub-basin and naturally only for lower flow rates.

4.7 Precipitation Data

Precipitation data for this study was acquired from a number of sources:

1. The GRCA Rain Gauge Network;

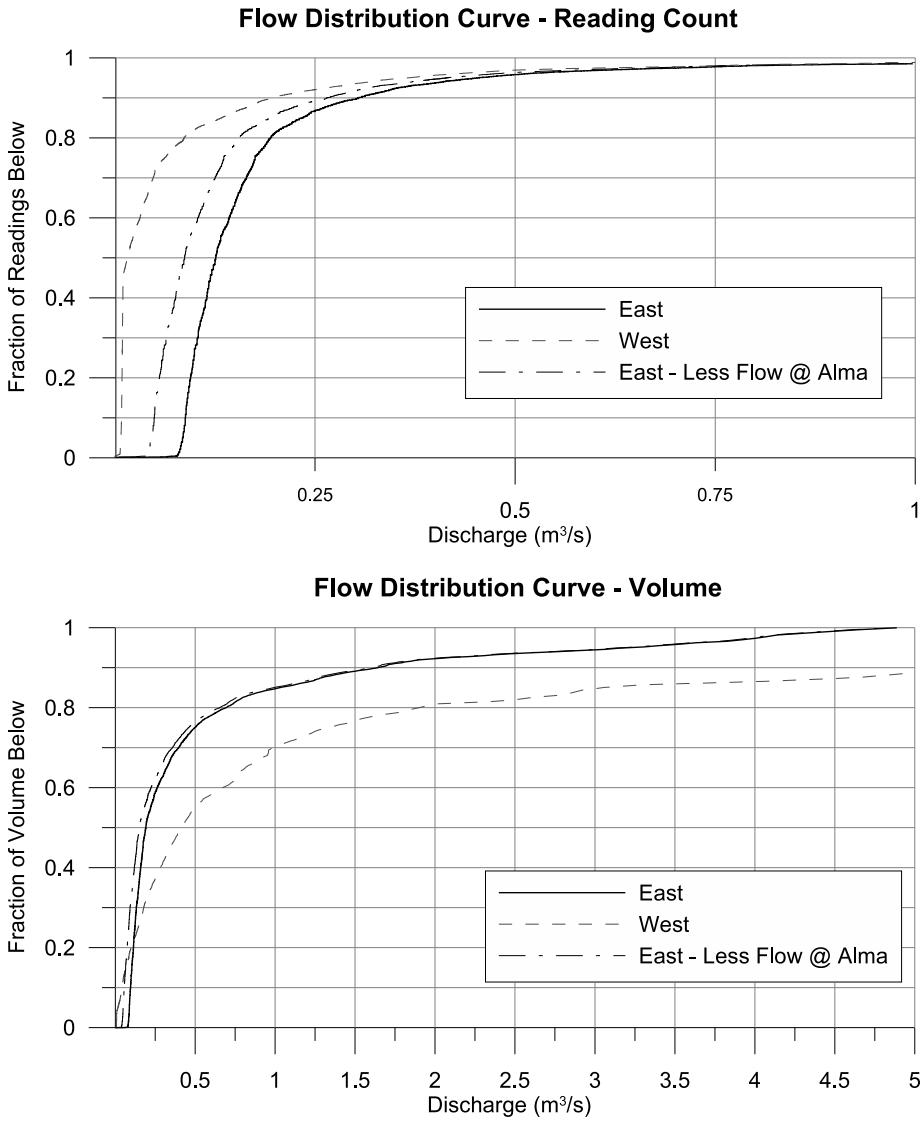

Figure 4.3: Flow Distribution Curves by Reading Count and Flow Volume

2. Study Site Tipping Bucket gauges operated for this study;
3. Daily rainfall measurements at the Alma Research Station;
4. RADAR Precipitation data provided by the King City Weather Radar station; and
5. The University of Waterloo Weather Station.

The study site tipping bucket data was very important in this study as it provided the non-snowfall precipitation data closest to the study site from 2005 to 2007. However, only two gauges were installed and no precipitation data was available from these gauges before the study began in 2005.

The rain gauge data provided by the GRCA were used extensively for the modelling in this study, as it provided hourly data in close proximity to the study site, and was available from January 2000. However, these data were provided as provisional and not quality assured. It was required to perform some independent quality assurance of precipitation data to ensure that the quantities and timing of the data was reasonably accurate.

The Alma research station located at the north end of the Canagagigue Creek collects daily rainfall measurements from a manual rain gauge. Because these data were collected only daily (whereas other data sources were hourly or sub-hourly) the data was used primarily as a quality assurance tool.

RADAR data provided by King City was useful in determining the timing and spatial distribution of the precipitation events, but the reported rainfall quantities were subject to errors in rainfall quantity estimation as is typical of RADAR products (Borga, 2002; Krajewski and Smith, 2002). Additionally, RADAR data was used when data was missing from the GRCA, Alma and Study Site gauges due to precipitation falling as snow not being recorded by tipping bucket rain gauges. The University of Waterloo Weather Station was also employed, primarily as an independent verification of precipitation event timing and magnitude. The precipitation data from the weather station was employed in the modelling efforts, but due to the relatively large distance away from watershed and the proximity of other gauges, the data was not a significant contributor to precipitation input.

A map of the locations of all the precipitation measurement locations employed in this study is shown in Figure 4.4. Rain gauges employed only for this study, the third-party

sourced data (GRCA and Alma Research Station) and the Waterloo weather station are identified. The GRCA Rain Gauge network is more extensive than shown here, but only the GRCA gauges within or immediately surrounding the Canagagigue Creek were employed. A summary of the measured rainfall for each of the captured runoff events is presented in Figure 4.1.

For details on how the precipitation data was collected, processed and quality assured see Appendix B.

4.8 Air Temperature Data

Air temperature data was provided by the University of Waterloo Weather Station, as well as the GRCA Woolwich Dam Location (see Figure 4.4 for locations). The rain gauge data loggers (RG01, RG02) included temperature sensors, but were not adequately protected from incident sunlight so were used for quality control purposes only.

4.9 Snow Surveys

Snow surveys were conducted to estimate snow water equivalent within the study basin and were conducted before the snow melt events for the 2006 and 2007 freshets. Four locations were chosen for snow surveys primarily based on permission by landowners providing access to the fields. Snow course samples were conducted March 3rd each year.

Snow course data was also provided by MNR for the region from 2003 to 2007. Depending on snow cover the MNR surveys were conducted twice a month, close to the 1st and 15th of each month.

Snow course data locations are presented in Figure 4.5. SNW01 to SNW04 are identified and represent the snow survey locations conducted as a part of this study. The remaining snow survey locations were provided by MNR. Data from each of these locations was included in the modelling effort in this study.

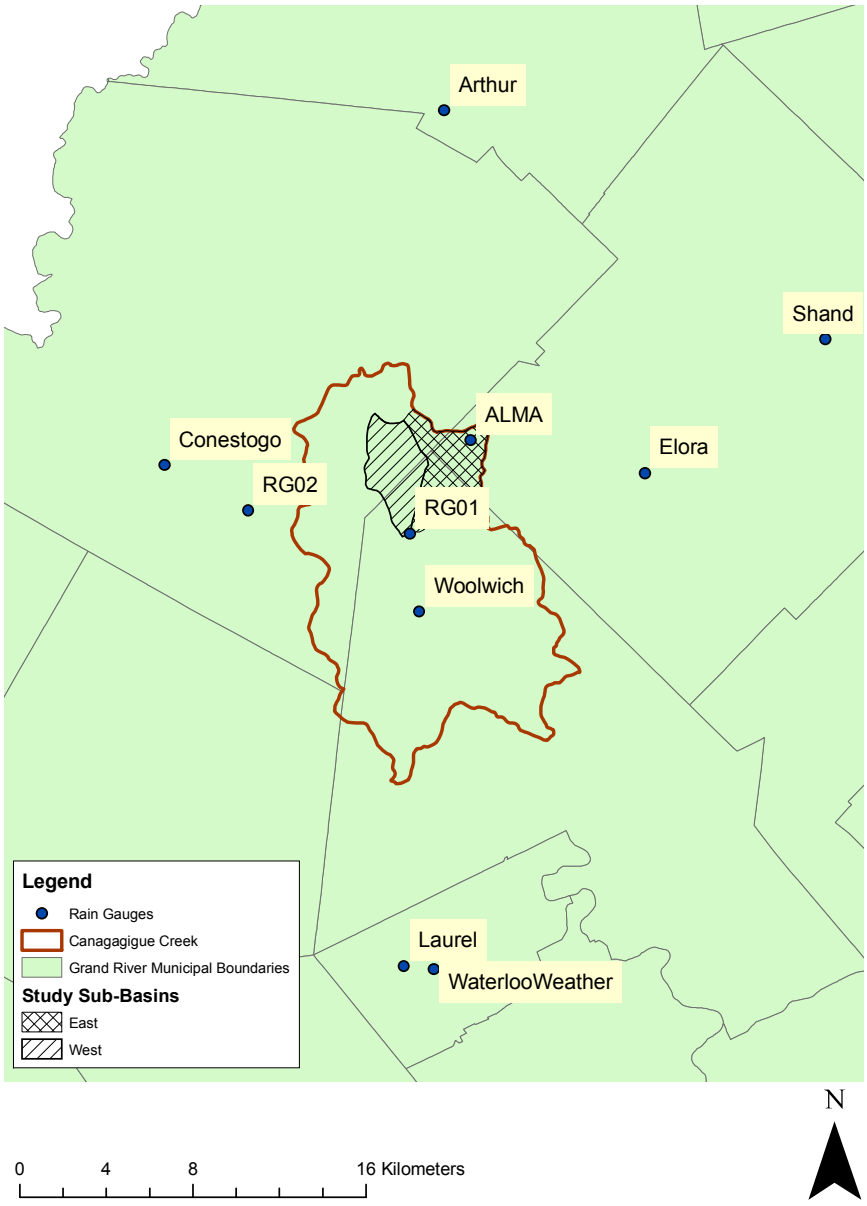

Figure 4.4: Rain Gauge Network

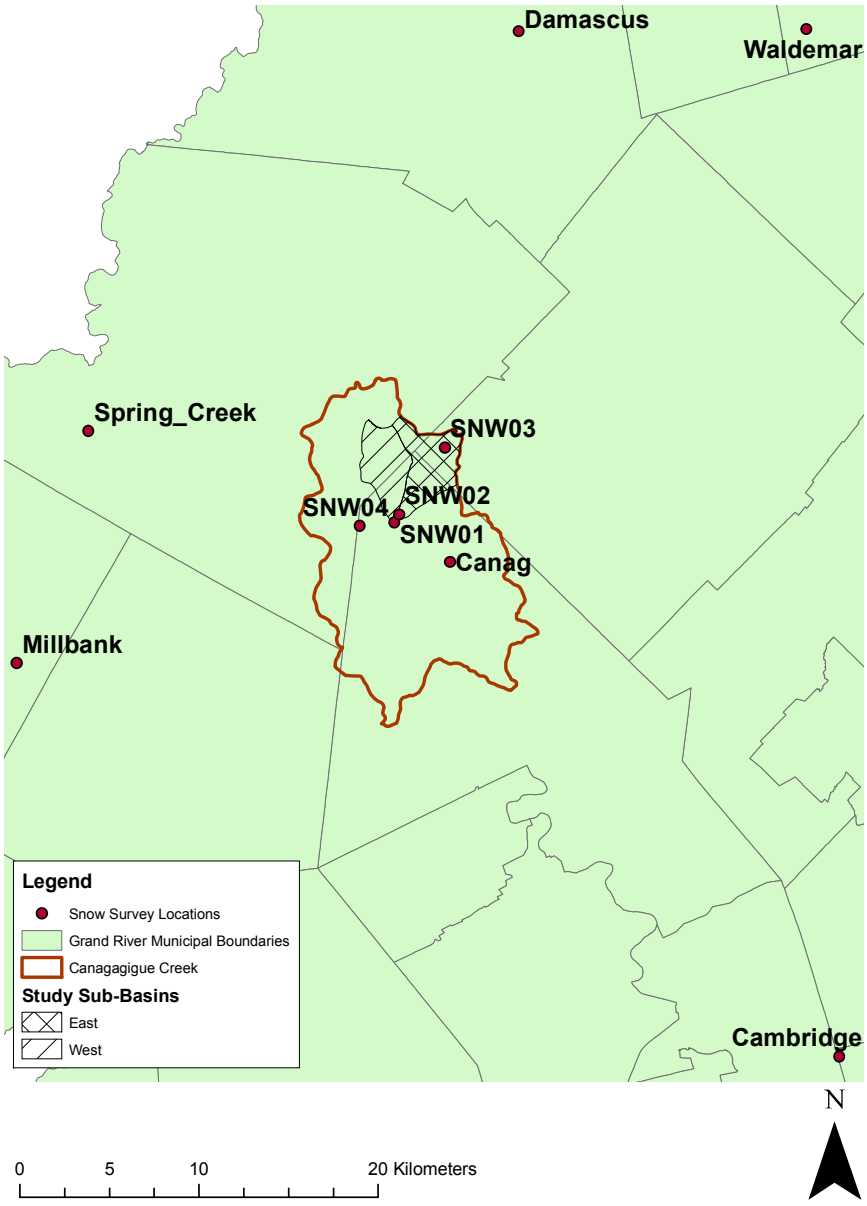

Figure 4.5: Snow Survey Locations

Event Code	Date	Total Event Precipitation (mm)			
		Elora	RG01	UW Weather Station	Woolwich Dam
EVT01	16-Jul-2005	12.6	22.4	25.8	27.8
EVT02	19-Aug-2005	37.0	64.4	0.0	30.4
EVT03	26-Sep-2005	42.0	82.4	34.6	45.2
EVT04	29-Sep-2005	14.0	32.4	15.0	14.6
EVT05	15-Nov-2005	29.4	46.4	35.4	35.0
EVT06	09-Mar-2006	61.8	34.8	47.0	46.0
EVT07	07-Apr-2006	13.6	12.4	11.6	14.8
EVT08	23-Apr-2006	35.8	23.0	27.6	32.0
EVT09	31-May-2006	12.8	20.6	41.4	29.0
EVT10	12-Jul-2006	20.4	25.2	47.4	24.2
EVT11	26-Jul-2006	20.0	19.9	17.6	22.0
EVT12	27-Sep-2006	25.6	22.0	22.4	26.2
EVT13	04-Oct-2006	3.4	5.4	11.0	5.4
EVT14	11-Oct-2006	19.4	28.0	16.2	24.4
EVT15	27-Oct-2006	29.6	40.8	29.2	19.4
EVT16	22-Mar-2007	7.8	11.2	n/a	9.8

Table 4.1: Total Precipitation by Captured Event and Rain Gauge Location

4.10 Streamflow and Dam Discharge Data

In addition to the stream flow data collected at the outlets of the East and West sub-basins, other flow data was collected within the Canagagigue Creek from the GRCA for the period of January 2000 to 2007. These data included hourly stream flow data exiting the Woolwich Dam, and at the Floradale, Elmira, and Below Elmira stream gauge stations and are presented in Figure 4.10. Floradale, Elmira and Below Elmira are stream flow measurement stations, whereas the Woolwich Dam is a calculated release from the controlled reservoir.

4.11 Sub-Basin Hydrological Response

The hydrological responses of each of the sub-basins were examined to determine the average time to peak for each of the two sub-basins. The hydrograph lag was determined by finding the time between the centroid of the contributing rainfall event and comparing that with the centroid of the runoff event (McCuen, 2005). Rainfall at the RG01 gauge

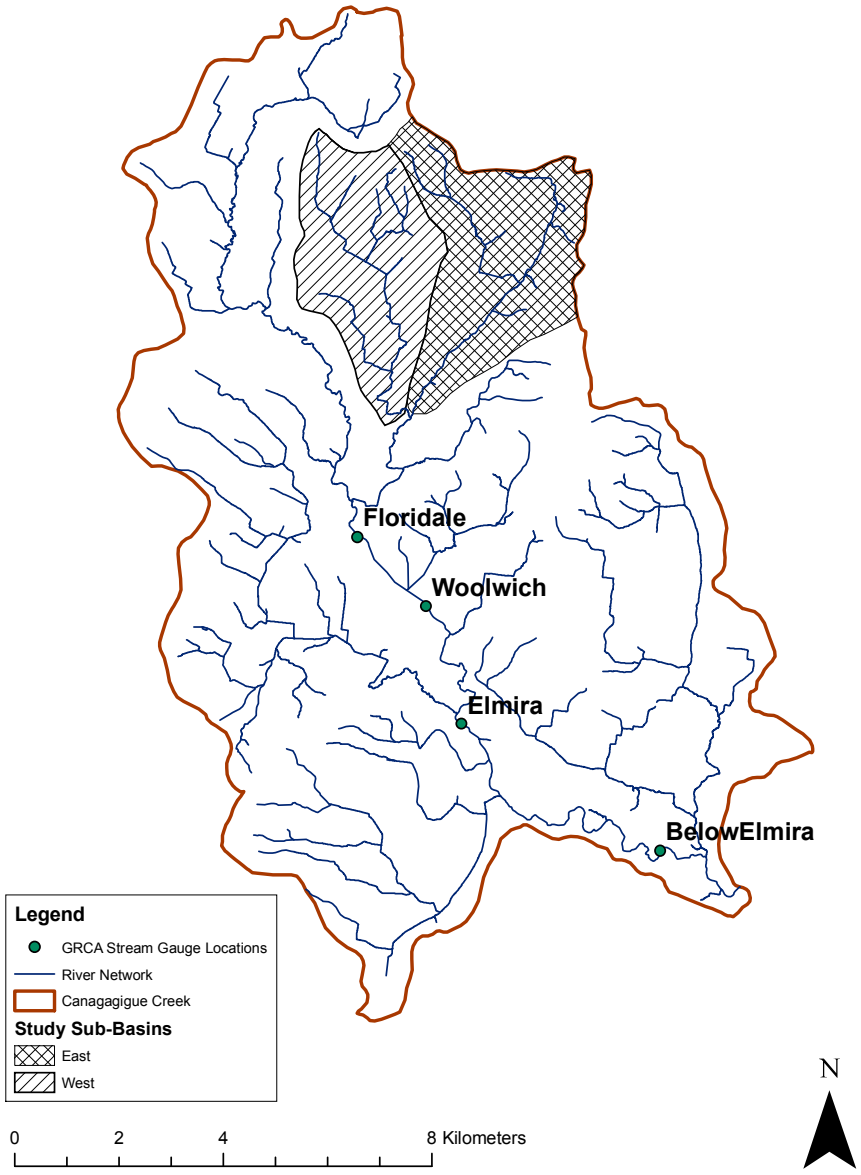

Figure 4.6: GRCA Streamflow Measurement Locations

was used to estimate the rainfall centroids. Calculations were performed directly on the database stored in the FSAM database tool. Figure 4.7 shows two plots: representing a) the hydrograph lag in hours as a function of rainfall intensity and b) a histogram of the difference between hydrograph lags between the east and west sub-basins. This figure shows that the hydrograph lag in the West sub-basin was consistently longer than the East sub-basin for all measured events, typically arriving 6 to 9 hours later. This again points to the fundamental differences in hydrological response in the watersheds due to antecedent conditions the East sub-basin channel being perennial, as well as local differences in slope, the East basin channel being steeper and the West basin having a higher effective roughness.

4.12 Chapter Summary

In this chapter the collection of a variety of data types for the hydrometric investigation of the study site was outlined. Topographic surveys showed that the two sub-basins tend to differ in terms of their channel morphology, with the main channel in the East sub-basin being steeper and with a more regular channel structure with an established flood plain. The West basin shows less slope and more irregular channel morphology due to incision.

Stage-discharge rating curves were developed for each of the sub-basins using velocity-area measurement calculations. The rating curves were extrapolated using a calibrated HEC-RAS model to provide a physically-based estimation of higher flows in the basins.

This chapter also outlined the collection of other meteorological data used for analysis and hydrological modelling purposes.

Hydrologically there were differences between the basins with the East basin having a perennial base flow condition whereas the West basin was shown to be ephemeral, going dry for several months during the summer and resuming flow during those periods only during large rainfall events. Hydrographic response was also quite different with the east sub-basin tending to respond more quickly than the West with an average hydrograph lag approximately 6-9 hours earlier than the West sub-basin.

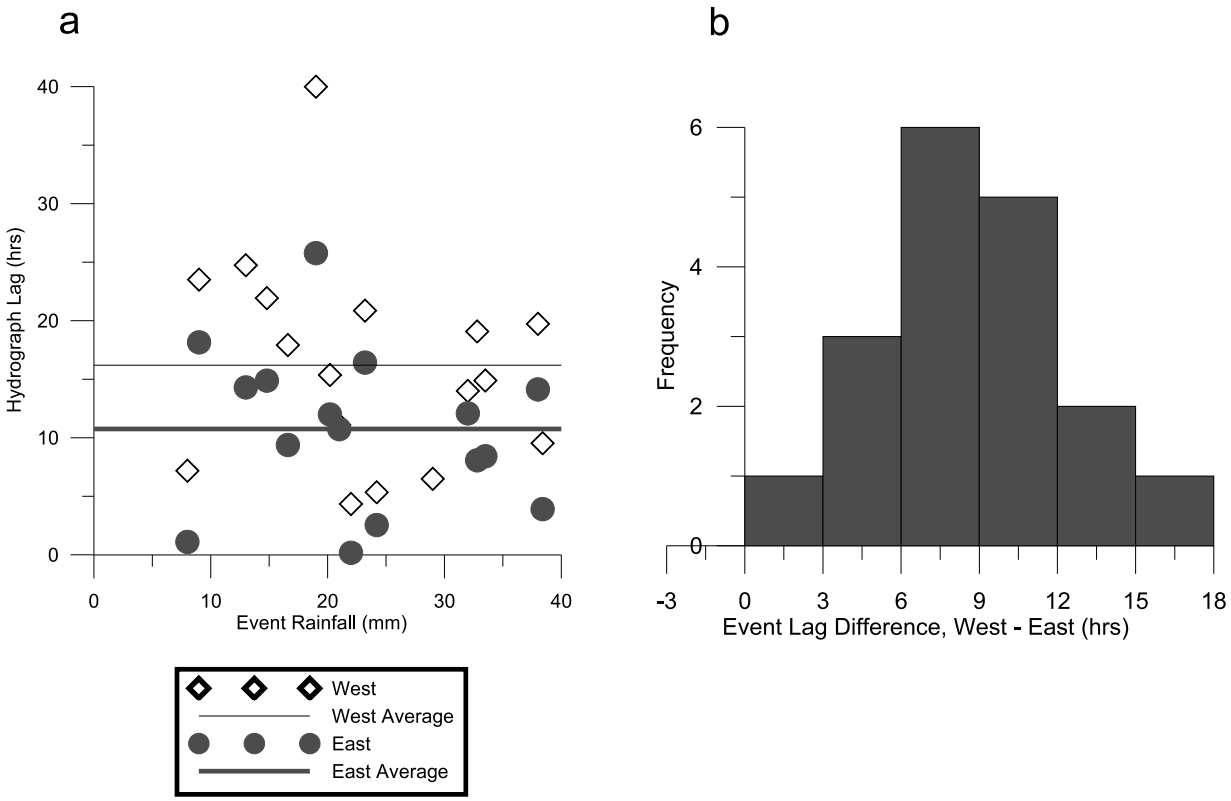

Figure 4.7: Hydrograph Centroid Lag - a) Hydrograph Lag as a function of rainfall intensity and b) Histogram of Hydrograph Lag difference between sub-basins (West-East)

Chapter 5

Hydrological Simulation

5.1 Introduction

Hydrological processes act as chemical transport drivers for non-point source pollution. For this study, a hydrological simulation was employed to provide a prediction of the hydrological response and facilitated subsequent analysis of chemical transport within the study site watershed. The objective of hydrological modelling was to produce accurate hydrograph responses from each sub-watershed, and also provide reasonable estimates of the hydrological processes such as contributions from interflow and modelling of water storage in the riparian wetlands.

WatFlood was chosen as the hydrological model to perform these tasks for a number of reasons:

- *Frequent time step:* For small watersheds with rapid hydrological response a short time step is required to capture the runoff events with an adequate resolution. WatFlood employs a sub-daily (hourly) time step.
- *Physically-based infiltration and runoff model:* WatFlood employs a physically-based runoff model which allows for more deterministic continuous modelling, and precludes reliance on empirical runoff modelling approaches (such as SCS curve numbers).

- *Established routing model:* The WATFLOOD model has been shown to contain a successful hydrological routing model.
- *Integrated riparian wetland model:* The WATFLOOD model includes a fully coupled hydrological model that links a riparian zone storage model to a channel routing model.

In this chapter the procedure for the WATFLOOD model configuration for the Canagagigue Creek and the study sub-basins is outlined. The calibration approach is identified and the results for the Canagagigue Creek and the study sub-basins are presented. Some discussion addressing the issues with modelling ephemeral channels with WATFLOOD and the observed performance of the riparian wetland sub-model conclude the chapter.

5.2 Hydrological Modelling Approach

There are several approaches that can be taken when hydrologically modelling a watershed. Refsgaard and Knudsen (1996) describe three primary classes of hydrological models: Empirical, Lumped Conceptual, Distributed Physically-based model. The authors concluded the best models in terms of performance and ability to match hydrological response are lumped and physically-based providing there is an adequate calibration period. Physically-based models provide an additional non-performance-based advantage as the parameter sets are based on physical processes – allowing for physical limits on permitted values and for shorter calibration periods if changes are made to land cover or land use data. Vieux (2001) similarly classified hydrological models in two types, those being either physics-based or conceptual, although with the understanding that some models may contain both conceptual and physically-based elements, and exist as a hybrid of the two classes. Vieux identifies the strength of physically-based models in similar terms as Refsgaard and Knudsen, in that a distributed physically-based model benefits from using model parameters that can be estimated and constrained by physical limits.

The WATFLOOD model is a physically-based, distributed hydrological model developed at the University of Waterloo (Kouwen, 2005). WATFLOOD has been employed successfully

as a hydrological predictor model on a number of watersheds at various scales throughout Canada and elsewhere (Bacchi and Ranzi, 2000; Cranmer et al., 2001; Kouwen et al., 2005; Bingeman et al., 2006). Although WATFLOOD was developed primarily as a flood forecasting model requiring a short time-step, its structure allowed it to be used for long term simulations in climate impact studies (Toth et al., 2006; Pietroniro et al., 2006b).

Although the primary purpose of the model is stream flow simulation and prediction using a distributed approach, research by others has used the hydrological framework to predict other parameters of concern, including water quality parameters (Dorner, 2004; Leon et al., 2004) and isotopic signatures (Stadnyk et al., 2005).

This chapter outlines the key modelling processes in the WATFLOOD hydrological model that have a direct or tangential relationship to model calibration and model development that is described in subsequent chapters. A more complete description of the model can be found in Kouwen et al. (1993) and Kouwen (2005). Additionally, this chapter outlines data acquisition and incorporation into the model for hydrological modelling purposes, the calibration approach and the model performance.

5.2.1 The WatFlood Hydrological Model and the GRU Concept

WATFLOOD is a suite of hydrological tools including a hydrological model (SPL) and a number of data pre-processing and post-processing tools to incorporate data sources into the model and to report model results and interface with other models and visualization tools (EnSim in particular). WATFLOOD is a gridded model that employs the Grouped Response Unit (GRU) concept (Tao and Kouwen, 1989). A GRU is a conceptual grouping of land surface areas with similar land use that are expected to have similar hydrological response. Each grid in the WATFLOOD model can contain one or more GRUs, dictated by the number of distinct land classes within the grid. Within grid connectivity is not considered in the WATFLOOD model, as all areas of similar land class are grouped to a single GRU, notwithstanding the position within the grid. The area of the GRU is proportional to the percentage of the associated land class within the grid. Hydrological parameters in WATFLOOD are generally associated with an identified land class and will control the hydrological response of each GRU within each grid.

River channels are classified in a similar manner to land classes within the WatFlood model, in that the river channel within each grid can be classified and associated with a distinct set of parameters, controlling routing and groundwater leakage within the model.

The GRU approach allows for a distributed modelling framework in which there are few watershed-specific parameters. Parameters are instead tied to land and river classes and usually the parameters can be transferred from one watershed to another within a physiographically similar region and provide good hydrological response (Leon, 1999; Cranmer et al., 2001).

Some identified limitations of the model include the regional groundwater model and the gridded nature of the watershed setup. The gridded nature of the model facilitates the inclusion of many distributed data sources, particularly radar and remotely sensed data. However the gridded approach does impose an arbitrary sub-basin delineation (considering a grid as a drainage unit) that does not necessarily comply with the topography of the watershed itself. This limitation diminishes in importance as the size of the modelled area increases beyond a few grids.

5.3 Watershed Model Set-up

The WatFlood model was configured for the entire Canagagigue Creek including the two study site sub-basins. This section outlines how the acquired data on the watershed was integrated into the model.

5.3.1 Watershed and Drainage Network Delineation

Generation of the model basin set-up for the Canagagigue Creek was done with the assistance of the EnSim hydrological modelling tool, ArcGIS and a 25 m resolution Digital Elevation Model (DEM) provided by the GRCA (GRCA, 2003a).

Watersheds may be delineated using computational techniques and DEM data by examining the gradients expressed by elevation differences across adjacent pixels and aggregating a conceptual surface flow upstream from a defined "outlet". As such, a topographically-driven flow field can be generated, and from this, flow accumulation from cell to cell, a

flow network and a drainage area contributing to the outlet are determined. Procedures for developing drainage areas and flow networks have been described by Jenson and Domingue (1988); Jensen (1991) and O'Donnell et al. (1999) among others and this process is incorporated into many GISs including ArcGIS and EnSim . The process prescribed within EnSim and followed in this study is as follows:

1. Create a depressionless DEM by filling local depressions or "pits" in the DEM so that local minima are removed;

2. Determine flow direction within each DEM grid element by determining the direction of maximum downward gradient when compared to each of the 8 adjoining cells;

3. Create a "flow accumulation" raster by summing up the number of cells that "contribute" to a particular DEM element;

4. Determine watershed area by identifying all DEM grid elements that contribute to a prescribed outlet; and

5. Determine drainage network by identifying all areas of high flow accumulation (i.e. channels) above some defined contribution threshold.

The watershed was delineated using the Depressionless DEM algorithm by Jensen (1991) incorporated into the EnSim software package. The EnSim tool was also used to section the watershed into specified 1 km grids and determined slopes, drainage areas, drainage directions and channel density. For further details on watershed generation in EnSim refer to the application manual (CHC, 2007).

Although automated drainage basin delineation does accelerate the generation of watershed delineation and drainage network generation for modelling, the most accurate way of delineating watersheds and drainage network is for a hydrologist familiar with the area to manually intervene with the aid of photographs and topographic maps (Ehlschlaeger, 1989). As such, with the aid of detailed areal photographs and delineated drainage networks provided by the GRCA, the drainage areas and drainage directions for each of the generated grids were modified manually to account for sub-basin boundaries within the

watershed and the published drainage network (GRCA, 2003b). Model drainage areas at hydrometric stations were compared to published drainage areas and compare favourably (within 10% error). Details of these results are shown in Apprendix B.

5.3.2 River Classes

WatFlood allows for the independent definition of river "classes" within the model. Each river class contains parameters which define water transport within the channel including: channel roughness, channel groundwater leakage parameters, channel geometry, and riparian zone conductivity and storage parameters. Each grid within the model must be assigned one river class, and grids with distinct characteristics should be assigned independent river classes (Kouwen, 2005). A number of the river class parameters cannot be measured directly and must be calibrated, namely roughness, wetland storage and conductivity. Other parameters that describe the geometry of the channels can be obtained through field and survey observations.

Three river classes were defined for the model: one class for the east basin main channel, one class for ephemeral tributaries within the study sub basins, and one for the remainder of the Canagagigue Creek. The two study sub-basins were extensively surveyed and the physical characteristics (i.e. bankfull areas) were well known for these two basins. Bankfull-drainage area relationships were generated for each of the sub-basins based on the measured data illustrated in Figure 5.1 (based on data presented in Chapter 4). For the main channel in the East basin a power-relationship of the type shown in Equation 7.6 was generated using a best-fit (minimized RMS error) approximation. The West basin and small tributaries contributing to the East basin showed a great deal of incision in the contributing channels, with no clear bankfull-drainage area relationship. However, the WatFlood model requires such a relationship to operate. The important observation that was made during the field season was that even during the snowmelt events of 2006 and 2007 very little evidence of water topping the banks was observed in the incised channels. The East basin main channel showed regular and pervasive topping of the banks during snowmelt events for all years observed. From a routing point of view it was important to capture this observation in the determination of a bankfull-drainage area relationship

within the WatFlood routing model, to avoid topping the banks under normal flow conditions in the incised channels.

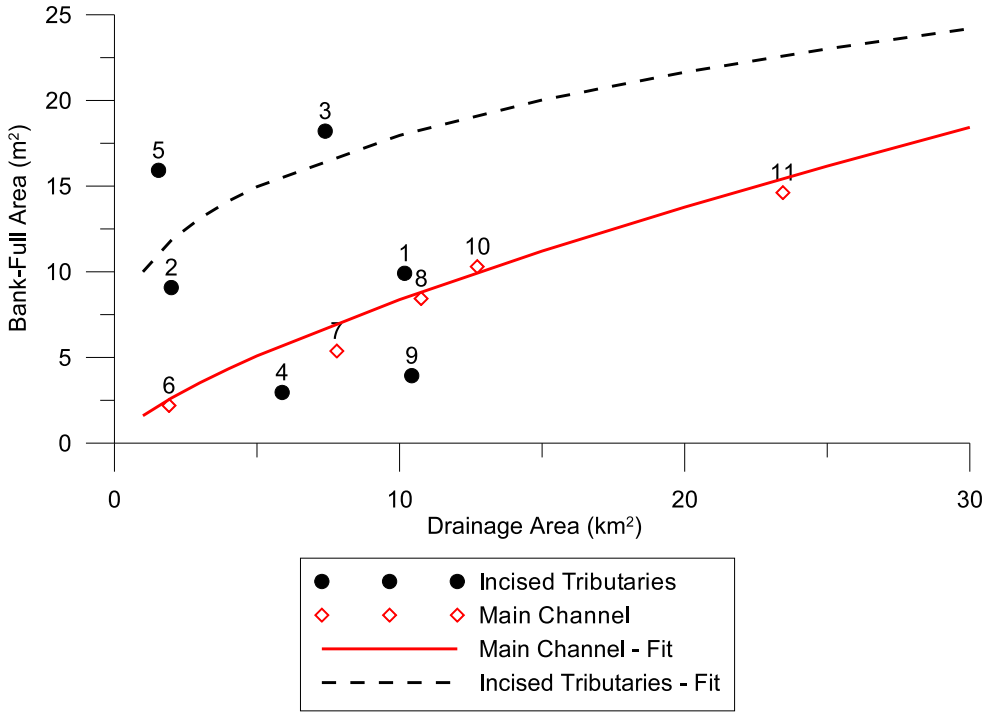

Figure 5.1: Bankfull - Drainage Area for Natural and Incised Channels with Fitted Relationships

Figure 5.2 illustrates this difference by plotting two cross sections and indicating bankfull area with coloured fill. It can be seen that for similar drainage areas the East basin main channel (East 7) had much less incision and a more pronounced flood plain than the West ephemeral channels (West 3). (A map of cross section locations is presented in Figure A.5.)

To incorporate this variability into the model a fit for the incised bankfull-drainage area was chosen that would conservatively choose a larger bankfull area and generally preclude bankfull flow. A fit for the bankfull-drainage area relationship was generated considering the three points with the greatest bankfull area for a given drainage area (sample points 2, 3, and 5). These points provided an outer envelope for the remainder of the incised

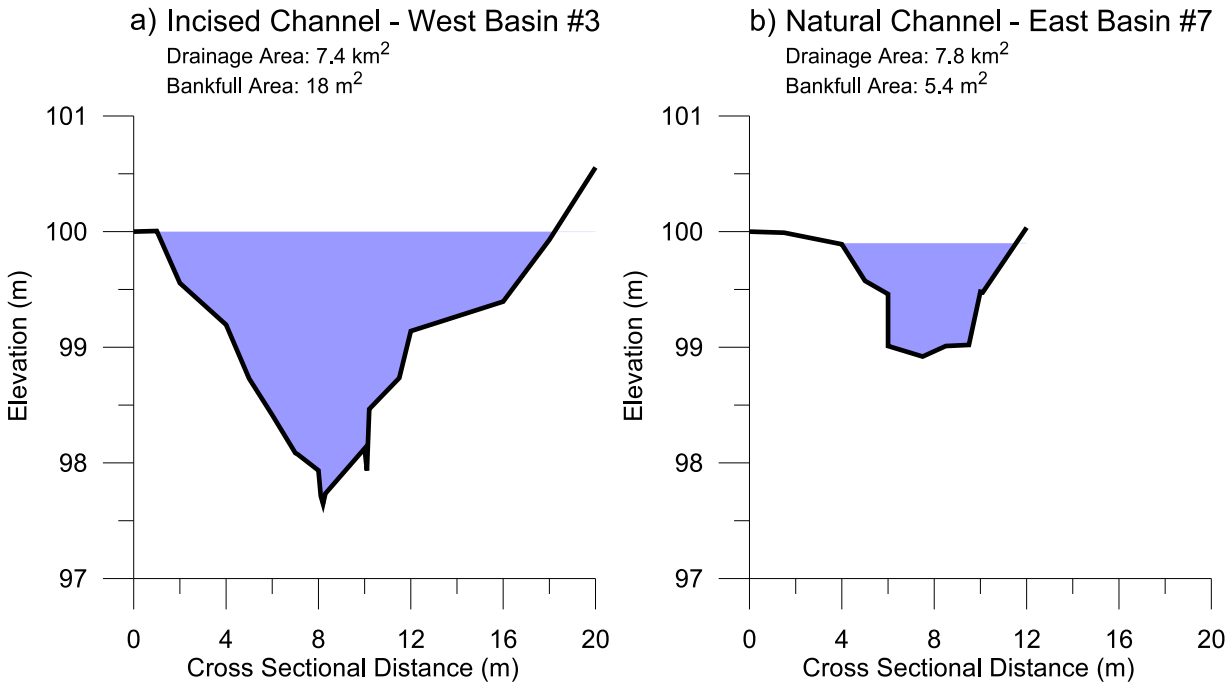

Figure 5.2: Bankfull Area for Incised Channels (a) and Natural Channels (b)

channels.

For the remainder of the Canagagigue Creek outside the two study sub-basins the relationship developed by Kouwen using bankfull-drainage area relationships for the entire Grand River was employed (Kouwen, 2005).

In addition to the determination of the bankfull area, the model also requires a channel width-depth ratio. The width-depth ratios were determined for both the natural and the incised channels by assuming a rectangular cross section and calculating the depth from the measured width and bankfull areas from cross sectional surveys. The average width-depth ratio of the cross sections surveyed was employed for each channel type.

5.3.3 Land-Use / Land-Class Data

In keeping with the GRU concept of the WatFlood model, it is expeditious to identify a number of hydrologically independent land classes or land uses within the modelled watershed. Although WatFlood does not have a limit as to the number of classes that can be introduced in the model, it is important to reduce the number of classes to the smallest reasonable number to ensure the model is not over-parameterized.

In determining land-use for hydrological modelling purposes the data provided by the GRCA and OMAFRA was considered as well as the wetland delineations provided by NRVIS (see Sections 3.2 and 3.3). It was determined through land-use truthing visits that the OMAFRA land-use map was most representative for the study area, although there was no distinction between wetlands and forests in the OMAFRA LULC map (all being classified as woodlots). Consequently, to determine unique hydrological land classes, the NRVIS wetland delineations were superimposed on the OMAFRA LULC, with the remaining classes being defined as is typical for the WatFlood Hydrological model in the Grand River Watershed– Forest, Bare, Crop, Wetland , Water and Urban/Impervious. Land use mapping from the OMAFRA LULC classification to the WatFlood model classification are shown in Table 5.1.

Soil types were originally considered when defining GRU land classes for the WatFlood model. As described by Vieux (2001), to account for variability in infiltration rates between soil types one may classify unique combinations of land-use and soil as

GRUs. However, the watershed shows very similar soil characteristics throughout as illustrated previously in Figure 3.5, especially within the two study sub-basins and areas upstream of the Woolwich dam, where loam and silty loam soils predominate. The only regions that are distinct from this classification are the organic and gravelly loam areas which lie along the East basin main channel corridor, which are already uniquely classified as riparian wetlands. Consequently, the land use was deemed to be the most important characteristic when defining GRU classes in WatFlood.

OMAFRA Land Class	**Watflood Model Land Class**
Mixed System	Crop
Corn System	Crop
Woodlot	Forest
Grain System	Crop
Hay System	Crop
Continuous Row Crop	Crop
Built Up	Impervious
Unclassified	Bare
Water	Water
Idle Agg > 10 yrs	Bare
Pasture System	Bare
Recreation	Bare
Extraction Pits	Bare
Idle Agg 5-10 yrs	Bare
Grazing System	Bare
Unclassified	Bare
Reforested Woodlot	Forest

Table 5.1: OMAFRA LULC to WatFlood Land Class Mapping

5.3.4 Precipitation Data

Precipitation data were collected from a variety of point sources that employed either tipping-bucket and weigh-scale gauges as well as distributed RADAR data (see Section

4.7). When data was available the point gauge precipitation measurements were distributed over the watershed area using a modified version of an inverse distance weighting method (IDWM) described by Wei and McGuinness (1973). Inverse distance weighting methods are recommended by in the ASCE Handbook of Hydrology for missing data (ASCE, 1996). When reliable gauge precipitation was not available within the area, particularly in winter months, the uncalibrated RADAR data from King city was applied.

Further details on how the precipitation data was processed and quality assured are described in Appendix B.

5.3.5 Snow Course Data and Distribution

The precipitation gauges employed in this study were tipping-bucket rain gauges, with the exception of the GeoNor® T-200B Series Precipitation Gauge at the University of Waterloo weather station. None of the tipping-bucket rain gauges provide an estimate of the quantities of snow on the watershed. Consequently data provided from snow surveys was required to provide corrections to the model estimated snow pack. A number of surveys were conducted within the study area prior to the 2006 and 2007 snowmelt events and these data were supplemented with snow survey data provided by the MNR (see Section 4.9). Snow water equivalent values collected at these point surveys were redistributed using the same rainfall distribution algorithm described in Section 5.3.4. This snow distribution routine resets the snow water equivalent for the entire watershed at the time of distribution, which was typically at the start of the month, or WATFLOOD event.

5.3.6 Stream Flow Data

The stream flow data was obtained from the two study sub-basins operated for this study (see Section 4.4) and from the GRCA monitoring stations (see Section 4.10). Stream flow and dam discharge data were provided by the GRCA for the period from January 2000 to January 2008 and included stream flow data at the Floradale gauging station (near Floradale Rd., upstream of the Woolwich Reservoir), the Woolwich Dam Discharge, Elmira gauging station (at Albert Street) and the Below Elmira gauging station (at County

Road 22, 3.5 km east of Elmira). The stream flow data were considered provisional by the GRCA and had not been corrected for data recording anomalies or changes in the stage discharge rating curves. The dam discharge data were also considered provisional and were generated based on the water levels, gate settings and established stage discharge coefficients. For both the dam and stream flow data, corrections to the provided data were necessary. Data that could be categorically discounted for physical reasons were removed from the simulations and were not otherwise adjusted. Details can be found in Appendix B.

5.4 Hydrological Model Calibration

The WatFlood hydrological model employs a number of essential parameters that cannot be precisely measured and, as with any hydrological model, requires some degree of calibration. Parameters may be estimated in two ways - they can be determined manually, relying on the modeller's experience, or they may be estimated using an optimization algorithm to obtain an "optimum" value based on a prescribed objective function. The first requires the modeller to adjust the parameter values systematically and within a prescribed range, again relying on experience in the model's performance under different conditions whereas the latter approach uses a systematic computational approach.

For this modelling exercise a combination of approaches was employed to calibrate the model to observed stream flow values. A WatFlood parameter set with reasonable performance had already been calibrated for the region during previous studies of the Canagagigue Creek watershed and the Grand River watershed (Leon et al., 2002; Kouwen, 2005; Dorner et al., 2006) . Systematic modifications to sensitive parameters were made to improve the model performance. The approach prescribed in the WatFlood manual (Kouwen, 2005) was followed for manual calibration.

5.4.1 Calibration Parameters and Procedure

The parameters that were calibrated within the WatFlood hydrological model included:

River Class Parameters:

1. *LZF* - lower zone drainage function (linear parameter)
2. *PWR* - lower zone drainage function (exponential parameter)
3. *R2N* - river channel roughness
4. *THETA* - porosity parameter for riparian wetlands
5. *KCOND* - conductivity of the riparian wetlands

Land Class Parameters:

1. *REC* - interflow depletion rate
2. *RETN* - maximum upper zone retention storage
3. *AK/FS* - surface drainage resistance
4. *AK2/FS* - upper zone drainage resistance
5. *R3* - surface roughness
6. *MF* - snow melt factor
7. *BASE* - base temperature for snow melt calculations

Further details as to the parameter characteristics and use within WatFlood are described in Kouwen (2005).

Due to the very short period of hydrological data obtained for the study site (March 2005 to December 2007), the hydrological calibration was conducted using hydrological data from downstream gauges provided by the GRCA that was available for a longer period (2000 to 2007). The hydrological model was calibrated for five specific hydrological periods between 2000 and 2004 using the supplied GRCA stream flow data. A warm-up period of 5 years using the 2000 calendar year meteorological data was employed to develop reasonable starting-point state variables. Throughout the calendar, short 1 to 2 month periods with good data availability and varied hydrological response were selected for model calibration.

Details of the events used for calibration and results are shown in Appendix B. Specific attention was paid to the stream flow gauge at Floradale, as this gauge has no upstream controlling structures and the two study sub-basins account for approximately one-half of the drainage area contributing to this stream flow station, making its performance the most representative of the study sub-basin performance. Additionally, the Elmira and Below Elmira GRCA stream flow gauges had measurements dominated by the reservoir releases at Woolwich Dam. The release quantities were found to be in error over several periods, making the calibration of the model to these stations questionable. In lieu of additional verification of the dam discharge data, the stream flow responses below Woolwich Dam were only considered qualitatively in the calibration procedure, as a means of checking for consistency in hydrological response throughout the watershed.

The selection of calibration criteria for hydrological models generally involves a matching of model response to a measured quantity, typically hydrograph response. How the model output is compared to the measured data is often project-specific and will depend largely on the objectives of the study. There is no universal metric to evaluate hydrological model performance (Beven, 2001). A widely used "fitness" measurement is the Nash-Sutcliffe efficiency coefficient (Nash and Sutcliffe, 1970):

$$R^2 = 1 - \frac{\sum_{i-1}^{n}(Q_i - Q_i')^2}{\sum_{i-1}^{n}(Q_i - \bar{Q})^2} \tag{5.1}$$

where R^2 is the Nash-Sutcliffe efficiency coefficient, n is the number of measured stream flow values, Q_i is a measured stream flow value, Q_i' is a simulated stream flow value and $\bar{Q}$ is the average measured flow rate for the simulation period. Nash-Sutcliffe is a statistical method based on the error variance of the time series data. A value of 1 represents perfect agreement between the simulation and observations, with lower values indicating less agreement. A Nash-Sutfliffe value of 0 represents a model performance no better on average than using the mean measured value, and values less than 0 are worse than this most basic model. The utility of the Nash-Sutcliffe metric has been criticized due to its sensitivity to small temporal shifts between the observed and measured hydrographic responses (Beven, 2001), but is nevertheless widely used.

Another common "fitness" measurement is comparing the total runoff volume between the measured and simulated data over a simulation period (Beven, 2001; Vieux, 2001). The relative difference in runoff volume is calculated using Equation 5.2:

$$D_v = \frac{V - V'}{V} \tag{5.2}$$

where V is the measured runoff volume for the simulation period and V' is the simulated runoff volume. The runoff volume difference provides no information about time-varied hydrological response, but is a good indication of whether hydrological continuity is being maintained within the model over the simulation period.

Calibration was initially done manually as per the recommendations in the WATFLOOD manual (Kouwen, 2005). Both the Nash-Sutcliffe and relative volume difference measurements were used with the manual calibration. Subsequently the pattern search algorithm described by Monro (1971) and incorporated into the WATFLOOD was run to further refine the parameter values and optimize the model performance. Details of the pattern-search implementation are more fully described in Kouwen (2005). The resulting WATFLOOD parameter file used for the subsequent simulations is presented in full in Section B.7.1.

5.4.2 Model Validation

The evaluation of model performance can involve a number of comparative metrics. Beven (2001) and Vieux (2001) suggest that in addition to comparing variance statistics (Nash-Sutcliffe) and volume comparisons, peak flows, known water levels or other data may be appropriate, depending on the requirements of the study. When considering water quality modelling, obtaining accurate event-based characterization is important. Nutrient fluxes are dictated largely by runoff volumes. Sediment transport fluxes are also controlled by event runoff volumes, however, the peak flows are also of importance due to the in-stream processes that drive sediment transport and the strong correlation of sediment concentrations to stream power. It is therefore deemed important to evaluate the hydrological model in terms of its ability to accurately predict the event peak values and the total event runoff volumes when assessing simulation quality. Although event loadings are the focus

of this research is is understood that baseflow conditions may be of particular importance for water resources policies including drinking water sourcing and fish habitat. However, the goal of the hydrological modelling in this research is to simulate total loading from sub-basins with a future goal to applying the loading model to larger watersheds (eg. the Grand River).

The model metrics used in the calibration approach, the Nash-Sutcliffe and Runoff Volume Difference metrics, were calculated for the entire non-snowmelt periods for each of the modelled calendar years using daily flows. The results are presented in Table 5.2.

Table 5.2 illustrates some of the issues in employing the Nash-Sutcliffe value over the entire period. Some periods were modelled well, particularly the Floradale station in 2002 and 2003 with relatively high Nash-Sutcliffe values and low runoff volume errors. During other periods and particularly with the two study sub-basins the model performed much less well as indicated by the low Nash-Sutcliffe values and runoff differences. However, one must consider the very long periods of low-flow between approximately June and September of each year. Matching the low-flow conditions with the WatFlood model proved difficult during the calibration period (See Appendix B.7) and the Nash-Sutcliffe and runoff volume comparison metrics suffered over these modelled periods. An illustration of the hydrological response over the calendar year 2006 is presented in Figure 5.3, which illustrates the long period in mid-summer when very few runoff events were realized.

As discussed above, the event-based performance is of particular interest in water quality modelling. To assess the model performance with regard to event-based performance, runoff event periods with valid rainfall and stream flow data were identified over the entire simulation period for the Floradale stream flow gauge, and the East and West sub-basin gauges. Figure 5.4 illustrates the performance of the model on an event basis for the entire 2000 to 2008 period. (Events used in the calibration procedure were excluded from this calculation.) In Figure 5.4, both the measured and simulated peak flows (a) and the measured and simulated runoff volumes (b) were compared and plotted with the 1:1 line representing a perfect model performance. It can be seen that the calibrated model did not systematically over- or under-estimate either the peak flows or the runoff volumes, but the runoff volumes were more accurately captured. Plotted relative error measurements can

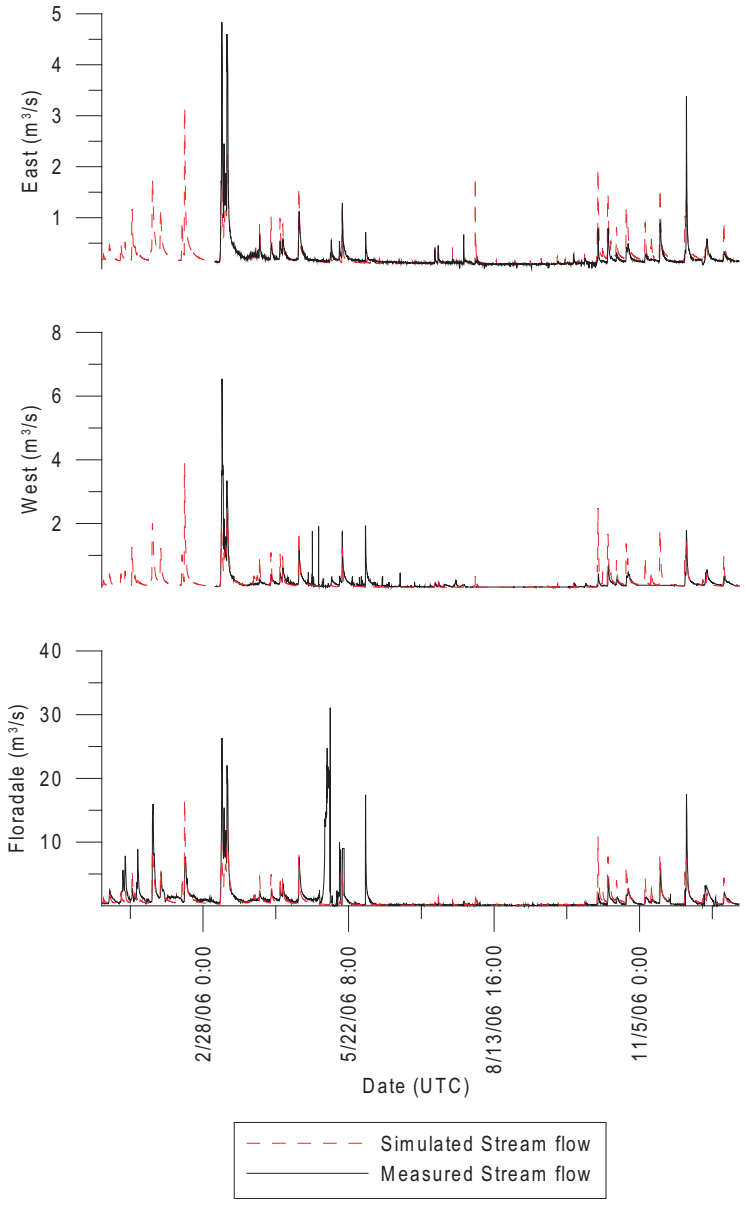

Figure 5.3: WatFlood model performance - 2006

	Nash-Sutcliffe			**Runoff Volume Difference (%)**		
Non-Snowmelt Period	Floradale	West	East	Floradale	West	East
2000	0.629	n/a	n/a	27.4	n/a	n/a
2001	-0.137	n/a	n/a	-16.3	n/a	n/a
2002	0.847	n/a	n/a	-1.6	n/a	n/a
2003	0.413	n/a	n/a	-34.3	n/a	n/a
2004	0.202	n/a	n/a	-32.8	n/a	n/a
2005	-0.023	0.202	0.043	-44.3	28.6	-9.0
2006	0.029	0.107	0.177	31.7	17.4	-14.1
2007	0.284	0.148	0.496	42.0	29.7	30.2

Table 5.2: Annual Non-Snowmelt Nash-Sutcliffe and Runoff Volume Differences in Calibrated Model

be a usefull graphical performance aid (James and Burges, 1982). Figure 5.5 shows the relative error in the peak flow and runoff volume estimates for each of the delineated events. Figure 5.5 illustrates the bias in the calibrated model to overestimating peak flow (by approximately 27% on average) and underestimating peak volumes (by 3.8% on average).

$$D_p = \frac{P - P'}{P} \tag{5.3}$$

Employing a relative error metric is useful to illustrate the degree of error, but the model is restricted to positive values, necessarily skewing the relative error positively. The model cannot simulate a negative peak, which naturally skews the mean to a higher relative error value. However, comparing the central tendencies of the distribution in Figure 5.5 shows that the number of over- and under-estimated events were similar in number for both the peak flow and runoff volume relative errors, indicating that the model over-estimated peak flow and runoff volume as often as it under-estimated them. This is illustrated by the low magnitude of the median values of the relative errors for both the peak flow and runoff volumes in Figure 5.5.

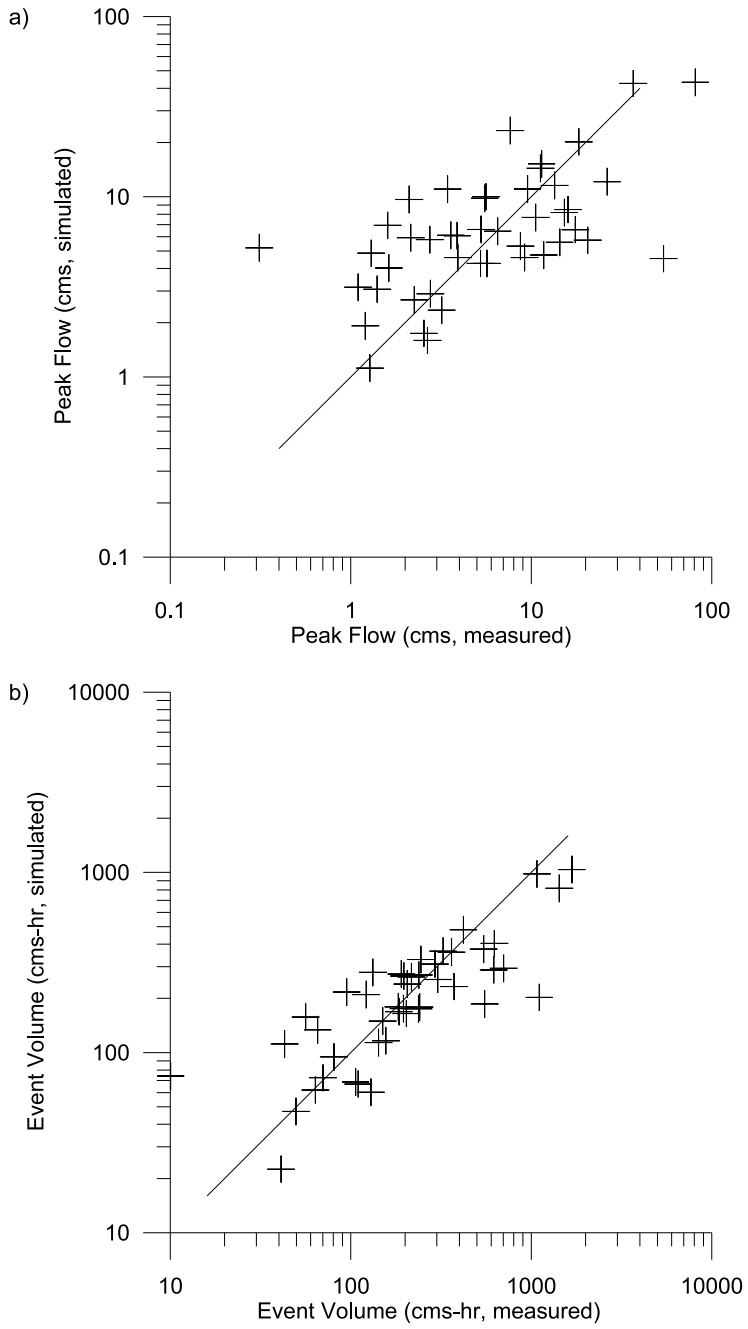

Figure 5.4: Event Peak Flow (a) and Runoff Volume (b) Comparison - Floradale Stream Flow Station

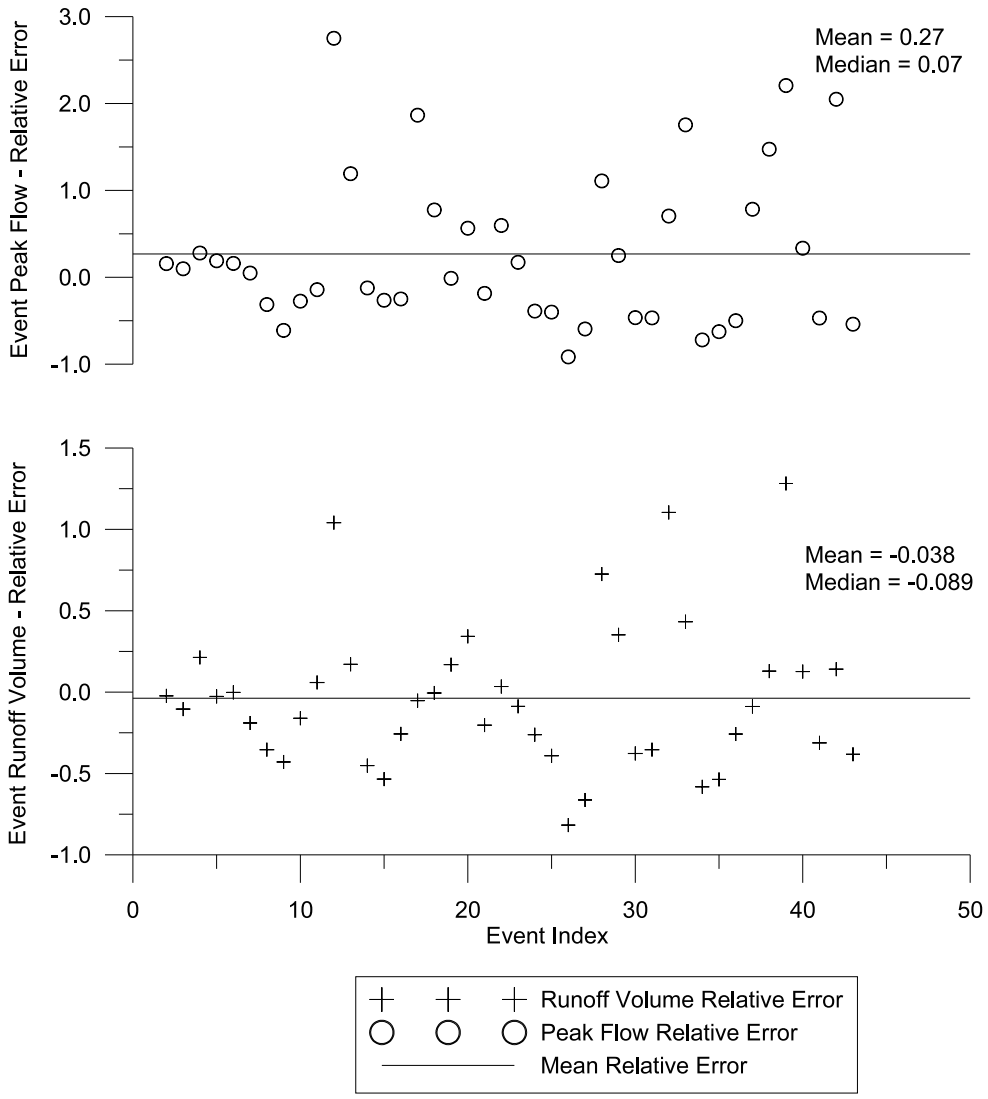

Figure 5.5: Event Peak Flow and Runoff Volume Relative Error - Floradale Stream Flow Station

5.4.3 Performance of Sub-Basins

The performance of the hydrological model in the East and West sub-basins was examined. Of particular interest was the difference in hydrological response between the East and West basins, particularly when antecedent conditions were dry (i.e. tributaries not in the main channel were dry). As witnessed in the field, after a period of low rainfall in the summer, when the flow would stop or nearly stop in the West basin, the timing of the hydrographs of the West sub-basin was delayed as compared to the East sub-basin. When the West stream went dry the storage within the channel would have to be satisfied before the hydrograph would make its way to the basin outlet. Additionally, considering the higher elevation of the West basin channel than the East basin channel, the dry summer months would position the water table well below the West channel, which would again provide additional storage to be satisfied. During smaller events (< 30 mm) when the basin was dry the change in hydrograph timing was clearly evident. For larger events, or events that occurred with more wet antecedent conditions the hydrograph timings of the two basins were more similar. Figures 5.6 and 5.7 illustrate this effect. Both events were of similar size (approximately 20 - 25mm). Figure 5.6 illustrates the hydrographic response with wet antecedent conditions in late April of 2006. The timing and overall runoff quantities were similar in both sub-basins. Figure 5.7 illustrates the hydrographic response with dry antecedent conditions in mid-July 2006. Here a shift in hydrograph timing in both basins was observed with a very pronounced shift in the West sub-basin. Also, the total runoff volume was much reduced in the West sub-basin.

Other researchers have observed timing complications in hydrograph routing relating to channel geometry, but these are often related to larger events where the flood plain has an influence. Vieux (2001) identified issues with flood routing in incised channels using trapezoidal geometries for large flows. The issues identified here indicate that similar issues can be observed with incised channels at lower flow rates where the irregularity of the channel can cause complications. Vieux (2001) showed improved routing can be obtained by incorporating rating curves for measured cross sections rather than assuming a geometry across the watershed.

The simulated and measured peak flows and runoff volumes for events in the East and

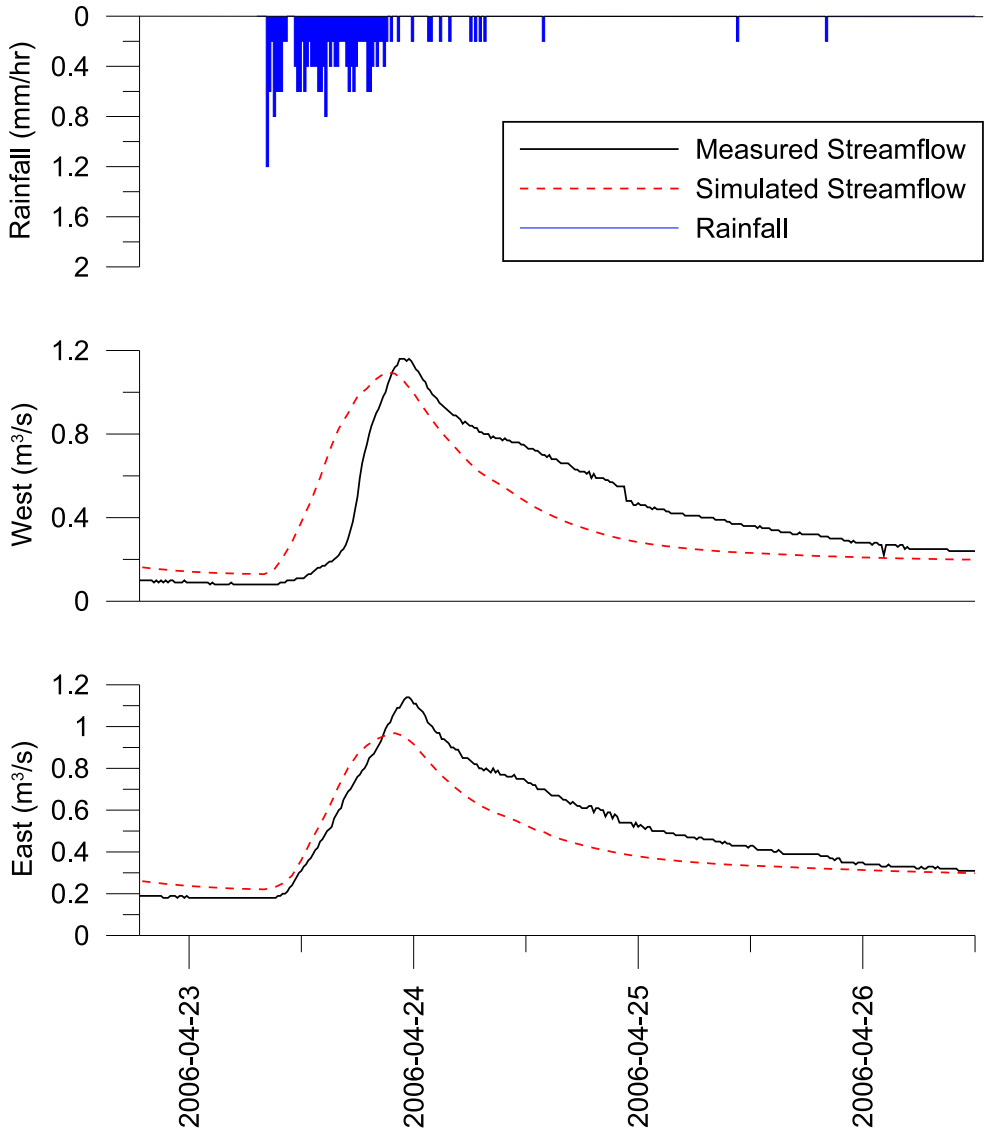

Figure 5.6: Hydrograph timing for wet antecedent condition event - Event 08

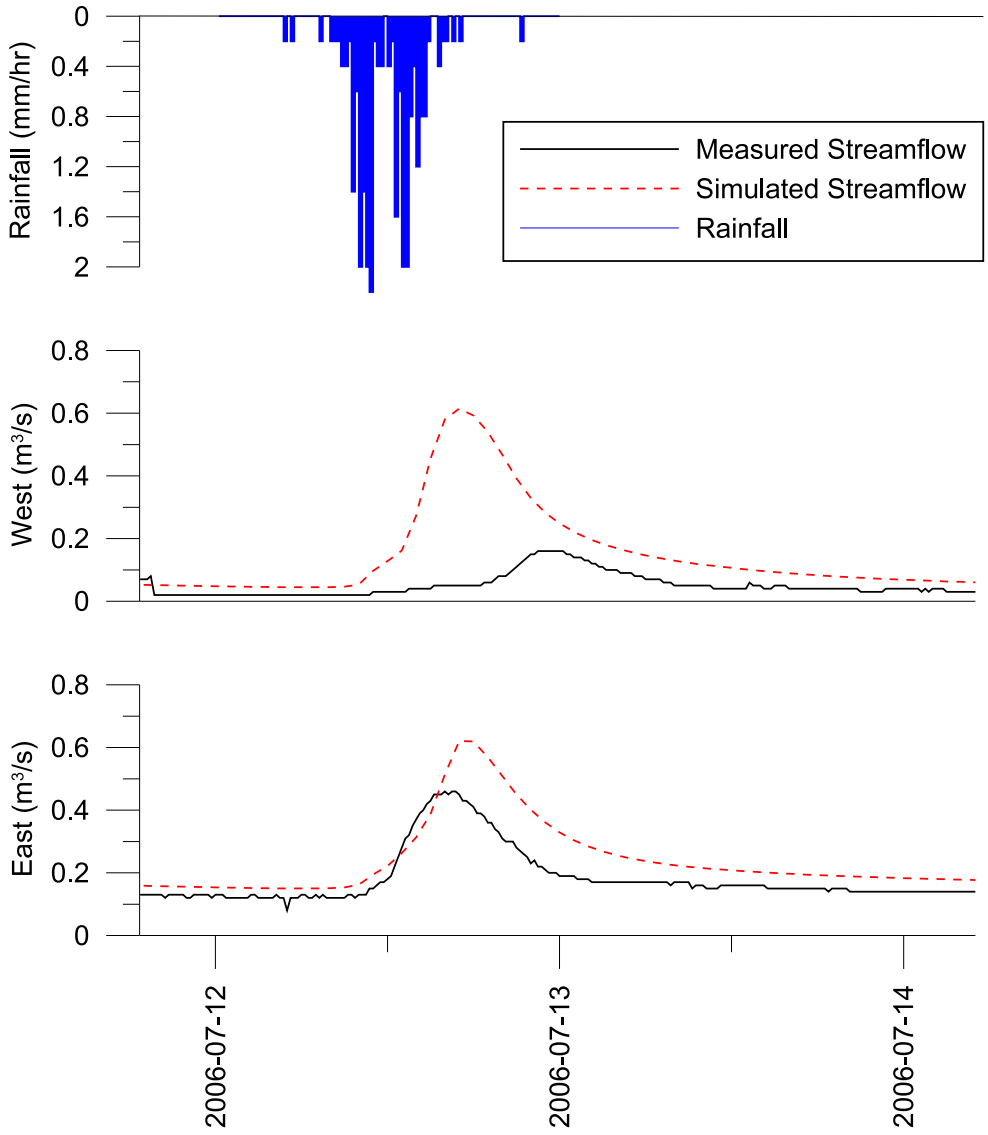

Figure 5.7: Hydrograph timing for dry antecedent condition event - Event 10

West sub-basins were compared as previously described for the Floradale station in Figure 5.4. To re-iterate, it is important to capture the flow volumes and the peak flows to ensure that the water quality modelling that is built upon the hydrological modelling is as accurate as possible. Figures 5.8 and 5.9 graphically illustrate the ability of the calibrated model to predict runoff volumes and peak flows for 28 rainfall events for the East and West sub-basins respectively. The event volumes and peak flows were extracted from a continuous model run over the entire simulation period (2000 to 2008). When compared with the 1:1 line the east sub-basin was modelled very well with good prediction of stream flow volumes at all event sizes and provided an unbiased prediction of peak flows. In contrast, the west sub-basin predictions of both peak flows and volume was less accurate, with the model over-predicting both peak volumes and peak flows. Of particular interest is the tendency for the model to substantially overestimate the peak flows for the smaller observed events. This observation agrees with the observations in the field and the hydrograph timing and volume issues observed in Figures 5.6 and 5.6 and points to what is perhaps a deficiency in the WatFlood routing model for dry headwater streams.

5.5 Hydrological Analysis for Water Quality

The calibrated WatFlood model showed a good ability to model the hydrological response of the two sub-basins, with the exception of the West sub-basin during dry antecedent conditions. It is of interest to examine the model's hydrological state variables with regard to their potential impacts on water quality modelling. Of particular interest is the degree of water storage in the riparian zones as indicated by the model, and the portion of runoff that was sourced from direct runoff, interflow and groundwater flow during events.

5.5.1 Wetland Storage

The modelling results showed a predictable annual wetland water storage pattern with maximum specific storage during the snowmelt period and early spring and with lower values during an extremely dry period in July and August. A representative plot of the 2002 year is shown in Figure 5.10. The west basin is not shown in Figure 5.10 because no

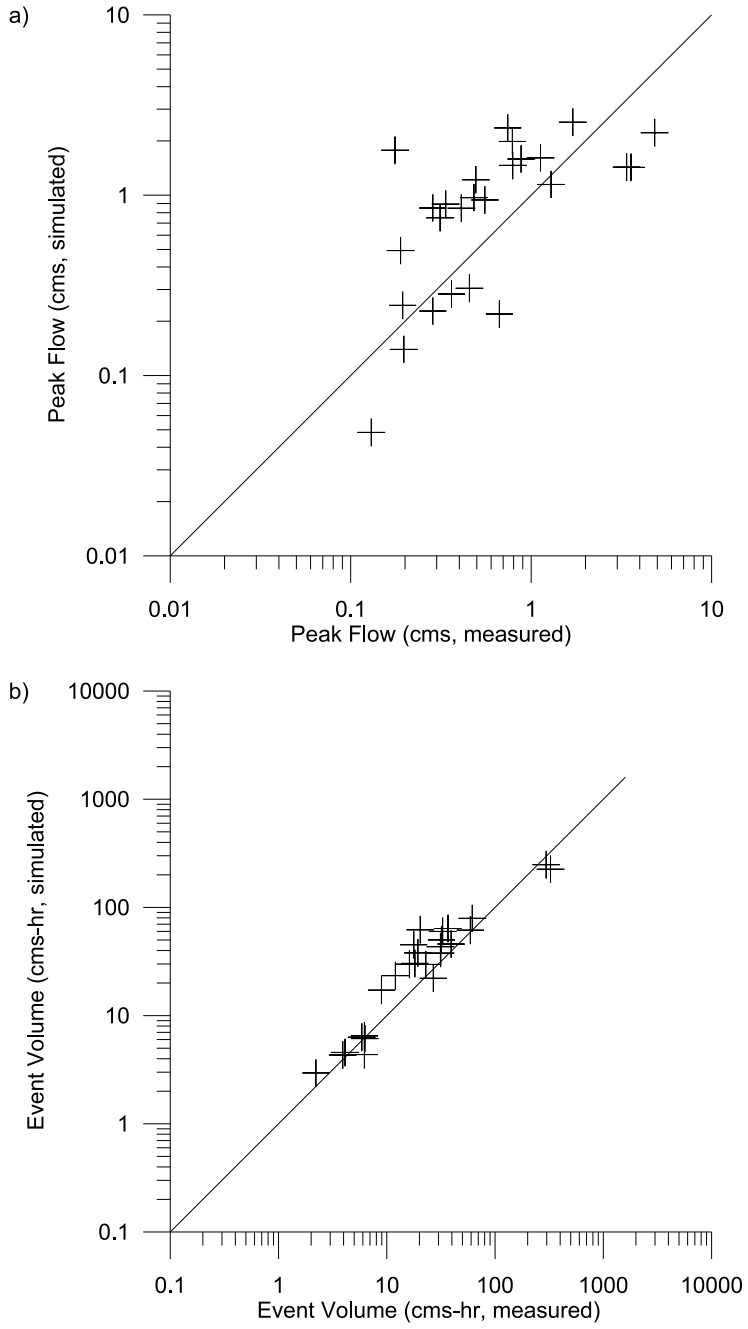

Figure 5.8: Event Peak Flow (a) and Runoff Volume (b) Comparison - East Sub-Basin

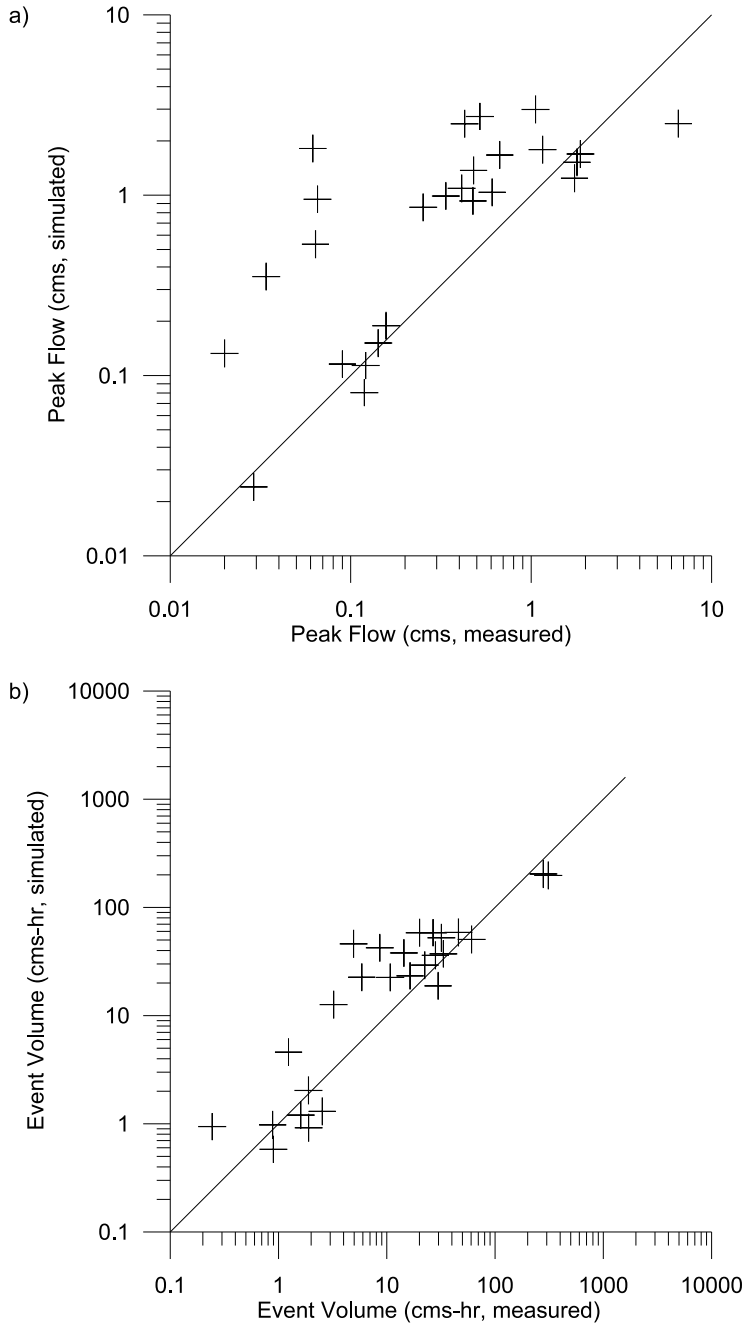

Figure 5.9: Event Peak Flow (a) and Runoff Volume (b) Comparison - West Sub-Basin

riparian zones exist for this sub-basin. This is of interest as the events with wet antecedent conditions showed less overall water quality improvements than the events with drier antecedent conditions in Chapter 6. The water quality modelling implications are that the wetlands will have more capacity to retain storm water during the extremely dry summer months than the wetter spring and fall months.

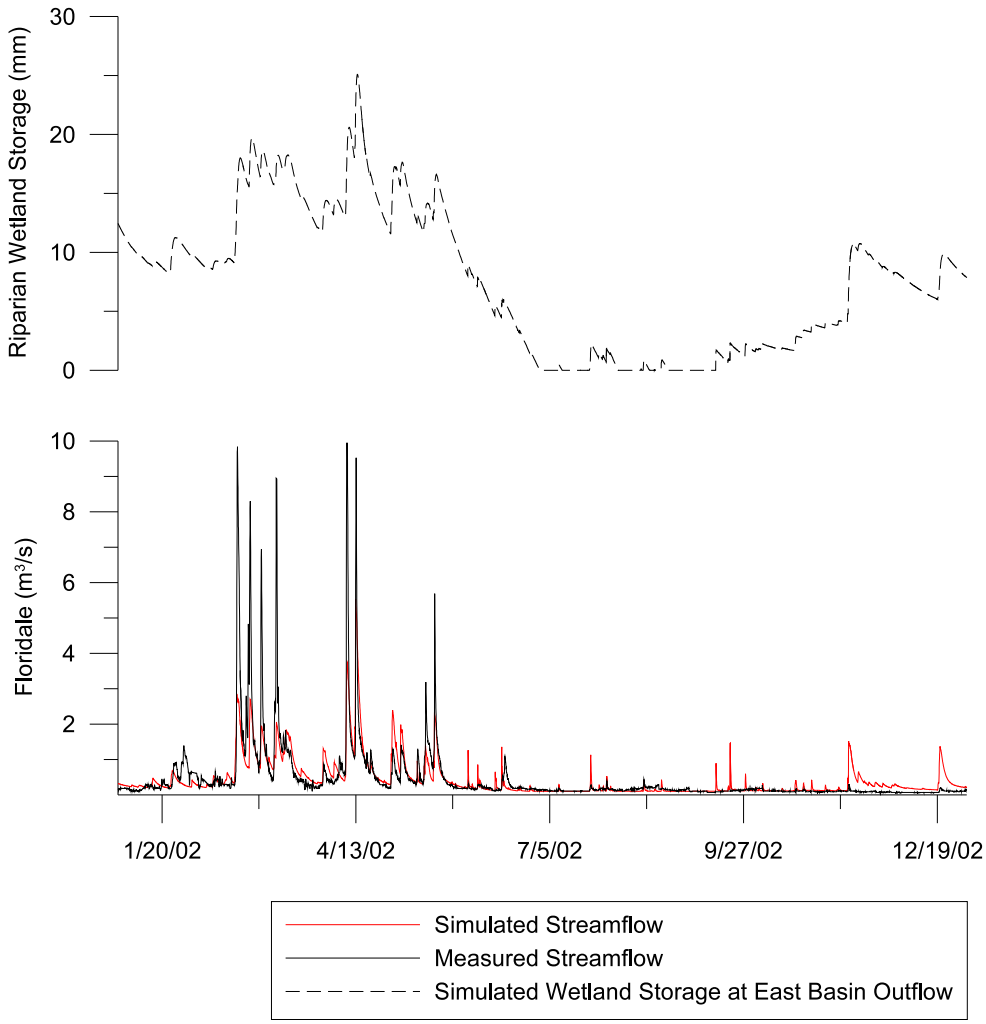

Figure 5.10: Wetland Storage Pattern - 2002

5.6 Discussion

The WatFlood hydrological model provides a reasonable hydrological simulation of the two study sub-basins and the larger upper Canagagiguge Creek basin to the GRCA Floradale gauge station. It is evident that the ephemeral nature of many of the contributing streams to the watershed reduces the effectiveness of the model during events that are preceded with dry in-stream conditions. The excellent performance of the East sub-basin, with most of the channels flowing constantly, is contrasted against the moderate performance for the West sub-basin and the entire upper Canagagigue to the Floradale gauge station.

The nature of the ephemeral creek routing problem is important for WatFlood as a hydrological model and for water quality modelling using the WatFlood framework. The contributing areas that have ephemeral streams in the Canagagigue Creek are not insignificant – the West sub-basin alone has a drainage area 12 km^2 representing 10% of the Canagagigue Creek drainage area and is almost entirely ephemeral. Additionally, many of these low-relief upstream drainage areas within the Canagagigue Creek are visibly ephemeral. This discovery provides interesting insight into issues relating to transport timing that are often considered scale issues with distributed models (Vieux, 2001). In fact, the issue of scale in this case is less relevant than the identification of physical processes that dominated flow routing that is not adequately considered in the model.

Further study into in-stream storage with detailed surveys or in-stream topographic data collection with modern 3D scanning equipment provide a data set that would allow for a modification of the routing model to accommodate ephemeral storage. When combined with the hydraulic and hydrological data collected in this study, a modification of the routing model to accommodate ephemeral storage could be properly justified. The modification of the WatFlood routing model is however out of the scope of this study. In lieu of a routing model that accounts for ephemeral storage within the model, further water quality modelling was largely restricted to events that were well-modelled hydrologically. Additionally, it is recommended that further research be conducted into employing rating curves in the WatFlood model when available as described by Vieux (2001) rather than using an assumed standard rectangular channel with a flood plain based on the up-stream

drainage area. It is clear that the channel geometry plays a critical role in the hydrology of this study area, and other similar basins in the region.

Chapter 6

Water Quality Sampling Methods and Results

6.1 Introduction

One of the objectives of this research project as identified in Chapter 1 was to determine if there are any measurable water quality differences between basins in the region that do not have riparian cover and those that have significant riparian protection on river corridor.

The region of Southern Ontario, Canada, has historically had a large quantity of wetland area due to the mild slopes and poor drainage of many of the regional soils. Within the Grand River watershed 60 - 85% of wetlands have been drained over time to facilitate agricultural activity and community development, however a number of wetlands in the region have remained unaltered in the riparian corridors of some streams and other low-lying areas. The Grand River Conservation Authority (GRCA) has attempted to actively preserve and protect wetlands in the region because of the water quality and ecological benefits of these systems (GRCA, 2003c). However, the water quality benefits of the riparian wetlands in the region have not been quantified. Many benefits of riparian wetlands in the region are not disputed, namely the benefits they offer as wildlife corridors, peak flow attenuation, and shelter for aquatic fauna, however these points are not addressed in this thesis.

Some ongoing surface water quality studies in the region have been conducted by the GRCA and the Ontario Ministry of the Environment (MOE) involving the regular collection of water samples for the analysis of water quality constituents (Cooke, 2006). These water quality analyses have been conducted on an infrequent basis with grab samples taken throughout the watershed approximately 8 times per year primarily during baseflow conditions. Although invaluable in determining background water quality conditions in the watershed this dataset was not likely representative of the water quality conditions in the watershed during runoff events. Richards (2002) identified that 80-90% of contaminants can be delivered during high-flow events that occur only 10% of the time and that characterization of loading during events is required for a full assessment of pollution loading from a drainage basin. In temperate climates like those in Southern Ontario, snow melt events are generally the most significant runoff events in a year and sediment and nutrient transport can be expected to be greatest during those times.

Modelling studies that have considered the effects of riparian wetlands have been conducted to predict water quality, nutrient and sediment loads in the Canagagigue Creek within the Grand River watershed in Southern Ontario. A recent study by Liu et al. (2008) predicted a 19% reduction in sediment loading in the riparian protected zone considering the presence of riparian zones in the watershed and employed the GRCA and MOE study data as a validating dataset. However, without event-based data these reported benefits during runoff events remain unvalidated.

The purpose of this study was to obtain high-frequency data over a range of hydrological conditions from two sub-watersheds with similar land use, soil and topographic characteristics but very different riparian wetland protection along the main stream corridor. Water quality parameters were collected primarily on an event basis to elucidate the degree of protection the riparian cover provides during the times when contaminant and nutrient transport is most active. The data set was collected in the same region as the modelling study conducted by Liu et al. (2008) and will provide future validation into water quality and wetland modelling efforts in the region.

6.2 Sample Collection

Water quality samples were collected during two separate programs in this study: an investigative program and an intensive sampling program. The investigative sampling phase was conducted first during the second half of 2004, and involved grab sampling at various locations in the north end of the Canagagigue Creek watershed upstream of the Woolwich Dam. The intensive sampling program followed from the investigative sampling program and involved more high-frequency water quality sampling at the outlet of the two selected study sub-watersheds for a two-year study period. For these two sampling phases water quality samples were collected during both runoff events and base-flow conditions. Samples were analyzed for total suspended solids (TSS), total nitrogen (TN), total phosphorus (TP), cations and anions including nitrate (NO_3^-). Other water quality constituents were analyzed including pH, turbidity, dissolved oxygen, temperature, cations and anions.

Water quality samples were collected during events using two float-triggered auto-samplers. During base-flow periods a grab sample was collected approximately monthly as per the sampling guidelines outlined by Richards (2002). Sampling locations were selected so as not to be influenced by flow confluences, back eddies, or unstable sections (USGS, 2005b). All samples were collected using 1-L polyethylene bottles. Samples bottles were prepared as per the inorganic constituent procedure outlined by USGS (2005a).

Grab samples were collected using the single vertical at the centroid of flow (SVC) method (USGS, 2005b). The centroids of the flow were determined from velocity profiles that were obtained from in-situ velocity measurements (see Section A.6). An average representative centroid was selected based on preliminary flow measurements over a number of high- and low-flow regimes.

Automatically collected samples were obtained using two Sigma 900 Standard Portable Auto-samplers that were equipped with a 24 1-litre bottle, suction-lift pump and a fixed-depth sample intake. Samples were collected in the 1-litre polyethylene sample bottles with a single intake rinse before pumping each sample. The auto-samplers were programmed with a variable interval sampling schedule to allow for more frequent sample collection during the rising limb of the stream hydrograph and more infrequent sample collection during the falling limb of the hydrograph. The auto-samplers were equipped with a float-

trigger to allow for the sampling program to be triggered by a water level rise. The intake was attached to a steel rod at the average centroid of flow for the cross section. The samples were kept cool within the auto-samplers with ice until collection twice a day during rainfall events.

6.3 Analytical Methods

Samples were transported directly to the University of Waterloo lab in iced coolers. Once transported to the University of Waterloo Environmental Lab the samples were stored in a refrigerator at 4°C until analysis was conducted. After samples were split and analyzed for nitrate the remaining samples were dosed with 2 mL of concentrated H_2SO_4 per 1-L sample, to bring their pH to below 2 for TN, TSS and TP analysis.

6.3.1 Turbidity, Electrical Conductivity and pH

Turbidity, Electrical Conductivity (EC) and pH were analyzed in the University of Waterloo Environmental Laboratory. The turbidity was determined using a HACH® Portable Turbidimeter Model 2100P. The Turbidimeter was calibrated periodically using HACH® Formazin at < 0.1, 20, 80, 100 and 800 NTU standard concentrations. Calibration was performed approximately every 3 months or when the instrument itself indicated a faulty calibration curve.

Electrical Conductivity was determined using a HACH® CO150 Portable Conductivity Meter and was used both in the field and in the laboratory, depending on the availability of the probe. The readings were taken in μS corrected for temperature using the automatic temperature correction (ATC) mode. The probe was calibrated using the Cell Constant Adjustment Calibration Method (HACH, 2000), which determined the conductivity correction coefficient with a NaCl standard.

pH was measured using an Orion® Benchtop pH/ISE meter, model 710A. The probe was periodically calibrated using a 2-point calibration technique using pH 7.00 and 10.01 standards.

6.3.2 Total Phosphorus

Total Phosphorus (TP) was analysed using a HACH® Odyssey DR/2500 manual spectrophotometer. 5mL samples were digested with a persulphate digestion method at 150°C for 30 minutes with an addition of H_2SO_4. Samples were then neutralized with NaOH and reacted with molybdate and ascorbic acid powder (HACH PhosPher3 Reagent)to provide a blue color the absorbance wavelength set to 880 nm. The QA standards employed were a 1.0 mg/L $PO_4^{3-}$to validate the spectrophotometer's built-in rating curve which were a a dilution of a purchased HACH® 50 mg/L standard (HACH Method 8190) (HACH, 2000).

The method detection limit (MDL) for the total phosphorus procedure was calculated using low concentration analytes in reagent water (Helsel and Hirsch, 1991). Quality assurance of the method was conducted by running a number of mid-range purchased standards to determine the degree of variability of the standards and plotting the degree of analyte recovery over time (APHA, 2005). The method detection limit for this method was 77 $\mu g/L$-P. Details for the MDL and QA are shown in appendix C.

6.3.3 Total Nitrogen

Total nitrogen (TN) was analysed to account for species other than nitrate/nitrite that would contribute to the overall nitrogen loading in the surface waters.

Total nitrogen was analyzed using a HACH Odyssey DR/2500 manual spectrophotometer. The HACH®Method 10071 Persulfate Digestion Method Test 'N' Tube™ was employed (HACH, 2000).

The MDL calculations for the Total Nitrogen method are shown in Appendix C. The degree of variability in repeat readings was very high with this method as illustrated in the very high MDL of approximately 1.3 mg-N/L. Consequently the TN readings were used as a check of other methods but was not considered as a reliable means of detailed quantification.

6.3.4 Nitrate (Colourmetric)

During the investigative sampling program, nitrate was analyzed using a colourmetric cadmium reduction method providing a measurement of combined nitrate/nitrite. The method followed was provided by HACH Method 8039 (HACH, 2000). This method was found to have large confidence limits (low precision) and to be technique sensitive as described in the method description. Nitrate measurement using this method was discontinued once the intensive sampling program began and access to the ion chromatograph was procured (see Section 6.3.5).

6.3.5 Anions and Cations

Anions and Cations were analysed using a Dionex Ion Chromatograph (IC). The anions that were analyzed included chloride (Cl^-), nitrite (NO_2^-), nitrate (NO_3^-), sulphate (SO_4^{2-}) and phosphate (PO_4^{3-}). Cations that were analyzed included sodium (Na^+), potassium (K^+), magnesium (Mg^{2+}), calcium (Ca^{2+}) and ammonium (NH_4^+).

The Dionex PeakNet® 5.1 Chromatography Workstation software was employed to extract the peak areas and peak heights from the conductivity and the UV emission time-series data. Calibration curves were generated with a seven point calibration curve made from UW Environmental Laboratory stock standard solutions. A purchased standard for nitrate at 10 mg/L as N was employed to ensure accurate concentrations for this particularly important anion and was included in every anion run.

Each sample was analysed twice. Samples with a coefficient of variation greater than 2.0% were flagged and analysed again if available.

Ion Chromatagroph Method - Anions

The Anion Method employed a Dionex 4mm IonPac® AS4A-SC column with a IonPac® AG4A-SC pre-column and either direct conductivity or UV detection with peak area quantitation. (Method 4110.C APHA (2005)).

The IC eluent for anion analysis consisted of a sodium carbonate / sodium bicarbonate solution (1.8 mM Na_2CO_3, 1.7 mM $NaHCO_3$) pumped at a rate of 2 mL per minute through

the column. The sample volume injected was 50 μLȦn acid regenerate of dilute H_2SO_4 to rinse the column after each injection. Anion samples were run through the column for 10 minutes. Two detectors were used for the anion IC runs including a CDM-II Conductivity detector for all anions, and a VDM-II UV Wavelength Detector for nitrate and nitrate ions.

The MDL values for chloride, nitrate and sulphate using the Conductivity detector were 56 $\mu g/L$, 63 $\mu g/L$-N and 57 $\mu g/L$ respectively. The MDL for Nitrate using the UV Wavelength detector was 61 $\mu g/L$-N. MDL calculations and QA for nitrate are shown in Appendix C. The MDL concentrations were slightly higher than those proposed in APHA (2005), although the differences could be attributed to variations in the methods and sample sizes.

Ion Chromatagroph Method - Cations

The cation method included a Dionex 4mm IonPac® CS16 column with an IonPac® CS16 pre-column. The IC eluent employed was 50 mM methanosulfonic acid (MSA) diluted with ultra-high purity (UHP) water. The dilution rate was varied to generate reasonable peak isolation with the CS16 column but was typically fixed to 50% MSA and 50% UHP.

The MDL values for Sodium, Potassium, Magnesium and Chloride using the Conductivity detector were 68 $\mu g/L$, 58 $\mu g/L$, 52 $\mu g/L$ and 112 $\mu g/L$ respectively. MDL calculations are shown in Appendix C.

Suspended Solids

Samples were analyzed for total suspended solids and fixed suspended solids based on Methods 2540 D and 2540 E from APHA (2005). The filters were pre-rinsed with UHP water and dried at 550°C before use. Typically 400 mL of agitated sample was filtered. However, in some circumstances less sample was used due to high solids content or because of a small amount of the sample collected.

Filters were weighed prior to filtering and after filtering and drying at 105°C for 1 hour to determine the total suspended solids (TSS). The filters were then placed into a muffle

furnace at 550 °C to remove the volatile solids for 1 hour and weighed again to determine the fixed suspended solids (FSS).

It was determined through analysis that turbidity was highly correlated with TSS and that if a turbidity reading of less than 10 NTU was detected then there would be generally no discernable TSS measurement in a 400 mL sample. That is, the required amount of 2.5 mg of suspended solids as specified by Method 2540 D could not be obtained from a 400 mL sample. In these cases the TSS analyses were not performed.

6.4 Sampling Programs

As discussed above, two phases in water quality sampling were conducted in this study: an investigative sampling program and an intensive sampling program. The investigative program involved the acquisition of a number of grab samples in the northern headwaters of the Canagagigue Creek during different seasons and flow conditions. The purpose of the investigative sampling program was to determine if there were water quality differences in the region due to the presence or absence of the riparian zones in the watershed. The investigative sampling was conducted during the summer and fall of 2004 (June to November).

After the investigative study period a more intensive sampling program was implemented, with the determination of the study sub-watershed, the set-up of the hydrometric instrumentation and the employment of the auto-samplers for event-based water quality sampling.

6.5 Investigative Sampling Program

The selected study site was identified as an area for potential research early in 2004. As identified in Section 3, the northern headwater of the Canagagigue Creek shows regions of relatively high wetland, and riparian wetland content. Initially the water quality parameters were estimated in the area based on grab-samples in the waters around the study during storm events to determine estimates of water quality parameters and to determine

if further, more detailed investigations were justified. This first sampling period was from March to October 2004 and was an investigative sampling period in the area around the study site. The goal was to gain some insight into the nature of the water quality in the surface waters, and to see if there was any measurable difference in receiving waters that had wetland cover and those that did not.

A number of designated sampling locations were employed in this study. Figure 6.1 shows a map of the study area and location of each of the sampling points. During the preliminary analysis phase of the study water quality grab samples were taken near bridge crossings, and may not be entirely representative of water quality in the stream.

The water quality samples were collected as grab-samples for the period of the investigative sampling and were analyzed for Total Phosphorus, Total Nitrogen and Nitrate employing the methods described above. Field trips to the Canagagigue Creek were conducted on a number of days. Times were targeted during runoff producing rainfall events, but other baseline measurements were taken as well. The autumn from September to November 2004 was a rather dry one with very few significant events. Sampling dates are presented in Table 6.1.

The data from the investigative sampling was analyzed to attempt to elucidate the differences due to riparian cover in the North Canagagigue Creek. The sampling locations were classified based on the degree of riparian content. Low riparian meant a much larger contribution of riparian cover than no riparian cover at the location or upstream of the location. High riparian meant almost complete riparian cover at the location and upstream

Sampling Date	**Daily Precipitation**
15-Jul-2004	5.6
03-Sep-2004	0.0
07-Sep-2004	4.8
09-Sep-2004	21.8
15-Oct-2004	10.0
02-Nov-2004	14.5
04-Nov-2004	23.2

Table 6.1: Investigative Sampling Program - Sampling Dates

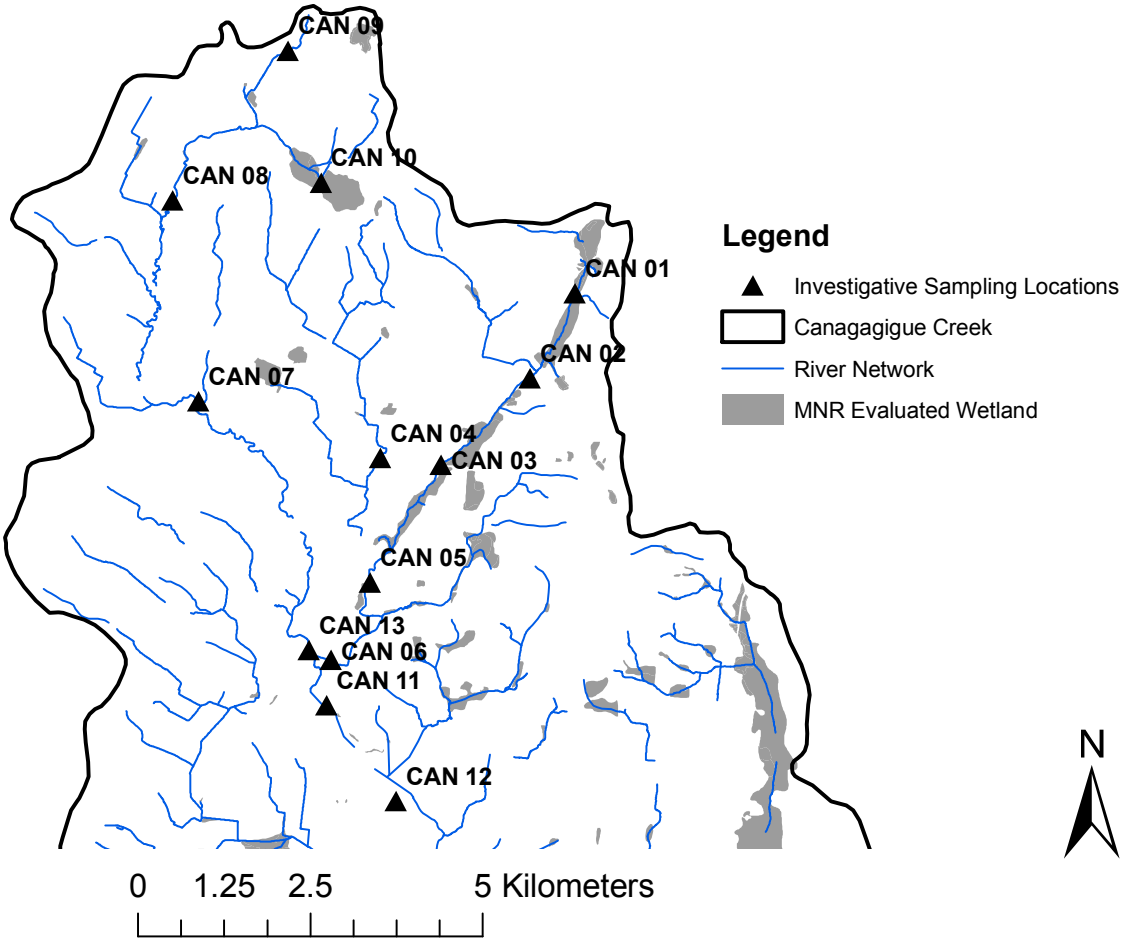

Figure 6.1: Investigative Sampling Program - Water Quality Sampling Locations

of the location. Although this is a subjective measure by which they are classified, it is believed to be a valid one. The resulting categorization partitioned the sampling locations as shown in Table 6.2. Essentially, the three sampling locations found in the high riparian sub-basin ("East" Basin) were classed as high riparian and all remaining sampling sites were classified as low riparian.

The samples were analyzed using the TP and TN methods described above in Sections 6.3.2 and 6.3.3 respectively. The nitrate concentrations for the investigative sampling were determined using the colourmetric method described in Section 6.3.4. There were several issues with the laboratory analysis in that the colourmetric nitrate technique often produced low recovery rates against standard solutions (60 - 80% were observed). This method was abandoned after the investigative sampling period for the ion chromatographic approach, which produced higher recovery with standard solutions.

The sampling results for TN, TP and nitrate are shown in the box and whisker plot in Figure 6.2. This figures shows that the maximum measured concentrations are higher for all three measured constituents in the low riparian protected receiving waters than the high riparian receiving waters, although statistically the riparian and non-riparian groups are not distinct when compared using a signed-rank or Mann-Whitney Non-parametric statistical test (Helsel and Hirsch, 1991). The statistical results are shown in Table 6.3 and show that none of the riparian and non-riparian concentration populations are distinct for each constituent even at the 10% confidence level. However, the total phosphorus data show the greatest statistical difference between the riparian and non-riparian data.

Riparian Class	**Site Number**
High Riparian	CAN-01, CAN-02, CAN-03
Low Riparian	CAN-04, CAN-05, CAN-06, CAN-07, CAN-08, CAN-09, CAN-13

Table 6.2: Investigative Sampling Program - Sampling Location Grouping

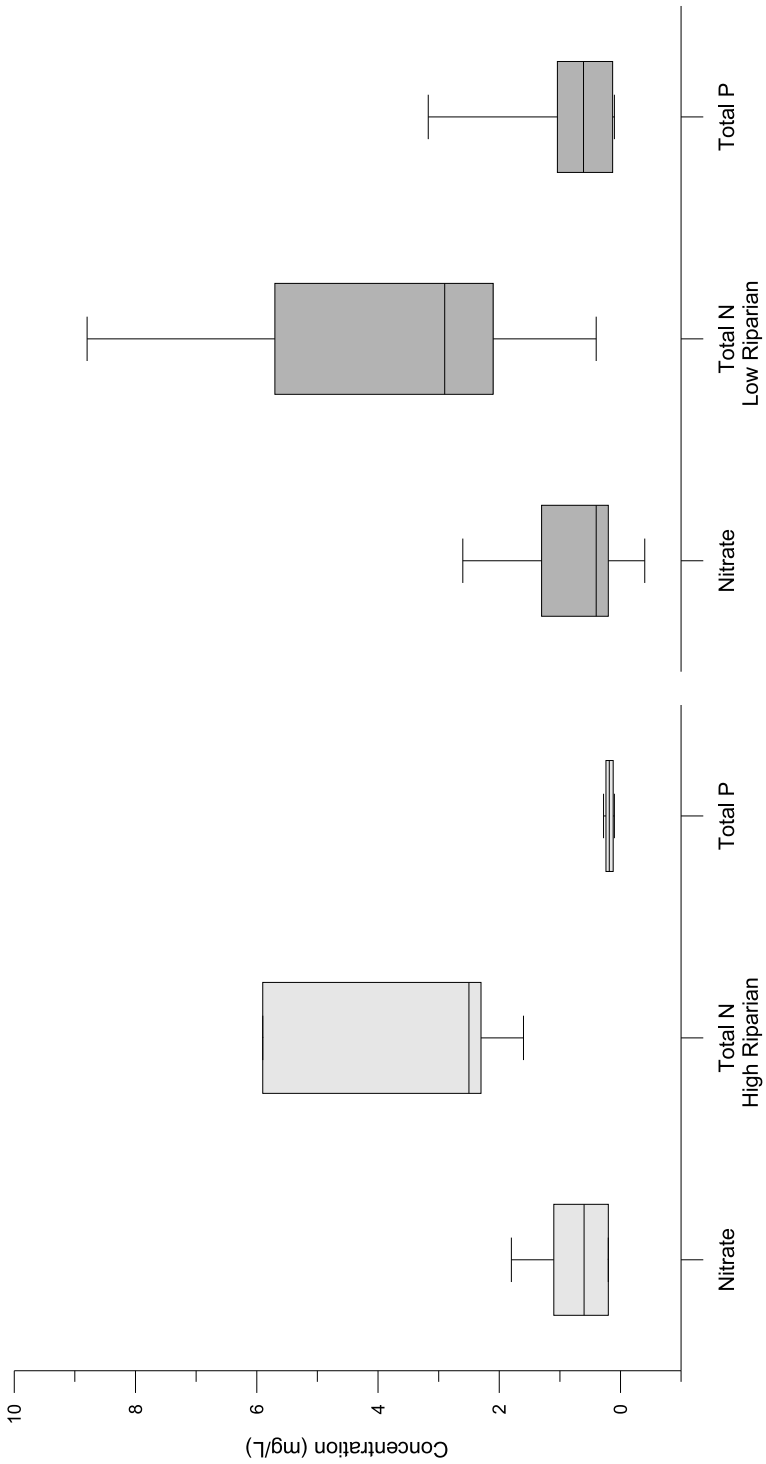

Figure 6.2: Investigative Sampling Program - Concentration Box Plot by Riparian Protection

Constituent	Mann-Whitney Statistic (p)
NO_3^-	0.836
TN	0.656
TP	0.118

Table 6.3: Investigative Sampling Program - Population Mann-Whitney Test Statistics

6.6 Intensive Sampling Program

The second sampling period involved more intensive water quality sampling in two delineated sub-watersheds Section 3. The intensive sampling program spanned from May of 2005 until after the snow melt in March of 2007. After the investigative sampling it was determined that grab sampling would be inadequate to describe the contaminant transport within the watershed and that high-frequency samples would be required during storm events to fully characterize the contaminant concentrations and fluxes leaving the sub-watersheds via the surface water. The subsequent sections in this chapter outline the findings from the intensive water quality sampling program.

The map shown in Figure 6.3 shows the water quality sampling locations for the intensive sampling period. The sampling period was for approximately 2 years from May 2005 to March 2007. The sampling was begun shortly after the establishment of the flow measurement stations described in Chapter 4.

6.6.1 Storm Events

A total of 16 runoff events were captured during the 2 year study period, including two multi-day snowmelt events. The events are itemized with their sampling durations in Table 6.4.

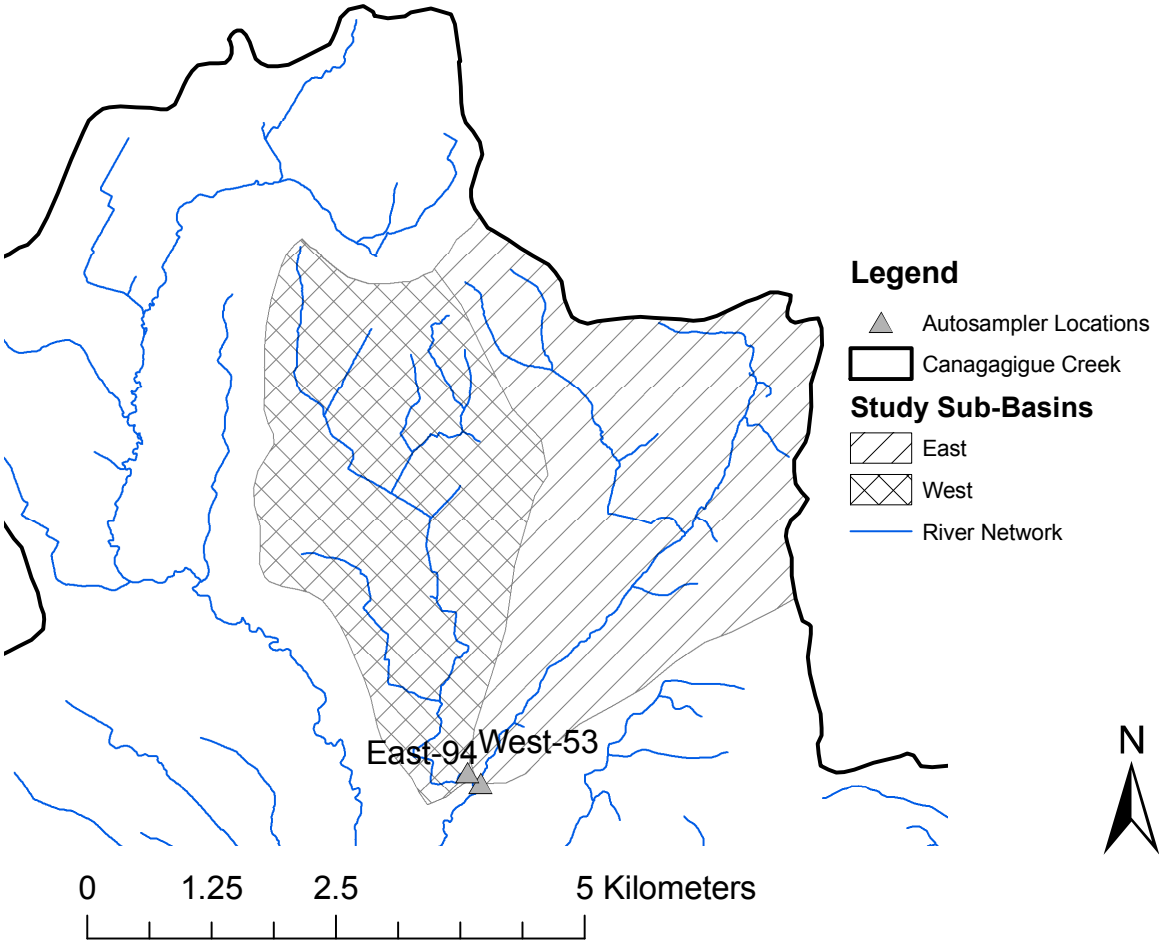

Figure 6.3: Intensive Sampling Program - Water Quality Sampling Locations

Event Code	**Description**	**Start Time (UMT)**	**End Time (UMT)**
EVT01	Event 2005-07-16	17-Jul-2005 03:00	18-Jul-2005 20:00
EVT02	Event 2005-08-19	19-Aug-2005 09:00	20-Aug-2005 22:00
EVT03	Event 2005-09-26	26-Sep-2005 09:00	27-Sep-2005 23:00
EVT04	Event 2005-11-15	29-Sep-2005 06:00	30-Sep-2005 02:00
EVT05	Event 2005-09-29	15-Nov-2005 22:00	17-Nov-2005 06:00
EVT06	Event 2006-Snowmelt	09-Mar-2006 15:00	14-Mar-2006 15:00
EVT07	Event 2006-04-07	07-Apr-2006 17:00	08-Apr-2006 23:30
EVT08	Event 2006-04-23	23-Apr-2006 13:00	27-Apr-2006 11:00
EVT09	Event 2006-05-31	31-May-2006 22:00	04-Jun-2006 08:00
EVT10	Event 2006-07-12	12-Jul-2006 00:00	13-Jul-2006 00:00
EVT11	Event 2006-07-26	27-Jul-2006 03:00	28-Jul-2006 12:00
EVT12	Event 2006-09-28	28-Sep-2006 03:00	30-Sep-2006 20:00
EVT13	Event 2006-10-04	04-Oct-2006 20:00	05-Oct-2006 04:00
EVT14	Event 2006-10-11	11-Oct-2006 17:00	13-Oct-2006 08:00
EVT15	Event 2006-10-28	28-Oct-2006 03:00	30-Oct-2006 23:00
EVT16	Event 2007-Snowmelt	22-Mar-2007 14:00	25-Mar-2007 23:30

Table 6.4: Captured Runoff Events - Sampling Periods

6.7 Intensive Sampling Program Results

6.7.1 Analyte Correlations

To account for missing data for some events some analyte correlations were investigated so that missing samples or analytes could be estimated. Other researchers have looked at similar processes in surface water quality studies (Vanni et al., 2001) and found strong correlations between particulate nutrients and suspended solids, as well as relationships between particulate and dissolved analytes of the same species.

Total nitrogen and nitrate concentrations were highly correlated during all seasons and for both sub-basins, nitrate representing 85% or more of the nitrogen loading on average. The relationships between TN and NO_3^- for all collected samples are presented in Figure 6.4a and Figure 6.4b for the East and West basins respectively. The plotted results show the strong, near 1:1, relationship between TN and NO_3^- with strong R^2 coefficients for the linear regression relationships. These relationships also clearly demonstrate that nitrate dominates the nitrogen loading in both sub-watersheds. This observation is consistent with other studies of nitrates in receiving waters in agricultural watersheds, particularly with tile drainage which can facilitate nitrate transport (Spaling, 1995; Vanni et al., 2001).

Although very similar, the TN and NO_3^- concentrations were of statistically distinct populations. An examination of the two paired sample populations using the non-parametric Signed-Rank (Wilcoxon) test (Helsel and Hirsch, 1991) showed the East and West basins exhibited TN and NO_3^- populations that were strongly distinct with the TN median statistically higher than the NO_3^- values for both basins ($p=0.005$ and $p=0.003$ for the East and West basins respectively). For the East basin samples the median difference was 0.68 mg/L-N and for the West basin samples the median difference was 1.5 mg/L-N.

Strong correlations were observed between measured turbidity values and total suspended solids concentrations. The turbidity measurements were much easier to acquire than the TSS values, and in some cases the TSS analysis was not performed, or too small a sample was collected by the auto-sampler. The strong relationship between the log-transformed values of measured TSS and turbidity are shown in Figures 6.5 showing the relationships for the East and West sub-basins respectively.

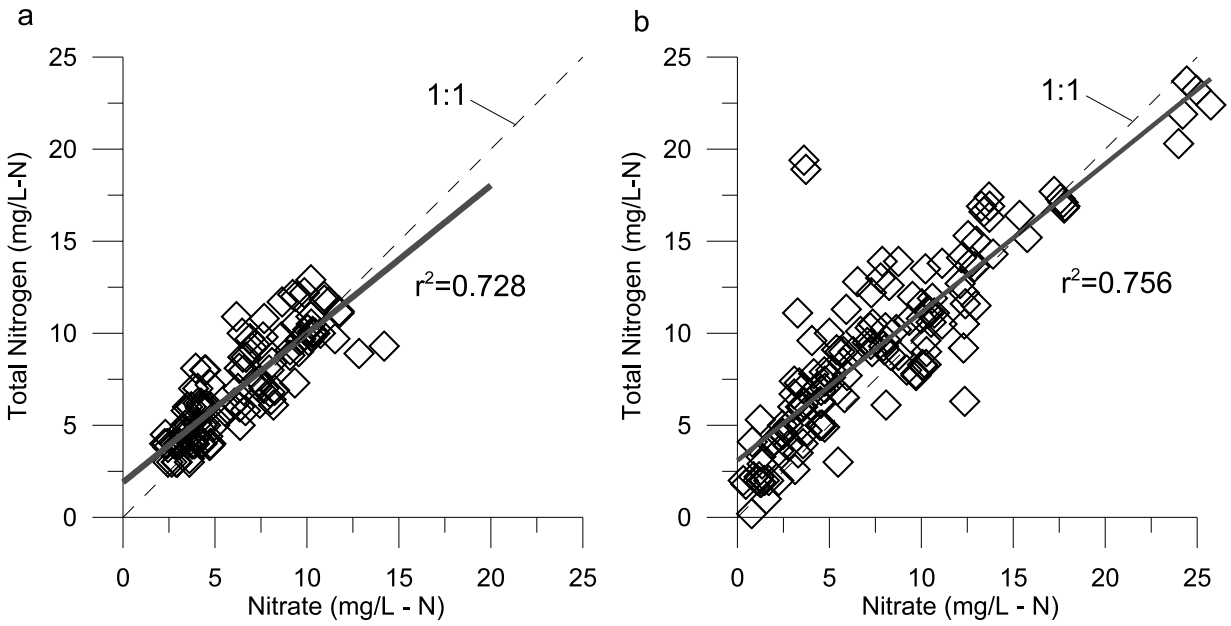

Figure 6.4: Nitrate - Total Nitrogen Regression relationships for the East (a) and West (b) Study Basins

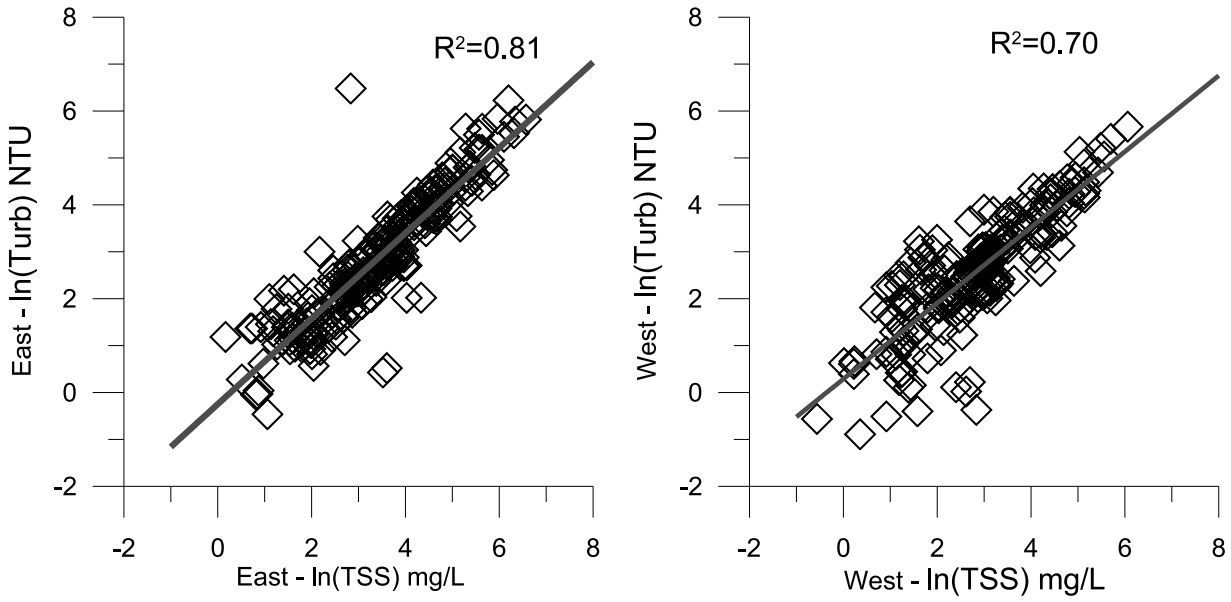

Figure 6.5: TSS - Turbidity Correlation

Relationships between total phosphorus and total suspended solids were suspected based on the observed water quality patterns during events. However, the relationship between TSS and TP was strong only in the east sub-basin. The west sub-basin showed no strong relationship between TP and the total suspended solids concentrations. Figure 6.6 shows this difference for the East and West sub-basins respectively. Here it can be seen that the west basin presented high total phosphorus concentrations even though the suspended solids concentrations were quite low. It is suspected that there was a greater degree of phosphorus loading that was not related to the solids transport coming from the ephemeral stream and the phosphorus could have other non-channel origins.

6.7.2 Data Interpolation and Flux Calculations

Nutrient and sediment fluxes over the study period were determined by first interpolating for missing data during the study period. Two interpolation techniques were employed in determining concentrations after Hill (1981) and Vanni et al. (2001): (1) a simple interpolation and (2) a flow-proportional rating curve. The flow-proportional rating curve was used preferentially as an interpolation technique, however, if the flow-proportional rating curve provided a linear regression coefficient of determination (R^2) value less than 0.5 the simple interpolation approach was employed (Hill, 1981; Macrae, 2003). However, for event-based loading estimates for sampled events the simple interpolation technique was employed over the flow-proportional technique due to the high sampling frequency during those events.

Hourly concentration data estimated using a simple interpolation technique was determined using equation (6.1):

$$C_h = C_{prev} + (C_{prev} - C_{after}) \frac{h - h_{prev}}{h_{after} - h_{prev}} \tag{6.1}$$

where C_h is the interpolated hourly concentration, h is the hour of the interpolated concentration, C_{prev} and C_{after} are the closest previously and subsequently measured concentrations respectively, and h_{prev} and h_{after} are times of the previously and subsequently measured concentrations.

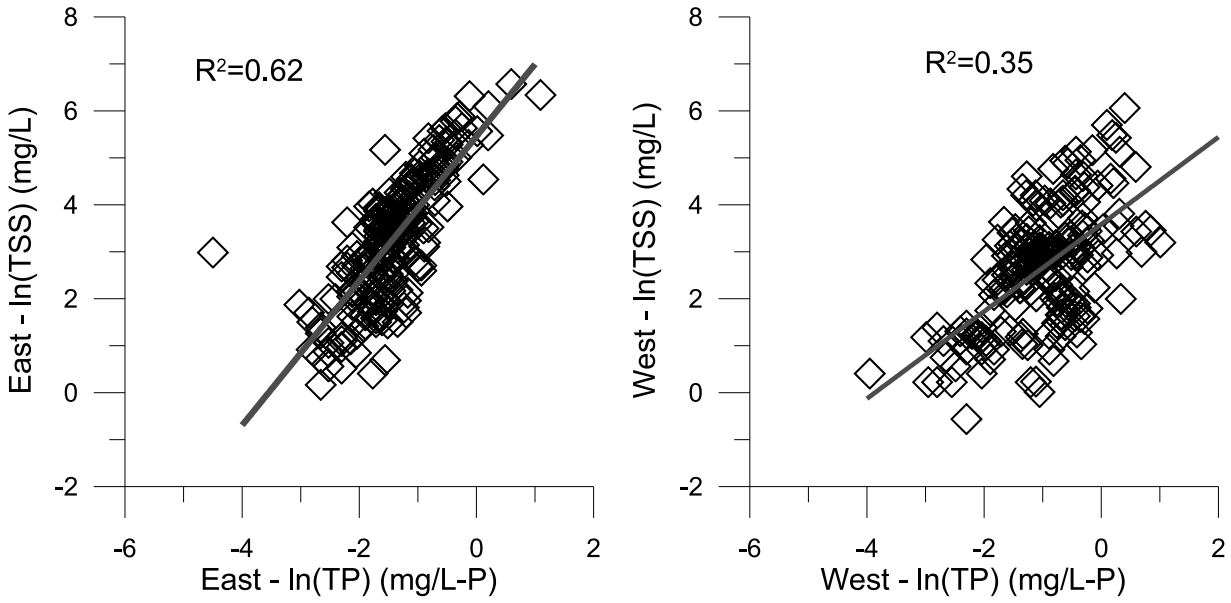

Figure 6.6: TSS - TP Correlation

Hourly concentration data estimated using a flow-proportional rating curve were determined using the log-transformation regression analysis technique described by Cohn et al. (1992). The regression models were fit to the data in equation (6.2):

$$\ln C_{RC} = \beta_1 \ln Q_h + \beta_2 \tag{6.2}$$

where C_{RC} is the predicted concentration at the interpolated hour and Q_h is the measured stream flow in at the interpolated hour. β_1 and β_2 are linear regression coefficients. Back-transformations from the logarithmic regression curve to a predicted concentration can be subject to bias (Cohn et al., 1992; Richards, 2002). The calculated logarithmic values of the nutrient or sediment concentrations to standard concentrations were determined using the quasi-maximum likelihood estimate (QMLE) as described by Ferguson (1986) to correct for biases associated with the logarithmic transformation. The QMLE bias-correction is presented in equation (6.3).

$$C_h = e^{\ln C_{RC} + \frac{\sigma^2}{2}} \tag{6.3}$$

where C_h is the bias-corrected interpolated concentration and σ^2 is the variance of the residual errors of the regression model.

Hourly nutrient and sediment fluxes were estimated by multiplying the interpolated concentration by the measured flow rate at the sub-watershed outlets. Daily and monthly fluxes were estimated by summing the hourly fluxes over the prescribed period. The estimation of daily average concentrations was done by dividing daily fluxes by the mean daily stream flow.

6.7.3 Water Quality Patterns

Water quality data was collected for 16 of the 26 observed events during the study period including two snow melt events and samples were also collected monthly during base-flow conditions.

Nutrient concentrations did not correlate well with flow with $\ln C - \ln Q$ relationships for TN, NO_3^- and TP having R^2 values less than 0.5. However, the total suspended solids data had a stronger relationship with flow rate. The sediment-stream flow data showed distinct differences between the "summer" (June-November) and "winter" (December-May) months. A single $\ln Q - \ln TSS$ relationship for the entire season tended to overestimate the loading during the winter snowmelt for each of the sub-basins. Consequently, to determine suspended sediment loading estimates between measured events two regression models were employed per site: one to predict the winter sediment loads and a second to describe the summer sediment loads. The parameters and regression performance for the sediment rating curves are shown in Table 6.5 for stream flows in m^3/s and TSS concentrations in mg/l. The summer rating curve for the West sub-basin did not have an adequate R^2 value and as such a simple interpolation scheme was used for that period for the West sub-basin. The TN, NO_3^- and TP hourly concentrations were determined using the simple interpolation technique.

Measured nutrient concentrations and daily averaged nutrient concentrations tended to be higher in the West sub-basin than the East sub-basin during the study period. The measured and daily averaged TSS concentrations, however, were higher in the East sub-basin than the West. The cumulative frequency distributions of daily flow-averaged

	East Sub-Basin		West Sub-Basin	
	Summer	**Winter**	**Summer**	**Winter**
β_1	1.60	1.27	0.38	1.12
β_2	6.07	3.74	3.69	3.87
R^2	0.56	0.72	0.15	0.61

Table 6.5: TSS Regression Model Parameters

concentrations for the two-year study period are presented in Figure 6.7 for NO_3^- (a), TN (b), TP (c) and TSS (d). The nitrate and TN frequency distributions show very similar patterns with approximately 75% of daily flow-averaged concentrations higher in the West basin than the East sub-basin, and with maximum daily concentrations much higher in the West sub-basin. Total phosphorus and total suspended solids concentrations are presented in Figure 6.7 with a logarithmic concentration scale due to the wide range of measured concentrations. Figure 6.7c shows that the TP concentration distribution was consistently higher in the West sub-basin than the East. Conversely, the TSS concentration distribution was consistently higher in the East than the West. This implies different TP sourcing mechanisms for the two sub-basins. In the East sub-basin the sediment mass (TSS) largely explains the TP loading, but in the West sub-basin high TP concentrations are observed even without high TSS concentrations, suggesting higher concentrations of phosphorus on the sediment delivered by the West sub-basin or higher concentrations of soluble phosphorus.

Maximum measured nitrate concentrations were observed in the West sub-basin as approximately 26 mg/L-N recorded during low-flow conditions in the fall of 2005. The average nitrate concentration in the West basin was 7.7 mg/L-N. In the East sub-basin the maximum nitrate concentration was 17 mg/L-N during the 2006 snow melt event, the average nitrate concentration was 6.0 mg/L-N and the average concentration measured during base flow conditions was 1.3 mg/L-N. Nitrate concentrations did not correlate well with flow rate for either sub-basin and tended to reach a maximum concentration during the recession curve of the stream flow hydrograph.

The nitrate concentrations showed a distinct pattern with the peak nitrate concentration occurring after the peak flow with the nitrate concentrations rising as the hydrograph

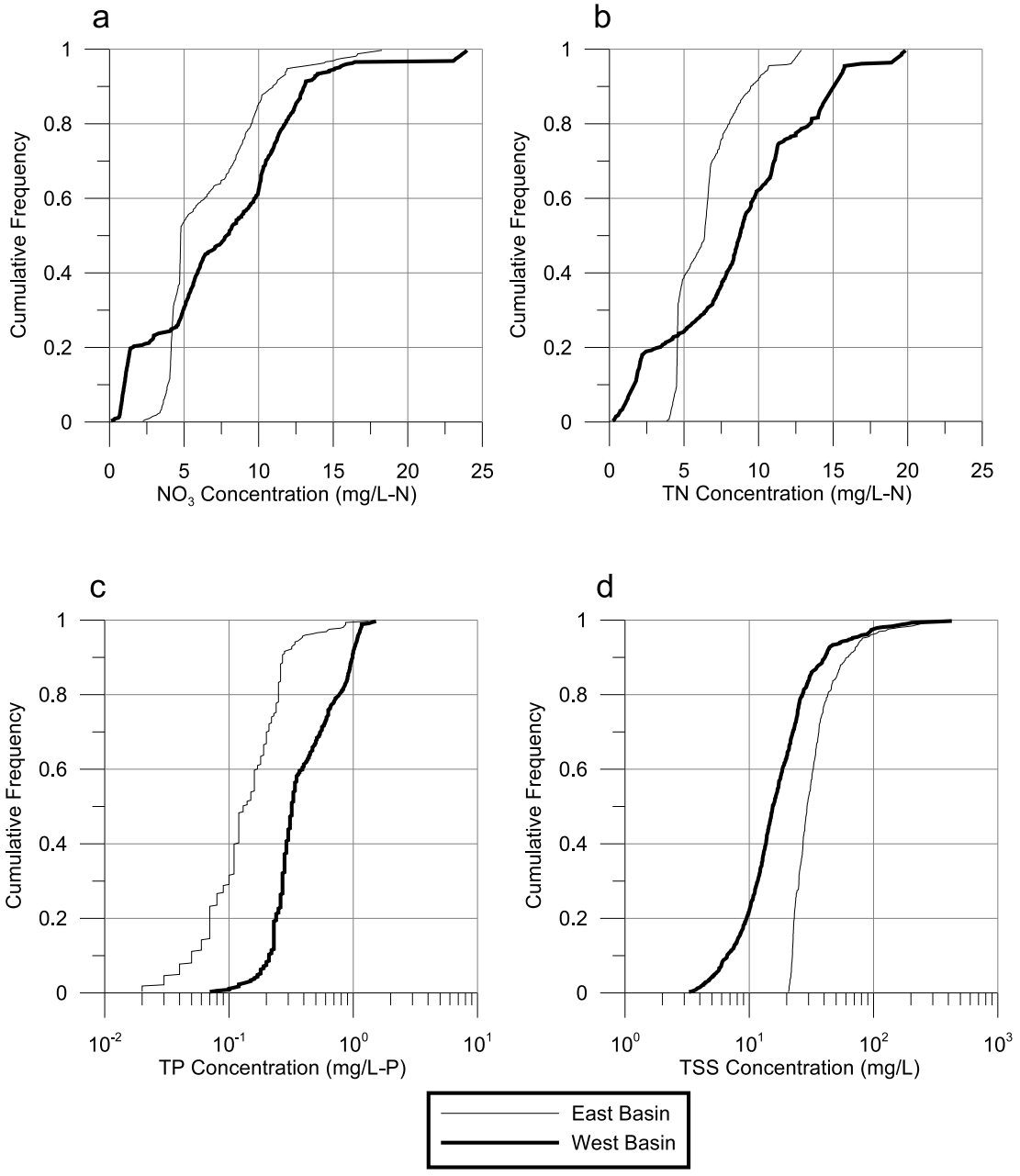

Figure 6.7: Probability fequency of daily average concentrations within the East and West Basins for NO_3^- (a), total nitrogen (b), total phosphorus (c) and total suspended solids (d)

fell. This pattern occurred at low and high flow conditions and in both study basins. The position of the high nitrate concentrations after the hydrograph inflection point indicates that the sourcing of nitrate nitrogen in these responses was from a more diffuse source of subsurface flow (see Figures 6.8 and 6.9). Vanni et al. (2001) showed very similar event-based nitrate patterns in agricultural watersheds, with the highest concentrations occurring during the receding portion of the hydrograph (near the recession inflection point) and attributed the greatest contributions to sub-surface or base-flow sources and similarly found that nitrate nitrogen accounted for the majority of the nitrate concentrations in the surface water samples collected. Similarly, Schilling and Helmers (2008) observed similar solute concentration patterns in a tile drained agricultural field and considered the high nitrate concentrations at the tail end of the events as a result of near-surface diffuse source groundwater.

Higher total suspended solids concentrations were measured in the East basin as compared to the West sub-basin. The maximum TSS concentration recorded in the East basin was 710 mg/L during the 2007 snow melt event and the maximum in the West basin was 430 mg/L during the 2006 snow melt event. The average base flow TSS concentrations measured in the East sub-basin was 11 mg/L. TSS showed similarities in concentration patterns with stream flow for both the East and West sub-basins. It is noted that the character of the sediments collected using the auto-sampler and manual sampling methods was noticeably different between the East and West sub-basins. The West sub-basin samples tended had a finer TSS, appearing to have higher clay-sized content than the East sub-basin samples. The difference between the samples was clearly visible, although no grain-size distribution measurements were conducted with the collected samples. The difference also was clearly identified when conducting the TSS analysis, as the West samples would take a much longer time to filter due to the presence of fines in the samples.

Figures 6.8 and 6.9 show TSS concentration time series for a low- and high-flow event respectively and are representative of those observed in many of the events. The graphs show that the TSS concentration patterns for the East and West sub-basins matched closely the flow patterns with the maximum TSS concentration occurring at the same time as the maximum peak flow in all cases. It was observed that for similar flow rates the East basin

tends to have a higher TSS concentration than the West basin.

The higher TSS concentrations in the East basin can be partially explained by local physical conditions. The creek bed slopes at the East basin is 15% greater than the slope at the west basin directly upstream of the sampling locations. Additionally, measured particles size distributions in the creeks show that the East basin has a finer median measured sediment. The D_{50} for the West basin was measured to be 22 - 35 mm and the D_{50} for the East was 8 - 15 mm. However, it was also observed that the West basin had a higher percentage of fines (clay sized partilces) in the sampled sediment than the East sub-basin. Finally, by visual inspection and stream survey it was observed that the riparian wetlands are very mature in the East basin with many felled trees and other recent woody debris in the stream channel. Although the riparian wetlands provided erosion protection in certain areas, natural flaura succession had released fine organic sediment at other locations.

Alma Research Centre Water Quality Analysis

As identified in Chapter 4, the Alma research station contributes a portion of the base flow to the headwaters of the East sub-basin. During the 2006 season water samples were collected from the Alma research station and analyzed in the same manner as the other samples collected manually at the sub-basin outlets. Eight samples in total were collected over the season during visits to the study site. Table 6.6 shows the average concentrations measured during the period.

Analyte	Mean Measured Concentration
TP (mg-P/L)	0.14
TN (mg-N/L)	1.33
NO_3^- (mg-N/L)	0.63
TSS (mg/L)	< 5

Table 6.6: Alma Research Station Effluent Water Quality

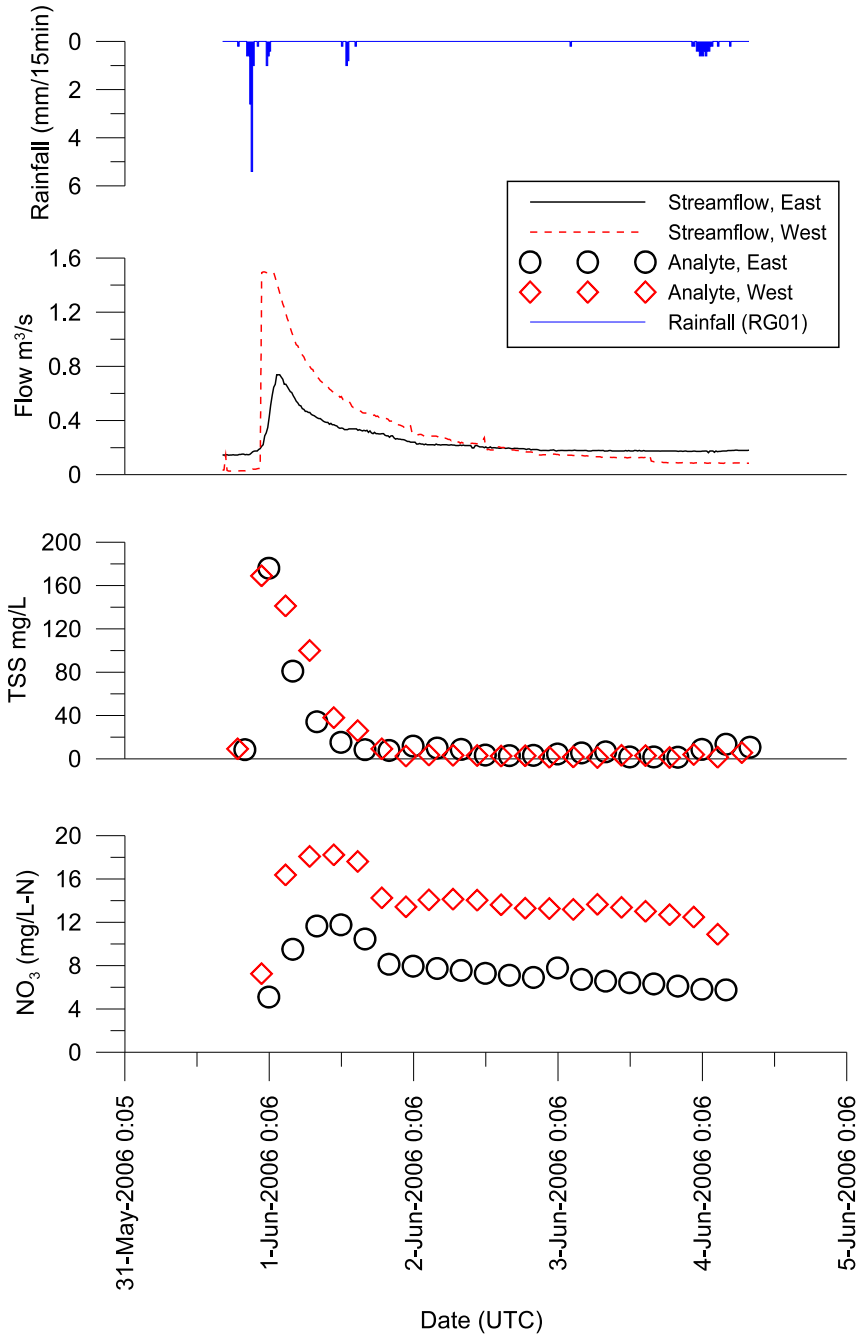

Figure 6.8: TSS and NO_3^-Time Series - Low-flow event - 1 June 2006

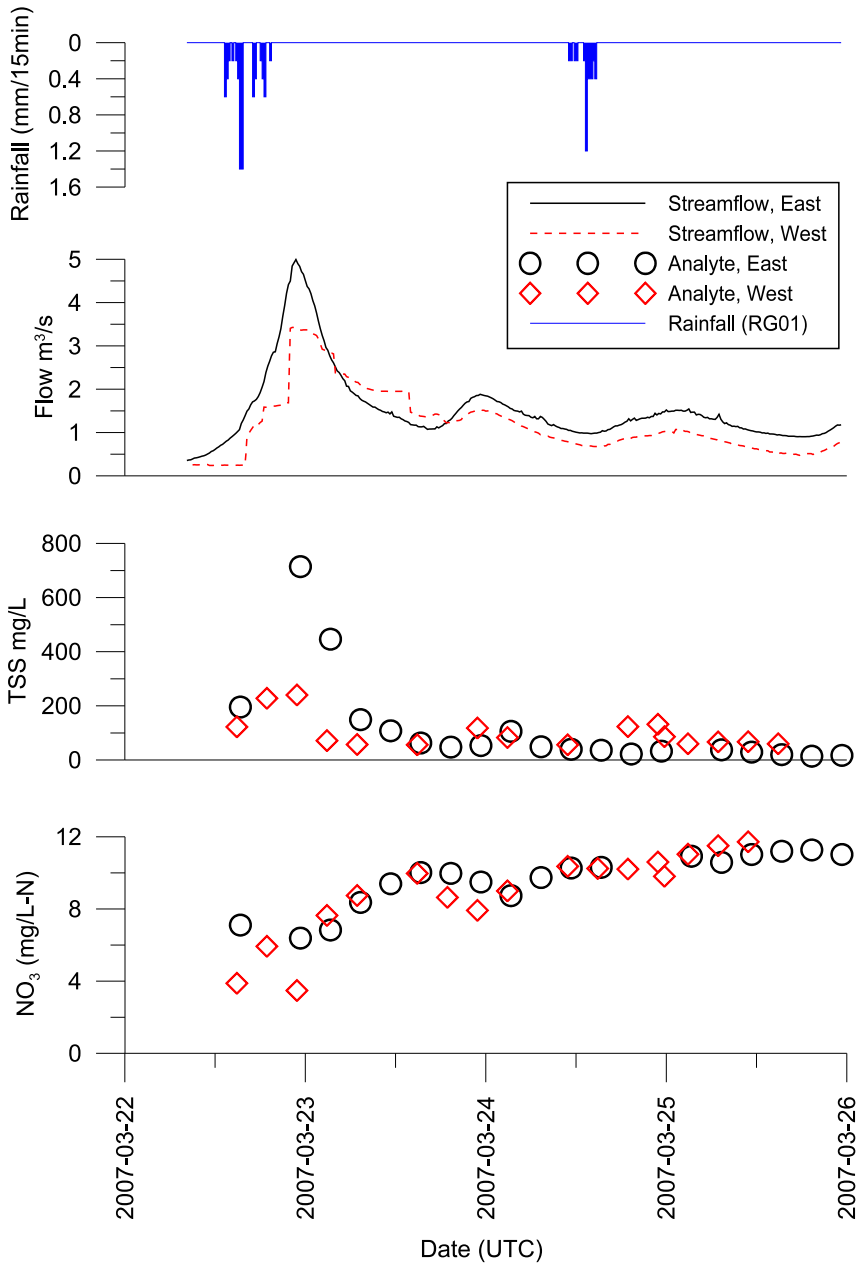

Figure 6.9: TSS and NO_3^-Time Series - Snow melt event - 22 March 2007

6.7.4 Event-Based Load Analysis

To compare the East and West basins contaminant loading contributions on an event basis, total mass loads were calculated for each captured event over the two year study period. Total event mass flows were determined by linearly interpolating the concentrations between sample intervals to points that corresponded with stream flow data derived from 15 minute stage recordings. The corresponding flux at each flow measurement point was calculated at each 15 minute interval. The total flux for an event was calculated by integrating over the duration of the event between 15 minute calculated fluxes. Events were delineated by the sampling starting point, determined by float trigger, and when the flow rate returned to 110% of the flow rate at the time the sampling started (Richards, 2002).

Figure 6.10 compares the loadings of the East and West basins of each of the monitored contaminants. The significance of the differences in event loading were determined by two-sided matched-pair signed-rank test for the event load for each constituent normalized to the drainage basin area. A multiplicative relationship was observed for the differences in loading between basins so the loading values were log-transformed to provide symmetric sets of differences. The estimate of the differences between the East and West loading measurements were determined using the Hodges-Lehmann estimator (Helsel and Hirsch, 1991). The results of the statistical analysis are presented in Table 6.7 identifying the estimated mass loading ratio between the East sub-basin (L_{East}) and the West sub-basin (L_{West}). The TSS, TP and NO_3^- events all showed a statistically significant higher loading in the East basin than the West basin (for $\alpha = 0.05$). Total nitrogen showed a higher average loadings in the East basin than the West although the difference was not statistically significant. The Hodges-Lehmann multiplicative estimator is presented in Table 6.7 and is an estimate of the magnitude difference between the loading of the two groups, with the positive Hodges-Lehmann estimator values indicating the East basin loading is estimated as larger for each of the analytes. Confidence intervals on the Hodges-Lehmann estimator are also presented in Table 6.7 and plotted on Figure 6.10.

The higher loading in the East basin was expected considering the event-based observations discussed above, including higher TSS concentrations in the East than the West

Analyte	Signed-Rank (p)	Hodges-Lehmann Multiplicative Estimator (L_{East}/L_{West})	Confidence Interval (α=0.05) low	high
TSS	0.004	4.95	1.61	6.10
NO_3^-	0.017	2.39	1.21	4.83
TN	0.156	1.75	0.85	3.67
TP	0.002	2.24	1.46	3.65

Table 6.7: Event Loading Signed-Rank Test Summary

under similar flow conditions. The nitrate and TN event based loadings were less significantly different between the East and the West basins. Nitrate and TN concentrations were frequently much higher in the West basin than the East basin. The rapid hydrologic response of the East basin would not always translate into a higher nitrogen load, particularly for the smaller events.

6.7.5 Average Monthly Load Analysis

Monthly averaged nutrient loading estimates were calculated for each of the nutrients and sediments for both of the sub-basins over the study period. The results are presented in Figure 6.11 showing all monthly loading for the months in which sampling was conducted as well as the monthly average flow rate for each of the sub-basins. Nitrate and TN showed similar monthly loading patterns over the study period with the highest loading during the snowmelt events (March 2006 and March 2007) for both the East and West basin and of similar magnitude for both sub-basins during those months. The West and East basins differed significantly however in the summer months with much higher nitrate and TN loading in the East basin than the West basin for June to September of 2006. This is directly attributable to the ephemeral nature of the West sub-basin as the flow levels were reduced considerably during those months. However, loading in the East basin for nitrate and TN was higher for all months with the exception of May 2006 (nitrate and TN) and December 2006 (TN only). It is important to note that May 2006 was the only month with a significantly higher average monthly flow rate in the West sub-basin.

TP showed similar loading patterns for both the East and West basin. The greatest

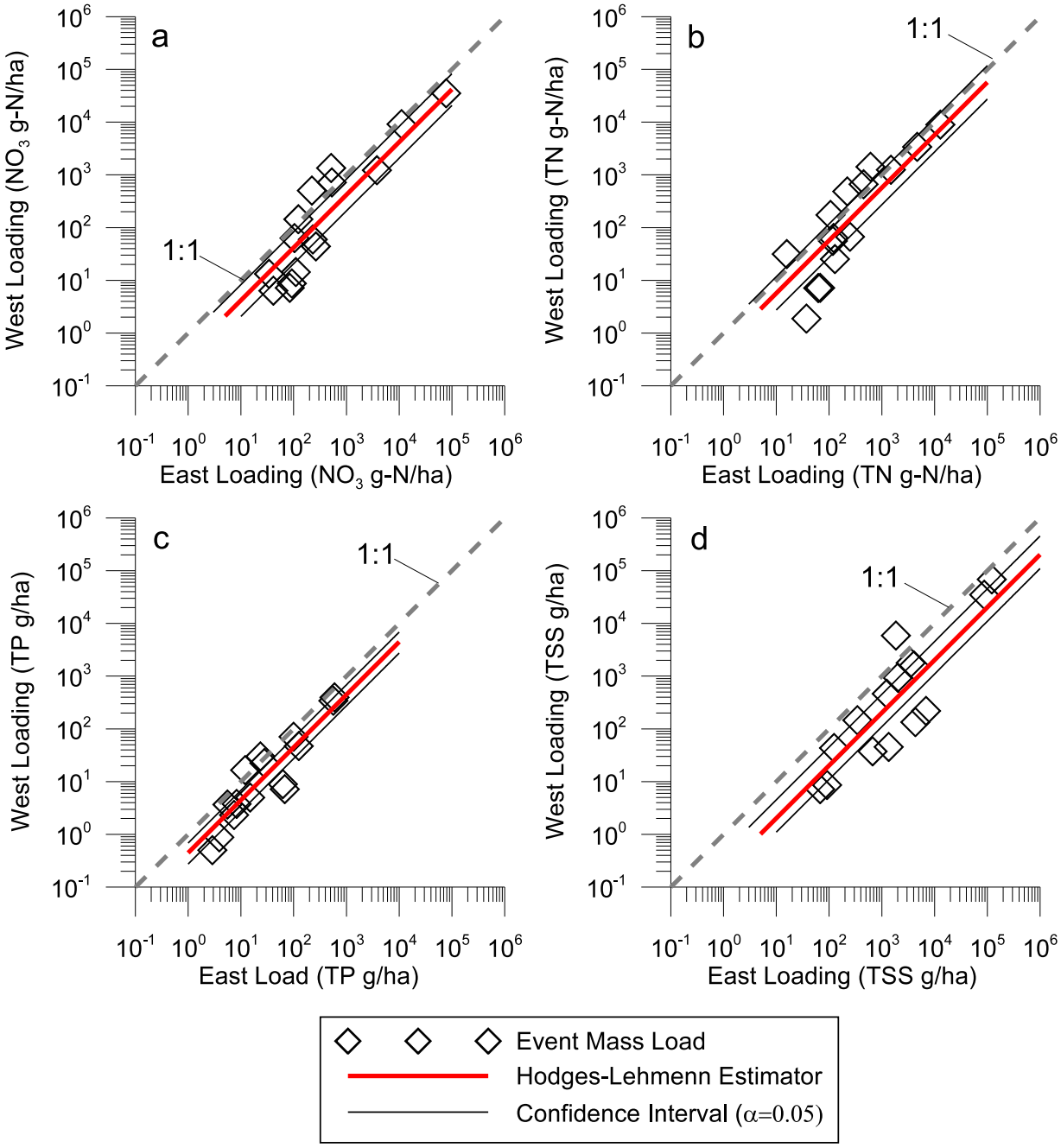

Figure 6.10: Event-Based Total Mass Flux Comparison in East and West basins for (a) Nitrate , (b) Total Nitrogen, (c) Total Phosphorus and (d) Total Suspended Solids

monthly loadings occurred during the winter snow melt events and the lowest loadings occurred during the summer low flow events. The summer loadings were higher for the East basin, however the difference was not as great as with the nitrogen species, in spite of the much higher flow rates in the East basin. This can be attributed to the much higher measured values of total phosphorus in the West sub-basin which resulted in high loadings in that basin even considering the low flow rates.

Suspended solids data showed a consistently higher loading in the East basin than the West basin for all months with the exception of May 2006. Sediment loadings were most similar for the winter snow melt events, particularly the 2006 snow melt event, with the greater differences in the summer months between June and November.

The average of the monthly load estimates over the study period is presented in Table 6.8, showing that on average each of the nutrients and sediment loadings were higher in the East sub-basin than the West sub-basin, the values of average TSS loading in particular being much higher. The two monthly averaged flux populations were subjected to the Wilcoxon Signed-Rank paired value test to see if the monthly average loads were significantly higher in one sub-basin or the other. The values of the Wilcoxon test statistic are shown in Table 6.8. At the 5% confidence level ($\alpha = 0.05$) the TSS, NO_3^- and TN monthly average loads in the East sub-basin were significantly higher than those in the West sub-basin. The TP monthly average loads were not significantly higher so as to be considered a distinct population.

The importance of the snowmelt period in terms of nutrient and solids loading is identified in Figure 6.11. Indeed, the months containing the snowmelt events (March 2006 and March 2007) accounted for the highest loading months for sites for most analytes.

	Average Monthly Load (kg/ha)		Wilcoxan Signed-Rank
Analyte	West sub-basin	East sub-basin	Statistic (p)
TSS	25.63	33.39	0.011
NO_3^-	2.76	3.36	0.011
TN	2.28	2.96	0.039
TP	0.12	0.14	0.109

Table 6.8: Average monthly nutrient and sediment load for study period

Table 6.9 presents the contribution of the snowmelt months to the total estimated loading over the period and contributions range from 34% to 64% of total estimated load. It is understood that certain months during the winter were missed in the total loading estimation due to snow and ice formation in the creeks, over emphasizing the importance of the snow melt in the statistics in Table 6.9. However, the contribution of the snowmelt to total loading remains the single most important event during the year when determining loading estimates in the region.

6.8 Discussion

The results obtained in this study seem to indicate that the riparian zones in this area have little positive effect on the nitrate and suspended sediment loading within the study area, or at least the benefits they provide are dominated by other conflicting processes. For the same rainfall event, the riparian protected East sub-basin will export nearly 5 times the TSS and approximately twice the nitrate, TN and TP loading than the West sub-basin which is without riparian protection. Average monthly loading estimates over the study period showed that TSS, TN and NO_3^- loading was significantly higher in the East basin than the West basin. TP monthly average loading was estimated to be higher in the East basin as well, but not significantly so. The estimated loading for nutrients in the East sub-basin was higher than the West sub-basin even though the daily average concentrations for nutrients were consistently higher in the West sub-basin. This is largely explained by

	Contribution of Snowmelt Months to Total Estimated Load	
	West sub-basin	East sub-basin
TSS	49%	64%
NO_3^-	44%	44%
TN	34%	40%
TP	40%	45%

Table 6.9: Percentage load contribution of snowmelt months (March 2006, March 2007) to total estimated load over study period

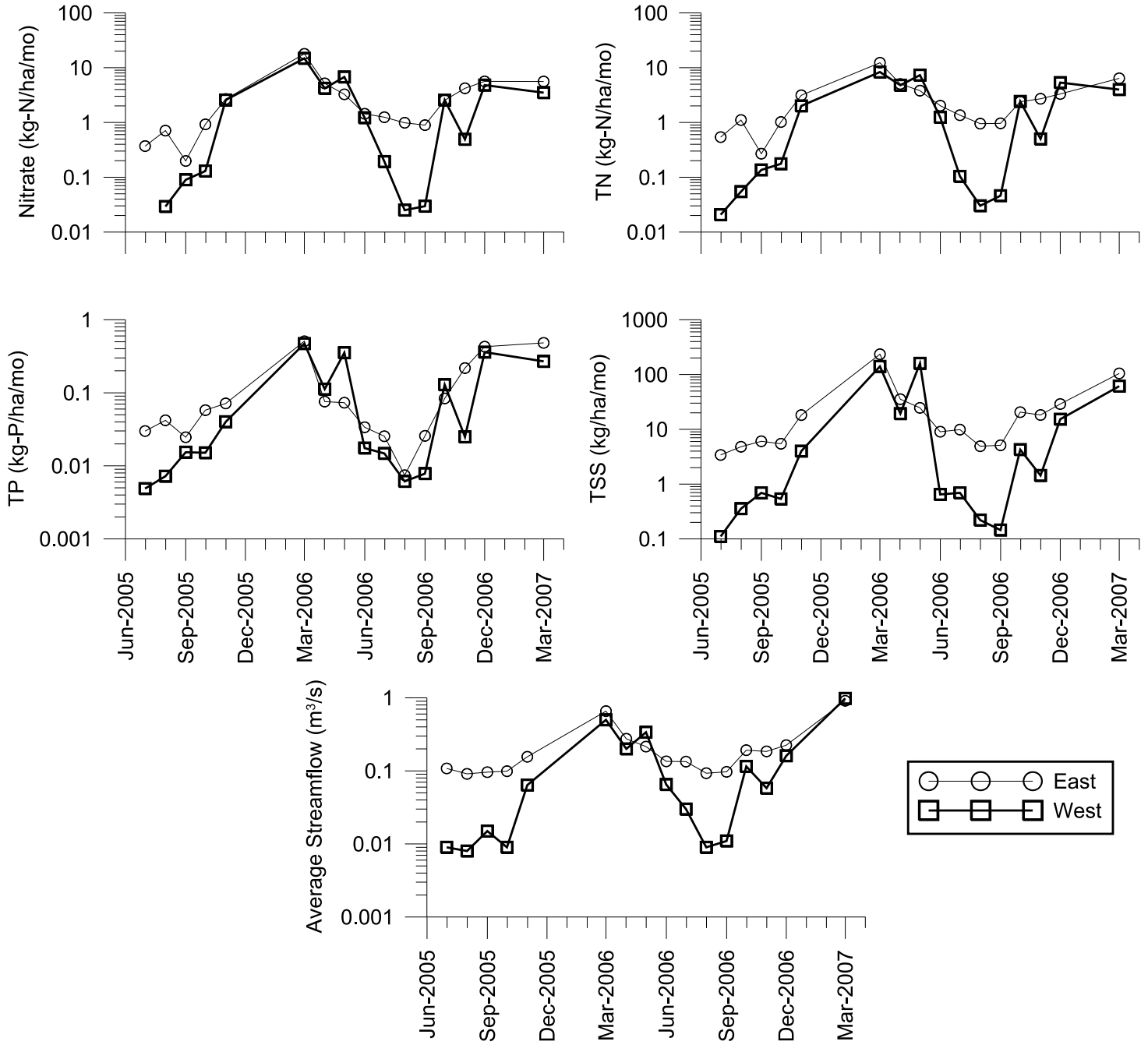

Figure 6.11: Monthly nutrient loading estimates and average monthly stream flow

the differences in hydrology of the two systems with the East sub-basin showing faster hydrologic response and more persistent flow in the summer months.

As contaminant loading was dominated by hydrology the ephemeral conditions of the unprotected basin provided for less overall contaminant loading. This is not surprising when considered in context of other best management practises. Phillips (1996) identified non-wetland riparian zones as better water quality mitigating systems than wetland buffers because of their ability to retain the contaminated water for longer. In effect, the ephemeral stream in this study was performing an analogous function to the non-wetland riparian buffer, although at the sub-watershed scale. The ephemeral stream released less water than the persistent, protected stream during an event and, therefore, contributing less flow downstream, albeit with higher nutrient concentrations.

The differences in the pollutant loadings between the riparian protected basin and the basin without riparian protection was attributed to hydrologic and geologic conditions, more than the presence or absence of riparian zones. Contrary to modelling results presented in previous studies, the presence of riparian zones in these areas did not appear to provide any measurable benefit to receiving waters with regard to nutrient or solids loading, either on an event-basis or a monthly averaged basis, although the nutrient levels were generally lower in the sub-basin with riparian protection. However, due to the integral nature of the study and the other hydrological and geological differences between the two sub-basins the presence or absence of the riparian wetlands is not the only factor to be considered. Further research needs to be conducted to incorporate these findings into modelling efforts to provide more accurate predictive models.

Chapter 7

Water Quality Sub-Model Development

7.1 Introduction

The goal of the research outlined in this chapter is to present improvements to the in-channel and riparian contaminant transport models for both the sediment and nitrogen simulations. The exiting WatFlood/AGNPS model was employed as a starting point. The enhancements made to the water quality model follow the sections in this chapter and include:

- Improved in-channel contaminant transport;
- Riparian wetland contaminant transport;
- In-stream water quality modelling for sediment and nitrate;
- Riparian upstream contaminant load partitioning methodology;
- Riparian wetland water quality modelling for sediment and nitrate; and
- Enhanced land surface processes for nitrogen modelling.

Two primary processes were added to the riparian and channel models: a first order decay process, and a sediment suspension-deposition model. These two processes are applied to both the riparian zones and the channels to estimate the fate of sediment and nutrients supplied from the upland non-point source models. The modularity of the development allowed the algorithms to be applied generally to the riparian wetland and channel elements with a large degree of code re-use.

7.2 In-Channel Contaminant Transport

This section describes the incorporation of a channel contaminant transport sub-model for the WatFlood / WATCLASS distributed model framework. The purpose of this model is to improve the contaminant in-stream routing in the WatFlood model and to improve the transport timing of the existing models using a physically-based in-channel mixing and transport sub-model that accommodates hydraulically coupled riparian wetlands. This was identified as a deficiency in the model in Chapter 1.

The introduction of a high precision advection dispersion model in Chapter 7 provides for a starting framework for integration of chemical decay and rate models for in-stream and riparian wetland processes.

This chapter outlines the WatFlood/AGNPS water quality component of the model as well as changes and enhancements that were added to allow for a more accurate simulation of the water quality data presented in Chapter 6.

The accurate spatial and temporal prediction of contaminant concentrations within a hydraulic/hydrologic modelling system requires a solution of the governing advective and dispersive processes to capture movement of the constituent within the flow field. Contaminant transport in rivers is controlled by the flow velocities and turbulent dispersion and the selected model should explicitly account for these processes while remaining mass conservative.

The modelling of contaminant transport in rivers typically assumes that the contaminants are vertically and laterally well mixed within the river and that the contaminant transport equations can be reduced to the one-dimensional (1D) advection-dispersion equa-

tion within the stream (Fischer, 1979). The 1D advection-dispersion equation employed for contaminant transport modelling is shown in Equation (7.1).

$$\frac{\partial(A\phi)}{\partial t} + \frac{\partial(UA\phi)}{\partial x} = \frac{\partial}{\partial x}\left(DA\frac{\partial\phi}{\partial x}\right) + S \tag{7.1}$$

where A is the flow cross sectional area of the channel $[L^2]$, D is the dispersion coefficient $[L^2/T]$. The dispersion coefficient incorporates both mechanical dispersion and molecular diffusion process, although for most fluvial systems the longitudinal mechanical dispersion processes dominate (Fischer, 1979; Rutherford, 1994). U is the mean cross-sectional velocity $[L/T]$, ϕ is the concentration of a constituent or solute $[M/L^3]$, t is time $[T]$, x is the distance in the downstream direction $[L]$, and S is a generic source or sink term $[M/LT]$.

The source/sink term may be further expanded to consider all possible additions or removal of the mass within the stream:

$$S = \sum_i \left(q_{LI}\phi_{LI}\right)_i + \sum_j \left(q_{LO}\phi\right)_j + AK_1\phi + AK_0 \tag{7.2}$$

where q_{LI} is the lateral flow into the stream (from lateral upstream contributing areas) and ϕ_{LI} is the concentration of the constituent in the lateral inflow, q_{LO} is the lateral flow leaving the stream (from exchange with riparian zones or drainage into the sub-surface), i and j are the number of lateral inflow and outflow sources, respectively, K_1 $[1/T]$and K_0 $[M/L^3T]$ are decay or source rate constants for first- and zero-order processes respectively.

In addition to the assumptions of complete lateral and vertical mixing within the channel the employment of (7.1) assumes that there is a complete decoupling of the flow and contaminant transport equations, which implies that that the flow fields are not affected by the constituent concentrations. This is a valid assumption except when considering bed-load sediment transportation where a fixed-bed model is no longer appropriate and the contaminant transport and fluid flow equations require a stronger coupling for accuracy (Lyn, 1987; Graf, 1998).

7.2.1 WatFlood Channel Routing Model Structure

The application of equations (7.1) and (7.2) require velocity and flow information predicted from data or a hydraulic model input. WatFlood, as a hydrologic driver, employs a storage routing approach to in-stream flow routing. The storage element resolution is that of a grid square within the model, the storage of the specified channel being dictated by the length of the channel within the grid and the channel geometry. The discharge from the channel into the next receiving element in WatFlood is dictated by the Manning equation. The storage routine approach is illustrated by (7.3) whereby the change in storage over a time step is the difference in inflow and outflow averaged over the time step.

$$\frac{I^n + I^{n+1}}{2} - \frac{O^n + O^{n+1}}{2} = \frac{\forall^{n+1} - \forall^n}{\Delta t} \tag{7.3}$$

where I represents inflow into the grid channel, O represents the flow out of the grid channel and $\forall$ represents the storage volume in the grid channel. The superscript n corresponds to the time step and Δt is the time-step increment. The outflow term in (7.3) is described by the Manning equation as shown in (7.4).

$$O^{n+1} = \frac{1}{n_R} \frac{A^{3/2} S_0^{1/2}}{w^{2/3}} \Bigg|^n \tag{7.4}$$

where n_R is the Manning roughness value for the channel, A is the cross sectional area, S_0 is the channel slope and w is the channel width. The superscripts containing n correspond to the time step. The sequence with which the grids are solved is important as upstream outflows are summed together to constitute the inflow to downstream receiving grids. Lateral inflows in a grid are added at the upstream end of the reach for each grid, routed through the channel within the grid before contributing to the downstream grid. Therefore (7.3) and (7.4) are solved for upstream grids first and the solution progresses successively downstream.

The determination of area in (7.4) is derived from the channel geometry equations in the WatFlood model. WatFlood assumes a wide rectangular channel with the hydraulic

radius of the channel being close the water depth. The width to depth ratio for a bank-full channel is specified by a width-depth ratio parameter for the prescribed channel type as outlined in (7.5)

$$R_{WD} = \frac{w_{bf}}{d_{bf}} = \frac{w_{bf}^2}{A_{bf}} \tag{7.5}$$

where R_{WD} is the width-depth ratio for a bank-full channel, w_{bf} is the bank-full width, d_{bf} is the bank-full depth, and A_{bf} is the bank-full cross sectional area. Values for the width to depth ratio and the bank full - drainage area relationships were obtained from stream cross sections measurements in the study sub-basins as described in Section A.3. Channel bankfull area within a grid in WATFLOOD is related to the drainage area upstream of that grid using an exponential equation (7.6).

$$A_{bf} = a_2 + a_3(A_{drain})^{a_4} \tag{7.6}$$

where A_{bf} is the cross sectional area of a channel, A_{drain} is the upstream drainage area, and a_2 a_3 and a_4 are fitted parameters obtained from cross-section data. Each of the fitted parameters are specific to a prescribed river class in the WATFLOOD model.

Riparian wetland routing is accomplished through a hydraulic coupling between the riparian wetland storage and the storage in the wetlands. In the WATFLOOD hydrological model, the model accounts for riparian wetland storage using a modified version of the Dupuis-Forcheimer equation adapted from Bear (1979) shown in Equation 7.7.

$$Q_{wet} = \frac{K_{cond}}{2} L_{wet} \left(h_{wet}^2 - h_{chan}^2\right) \tag{7.7}$$

where Q_{wet} is the wetland outflow (positive being from the wetland to the channel), K_{cond} is the calibrated wetland conductivity, h_{wet} is the height of the water level in the wetland, h_{chan} is the height of the water in the channel and L_{wet} is the coastal length of the riparian wetland within the grid element. The flow area state variable for the channel is described by a rectangular relationship

$$A = h_{chan} w_{bf} \tag{7.8}$$

where A is the channel area.

Storage in the riparian wetland class is driven by the specified porosity of the wetland class, the areal cover of the riparian wetland and the measured channel depth.

$$\forall_{wet} = A_{wet} d_{bf} \theta_{wet} \tag{7.9}$$

where $\forall_{wet}$ is the maximum storage in a grid-element riparian wetland class, A_{wet} is the areal cover of a the riparian wetland class in a grid, d_{bf} is the bankfull height of the channel (as specified by Equation 7.5) and θ_{wet} is the porosity parameter for the wetlands which is calibrated in the model.

Large scale watershed basins of the size of the Grand River do not appear to be overly sensitive to the Bank-full Drainage Area relationship as pertaining to flood routing (N. Kouwen, personal communication), however, as the depth of the channel at any location predicts the storage hydraulic storage available by a riparian wetland it is considered important in assessing wetland contributions to the hydrology and the need to validate the channel geometry is important.

7.2.2 WatFlood Contaminant Transport Model

The original contaminant transport model included in WATFLOOD builds upon the storage routing model employed by the WATFLOOD flood routing model and calculates constituent movement using an analogous storage routing approach which is in effect a complete mixing-cell model (Leon, 1999). The mass balance for each solute in each grid element M is calculated using (7.10)

$$\frac{M^{n+1} - M^n}{\Delta t} = \frac{M'^{n+1}_{in} + M'^{n}_{in}}{2} - \frac{M'^{n+1}_{out} + M'^{n}_{out}}{2} \tag{7.10}$$

where M' represents the mass flux in or out of the element as denoted by the sub-scripts, M represents the mass of the solute in the element and the time step is represented by Δt. This equation is solved considering equations (7.11) and (7.12) relating M'_{out} to the mass,

storage and flow in the element

$$M'^{n+1}_{out} = Q^{n+1}_{out}\phi^{n+1}\Delta t \tag{7.11}$$

$$\phi^{n+1} = \frac{M^{n+1}}{V^{n+1}} \tag{7.12}$$

where ϕ is the solute concentration, the volumetric outflow Q^{n+1}_{out} and storage V^{n+1} are known for all time steps (provided from the WATFLOOD hydrologic model). The remaining variables are determined through an iterative solution of Equation 7.10 and 7.11 until a convergence tolerance in the incremental change in M'^{n+1} is reached (0.1% is prescribed in the current WATFLOOD model with a maximum of 50 iterations permitted). The storage routing is solved for each grid in the reach sequentially. For receiving grids, the combined input fluxes from all upstream contributing grids are added to the M'_{in} value for the receiving grid. This contaminant transport model will hereafter be referred to as the "storage routing" contaminant transport routine.

7.2.3 Storage Routing Contaminant-Transport Limitations

The existing contaminant routing model is subject to a number of limitations. Particularly, it does not explicitly consider dispersion, and dispersive processes are manifest only in the numerical dispersion inherent in the mixing-cell approach. This may not be of concern when considering average loadings over large periods of time. However, if event-based data is to be analyzed, or other grab-sample or point data were collected and compared using the WATFLOOD model, the need to accurately account for dispersive processes becomes important. Additionally, the mass preservation or conservation of the routine is suspect due to the iterative nature of the solution to converge on a mass flux rather than directly calculating fluxes based on state variables.

Figure 7.1 illustrates the issues associated with the storage routing algorithm with regards to contaminant transport. Shown in this figure are several conservative tracer plumes modelled with the WATFLOOD hydrological model on the Grand River watershed with different grid resolutions. The hydrologic response for each of these scenarios is

identical but with different grid sizes one observes stark differences in the shape of the tracer plume. The dispersion in this model is controlled entirely by the grid resolution. Vieux (2001) and Beven (2001) have highlighted the importance of scale in hydrological modelling, particularly with regard to roughness, slope and other model parameters that operate on a finer scale than that of the gridded model, requiring a distinct value at different grid scales. The problem identified here with contaminant transport in WATFLOOD requires attention as the in channel mixing parameter *is* the grid scale. That is, the mixing parameter is inseparable from the model discretization.

The introduction of a physically-based contaminant-transport sub-model is seen as an important next step in the evolution of the WATFLOOD/WATCLASS distributed hydrologic model framework. Efforts are underway to model isotopic tracers (Stadnyk et al., 2005), water temperature as well as nutrients, pathogens and other water borne constituents (Leon et al., 2004; Dorner et al., 2006). The implementation of a physically-based contaminant routing model that accounts for channel velocity and dispersion in the main channel and is mass conservative is required.

7.2.4 Enhancements to WatFlood In-Channel Contaminant Transport

The modelling approach taken when developing the solute channel routing code was to modularize the contaminant transport processes and separate the water quality transport code from the WATFLOOD code. This collection of routing routines (named SOLROUTE) maintains its own state variables for flow and solute concentrations, receives hydrologic data from the WATFLOOD model and contaminant loading data from the AGNPS submodel via programmatic pointers in the WATFLOOD controlling subroutines. Although the primary purpose was integration with the WATFLOOD model, the modularization of the code provides for sourcing of hydrologic and contaminant loading data from any source and the execution of the SOLROUTE code in isolation. This approach is valuable for unit testing of the algorithms against known analytical solutions and for portability, allowing the solute transport model to be run in conjunction with other models or merely model output (i.e. EnSim R2C files of gridded outflow hydrographs). Ultimately, the only code

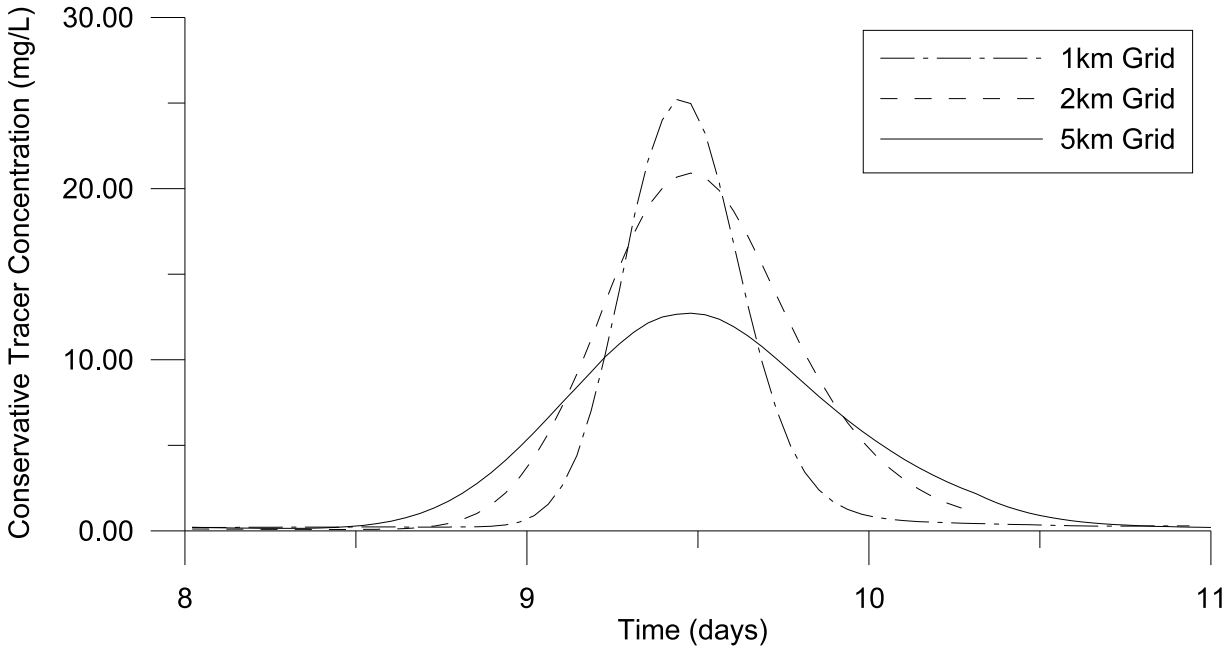

Figure 7.1: Storage Routing A-D Model - Grid Size Dependence

requiring updating is the interface code that communicates between the hydrologic and contaminant loading source models.

This data integration relationship is presented in Figure 7.2. Here the data flow between the models is illustrated, where the Hydrologic and Contaminant inputs from WatFlood and AGNPS are coded (solid lined boxes) via interface code to the SOLROUTE modules. However, the design of the routine is such that further integration with hydrology or water quality time series data may be easily integrated in the future including WATCLASS hydrological or thermal data and the nascent MESH model (Pietroniro et al., 2006a) currently in development by Environment Canada (indicated with dashed line boxes). All of these models employ the GRU structure facilitating integration with the SOLUTE routing code.

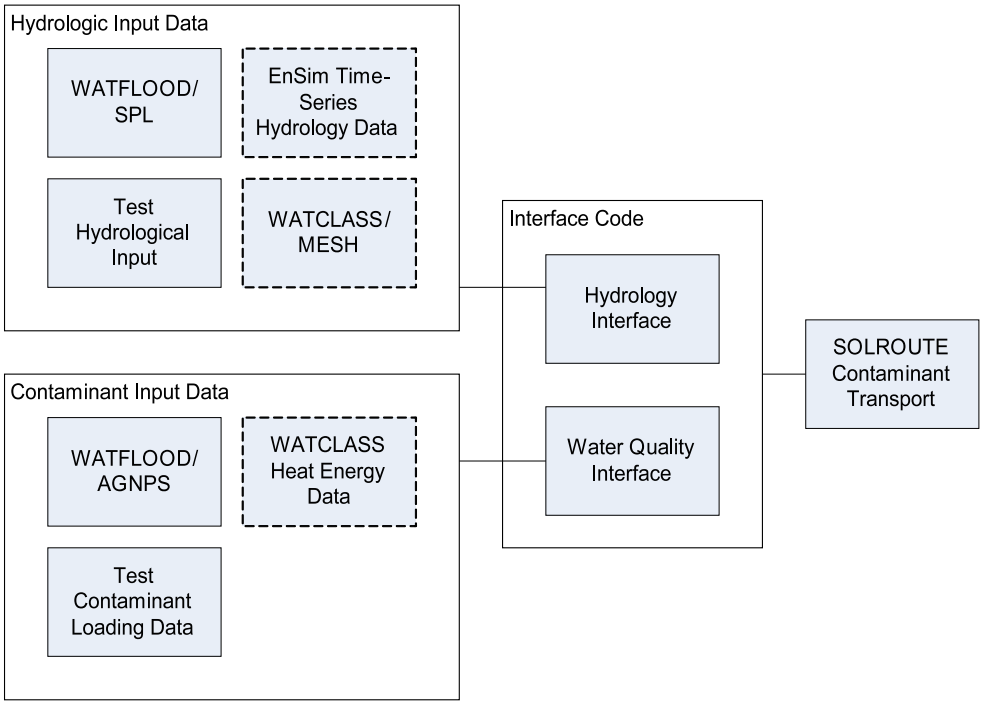

Figure 7.2: WatFlood Solute Routing Integration

As described previously in Section 7.2.1 the current routing employed by WatFlood is a storage-routing technique. This approach provides limitations in terms of contami-

nant transport and flood-wave routing as compared to kinematic-wave and dynamic-wave routing due to a lack of explicit velocity characterization (Chapra, 1997; Julien, 2002). The modification of the routing technique was beyond the scope of this research. However, with a modular design approach for the SOLROUTE subroutines, changes to the hydraulic routing approach will be transparent to the solute routing code requiring only modification to the interface code and pointers to the hydrologic state variable data.

7.2.5 Extensible Contaminant Transport Model Structure

The modularity of the code was not only considered in how the model is integrated with external hydrology and contaminant sourcing modules. The selection of the routing routine, the number of solutes modelled and the equations used in reaction calculations were also designed to be modular in structure. The design of the interface code will allow the modeller to choose which contaminant routing routine to use, the time step adjustments, the number of constituents to model and the process equations to use in determining the fate of the constituents. The underlying structural goal in developing this code base was to allow for easy integration into multiple hydrological and water quality source models, and also to allow any additional development to be facilitated by the extensibility of the code structure.

7.2.6 Modular Input File Structure and WatFlood Integration

The input data required for the application was abstracted from the data required by the WatFlood model, although the event-based structure of the WatFlood model was adhered to for this implementation. WatFlood employs an event-based file structure, with each "event" identified by a single file that points to a number of other input files required for the model to run for that time period. Typically events are prescribed as month-long periods in the WatFlood model but can be shorter or longer in duration. Extended simulations can be run by chaining events together in a sequence. The file structure for the integrated water quality model involved a similar file structure approach. A single pointer was added to the WatFlood event file to point to a water quality data

(WQD) file for that event. Each event WQD file would in turn point to the required input files for the water quality model to operate. This approach minimized the degree of intrusion to the WATFLOOD code base and allowed for complete removal of the required water quality files if simulations omitting water quality processes were desired. Figure 7.3 identifies the event-based file structure modified for the inclusion of water quality parameters and input data.

7.2.7 Sub-Grid Discretization

In order to improve the flexibility and precision of contaminant transport algorithms a grid sub-element data structure was constructed which segmented the channel of each WATFLOOD grid into a specific number of smaller, equally sized computational segments Figure 7.4 shows a schematic representation of the sub-grid elemental structure of the storage routing model illustrating how each WATFLOOD Grid channel i may be subdivided into N channel elements. This is an established computational approach where the reach (or grid) length defines the reach characteristics but the computational domain is subdivided to provide a more spatially accurate numerical solution (Foster, 1982; Chapra, 1997).

The number of sub-grid elements within a grid can be any positive integer value. Solutes are routed downstream through each of the elements within the grid. The calculated outflow from the last element in the grid's channel is added to the first element of the receiving grid, as dictated by the chosen contaminant transport scheme. Figure 7.5 illustrates this relationship schematically, where solute output from the final elements in Grids A, B, and C contribute to the first element in the receiving grid D.

7.2.8 Contaminant Transport Algorithm Selection

Considering the established weaknesses of the original contaminant transport routine a number of options for improved contaminant transport were considered. Three separate contaminant transport algorithms were selected for inclusion into the SOLROUTE contaminant transport library:

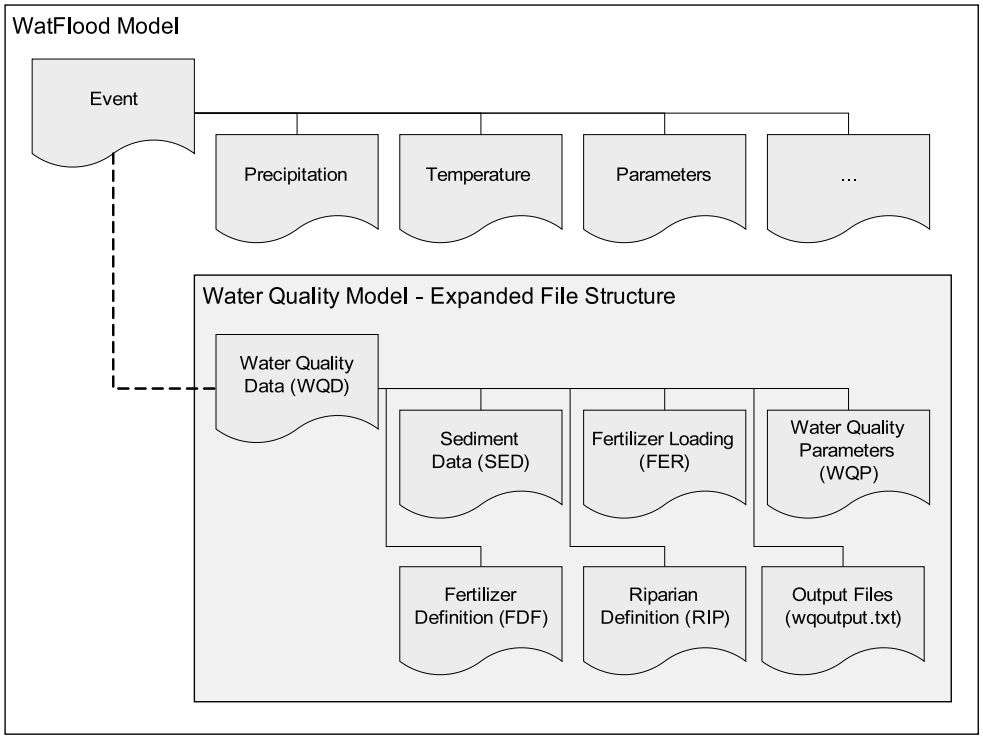

Figure 7.3: Water Quality Model Input File Structure and WatFlood Integration

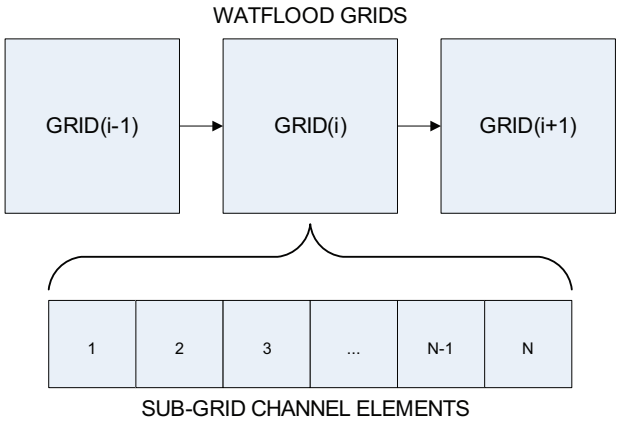

Figure 7.4: WATFLOOD Grid and Sub-Grid Elements

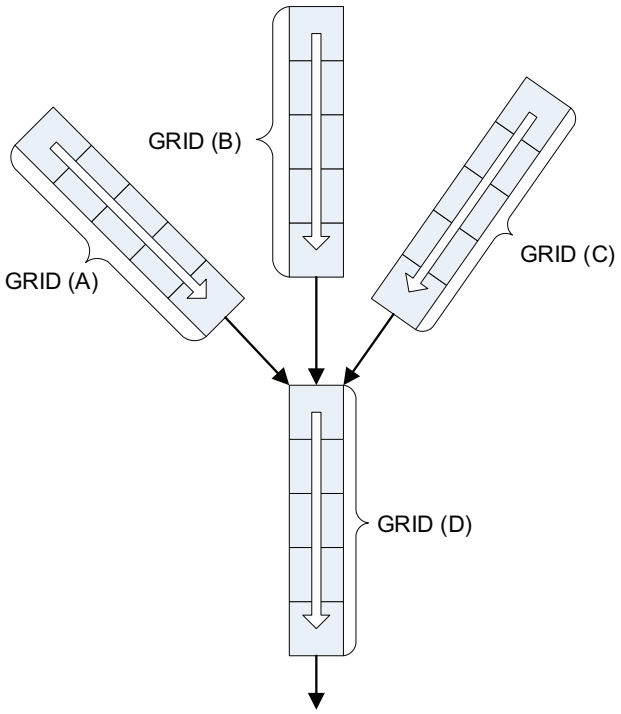

Figure 7.5: Sub-Grid Element Routing Network

1. Sub-grid Storage Routing;

2. The QUICKEST Finite-Volume advection-dispersion scheme; and

3. A Holly-Preissmann/Crank-Nicholson (HPCN) split operator scheme.

These three algorithms were chosen because they represent three fundamentally different approaches to solving the advection-dispersion problem in a framework such as the WatFlood model.

The Sub-grid Storage Routing scheme is a re-coding of the existing storage routing algorithm described in Section 7.2.2 but on an "element" basis rather than a "grid" basis. This routine was coded as an existing benchmark, so that other algorithms could be compared to the WatFlood unmodified base case in a test framework.

The QUICKEST routine is a finite-volume explicit third-order accurate 3 point upwinding scheme developed by Leonard (1979). It has received wide use over a number of decades and the scheme provides an accurate and reasonably stable solution to highly advective computational problems (Leonard and Noye, 1990; Leonard, 1991; Wallis and Manson, 1997).

The Holly-Preissmann/Crank-Nicholson scheme is a split-operator finite difference scheme that solves the advection and dispersion components of the transport equation in two steps. A fourth-order accurate Lagrangian approach is employed to solve the hyperbolic advection problem, whereby the concentration profile itself is advected (Holly and Preissmann, 1977). The dispersive fluxes are determined employing the implicit Crank-Nicholson method to solve the diffusion equation in a separate calculation (Chapra, 1997).

The development and description and implementation of the Storage, QUICKEST and HPCN transport algorithms is provided in detail in Appendix D, Sections D.2.1, D.2.2, and D.2.3 respectively.

Once implemented, the coded contaminant transport algorithms were evaluated through a number of test cases to assess their performance. Test cases for which analytical solutions are available were employed to assess the performance of each algorithm:

- the advection and dispersion of an instantaneous point source; and

- the advection of a sharp front from a continuous source.

Algorithms were evaluated based on their accuracy, stability, peak attenuation, oscillations and mass conservation as compared to an analytical solution of the advection-diffusion equation in the test cases. Algorithms were evaluated on sub-grid and multi-grid test cases. The WATFLOOD model structure provides potential problems with respect to contaminant transport. The computational domain in WATFLOOD, as dictated by the gridded GRU structure, is broken into a large number of small reaches with a large number of connecting nodes. The boundary conditions at these nodes presents potential problems requiring controlled assessment in a test framework. The performance of the three algorithms was assessed and then source and sink calculations were added after the preferred algorithm was selected.

7.2.9 Evaluation of Contaminant Transport Schemes

An evaluation of the routing schemes was conducted to determine which of the storage, QUICKEST and HPCN schemes provided the greatest accuracy and general utility for use in the SOLROUTE routine to determine the validity of each of the coded routines.

Examining the migration of a steep curve in an advection-only condition provides a reasonable assessment of the reliability of the model. The advection of a sharp front represents one of the most difficult scenarios to model accuracy using the advection-diffusion equation due to the rapidly changing terms. Models tend to extrapolate and exhibit oscillations or dampen the front with excessive numerical dispersion.

Computational tests were conducted to determine the ability of the QUICKEST and Holly-Priessman/Crank-Nicholson (HPCN) models, as employed in the framework, to model the AD equation from a point contaminant input along the length of a grid. The unit test employed was within the stability envelope of the QUICKEST, Storage and HPCN routing schemes and were compared to the analytical solution of the one dimensional advection-dispersion equation.

The schemes were compared by examining mass conservation looking at the total system relative error

$$E_{mass} = \left| \frac{M_o - M_s}{M_o} \right| \tag{7.13}$$

where M_o is the observed, or analytical total mass in the system, M_s is the total mass in the system simulated by the model and E_{mass} is the system relative error. Concentration profiles are compared by looking at the concentration relative error at a particular point in time

$$E_{conc}(x) = \frac{\phi_o(x) - \phi_s(x)}{\phi_{sp}} \tag{7.14}$$

where $\phi_o(x)$ is the observed or analytical concentration as a function of distance along the channel, $\phi_s(x)$ is the simulated concentration as a function of distance and ϕ_{sp} is the simulated peak concentration over all of (x). $E_{conc}(x)$ is the concentration relative error as a function of distance.

These two metrics were used to validate the advective and diffusive transport within the selected algorithms as implemented in the SOLROUTE routine, and were evaluated in a number single- and multi-grid of unit tests. The details of these tests are found in Appendix D, Section D.2.4. Results of these tests revealed a number of findings:

- In single grid, multi-element tests with point and step constituent addition both the QUICKEST and HPCN schemes show good mass conservation ($E_{mass} < 10^{-4}$) whereas the storage routing routine shows poor mass conservation ($E_{mass} > 10^{-2}$).

- In single grid, multi-element tests with point and step constituent addition both the QUICKEST and HPCN schemes match the analytical solution profiles with oscillation errors located at points of steep gradient. The storage routing routine is unable to match the analytical solution profile.

- In multi grid, multi-element tests with point and step constituent addition the QUICKEST routine out-performs the HPCN and the storage routing routines. The storage routing routine show similar mass conservation error as with the single-grid tests. The HPCN routine shows errors accumulating at the grid-grid interface due

to inaccurate interpolation of the concentration and derivative gradients after application of the Crank-Nicholson dispersion routine.

The simple tests performed to analyze the performance of the various contaminant transport models illustrated the clear problems with the storage routing currently employed the WATFLOOD routing model with regard to the ability to model constituent dispersion and advection, but also the lack of mass conservation in the model. The poor performance of the storage routing algorithm when subjected to point concentration additions is clearly evidenced. This routine inaccurately models the timing and the dispersion of the contaminant plume and demonstrated a high degree of inaccuracy with regard to mass conservation, even within a very simple steady-state flow environment.

Both the HPCN and the QUICKEST transport routines performed very well within the sub-grid routing model tests, showing a high degree of accuracy modelling both advective and dispersive flow. The HPCN routine showed somewhat greater accuracy and mass conservation that the QUICKEST model in the advective tests.

The QUICKEST transport routine showed better mass conservation on a grid-to-grid basis than the HPCN routine. Although the HPCN routine shows promise, more work needs to be done to estimate the concentration gradients near the boundary to accurately advect the concentrations. Some numerical dispersion and mass conservation occurred with the QUICKEST scheme at the upstream boundary condition for each grid due to the lower-order advective approximation at that location, but on balance was the better choice.

Stability remains a potential issue with the QUICKEST routine for highly dispersive flow, but considering the generally advective nature of fluvial transport processes the issue will be addressed on a case-by-case basis. That is, if the stability criterion are violated due to very low velocities and relatively high dispersion values, special considerations can be made. This was done for reservoirs within the WATFLOOD model and is discussed below in Section 7.2.11.

7.2.10 Integration with WatFlood

As a final test, the contaminant transport equations were integrated with the calibrated WatFlood model for the Canagagigue creek (see Chapter 5). The selected QUICKEST model was employed in the WatFlood model and the HPCN routine was not employed considering the mass conservation issues at the grid interfaces. The Storage routine was employed as well as a benchmark comparison.

Integration included linking the hydrologic data from the WatFlood model using an interface module. The hydrologic data was updated in step with the WatFlood model time steps, as a Courant number less than one, which is enforced in the WatFlood model is required for stability of the first-order upwind scheme used in the upstream grid elements. Consequently the time steps dictated by WatFlood were used in SOLROUTE but were divided by the number of elements per grid. For example, a 900 second time step in WatFlood would be 90 seconds in SOLROUTE if there were 10 computational elements per grid. Figure 7.6 outlines the integration in a flow-chart that illustrates the interface locations tasks performed by the WatFlood model, the interface code and the water quality model.

The test involved the transport of a point instantaneous addition of a conservative tracer at a location below the Woolwich Dam during the spring runoff season of 2000. A mass addition of 2000 (arbitrary units) was added on 30 Apr 2000 00:00 to the centre of a grid on the main channel (UTM coordinates easting: 535 500, northing: 4828 500) and was transported to the watershed outlet. The timing was selected due to the relatively dynamic nature of the flow field at that time. The test was selected to determine mass conservation within the WatFlood model outside of a test framework. No analytical solution is possible for this scenario so assessment of the precise accuracy of the dispersion profile is not possible. The model was run with a varying degree of sub-grid discretization and dispersion coefficients for both the QUICKEST and storage routing routines.

Figure 7.7 shows the contaminant profile from the QUICKEST routine at a location just upstream of the watershed outlet (WatFlood grid centred at 540 500, 4824 500) and represents the total mass stored in that grid as a function of time as the transported solute moved through the grid. For each of the four presented runs the dispersion parameter was

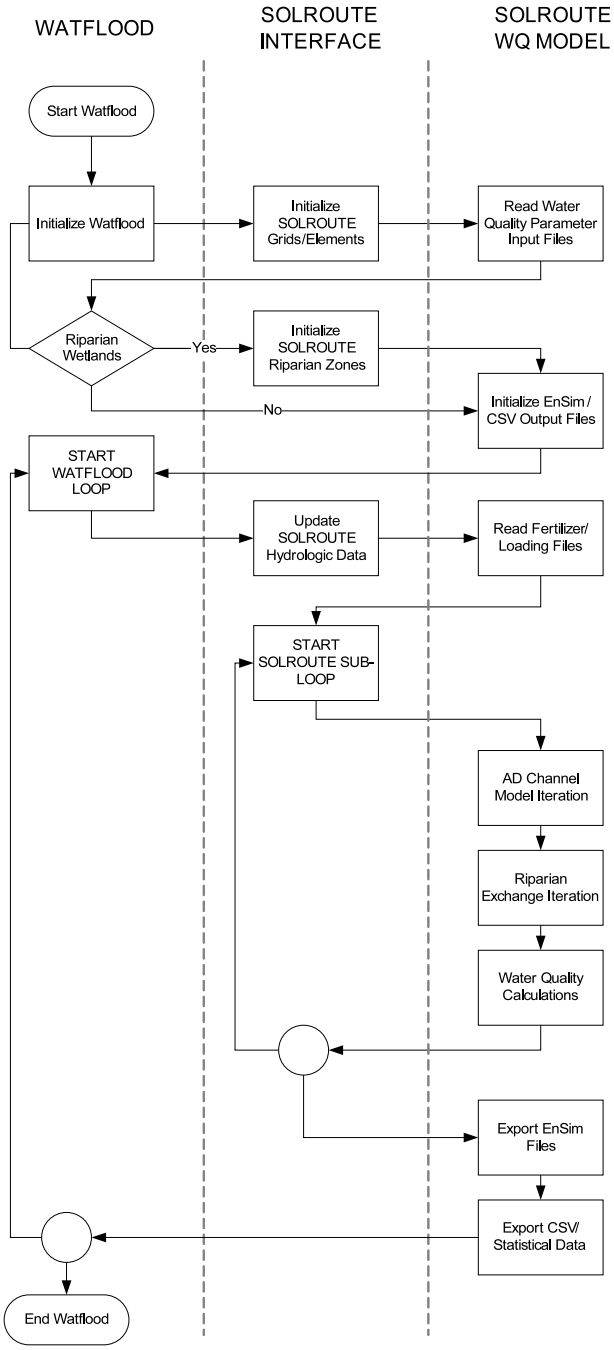

Figure 7.6: WatFlood- Solroute Integration Flow-Chart

fixed to $10m^2/s$ and the grid resolution was varied from 5 elements per grid to 40 elements per grid. The legend entries "QXX_DYY" in Figure 7.7 correspond to XX elements per grid with a dispersion factor of YY m^2/s. The QUICKEST routine showed good convergence to a solution as the element resolution was increased, with only very small differences between the Q10_D10, Q20_D10 and Q40_D10 simulations. As expected, the coarser element resolution produced a greater degree of numerical dispersion, especially considering the upstream element of each grid employed only a first-order accurate advective scheme, and a coarser element resolution would have a greater proportion of the elements operating at a lower order of accuracy.

The QUICKEST routine showed good mass conservation within the WatFlood modelling framework. Figure 7.8 illustrates the degree of mass conservation within the model for the above simulation. The system mass error never exceeded 0.1% for any of the grid resolutions. The occasional sharp drops in mass error are due to a change in the total mass error from positive to negative values or vice-versa, similar to what was observed in D.7.

By contrast Figure 7.9 illustrates the same simulation conducted with the storage routing routine with three different sub-grid resolution where "SXX" corresponds to a storage routing simulation in WatFlood with XX elements per grid. The storage routine produced breakthrough curves that did not converge to a solution with increasing sub-grid resolution. Although the time to peak was constant for all sub-grid resolutions (and identical to the QUICKEST model when compared with Figure 7.7) the spread of the curve varied substantially from one resolution to another. As discussed above, this is a limitation of the routine that is important to recognize, as it has clear implications for solute mixing, breakthrough timing and peak estimation. The storage routing routine also showed relatively poor mass conservation within the WatFlood model as observed before within the unit test scenarios. The mass conservation graphs for the simulation are presented in Figure 7.10 where it is seen the relative mass error within the simulation clearly depends on grid resolution and consequently time step, as the time step increment will scale directly with the grid element size to maintain CFL stability criteria. The total system error ranged from over 10% for the simulation with 5 elements per grid to as low as 2% with 20 elements per grid.

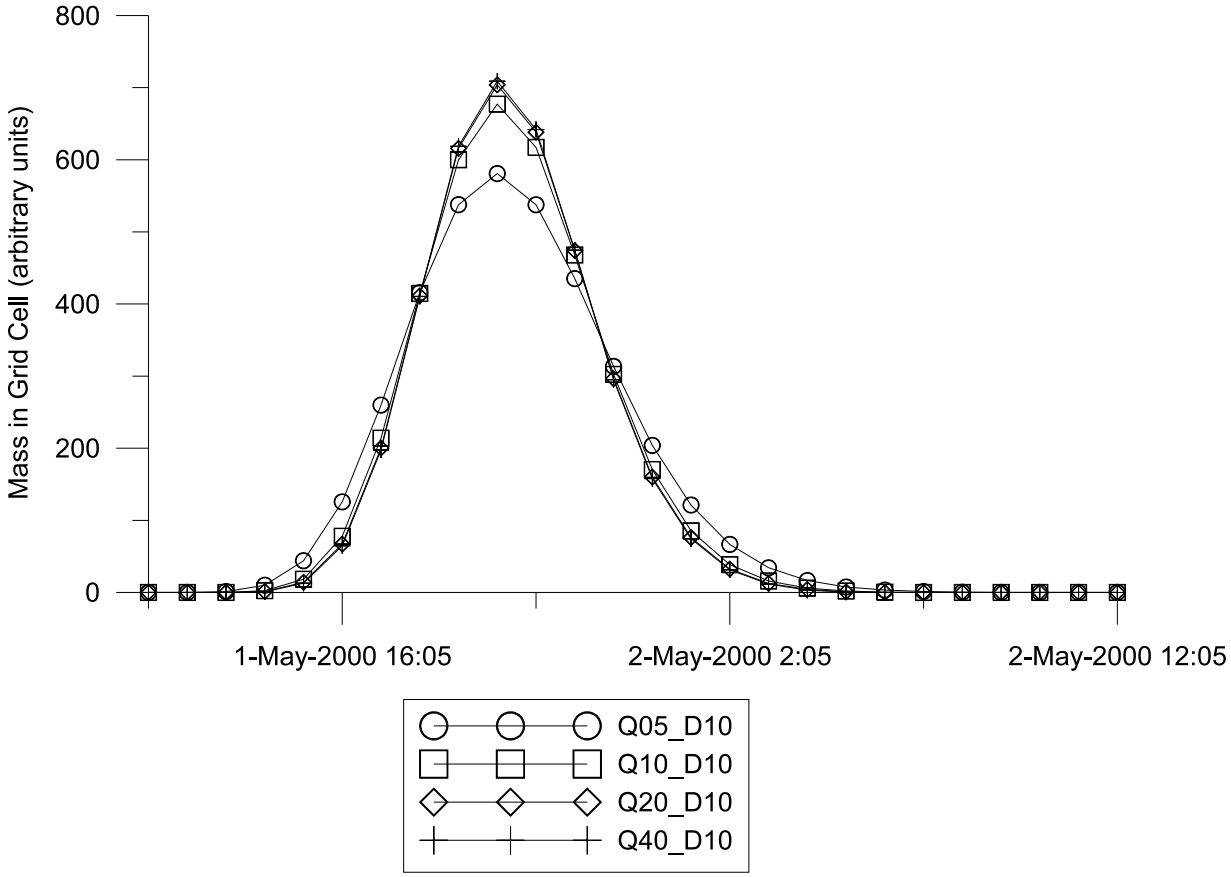

Figure 7.7: QUICKEST Model in WATFLOOD - Breakthrough profiles with varied grid element resolutions

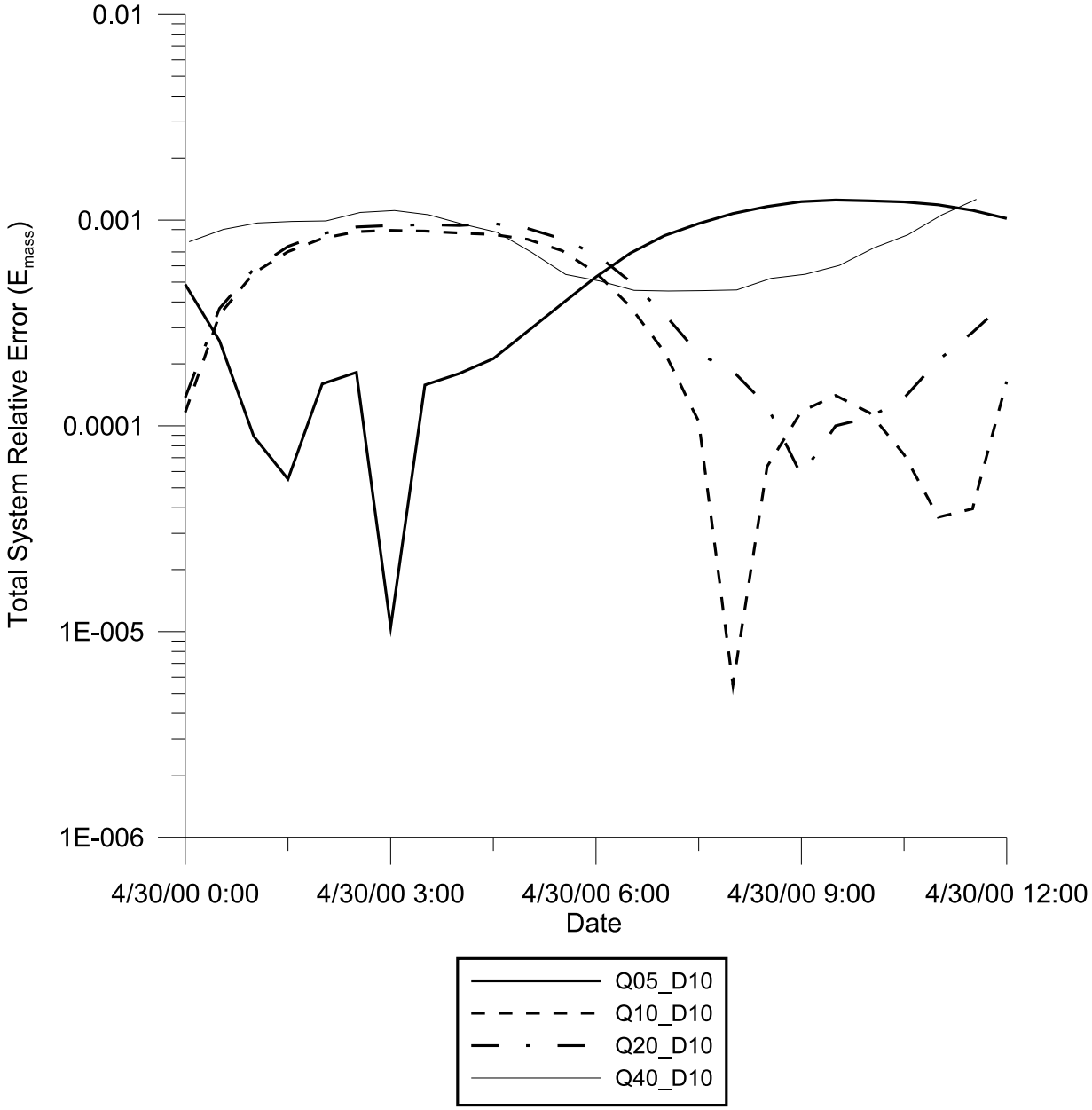

Figure 7.8: QUICKEST Model in WatFlood - Mass conservation with varied sub-grid element resolutions

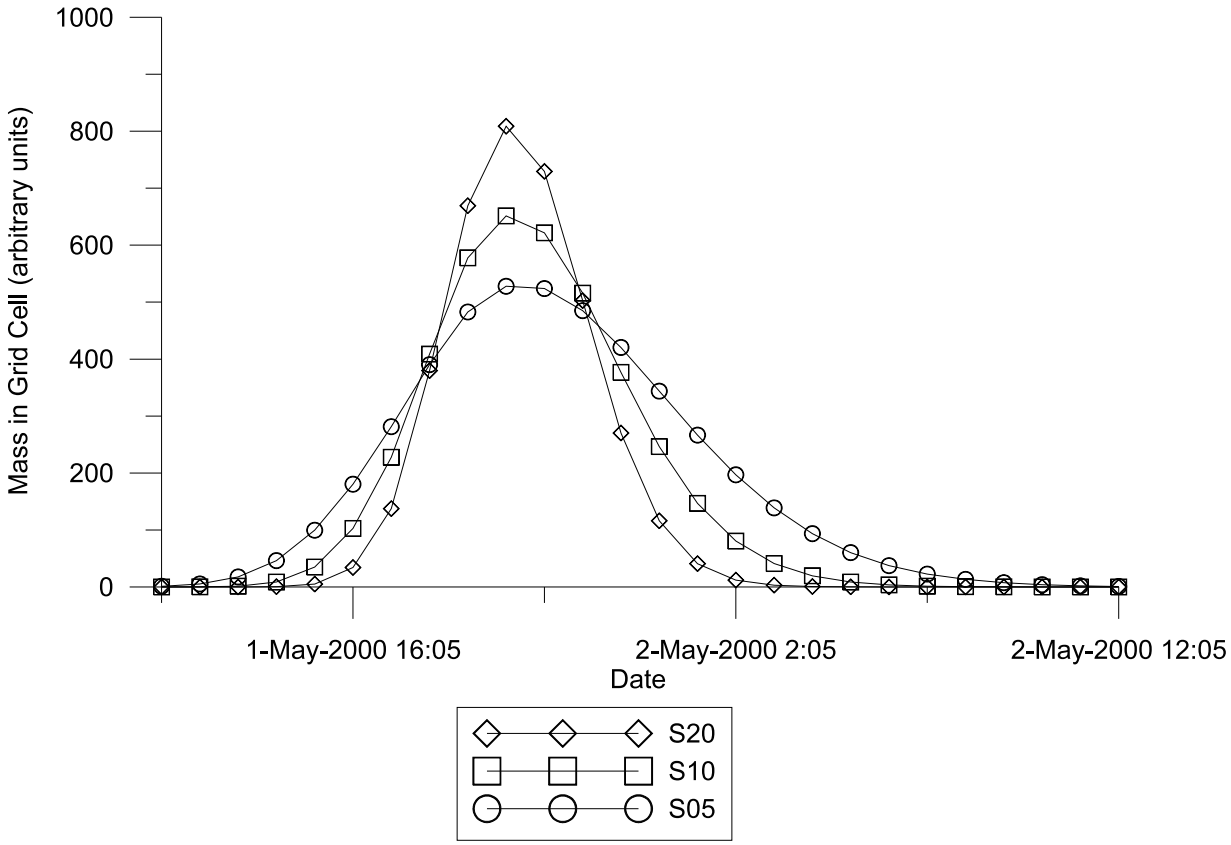

Figure 7.9: Storage Routing Model in WATFLOOD - Breakthrough profiles with varied grid element resolutions

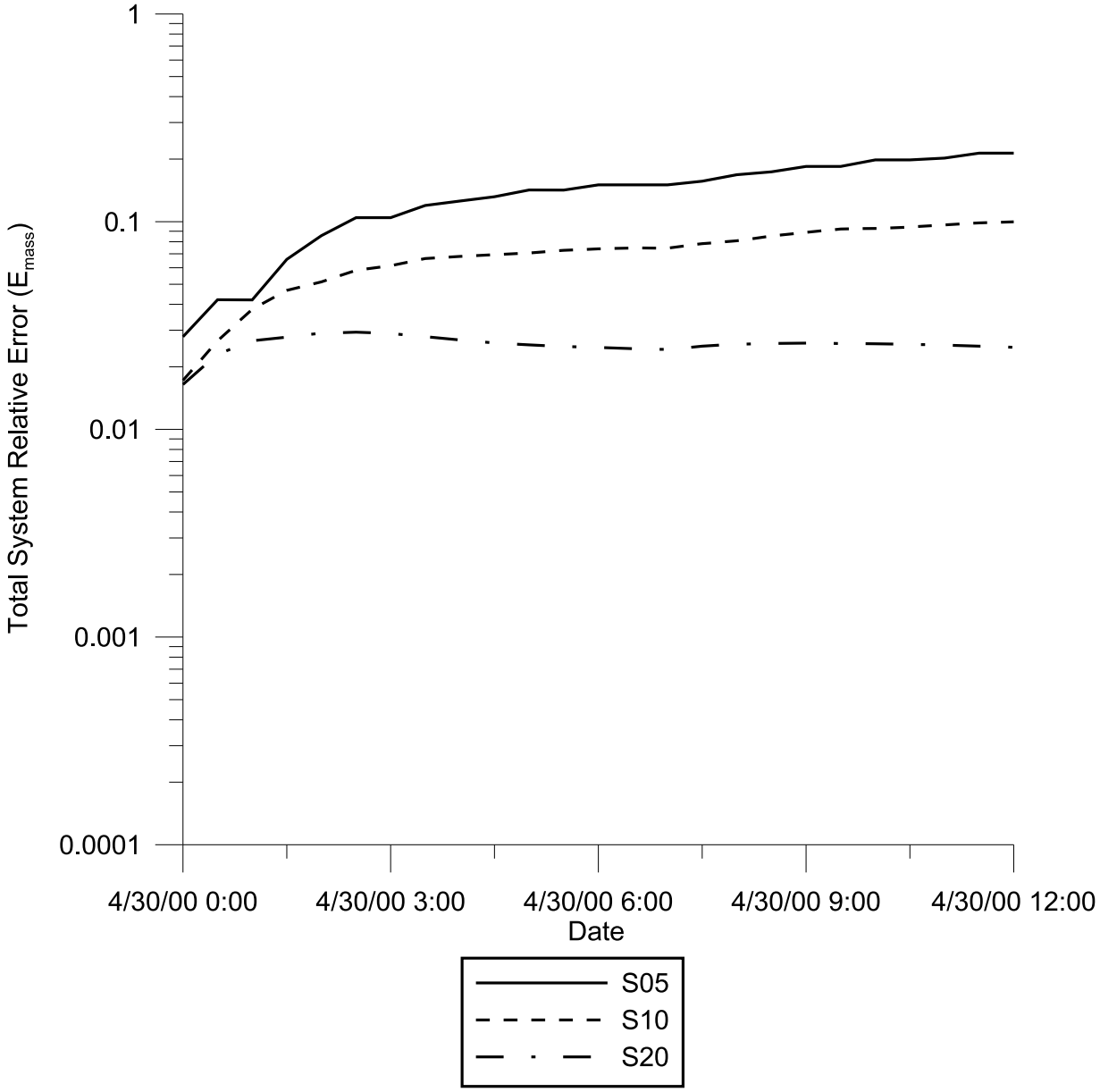

Figure 7.10: Storage routing in WatFlood - Mass conservation with varied sub-grid element resolutions

7.2.11 Reservoir Considerations

The WATFLOOD hydrological model includes a set of subroutines to account for the presence of lakes and reservoirs in a watershed. The Canagagigue Creek model (see Chapter 5) contains a reservoir at the centre of the watershed behind the Woolwich Dam. The WATFLOOD model simulates reservoirs but does not necessarily take explicit account of storage within the reservoirs, and relies on release data to dictate dam discharge in the Canagagigue Creek case. In this contaminant transport sub-model, contaminants were routed through the reservoirs using the QUICKEST scheme. However, because the hydraulic data provided by the WATFLOOD model is not reliable for reservoirs some variables require forcing in the QUICKEST model. The storage is set to an arbitrarily high value for each reservoir grid ($1x10^6$ m^3), and the dispersion value is fixed to zero throughout the grid to maintain stability due to the very small velocities. For the sediment transport routine the sediment carrying capacity is forced to zero for the reservoir allowing for the settling of sediment, but no resuspension of the sediments. Accurate modelling of reservoirs will require some adjustment to the WATFLOOD model to more accurately model storage. A more accurate reservoir contaminant transport model is a recommended future development.

7.2.12 Performance Benchmarking

In addition to the examination of the accuracy of the routine an assessment of the computational expense was also desirable. Consequently both the QUICKEST and Storage routing routines were benchmarked for performance within the WATFLOOD basin. The same point instantaneous injection was performed as above. Tests were run on an Intel® T2300 1.67GHz processor. Table 7.1 outlines the time taken for the Canagagigue Model to run for a 68 day simulation with different contaminant transport models and different sub-grid resolutions. The WATFLOOD model on its own required 40 seconds to run. The WATFLOOD model was then run with solute data management enabled, which was the handling routine that updated solutes from time step to time step, calculated grid totals and other statistical data. As these processes were performed in all simulations and were not directly related to the algorithm performance it was important to separate the time

commitment for these processes in the model runs. Finally the simulation was run for the full QUICKEST and Storage routing algorithms. Table 7.1 clearly shows the improved performance of the QUICKEST model over the storage routing algorithm with the storage routing algorithm taking more than 7 times as long to run. If the processing time taken for WatFlood and data management are removed from the calculation the QUICKEST algorithm is over 10 times more efficient than the storage routing algorithm. Figure 7.11 illustrates the increase in computation time dedicated to the algorithm solution for the QUICKEST and Storage routing routines as the sub-grid resolution increases. The increase is approximately a factor of 4 for every doubling of grid size, which follows from a doubling of the number of computation elements and a doubling of the number of time steps required for stability. The difference between the QUICKEST algorithm and the Storage routing algorithm is a factor of 10 in favour of the QUICKEST algorithm within the WatFlood at all sub-grid resolutions.

Elements per Grid	**WatFlood**	**WatFlood with Data Management**	**QUICKEST**	**STORAGE**
5	40	54	67	243
10	40	75	150	833
20	40	168	448	3 185

Table 7.1: Contaminant Transport Routine Performance - Simulation Time by Routine and sub-grid resolution (seconds)

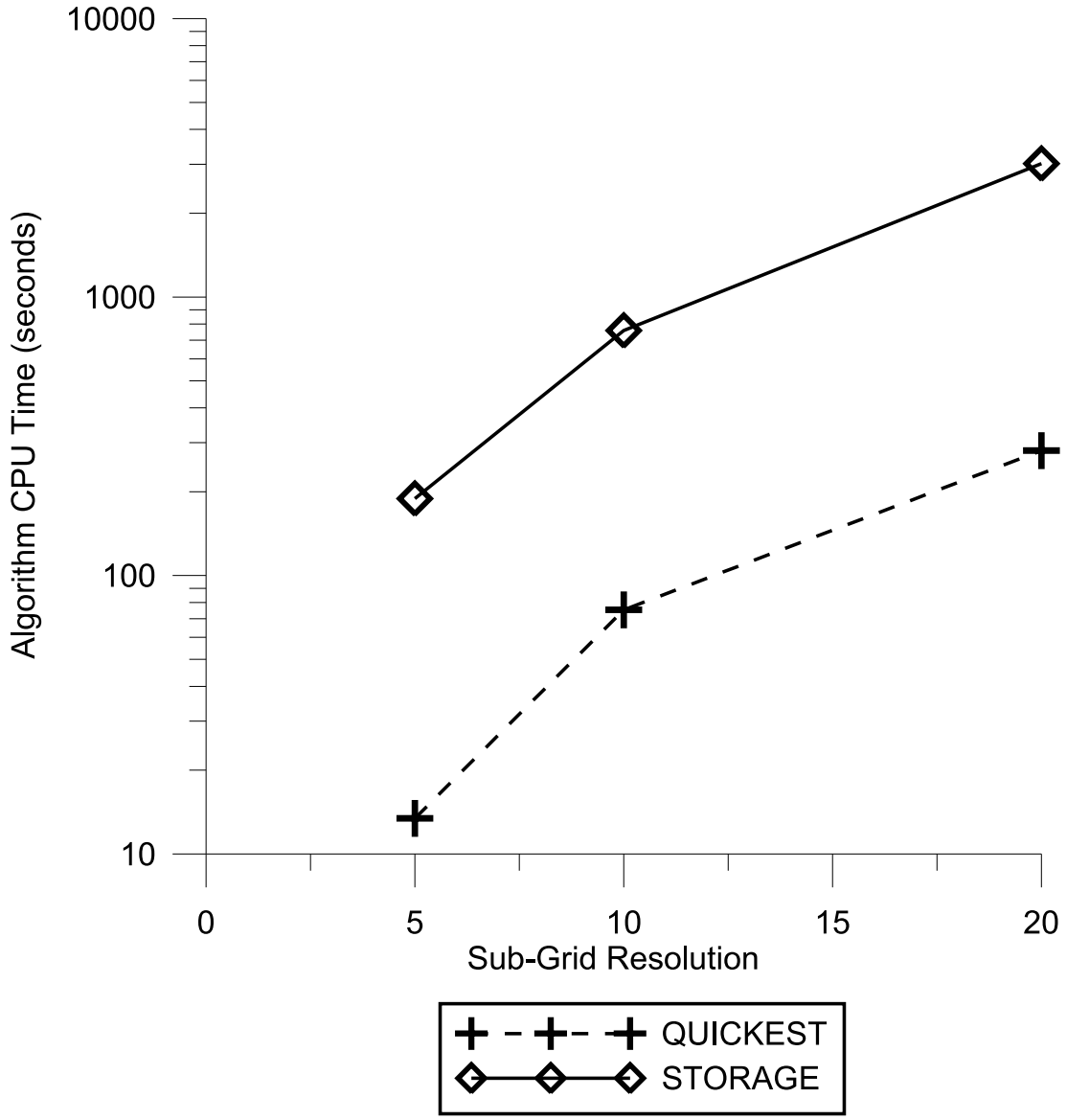

Figure 7.11: Algorithm Performace Based on Grid Resolution

7.3 Riparian Contaminant Transport

The riparian wetlands that are coupled with the main channel in WATFLOOD required representation in the SOLROUTE water quality transport model. A similar discretization approach was taken with riparian wetland segmentation as was taken with the channel discretization in that the channel length was divided into elemental segments. The relationship between the channel sub-grid elements and the riparian wetland sub-grid elements are presented in Figure 7.12.

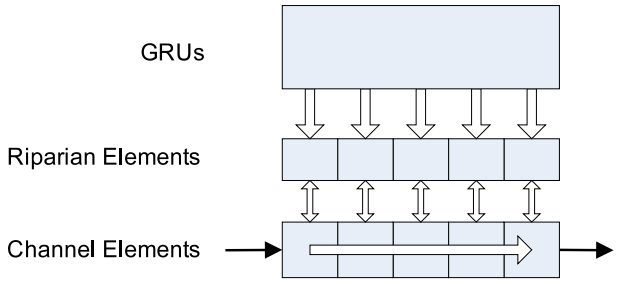

Figure 7.12: Riparian Sub-Grid Elements Schematic

Riparian wetland zones, if defined for a grid, assigned the same number of sub-grid elements as the adjoining channel. No flow between the riparian elements is permitted and the transport into and out of each riparian sub-grid element is with adjacent channel element. Riparian elements may, however, have contaminant loading from the GRU that contributes to the stream. Loading from the GRUs to the riparian elements is one way, and loading is averaged equally over all riparian elements (although it can be adjusted using the model interface code).

Solute transport calculations between the channel and riparian elements are modelled using advective and dispersive processes between the elements. The advective flux is determined if the flow rate between the riparian zone and the channel is known, which is the case with the WATFLOOD model.

$$\frac{\partial M_{rip}}{\partial t} = \begin{cases} Q_{wl}\phi_{chan} & \text{if } Q_{wl} > 0 \\ Q_{wl}\phi_{rip} & \text{if } Q_{wl} \leq 0 \end{cases} \tag{7.15}$$

where $\frac{\partial M_{rip}}{\partial t}$ is the rate of change in the solute mass in the riparian zone, Q_{wl} is the flow between the channel and the riparian element (where flow to the riparian zone is positive), ϕ_{chan} is the concentration of the solute in the channel and ϕ_{rip} is the concentration of the contaminant within the wetland pore water. Concentrations and mass within the riparian wetland element are updated with changes in the storage of the element as per (7.12). The riparian storage is provided by the hydrological input to the model.

A dispersive model was also included in the riparian transport model, which allowed the contaminants to disperse or exchange between riparian zone to the channel without any net flow between the two regions. The dispersive transport between the riparian and channel regions was accomplished using a standard dispersion equation

$$\frac{\partial M_{rip}}{\partial t} = A_{rip} K_{rip} \frac{\partial \phi}{\partial x} \tag{7.16}$$

where the spatial gradient represents the changes in concentration across the riparian-channel interface, K_{rip} is a dispersion constant, and A_{rip} is the effective area connecting the channel to the riparian zone. Considering the temporal change in concentration in the riparian zone as a reference for (7.16) and that the spatial dimension is not fully qualified in this model the equation is rearranged

$$\frac{\partial M_{rip}}{\partial t} = A_{rip} K'_{rip} \left(\phi_{chan} - \phi_{rip}\right) \tag{7.17}$$

where K'_{rip} represents a new calibration constant which is a combination of the dispersion constant and the effective spatial dimension linking the riparian zone and the channel. The interface area is calculated based on provided depth information from the hydrological model. In this case the area is defined as the product of the length of the channel for the element and the minimum of the riparian and channel depths. This is illustrated graphically in Figure 7.13.

The riparian transport coupling of (7.15) and (7.17) with the channel was simulated using a modular computational step after the routing algorithm step had completed. The solution to the equations' concentration changes were calculated with a 4^{th}-order Runge-Kutta formulation (Press et al., 1992).

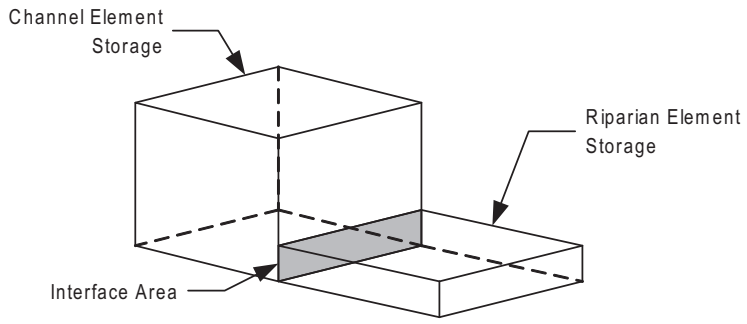

Figure 7.13: Riparian-Channel Diffusion Computational Area

To maintain positive concentrations in the riparian zones an additional limiting function was applied to the contaminant transport within the riparian transport model. The in-channel transport is currently not restricted from obtaining negative concentrations. This is a rare occurrence with natural dispersion in the channels. However, to prevent negative oscillations generated from the QUICKEST algorithm at the sharp front of an advective wave from contributing negative concentrations to the riparian zone the storage in the riparian zones is forced to positive values. That is, the flux from the creek is limited to result in a non-negative value in the riparian zone elements.

To assess the effects of the riparian sub-model, a riparian exchange unit test was conducted and the results are shown in Figure 7.14. This figure compares the routing of a point addition of a contaminant at a downstream distance of 200 (arbitrary units) and the contaminant was transported downstream with and without riparian exchange. For the riparian exchange scenario the riparian storage was set to 10% of the channel storage with a riparian-channel dispersion coefficient of 0.5 m/s. The effect of riparian exchange is clearly evidenced with the exchange producing a contaminant tail and reduced peak concentration. The riparian exchange routine showed similar mass conservation to the QUICKEST routine without riparian zone coupling.

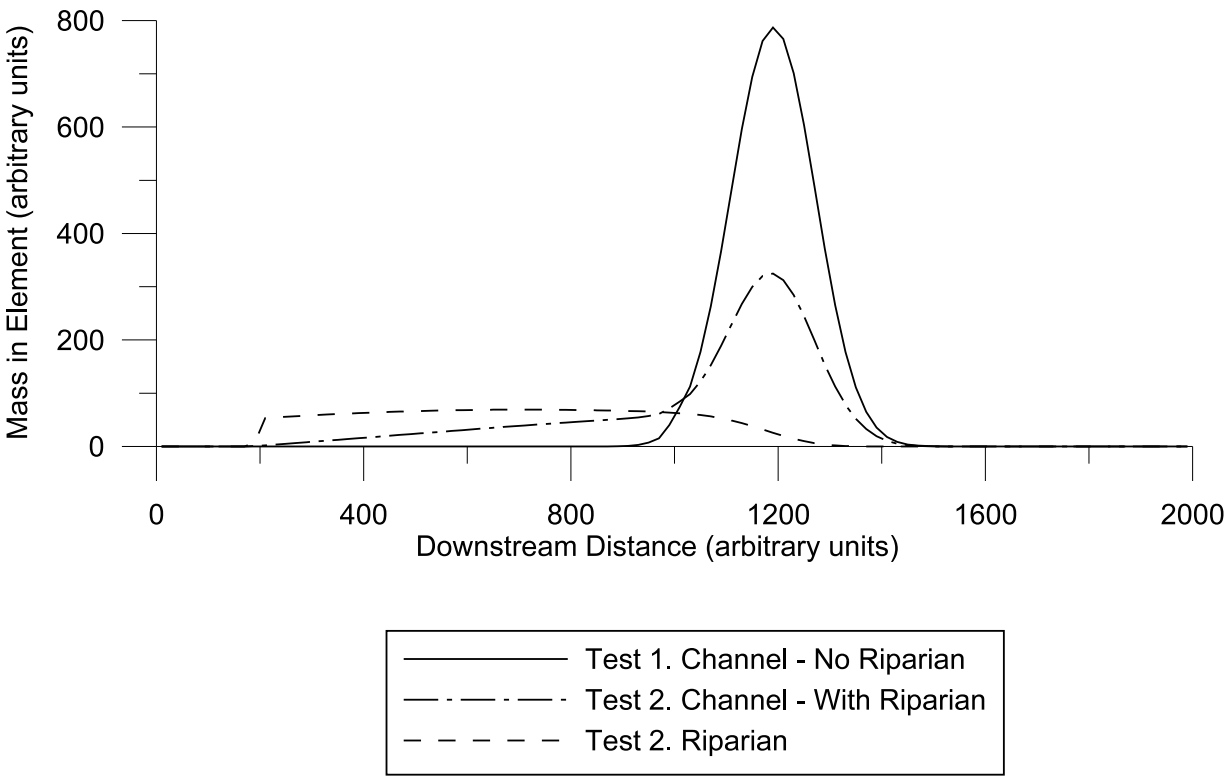

Figure 7.14: Riparian-Channel Exchange Test

7.4 In-Stream Water Quality Modelling

The WATFLOOD/AGNPS model included some accounting for species fate within the stream corridor. The approach outlined in Leon (1999) was a decay or depositional approach for all transported constituents. Specifically, each grid channel a mass balance was conducted over a time step.

$$M_{out} = M_{in} + M_{store} - M_{dec} \tag{7.18}$$

where M_{out} is the mass leaving the grid channel, M_{in} is the mass entering the channel from all sources over the time step, M_{store} is the mass in storage during the time step and M_{dec} is the mass that decayed or was deposited on the stream bed during the time step. Mass depletion or removal was calculated as a fraction of the total mass in the grid channel

$$M_{dec} = K_{ag} \left(M_{in} + M_{store} \right) \tag{7.19}$$

where K_{ag} is a decay coefficient (value between 0 and 1) that applies to a particular constituent at the watershed scale. Combining (7.18) with (7.19) provides the in-stream water quality conservation equation employed in the existing WATFLOOD/AGNPS model for each of the modelled constituents (suspended solids, nitrogen, and phosphorus)

$$M_{out} = (1 - K_{ag}) \left(M_{in} + M_{store} \right) \tag{7.20}$$

where the total mass leaving is linearly related to the sum of the total mass entering the grid and the mass stored in the grid.

In the original development of the WATFLOOD/AGNPS model a general need for improvement of in-stream processes was identified (Leon, 1999). One of the primary concerns discovered in this study with the WATFLOOD/AGNPS in-stream sub-model is that there is no capacity for sediment resuspension or sourcing from the stream bed. This is a considered a significant deficiency in the model with regard to the Canagagigue Creek watershed study. Modelling and physical observations both show very few occurrences of overland flow during the study period as outlined in Chapters 4 and 5. Other studies in the Canagagigue

Creek have shown similar observations of very little overland flow (Dorner et al., 2006). However, significant sediment loading was clearly observed in the study site, even during small events (see Chapter 6). As the soil loss equation for the land surface is predicated on overland flow, not having any sediments sourced from the channel limits the ability of the model to simulate the observed data and would underestimate sediment loading.

Additionally, although the introduction of a decay coefficient is valid and has been employed by a number of models (USACE, 1995; Woolhiser et al., 1990; Neitsch et al., 2001; Chapra et al., 2007), the approach outlined above has weaknesses. In the WatFlood/AGNPS approach the deposition rate constant is not a function of the time step, with the consequence being that the same mass fraction will be deposited regardless of the size of the time step taken. If the time step in the WatFlood model were fixed then the time step size would be implicit in the value of K_{ag} in (7.19). However, as identified in Chapter 7, the WatFlood model scales the time step inversely with the velocity in the channel to maintain a stable Courant condition, and the time step itself can be forced to have an arbitrarily finer temporal resolution if necessary. A direct consequence for the stream decay model is that during high flow conditions the time step frequency will increase and consequently a greater fraction of the constituents will settle or decay. This is the opposite effect one would expect to see in most fluvial environments.

The above issue relating to time step problems for sediment deposition was partially resolved by Dorner (2004) through the addition of a time step duration term in (7.19) effectively converting it to a first order decay equation. Sediment was removed through an estimate of a settling velocity shown in (7.21)

$$v_s = 0.033634\alpha(\rho_s - \rho)d_s^2 \tag{7.21}$$

where v_s is the settling velocity ($m\,d^{-1}$), α is a dimensionless shape factor (1 representing a perfect sphere), ρ_s and ρ are the densities of the sediment particles and the medium, respectively ($g\,cm^{-3}$)and d_s is the diameter of the sediment particle (μm). If a depth of water can be estimated then the removal rate can be approximated by dividing the settling velocity by the height of the water column (Chapra, 1997)

$$K_s = \frac{v_s}{h} \tag{7.22}$$

where K_s is the settling rate and h is the height of the stream or water column.

The lack of sediment resuspension simulation was not resolved and remained a modelling issue in the study conducted as resuspension of sediments from the stream bed was suspected to be a major contributor to in-stream microbial concentrations (Dorner et al., 2006). An additional limitation is that no riparian zone considerations are included in the existing model as the development of the AGNPS sub-model pre-dated the introduction of the wetland sub-routines in the WATFLOOD hydrological model.

7.5 Reactive Transport Calculations

Integrating the reactive transport calculations into the SOLROUTE contaminant transport models required coupling of the transport and reactive fate models. Reactive transport calculations were implemented into the QUICKEST finite volume routine to allow for mass addition and removal based on specified physical processes in the channel and riparian wetland elements relating to sediment and nitrate.

The reactive source and sink functions were abstracted from the contaminant transport QUICKEST routine to allow for flexibility in implementation and computational sequence. Several approaches to integrating the source-sink processes with the transport processes were considered. A global implicit approach is considered the most accurate, with transport and reactive processes being solved simultaneously in a time-step but considering the explicit nature of the transport algorithm, a global implicit approach was infeasible and discounted. Two implicit approaches were considered for the reactive calculation routine: a sequential non-iterative approach SNIA originally conceived by Yanenko (1971), and the Strang-splitting approach (Strang, 1968). A sequential iterative approach (SIA) also known as the iterative split operator (ISO) approach, which solves the transport and reactive components iteratively was also considered. Steefel and MacQuarrie (1996) showed that the SIA approach can provide results as accurate as a completely coupled system in multicomponent modelling in porous media, but suffers from the added computational

cost of multiple iterations. The SIA approach was only considered if the non-iterative approaches provided inaccurate results.

The SNIA approach involves a splitting of the reactive transport problem into two separate computational steps. First the constituents are transported for the full time step and then the constituents are reacted over the full time step. This method is also called the fully implicit method or the method of fractional steps (Yanenko, 1971) and benefits from being easy to implement, but can show inaccuracies for larger time-steps as the two processes which in fact occur at the same time are processed independently. The computational sequence for the SNIA is shown in (7.23).

$$\begin{aligned} \frac{\left(\phi_i^* - \phi_i^n\right)}{\Delta t} &= L(\phi_i)^n \\ \frac{\left(\phi_i^{n+1} - \phi_i^*\right)}{\Delta t} &= R(\phi_i) \end{aligned} \tag{7.23}$$

where ϕ is the constituent concentration, the n superscript represents the time step increment and the superscript $*$ represents an intermediate computational step and Δt is the time step. L represents a transport operator and R represents a reactive operator.

The Strang-Splitting approach is a slight modification to the SNIA approach but in three steps where the transport equations are solved at a half time step, the reaction equations are solved at the full time step, and the transport equations are solved again at the half time step (Strang, 1968) and illustrated in (7.24).

$$\begin{aligned} \frac{\left(\phi_i^* - \phi_i^n\right)}{\Delta t/2} &= L(\phi_i)^n \\ \frac{\left(\phi_i^{**} - \phi_i^*\right)}{\Delta t} &= R_i(\phi_i) \\ \frac{\left(\phi_i^{n+1} - \phi_i^{**}\right)}{\Delta t/2} &= L(\phi_i)^{**} \end{aligned} \tag{7.24}$$

where the defined variables are the same as for (7.23) and the superscript value $**$ represents a second intermediate computational step. The SIA approach has shown to greatly increase computational expense and can result in instabilities under certain situations (Steefel and

MacQuarrie, 1996). Considering the reasonable accuracy of the model (described below) the SNIA approach was implemented and the extra computational expense associated with the SIA ruled it out for this stage of the model development.

The analysis of the implemented rate equations typically involved a first-order removal equation, or similar formulation. The dimensionless decay coefficient (7.25) was used in reporting of model performance in the test framework and used in this chapter

$$\lambda = K_1 \Delta t \tag{7.25}$$

where λ is the dimensionless decay coefficient, K_1 is the first order decay or removal rate $[T^{-1}]$ and Δt is the computational time step $[T]$.

7.6 Suspended Sediment Transport Calculations

To account for the important process of deposition and resuspension in the contaminant transport model a new approach was required to that identified in Section 7.4. The goal was to introduce a physically-based process model that would account for sediment deposition and resuspension based on the velocity and flow state-variables provided by the WATFLOOD model. Some approaches to in-channel sediment transport are discussed below along with the selected formulation for this model development.

The KINEROS2 model is a runoff and erosion model (Woolhiser et al., 1990) which for in-channel sediment transport employs a stream-power and sediment transport equilibrium approach to determining the transport capacity

$$\frac{\partial \phi_{sed}}{\partial t} = \frac{e_c}{A} = c_g(\phi_{sed\_max} - \phi_{sed}) \tag{7.26}$$

where ϕ_{sed} is the concentration of the suspended sediment in the water column element, e_c is the erosion rate per unit length of channel $[ML^{-1}T^{-1}]$, c_g is a calibrated or estimated parameter $[T^{-1}]$, ϕ_{sed_max} is the maximum transportable concentration of solids in the channel, ϕ_{sed} is the actual transported concentration in the channel and A is the cross sectional area of flow. The maximum estimated value for c_g is the settling velocity (v_s)

divided by the water height (h). The settling velocity is estimated as the terminal velocity for a sphere in water of a specified diameter d. The erosion rate can be positive or negative depending on the concentration of sediment in the stream relative to the maximum carrying capacity.

The maximum channel concentration in KINEROS2 is estimated using (7.27)

$$\phi_{sed\_max} = \frac{0.05}{d_s \left(\gamma_s - 1\right)^2} \sqrt{\frac{Sh}{g}} \left(\Omega - \Omega_c\right) \tag{7.27}$$

where d_s is the particle diameter, γ_s is the particle specific gravity, S is the water surface slope, h is the water depth and Ω is the stream power which is the product of the mean channel velocity and the water surface slope US. KINEROS2 also employs a minimum stream power required before sediment suspension takes place Ω_c which is estimated at 0.004. With the explicit identification of the sediment diameter in (7.27) the KINEROS2 model allows for the simulation of a number of independent sediment sizes.

The SWAT model (Neitsch et al., 2001) solves the in-channel sediment transport problem in a similar manner to KINEROS but more parametric approach in-stream sediment transport which was adapted after Arnold et al. (1995) and involves a simplified stream-power approach. The rate at which suspended sediment is deposited from the water column or re-entrained into the water column from the channel is determined by a first order rate equation related to the difference between the sediment carrying capacity concentration in the stream and the actual concentration within the stream.

$$\frac{\partial \phi_{sed}}{\partial t} = \begin{cases} -K_{sed\_dep} \left(\phi_{sed\_max} - \phi_{sed}\right) & \text{if } \phi_{sed} \geq \phi_{sed\_max} \\ K_{sed\_res} C_{ch\_er} \left(\phi_{sed} - \phi_{sed\_max}\right) & \text{if } \phi_{sed} < \phi_{sed\_max} \end{cases} \tag{7.28}$$

where ϕ_{sed} is the concentration of the suspended sediment in the water column element, K_{sed_dep} is the sediment deposition rate constant, K_{sed_res} is a resuspension rate constant and C_{ch_er} is a channel erodibility factor. The relationship in (7.28) is identical to (7.26) except that the suspension and deposition rate constants in (7.28) differ depending on the direction of the sediment movement.

The maximum transported stream concentration is estimated using (7.29)

$$\phi_{sed\_max} = C_{sed} u^{K_{sed}} \tag{7.29}$$

where ϕ_{sed_max} is the maximum sediment concentration that can be carried by the stream, u is the stream velocity and C_{sed} and K_{sed} are fitted parameters with K_{sed} generally having a value between 1.0 and 2.0 (Neitsch et al., 2001). The SWAT modelling approach is more generic in that the suspended sediment diameters are not explicitly stated and the reported values represent a total suspended solids estimate. That is the calibration parameters have an implicit association with the particle diameters, settling rates and densities, etc.

Selected Modelling Approach

In this modelling study a stream-power in-channel sediment transport approach was taken, as the parameterization shown in the KINEROS2 and SWAT models is in line with the data types collected or modelled in this study. Of the approaches reviewed a combination of approaches was adopted. No measurement of sediment sizes distributions in collected TSS samples were conducted. As such a discrete sediment distribution modelling approach could not be used. Rather suspended solids were modelled as a single lumped constituent. Instead of employing a generic deposition and resuspension rate constant, estimates of the settling velocity (v_{sed_dep}) and resuspension velocity (v_{sed_res}) were employed. In this way the values for resuspension rates could be physically estimated. The actual rate constant would then be calculated based on the stream depth calculated in the WATFLOOD hydrological model using (7.22). The KINEROS2 approach is certainly more physically-based and rigorous approach than that of the SWAT model, but would require more data to properly assess its performance. Investigating the applicability of the KINEROS2 approach in SOLROUTE is recommended as a future endeavour.

The stream-power sediment transport and deposition routine was added to the SOLROUTE modelling framework as a modular set of functions that can act on any particular solute index in the framework. Calibration parameters are stored in a water quality parameter (WQP) file and each WATFLOOD river class is assigned its own set of five sediment

parameters ($C_{sed}, K_{sed}, v_{sed\_dep}, v_{sed\_res}, C_{ch\_er}$). Stream flow, average velocity and channel storage are supplied from the WATFLOOD model for each time step. An Euler approach was used to calculated the change in concentration within a grid element at each time step according to the following

$$\phi_{sed}^{n+1} = \begin{cases} \phi_{sed}^{n} + K_{sed\_res} C_{ch\_er} (\phi_{sed\_max}^{n} - \phi_{sed}^{n}) \Delta t & \text{if } \phi_{sed\_max}^{n} < \phi_{sed}^{n} \\ \phi_{sed}^{n} + K_{sed\_dep} (\phi_{sed\_max}^{n} - \phi_{sed}^{n}) \Delta t & \text{if } \phi_{sed\_max}^{n} \geq \phi_{sed}^{n} \end{cases} \tag{7.30}$$

$$K_{sed\_res} = \frac{v_{sed\_res}}{h} \tag{7.31}$$

$$K_{sed\_dep} = \frac{v_{sed\_dep}}{h} \tag{7.32}$$

where K_{sed_res} and K_{sed_dep} are the resuspension and deposition rate constants respectively, v_{sed_res} and v_{sed_dep} are the resuspension and deposition velocities respectively, h is the water depth in the channel, ϕ_{sed} is the sediment concentration with superscripts denoting time steps. The max concentration, ϕ_{sec_max} is calculated directly by (7.29) using the direct velocity from WATFLOOD for the time step.

There is no accounting in the SOLURUTE code for quantities suspended or deposited on the stream bed in this version of the model. Sources are considered available at all times and, as mentioned above, the deposition and resuspension is not translated to any morphological change in the stream geometry. Additionally flood plain and main channel deposition and resuspension is not distinguished in this version of the model.

The performance of the in-channel sediment transport model is presented in Appendix D, Section D.3. The simulation illustrates the routines ability to accurately simulate analytical solution in the test framework and its tendency for convergence to the analytical solution with reduction in grid element size.

7.6.1 Solute Decay Equations

First order decay was integrated into the SOLROUTE framework by adding a modular first-order decay function that can apply to any solute index in the modelling framework.

A variety of constituents exhibit first-order rate transformations in channels, or are traditionally modelled using first-order rate equations including oxidation reactions, phosphate sorption, BOD and CBOD reduction and various nitrate transformation processes (USACE, 1995), and the incorporation of a generic first order transformation routine was similarly desirable in the SOLROUTE framework, particularly for modelling nitrate transformations.

Integration with SOLROUTE

The decay equation 7.33 was implemented for both the riparian and channel elements in the SOLROUTE model. The approach was similar to (7.30) in that a single step Euler solution was employed to calculate solute losses due to 1st order decay.

$$\phi^{n+1} = \phi^n e^{-K_{dec}\Delta t} \tag{7.33}$$

where ϕ^{n+1} is the concentration transformation Δt is the time step ϕ^n is the concentration prior to transformation and K_{dec} is a first order decay coefficient. K_{dec} can be a function of a number of other state variables including other constituent concentrations or physical conditions such as temperature. The values prescribed for K are maintained in the water quality parameter file by defined river class.

The performance of the in-stream decay procedure in a test framework and in the WatFlood model is presented in Appendix D, Section D.4. Here the procedure shows a degree mass conservation comparable to the QUICKEST avection-dispersion routine both in the test framework and integrated into the WatFlood model, and an ability to accurately simulate the analytical solutions to the advection-dispersion equation with decay in a test framework.

7.7 Riparian Wetland - Channel Constituent Load Partitioning

Sediment and nutrient loads from the GRUs to the receiving waters may or may not pass through a riparian wetland, depending on the configuration of wetlands in the watershed. For the WATFLOOD model the presence or absence of the riparian wetland is uniform along the channel. That is, if a riparian wetland exists within a GRU then the riparian wetland exists along the whole channel. It's "size" is dictated by its areal extent and its storage parameters (see Section 5.4).

Riparian wetland protection in a basin was determined on a grid by grid basis. That is, for each grid with riparian wetlands the channel coast was examined and the fraction of the channel coast that was protected by riparian wetlands was determined. This procedure is illustrated in Figure 7.15. The extent of a single WATFLOOD grid is shown with the riparian wetlands shown and the river network channels also included. Added is a calculated 10 meter buffer around the river network which was designated as the minimum acceptable riparian wetland cover to be considered in Section 3.2. This length selection was arbitrary, but this distance was chosen was identified as a minimum riparian buffer size by some authors (US-EPA, 2005). The extent of riparian cover (R_C) was calculated by determining length of the main channel in each grid, doubling that length to determine the total coastal channel extent and then determining the fraction of that coastal length that is protected by 10 m or more of riparian wetland. In Figure 7.15 the WATFLOOD grid had 1060 m of channel length with 56% of the channel length protected by riparian wetlands.

Constituent loading in this model is abstracted from the WATFLOOD hydrology for the purposes of contributions to wetlands and the channel. Whereas the WATFLOOD model is coded to contribute all water from the GRUs in a grid to the riparian wetland, the water quality model will load constituents proportionally to the degree of riparian wetland cover within the grid. Employing Figure 3.2 as an example, 56% of the nutrient and sediment load from the upland areas will be contributed to the riparian wetland, and the balance will be discharged directly into the channel. The dimensions of the riparian wetland are determined by using the area of the riparian wetland and the fraction of the coastal area

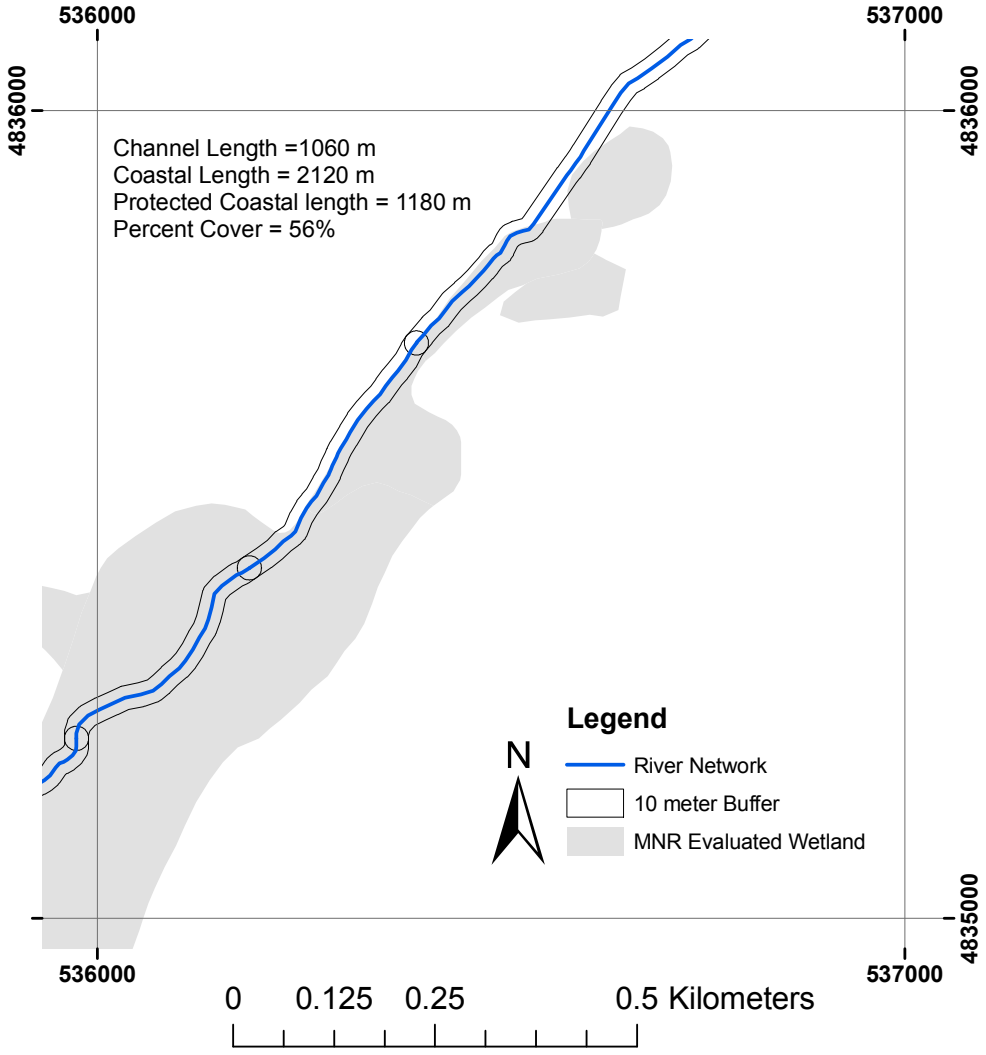

Figure 7.15: Riparian Wetland Cover Calculation - Sample WatFlood Grid

protected. The average distance from the upstream channel is then the area of the riparian wetlands divided by the protected coastal area. Although not an ideal approach, as some areas within a grid may have much thinner cover than others, it is considered reasonable considering the other large-scale hydrological assumptions relating to riparian wetland connectivity. The riparian cover is stored in a gridded format in a the riparian definition file (RIP) in Appendix D.

The dimensions of the riparian wetland are assumed based on the provided area of the riparian wetland in the WATFLOOD input file and the extent of riparian protection using the following equation

$$W_{wet} = \frac{A_{wet}}{2R_C L_C} \tag{7.34}$$

where W_{wet} is the average riparian wetland width, or distance from the contributing GRU to the receiving channel, A_{wet} is the total riparian area in the grid, R_C is the ratio of riparian cover over the channel (1.0 being complete cover, 0.0 being no cover) and L_C is the channel length. The factor of 2 is included as the total channel coastal length is twice the channel length. A schematic of the process is presented in Figure 7.16.

Using the example outlined in Figure 3.2, the total areal extent of the riparian wetlands for that grid cell represents 15.9 % of the grid area which for this WATFLOOD grid is 1.15 km^2. The riparian wetland area is therefore approximated as 0.182 km^2. The width of the riparian wetland is calculated from (7.16) and assumed to be the mean width of 153 m over 56% of the coastal length.

7.8 Riparian Wetland Suspended Sediment Processes

Riparian wetlands are well documented as effective agents for the removal of suspended sediments from overland sources and can protect receiving waters from suspended sediment pollution (see Section 2.3). This is accounted for by the several important properties of the riparian wetlands, namely milder slopes and increased vegetation roughness that act to reduce overland flow velocities and turbulence and allow for sediment deposition.

Several existing water quality models have taken approaches to estimating the potential

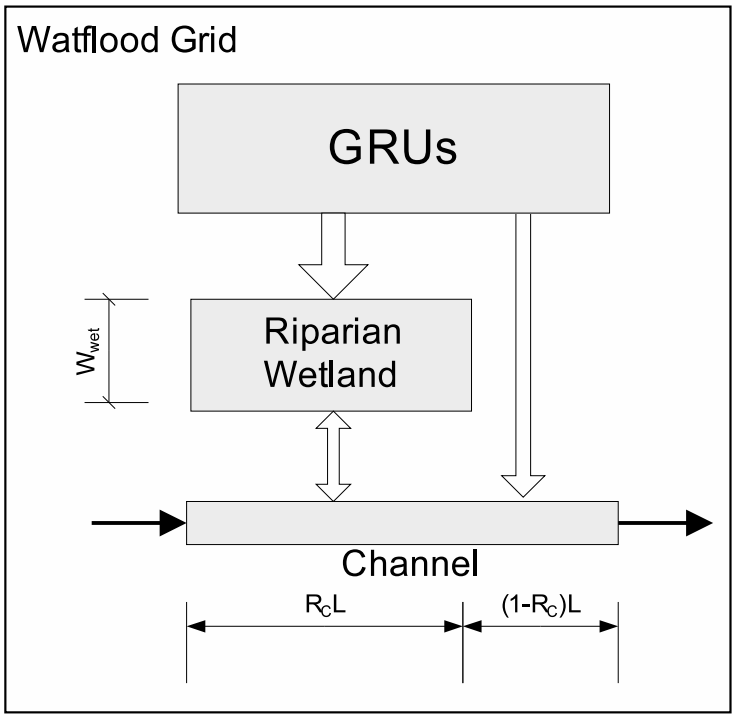

Figure 7.16: Riparian Width Calculation Schematic

impacts of riparian buffer zones on water quality as related to suspended sediment. The SWAT model employs a "filter strip" model, which employs a removal efficiency based on the length of the filter strip for sediment, nutrients and bacteria loading (Neitsch et al., 2001)

$$\frac{\phi}{\phi_0} = 0.367 \left(w_{fs}\right)^{0.2967} \tag{7.35}$$

where ϕ are ϕ_0 are the final and initial concentrations of the constituent, respectively, and w_{fs} is the width of the filter strip in meters.

Work by Liu et al. (2008) adapted the sediment removal processes of water bodies as modelled in the SWAT model and applied the same processes to simulate riparian wetlands sediment removal efficiency. This approach employs a static, user-specified equilibrium concentration for the water body (riparian wetland) and the quantity of sediment leaving is calculated using a first-order decay equation

$$\phi_{sed}^{n+1} = \begin{cases} \left(\phi_{sed}^{n} - \phi_{sed\_eq}\right) e^{-k_s t d_{50}} + \phi_{sed\_eq} & \text{if } \phi_{sed}^{n} > \phi_{sed\_eq} \\ \phi_{sed}^{n} & \text{if } \phi_{sed}^{n} \leq \phi_{sed\_eq} \end{cases} \tag{7.36}$$

where ϕ_{sed_eq} is the specified equilibrium sediment concentration, ϕ_{sed} is the sediment concentration leaving the water body with the superscripts representing the (daily) time step sequence, k_s is the decay coefficient and d_{50} represents the median sediment diameter (Neitsch et al., 2001). Total sediment removal is determined through a mass-balance approach

$$M_{sed}^{n+1} - M_{sed}^{n} = (\phi_{sed}^{n+1} - \phi_{sed}^{n})\forbar{V} \tag{7.37}$$

where M_{sed} is the mass of sediment in the water body (riparian wetland) and $\forbar{V}$ is the volume of the water body. Total mass leaving the riparian wetland follows from the above as the concentration in the water body ϕ_{sed} multiplied by the flow leaving the water body into the receiving channel. This approach requires the estimation of a equilibrium concentration for each wetland as well as the settlement coefficient.

Other work by Muñoz Carpena et al. (1999); Muñoz Carpena and Parsons (2004) have

incorporated sediment depositional processes into a detailed finite difference model VFS-MOD. This model simulates the field scale hydrology of the upland areas contributing to a vegetated filter strip and the sediment loading and deposition along the filter strip. The model includes a detailed hydraulic model as well as a sediment transport and deposition routine at the field scale. The sediment deposition routine employed was developed at the University of Kentucky (Barfield et al., 1979; Hayes et al., 1979) and has since been referred to as the "University of Kentucky filter strip sedimentation model" (Muñoz Carpena et al., 1999; Abu-Zreig et al., 2001; Muñoz Carpena and Parsons, 2004). Validation of the model by Muñoz Carpena et al. (1999) and Abu-Zreig et al. (2001) indicated that the model performed well both hydrologically and as a sediment transport simulator provided channelization did not occur within the vegetated filter strips. Field studies conducted by Dosskey et al. (2002) identified that when flow does not remain distributed in vegetated filter strips but rather channelizes or concentrates it can have a significant impact on a filter strip's capacity for sediment reduction greatly influencing the effective area. Although clearly an important process, concentration of flow was not considered in this modelling effort, primarily because of the difficulty in assessing the degree of flow concentration in riparian wetlands at a watershed scale.

One of the challenges in incorporating a sediment removal routine into the WatFlood model is a lack of known, measured or otherwise approximately determined parameters that affect the influence of riparian wetlands on their ability to intercept sediment from upland sources. The density and character of the vegetation, local slopes, degree of channelization, and effective length were identified as particularly important (Muñoz Carpena et al., 1999). Although these are readily identifiable at a field scale, at the watershed scale the estimation of these parameters becomes difficult. In this research a simple parametric approach was taken to the removal of sediment loading due to the riparian wetland areas and assigned on a per-river class basis. It was decided that the approaches used in the SWAT manual for filters strips was not adequately physically based. Also, the approach taken by Liu et al. (2008) did not appear to conform with the observed physical state of the riparian wetlands. Although the riparian wetlands were often saturated they rarely were inundated so as to be called "water bodies" and did not look to behave like "ponds" or "impoundments" as

the process equations were described by Neitsch et al. (2001).

The approach taken is based on the roughness and slope of the riparian wetland. An estimation of the flow velocity is determined from a modified version of the Manning equation which relates the flow rate to the Manning's roughness value (n_R)of the riparian wetland, the slope of the riparian wetland and the depth of flow. The depth of flow is calculated based on the surface runoff flow rates provided by the WATFLOOD hydrological model. Manning's roughness values could be estimated from the literature, and the slopes employed for the wetlands were estimated from the cross sections taken at various locations within the watershed (see Section A.3). The Manning formulation takes the following form

$$Q = VA = 1.49A\frac{S^{1/2}h^{5/3}}{n_R} \tag{7.38}$$

where V is the velocity S is the energy slope which is assumed to be the wetland slope, h is the water depth, A is the cross-sectional area of flow, Q is the total flow and n_R is the defined Manning's roughness coefficient. This calculated velocity is then employed to determine the carrying sediment carrying capacity of the riparian wetland. This is the same physical principle employed in both the KINEROS2 and the VFSMOD models (Woolhiser et al., 1990; Muñoz Carpena and Parsons, 2004, 2005).

The physical deposition was modelled in the same way as the in-stream sediment deposition was, namely using parameters to specify the carrying capacity rating curve for the sediment and a deposition or settling rate constant as illustrated in (7.29) and (7.30). No resuspension was assumed in the riparian wetlands for this model.

This approach, although not as physically rigorous as VFSMOD in particular, provides an opportunity to evaluate the effectiveness and sensitivity of riparian wetlands at removing sediments within the modelling framework. This approach is more physically-based than (7.35) and depends on the calculated velocities, but makes assumptions that the impact of the riparian wetland is uniform for all river classes, that the sedimentation rate is uniform for all storm intensities and vegetation types and seasons for a particular river class.

The riparian wetland sediment removal processes were integrated with the existing hydrological and water quality model by linking to a number of state variables provided by the model. The sediment concentration in the runoff flow is provided by the sediment

transport sub-model. The volume of the surface runoff is also provided by the WATFLOOD model, thereby providing a total contaminant flux. For each grid the flux is apportioned proportionally to the riparian wetlands and the channel based on the degree of riparian cover (R_C) in each grid for each time-step. The degree of removal is based on the instantaneous deposition rate. The deposition rate is calculated using sediment carrying capacity and the sedimentation rate or settling velocity for the riparian wetland. The slope and roughness of the wetland are defined as wetland parameters. The depth of the overland flow is determined by the quantity of overland flow contributed to the riparian wetland Q from all contributing GRU land classes, and considering that the total cross sectional area can be defined

$$A_{of} = 2L_C R_C h \tag{7.39}$$

with the value of h solved from (7.39) and (7.38), the velocity is determined based on the Manning equation described in (7.38). The calculation is performed on a single-element basis for the entire riparian wetland area for the grid. That is, there is no explicit discretization within the riparian wetland. The approach taken for sediment removal is similar to that employed by (Liu et al., 2008) and (Neitsch et al., 2001) in determining removal rates for filter strips and impoundments. A steady state assumption is made over the riparian wetland and the removal rate is based on the theoretical travel time between the edge of the GRU and the channel based on the calculated overland velocity. With the hydraulic characteristics of the flow provided by (7.39) and (7.38), the mean travel time is assumed to be the mean riparian wetland width divided by the velocity. The removal rate is then determined through the sediment settling rate parameters. The full removal rate equation for riparian wetlands is then defined as

$$\phi_{exit} = \begin{cases} \phi_{max} + (\phi - \phi_{max})\, e^{-K_d \frac{W}{V}} & \text{if } \phi > \phi_{max} \\ \phi & \text{if } \phi \leq \phi_{max} \end{cases} \tag{7.40}$$

where ϕ_{exit} is the concentration of the suspended sediment leaving the wetland, ϕ_{max} is the maximum sediment carrying capacity based on the flow conditions and the sediment suspension parameters, ϕ is the flow weighted average concentration of the sediment in the

flow from the contributing upland GRUs. K_d is the sediment deposition rate constant, W is the calculated riparian width or distance to the channel from the GRU, and V is the calculated flow velocity. As discussed above, there is no capacity for resuspension of the trapped sediments in this version of the model. The result of equation (7.40) is a variable sediment removal rate equation based on the instantaneous flow velocity, riparian wetland width and sediment settling properties.

7.9 Riparian Wetland Nitrate Processes

Several approaches have been taken when modelling the impacts of riparian wetlands on nitrogen species. As outlined in Section 2.3.3, the modelling approaches have varied from first-order decay models such as that described by Crumpton (2001), to complete carbon-nitrogen models that include both carbon and nitrogen species cycling within the model, as well as litter decay, seasonal plant uptake, etc. in REMM (Inamdar et al., 1999b).

In this modelling effort a fully integrated carbon-cycling model was not considered an ideal integration alternative, considering many of the required input parameters are not considered in the WatFlood/AGNPS modelling framework, and the REMM model in particular is dedicated to field scale analysis. Additionally, riparian wetlands are expected to cycle nitrogen through groundwater uptake during plant growth and mineralization of nitrogen thorough decay of litter and other organic material. These processes were not considered at this stage of model development and a simpler model was considered for assessment.

A watershed scale riparian wetland treatment model as described by Crumpton (2001) was employed to describe the reduction of nitrate concentrations in a riparian wetland using a first-order aerial decay equation shown in (7.41)

$$J = k'_{20} C \theta_T^{(T-20)} \tag{7.41}$$

where J is the nitrate loss rate $[ML^{-2}T^{-1}]$, k'_{20} is the areal decay rate $[LT^{-1}]$ C is the nitrate concentration $[ML^{-3}]$, θ_T is the rate correction constant, and T is the temperature $[^{\circ}C]$. No nitrate formation was considered in nitrate reduction model (Crumpton, 2001).

The incorporation of (7.41) into the riparian water quality model was similar to the original equation except that instead of an areal nitrate reduction, the estimate of the stored volume in the riparian wetlands as provided by the WATFLOOD model was used and through integration over time (7.41) becomes

$$\frac{\phi}{\phi_0} = e^{k_{20}\theta^{(T-20)}t} \tag{7.42}$$

where ϕ_0 is the initial concentration of nitrate in the riparian wetland and ϕ is the final concentration, t is the time variable and k_{20}, T, and θ as as per (7.41) except the units of k_{20} are not areal but rather over the whole reacting volume $[T^{-1}]$. Values for θ and k_{20} were integrated into the WATFLOOD model and stored in the water quality parameter file (See Appendix D).

7.9.1 Water Temperature Estimation

The water quality model allows for direct input of stream water temperature data if available. If water temperature is unavailable it can be estimated based on an auto-correlation function described by Stefan and Preud'homme (1993) that relates the stream temperature to measured air temperature. Stefan and Preud'homme (1993) measured relationships for a number of streams and fit an average autocorrelation function for 11 rivers and streams of various sizes to the following autocorrelation function

$$T_w(t) = A_t + B_t T_a(t - \delta) \tag{7.43}$$

where T_w and T_a are the temperatures of the air and water respectively, t is the time series and A_t, B_t and δ are fitting parameters, δ being the effective lag between the air temperature and the surface water temperature. Default values for A and B are 5.0 and 0.75 as recommended by Stefan and Preud'homme (1993), but can be modified in the water quality parameter file (WQP). The model also allows for an established lag in water temperature in δ which is also specified in the water quality parameter file. River temperature parameters are defined by river class. In this model the stream temperature and the riparian wetland temperatures were considered identical.

7.9.2 Illustrative Riparian Nitrogen Process Simulation in the WatFlood Model

The processes that determine nitrate nitrogen fate in riparian wetlands are best illustrated with a simulation of the WatFlood model with nutrient loading to riparian wetlands. Figure 7.17 illustrates the process relationships for a 3 year simulation for the riparian wetland in a single WatFlood grid, including the cumulative nitrogen loading and fate, either by dentirification or by removal to the stream channel, and some of the controlling state variables in the model. Ultimately the nitrogen loaded to a riparian wetland is either carried out to the stream by lateral flow from the wetland to the stream or the nitrogen is removed from the system by denitrification processes outlined in (7.42). Figure 7.17 illustrates the temporal variability of those competing processes. The denitrification or nitrogen removal rates are temperature sensitive with higher rates of removal in the summer months and much lower rates during the colder months (Figure 7.17c), which corresponds to the patterns of denitrification simulated (Figure 7.17b). Hydrological processes also have a significant influence on nitrogen fate within the riparian wetlands. During autumn, winter and spring months, the flow hydrological loading to the wetlands is higher with higher flow through rates observed (Figure 7.17a). Consequently, during the wet, cold months nitrogen tends to follow the water through the wetland and into the stream channel. During the summer, flows to the riparian zone from upland sources is reduced and for some periods actually reverses with flow coming into the wetlands from the channel. In these summer circumstances, the retention times of the riparian wetlands are much longer, allowing for denitrification to dominate in these periods of the simulation.

7.10 Land Surface Process Modification

Although not included in the original scope of this research, some modelled process changes were required in the land surface water quality modelling of the WatFlood/AGNPS model to conform with observed physical processes in the field, particularly regarding nitrogen modelling. The WatFlood/AGNPS nutrient transport model has been employed in a number of published studies (Leon et al., 2001, 2002, 2004) and any modifications

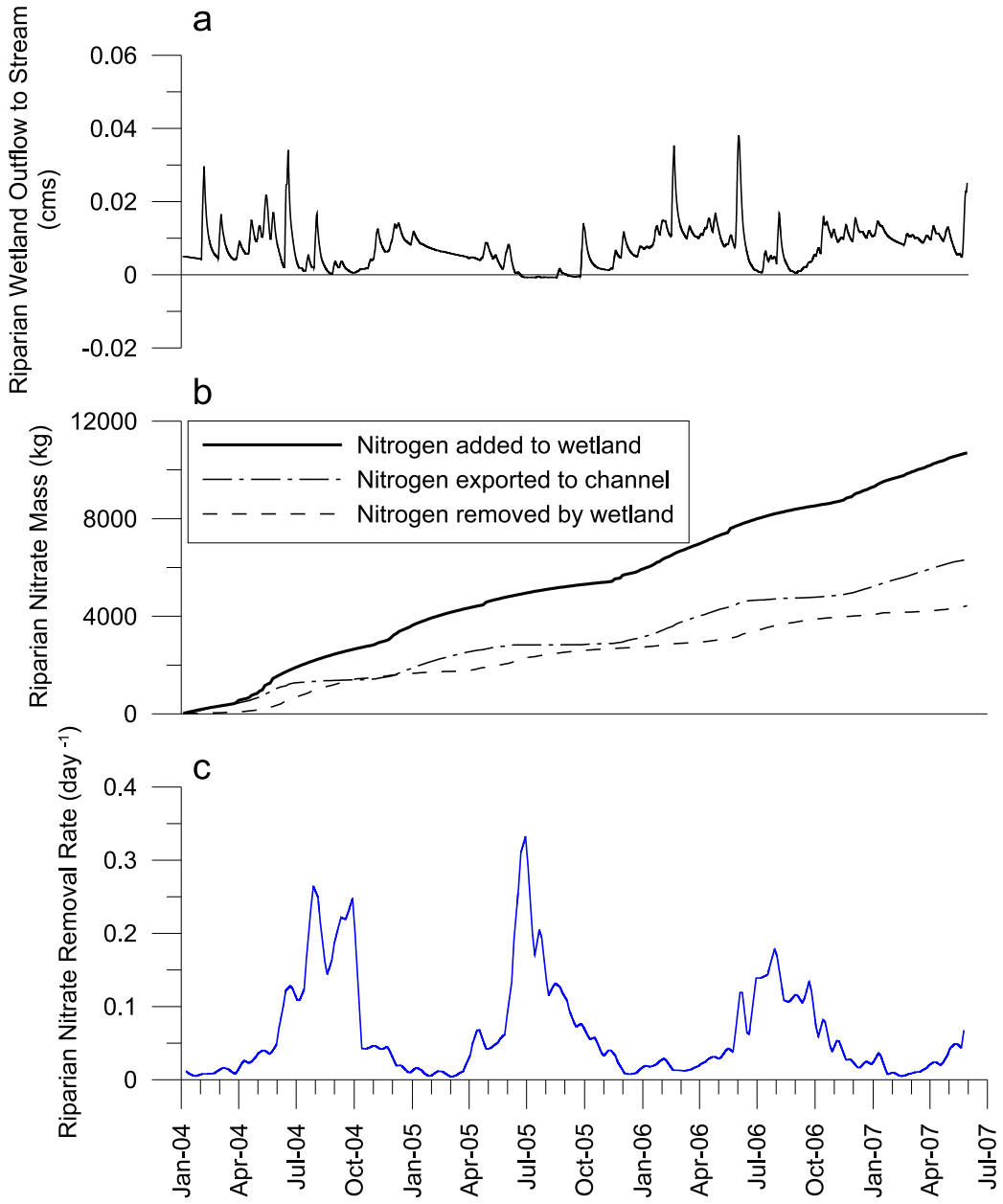

Figure 7.17: Illustrative Simulation of Riparian Loading to a Wetland in a WatFlood Grid - a) Flow from wetland to channel, b) riparian wetland nitrogen loading and fate, and c) riparian nitrate removal or denitrification rate

to the existing model were designed to be minimal. However, the WatFlood/AGNPS model was developed with a primarily event-based focus. That is, an event was initialized with nutrient loading and concentration levels at the start of a month-long event in the WatFlood upper zone groundwater storage and the simulation would continue from that point. The current research required continuous simulation over several years, rather than weeks. Processes that were considered to be insignificant or making little change in the previous studies on the time scale of weeks became important at longer time scales. Additionally, the previous study areas modelled using the existing WatFlood/AGNPS model seemed to not be impacted significantly by groundwater nitrogen contributions, which is not the case with the Canagagigue Creek study site. Some adjustments to the model were necessary to account for some processes that were found missing in the existing model. These processes included:

1. Inclusion of ammonia nitrogen species modelling;
2. Adjusting runoff to include nitrogen in interflow contributions;
3. Movement of mobile nitrogen to groundwater (lower zone storage);
4. Contribution of groundwater nitrogen to the receiving channel;
5. Nitrogen uptake by crops; and
6. Mineralization of applied fertilizer nitrogen.

This section will outline some of the salient features of the WatFlood/AGNPS model, which is fully described in Leon (1999) and Leon et al. (2001), and the modifications made to it for successful modelling of the Canagagigue Creek study area.

7.10.1 WatFlood Sub-Surface Storage and Transport

It is useful to review the basic WatFlood sub-surface transport model to explain modifications made to nitrogen transport in the following sections. Full explanation of the WatFlood model can be found in Kouwen (2005). WatFlood is described as having

a "3-layer" groundwater model with an upper zone, and intermediate zone and a lower zone for groundwater modelling, and additionally surface water storage, above the ground surface is modelled. Figure 7.18 provides a simple schematic illustration of these modelled storage areas with flow dictions provided. The upper zone (UZ) is described as the saturated zone, the intermediate zone (IZ) storage is described as the unsaturated zone, and the lower zone (LZ) is also a saturated groundwater zone but representing deep storage unaffected by evapotranspirative processes. During rainfall events, water may pond at the surface (S) if the precipitation rate is in excess of the infiltration rate. In the case of ponding in surface storage, after a certain storage is reached surface runoff may occur. Water storage is maintained as a state variable in the WATFLOOD model in the upper zone, lower zone and surface specified storage and these three zones may contribute flow to the grid channel, as illustrated by Q_s, Q_{uz} and Q_{lz} in Figure 7.18. Flow may infiltrate from the surface to the upper zone (Q_{inf}), and the upper zone may in turn drain to the lower zone (Q_{dr}). The surface storage, upper zone and intermediate zones were specific to land class within a grid. That is, there were the same number of these zones as there were prescribed land classes. The lower zone storage was common to the entire grid, and the drainage from the various land classes in that grid are pooled in a common lower zone storage before contributing to the receiving channel.

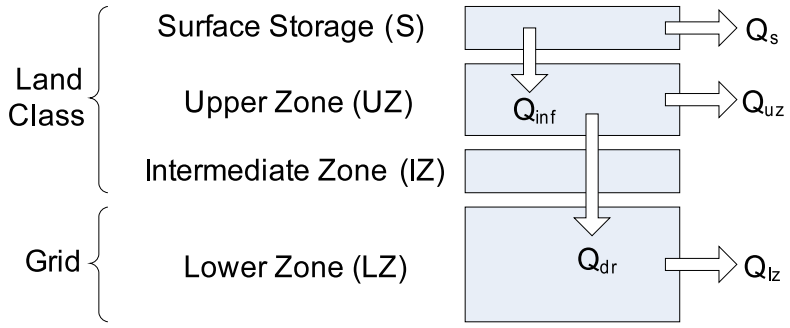

Figure 7.18: WATFLOOD Storage Zones Schematic

7.10.2 WatFlood/AGNPS Nitrogen Model Summary

The existing nitrogen model included a two "pool" approach. Nitrogen was marked as "available" and "unavailable" in the WATFLOOD/AGNPS model. Available nitrogen was mobile and able to be transported to the receiving waters and, in a physical sense, represented highly mobile nitrate and nitrite species and to a lesser degree ammonia although it is not clearly specified in Leon (1999) or Leon et al. (2001) what measured nitrogen species are being compared to modelled results. The unavailable nitrogen state variable in the model was used during fertilizer application but remained unused during the running of the simulation itself. It represents the fraction of the fertilizer nitrogen applied that is not available for transport. The two modelled pools described above were modelled at the near surface, although depletion or transformation of either pool was not considered in the WATFLOOD/AGNPS model. Available and unavailable nitrogen remained unchanged during the simulation.

The theory employed in determining the mobility of available (soluble) nitrogen involves an empirical approach to nitrate and nitrite nitrogen distribution in the subsurface. Mobile nitrogen takes the form of nitrate and nitrite which, having a negative charge, will be repelled from similarly charged soil particles. Consequently mobile nitrogen is expected to flush more quickly from the sub-surface than negatively charged (or uncharged) solutes would as small pore volumes would repel nitrate, leaving the larger pore volumes with larger nitrogen concentrations. As a consequence the effective nitrogen concentration in waters leaving the modelled sub-surface volume will vary with the flushed water volume with higher concentrations in the first, smaller flush and with concentrations dropping as the flush volume increases. A generic form of the equation used in the WATFLOOD/AGNPS model is presented in (7.44)

$$\phi_{nuz} = \frac{N}{Q_o} e^{\frac{Q_o}{(1-\theta)S}} \tag{7.44}$$

where ϕ_{nuz} is the concentration in the flow leaving the subsurface region in the upper zone $[kg - N/ha/mm]$ N is the available nitrogen $[kg - N/ha]$, Q_o is the flow leaving the subsurface over a time step $[mm]$, S is the storage in the subsurface during the time

step $[mm]$ and θ is a dimensionless availability coefficient controlling the rate of release of available nitrogen. Q_o is the total flow leaving the modelled sub-surface and as such could be partitioned and have multiple destinations (for example, simultaneous lateral and drainage flow). A variation on this approach is employed in a number of NPS source models (Young et al., 1989; Leon, 1999; Neitsch et al., 2001).

Soil nitrogen concentration was also modelled in the original WATFLOOD/AGNPS, and it was done by leveraging the sediment transport module and applying a nitrogen loading factor and enrichment ratio which converted a suspended sediment mass to an nitrogen mass. This methodology is described in detail in Leon (1999). In this study almost all of the nitrogen observed in the study site channels took the form of soluble nitrate nitrogen (see Section 6.7.1) and there was little correlation with sediment concentrations. As such the available data was seen as inadequate for assessing the attached nitrogen transport model available in WATFLOOD/AGNPS and was not considered further.

7.10.3 Nitrogen Pool Modelling Approach

The original two-pool nitrogen approach was modified in favour of a three-pool nitrogen approach. The introduction of a continuous model required the consideration of other processes, including drainage to lower zones and crop nitrogen uptake. A third pool was considered essential for the modelling of ammonia nitrogen in the model. Ammonia nitrogen is an important nitrogen species and does not easily fit in either of the pools described in the original model. That is, ammonia is relatively immobile and will not migrate readily when incorporated into soil similar to organic nitrogen in this regard, but is available for plant uptake like nitrate and other mineral nitrogen species (Tate, 1995). Also, when fertilizers are applied, often the mineral nitrogen is an important component, and with urea and certain manures the ammonia nitrogen fraction can be substantial (Chadwick et al., 2000). Consequently it was felt a third ammonia nitrogen pool was required for accurate modelling and was included in the hydrological upper zone.

7.10.4 AGNPS Nitrogen Mobility

As discussed above, the nitrate transport model uses an empirical nitrogen availability approach, which controls the nitrogen mobility. Nitrogen pools are separated into available (nitrate and nitrite) and unavailable and the added ammonia nitrogen pool.

One of the limitations in the original model described by Leon (1999) is that nitrogen only migrated to the receiving waters in the surface flow (Q_s). This decision was ostensibly made in the adaptation of the Soil Conservation Service (SCS) curve number runoff model to the WatFlood runoff model. However, when comparing the two models WatFlood employs both the interflow (Q_{uz}) and surface flow (Q_s) when determining total runoff. As such, the WatFlood/AGNPS model was modified to include interflow and surface flow as carrying nitrogen in surface runoff.

The empirical nature of the original WatFlood/AGNPS nitrogen transport approach, designed for event-based model, was found to not operate well on a continuous basis in the WatFlood model. With moderate runoff rates the ratio of the delivered concentration to the receiving waters could be one or two orders of magnitude higher than the concentration in the pore water. This was found to produce unrealistic results within the WatFlood model with entire grid upper zones being drained of nitrate completely in a single time step. Consequently, the empirical nitrogen enrichment equation was abandoned at this stage of the model with instead a standard completely mixed, mass balance approach being employed

$$\phi_{nuz} = \frac{N_{uz}}{S_{uz}} \tag{7.45}$$

where ϕ_{nuz}, is the concentration of teh nitrate in the upper zone $[kg-N/ha/mm]$ N_{uz}, is the mass of nitrate in the upper zone $[kg-N/ha]$ and S_{uz} is the upper zone storage $[mm]$, with the concentrations in the runoff and the drainage being the same. It is recommended that nitrate enrichment options be examined, in particular ones that fit in with the physically-based nature of the model philosophy, for future development.

The mass movement of nitrogen into the lower zone storage over a time step is described by

$$\frac{dN}{dt} = \sum_{i=1}^{n} \phi_{ni} Q_{dri} \tag{7.46}$$

where N is the mass concentration in the lower zone $[kg - N/ha]$, t is time $[hr]$, ϕ_{nuz} is the calculated upper zone nitrogen concentration from (7.45) and Q_{dr} is the drainage flow rate $[mm/hr]$ moving from the upper zone to the lower zone. The index i represents each of the n land classes in the WATFLOOD model, each of which will contribute to the total lower zone storage in a WATFLOOD grid. Hours are used (7.46) as the land use runoff and drainage time step is fixed to hourly in the WATFLOOD model.

The lower zone storage was assumed to be a completely mixed area of storage. Nitrogen added through (7.46) was averaged over the lower zone storage volume within a WATFLOOD grid cell. The calculation of the movement of mobile nitrogen out of the lower zone storage was calculated by assuming the mass added to the channel was a function of the flow out of the lower zone into the channel and the concentration of nitrogen in the lower zone

$$\phi_{nlz} = \frac{N_{lz}}{S_{lz}} \tag{7.47}$$

where ϕ_{nlz} is the mobile nitrogen concentration in the lower zone $[kg - N/ha/mm]$, N_{lz} is the mass of nitrogen in the lower zone $[kg - N/ha]$ and S_{lz} is the lower zone storage $[mm]$. The total loading to the channel is describe by

$$\frac{dN}{dt} = \phi_{nlz} Q_{lz} + \sum_{i=1}^{n} \phi_{nuzi} \left(Q_{uzi} + Q_{si} \right) \tag{7.48}$$

7.10.5 Crop Nitrogen Uptake

Seasonal nutrient uptake estimates for crops of various types are available from regional government agencies (OMAFRA, 2002). The nitrogen uptake is necessarily expected to occur over the growing season but the rate at which the nitrogen is contained in the crops requires explicit attention in a hourly water balance model like WATFLOOD/AGNPS. Nitrogen uptake estimates were made using a macro-scale uptake approach based on a polynomial function and the expected total nitrogen uptake of a particular crop. Equations

(7.49) and (7.50) provide a quadratic growth profile for the crops with the maximum nitrogen uptake occurring at the middle of the growing season with zero growth rate at the start and the end of the season (Saâdi and Maslouhi, 2003).

$$\frac{dN}{dt} = \begin{cases} A_N t(G-t) & \text{for } t < G \\ 0 & \text{otherwise} \end{cases} \tag{7.49}$$

$$A_N = \frac{6N_{max}}{G^3} \tag{7.50}$$

where G $[d]$ is the length of the growing season , t $[d]$ is the time from the start of the growing season , N $[kg/ha]$ is the quantity of nitrogen taken up by the crop at time t, A_N is a parabolic shape parameter, and N_{max} is the maximum nitrogen storage for a crop at harvest time $[kg/ha]$. A_N in (7.50) is determined by integrating (7.49) from $t = 0$ to $t = G$ and setting total nitrogen uptake mass to N_{max}. This nitrogen uptake approach has the advantage that it is straight forward to implement with the only required parameters being the emergence and harvest dates and the expected cumulative nitrogen content at the date of harvest. At the watershed scale this approach to nutrient uptake is considered appropriate and representative of the average uptake values, and in keeping with a WATFLOOD macro-scale modelling philosophy.

The duration of the growing season in the Wellington region was determined using data from OMAFRA (2008b) which set the average season start date at May 19 for the region (Guelph). The date of plant emergence and uptake is more difficult to discern but the requirement of 180 crop heat units for emergence of corn, the predominant crop in the region, is on average acquired by the region on the 1st of June. This date was set as the start date for the crop nitrogen uptake for the model. The season end for the region (Guelph) is on average September 30. This was marked as the date of harvest and the end of crop nitrogen uptake by the model. These dates were hard-coded into the water quality model, but could be abstracted to the water quality input file at a later date.

With the growing season, total nitrogen uptake specified, the nitrogen uptake profiles can be generated for the crop land use. For example, Figure 7.19 illustrates the nitrogen uptake profile for corn which has an estimated total nitrogen uptake of 135 kg/ha.

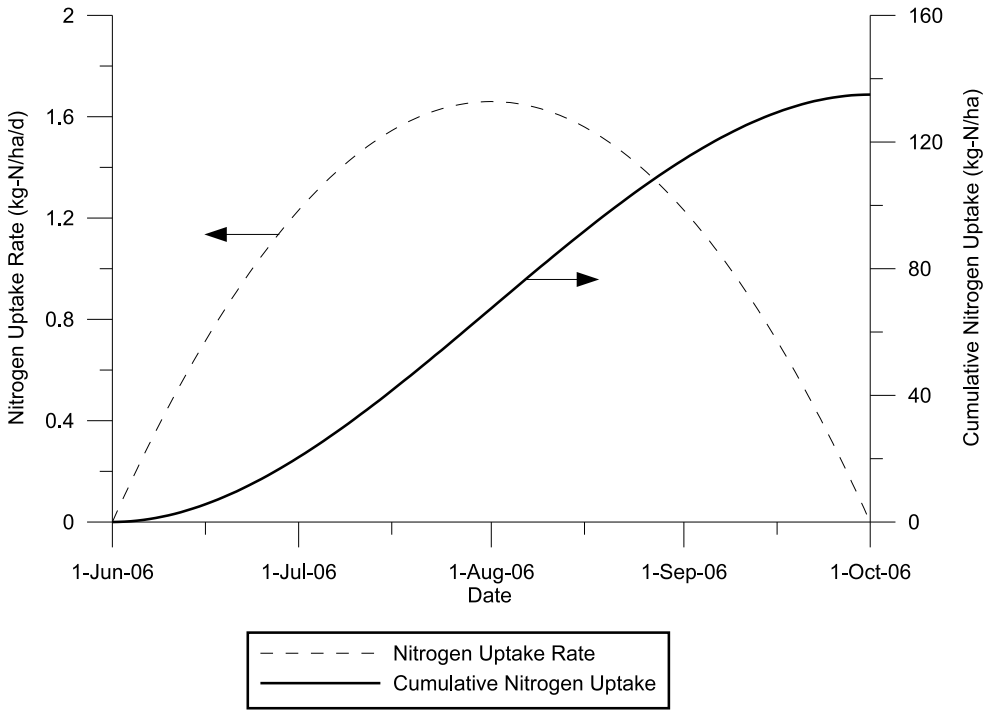

Figure 7.19: Nitrogen Uptake Profile - Corn

When modelling nutrient uptake by crops, nitrogen was taken from the available nitrogen and the ammonia pool proportional to the pool concentration using a daily rate calculated value from (7.49) and (7.50). The uptake rate was calculated for each day based on the time from crop emergence and was applied to the hourly time step of the WATFLOOD model. Nutrients were taken up if available from the upper zone "available" and ammonia pools to a maximum of that permitted by the crop uptake equations. If insufficient available nutrients were available in the upper zone then the concentrations in the upper zone were reduced to zero in that time step. No nutrients were taken up by crops from the lower zone. There was also no accounting for the development of root depth for nutrient uptake form the upper zone. All available nutrients in the upper zone were accessible for plant uptake.

7.10.6 Fertilizer Application

The existing WATFLOOD/AGNPS model did not allow for any adjustment or timing of the fertilizer loading during a simulation, requiring that the simulation begin with the applied fertilizer values. The model was modified to allow for more flexible loading combinations as was required for continuous simulations. A fertilizer loading file (FER) was incorporated in the model for each event which contains a list of hourly data describing the quantity, type, and loading location of the fertilizer. The FER file links to a fertilizer database file, which describes the character of the applied fertilizer in terms of quantity of nitrogen and phosphorus and the fraction of availability of each fertilizer type (i.e. contributions to each nitrogen pool). This is a direct adaptation from Leon (1999) fertilizer loading method except with additional temporal and spatial flexibility. If the fertilizer file is missing for an event (month) then the model assumes that no fertilizer loading will take place during the event. An important point to raise is that the unavailable nitrogen applied in fertilizer represents an organic nitrogen addition that can be mineralized. The total organic nitrogen in an added manure, for example, is not ultimately available for mineralization and may vary considerably, depending on the character of the manure, from as low a 0 to higher than 50% based on laboratory studies (Klausner et al., 1994; Eghball et al., 2002; Van Kessel and Reeves, 2002). The model requires a knowledge of the amount of mineralizable nitrogen in

the applied "unavailable" nitrogen pool. Similarly the amount of "available" and ammonia nitrogen must be prescribed when fertilizer is applied in the model. Additionally, for calibration and sensitivity purposes a loading formula was introduced into the model to allow a programmatic approach to load estimation (see Section 8.3.3).

7.10.7 Fertilizer Mineralization and Nitrification

The inclusion of organic fertilizer mineralization processes in the model was seen as an important step required for long-term nitrogen simulation in a watershed model. Many modelling efforts have been conducted to mathematically express the rate of organic fertilizer mineralization, many of which rely on the original work by Stanford and Smith (1972) who approximated organic nitrogen mineralization using a first order decay model.

$$\frac{dN_{org}}{dt} = -k_{min}N_{org} \tag{7.51}$$

where N_{org} is the concentration of mineralizable organic nitrogen $[ML^{-3}]$, k_{min} is the mineralization rate constant $[T^{-1}]$ and t is time $[T]$. The Stanford and Smith (1972) approach involves a laboratory incubation procedure conducted over a number of weeks, and although the transferability of the laboratory results to a field situation raises issues with the treatment of the soil samples in the procedure, (7.51) is the most widely used modelling approach (Tate, 1995). Mineralized organic nitrogen is contributed to the ammonia pool in this model.

Benbi and Richter (2002) conducted a thorough review of approaches to modelling organic nitrogen mineralization in soils by comparing incubation study results and the various modelling approaches. Modelling approaches typically involved first order decay of the organic nitrogen pools with rate modifiers based on temperature and soil moisture availability. The authors of this study suggested nitrogen mineralization modelling required two organic pools, one for "fresh" organic nitrogen and the other for "recalcitrant" organic nitrogen. This separation was required to account for the rapid release of mobile nitrogen during the first days of incubation and then the gradual release of mobile nitrogen over subsequent weeks which would not otherwise fit a first-order decay model.

For this model application, the time frames were on the order of months, and with the exception of a storm event immediately following a manure application, the impact of a short, relatively rapid release of mobile nitrogen from the organic nitrogen pool would be unnoticed in the model output. The existing "available", "unavailable" and ammonia nitrogen partitioning was considered acceptable for the purposes of this model and only one "recalcitrant" organic pool was considered with an associated decay coefficient. Additionally, in the interest of parsimony in model development, this approach required the estimation of a single decay coefficient rather than two for nitrogen mineralization.

Nitrification of ammonia was another kinetic process requiring simulation in the model. A first order decay approach was employed as with organic nitrogen mineralization (Jury et al., 1976)

$$\frac{dN_{NH_4}}{dt} = -k_{nit} N_{NH_4} \tag{7.52}$$

where N_{NH_4} is the ammonia nitrogen concentration $[ML^{-3}]$, k_{nit} is the nitrification rate constant $[T^{-1}]$ and t is time $[T]$. The change in the ammonia nitrogen pool contributed to the available nitrogen pool.

The rate constants included in (7.52) and (7.51) are subject to modifications based on environmental conditions, particularly temperature and soil moisture (Das et al., 1995; Tate, 1995; Antonopoulos, 1999; Benbi and Richter, 2002; Eghball et al., 2002). Typically the rate coefficient is modified by factors that correct a rate constant for changes in temperature or soil water availability as below (Antonopoulos, 1999)

$$k_{eff} = k_0 e_{sw} e_t \tag{7.53}$$

where k_0 is the original prescribed rate constant at a particular temperature and soil water condition, k_{eff} is the effective temperature corrected for existing soil water and temperature conditions and e_{sw} and e_t are soil water and temperature correction factors respectively. The estimation of the effect on reaction rate constants due to temperature was conducted using a Q_{10} relationship, which describes a change in the kinetic rate constant with a 10°C change in temperature (Johnsson et al., 1987)

$$e_t = {Q_{10}}^{(T_s - T)/10} \tag{7.54}$$

where e_t is the temperature correction factor, Q_{10} is multiplication factor for a change in temperature of 10°C, T_s is the soil temperature and T is the base temperature upon which the original rate constant was based. Typically Q_{10} is 2 to 3 and the base temperature is typically 20°C (Saâdi and Maslouhi, 2003).

The effects of extreme wetness and dryness on the decay coefficients was considered in the modification of decay rates. The model employed a parabolic rate reduction coefficient for low soil water content outlined by Antonopoulos (1999) which was modified from the original approach described by Johnsson et al. (1987).

$$e_{sw} = \begin{cases} \left(\frac{1}{\theta} - \frac{1}{\theta_d}\right) / \left(\frac{1}{\theta_l} - \frac{1}{\theta_d}\right) & \theta_l > \theta \geq \theta_d \\ 1.0 & \theta_h > \theta \geq \theta_l \\ e_s + (1 - e_s)\left(\frac{1}{\theta_s} - \frac{1}{\theta}\right) / \left(\frac{1}{\theta_s} - \frac{1}{\theta_h}\right) & \theta_s > \theta \geq \theta_h \end{cases} \tag{7.55}$$

where θ_d is the soil water content near dryness $[cm^3 cm^{-3}]$, θ_s is the saturated soil water content, θ_l is a lower limit of soil water content for maximum biological activity (assumed near wilting point), θ_h is an upper limit of soil water content for maximum biological activity (estimated at field capacity), e_s is a saturation coefficient (estimated at 0.6). The principle of (7.55) is that for a range of soil moistures a maximum mineralization rate can be expected, but for extremely dry or wet conditions a reduction in that rate constant can be expected. Dry conditions have a more pronounced effect on the rate adjustments that wet conditions, and below θ_w no mineralization is expected.

The equation prescribed in (7.55) was linked to the WATFLOOD state variables. Based on recommendations by Antonopoulos (1999), threshold values for the soil capacity curve should be prescribed by soil water tension values, which determine biological availability of water. However, due to the limitations of the groundwater modelling approach in WATFLOOD capillary potential or soil tension is not explicitly modelled. Field capacity and the permanent wilting point were prescribed in the model which were corresponded to θ_h and θ_l respectively and soil saturation levels prescribed in the WATFLOOD model were

also employed in (7.55). Based on simulations run on the calibrated WatFlood model for the Canagagigue Creek basin from 2000 to 2007 approximately 0.1% of simulated hours showed soil moistures at or below the prescribed wilting point, and 11.6% of the simulated hours showed upper zone storage values in excess of the field capacity in agricultural class GRUs.

7.10.8 Estimation of Soil Temperature

The estimation of soil temperature was an important step in estimating the kinetic rate coefficients in the model. For this estimation soil temperature data from the University of Waterloo weather station was employed. During 1999 to 2000 soil temperature data was collected at the University of Waterloo Weather Station at 0.05 m, 0.10 m, and 0.20 m depths. Although the upper zone storage has no prescribed depth, the 0.20 m depth was selected as the most representative of soil temperatures for that layer as rooting depths are anticipated to be in excess of 0.20 m for most crops (Verhallen and Roddy, 2003). A regression equation was developed that related the 11 day running average of atmospheric temperature to the soil temperature at 0.20 m. This is similar to the approach outlined by Zheng et al. (1993) except simplified to rely on the regression equation and not adjusting the soil temperature for precipitation and snow cover effects. It was assumed that the soil temperature / air temperature relationships at the University of Waterloo Weather station were similar to those observed at the field site. It is acknowledged that land cover affects will have an effect on soil temperature (Zheng et al., 1993; Kang et al., 2000) however, these effects were not considered in this stage of model development.

The regression equation was developed by taking the 15 minute data collected at the UW Weather station in 1999, determining the 11 day running average of atmospheric temperature and developing a linear regression equation to match the soil temperature data. This regression equation was then compared to the 2000 season to validate its applicability. Figure 7.21 shows the linear fit for the 1999 season for which the coefficient of determination (R^2) was 0.97, indicating that the soil temperature can be largely explained by atmospheric temperature patterns alone in this region. The calibration and validation periods for this linear model are shown in Figure 7.20.

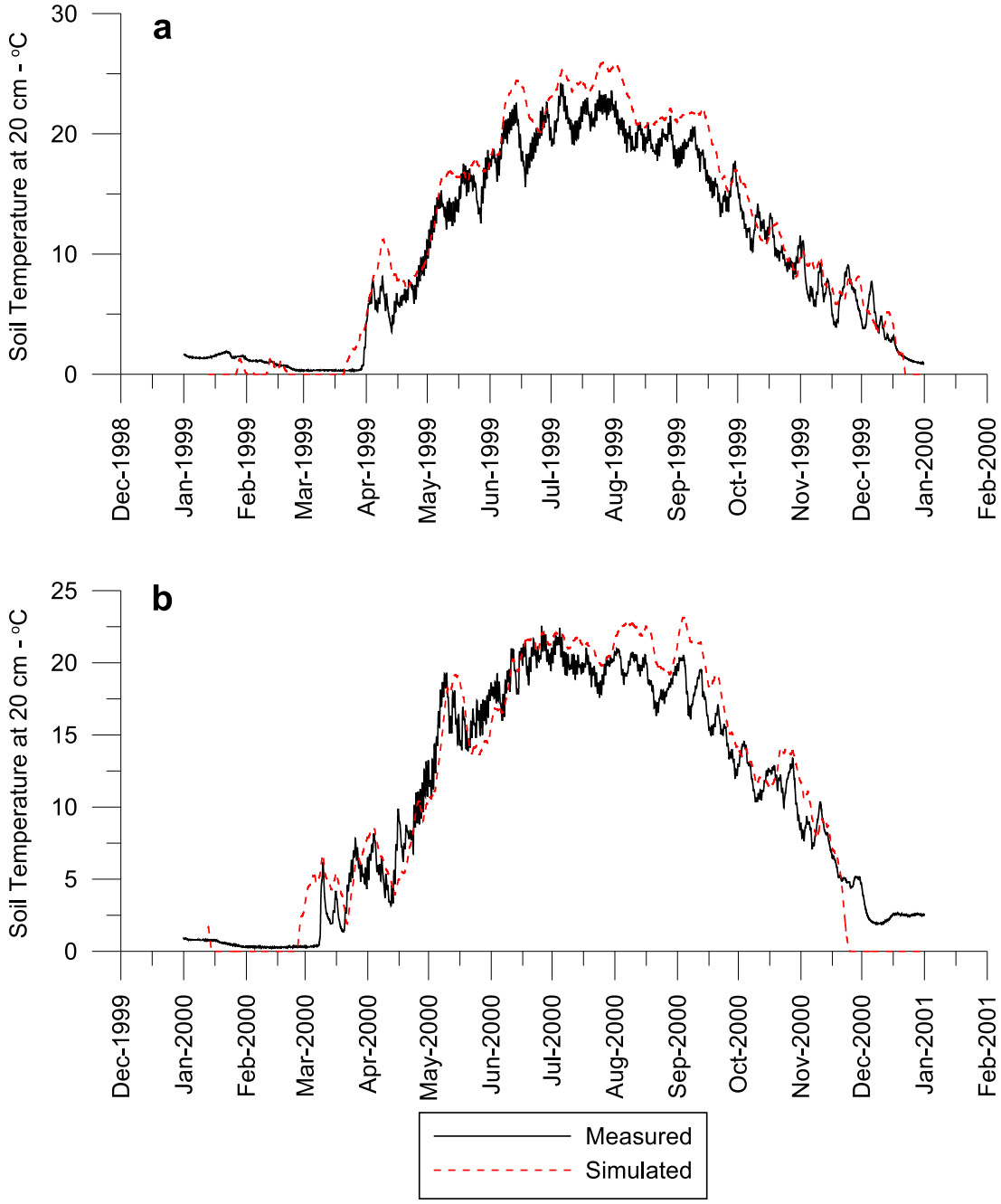

Figure 7.20: Soil Temperature Estimation Profiles a) 1999 Calibration b) 2000 Validation

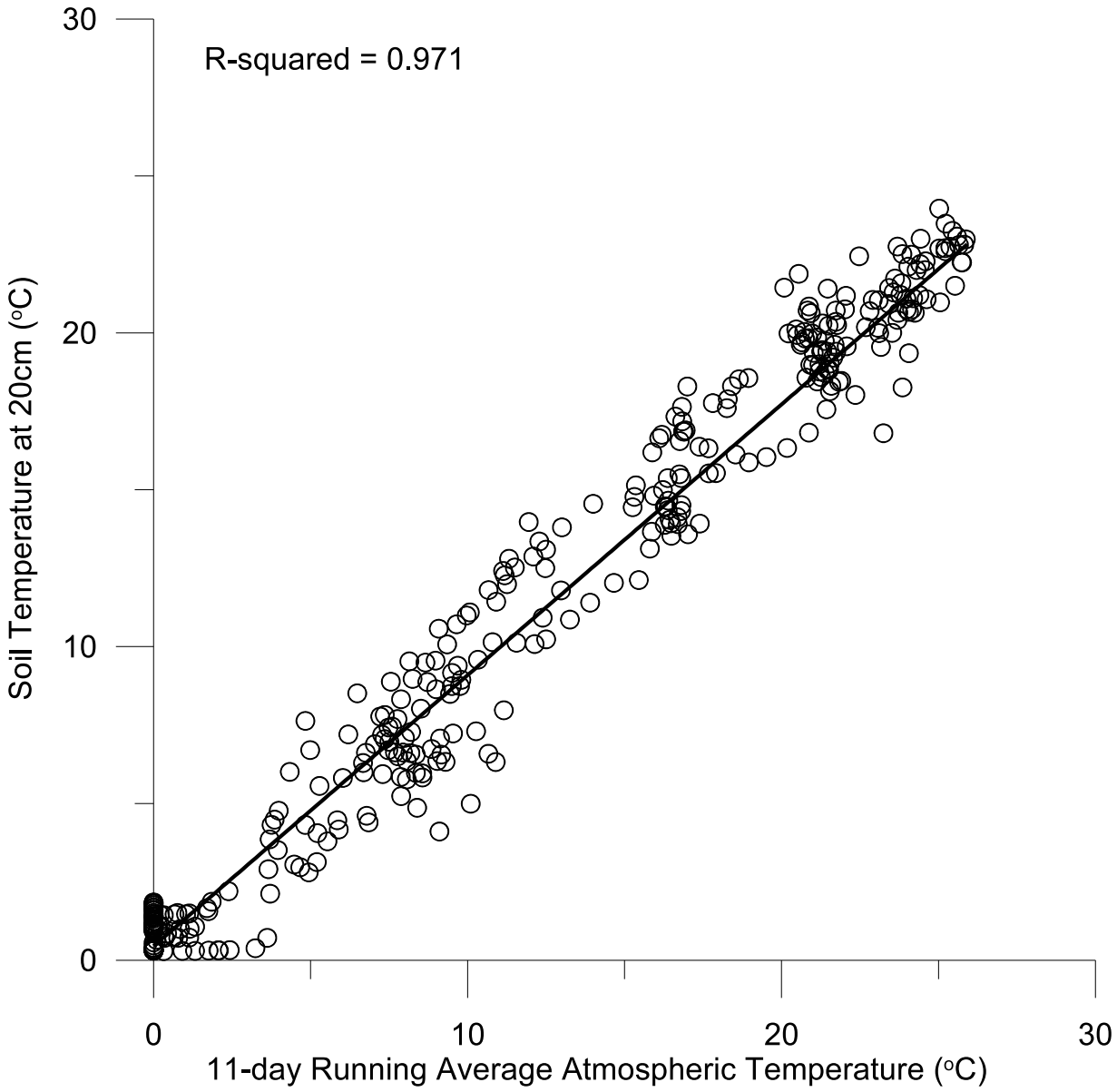

Figure 7.21: Soil Temperature Estimation Calibration - University of Waterloo Weather Station

The calibrated soil temperature relationship was coded into the model, but the regression parameters could be moved to a water quality input file in the future. Ultimately this model may be merged with the MESH / WATCLASS model, which will provide soil temperatures at depth as modelled state variables.

7.10.9 Illustrative Nitrogen Process Simulation in the WatFlood Model

The operation of the nitrogen model within the WatFlood hydrological model can be best illustrated with a sample simulation. Figure 7.22 shows the nitrogen mass storage results for a single WatFlood grid during a multi-year simulation with simulated crop growth and with fertilizer application in May and October of each year as a combination of organic and ammonia nitrogen. Also included in Figure 7.22a is the simulated soil temperature in the upper zone of the grid. The model shows a fluctuation in organic or unavailable nitrogen which spikes with fertilizer application and decays to the ammonia pool steadily, but as a clear function of the soil temperature. Ammonia nitrogen shows a similar pattern, but does not maintain a steady minimum concentration in the upper zone as ammonia decays to "available" nitrogen and nitrate. Available nitrogen shows a sharp increases after fertilizer application as high ammonia concentrations are oxidized, but drop quickly as crop uptake increases over the summer. Available nitrogen also drops suddenly during storm events which carry nitrogen to the streams and to the groundwater. The mass in the lower zone groundwater is responsive to the upper zone drainage, and reductions in available nitrogen in the upper zone are reflected in an increase in the nitrogen levels in the lower zone.

Interestingly, in this simulation, with identical fertilizer loading and crop nitrogen demand in each year, the four simulated years show a fair degree of variability. Simulated years 2003, 2004 and 2006 show inadequate fertilizer loading with available nitrogen reducing to close to zero roughly half way through the growing season, with 2004 and 2006 showing the lowest nitrogen availability for crop uptake. 2005 shows a better nitrogen balance with available nitrogen only going near zero for a short period. The variability is explained in the observed hydrological patterns. In the spring of 2004 there was above

average rainfall, infiltration and runoff, reducing the amount of available nitrogen for that simulated year. For the 2006 season, nitrogen was lost during the wet winter of 2005/2006 which resulted in less available nitrogen for the 2006 growing season. Both of these patterns are strongly visible in the lower zone nitrogen plot which receives drainage from the upper zone (Figure 7.22c). This simulation shows the effect of hydrology and hydrological conditions on the nitrate movement and the impact it can have on fertilizer loading requirements. Nutrient management plans in Ontario do not account for hydrological conditions in determining recommended fertilizer loading, relying on a nutrient balance approach with consideration to the surface soil characteristics (Harman et al., 2000).

7.10.10 Omitted Nitrogen Processes

A number of nitrogen fate processes were not considered in this model. Volatilization of ammonia-nitrogen to the atmosphere was not considered. Volatilization is a relatively rapid process and can be minimized through the incorporation of a fertilizer into the soil through tillage or other injection practises. For Ontario farmers OMAFRA has published fertilizer application guides, which help estimate the quantities of ammonia in selected fertilizers and the quantities that will be lost to volatilization depending on the duration of storage, manure type and incorporation method (OMAFRA, 2008b). In this model it was assumed that the prescribed method of application was considered in the definition of the fertilizer application file and the quantities of ammonia and mineralizable organic nitrogen remaining in the soil could be prescribed.

Ammonia transport was not considered in this model. Ammonia is not highly mobile in a soil matrix and can bind to soil particles when in soil solution due to its positive charge (Johnsson et al., 1987). Additionally, ammonia is generally rapidly transformed to nitrate by nitrifers (Tate, 1995). Other researcher have employed isotherms to estimate the degree of adsorption to the soil matrix and ammonia transport was considered based on the isotherm equilibrium (Saâdi and Maslouhi, 2003; Scott, 2006). As nitrate nitrogen dominated all water samples collected, ammonia transport was not considered a significant process in our study site and ammonia was presumed immobile in this model. This may not be the case in other regions and deserves further investigation if the developed model

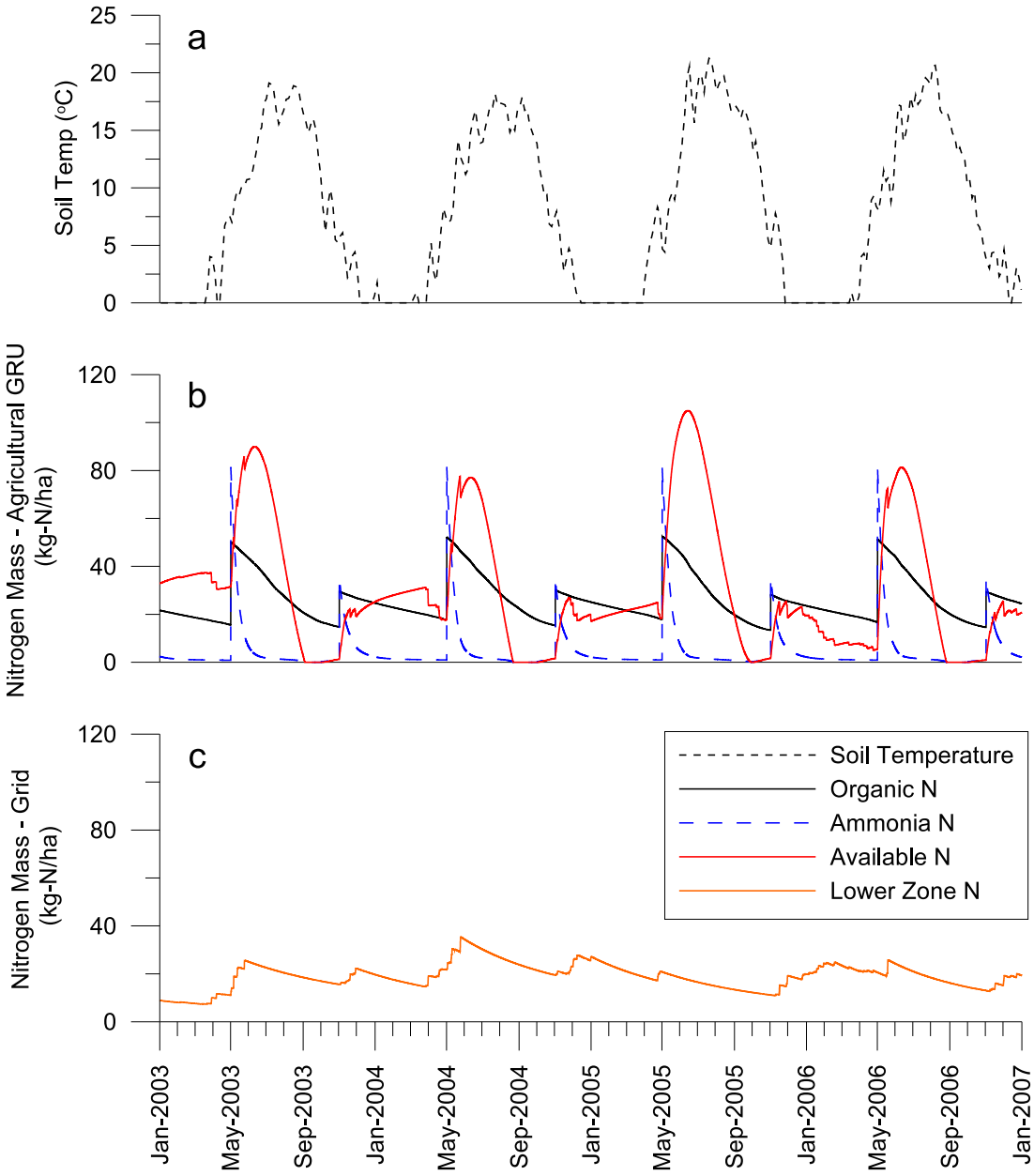

Figure 7.22: Nitrogen process results in a WATFLOOD grid for an illustrative multi-year simulation a) soil temperature, b) upper zone nitrogen species, c) lower zone nitrogen species

is applied to another watershed.

Litter or residue organic nitrogen was not considered explicitly in this model. The model can account for organic nitrogen residue after cropping through the inclusion of an additional fertilizer loading estimate after cropping. This can be considered an organic mineralizable nitrogen contribution that can be applied at an appropriate time after the harvest. These nitrogen additions will necessarily be subjected to the single mineralization rate constant prescribed in the model. Similarly, nitrogen fixation by legumes is not considered in this model and organic nitrogen left available after cropping of legumes must be considered in a similar manner to crop residue. OMAFRA (2008b) provides approximations of nitrogen available from the previous crop.

Denitrification in the upper and lower zone storage regions is not considered in this model. The importance of denitrification has been contested in the literature over the years. Modelling of several fields with a multi-layer nitrogen fate model conducted by Johnsson et al. (1987) indicated that denitrification accounted for less than 2% of the nitrogen removal, the largest components being plant uptake and drainage. However, other researches have pointed to a possible larger contribution due to denitrification, perhaps highter than 50% according to some mass balance models (Barry et al., 1993; Brink et al., 2008). In a mass balance analysis by Puckett et al. (1999) for an agricultural area in Minnesota suggested that deep water denitrification accounted for 10% of the nitrate removal in the system and that approximately half of the nitrate which leached to deep water was ultimately denitrified. In this stage of model development the denitrification at the GRU and grid levels was not considered, but should be examined for future development.

7.11 Discussion

In this chapter the development, testing, analysis and implementation of a more advanced contaminant transport routine for the WatFlood modelling framework is presented. The selected algorithm (QUICKEST) was shown to be much more accurate than the original storage routing routine. The ability of the new model to account for advective and disperive characteristics in contaminant transport was presented and the higher degree

of mass conservation of the model was also shown. Additionally the implementation of the QUICKEST model into WATFLOOD was shown to be much more efficient than the storage routing routine with a 10-fold savings in computation time while at the same time showing a 20- to 30-fold increase in mass conservation accuracy in tests conducted with WATFLOOD.

Also in this chapter, the development of in-channel and riparian nitrate and sediment decay and transformation equations and their integration into the SOLROUTE modelling framework and the WATFLOOD hydrological model is presented. The implemented processes include sediment resuspension and deposition in the channel and during overland flow in the riparian wetlands. The unit tests show good accuracy and mass conservation.

The use of an Euler technique for calculating contaminant decay, deposition and resuspension is sub-optimal given the known problems with the technique in over- or underestimating values during sharp gradients. Although the test framework simulations showed that the routines are accurate and converge on the desired solution with increased spatial and temporal resolution, it is recommended and planned that the 4^{th}-Order Runge-Kutta routine used in the riparian hydraulic exchange code (see Section 7.3) be employed in these calculations to improve the order of accuracy of the calculations.

The average riparian width calculations are an over-simplification of the local geometry. The arithmetic mean is likely to provide a more conservative estimate of the protection of the channel by the riparian zones. A geometric mean could provide a more accurate representation for the average width of the channel. However, more detailed connectivity calculations would be required for this type of assessment, the impacts of which are perhaps worth investigating in future research.

The calculation of sediment deposition within the riparian wetland is discretized using a single computational cell. This approach greatly oversimplifies the dynamics of sediment deposition, and the full VFSMOD model, by comparative example, provides a full discretization of the vegetated filter strip. In this way the impact of the length of the filter strip can be more fully qualified and have a direct impact on the degree of sedimentation. The employed simplification is believed to be a good developmental first step and provides at least an insight in to the sensitivity of the sediment loading to riparian wetland filter-

ing within a sub-watershed context. More complexity in the modelling approach could be investigated in the future, but a simpler approach could be adequate for watershed scale and is in line with the WATFLOOD macro-scale approach to hydrological modelling.

No modifications were made to the WATFLOOD wetland hydrological model. It is understood that the segmentation introduced in Section 7.7 to partition the contaminant loads should be equivalently applied to the WATFLOOD model hydrology to provide consistency between the hydrological and water quality paths. Indeed the entire wetland hydrological model could be expanded for a more flexible discretization in regard to sediment and nutrient transport as well as hydraulically and hydrologically. Further discretization may provide improved modelling accuracy and could be investigated further however, as discussed above, a simple approach like the one taken could be sufficient for modelling at the watershed scale.

The equations used to determine nitrate removal in the wetlands represents a very simplistic approach. The model is a simple mixing cell approach and does not account for vertical or lateral variability within the wetland. The employed equations do not account for other processes or state variables that can limit the riparian wetland nitrate processes including availability of carbon, dissolved oxygen, plant uptake or nitrate release from the riparian wetlands. Availability of data to support these extra processes could warrant their addition to the model in future work.

Temperature modelling is employed using the empirical stream temperature model by Stefan and Preud'homme (1993). A more deterministic modelling approach would be beneficial. Approaches included in CE-QUAL-RIV1 (USACE, 1995) and QUAL2K (Chapra et al., 2007), which focus more closely on the physics of heat exchange between the channel water, the channel surface and the atmosphere would be beneficial if included in the existing framework. This could be considered as a future implementation in the model in conjunction with the integration with the WATCLASS and MESH models.

The incorporation of the SNIA provided accurate results when SOLROUTE was executed using the test framework, and mass conservation in WATFLOOD at standard time steps. The introduction of a SIA approach could improve the accuracy of the coupling approach and is recommended.

Sedimentation velocities and fluid shear stresses will be dependant on the fluid viscosity, which of course is highly temperature-dependant. No considerations were made for viscosity changes in this model, which would effectively adjust the sediment carrying capacity, deposition, and resuspension rates with changes in water temperature. This is an identified limitation and is marked for future work.

Finally, the soil-nitrogen processes were introduced to the model to allow for continuous simulation of nitrogen-related processes. A number of processes were introduced including fertilizer addition, organic nitrogen mineralization, ammonia nitrification, plant uptake and nitrate transport processes to the channel and lower zone storage. A number of identified nitrogen processes were not included in the model. Some investigation into these omitted processes, denitrification in particular, could provide improved model performance.

Chapter 8

Water Quality Modelling Results

8.1 Introduction

This chapter outlines the application of the WatFlood/AGNPS model with enhancements described in Chapter 7 to the study site data described in Chapters 4 and 6. The chapter is separated into two sections, the first focusing on suspended sediment modelling and the second section on nitrate nitrogen modelling. In each of the sections the methods employed for parameter estimation, calibration, validation, performance analysis and sensitivity are described.

In all simulations a 10-element sub-grid discretization was employed in the SOLROUTE contaminant transport routine and no dispersive mixing between the channel and the riparian wetlands was employed. The transfer of solutes in and out of the riparian wetlands was driven by net hydrological movement.

8.2 Sediment Transport Modelling

The sediment transport model was executed over the period of June 2005 to May 2007 which overlapped the periods of water quality data simulation. A two year hydrologic spin-up period was employed before starting the simulation, the state variables of which were loaded via WatFlood resume files (Kouwen, 2005).

8.2.1 Parameter Estimation

For the sediment transport modelling several key parameters within the established WATFLOOD/AGNPS land surface sediment sourcing model had to be estimated . In addition to hydrological parameters such as slope, flow conditions, etc. provided by the WATFLOOD model, the sediment sourcing model requires information relating to the soil character and erodability. The required parameters are presented in Table 8.1 and include the land surface parameters from the original WATFLOOD/AGNPS model with the sediment source formulations derived from the Hartley Model (Hartley, 1987b,a), and the newly added parameters for channel and riparian sediment processes.

Parameter	Description	Units	Scope	File
Land Surface				
d50	median soil particle diameter	mm	distributed	*.SED
sg	soil specific gravity	-	distributed	*.SED
erod	erodibility	g/J	distributed	*.SED
a	carrying capacity parameter	-	watershed	*.WQP
b	carrying capacity parameter	-	watershed	*.WQP
gc	vegetative ground cover factor	-	land class	*.WQP
cf	canopy cover factor	-	land class	*.WQP
Channel				
Cs	carrying capacity fitting parameter	-	river class	*.WQP
Ks	carrying capacity fitting parameter	-	river class	*.WQP
Vsd	depositional velocity	m/s	river class	*.WQP
Vsr	resuspension velocity	m/s	river class	*.WQP
Cer	erodibiltiy protection factor	-	river class	*.WQP
Riparian				
nr	hydraulic roughness	-	river class	*.WQP
S0	slope	-	river class	*.WQP
Csr	carrying capacity fitting parameter	-	river class	*.WQP
Ksr	carrying capacity fitting parameter		river class	*.WQP
Vsdr	depositional velocity	m/s	river class	*.WQP
River Mixing				
disp	dimensionless dipsersion coefficient	-	river class	*.WQP

Table 8.1: Sediment Modelling Parameters

The first three parameters $d50$, sg and $erod$ are distributed parameters, with each WATFLOOD grid cell being assigned a representative value. The values assigned for the various parameters were determined from a lookup table provided by Leon (1999) that was adapted from AGNPS which linked the soil type to values of $d50$, sg and $erod$. The predominant land class in a WATFLOOD grid as defined by the soil map shown previously in Figure 3.5 (p. 33) was used as the representative soil class in the grid. The majority of the cells within the Canagagigue Creek model were classified as "Loam" or "Sandy Loam", and the associated SED file used in the model is found in Appendix D.

The overland carrying capacity is defined by (8.1) from Hartley (1987b)

$$\phi_{sed} = a \left(\frac{\tau}{\tau_c} \right)^b \tag{8.1}$$

where ϕ_{sed} is the sediment concentration in the overland flow, τ and τ_c are the active and critical shear stresses respectively and a and b are fitted parameters that were calibrated to field data in the original reference to 6.6×10^{-4} and 1.61 respectively (Hartley, 1987b; Leon, 1999).

The origin of the "Channel" "Riparian" and "River Mixing" parameters listed in Table 8.1 are all described in Chapters 7. The riparian wetland Manning's n coefficients were estimated from Vieux (2001) as a grassed cover (estimated:0.45, range:0.39–0.63). The slopes of the riparian wetlands were determined from the cross sectional data obtained during site surveys (Section A.3). The dimensionless dispersion value was allowed a possible range of 30 – 3000 as suggested by Rutherford (1994).

The fall velocity values were initially estimated by using Stoke's law for falling spheres (Streeter and Wylie, 1985)

$$v_s = \frac{2(\rho_s - \rho) g r^2}{9\mu} \tag{8.2}$$

where v_s is the fall velocity, ρ_s is the sediment density, ρ is the fluid density g is the acceleration due to gravity and r is the particle radius and μ is the fluid dynamic viscosity. For fine sands and silts, with assumed spherical shapes in dilute solution in water at 15 °C the estimated fall velocities were $1 \times 10^{-5} m/s$ to $1 \times 10^{-3} m/s$.

8.2.2 Calibration Procedure

Model calibration was determined using a pattern search hill-climbing algorithm similar to the one described in Section 5.4 for use in the WatFlood model. Whereas the optimization routine used for the hydrological model is incorporated into the model itself, for the adjustment of the water quality parameters required the development of a separate series of computer programs that would make systematic adjustments to the water quality parameter files and assess the variation against a prescribed objective function. Additionally, the WatFlood optimization routine required matched hourly data for calibration, which functions well with regular hydrometric data, but functions less well for irregularly collected water quality data.

Because the measured data were acquired at intervals that did not coincide with the hourly reporting of the WatFlood/AGNPS model, a preprocessing step was conducted before each statistics calculation to determine the value at the time of sampling though a linear interpolation between the modelled data points.

Several efficiency functions were considered in this model and for the calibration of the sediment model parameters. The first was an ordinary least squares estimator (OLS) [1] shown in (8.3), a square-root least squares estimator (SLS) shown in (8.4), a Nash-Sutcliffe efficiency formulation shown in (8.5), and a normalized ordinary least squares efficiency function (8.6) were calculated.

[1] The use of acronyms for ordinary least squares is somewhat confused within the literature alternatively presented as Ordinary Least Squares (OLS) and Simple Least Squares (SLS). In this document the calculation in (8.3) is referred to as OLS and (8.3) is referred to as SLS.

$$F_{OLS} = \sum_{i=1}^{n} (S_i - O_i)^2 \tag{8.3}$$

$$F_{SLS} = \sum_{i=1}^{n} \left(\sqrt{S_i} - \sqrt{O_i}\right)^2 \tag{8.4}$$

$$F_{NASH} = 1 - \frac{\sum_{i=1}^{n} (S_i - O_i)^2}{\sum_{i=1}^{n} (S_i - \bar{O})} \tag{8.5}$$

$$F_{NOLS} = \frac{\frac{1}{n}\sqrt{\sum_{i=1}^{n} (S_i - O_i)^2}}{\frac{1}{n}\sum_{i=1}^{n} O_i} \tag{8.6}$$

where F is the efficiency function value, S_i and O_i are the i^{th} simulated and observed values respectively, n is the number of simulation-observation pairs, and $\bar{O}$ is the average of all observed values. The OLS formulation is widely used and it's variant, SLS, provides a similar approach but with square-root transformation places more relative weight to lower values than higher values. The Nash-Sutcliffe efficiency criterion (NASH) is widely used in assessing hydrological performance and a coefficient value of zero or less implies that the mean value of sampled data provides a better estimate than the model itself. A modification of the ordinary least squares equation (8.3) was made to normalize it against the average observed values by calculating the root mean squares value (RMS) and dividing it by the mean of observed values, the normalized ordinary least squares estimator (NOLS) in (8.6). The NOLS estimator provides an estimation of the error relative to the mean of the observed values.

All of the above formulations were coded into the optimization statistics program as options for evaluation. It is noteworthy that for all equations a zero value represents a perfect fit with higher values representing worse fits with the exception of (8.5), for which 1.0 is a perfect fit and lower values represent worse fits.

The calibration of the model required the combination of data from both East and West sub-basins. As such, the system objective function required a weighted combination of the efficiency functions from the two sub-basins. A generic weighted objective function was coded to allow for a combination of data pairs to be compared after every run with a

flexible weighting scheme shown in (8.7).

$$F_S = \sum_{i=1}^{n} (a_i + b_i F_i^{c_i}) \tag{8.7}$$

where F_S represents the system objective function, a_i, b_i, and c_i represent additive, multiplicative and exponential weights to be assigned to a particular efficiency function value F_i, and n represents the number of efficiency functions to be combined.

For this calibration effort, the model suspended solids values were compared to the measured suspended solids data for both the east and west sub-basins for the period from 1 July 2005 to 1 Apr 2006. This period included the first monitoring season up to and including the 2006 snow melt. Through observation of the efficiency functions during sample simulations it was determined that the normalized equations (8.5) and (8.6) provided the most useful metrics as the normalized values allowed for additive comparison between the East and West sub-basin performance. The normalized ordinary least squares estimator was used as an objective function for calibration. The system calibration objective function included the NOLS results combined for the west and east basins by simple equal additive weighting of the two functions. The values for the parameters identified (8.7) are shown in Table 8.2.

Objective Function Weighting Parameter	Sub-Basin	
	West	East
a_i	0	0
b_i	0.5	0.5
c_i	1	1

Table 8.2: Sediment Objective Function Weighting Parameters

Calibrated Parameters

The parameters that were calibrated are listed in Table 8.3 along with their acceptable ranges (Min, Max) and their ultimate calibrated values (Value). The "Index" column in Table 8.3 indicates the land class or river class index. River class index "2" represents

the West sub-basin and river class "3" represents the East sub-basin. The erodability coefficient C_{er} is omitted from the calibration as it performs the same function as the resuspension rate. C_{er} was left at unity and the resuspension velocity V_{sr} was permitted to vary.

Parameter	Index	Value	Min	Max
River Mixing				
D_{par}	2	2.35×10^3	3.00×10^1	3.00×10^3
D_{par}	3	2.09×10^3	3.00×10^1	3.00×10^3
River Sediment				
C_s	2	1.62×10^3	1.00×10^3	5.00×10^3
C_s	3	3.27×10^3	1.00×10^3	5.00×10^3
K_s	2	1.85×10^0	1.00×10^0	3.00×10^0
K_s	3	2.59×10^0	1.00×10^0	3.00×10^0
V_sd	2	1.07×10^{-3}	1×10^{-4}	1×10^{-2}
V_sd	3	3.01×10^{-4}	1×10^{-4}	1×10^{-2}
V_sr	2	1.05×10^{-3}	1×10^{-4}	1×10^{-2}
V_sr	3	2.00×10^{-4}	1×10^{-4}	1×10^{-2}
Riparian Sediment				
n_r	3	2.69×10^{-1}	1.00×10^{-1}	6.00×10^{-1}
S_0	3	2.00×10^{-4}	1.00×10^{-5}	1.00×10^{-3}
C_{sr}	3	4.22×10^3	1.00×10^3	5.00×10^3
K_{sr}	3	1.35×10^0	1.00×10^0	3.00×10^0
V_{sdr}	3	1.52×10^{-3}	1×10^{-4}	1×10^{-2}

Table 8.3: Calibrated Sediment Parameters

The East basin showed generally higher efficiency values in the calibration period for all efficiency functions in Table 8.4 with the exception of the SLS formulation, for which the East and West sub-basins show similar responses. The SLS applies extra weight to lower flows, implying that the calibrated model performed better at the higher values in the East than the West, but base-flow modelling was slightly better in the West than the East. Figure 8.1 shows the concentration comparison for the measured and simulated TSS concentrations for the East and West sub-basins. It shows a greater degree of model convergence on the East basin and much more scatter on the West sub-basin, a pattern which was also observed in the flow volume and peak volume simulation results presented in

Chapter 5 (see Figures 5.8 and 5.9). Table 8.4 provides a summary of the various objective function values for each of the sub-basins and the average for the two sub basins.

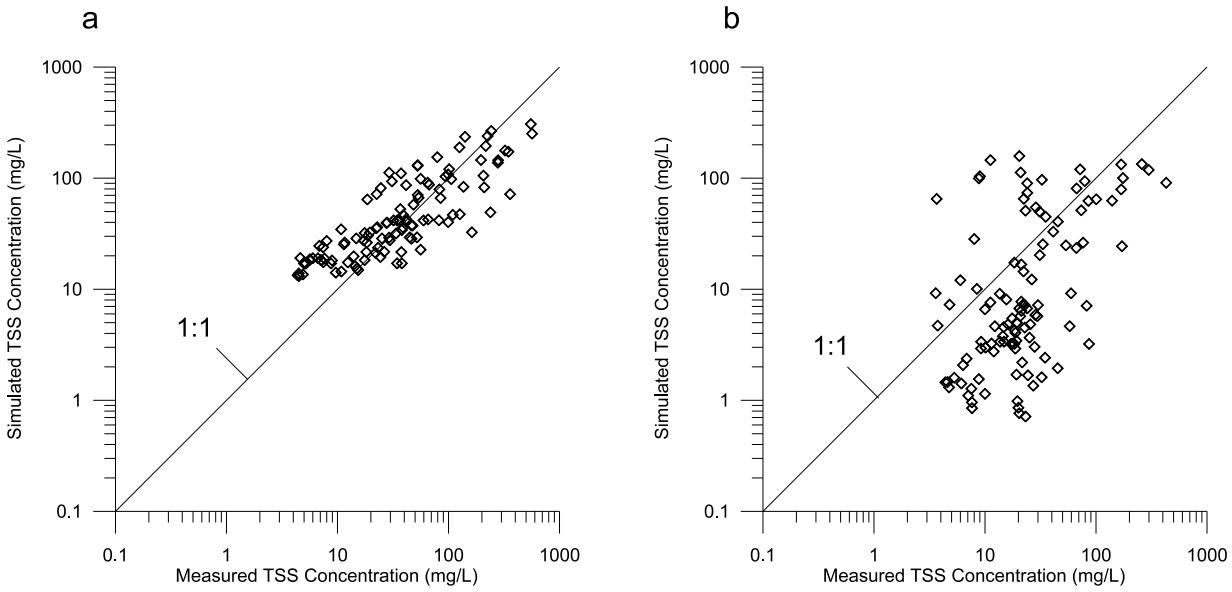

Figure 8.1: Measured and Simulated TSS Concentration Comparison for Calibration Period - a) East Sub-basin and b) West Sub-basin

The East basin showed little bias in the calibrated results shown in Figure 8.1, with equal scatter on both sides of the 1:1 line. The West basin showed some bias, with simulated TSS concentrations less than measured on average for the calibration period, but also showing a greater degree of scatter around the 1:1 line. It is noteworthy that during sample analysis the measurement of TSS concentrations below 1.0 mg/L was not generally possible, which is noted by the lack of sampled data below this value in Figure 8.1b. The

Efficiency Formula	East	West	Combined
OLS	350 563	701 126	525 845
SLS	1 759	1 510	1 634
NASH	0.439	0.217	0.328
NOLS	0.093	0.121	0.107

Table 8.4: Sediment Calibration Period Objective Function Values

model results were not restricted by these lower limit concentrations in the simulations and consequently produce a population of samples well below the simulated concentration of 1.0 mg/L. This disparity between the measured and modelled data resulted in a disparity that was manifested as skew when plotting 1:1 plots in this manner.

The calibrated parameter values shown in Table 8.3 highlight differences between the two sub basins. The East sub-basin had much higher values for C_s and K_s which indicate a higher sediment carrying capacity, which was observed in the measured data in Chapter 6.

8.2.3 Validation Results

Validation is a testing process applied to a model that compares simulated output with measured observations employing data not used in development (eg. calibration). A valid model will produce satisfactory results when compared with new data which is an indication that the model structure and forumulation is "correct", in that it can simulate an aspect of the modelled system. The validation of the water quality model with regard to sediment transport simulation was conducted in three different ways: the ability of the model to match measured sediment concentrations, the model's ability to reproduce measured event-based sediment loads, and the ability of the model to match monthly loading estimates. These differing temporal scales allow for an examination of the utility of the model. The matching of instantaneous measured concentrations is the most challenging as it requires a high degree of accuracy and timing precision for all hydrological and water quality processes for accurate simulation. However, event-scale and monthly-scale comparisons are more forgiving, for although the precise timing and therefore concentrations may not be well matched, over the scale of several days or a month the model may produce similar modelled and measured quantities.

Validation - TSS Concentration Comparisons

The calibrated model was first compared against the measured TSS concentration data outside of the calibration period. This period included the measured TSS data in the East

and West Sub-basins from 1 May 2006 to 1 April 2007.

Table 8.5 shows the calculated statistics for the validation period. When compared with the calibration period results in Table 8.4 the validation period showed markedly worse statistical values. Of particular interest are the NASH and NOLS values, which were normalized to the average measured values. The NASH values for the east basin remained above zero for the east sub basin, indicating that the model performed better than the mean value as an estimation of the measured TSS concentration values. The West basin performed worse, with the NASH value being negative, implying an average value was a better estimation than the model for the estimating the measured TSS concentration values for that sub basin. It is important to note, however, sample values are sparse and represent a very small portion of the overall simulation period, and that the NASH and NOLS values are very sensitive to hydrograph timing. The model should not be discounted entirely on such grounds.

Efficiency Formula	East	West	Combined
OLS	1 025 000	235 000	630 000
SLS	1 580	1 230	1 400
NASH	0.160	-0.145	0.008
NOLS	0.146	0.166	0.156

Table 8.5: Sediment Validation Period Objective Function Values

Figure 8.2 shows the combined comparison of the simulated and measured concentrations for the East and West sub-basins, with the calibration and validation data sets shown on the same plot for comparison. One can observe the generally uniform distribution around the 1:1 line but with larger degrees of variation for both the East and West basin for the validation data set. The tendency of the model to overestimate at low flows can be attributed to the in-channel sediment transport model employed. In the model some TSS will be transported under even the lowest flow regime. In fact, there is likely a shear-stress or stream power threshold that must be overcome before significant TSS will appear in the stream. This approach considered adequate for this study because the interpolation procedure to simulate monthly flows makes a similar assumption, and that the low flow regimes represent a relatively small total contribution when compared to the larger runoff

events.

Validation - TSS Event Loading Comparisons

The model was also validated against the calculated event loads for the intensively sampled events during the sampling period. The method for event-based sediment loads calculation from measured data was described in Section 6.7.4. Event-based load calculations from simulated data were calculated in a similar way, with the start and end time of the event prescribed from the measured data calculation and the total mass flux was determined through integration of the modelled hourly flow and concentration data over the event period. The same integration algorithm code was employed for the simulated event loads as for the measured event loads.

Figure 8.3 shows the simulated and measured event loads for TSS. The events are identified as either belonging to the calibration or validation period, although it should be noted that the event loading was not considered in the objective function *per se*. The model simulated the east basin event loads more accurately than the west sub basin. In both cases the largest events were not modelled well and exhibited the greatest absolute error. This was attributed to the lack of snow melt volume in the simulation resulting in an underestimation of the total flux mass for both sub-basins in both seasons.

Validation - TSS Monthly Loading Comparisons

To validate the model's ability to simulate monthly loading estimates, the calibrated flow and sediment concentration results were employed to calculate average monthly sediment fluxes. These simulated values were compared with the monthly flux values calculated in Chapter 6 and presented in Figure 6.11. The results of the monthly-averaged simulation data comparison to the measured monthly data for the East and West sub basins are presented in Figures 8.4 and 8.5, respectively. In these figures the TSS loading patterns were well matched for the East sub basin, with the clear exceptions of March 2006, and March 2007. In both of these months the simulation greatly underestimated the runoff volumes due to errors in the estimation of the snow melt in the model. The underestimation of the snow pack for the runoff resulted in greatly reduced sediment loading estimates. The

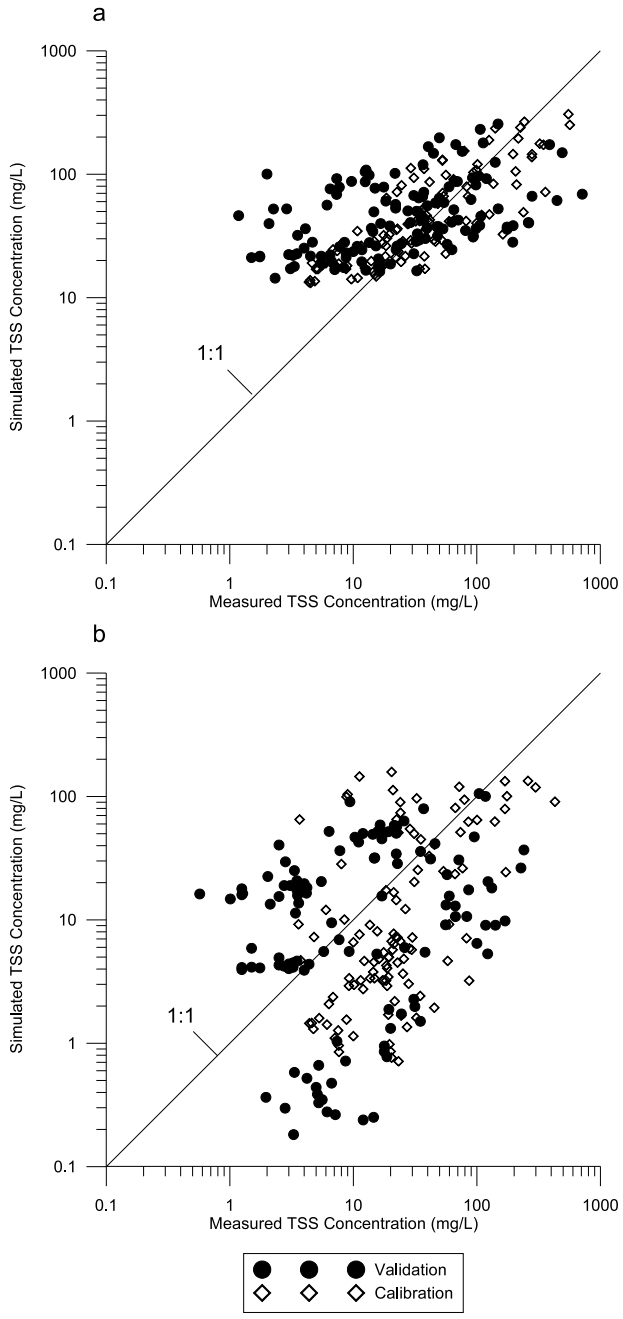

Figure 8.2: Sediment Concentrations - Model Calibration and Validation for a) East Sub-Basin and b) West Sub-Basin

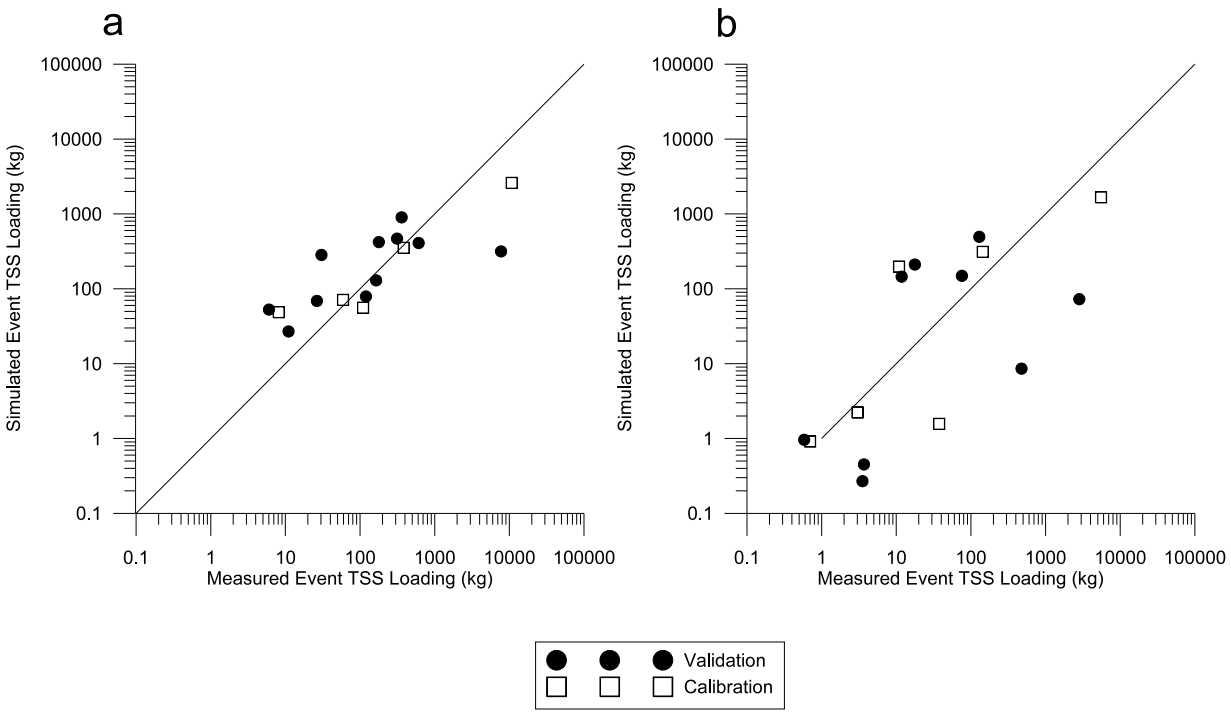

Figure 8.3: Sediment Model - Event Load Comparison for a) East Sub-Basin and b) West Sub-Basin

West sub basin showed a similar matching of the observed monthly patterns in TSS loading with the exception of three months: March 2006, May 2006 and March 2007. The months of March 2006 and March 2007 were underestimated for the same reasons as described for the East basin above. The May 2006 month had an observed event that was much larger than modelled which skewed the loading for that month.

The comparison of the monthly loading on a 1:1 plot for both the East and West sub-basins is presented in Figure 8.6. For the East sub-basin the fit was very good with the only two points that did not fit well on the 1:1 line being the points representing the two snow melt months. The West basin had a poorer fit, but as with the East sub-basin the two points with the greatest error were those representing the snow melt months. Adjustment of the degree of snow pack was conducted to examine the effect on model performance in a subsequent section (see Section 8.2.5).

The goodness of fit observed in Figures 8.6 requires qualification. The loading estimates based on measured data were determined by an exponential relationship with flow rate or interpolated fit (see Section 6.7.5). For the east sub-basin a reasonable fit was found using an exponential relationship for the entire measurement period, and for the West sub-basin an exponential relationship was found to fit for the higher flow (winter) months. If the dominant process that determines sediment loading in the stream is a flow-based carrying capacity as identified by (7.30) (see Section 7.6) then the "measured" and "simulated" monthly loading estimates identified in Figure 8.6 would be necessarily similar. As described in Section 8.2.4 below, this was observed to be the case.

8.2.4 Model Sensitivity

The determination of the degree of sensitivity of the model to adjustment in the estimated and model parameters is important in that it helps elucidate the dominant model processes that contribute to simulated sediment concentration profiles and loading. The sensitivity of the sediment transport model to adjustment of the calibrated and estimated parameters was assessed using the normalized sensitivity coefficient approach outlined by McCuen (1973). In this approach the sensitivity coefficient is determined through relative change in model output due to a known change in a parameter value. The equation for the

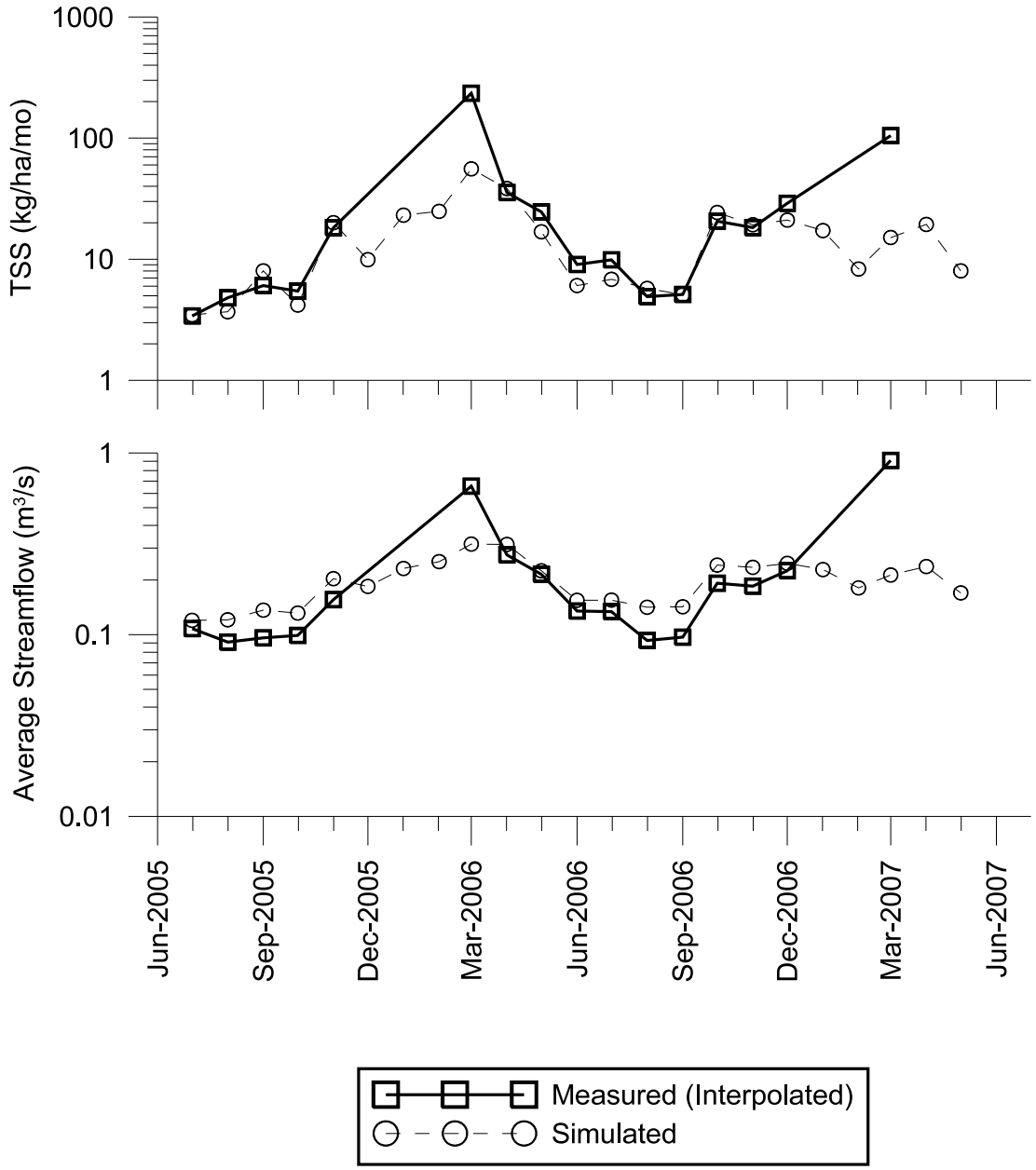

Figure 8.4: Monthly Sediment Load - Measured vs. Simulated - East Sub-Basin

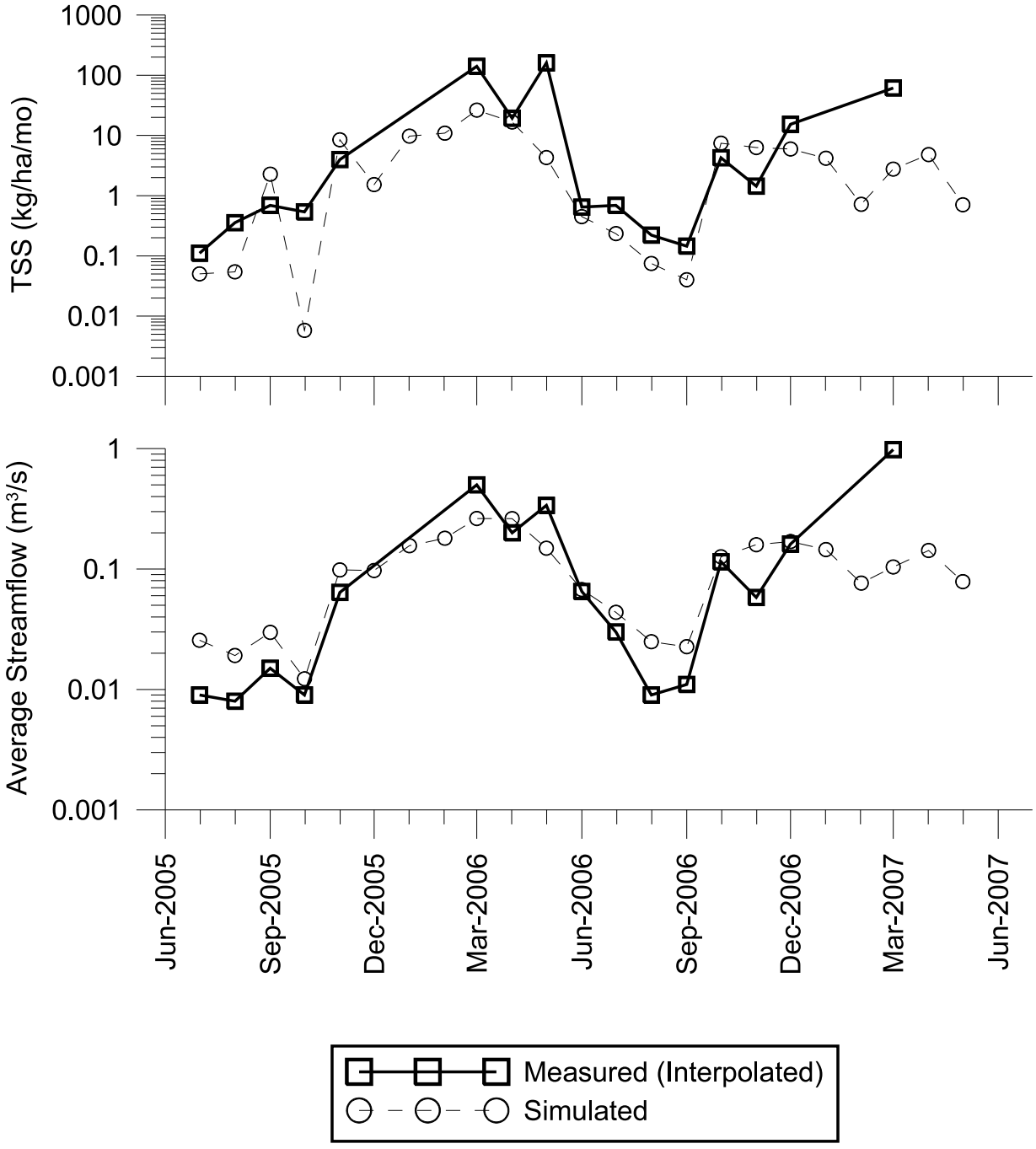

Figure 8.5: Monthly Sediment Load - Measured vs. Simulated - West Sub-Basin

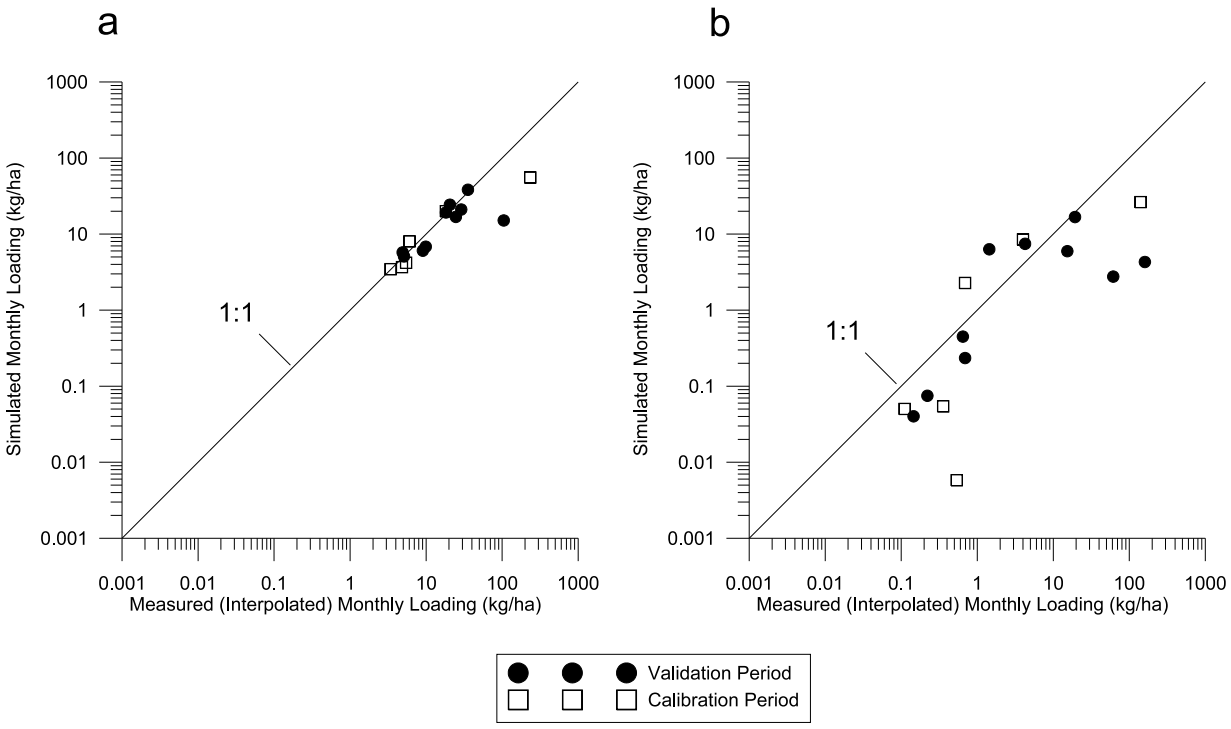

Figure 8.6: Monthly Measured and Modelled TSS Loading Comparison - a) East Sub-Basin and b) West Sub-basin

sensitivity coefficient is presented in (8.8)

$$R_s = \frac{\Delta F_0}{F_0}\frac{F_i}{\Delta F_i} \tag{8.8}$$

where R_s is the relative sensitivity, F_0 is the reference case model output, ΔF_0 is the change in model output due to parameter perturbation, F_i is the reference case parameter value, and ΔF_i is the change in parameter value or parameter perturbation.

For this sensitivity analysis the same objective function values were employed as with the calibration procedure: the Normalized ordinary least squares (NOLS) and the Nash-Sutcliffe (NASH) objective functions. Each model parameter was adjusted by 5% and the resulting changes in the objective functions were recorded. The sensitivity results are presented in Appendix D, Section D.6. The entire simulation period (Jan 2005 to May 2007) was considered in the analysis. In addition to the sediment model parameters specified above, some additional scale parameters were adjusted to examine the effect of estimated parameter values in the original AGNPS model. These included adjustment to the overland-flow sediment transport parameters a and b. Additionally, to change values in the estimated distributed soil type data $d50$, spg and $erod$, three corresponding factors were introduced to the model $d50f$, $spgf$, $erodf$. These three factors represent a multiplicative adjustment with 1.0 being the exact values stored in the sediment (SED) file.

The sensitivity results to the NOLS objective function illustrated the models sensitivity to matching point measurements. The most sensitive parameters for both basins were the sediment carrying capacity coefficients C_s and K_s. The sedimentation and resuspension velocities were the next most sensitive followed by the river dispersion coefficients. The model's sensitivity to total loading reveals that the sediment carrying capacity coefficients are also the most important with regard to sediment delivery from the watersheds. The other parameters like settling velocities and dispersion coefficients, which have a somewhat important role in matching the sediment time series (matching the NOLS objective function) are not important in total sediment delivery from the sub-basin.

The land surface parameters including both the riparian and land surface sourcing parameters were insensitive. These results show that the dominant processes as described

by the model are the in-channel processes, primarily the parameters that set the sediment carrying capacity of the stream. The dimensionless dispersion coefficient was not as sensitive but showed some impact on the model's ability to predict the sediment concentrations. The land surface parameters, including the riparian parameters, were not sensitive, which implies that any contributions made to the stream are quickly dominated by in stream process including sediment suspension and deposition. Additionally, the frequency of events that contribute to overland flow are few during the simulation, necessarily contributing infrequent sediment loading from overland. As a direct consequence the riparian retention parameters are also insensitive as they depend on upstream sediment loading to have an impact on in-stream concentrations.

It is believed that there are a number of factors that contribute to the model's insensitivity to land surface sediment parameters. The land surface sediment delivery model is physically based, and as such requires a reasonable estimate of land slope, water depths, etc. However, with a discretization limit of 1km in the WATFLOOD model, any local steep slopes that are observed at the sub-kilometre scale will be smoothed, and rill and gully erosion cannot be considered as the runoff is simulated as an approximation of sheet flow (average depth) in the sediment delivery sub-model (Leon, 1999). This modelling artifact is understood and has been investigated recently by Rojas et al. (2008) using the CASC2D-SED model. The authors found reduced accuracy with grid resolutions greater then 150m in a study of Goodwin Creek experimental watershed. Although the modelling approaches are different than those presented here, the principle of averaging the topology over a large area can have direct consequences with regard to sediment delivery. Empirical approaches, like the USLE and its variants, can be corrected for grid size and other variations to more closely match modelling results and are not physically as constrained (Julien and Frenette, 1987; Das et al., 2008).

The model was also examined as to its sensitivity to the WATFLOOD hydrologic parameters. The same sensitivity analysis was conducted as with the water quality parameters with a 5% perturbation in values and an assessment of the change in absolute objective function values and the total sediment loading. The sensitivity analysis results are shown in Appendix D, Section D.6.1. The paramters adjusted for the hydrologic sensitivity anal-

ysis are discussed in Chapter 5 and in Kouwen (2005) and summarized in Appendix D, Table D.1.

The sensitivity results showed that the sediment transport model fit is most sensitive to infiltration and surface roughness parameters in the GRU (AK, R3) as well as retention storage (RETN) and depression storage (DS). All of these parameters influence greatly the shape of the storm hydrograph and, considering the dependence of the sediment model on in-stream characteristics, influence of these parameters on model fit is expected. Additionally, a number of channel parameters are sensitive to sediment model fit, primarily the channel roughness (R2N) which will influence the velocity and therefore the sediment carrying capacity, and the geometry parameters (aa2,aa3, and aa4) which dictate the cross sectional area and also influence the flow velocity.

The effect of parameter perturbations on total sediment loading showed similar sensitive parameters to that of objective function fit, with the notable exception of the groundwater parameters (lzf, pwr) and the conductivity wetland parameters (kcond). These parameters have a strong effect on loading as they dictate the inter-event flow conditions which can contribute small sediment concentrations, but over long periods of time. These parameters have less effect on the model fit sensitivity as the majority of samples were collected during runoff events.

8.2.5 Snow Ablation Adjustment

The errors associated with the snow melt months were further investigated by adjusting the snow pack in the WatFlood model to match the observed snow melt runoff. This was accomplished by updating the snow volumes in the model so that the total runoff for the month matched more closely the observed runoff volumes. The WatFlood model contains a snow adjustment factor in the event file (eventsnowscalefactor) which allows for the adjustment of the total snow content for the entire model by this factor. The snow scale factor was adjusted for the months of March 2006 and March 2007 to best match the total runoff for both the East and West basins. Additionally some parameters in the model were adjusted to ensure the timing of the snow melt matched what was observed in the field for the 2006 season. The results of the adjusted monthly data for the East

and West sub-basins are presented in Figures 8.7 and 8.8 respectively. A comparison of the measured and simulated monthly loadings for both sub-basins with the snow pack quantities adjusted is presented in Figure 8.9. It can be seen that through the adjustment of the snow melt quantities, without a re-calibration of the parameters, the simulation of the TSS loadings improve dramatically although the simulation does now over-estimate the loadings of those two snowmelt months. In Figure 8.9b the largest absolute outlier that remained was the month of May 2006, which also represented a month when the modelled and measured hydrological response of the basin did not match well. A re-calibration of the sediment transport with the corrected flow would certainly improve on the simulated results further. This simple adjustment of the model shows the great degree of sensitivity of the model to errors in the hydrology of the system.

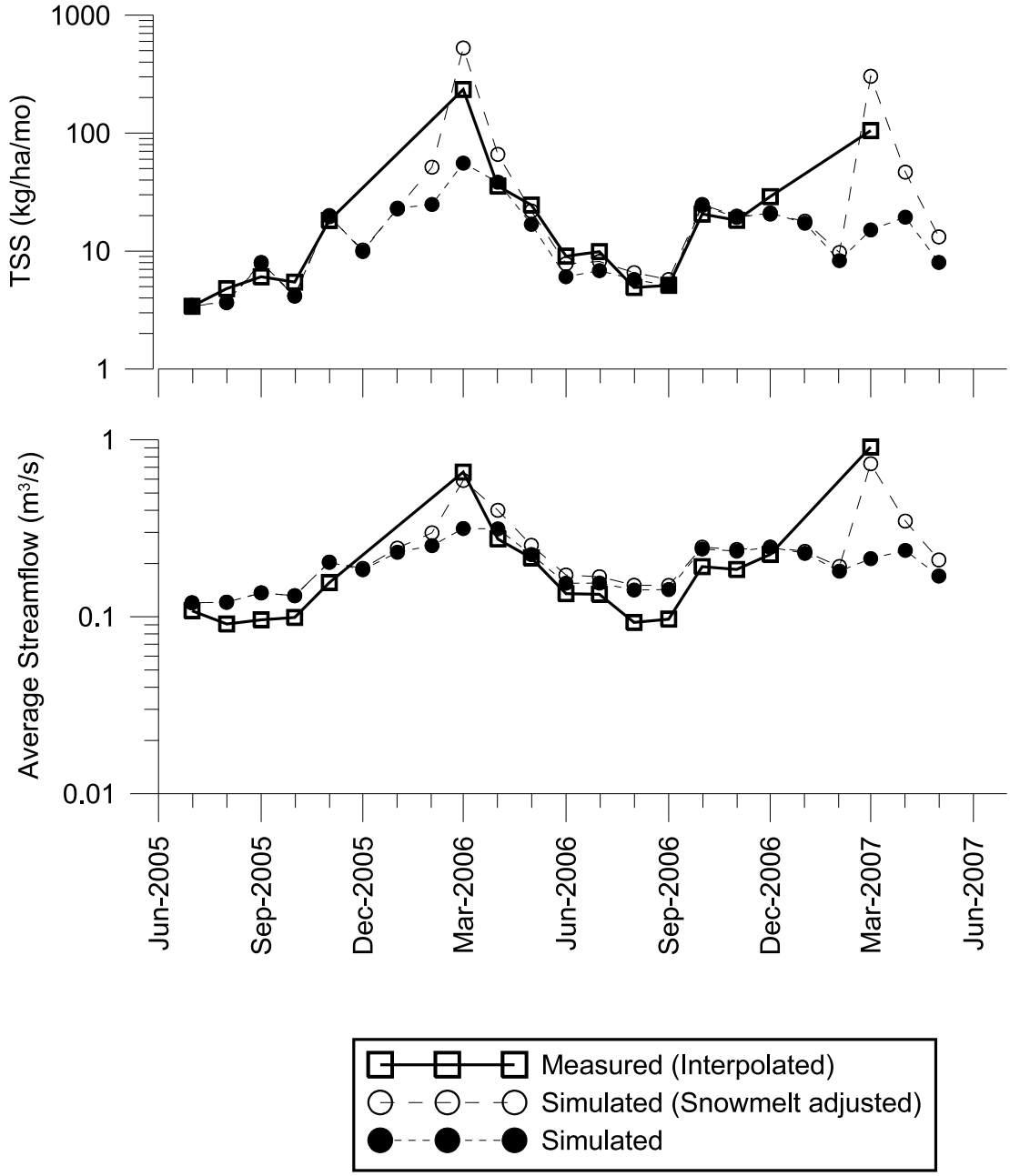

Figure 8.7: Monthly Sediment Load with Adjusted Snow Pack - Measured vs. Simulated - East Sub-Basin

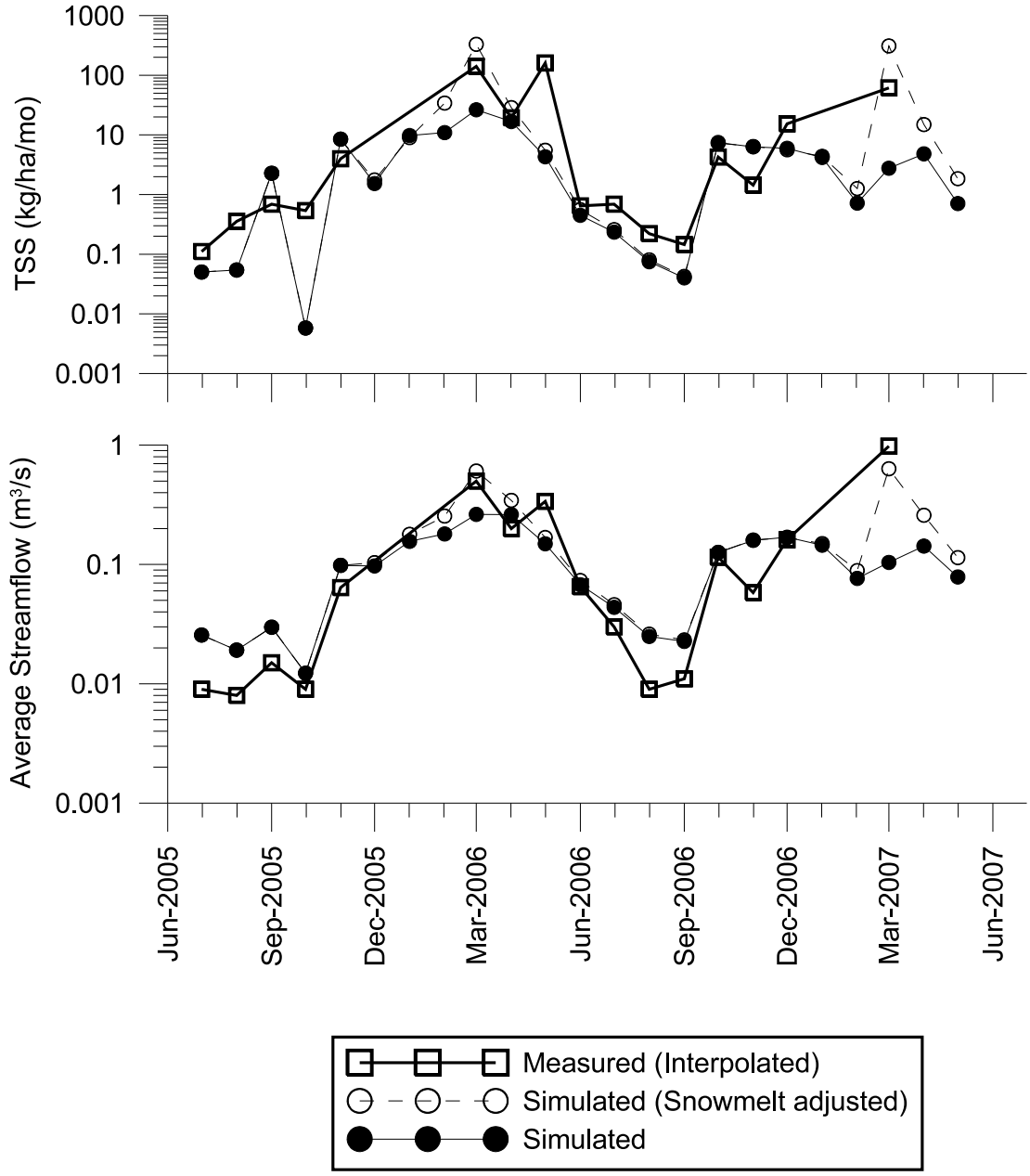

Figure 8.8: Monthly Sediment Load with Adjusted Snow Pack - Measured vs. Simulated - West Sub-Basin

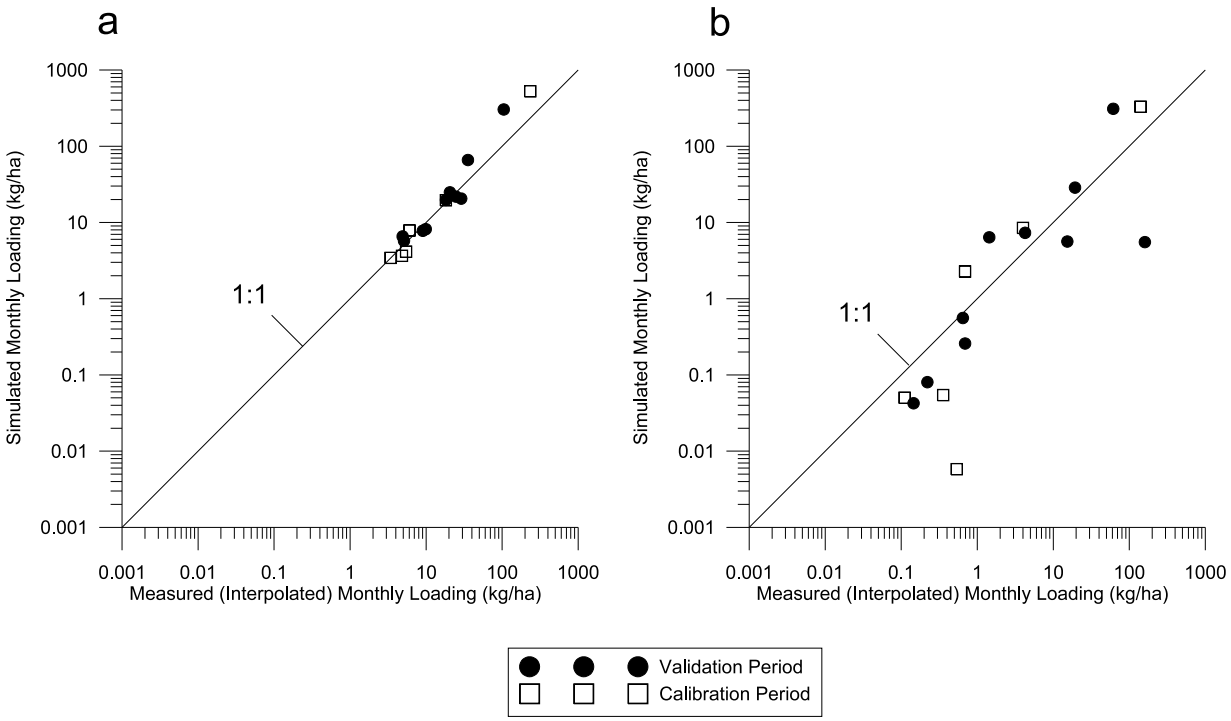

Figure 8.9: Monthly Measured and Modelled TSS Loading Comparison with Adjusted Snow Pack - a) East Sub-Basin and b) West Sub-basin

8.3 Nitrate Transport Modelling

The Canagagigue Creek simulations using the nitrate transport model required the estimation of a number of parameters for mineralization, nitrification and nitrate removal processes. Additionally, the simulation required an estimate of the crop nutrient uptake as well as the fertilizer type and application as described in Chapter 7. This section begins with the estimation of these values, then calibration, validation and sensitivity results follow.

All nitrate simulations were conducted with a three year spin-up period with the same parameter and loading rules. It was observed that two years were required for the nitrogen state variables to reach steady state, and a three-year spin-up provided a reasonable buffer.

8.3.1 WatFlood/AGNPS Model and Parameter Estimation

The WatFlood/AGNPS nutrient water quality model uses a simple nitrogen balance approach to determining nitrogen concentrations in receiving waters as described in Chapter 7. For the nitrate transport model several key parameters had to be estimated within the established WatFlood/AGNPS land surface sediment sourcing model. The nitrogen transport module requires estimation of the following: nitrate concentration in the rainfall (N_{crn}), the mineralization rate of organic nitrogen (k_{min}), the nitrification rate of ammonia (k_{nit}), the land surface nitrogen process temperature correction coefficient (Q_{10}). The riparian nitrate removal coefficient (k_{20}) and temperature correction coefficient (θ_T). Crop nitrogen uptake estimates (N_{max}) were also required for the agricultural land class in the model. And estimates were required for nutrient loading quantities, character and timing, cropping dates and residual organic nitrogen from stover, or crop residue. A number of the nitrogen decay factors employed in the event based model are still present in the WQP file, including the nitrogen decay factor (N_{dec}) and empirical enrichment and delivery coefficients (N_{rec}, N_{lec}, N_{dec}, N_{cpw}) but have been deprecated and is now supplanted by physically-based and time-variable processes (see Section 7.6). The methodology for the selection of the above unknown parameters is outlined below. Table 8.6 outlines the parameters available in the nitrogen process sub-model.

Parameter	Description	Units	Scope	File	Notes
Grouped Response Unit					
N_{crn}	nitrogen rainfall	mg/L	watershed	*.WQP	
N_{rec}	nitrogen runoff	1/mm	watershed	*.WQP	deprecated
N_{lec}	nitrogen leaching	1/mm		*.WQP	deprecated
N_{dec}	carrying capacity	-	watershed	*.WQP	deprecated
N_{cpw}	nitrogen pore water	mg/L	watershed	*.WQP	deprecated
N_{snc}	soil nitrogen	g N / g	land class	*.WQP	deprecated
k_{min}	organic nitrogen mineralization	day^{-1}	watershed	*.WQP	
k_{nit}	ammonia nitrification	day^{-1}	watershed	*.WQP	
Q_{10}	temperature correction	-	watershed	*.WQP	
$omaff$	fertilizer loading factor	kg-N ha^{-1}	land class	*.WQP	
$residf$	residual factor	-	land class	*.WQP	
upf	nitrogen uptake factor	-	land class	*.WQP	
Channel					
A_t	temperature fitting parameter	-	river class	*.WQP	
B_t	temperature fitting parameter	-	river class	*.WQP	
δ	temperature fitting parameter	day	river class	*.WQP	
Riparian					
k_{20}	decay parameter	day^{-1}	river class	*.WQP	
θ_T	temperature correction factor	-	river class	*.WQP	

Table 8.6: Nitrate Sub-Model Parameters

8.3.2 Crop Nitrogen Uptake Estimates

Crop nitrogen uptakes estimates were determined by taking a weighted areal average of the crops employed in the region based on photographic surveys. In fact, over the period, the crops were regularly rotated in the area. However, data regarding these cropping sequences was not available. Consequently, the best crop estimate was determined using the known crop distributions based on collected photographic surveys. Photographic survey results were presented in Section 3.3. The nutrient uptake rates for various crops are presented by OMAFRA (2008b) and also available from the Canadian Fertilizer Institute (CFI, 2001) which produces an estimate of nitrogen uptake and removal at the time of harvest. Heard and Hay (2006) found that the CFI estimates for prairie crop nutrient uptake and removal generally matched other regional studies, although uptake rates are dependant on a number of factors including climactic conditions, nutrient loading rates and timing. Figures from CFI (2001) and OMAFRA (2008b) are summarized below in Tables 8.7, 8.8, and 8.9 which present the estimated annual nitrogen removal rates, nitrogen uptake rates, and previous crop nitrogen remaining after removal respectively. All annual uptake and removal rates have been converted to kg / ha for a standard estimated crop yield. The removal rates cited by OMAFRA and CFI are similar although the CFI numbers are consistently higher for each crop. The CFI report identified both uptake and removal rates for various crops, the difference being the nitrogen remaining on field after harvest. OMAFRA provides a nitrogen removal rate in addition to a previous crop nitrogen estimate to indicate the degree of nitrogen available after harvest (Table 8.9). It is identified in CFI (2001) that the uptake for soybeans and other legumes in Table 8.8 comes primarily from the atmosphere.

The crop nitrogen uptake in the model was assigned to the N_{max} parameter for the

	Annual Crop Nitrogen Removal (kg-N/ha)	
	OMAFRA (2008b)	CFI (2001)
Grain Corn	135	168 - 188
Wheat	101 - 165	179 - 201
Soybean	217	224 - 251

Table 8.7: Crop Nitrogen Annual Removal Rates

	Annual Crop Nitrogen Uptake (kg-N/ha)
	CFI (2001)
Grain Corn	190 - 269
Wheat	157 - 179
Soybean	258 - 325

Table 8.8: Crop Nitrogen Annual Uptake

	Annual Previous Crop Nitrogen (kg-N/ha)	
	OMAFRA (2008b)	CFI (2001)[1]
Corn	11 - 34	22 - 81
Wheat	-	22
Soybean / Legumes	45	34 - 74

[1]calculated from Tables 8.7 and 8.8

Table 8.9: Previous Crop Nitrogen

"agriculture" GRU class. The single parameter was estimated based on an area weighted average of each of the crops with the exception of soybean, which generally acquires nitrogen from the atmosphere. Using the uptake ranges outlined above the weighted average of the fertilizer nitrogen uptake for the region was 98 – 184 $kg - N/ha$ over a growing season.

8.3.3 Nitrogen Loading Estimates

Fertilizer loading as applied to agricultural fields in a watershed can be very difficult to estimate. The timing, quantity and character of the fertilizers applied to agricultural fields in the study region was not recorded and so had to be estimated based on other available surrogate data. Researches have estimated fertilizer loads in watersheds using a number of methods including matching the fertilizer application to crop uptake requirements, the adherence to regional fertilizer loading recommendations provided by government authorities, the application of manure fertilizer based on livestock census or survey data or some combination of these methods. No detailed fertilizer application data for the area was available. Consequently, a loading estimate function was required to estimate the applied fertilizer loading in the study area, based on average land use, photographic surveys, and OMAFRA fertilizer application guidelines similar to an approach outlined by Scott (2006).

Fertilizer Application Timing and Quantity Variability

The regional provincial agricultural ministry (OMAFRA) provides detailed guidelines for farmers for recommended annual applications rates of nitrogen based on a number of factors including fertilizer application history, cropping history and manure or fertilizer characteristics and application rates. Even with the prescribed loading guidelines the nitrogen application can be expected to vary. Nitrogen annual loading rates are in Southern Ontario as recommended by OMAFRA (2008b) vary from 168 kg/ha to 213 kg/ha, wheats have a recommended nitrogen loading rates from 71 kg/ha to 151 kg/ha, forage fields have recommended loading rates from 56 to 112, without legumes, etc. Based on these figures the variability in nitrogen loading can be from $\pm 8\%$ to $\pm 57\%$. This variation in possible nutrient application was built into the mode application function with a loading variability of $\pm 20\%$ from prescribed guidelines.

Determining the exact timing of fertilizer loading is difficult but in the region it was observed that fertilizer was generally applied at the beginning and the end of the growing seasons and manure was typically applied. Similar conclusions were drawn from studies conducted by Scott (2006) when examining nitrate loading in the Grand River watershed. In the model the timing of the application was not allowed to vary and loadings were applied at the start or the end of the end of the growing season every year as constrained by the model (see Section 7.10.5).

Regional Manure Fertilizer

With a large number of Mennonite communities in the region manure application to fertilize fields is common (Scott, 2006; Cooke, 2006). Through observations of the field site and discussions with local farmers the predominant nutrient loading is through the application of cattle and swine manure, and the applications tend to occur at the start of the growing season in early spring or after the growing season in the early fall. On some occasions it was observed that manure was being spread on fields before the snow melt, although this is not recommended by provincial guidelines.

Statistics Canada provides estimates of livestock head counts for various census years for all of Canada, including the three municipal townships containing the Canagagigue

Creek watershed: Centre Wellington and Mapleton (Wellington County) and Woolwich (Municipality of Waterloo). Scott (2006) performed a basic manure accumulation estimate analysis for the entire Grand River Watershed county by county employing livestock head counts provided by Statistics Canada, estimated manure production levels by livestock type provided by OMAFRA, and crop application area based on GRCA LULC maps. Annual summaries of the estimated loading rates for census data years are presented in Table 8.10. Other assumptions implicit in this technique was that the manure produced in one county would be applied to farm fields in the same county, which could not be verified. Additionally fertilizer application periods were considered with application of manure before and after the growing season with approximately 56% of the manure being applied before and the balance after the growing season, based on estimates of manure storage capacity in the region.

Table 8.10 shows manure availability that is well below the nutrient uptake requirements for the crops considered in this region (Tables 8.7 and 8.8). This was identified by Scott (2006) and the nitrogen deficit was assumed to be made up through the addition of artificial fertilizer in the form of urea when necessary as it was cited as the most common artificial fertilizer in the region. Referring to analysis of the regional manure supply for the three townships based on livestock head count 81 – 92% of the available nitrogen from manure is from cattle, the balance being from pig (4 – 15%) and poultry (3 – 4%). Ammonia content can be estimated from the source of the manure. Dairy cattle manure has higher ammonia content than other cattle type (OMAFRA, 2002). Census estimates show that slightly less than half the cattle in the region is dairy (37 – 50%). Considering loading in

Estimated Manure Application by Township (kg-N /ha)

Year:	1981	1986	1991	1996
Centre Wellington	54.2	45.0	41.5	52.8
Mapleton	56.0	55.6	50.5	84.5
Woolwich	56.3	53.1	49.4	68.5
Township Average - Grand River Watershed	48.6	46.1	47.0	49.0

Table 8.10: Regional Manure Application Estimates - Adapted from Scott (2006)

the region as an amalgam of the available manure types provided by OMAFRA (2002) the ammonia content for manure in the region on average is estimated between 18 and 27%. Total available manure nitrogen available for application in any given year was taken to be the 1996 average for the three counties containing the study site, or 69 kg-N/ha, with 20% of the available nitrogen being as ammonia.

Fertilizer Loading Function

Determining the amount of additional fertilizer added to fields was determined using the fertilizer loading guidelines provided by the OMAFRA NMAN Worksheet as a primary guide (OMAFRA, 2008a). The OMAFRA Nutrient Management workbook provides guidelines as to the quantities of manure nitrogen to be applied to a field based on cropping and fertilizer application history. Guidelines such as these are designed to provide adequate nitrogen for crop uptake yet minimize the over application of nitrogen which can lead to a nitrogen surplus and movement of nitrogen into ground and receiving waters. Although the effectiveness of these methods has been brought into question by some researchers and environmental organizations (Harman et al., 2000), it is presumed that the applied fertilizer loadings in the region can be approximated by these recommendations. The OMAFRA loading function can be summarized as

$$N_{fert} = N_{crop} - N_{NH_4^+} - N_{NO_3^-} - 0.10(N_{org_{-1}}) - 0.05(N_{org_{-2}}) - 0.02(N_{org_{-3}}) \qquad (8.9)$$

where N_{fert} is the quantity of *available* nitrogen fertilizer added in a year $[kg - N/ha]$ with the non-mineralizable portion of nitrogen not included in that figure. N_{crop} is the annual nitrogen requirement of the crop, $N_{NH_4^+}$ and $N_{NO_3^-}$ are the quantities of ammonium and nitrate in the soil at the start of the growing season respectively and $N_{org_{-i}}$ is the amount of organic nitrogen applied to the soil during previous year i. Equation (8.9) estimates organic nitrogen contribution for a year assuming 10% of organic nitrogen from a fertilizer application will be available in the second year, 5% will be available in the second year and 2% will be available in the third year. For nitrogen application in the

model, the crop uptake is estimated, based on OMAFRA published estimates, the NH_4^+ and NO_3^- quantities are state variables in the model and the application history is also known. Fertilizer is applied first as available manure, and then the balance is made up through the addition of ammonium which is to simulate the addition of urea or similar chemical fertilizer.

Residual Estimates

Based on the estimates of agriculture crop area obtained from photographic surveys (see Chapter 3) and using a weighted average of the nitrogen uptake and organic nitrogen residual, the range of annual fertilizer nitrogen uptake was 98 – 184 kg-N/ha. Residual estimates ranged from 14 – 65 kg-N/ha or 14 – 35% of the crop uptake on average. These ranges were employed in driving the fertilizer loading in (8.9).

Model Implementation

The rules for fertilizer loading are described in Appendix D using a pseudocode algorithm structure presented in Figure D.20. This algorithm employs the above data to determine the quantities of nitrate nitrogen applied while preserving the annual loading requirements set out by (8.9). The exception is that all manure produced is applied to the fields regardless of the crop demand. In the model the calculations of the crop uptake rate, the crop percentage residual and the nitrogen required are all adjusted within the parameter file to allow for the variability in the input data. Crop uptake is set by upf, the crop residual percentage is set by $residf$ and the recommended loading rate calculated by (8.9) is multiplied by $omaff$ in the model to adjust total fertilizer application quantities.

8.3.4 Nitrogen from Rainfall

Nitrogen from rainfall was not measured directly. A number of rainfall samples were collected in fall of 2005 to ascertain the degree of nitrogen in the rainfall but concentrations were very low, at or near the detection limit for nitrate. Previous modelling by Leon (1999) in southern Ontairo presumed 1 mg-N/L of nitrogen in the rainfall. A field study by

Rudolph and Parkin (1998) estimated total nitrogen loading from atmospheric sources to be 13 - 15 kg-N/ha for a field site at Kintore, ON, between Waterloo and London. With an average annual precipitation in the region of approximately 900 mm /yr, this is equivalent to approximately 1.6 mg-N/L on average. An allowed range of 0 to 1.6 mg-N/L in rainfall was assumed in the model.

8.3.5 Nitrogen Mineralization and Nitrification Rates

The nitrate transport model required an estimated for the mineralization rate of organic nitrogen to ammonia nitrogen (k_{min}), the nitrification rate of ammonia nitrogen (k_{nit}) and the temperature adjustment factor applicable for region(Q_{10}).

Of the net organic nitrogen mineralization rates in soils reported in the literature Stanford and Smith (1972) is among the most cited, where in a laboratory experiment of 39 differing soils the reliable rates estimate for k_{min} was $.054 \pm .009\, week^{-1}$ or $7.71 \pm 1.29 \times 10^{-3}\, day^{-1}$. Campbell et al. (1984) conducted a number of nitrogen mineralization test on Canadian prairie soils and found a range of k_{min} values at 25°C from $0.014 - 0.10\, week^{-1}$ or $2.0 \times 10^{-3} - 1.4 \times 10^{-2}\, day^{-1}$. The range provided by Campbell et al. (1984) was used as a possible range organic nitrogen mineralization rates in the model.

Nitrification rates have been reported in the literature, which tend to be significantly more rapid than mineralization rates in soils (Tate, 1995). Johnsson et al. (1987) employed a k_{nit} value of 0.20 day^{-1} Saâdi and Maslouhi (2003) and Jury et al. (1976) both employed a k_{nit} value of 0.24 day^{-1}. The measured values in the literature are of the same order of magnitude so in the model the nitrification rates were allowed to vary slightly around the reported ranges, from 0.1 day^{-1} to 0.4 day^{-1}.

The temperature adjustment factor, Q_{10}, represents the factor change for a rate constant with a temperature change of 10°C. Saâdi and Maslouhi (2003) used a value of 2 for Q_{10} in their modelling studies. However Campbell et al. (1984) examined mineralization rates in Canadian soils and found that a range of Q_{10} values from 2 to 3 was observed. Andersen and Jensen (2001) found in laboratory mineralization studies with manure that in low temperatures the calculated Q_{10} value for gross mineralization could be markedly higher in the 3-9°C range than the 9 - 15°C range, indicated the breakdown of certain recalcitrant

substances can be slower in colder temperatures, with calculated Q_{10} values as high as 9.9. It was clear from the literature that the need to make allowances for variable temperature dependence in a cold Canadian environment was necessary. In this modelling effort the Q_{10} parameter was provided an allowable range from 2 to 3.

8.3.6 Riparian Wetland Nitrate Removal

An estimate of the first order decay removal rate (k_{20}) and temperature activity coefficients (θ_T) for the riparian wetlands was required for the riparian wetland model originally presented by Crumpton (2001). Crumpton provided a precise estimate of $0.15\,m\,day^{-1}$ for a depth averaged model, and Gale et al. (1993) estimated a nitrogen removal rate range between 0.086 to 0.214 day^{-1}. Crumpton (2001) and Kadlec and Knight (1996) suggest a temperature activity coefficient of $\theta_T = 1.09$. Bachand and Horne (1999) suggests a range of activity coefficients from $\theta_T = 1.15 - 1.22$. Riparian nitrate removal rates reported in the literature vary significantly, and are often reported on an aerial basis as a zero-order removal rate. Many other studies exist that have examined nitrate removal in riparian wetlands based on field mass balance studies and tend to report nitrate removal rates as a percentage of loading or mass removal per hectare per year (Peterjohn and Correll, 1984; Hill, 1996; US-EPA, 2005). It was decided that the range of first order removal provided by Crumpton (2001), Kadlec and Knight (1996), Bachand and Horne (1999) and Gale et al. (1993) would be used in the calibration of the riparian wetland nitrate removal model. For this model a range of possible denitrification rates for riparian wetlands was selected. A zero riparian removal was considered a lower limit, and the upper limit was 0.21 day^{-1} and the activity coefficient was permitted to vary from 1.09 to 1.22.

8.3.7 Calibration Procedure

The calibration procedure employed used a similar approach to the sediment calibration procedure identified in Section 8.2.2. The measured nitrate concentrations were compared to the simulated concentrations based on the WatFlood/AGNPS model to assess model performance and the identical efficiency functions were employed. The calibrated param-

eter values and parameter bounds are shown in Table 8.11.

Parameter	Index	Value	Min	Max
GRU Nitrate				
N_{crn}	n/a	0.418	0	1.6
k_{min}	n/a	0.009	0.002	0.014
k_{nit}	n/a	0.328	0.1	0.4
Q_{10}	n/a	2.578	2	3
upf	n/a	102.493	98	184
$residf$	n/a	0.153	0.14	0.35
$omaff$	n/a	0.867	0.8	1.2
Riparian Nitrate				
k_{20}	3	0.004	0	0.21
θ_T	3	1.197	1.09	1.222
River Temperature				
A_t	3	4.419	4	6
B_t	3	0.767	0.5	1
δ	3	6.476	5	10

Table 8.11: Nitrate Parameters Optimized

8.3.8 Model Performance

As with the sediment model, the nitrogen model was calibrated against the first year of data and then validated against the second year of data. The objective function was an equally weighted normalized least squares function combined for the east and west sub-basins (see Table 8.2). The results of the calibration and validation are shown in scatter-plot in Figure 8.10, and numerically in Table 8.12 and Table 8.13. The nitrate statistical scores are different in character from the sediment scores as the sediment values vary by orders of magnitude whereas the nitrate concentrations are observed over a much shorter range. However, the NASH scores for the nitrate model are worse than the sediment model. Of note is that the validation period generally performs better than the calibration period. Similar to the sediment model, the east sub-basin, which has a better hydrological fit, shows the best performance of the two.

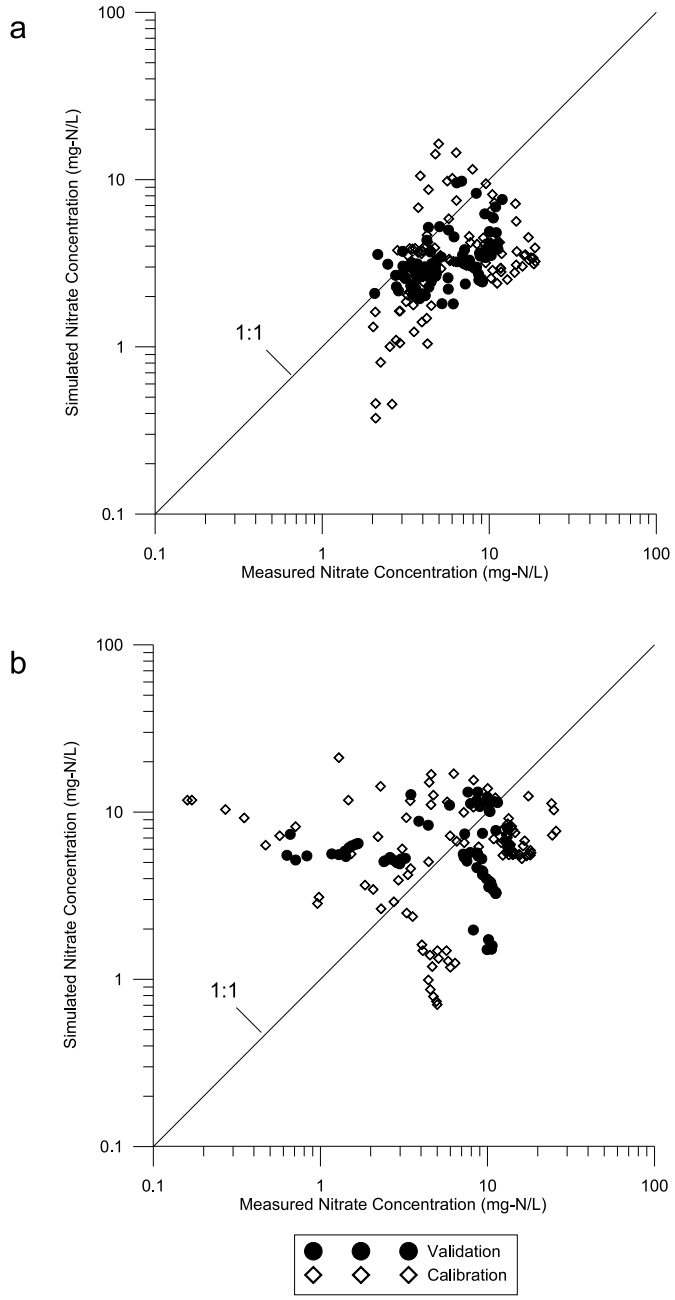

Figure 8.10: Measured and Simulated Nitrate Concentration Comparison - a) East Sub-basin and b) West Sub-basin

Statistic	East	West
NOLS	0.093	0.089
NASH	-0.658	-0.311
OLS	3683.703	4704.462
SLS	117.765	164.608

Table 8.12: Nitrate Model Calibration Statistics

Statistic	East	West
NOLS	0.053	0.072
NASH	-1.028	-0.481
OLS	1667.028	3282.460
SLS	76.180	119.819

Table 8.13: Nitrate Model Validation Statistics

The event-based loading predicted by the model and the estimated loading calculated in Chapter 6 were compared and are presented in Figure 8.11. As clearly observed the east basin event loads are much more accurately simulated than the west basin loads. As with the sediment modelling for the east and west basins the outliers represent the snow melt events which were not captured well in the hydrologic model. Considering most of the sampling points for nitrate nitrogen collection were obtained during sampling events it follows that the event loading estimates would similarly be better for the east basin, which simulated more closely the observed event concentrations. An observation of note regarding event loading in the West basin is that smaller events tend to be over estimated in the model. This can explained by the hydrological problems with the model in ephemeral streams outlined in Chapter 5 where low- or no-flow conditions are not well simulated during summer months. These summer events represent the smallest loading events and with an over-estimation of simulated flow, event-based loading simulation estimates would be expected to be much higher than observed.

Monthly loading was also compared, with the monthly loading estimates calculated in Chapter 6 for nitrogen compared to simulated model output. The results are presented for the West and East sub-basins in Figures 8.12 and 8.13 respectively. Both the east and west simulations are characterized by a lack of variation in simulated loading as compared

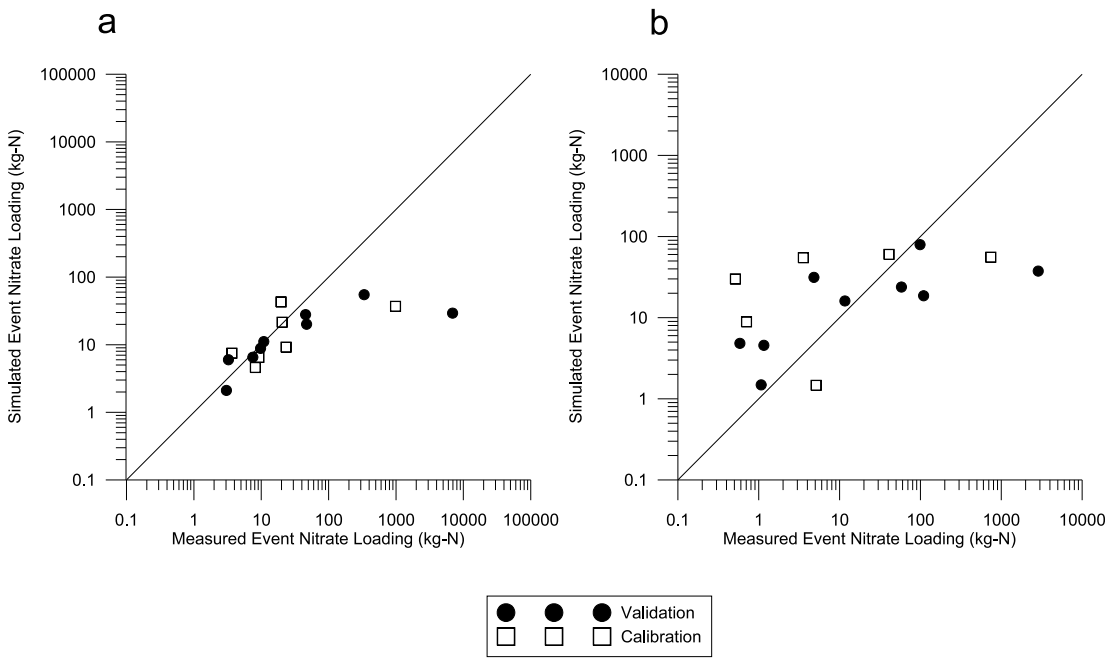

Figure 8.11: Nitrate Event load comparision for a) East sub-basin and b) West sub-basin

to the measured loading estimates. In the west basin the high winter and very low summer loadings are not entirely captured, with the trend visible but the amplitude of the seasonal change not simulated. The East basin shows a similar small change in loading with season, although the calibration of east model has placed the loading closer to the lower range of the loading amplitude. This tendency is also presented when the simulated and measured (interpolated) monthly loads are compared on a 1:1 plot shown in Figure 8.14. For both the east and west sub-basins the model underestimates the months with the higher loads and overestimates the months with lower loads. The discrepancy between the monthly and the event loading estimate accuracy can be partially explained by the nature of the calibration procedure. Nitrate events are characterized by a dip in nitrate concentration with a gradual increase in concentration toward the end of the event as diffuse flow contributes higher nitrate concentrations. The model will be sensitive to the concentration delivered from the model upper zone storage more than in the lower zone. However, for monthly loading estimates the lower zone dictates the background concentrations for large time periods, which can be much higher post event than during the peak flows themselves. Furthermore the storage in the lower zone of a GRU tends to be large, with retention times in the order of 100 days (see Section 8.3.10). Concentration changes in the lower zone are slow to take place in the model. However, the sampling data showed that the concentrations at the tail end of the events could vary substantially, especially in the West sub-basin. Trailing concentrations could be lower than 10 mg-N/L in the summer in that basin but as high as 25 mg-L/N in the fall and spring months. The implication here is that the hydrological model simplified mixing-cell storage may not accurately represent the equivalent "storage" processes observed in the field. Other models including LASCAM (Viney and Sivapalan, 1999) which operates in a similar conceptual way to the WatFlood model have added additional storage zones at the near surface to account for these timing changes to solute delivery to the receiving channel, although in this particular case it is groundwater salinity that was considered. Approaches such as these are worth investigation to enhance the solute transport approach in WatFlood at the GRU level.

When examining the nitrate concentration profiles on an event-basis the strengths and weaknesses of the modelling approach are somewhat illuminated. Figure 8.15 shows a

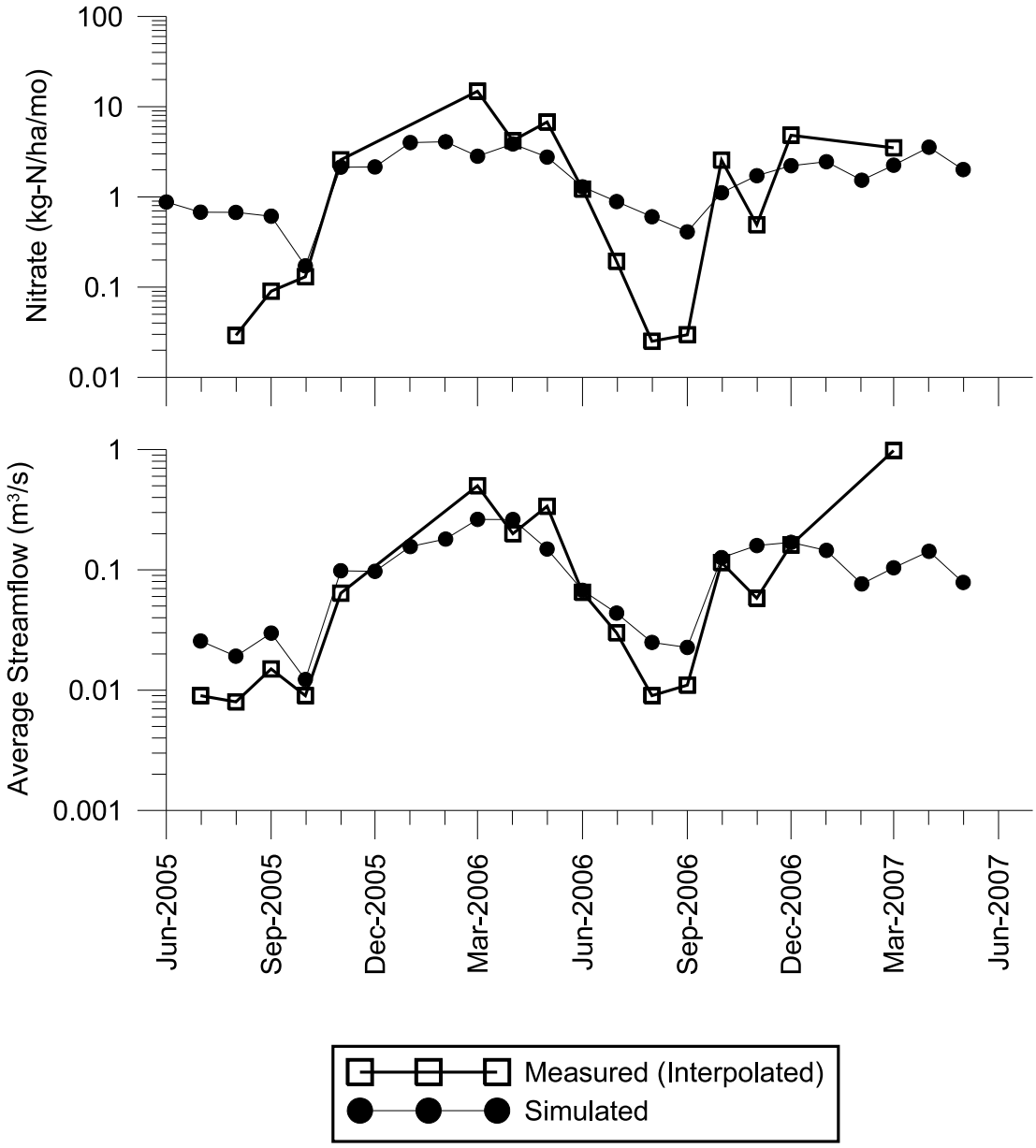

Figure 8.12: Monthly Nitrate Load - Measured vs. Simulated - West Sub-Basin

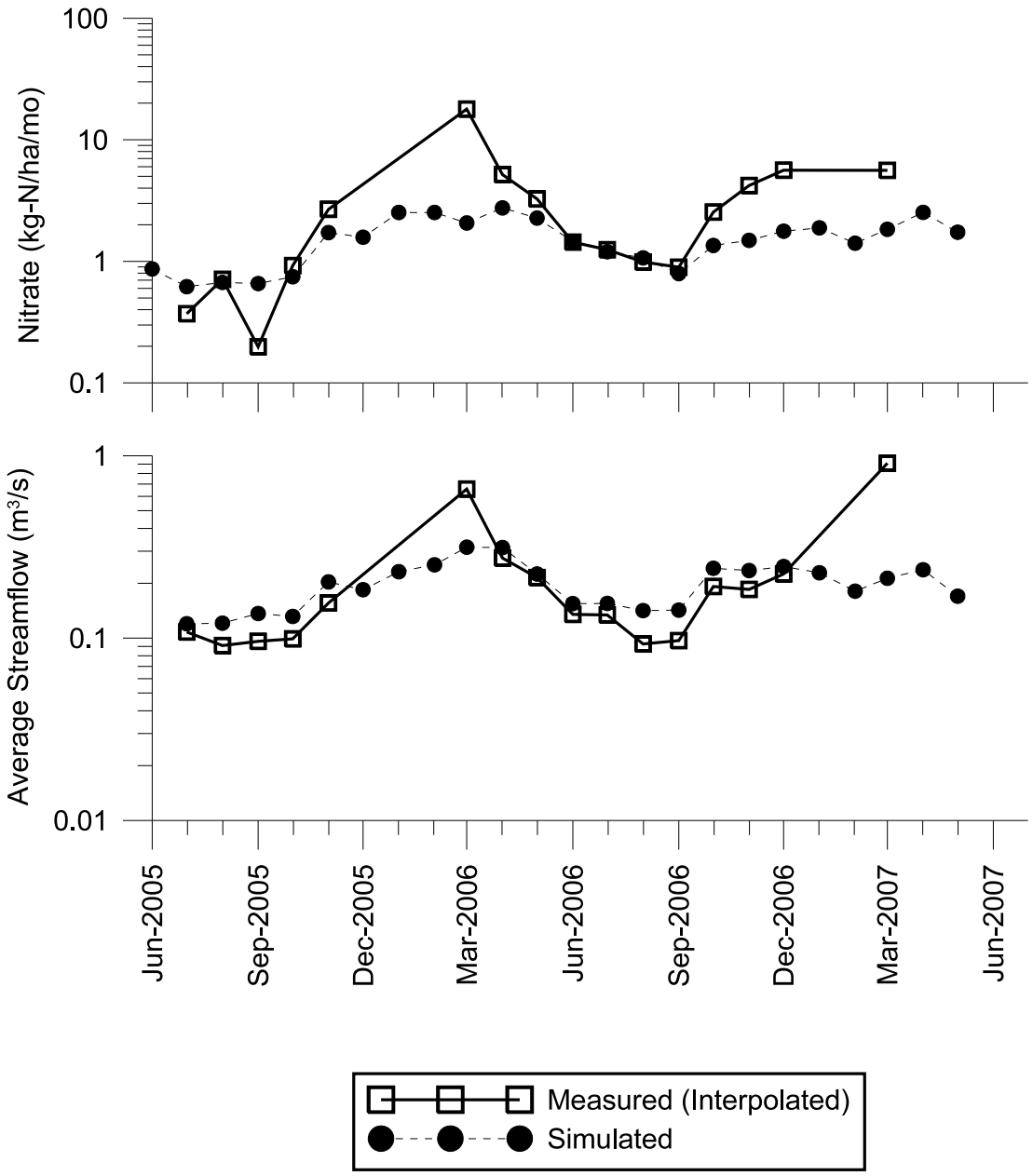

Figure 8.13: Monthly Nitrate Load - Measured vs. Simulated - East Sub-Basin

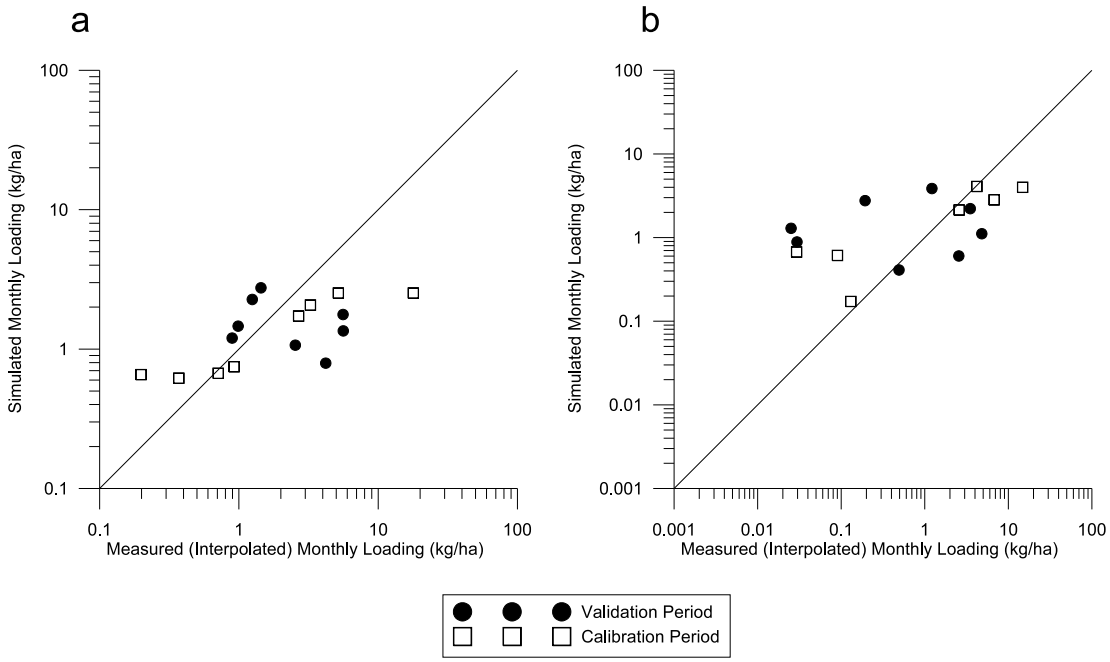

Figure 8.14: Nitrate Monthly Load Comparison - a) East Sub-Basin and b) West Sub-Basin

simulated and measured concentration profile for Event 2 in the East sub-basin. In this well modelled event one can see the contributions to the profile with first a spike in concentration from the flushing of the upper zone, then a dip in concentration as relatively low nitrate concentration water moves though the upper zone and then an increase in concentration as the groundwater "diffuse flow" contributes to the stream. In this figure the processes seem to be well modelled with some clear issues in timing and perhaps a small error in groundwater concentration with the simulated groundwater contribution being too low in the simulation with the groundwater concentrations are ranging between 2 and 3 mg-N/L.

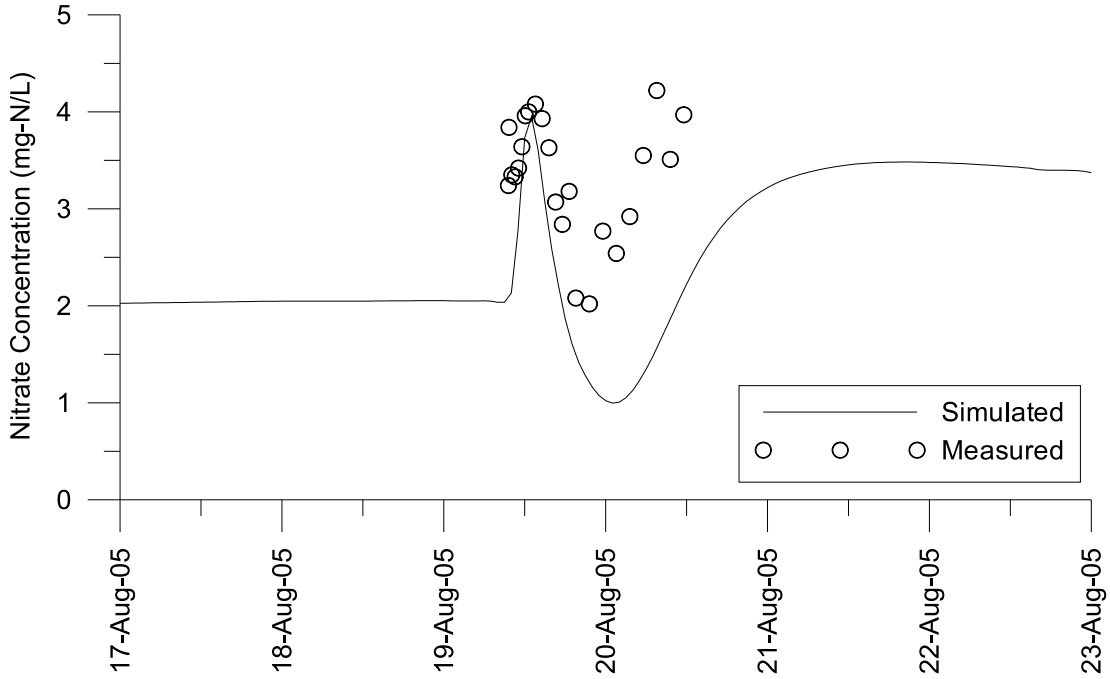

Figure 8.15: Measured and Simulated Nitrate Concentration Profile - Event 2, East sub-basin

A less well modelled event only a year later is shown in Figure 8.16. In this event we see a similar profile as the previous event in both the simulated and modelled results with the high initial concentration, a drop in concentration as low-nitrate water comes through the interflow zone and then a rise in nitrate with increasing groundwater contribution. In this event the profile and timing match well but the simulated groundwater concentration

is very low. Note that the groundwater concentration is still within 2 to 3 mg-N/L in the simulation whereas in the measured data the contribution from groundwater (as described by the model) would appear to be somewhere between 4 and 5 mg-L.

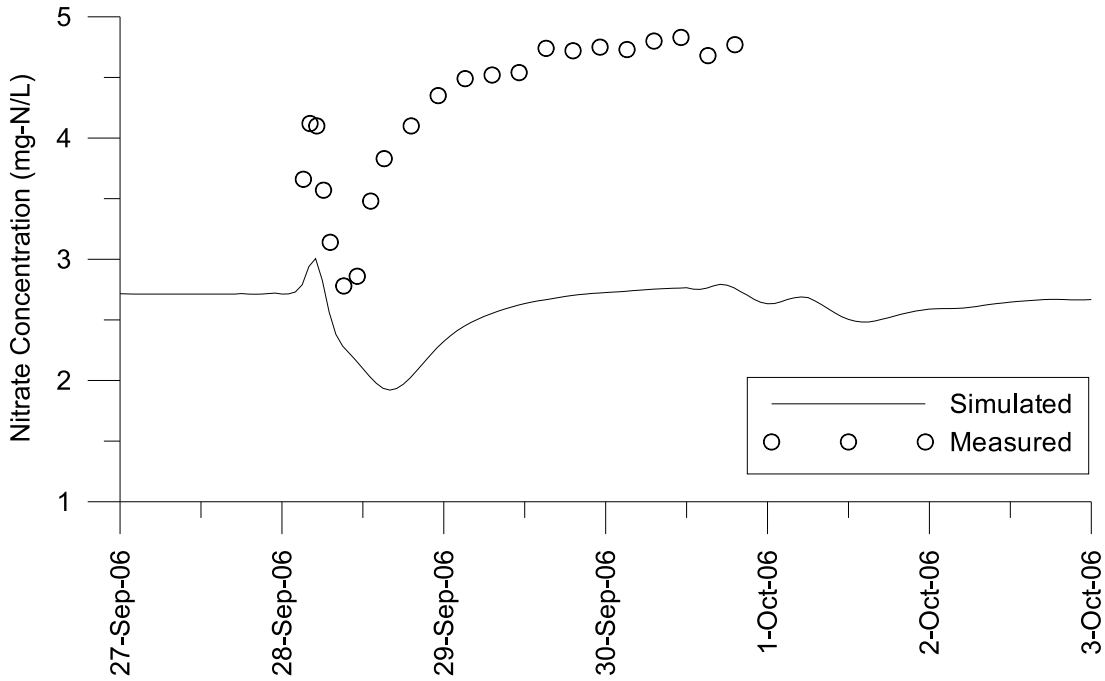

Figure 8.16: Measured and Simulated Nitrate Concentration Profile - Event 12, East sub-basin

Finally the examination of a snow melt event shows a very poorly modelled nitrate concentration profile in Figure 8.17. In this event the observer concentration profile is not well simulated, although small undulations in the simulation hint at the observed pattern. Again the background concentration in the simulated model is low, in this case near 4 mg-N/L, and although higher than at other times in the season it is not near the observed "diffuse flow" concentrations near 20 mg-N/L.

This analysis would seem to show that the model, although simulating the timing patterns with a degree of accuracy, is not adequately accounting for nitrate storage and release in the model with regard to groundwater. In the model the groundwater or lower zone storage is relatively large with long residence times. The concentrations in this zone

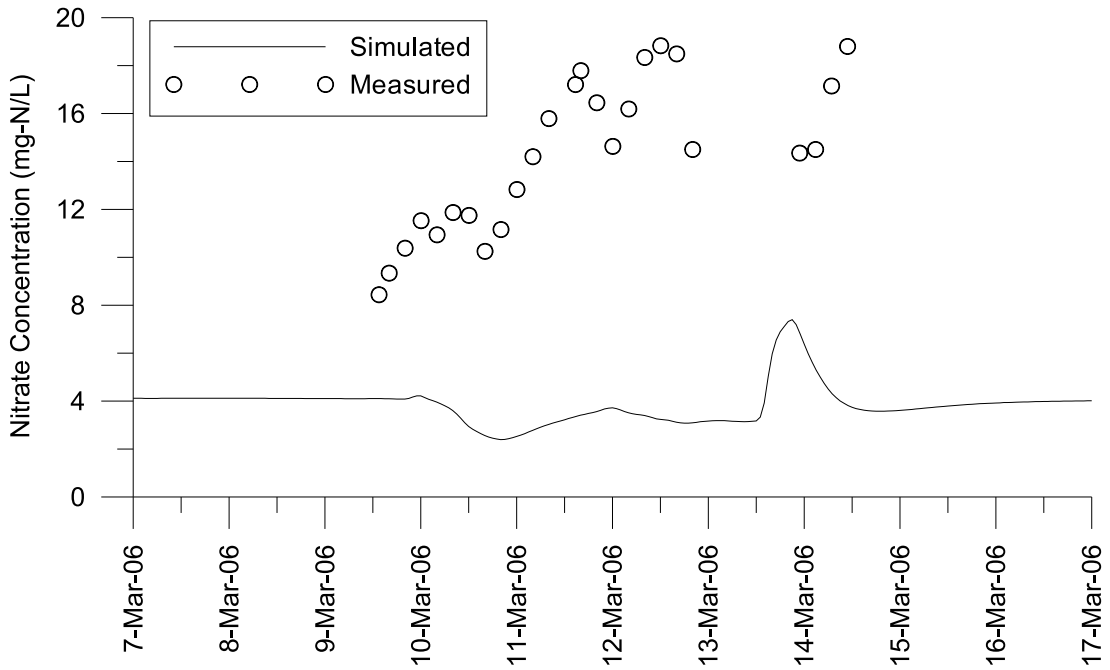

Figure 8.17: Measured and Simulated Nitrate Concentration Profile - Event 6 (Snowmelt), East sub-basin

do change seasonally, but only to a small degree. In the observed data the "groundwater" contributions or contributions from a diffuse source seem to vary substantially over the season with very high concentrations during the fall and snow melt events and lower concentrations in the summer. It is believed that through further calibration the model could be adjusted to still produce reasonable hydrology and have lower residence times to account for the changes in the seasonal groundwater fluctuations. However, it could also be that the simplicity of the completely mixed 2-zone groundwater model as it exists may not accurately account for the seasonal variability of nitrate delivery in this study site (see Section 8.3.11).

8.3.9 Nitrate Model Sensitivity

The sensitivity of the model as it pertained to nitrate nitrogen modelling was conducted in a similar manner as outlined in Section 8.2.4. The sensitivity of the objective function to perturbations of calibrated model parameters was investigated as well as the sensitivity of the model to total nutrient loading over the modelling period (1 January 2005 – 1 May 2007). Each model parameter was adjusted by 5% and the resulting changes in the objective functions were recorded using (8.8). The sensitivity analysis is presented in Appendix D, Section D.6.2. Sensitivity analysis showed that the parameters relating to nutrient loading, including crop residual ($residf$), crop uptake (upf) and loading factor ($omafff$) all have the most significant effect on model fit and ultimately the nitrogen stream loading estimates. The sensitivity to loading parameters can be explained as the OMAFRA guidelines prescribe nutrient loadings very close to and slightly in excess the crop uptake estimates. Loading in excess of those estimates by increasing the loading factor or increasing crop residual will allow for more nitrogen loading to the groundwater and to the receiving waters during rainfall events. Nitrogen transformation constants are also important for both the loading and model fit sensitivities including the organic nitrogen mineralization rate (k_{min}) and the temperature correction coefficient (Q_{10}), and to a lesser degree the nitrification rate (k_{nit}). These parameters dictate the rate at which organic and ammonia nitrogen transforms to nitrate, and a more rapid transformation, particularly in the spring and fall months, will make available more nitrate for transport

to the groundwater and channel. The nitrogen content in the rainfall (N_{crn}) is not a sensitive parameter, and simulated nitrogen concentrations in the channel are dominated by agricultural inputs. In addition to the above parameters, the total loading is also somewhat sensitive to the riparian rate parameters and the temperature parameters in the East basin. In particular, the river temperature parameters (A_t, B_t) and the riparian removal temperature correction parameter (theta) are very sensitive, followed by some slight sensitivity to riparian rate parameter (k_{20}). The nitrogen loading rate is sensitive to these parameters as the higher temperatures and rate constant will remove more nitrogen in the riparian zones before it is transported to the receiving channel.

8.3.10 Riparian Wetland Contribution to Nitrate Removal

The degree of riparian wetland contribution to nitrate removal was assessed, and it was found in the current calibrated model that nitrate removal by the riparian wetlands was insignificant. Separate simulations were run with and without riparian wetland processes activated in the model for the east sub-basin. Figure 8.18 shows the East basin monthly nitrate loading with and without wetlands included and the simulations with and without riparian wetland processes are indistinguishable. Of the total nitrate loading to the riparian zones in the east sub-basin the expected nitrate removal is approximately 0.36%. This can be explained by two contributing factors: the relatively slow nitrate removal rate and the relatively short retention times within the riparian wetlands simulated in the WatFlood model. As illustrated in Section 7.9 the riparian wetland model is capable of removing nitrate under favourable conditions, but the calibrated model was constrained during calibration to match a single fertilizer loading function across the entire watershed. The measured data in Chapter 6 showed higher nitrogen event loading in the East sub-basin than the west sub-basin. With similar land use and loading quantities the calibration of the model would necessarily attempt to increase the east-basin loading and reducing the treatment effects of the riparian wetland would be a natural consequence.

Assuming that fertilizer loading patterns in the two basins are comparable year-over-year, accounting for the differences in nitrate loading requires investigation into the flow transport pathways. The removal of nitrate from a system via denitrification is a time-

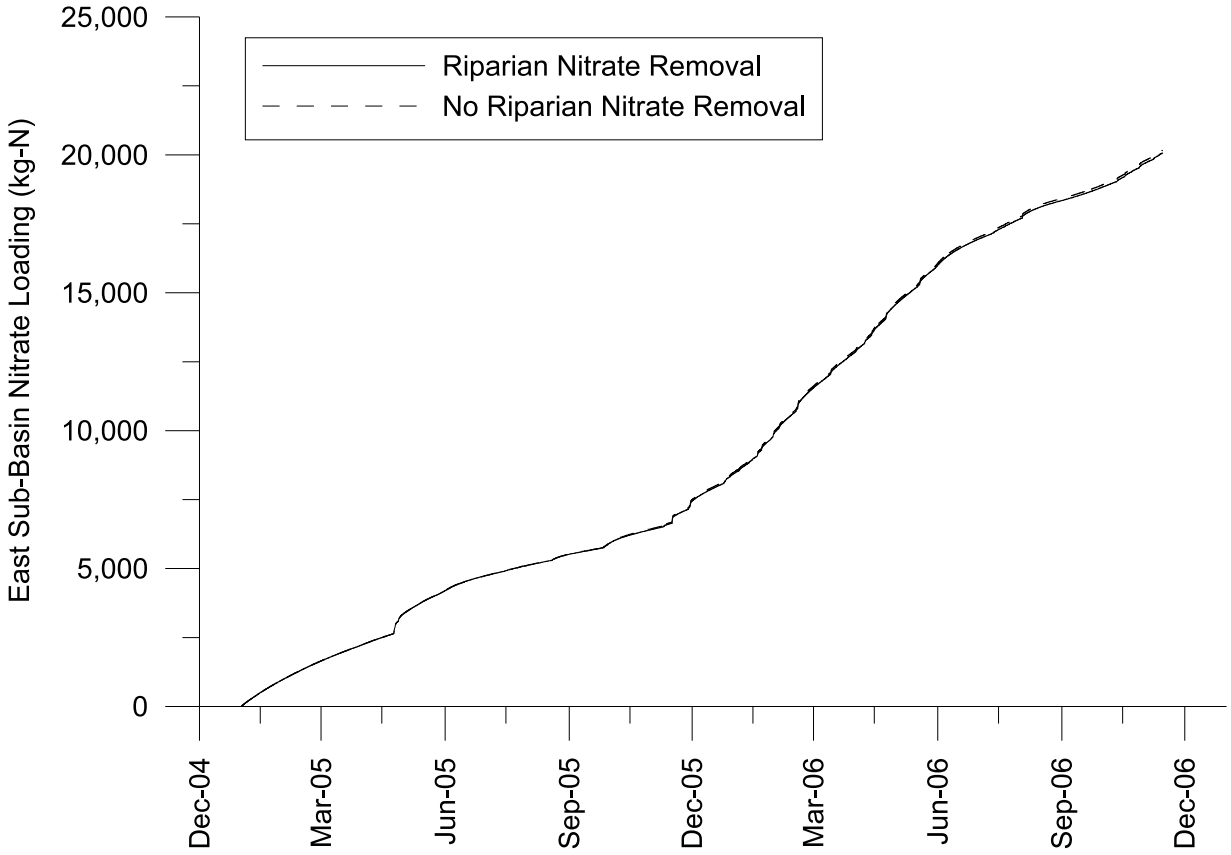

Figure 8.18: Riparian Contribution to Nitrate Removal - Cumulative Nitrate Loading, East Sub-Basin

sensitive process requiring low-oxygen environments and available carbon. Other than the riparian wetlands, the next most likely modelled region for nitrate removal would be the lower zone storage. A residence time analysis was conducted on a number of hydrologic features in the calibrated WATFLOOD model to determine where the water transporting the nitrate would reside longest in the hydrological flow paths. An equation was used to determine the instantaneous residence time of a WATFLOOD storage element

$$T_{Ri} = \frac{S_i}{Q_{out_i}} \tag{8.10}$$

where for time step i, T_R is the instantaneous residence time $[T]$, S is the instantaneous storage of the zone at that end of the time-step $[L^3]$ and Q_{out} is the volumetric flow rate leaving the storage zone during the time step $[L^3T^{-1}]$.

Figure 8.19 shows instantaneous residence times for the riparian wetland zones in two grid cells in the Canagagigue Creek model with differing quantities of riparian wetlands. Also included in Figure 8.19 for comparison is the residence time profile of the lower zone storage which was indistinguishable between the two grids.

In Figure 8.19 the two selected grids represent an upper and lower limit of riparian wetland cover for those grids with riparian cover in the east sub-basin, with 6% aerial cover being close to the minimum and 13% being close to the maximum. The residence times for the riparian zones is naturally and clearly based on aerial extent, as the amount of storage increases with greater aerial extent. However, the calculated residence times for riparian zones are shown to vary by several orders of magnitude depending on hydrologic conditions. On average the instantaneous residence times are relatively short with mean residence times on the order of days. The high riparian wetland cell in Figure 8.19 has a median instantaneous residence time of 16 days, and the lower riparian content wetland cell has a median residence time of 2.5 days. For summer seasons (July to October) the residence times can increase substantially. Occasionally the instantaneous residence times approach infinity in the summer seasons (observed in Figure 8.19 at locations with discontinuities in the graph lines) for short periods. This occurs when the flow out of the wetland is zero or less than zero (i.e. the riparian zone is not discharging to the channel and may be receiving water from the channel). These residence times make logical

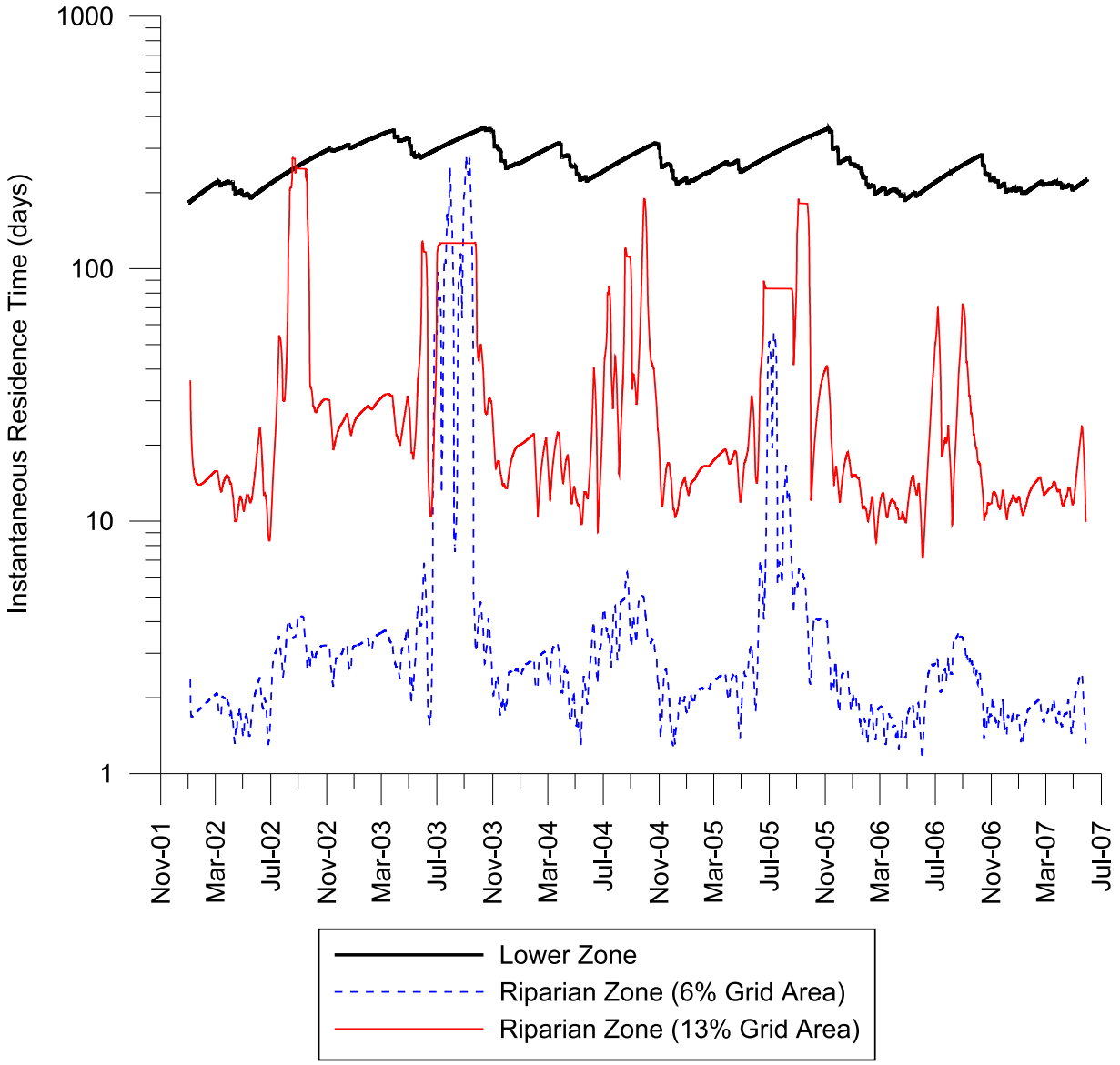

Figure 8.19: Instantaneous Residence Times for Riparian Wetland and Lower Zone storage

sense, with the highest flow-through rates being in the spring and fall seasons, reducing residence times, and less flow-through in the dryer summer months. However, even with high instantaneous residence times in the summer, these periods of hydraulic retention are relatively short. Furthermore, during periods when the nutrient loading to the receiving channel is the greatest and nutrient retention would be most beneficial (spring and fall) the residence times are shortest. It is clear that in reality the completely mixed model is not accurate for riparian wetlands. There would exist distinct flow paths with differing residence times, however as a large scale approximation this modelling exercise shows the relatively reduced importance of riparian wetlands in this hydrological context.

The residence times for the lower zone groundwater is 1 to 2 orders of magnitude longer in duration than the riparian wetlands. If any denitrification is occurring in the groundwater, the long residence times could allow for significant reduction. By comparison the riparian wetlands have relatively short retention times on the order of 1 to 10 days, with longer retention times in the summer months. It would seem, based on the modelling results, that the importance of the riparian zones can be limited by hydrologic conditions, and in this particular study area, other processes not currently available in the model, including deep water denitrification, could do more to explain loading differences than the riparian wetlands.

8.3.11 Groundwater Consideration in Nitrate Modelling with WatFlood

The WatFlood model has two types of sub-surface flow that contribute to the receiving channel in the grid, "interflow" and "baseflow", which contribute water to the channel from the "upper zone" and "lower zone" storage respectively. These are abstracted storage locations that are separated programmatically to account for different hydrological processes. Namely, the upper zone storage location is subject to evapotranspiration and the lower zone storage is not. The storage maintained in each of these storage locations is primarily a function of the equations that control the rate of release of water from the location. Of particular interest is that within the model the amount of baseflow is related to the quantity of storage in a power relationship. In the WatFlood model if there is any storage in

the lower zone there will be some contribution to baseflow. However, contribution from the upper zone only occurs when a minimum retention storage requirement is satisfied at which point flow beings. Finally the zones are considered completely mixed in the model with additions of constituent mass being immediately distributed within the mixing cell and contributing to the channel once flow begins. All of these factors have direct consequences for water quality modelling of nitrate. The lower zone represents a large pool of storage with long retention times constantly delivering to a receiving channel a source of relatively constant nitrate concentration. The upper zone will store solutes between rainfall events and then is very quickly, and often completely flushed during rainfall events contributing high concentration pulses during a start of an event, and then low concentration water for the remainder. Perhaps somewhat fortuitously this combination of processes matches the observed concentration profiles very well in some cases (Section 8.3.8). However, one observes that the large and slow moving groundwater storage tends to reduce the variability of nitrate concentration in the groundwater simulation. To reduce the storage would be one adjustment to the model that could increase the temporal variability, however, this would imply that during some events, snow melt in particular, the groundwater concentrations have elevated to in excess of 20 mg-L/N. It seems unlikely that this degree of variability would be occurring in deep groundwater. Rather it is probably more likely that the variability would be due to nitrate storage in the relatively near surface that is activated hydrologically by very intense events that flush nitrate from the soil in a diffuse flow pattern. Indeed, detailed research on a tile drain solute delivery by Schilling and Helmers (2008), where very similar nitrate profiles to those in this study were observed, suggested that after a flush preferential flow paths contributed to relatively low nitrate concentrations to tile trains followed by a "diffuse flow" higher-concentration contribution to the drains. To more accurately model the transient nature of nitrate storage in the upper zone which in the WatFlood model would contribute to the tile drainage, one would have to re-think the storage-flow-concentration relationships in that zone to improve the model performance. The inclusion of another storage component or relationship that describes the variability in the sources of interflow contribution in the model could be beneficial. As mentioned above, other models such as LASCAM (Viney and Sivapalan, 1999) have

introduced multiple upper zone storage zones to account for variability in concentration delivery to channels from the land surface in this way.

It should be noted that the previous implementations of the WatFlood/AGNPS model was focused on surface water modelling: sediments or pathogens attached to sediments (Dorner et al., 2006), and regions that appear to have been modelled well only considering surface or near-surface contaminant sources (Leon, 1999; Leon et al., 2001, 2002).

8.4 Discussion

The calibration and sensitivity procedure for this chapter has isolated the water quality processes from the hydrological processes when analyzing system response. It is recommended that with more time and computational resources a complete calibration with a combined objective function for both water quality and hydrological parameters simultaneously be conducted. This approach may constrain the hydrology more effectively in the calibration process.

The surface transport processes are much more accurate in the model than the sub-surface processes. TSS transport is dictated by hydraulic processes which are approximately simulated in the model. When the WatFlood model displayed reasonably accurate flow and other hydrologic parameters in the stream the model performed reasonably well. This is in large part due to the relative lack of importance of the sub-surface storage state variables in determine in-stream concentrations. Provided the surface flow rates, whether overland or in channel were reasonably simulated the sediment transport model performed reasonably well.

The success with which the east basin is modelled points to the contributing mechanisms and sheds some light on the dominant processes in the two sub-basins. It is clear that the dominant process in the east basin is in-stream transport of sediment. The event based data is very well modelled and the most sensitive parameters and when compared to the sediment rating curve, the models are almost identical. This would indicate that for the riparian-protected basin understanding the stream flow-sediment relationship is a

reasonable model for predicting sediment concentrations and loading. However, for the west basin, this relationship is not so strong. The stream flow flow-sediment relationship is much less strong and other parameters contribute more significantly to sediment loading. Combining this observation with observations made in Section 6.7.3 regarding the greater presence of fines soils in the collected TSS samples suggests that the riparian zones are having an effect on the *nature* of the sediment loading, if not the quantity. The riparian zones seem to be reducing the presence of fine sediment in the receiving waters, although the riparian protected channel contributes sediment itself. Clearly there are two processes involved: the channel-based and the field-based. Further investigation into delineating the sources of the sediment would go some way to qualifying the benefits of riparian wetlands to receiving waters in relation to sediment loading and delivery.

The nitrate transport model showed less success than the sediment transport model, although there existed much more uncertainty in the inputs for that sub-model.

The estimates of crop uptake, mineralization, and loading are linked to an agricultural land class GRU. This is in line with the general macro-scale modelling approach taken by WatFlood where average responses based on parameters that can be estimated or averaged over a large scale are employed. In fact, a higher degree of resolution could be investigated through the introduction of cropping sequences and estimated responses based on prescribed cropping sequences over a number of different land classes. Investigating alternative loading sequences could reveal sensitivities to loading parameters and sequences. Farming activity that disturbs the soil including cropping, tilling, and other activities is not explicitly considered in the model at this stage and deserves attention in future model iterations.

Finally, the presence of the riparian processes, including sediment retention and nitrate removal, were not the most important processes when attempting to simulate the observed water quality patterns. In both cases other processes dominated or controlled constituent delivery in the model. With sediment delivery this was due to the lack of observed surface water transport and hence minimal sediment delivery to the riparian wetlands, although with a process simulating sediment contribution from tile drains this could change. With nitrate transport the situation was different. Much of the delivered nitrate

was necessarily transported to the riparian wetlands but the calibration of the model and the higher observed loadings in the east basin meant that riparian wetland nitrate removal was minimized to provide the best simulation results. With the addition of deep water denitrification, which could contribute to nitrate removal in the West sub-basin, the effects of nitrate removal in the riparian wetlands could be different.

Chapter 9

Conclusions and Recommendations

This study was designed to examine the influence of riparian wetlands in mitigating non-point source pollution in a southern Ontario agricultural watershed taking a watershed scale approach. The field study, which examined the hydrology and the water quality of two similar sub-basins but with different degrees of riparian wetland cover, the west basin having little riparian protection and the east basin having a high degree of riparian wetland protection. The field studies showed that the basin with riparian protection produced higher event based and continuous loading of sediment and nutrients, although the basin without riparian protection tended to show higher in-stream concentrations of most nutrients. The disparity was explained partially by the differing hydrologic and conditions between the two sub basins.

The WatFlood hydrologic model was significantly enhanced to deal with contaminant transport in the stream corridor using the QUICKEST advective-dispersive algorithm, which provided better mass conservation, more control over numerical dispersion in the WatFlood model and improved computational efficiency. Additionally the model was enhanced to include in-stream sediment processes, riparian sediment and nitrate nitrogen fate processes and land surface nitrogen processes to allow for continuous water quality simulation. The enhancements to the WatFlood provide significant enhancements to the exiting water quality modelling framework.

In computer simulations of the sub-basins for total suspended solids it was found that

the model simulation was very sensitive to in-stream sediment carrying capacity parameters, with overland sediment contributions being much less important. This was largely due to the relatively rare contributions of overland flow in the model which corresponded to observations. The east basin was better simulated than the west which was partly attributed to a better hydrologic model performance in that sub-basin. It was also suggested that the irregularity of the west channel and the unaccounted for influence of tile drains in that sub-basin would have compromised simulation performance in that sub-basin. The presence or absence of the riparian zones was shown to be relatively unimportant in the calibrated model with regard to simulation accuracy or sensitivity.

Nitrate nitrogen simulation was less well modelled when compared to the sediment simulations. Although nitrate profile trends were accurately simulated generally, the storage approach in the WatFlood model appears to not match or adequately model the variability in nitrate storage and delivery observed in the field study.

Generally, the enhancements to the model provided improved modelling performance for the WatFlood water quality model. However, in this setting it appears that the water quality benefits of the presence of riparian wetlands in terms of sediment and nutrient loadings are not observed either in the measured data or the simulations. However, this model development provides insights into specific areas of improvement required for the WatFlood suite of models to more accurately simulate nitrate and suspended sediment transport. Additionally, the modelling developments conducted in this study over two relatively small watersheds with extensive data collection have provided insights into using the WatFlood/AGNSP model at larger scales, particularly in the Southern Ontario regions. In particular data requirements for modelling have been elucidated particularly with regard to the changes in contaminant profiles during runoff events for nitrogen and sediment constituents. The field work highlighted some important differences between the sub-basins that make the isolation of riparian influences difficult. In particular the geologic and hydrologic differences between the two sub-basins could contribute to the differences nutrient and sediment loading masking benefits possibly awarded by the riparian wetlands.

9.1 Recommendations

Listed here are a number of recommendations for improvement or extension of this research.

9.1.1 Larger Modelling Domain

It would be a natural extension of this research to apply the existing model now to the Grand River basin in its entirety employing the MOE data set (Cooke, 2006). Additionally, event-based sampling could be conducted at targeted watersheds with larger drainage areas to increase our understanding of event-based transport at larger scales with the assistance of the enhanced WatFlood model.

9.1.2 Extended Study Period

It is recommended that the study period be extended for this study site to refine the hydraulic, hydrologic and water quality measurements. For example, the rating curves developed were done over a relatively short period (3 years) and could benefit from the capture of more flow measurements. The water quality trends identified would benefit from several more seasons of measurement. And the measured hydrological responses of the two study sub-basins is relatively short (2 years). To develop meaningful hydrological relationships for the sub-basins, not the entire Canagagigue Creek, several more years of monitoring would be beneficial.

9.1.3 Hydrology of Small, Ephemeral Basins

The WatFlood model shows some deficiencies when modelling smaller basins with ephemeral conditions. It is clear from the modelling results that the model does not adequately account for in-stream storage, and the changes in river routing that arise when the streams go dry. In fact, the WatFlood model does not ever allow a stream to truly go dry, with a constant background flow of 0.001 m^3/s enforced. Some further investigation into the storage routing model for the WatFlood model could make it more generally applicable to small watersheds that have a large proportion of ephemeral contributors, or river

systems in more arid climates that can periodically go dry.

9.1.4 Riparian Wetland Hydrology

The WatFlood riparian wetland sub-model was developed and integrated into the model based on work done by R. McKillop at a headwater wetland in Southern Ontario (McKillop et al., 1999). The model is based on established physical models but the model itself has never been validated within the WatFlood modelling framework. The Canagagigue Creek study site represents an ideal opportunity to validate the wetland sub-model within a model framework at a sub-catchment scale.

9.1.5 Mixing in incised and well-formed channels

The Canagagigue Creek study site provides an ideal opportunity to examine the differences in in-channel mixing within a well formed natural channel with an established flood plain and a network heavily insiced channels. The establishment of detailed stage-discharge rating curves and some preliminary conservative tracer studies paves the way for some detailed mixing analysis that would be valuable in contaminant transport modelling within southern Ontario within headwaters.

9.1.6 Examination of other nitrogen fate processes

To account for the differences between the east and west sub-basins regarding nitrate transport further investigations need to be made into other possible nitrogen fates within an agricultural watershed, namely groundwater dentitrification outside of the riparian zones and the potential sourcing of nitrogen from a mature riparian wetland. The riparian protected sub-basin discharged significantly more nitrogen to the receiving water than the unprotected basin. If the loadings can be assumed similar then another nitrogen fate or source must be considered to account for these differences. Further simulation efforts experimenting with new processes could shed light on this disparity.

9.1.7 Recommendations for Water Quality Model Improvement

This application of the water quality model included highlighted some areas of possible improvement. Some of the more salient areas requiring attention in this model include:

1. Denitrification considerations in areas other than riparian wetlands.
2. Ephemeral storage model enhancements to include base flow discharge threshold levels and channel storage and deposition.
3. Upper zone solute concentration transport adjustment, to temporal nitrate transport patters to tile drains.
4. Sediment transport through the sub-surface due to tile drains.
5. Differentiation of sediment transport due to grain size, to account for partitioning effects of tile drain sediment delivery and overland delivery.

References

AAFC (2000). *Canadian Soil Information System: National Soil Database*. Agriculture and Agri-Food Canada.

AAFC (2002). Long term land use trends for water quality protection: Ten years of monitoring in the south tobacco creek watershed. Technical report, Agriculture and Agri-Food Canada - Prairie Farm Rehabilitation Administration, A22-270 /2002E.

Abbott, M., Bathurst, J., Cunge, J., O'Connell, P., and Rasmussen, J. (1986). An introduction to the european hydrological system - systeme hydrologique europeen, "she", 1: History and philosophy of a physically-based, distributed modelling system. *Journal of Hydrology*, 87(1-2):45–59.

Abbott, M. B. and Basco, D. R. (1989). *Computational fluid dynamics : an introduction for engineers*. Longman Scientific and Technical ; Wiley, Harlow, Essex, England New York, NY.

Abu-Zreig, M., Rudra, R. P., and Whiteley, H. R. (2001). Validation of a vegetated filter strip model (vfsmod). *Hydrological Processes*, 15(5):729 – 742.

Alvord, H. and Kadlec, R. (1996). Atrazine fate and transport in the des plaines wetlands. *Ecological Modelling*, 90(1):97 – 107.

Andersen, M. and Jensen, L. (2001). Low soil temperature effects on short-term gross n mineralisation-immobilisation turnover after incorporation of a green manure. *Soil Biology and Biochemistry*, 33:511–521.

Antonopoulos, V. Z. (1999). Comparison of different models to simulate soil temperature and moisture effects on nitrogen mineralization in the soil. *Journal of Plant Nutrition and Soil Science*, 162(6):667–675.

APHA (2005). *Standard methods for the examination of water and wastewater*. American Public Health Association, Washington, D. C., 21st edition.

Arnold, G. and Fohrer, N. (2005). Swat2000: current capabilities and research opportunities in applied watershed modelling. *Hydrological Processes*, 19:563 – 572.

Arnold, J. G., Williams, J. R., and Maidment, D. R. (1995). Continuous-time water and sediment-routing model for large basins. *Journal of Hydraulic Engineering*, 121:171–83.

ASCE (1996). *Hydrology handbook*. ASCE manuals and reports on engineering practice, no. 28. New York, 2nd ed. edition.

Bacchi, B. and Ranzi, R. (2000). Raphael: Runoff and atmospheric processes for flood hazard forecasting and control. Technical report, EC, Directorate General XII, Programme Environment and Climate 1994-1998, University of Brescia.

Bachand, P. A. M. and Horne, A. J. (1999). Denitrification in constructed free-water surface wetlands: Ii. effects of vegetation and temperature. *Ecological Engineering*, 14(1-2):17–32.

Barfield, B. J., Tollner, E. W., and Hayes, J. C. (1979). Filtration of sediment by simulated vegetation i. steady-state flow with homogeneous sediment. *Transactions of the American Society of Agricultural Engineers*, 22(3):540–545.

Barnes, H. H. J. (1987). *Roughness Characteristics of Natural Channels*. U. S. Geological Survey, water supply paper 1849 edition.

Barry, D. A. J., Goorahoo, D., and Goss, M. J. (1993). Estimation of nitrate concentrations in groundwater using a whole farm nitrogen budget. *J Environ Qual*, 22(4):767–775.

Bear, J. (1979). *Hydraulics of groundwater*. McGraw-Hill International Book Co., London ;New York.

Benbi, D. K. and Richter, J. (2002). A critical review of some approaches to modelling nitrogen mineralization. *Biology and Fertility of Soils*, 35(3):168 – 183.

Beven, K. J. (2001). *Rainfall-runoff modelling : the primer*. John Wiley, Chichester, England ; Toronto.

Bingeman, A. K., Kouwen, N., and Soulis, E. D. (2006). Validation of the hydrological processes in a hydrological model. *Journal of Hydrologic Engineering*, 11(5):451–463.

Blaustein, A. R. and Kiesecker, J. M. (2002). Complexity in conservation: lessons from the global decline of amphibian populations. *Ecology Letters*, 5(4):597–608.

Borga, M. (2002). Accuracy of radar rainfall estimates for streamflow simulation. *Journal of Hydrology*, 267(1-2):26–39.

Brink, C. v. d., Zaadnoordijk, W. J., Burgers, S., and Griffioen, J. (2008). Stochastic uncertainties and sensitivities of a regional-scale transport model of nitrate in groundwater. *Journal of Hydrology*, 361(3-4):309–318.

Brinson, M. (1988). Strategies for assessing the cumulative effects of wetland alteration on water quality. *Environmental Management*, 12(5):655–662.

Bullock, A.; Acreman, M. (2003). The role of wetlands in the hydrological cycle. *Hydrology and Earth System Sciences*, 7(3):358–389.

Campbell, C. A., Jame, Y. W., and De Jong, R. (1988). Predicting net nitrogen mineralization over a growing season: Model verification. *Canadian Journal of Soil Science*, 68:537–552.

Campbell, C. A., Jame, Y. W., and Winkleman, G. E. (1984). Mineralization rate constants and their use for estimating nitrogen mineralization in some canadian prarie soils. *Canadian Journal of Soil Science*, 64:333–343.

Carpenter, S., Caraco, N., Correll, D., Howarth, R., Sharpley, A., and Smith, V. (1998). Nonpoint pollution of surface waters with phosphorus and nitrogen. *Ecological Applications*, 8(3):559–568.

Cey, E., Rudolph, D., Aravena, R., and Parkin, G. (1999). Role of the riparian zone in controlling the distribution and fate of agricultural nitrogen near a small stream in southern ontario. *Journal of Contaminant Hydrology*, 37(1):45 – 67.

CFI (2001). Nutrient uptake and removal by field crops-eastern canada. Technical report, Canadian Fertilizer Institute.

Chadwick, D. R., John, F., Pain, B. F., Chambers, B. J., and Williams, J. (2000). Plant uptake of nitrogen from the organic nitrogen fraction of animal manures: a laboratory experiment. *Journal of Agricultural Science*, 134:159–168.

Chapman, L. J. and Putnam, D. F. (1984). *Physiography of southern Ontario*. Ontario Geological Survey, 3rd edition.

Chapra, S., Pelletier, G., and Tao, H. (2007). *QUAL2K: A Modeling Framework for Simulating River and Stream Water Quality (Version 2.07)*.

Chapra, S. C. (1997). *Surface water-quality modeling*. McGraw-Hill, New York.

Chapra, S. C. and Robertson, A. (1977). Great lakes eutrophication: The effect of point source control of total phosphorus. *Science*, 196(4297):1448–1450.

CHC (2007). *EnSim Hydrologic Reference Manual*. Canadian Hydraulics Center (CHC), National Research Council of Canada (NRC).

Chow, V. T. (1959). *Open-channel hydraulics*. McGraw-Hill, New York.

Cirmo, C. P. and McDonnell, J. J. (1997). Linking the hydrologic and biogeochemical controls of nitrogen transport in near-stream zones of temperate-forested catchments: a review. *Journal of Hydrology*, 199(1-2):88–120.

Cohn, T., Caulder, D., Gilroy, E., Zynjuk, L., and Summers, R. (1992). The validity of a simple statistical model for estimating fluvial constituent loads: An empirical study involving nutrient loads entering chesapeake bay. *Water Resources Research*, 28(9):2353–2363.

Cooke, S. (2006). Water quality in the grand river: A summary of current conditions (2000-2004) and long-term trends. Technical report, Grand River Conservation Authority.

Cooper, J., Gilliam, J., Daniels, R., and Robarge, W. (1987). Riparian areas as filters for agricultural sediment. *Soil Science Society of America Journal*, 51(2):416–420.

Cordone, A. and Kelley, D. (1961). The Influence of Inorganic Sediment on the Aquatic Life of Streams. *California Fish and Game*, 47(2):189 – 228.

Courant, R., Friedrichs, K., and Lewy, H. (1967). On the partial difference equations of mathematical physics. *IBM Journal*, pages 215–234. English translation of the German original published in Mathematische Annalen 100, 32-74 (1928).

Cowan, W. L. (1956). Estimating hydraulic roughness coefficients. *Agricultural Engineering*, 37(7):473–475.

Cranmer, A. J., Kouwen, N., and Mousavi, S. G. (2001). Proving watflood: modelling the nonlinearities of hydrologic response to storm intensities. *Canadian Journal of Civil Engineering*, 28(5):837–855.

Crumpton, W. (2001). Using wetlands for water quality improvement in agricultural watersheds; the importance of a watershed scale approach. *Water Science and Technology*, 44(11):559 – 564.

Das, B. S., Kluitenberg, G. J., and Pierzynski, G. M. (1995). Temperature dependence of nitrogen mineralization rate constant; a theoretical approach. *Soil Science*, 159(5):294–300.

Das, S., Rudra, R., Gharabaghi, B., Gebremeskel, S., Goel, P., and Dickinson, W. (2008). Applicability of annagnps for ontario conditions. *Canadian Biosystems Engineering*, 50:1.1 – 1.11.

Devito, K., Fitzgerald, D., Hill, A., and Aravena, R. (2000). Nitrate dynamics in relation to lithology and hydrologic flow path in a river riparian zone. *Journal of Environmental Quality*, 29(4):1075 – 1084.

Dingman, S. L. (1994). *Physical hydrology*. Prentice Hall, Englewood Cliffs, N.J.

Dorner, S. M. (2004). *Waterborne Pathogens: Sources, Fate, and Transport In a Watershed used for Drinking Water Supply*. Phd, University of Waterloo.

Dorner, S. M., Anderson, W. B., Slawson, R. M., Kouwen, N., and Huck, P. M. (2006). Hydrologic modeling of pathogen fate and transport. *Environmental Science and Technology*, 40(15):4746–4753.

Dortch, MS; Gerald, J. (1995). Screening-level model for estimating pollutant removal by wetlands. Technical Report Technical Report WRP-CP-9, US Army Corps of Engineers - Waterways Experiment Station.

Dosskey, M. G., Helmers, M. J., Eisenhauer, D. E., Franti, T. G., and Hoagland, K. D. (2002). Assessment of concentrated flow through riparian buffers. *Journal of Soil and Water Conservation*, 57(6):336–343.

Duff, J. H. and Triska, F. J. (1990). Denitrifcations in sediments from the hyporheic zone adjacent to a small forested stream. *Can. J. Fish. Aquat. Sci.*, 47(6):1140–1147.

Eghball, B., Wienhold, B., Gilley, J., and Eigenberg, R. (2002). Mineralization of manure nutrients. *Journal of Soils and Water Conservation*, 57(6):470–473.

Ehlschlaeger, C. (1989). Using the at search algorithm to develop hydrologic models from digital elevation data. In *Proceeding of the International Geographic Information System (IGIS) Symposium*, pages 275–281, Baltimore, MD.

Environment Canada (2007). Canadian climate normals 1971-2000. Internet. http://climate.weatheroffice.ec.gc.ca/climate_normals/.

Ferguson, R. (1986). River loads underestimated by rating curves. *Water Resources Research*, 22(1):74–76.

Fischer, H. B. (1979). *Mixing in Inland and Coastal Waters*. Academic Press, New York ; Toronto Academic Press, 1979.

Foster, G. R. (1982). Modeling the erosion process. In Haan, C. T., Johnson, H. P., and Brakensiek, D. L., editors, *Hydrologic Modeling of Small Watersheds*, pages 297–380. ASAE, St. Joseph, Michigan.

Gale, P., Reddy, K., and Graetz, D. (1993). Nitrogen removal from reclaimed water applied to constructed and natural wetland microcosms. *Water Environment Research*, 65(2):162 – 168.

Gilliam, J. (1994). Riparian wetlands and water quality. *Journal of Environmental Quality*, 23(5):869 – 900.

Goss, M. J., Barry, D. A. J., and Rudolph, D. L. (1998). Contamination in ontario farmstead domestic wells and its association with agriculture:: 1. results from drinking water wells. *Journal of Contaminant Hydrology*, 32(3-4):267–293.

Government of Ontario (2002). Nutrient Management Act. Ontario Regulation 294/04.

Graf, W. H. (1998). *Fluvial hydraulics : flow and transport processes in channels of simple geometry*. Wiley.

GRCA (2003a). Grand river watershed data - digital elevation model.

GRCA (2003b). Grand river watershed data - vector gis data.

GRCA (2003c). Wetlands policy. Technical report, Grand River Conservation Authority, Cambridge, Ontario.

HACH (2000). *HACH Water Analysis Handbook*. HACH Company.

Haestad Methods Inc., Totz, C., and Klotz, D. (2003). *Floodplain modeling using HEC-RAS*. Haestad Press, Waterbury, CT, 1st edition.

Harman, J., McLellan, J. E., Rudolph, D. L., Heagle, D. J., Piller, C., and Denhoed, S. E. (2000). A proposed framework for managing the impact of agriculture on groundwater. Technical report, Sierra-ALERT Coalition, Sierra Club of Canada.

Hartley, D. M. (1987a). Simplified process model for water and sediment yield from single storms part ii: Performance. *American Society for Agricultural Engineers, Transactions*, 30(3):718 – 723.

Hartley, D. M. (1987b). Simplified process model for water sediment yield from single storms part i: Model formulation. *American Society for Agricultural Engineers, Transactions*, 30(3):710 – 717.

Hayes, J., Barfield, B., and Barnhisel, R. (1979). Filtration of sediment by simulated vegetation ii. unsteady flow with non-homogeneous sediment. *Transactions of the American Society of Agricultural Engineers*, 22(5):1063–1067.

Heard, J. and Hay, D. (2006). Nutrient content, uptake pattern and carbon:nitrogen ratios of prairie crops. In *Proceedings of Manitoba Agronomists Conference, 2006*.

Helsel, D. and Hirsch, R. (1991). Statistical methods in water resources. In *Techniques in Water Resources Investigations of the United States Geological Survey*, volume 4, chapter A3 Hydrologic Analysis and Interpretation. USGS.

Hill, A. (1981). Stream phosphorus exports from watersheds with contrasting land uses in southern ontario. *Water Resources Bulletin*, 17(4):627–634.

Hill, A. (1990). Ground water flow paths in relation to nitrogen chemistry in the near-stream zone. *Hydrobiologia*, 206(1):39–52.

Hill, A. and Waddington, J. (1993). Analysis of storm run-off sources using oxygen-18 in a headwater swamp. *Hydrological Processes*, 7(3):305 – 316.

Hill, A. R. (1996). Nitrate removal in stream riparian zones. *Journal of Environmental Quality*, 25(4):743–755.

Holly, F. and Usseglio-Polatera, J. (1984). Dispersion simulation in two-dimensional tidal flow. *Journal of Hydraulic Engineering*, 110(7):905–926.

Holly, F. M. and Preissmann, A. (1977). Accurate calculation of transport in two dimensions. *Journal of the Hydraulics Division, American Society of Civil Engineers Vol.103*, p 1259-1277:2 append.

Inamdar, S., O'Leary, N., Mitchell, M., and Riley, J. (2006). The impact of storm events on solute exports from a glaciated forested watershed in western new york, usa. *Hydrological Processes*, 20:3423 – 3439.

Inamdar, S. P., Lowrance, R. R., Altier, L. S., Williams, R. G., and Hubbard, R. K. (1999a). Riparian ecosystem management model (remm): Ii. testing of the water quality and nutrient cycling component for a coastal plain riparian system. *American Society for Agricultural Engineers, Transactions*, 42(6):1691 – 1707.

Inamdar, S. P., Sheridan, J. M., Williams, R. G., Bosch, D. D., Lowrance, R. R., Altier, L. S., and Thomas, D. L. (1999b). Riparian ecosystem management model (remm): I. testing of the hydrologic component for a coastal plain riparian system. *American Society for Agricultural Engineers, Transactions*, 42(6):1679 – 1689.

Jaffe, D. A. (1992). The nitrogen cycle. In Butcher, S. S., Charlson, R. J., Orians, G. H., and Wolfe, G. V., editors, *Global Biogeochemical Cycles*, chapter 12, pages 263 – 284. Academic Press.

James, L. D. and Burges, S. J. (1982). Selection, calibration, and testing of hydrologic models. In Haan, C. T., Johnson, H. P., and Brakensiek, D. L., editors, *Hydrologic Modeling of Small Watersheds*, pages 437–472. ASAE, St. Joseph, Michigan.

Jensen, S. K. (1991). Applications of hydrologic information automatically extracted from digital elevation models. *Hydrological Processes*, 5(1):31–44.

Jenson, S. K. and Domingue, J. O. (1988). Extracting topographic structure from digital elevation data for geographic information system analysis. *Photogrammetric Engineering and Remote Sensing*, 54(11):1593–1600.

Johnsson, H., Bergstrom, L., Jansson, P.-E., and Paustian, K. (1987). Simulated nitrogen dynamics and losses in a layered agricultural soil. *Agriculture, Ecosystems & Environment*, 18(4):333–356.

Julien, P. Y. (2002). *River mechanics*. Cambridge University Press, Cambridge ; New York.

Julien, P. Y. and Frenette, M. (1987). Macroscale analysis of upland erosion. *Hydrol. Sci. J.*, 32(3):347358.

Jury, W. A., Gardner, W. R., Saffigna, P. G., and Tanner, C. B. (1976). Model for predicting simultaneous movement of nitrate and water through a loamy sand. *Soil Science*, 122(1):36 – 43.

Kadlec, R. and Knight, R. (1996). *Treatment Wetlands*. Lewis Publishers.

Kang, S., Kim, S., Oh, S., and Lee, D. (2000). Predicting spatial and temporal patterns of soil temperature based on topography, surface cover and air temperature. *Forest Ecology and Management*, 136(1-3):173–184.

Kapoor, A. and Viraraghavan, T. (1997). Nitrate removal from drinking water-review. *Journal of Environmental Engineering*, 123(4):371–380.

Karr, J. R. and Gorman, O. T. (1975). Effects of land treatment on the aquatic environment. *Non-Point Source Pollution Seminar Section 108(a) Demonstration Projects Progress Reports, Held at Chicago, November 20, 1975.Report EPA-905/9-75-007, (1975).p 120-150*, 31 ref. EPA G005103:G005140.

Kennedy, G. and Mayer, T. (2002). Natural and constructed wetlands in canada: An overview. *Water Quality Research Journal of Canada*, 37(2):295 – 325.

Klausner, S. D., Kanneganti, V. R., and Bouldin, D. R. (1994). An approach for estimating a decay series for organic nitrogen in animal manure. *Agronomy Journal*, 86(5):897–903.

Kouwen, N. (1988). Watflood: a real-time, microcomputer-based data management and flood forecasting system based on real-time weather radar. *Canadian Water Resources Journal*, 13(1):62–77.

Kouwen, N. (2005). *WATFLOOD-SPL9 Hydrological Model and Flood Forecasting System - Manual*. University of Waterloo.

Kouwen, N., Danard, M., Bingeman, A., Lu, W., Seglenieks, F. R., and Soulis, E. D. (2005). Case study: Watershed modeling with distributed weather model data. *Journal of Hydrologic Engineering*, 10(1):23–38.

Kouwen, N., Soulis, E. D., Pietroniro, A., Donald, J., and Harrington, R. A. (1993). Grouped response units for distributed hydrologic modeling. *Journal of Water Resources Planning and Management*, 119(3):289 – 305.

Krajewski, W. F. and Smith, J. A. (2002). Radar hydrology; rainfall estimation; 25 years, advances in water resources. *Advances in Water Resources*, 25(8-12):1387–1394.

Leon, L., Booty, W., Bowen, G., and Lam, D. (2004). Validation of an agricultural non-point source model in a watershed in southern ontario. *Agricultural Water Management*, 65:59 – 75.

Leon, L., Soulis, E. D., Kouwen, N., and Farquhar, G. (2001). Nonpoint source pollution: A distributed water quality modeling approach. *Water Research*, 35(4):997 – 1007.

Leon, L. F. (1999). *Integral System for Nonpoint Source Pollution Modeling in Surface Waters*. Phd, University of Waterloo.

Leon, L. F., Soulis, E. D., Kouwen, N., and Farquhar, G. J. (2002). Modeling diffuse pollution with a distributed approach. *Water Science and Technology*, 45(9):149–156.

Leonard, B. P. (1979). A stable and accurate convective modelling procedure based on quadratic upstream interpolation. *Computer Methods in Applied Mechanics and Engineering*, 19(1):59–98.

Leonard, B. P. (1991). The ultimate conservative difference scheme applied to unsteady one-dimensional advection. *Computer Methods in Applied Mechanics and Engineering*, 88(1):17–74.

Leonard, B. P. and Noye, J. (1990). Second- and third-order two-level implicit fdms for unsteady one-dimensional convection diffusion. In *Computational Techniques & Applications: CTAC-89*, pages 311–317. New York.

Leopold, L. B., Wolman, M. G., and Miller, J. P. (1992). *Fluvial Processes in Geomorphology*. Dover.

Liu, Y., Yang, W., and Wang, X. (2008). Development of a swat extension module to simulate riparian wetland hydrologic processes at a watershed scale. *Hydrological Processes*.

Lowrance, R., Todd, R., and Asmussen, L. (1984a). Nutrient cycling in an agricultural watershed: Ii. streamflow and artificial drainage. *Journal of Environmental Quality*, 13(1):27 – 32.

Lowrance, R., Todd, R., Fail, J., Hendrickson, O., and Leonard, R. (1984b). Riparian forests as nutrient filters in agricultural watersheds. *Bioscience*, 34(6):374 – 377.

Lowrence, R., Todd, R. L., and Asmussen, L. E. (1983). Waterborne nutrient budgets for the riparian zone of an agricultural watershed. *Agriculture, Ecosystems & Environment*, 10(4):371–384.

Lyn, D. A. (1987). Unsteady sediment-transport modeling. *Journal of Hydraulic Engineering*, 113:1–15.

Macrae, M., English, M., Schiff, S., and Stone, M. (2007). Intra-annual variability in the contribution of tile drains to basin discharge and phosphorus export in a first-order agricultural catchment. *Agricultural Water Management*, 92(3):171–182.

Macrae, M. L. (2003). *Temporal Variability in Nutrient Transport in a First-Order Agricultural Basin in Southern Ontario*. PhD thesis, University of Waterloo.

Mayer, P. M., Reynolds, S. K., J., and Canfield, T. J. (2005). Riparian Buffer Width, Vegetative Cover, and Nitrogen Removal Effectiveness: A Review of Current Science and Regulations. Technical Report EPA/600/R-05/118, US Environmental Protection Agency.

McCuen, R. (1973). The role of sensitivity analysis in hydrologic modeling. *Journal of Hydrology*, 18(1):37–53.

McCuen, R. H. (2005). *Hydrologic analysis and design*. Pearson Prentice Hall, Upper Saddle River, N.J., 3rd edition.

McKillop, R. (1997). *Modelling the Rainfall-Runoff Response from a Headwater Wetland*. PhD thesis, University of Waterloo.

McKillop, R., Kouwen, N., and Soulis, E. D. (1999). Modeling the rainfall-runoff response of a headwater wetland. *Water Resources Research*, 35(4):1165 – 1177.

Mitsch, W. and Gosselink, J. (2000). The value of wetlands: importance of scale and landscape setting. *Ecological Economics*, 35(1):25 – 33.

Mitsch, W. J. and Gosselink, J. G. (1993). *Wetlands*. Van Norstrand Reinhold, 2nd edition.

MNR (2002). *Natural Resources and Values Information System*. The Ontario Ministry of Natural Resources.

Monro, J. (1971). *Direct search optimization in mathematical modelling and a watershed application*. NOAA Technical Memorandum. NWS-HYDRO-12.

Muñoz Carpena, R. and Parsons, J. E. (2004). A design procedure for vegetative filter strips using vfsmod-w. *Transactions of the American Society of Agricultural Engineers*, 47(6):1933–1941.

Muñoz Carpena, R. and Parsons, J. E. (2005). *VFSMOD-W: Vegetative Filter Strips Hydrology and Sediment Transport Modelling System*. University of Florida. Version 2.

Muñoz Carpena, R., Parsons, J. E., and Gilliam, J. W. (1999). Modeling hydrology and sediment transport in vegetative filter strips. *Journal of Hydrology*, 214(1-4):111–129.

Nash, J. E. and Sutcliffe, J. V. (1970). River flow forecasting through conceptual models part i – a discussion of principles. *Journal of Hydrology*, 10(3):282–290.

Neitsch, S., Arnold, J., Kiniry, J., and Williams, J. (2001). *Soil and Water Assessment Tool (SWAT) User's Manual - Version 2000*. Temple, Texas.

Novotny, V. and Olem, H. (1994). *Water Quality: Prevention, Identification, and Management of Diffuse Pollution*. Van Nostrand Reinholdt.

O'Donnell, G., Nijssen, B., and Lettenmaier, D. P. (1999). A simple algorithm for generating streamflow networks for grid-based, macroscale hydrological models. *Hydrological Processes*, 13(8):1269–1275.

Oenema, O., van Liere, L., and Schoumans, O. (2005). Effects of lowering nitrogen and phosphorus surpluses in agriculture on the quality of groundwater and surface water in the netherlands. *Journal of Hydrology*, 304(1-4):289–301.

OMAFRA (2002). *Publication 811 - Agronomy Guide for Field Crops*. Ontario Ministry of Agriculture, Food, and Rural Affairs.

OMAFRA (2003). *Buffer strips*. Best management practices. Ontario Ministry of Agriculture and Food, Toronto.

OMAFRA (2008a). Best management practices. Online. http://www.omafra.gov.on.ca/english/environment/bmp_books.htm.

OMAFRA (2008b). *Publication 818 - Nutrient Management Workbook*. Ontario Ministry of Agriculture, Food, and Rural Affairs.

Peterjohn, W. and Correll, D. (1984). Nutrient dynamics in an agricultural watershed: observations on the role of riparian forest. *Ecology*, 65(5):1466–1475.

Phillips, J. D. (1996). Wetland buffers and runoff hydrology. In Malamoottil, G., Warner, B. G., and McBean, E. A., editors, *Wetlands: Environmental Gradients, Boundaries, and Buffers*, chapter 14, pages 207–220. Lewis Publishers.

Pietroniro, A., Fortin, V., Kouwen, N., Neal, C., Turcotte, R., Davison, B., Verseghy, D., Soulis, E. D., Caldwell, R., Evora, N., and Pellerin, P. (2006a). Using the mesh modelling system for hydrological ensemble forecasting of the laurentian great lakes at the regional scale. *Hydrology and Earth System Sciences Discussions*, 3:2473–2521.

Pietroniro, A., Toth, B., Leconte, R., Peters, D. L., Prowse, T. D., Kouwen, N., and Conly, F. M. (2006b). Modelling climate change impacts in the peace and athabasca catchment and delta: Iii - integrated model assessment. *Hydrological Processes*, 20(19):4231–4245.

PLUARG (1978). *Summary of the Final Report to the International Joint Commission from the International Reference Group on Great Lakes Pollution from Land Use Activities - PLUARG*. International Reference Group on Great Lakes Pollution from Land Use Activities.

Press, W. H., Teukolsky, S. A., Vetterling, W. T., and Flannery, B. P. (1992). *Numerical recipes in FORTRAN : the art of scientific computing*. Cambridge University Press, Cambridge England, 2nd edition.

Puckett, L. J., Cowdery, T. K., Lorenz, D. L., and Stoner, J. D. (1999). Estimation of nitrate contamination of an agro-ecosystem outwash aquifer using a nitrogen mass-balance budget. *J Environ Qual*, 28(6):2015–2025.

Rantz, S. E. (1981). Measurement and computation of streamflow: volume 1: measurement of stage and discharge. Technical report, United States Geological Survey.

Refsgaard, J. C. and Knudsen, J. (1996). Operational validation and intercomparison of different types of hydrological models. *Water Resources Research*, 32(7):2189–2202.

Region of Waterloo (2004). Water and wastewater monitoring report. Technical report, Region of Waterloo.

Richards, P. (2002). Estimation of pollutant loads in rivers and streams: A guidance document for nps programs. Technical report, Report to the U.S. Environmental Protection Agency, Tiffin, Ohio.

Rojas, R., Velleux, M., Julien, P. Y., and Johnson, B. E. (2008). Grid scale effects on watershed soil erosion models. *J. Hydrologic Engrg.*, 13(9):793–802.

Rudolph, D. and Parkin, G. (1998). Partition of solutes from agricultural fields within the hydrologic system at two sites in southern ontario and the subsequent impact on adjacent aquatic ecosystems. Technical Report RES/MON-010/97, Agriculture and Agri-Food Canada, Pest Management Research Centre.

Rupert, M. G. (2008). Decadal-scale changes of nitrate in ground water of the united states, 1988-2004. *J Environ Qual*, 37(5 Supplement):S–240–248.

Rutherford, J. C. (1994). *River mixing*. Wiley, Chichester England ; Toronto.

Saâdi, Z. and Maslouhi, A. (2003). Modeling nitrogen dynamics in unsaturated soils for evaluating nitrate contamination of the mnasra groundwater. *Advances in Environmental Research*, 7(4):803–823.

Schilling, K. E. and Helmers, M. (2008). Tile drainage as karst: Conduit flow and diffuse flow in a tile-drained watershed. *Journal of Hydrology*, 349(3-4):291–301.

Schimel, J. P. and Bennett, J. (2004). Nitrogen mineralization: Challenges of a changing paradigm. *Ecology*, 85(3):591–602.

Scott, M. E. A. (2006). Grand river watershed analysis of nitrate transport as a restult of agricultural inputs using a geographic information system. Master's thesis, University of Waterloo.

Shuman, J. R. (2005). Agricultural bmps, nutrient load reductions, and watershed restoration -the octoraro creek watershed and the chesapeake bay. In *Proceedings of the 3rd Conference on Watershed Management to Meet Water Quality Standards and Emerging TMDL*, pages 415–422. American Society of Agricultural Engineers.

Singh, V. P. and Frevert, D. K., editors (2006). *Watershed Models*. Taylor & Francis.

Sliva, L. and Dudley Williams, D. (2001). Buffer zone versus whole catchment approaches to studying land use impact on river water quality. *Water research*, 35(14):3462–3472.

Spalding, R. F; Exner, M. E. (1993). Occurrence of nitrate in groundwater-a review. *Journal of Environmental Quality*, 22:392–402.

Spaling, H. (1995). Analyzing cumulative environmental effects of agricultural land drainage in southern ontario, canada. *Agriculture, Ecosystems & Environment*, 53(3):279 – 292.

Stadnyk, T., St Amour, N., Kouwen, N., Edwards, T. W. D., Pietroniro, A., and Gibson, J. J. (2005). A groundwater separation study in boreal wetland terrain: The watflood hydrological model compared with stable isotope tracers. *Isotopes in Environmental and Health Studies*, 41(1):49–68.

Stanford, G. and Smith, S. J. (1972). Nitrogen mineralization potentials of soils. *Soil Sci Soc Am J*, 36(3):465–472.

Steefel, C. I. and MacQuarrie, T. B. (1996). Approaches to modeling of reactive transport in porous media. In C., L. P., Steefel, C. I., and Oelkers, E. H., editors, *Reactive Transport in Porous Media*, volume 34, pages 83–129. Minerological Society of America.

Stefan, H. and Preud'homme, E. (1993). Stream temperature estimation from air temperature. *Water Resources Bulletin*, 29(1):27–45.

Strang, G. (1968). On the construction and comparison of difference schemes. *SIAM Journal on Numerical Analysis*, 5(3):506–517.

Streeter, V. L. and Wylie, E. B. (1985). *Fluid mechanics*. McGraw-Hill, New York ; Toronto.

Tate, III, R. L. (1995). *Soil Microbiology*. John Wiley & Sons.

Toth, B., Pietroniro, A., Conly, F. M., and Kouwen, N. (2006). Modelling climate change impacts in the peace and athabasca catchment and delta; i, hydrological model application. *Hydrological Processes*, 20(19):4197–4214.

US-EPA (2001). *Better Assessment Science Integrating point and Non-point sources (BASINS), Version 3.0*. United States Environmental Protection Agency - Office of Water, epa-823-b01-001 edition.

US-EPA (2003). Definition and procedure for the determination of the method detection limit. In *USEPA Title 40*, volume 136. US EPA.

US-EPA (2005). *National Management Measures to Protect and Restore Wetlands and Riparian Areas for the Abatement of Nonpoint Source Pollution*, volume EPA-841-B-05-003. United States Environmental Protection Agency - Office of Water, Washington, DC.

USACE (1995). *CE-QUAL-RIV1: A Dynamic, One-Dimensional (Longitudinal) Water Quality Model for Streams*. U.S. Army Corps of Engineers, Vicksburg, MS, instruction report el-95-2 edition.

USGS (1999). *The Quality of Our Nations Waters: Nutrients and Pesticides*, volume USGS Circular 1225. USGS, Reston, VA.

USGS (2005a). Cleaning of equipment for water sampling. In *National Field Manual for the Collection of Water-Quality Data*, volume 9 of *Techniques of Water-Resources Investigations*, chapter A3. U.S. Geological Survey.

USGS (2005b). Collection of water samples. In *National Field Manual for the Collection of Water-Quality Data*, volume 9 of *Techniques of Water-Resources Investigations*, chapter A4. U.S. Geological Survey.

Uusitalo, R., Turtola, E., Kauppila, T., and Lilja, T. (2001). Particulate phosphorus and sediment in surface runoff and drainflow from clayey soils. *J Environ Qual*, 30(2):589–595.

Van Kessel, J. S. and Reeves, J. B. (2002). Nitrogen mineralization potential of dairy manures and its relationship to composition. *Biology and Fertility of Soils*, 36(2):118–123.

Vanni, M., Renwick, W., Headworth, J., Auch, J., and Schaus, M. (2001). Dissolved and particulate nutrient flux from three adjacent agricultural watersheds: A five-year study. *Biogeochemistry*, 54(1):85–114.

Vennard, J. K. and Street, R. L. (1976). *Elementary fluid mechanics*. Wiley, New York ; Toronto, 5th edition.

Verhallen, A. and Roddy, E. (2003). *Irrigating Vegetable Crops*. Ontario Ministry of Agriculture Food and Rural Affairs.

Vieux, B. E. (2001). *Distributed hydrologic modeling using GIS*. Kluwer Academic Publisher, Dordrecht.

Viney, N. R. and Sivapalan, M. (1999). A conceptual model of sediment transport: application to the avon river basin in western australia. *Hydrological Processes*, 13(5):727–743.

Wall, G. J., Dickinson, W. T., and van Vliet, L. J. P. (1982). Agriculture and water quality in the canadian great lakes basin: Ii. fluvial sediments. *J Environ Qual*, 11(3):482–486.

Wallis, S. G. and Manson, J. R. (1997). Accurate numerical simulation of advection using large time steps. 24(2):127–139.

Wei, T. and McGuinness, J. (1973). Reciprocal distance squared method, a computer technique for estimating area precipitation. Technical Report ARS-Nc-8, US Agricultural Research Service.

Whigham, D., Chitterling, C., and Palmer, B. (1988). Impacts of freshwater wetlands on water quality: a landscape perspective. *Environmental Management*, 12(5):663–671.

Woolhiser, D. A., Smith, R. E., and Goodrich, D. C. (1990). *KINEROS, a kinematic runoff and erosion model; documentation and user manual*. U. S. Department of Agriculture, Agricultural Research Service, USA. AAS-77.

Yanenko, N. N. (1971). *The Method of Fractional Steps: The Solution of Problems of Mathematical Physics in Several Variables*. Springer-Verlag. English Translation Edited by M. Holt.

Young, R., Onstad, C., Bosch, D., and Anderson, W. (1989). Agnps: A nonpoint-source pollution model for evaluating agricultural watersheds. *Journal of Soil and Water Conservation*, 44(2):168 – 173.

Zhang, C. (2007). *Fundamentals of environmental sampling and analysis*. Wiley-Interscience, Hoboken, N.J.

Zheng, D., Hunt, Jr, E., and Running, S. (1993). A daily soil temperature model based on air temperature and precipitation for continental applications. *Climate Research*, 2(3):183–191.

Glossary

ADV Acoustic Doppler Velocimeter, p. 295.

AGNPS Agricultural Non-Point Source Pollution Model (Young et al., 1989), p. 24.

ASCE American Society of Civil Engineers, p. 70.

BMP Best Management Practise or Better Management Practise, p. 2.

CANSIS Canadian Soils Information System, p. 31.

CFL Courant-Friedrichs-Lewy - convergence condition for explicit numerical time-marching schemes (Courant et al., 1967), p. 142.

CSTR Continuous Stirred-Tank Reactor model, p. 21.

DEM Digital Elevation Model, p. 63.

EnSim EnSim Hydrologic - Visualization and Analysis tool for Hydrologic Applications. EnSim is the former name of "Green Kenue" developed by the Canadian Hydraulics Centre of the National Research Council of Canada, p. 129.

FDC Flow Distribution Curve, p. 50.

FSAM Field Sampling Asset Management System, p. 45.

GIS Geographic Information System, p. 21.

GRCA Grand River Conservation Authority, p. 2.

GRU Grouped Response Unit (Kouwen et al., 1993), p. 23.

HEC-RAS Hydrologic Engineering Centre River Analysis System by the US Army Corp of Engineers, p. 7.

IJC International Joint Commission - an independent bi-national (Canada and USA) organization established to resolve treaty disputes and to advise governments on issues of scientific concern, p. 12.

KINEROS2 Kinematic Runoff and Erosion Model (Version 2) (Woolhiser et al., 1990), p. 158.

LULC Land Use / Land Cover, p. 36.

MDL Method Detection Limit, p. 93.

MESH Modélisation Environnementale Communautaire Surface and Hydrology Modelling System, p. 3.

MNR Ontario Ministry of Natural Resources, p. 7.

MOE Ontario Ministry of the Environment, p. 12.

NASH Nash-Sutcliffe efficiency criterion (Nash and Sutcliffe, 1970), p. 201.

NOLS Normalized ordinary least squares efficiency criterion, p. 201.

NPS Non-Point Source, p. 1.

NRVIS Natural Resources and Values Information System, p. 31.

OLS Ordinary least-squares estimator, p. 200.

OMAFRA Ontario Ministry of Agriculture, Food and Rural Affairs, p. 2.

PLUARG The Great Lakes Pollution from Land Use Activities Study, p. 12.

PWQMN Ontario's Provincial Water Quality Monitoring Network, p. 12.

R2C EnSim file format for storing gridded time-series data. The format is used extensively within the WATFLOOD model for input and output of hydrologic data., p. 129.

RDBMS Relational Database Management System, p. 45.

REMM Riparian Ecosystem Management Model (Inamdar et al., 1999a,b), p. 22.

RMS Root mean squares efficiency criterion, p. 201.

RUSLE Revised Universal Soil Loss Equation, p. 23.

SCS Soil Conservation Service, the former name of the U.S. Natural Resources Conservation Service (NRCS), p. 23.

SED Distributed Sediment Data File (*.SED), p. 214.

SLS Square-root least squares, p. 200.

SNIA Sequential non-iterative approach, p. 156.

SPSS Statistical analysis and data management system, p. 45.

SWAT Soil and Water Assessment Tool (Neitsch et al., 2001), p. 167.

TN Total Nitrogen, p. 91.

TP Total Phosphorus, p. 91.

TSS Total Suspended Solids, p. 21.

US-EPA United States Environmental Protection Agency, p. 34.

VFSMOD Vegetated Filter Strip Model (Muñoz Carpena and Parsons, 2004), p. 168.

WQP Water Quality Parameter file (*.WQP), p. 160.

Nomenclature

α dispersion parameter (reciprocal of Péclet number) $[-]$

Δt time step $[T]$

Δx channel element incremental length $[L]$

δ water temperature estimation lag coefficient $[T]$

γ_s particle specific gravity $[-]$

λ dimensionless decay coefficient $[-]$

M' mass flux of constituent into or out of element $[M/T]$

μ fluid dynamic viscosity $[L^2/T]$

Ω stream power $[L/T]$

Ω_c critical stream power for sediment transport $[L/T]$

ϕ concentration of a constituent or solute $[M/L^3]$

ϕ_{chan} constituent concentration in the channel $[M/L^3]$

ϕ_o observed constituent concentration $[M/L^3]$

ϕ_{rip} constituent concentration in the riparian wetland $[M/L^3]$

ϕ_{sed_max} maximum sediment concentration based on stream carrying capacity $[M/L^3]$

ϕ_{sed} sediment concentration $[M/L^3]$

ϕ_s simulated constituent concentration $[M/L^3]$

ρ fluid density $[M/L^3]$

ρ_s sediment particle density $[M/L^3]$

θ soil water content $[L^3/L^3]$

θ_T rate correction constant for temperature $[-]$

θ_{wet} wetland porosity parameter $[-]$

$\forall$ volume in a grid channel $[L^3]$

$\forall_{wet}$ maximum wetland water storage volume$[L^3]$

A flow cross sectional area of the channel $[L^2]$

A_t water temperature estimation coefficient $[-]$

a_2 watershed drainage area to bank-full channel area parameter $[-]$

a_3 watershed drainage area to bank-full channel area parameter $[-]$

a_4 watershed drainage area to bank-full channel area parameter $[-]$

A_{bf} bank-full channel area $[L^2]$

A_{drain} watershed drainage area $[L^2]$

A_{of} overland flow cross sectional area $[L^2]$

A_{rip} effective area connecting the channel to the riparian zone $[L^2]$

A_{wet} wetland areal cover $[L^2]$

B_t water temperature estimation coefficient $[-]$

C Courant number [−]

C_{ch_er} erodability factor [−]

C_{sed} maximum sediment carrying capacity multiplicative parameter [−]

D dispersion coefficient $[L^2/T]$

d depth of channel $[L]$

d_s particle diameter $[L]$

d_{50} median sediment diameter) $[L]$

d_{bf} bank-full channel depth $[L]$

D_{par} dimensionless longitudinal dispersion parameter [−]

E_{conc} concentration relative error [−]

E_{mass} system mass relative error [−]

e_{sw} soil water rate constant correction coefficient [−]

e_t temperature rate constant correction coefficient [−]

g acceleration due to gravity $[L/T^2]$

h height of channel water column $[L]$

h_{chan} height of water within channel $[L]$

I inflow into grid channel $[L^3/T]$

J nitrate loss rate $[M/L^2T]$

K'_{rip} riparian channel dispersion calibration constant $[L/T]$

K_0 zero-order decay or source rate constant $[M/L^3T]$

K_1 first-order decay or source rate constant $[1/T]$

K_s particle settling rate $[1/T]$

k_0 unadjusted rate constant $[1/T]$

k_{20} first order decay rate at 20 °C $[1/T]$

k'_{20} areal decay rate at 20 °C $[L/T]$

K_{ag} in-channel zero-order decay coefficient $[-]$

K_{dec} in-channel first order decay coefficient $[1/T]$

k_{eff} temperature and moisture corrected rate constant $[1/T]$

K_{rip} riparian channel dispersion coefficient $[L^2/T]$

K_{sed_dep} sediment deposition rate $[1/T]$

K_{sed_res} sediment resuspension rate $[1/T]$

K_{sed} maximum sediment carrying capacity exponential parameter $[-]$

L_C channel length $[L]$

M mass of constituent in element $[M]$

M_o observed system mass $[M]$

M_{rip} constituent mass in the riparian wetland $[M]$

M_s simulated system mass $[M]$

n_R Manning roughness $[-]$

O outflow from grid channel $[L^3/T]$

Pe Péclet number $[-]$

Q volumetric flow rate$[L^3/T]$

Q_{10} temperature correction factor $[-]$

q_{LI} lateral flow into channel per unit length $[L^2/T]$

q_{LO} lateral flow out of channel per unit length $[L^2/T]$

Q_{wl} flow from the channel to the riparian wetland $[L^3/T]$

R_s relative sensitivity coefficient $[-]$

R_C fraction of riparian protection along a channel $[-]$

R_{WD} width-depth ratio for a bank-full channel $[-]$

S mass source or sink term per unit channel length $[M/LT]$

S_0 channel slope $[-]$

T temperature $[^\circ C]$

t time $[T]$

T_a air temperature $[^\circ C]$

T_w water temperature $[^\circ C]$

T_s soil temperature $[^\circ C]$

U mean cross-sectional velocity $[L/T]$

u channel velocity $[L/T]$

u^* shear velocity $[L/T]$

v_s settling velocity $[L/T]$

w channel width $[L]$

w_{bf} bank-full channel width $[L]$

w_{fs} filter strip width $[L]$

W_{wet} average wetland width (distance from GRU to channel) $[L]$

x distance $[L]$

Appendix A

Hydraulic Measurements

A.1 Summary

This appendix outlines the hydraulic measurements and modelling efforts undertaken at the Canagagigue Creeek study site. Sections include the set-up of the flow measurement stations, topographic survey results, stage calibration, discharge measurements and flow centroid calculations.

A.2 Flow Measurement Installations

A schematic of the hydraulic installations for the measurement of river stage are shown in Figure A.1. The installations consisted of 12" PVC Piping that were secured vertically by 3 lengths of re-bar that were hammered into the stream bed. The pipe was perforated at the base to allow for free exchange of water. The perforations were aligned in the downstream direction. At the top of the PVC Piping near the flange a platform was installed and placement for a CP-XA Chart-Pac^{TM}Data Logger by Lakewood Systems and a FS-15 Level Transducer with a float-counterweight assembly. The voltage output of the transducer was recorded by the logger every 15 minutes along with ambient temperature. A slit was cut into the platform to allow for the float-counterweight and connecting cable to be installed and attached to the level transducer. A protective cover was constructed to fit the top of the pipe and was put in place to protect the logger apparatus. Although temperature was recorded by the logger, it was not used for modelling

due to the fact that incident solar radiation on the cover would elevate the temperature within the chamber at the top of the apparatus. However, the temperature proved to be useful in comparing readings between loggers if the internal logger clock in one logger was found to have lost time. The diurnal temperature fluctuations could be aligned and the time corrected.

Photographs of each installation are shown in Figures A.2 and A.3. Figure A.2 shows the stilling well with the protective aluminium cover installed on the East Sub-Basin. Figure A.3 shows the West Sub-Basin installation with the aluminium cover removed exposing the ChartPac^{TM}Data Logger.

A.3 Survey Information

It was anticipated at the outset of this study that the short 2-year time frame and limited resources for the collection of stage-discharge relationship data would impact the development of effective rating curves. It was necessary to extrapolate data beyond the measured rating curves during high flow situations, and it was desirable to do this based on physical principles. A hydraulic model was developed using for the area near the stream confluence using topographic data to allow for a physical basis for extrapolation of the rating curve.

Topographic surveys of the study site were conducted to determine the characteristics of the stream from the sampling locations to the confluence and from the confluence to the nearest control point at the bridge at Sandy Hills Dr. Surveys were conducted on 24 March 2005, 2 April 2006, 23 November 2006, 5 January 2007 and 26 November 2007. The survey data are presented superimposed on a map presenting the local road network and published drainage network in Figure A.4.

Cross section data at road-crossings within the watershed upstream from the confluence study area were collected using a level with stadia to determine the bank-full areas as related to drainage areas. These data are important for determining hydraulic, routing and shear stress conditions at various locations within the watershed and are a necessary data input for the WatFlood hydrologic model. Figure A.5 shows the indexed locations of measured cross sections. Care was taken to select a number of locations within each of the study sub-basins and each of the major contributing tributaries.

The drainage area for each cross section location was determined using a digital elevation model and determining contributing drainage areas using the ArcGIS Spatial Analyst. Figure

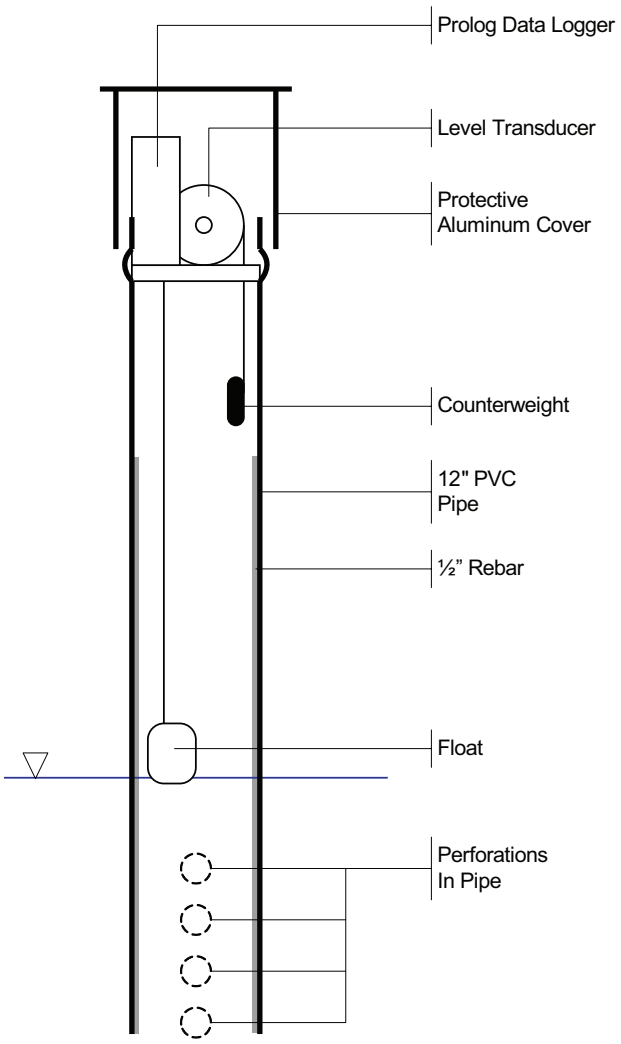

Figure A.1: Stage Measurement Installation Schematic

Figure A.2: Float Installation - East Sub-Basin (26-Sep-2005)

Figure A.3: Float Installation - West Sub-Basin (14-Apr-2005)

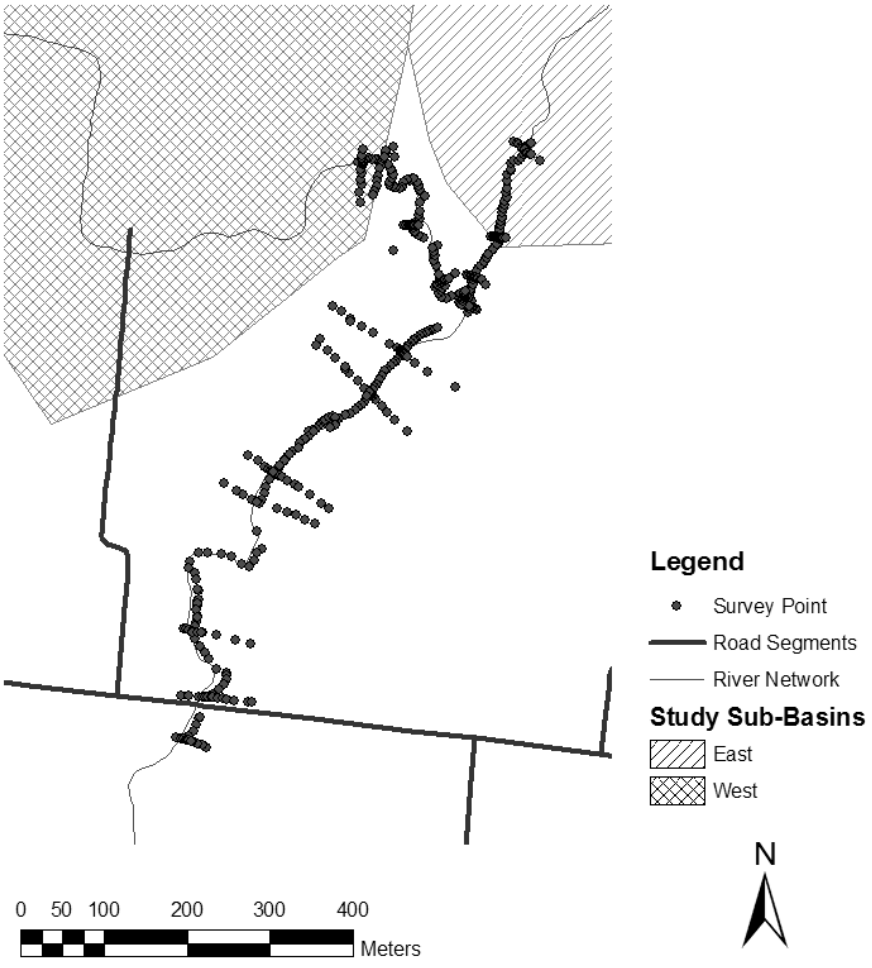

Figure A.4: Map of Study Site - Topographic Survey Data

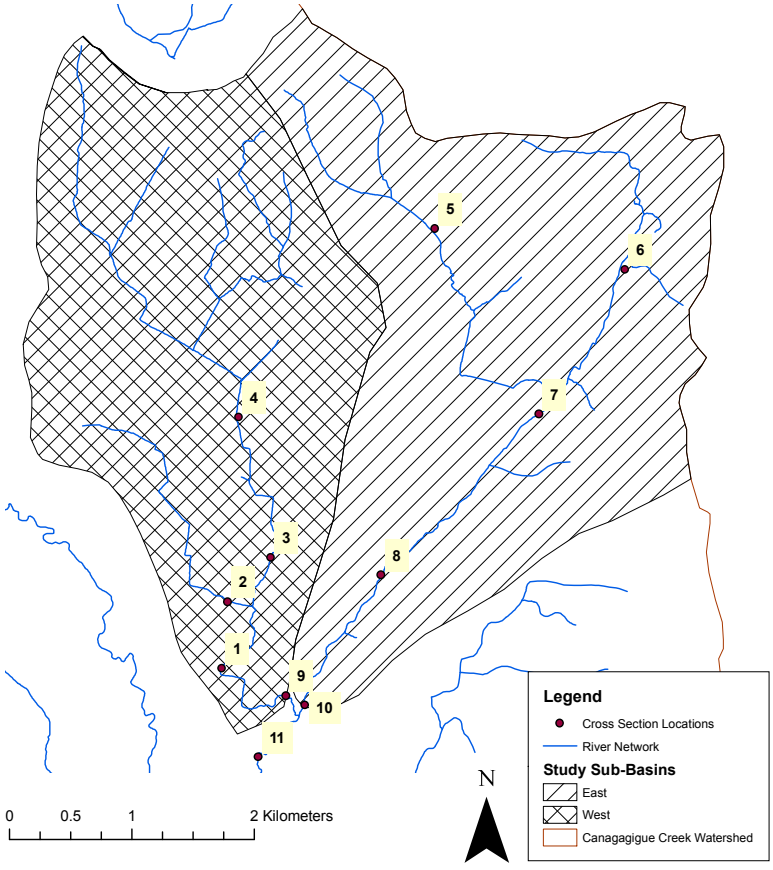

Figure A.5: Level Stream Cross-Section Measurement Locations

A.6 illustrates the relationship between the bank full area and the drainage area at the cross-section measurement location. Labels in Figure A.6 correspond to the location indices in Figure A.5.

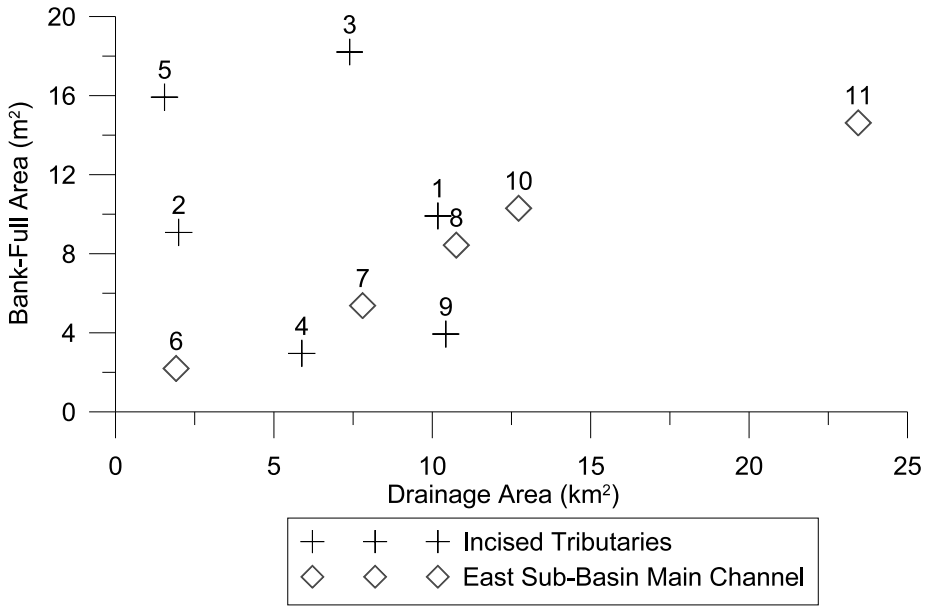

Figure A.6: Bank-Full Area vs. Drainage Area

Figure A.6 is informative as it illustrates the differences between the perennial main channel in the east sub basin (Locations 6,7,8,10, and 11) and remaining contributing drainage tributaries that often dry up over the summer (Locations 1,2,3,4,5, and 9). The perennial main channel in the East sub-basin and down stream shows a strong monotonic relationship between drainage area and bank full area with a relatively small channel and a wide flood plain. The remaining channels exhibit a strong degree of incision with very steep banks and no active flood plain. There is no relationship between the drainage area and the bank-full area of the channel for these reaches.

A.4 Stage Calibration

The float-counterweight level loggers report the stage within the stilling wells as a voltage which was logged to the data-loggers at 15 minute intervals. Voltage readings were calibrated to measured stage elevation. Periodic measurements were taken at the stilling wells to provide a record of the surface elevation at specific times based on the reference elevations provided from the topographic surveys. Stage measurements were entered into the FSAM Database and calibration datasets were created by linearly interpolating the float voltage measurements to match the time of tape measurement. The results are shown in Figure A.7. The relationships were entered into the FSAM Database and used to update the logger voltage data to local elevation data as the logger data was uploaded into the database. The results show a strong linear relationship over the observed range as is expected with the float-counterweight transducers employed. The float-counterweight systems were susceptible to freezing in the winter and were disassembled during the winter months and re-installed prior to the snowmelt. Consequently a separate stage-voltage relationship was required for each of the seasons, as it was difficult to re-orient the float-chain at precisely the same location from year to year. There were sometimes several regression relationships for one site location (as with Figure A.7 for 2005). This was due to an interruption or slip of the float-counterweight from the transducer. It was not always possible to to match the previous position of the transducer and a separate calibration period was required. Details of the installations themselves can be found in Appendix A. For the 2007 season the float counterweight was installed in the opposite orientation to the previous years, explaining the negative slope for that season as seen in Figure A.7.

A.5 Discharge Measurements

Flow discharge was measured at stable cross sections near the stilling well for each of the sub-basins using the velocity-area method (Dingman, 1994). Velocities were measured using a Marsh-McBirney Flo-Mate™ 2000 Portable Electromagnetic velocity meter. The Flo-Mate™ 2000 flow meter was employed because of it's utility when placed in weedy portions of the stream, where a propeller meter would not function. A ten-second average was employed on the instrument to determine the velocity at sampling points. Velocity measurements were recorded when the ten-second average reading stabilized. The Flo-Mate™ had been previously calibrated at the

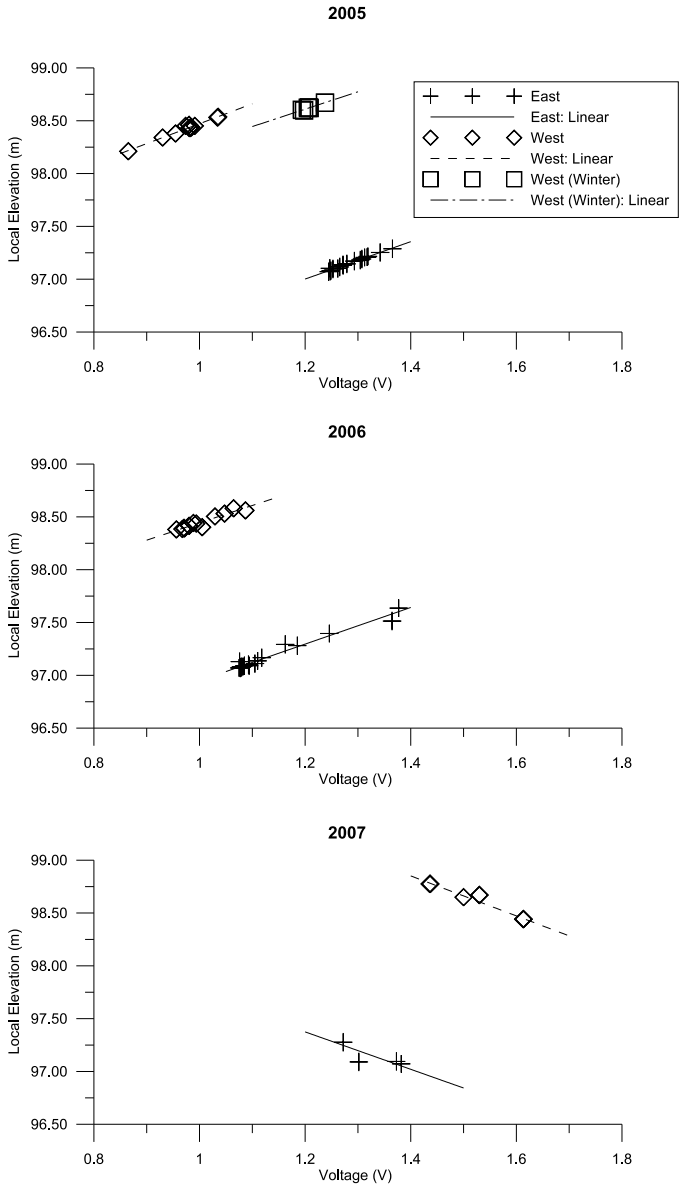

Figure A.7: Stage vs. Logger Voltage Relationship – 2005, 2006 and 2007 Seasons

National Water Research Institute (NWRI), Burlington, Ontario for velocity ranges from 0.02 to 2.76 m/s and was verified in the University of Waterloo hydraulics lab with a SonTek® Acoustic Doppler Velocimeter (ADV).

Cross sectional locations that were used for discharge measurements are shown in Figure 4.1. Only one cross section was employed for the East section. Two cross section locations were employed for West section. The primary cross section for the west which was closest to the stilling well was wide and often had very low velocities in low flow conditions. A second cross section was employed downstream with a narrower section to provide increased, more accurately measurable velocities across the section.

Velocity measurements were taken at regular intervals across the cross section and it was ensured at least two velocity measurements were taken at each position across the creek. Attempts were made to get reasonably close to the Two-Point Measurement locations (20% and 80% of the depth) as per Dingman (1994). However, due to the typically shallow conditions of the stream and the 5 cm increments of the velocity meter measuring rod, velocity measurements were taken at the nearest whole increment on the measuring rod. Velocity profiles in narrow streams do not always exhibit logarithmic velocity profiles and extra measurement points were required to interpolate the velocities and flows (Dingman, 1994). Employing 2 or 3 velocity measurement points at each cross-sectional location is believed to be a very conservative approach to stream measurement under the observed conditions as the stream depths were rarely greater than 0.75 m which is the maximum depth requirement by the U.S. Geological Survey to use only a single velocity point velocity per measurement location (Rantz, 1981).

Discharge measurements were calculated by using a linear interpolation between velocity measurements over the cross sectional area of the creek. The Surfer™ software package by Golden Software was used to generate the interpolated grid of velocities within the creek using the Delaunay linear interpolation and triangulation technique. The triangular surfaces are used to calculate the velocities in a regular grid and integrated over the cross sectional area.

Boundary values were included with the measured values to force a valid grid structure. Velocities at the channel edge were set to zero. Velocities at the water surface at a longitudinal sampling location were assumed to be equivalent to the velocity measurement taken nearest the surface. A sample of the interpolated velocity profile is shown in Figure A.8. Part A of this figure presents the velocity sampling points employed in generating the velocity profile contour plot, including the boundary values at the river bed and water surface. Part B of this figure shows

the generated velocity contour plot based on the Delaunay interpolation algorithm. The contour plot in Figure A.8 illustrates the observed general deviation from the logarithmic velocity profile which is generally assumed.

A.6 Flow Centroid Calculations

The location of the centroid of the flow across the stream width was required for the determination of water quality sampling locations as per (USGS, 2005b). The centroids of the flow fields were calculated for the east and west sub-basins using the flow profiles similar to that shown in Figure A.8. Centroids were calculated using the linearly interpolated data grid for various flow regimes. It was found that for each of the sub-basins the centroids remained relatively constant for the flow profiles measured. Figures A.9 and A.10 illustrate the centroidal variation as a function of flow through the channel. The flow centroid for the east sub-basin channel was approximately 2.5 m from a fixed left-bank marker. The flow centroid for the west sub-basin channel was 2.9 m from a fixed left-bank marker.

A.7 Flow-Discharge Rating Curve Development

The relationships in the rating curves were used to convert the measured elevations using the float and pressure transducer data to calculated discharge rates. The final rating curves were determined using a calibrated HEC-RAS hydraulic model that best fit the measured data. This approach was taken because it was difficult and dangerous to take flow measurements at the maximum flow rates during the spring snowmelt events. The employment of a hydraulic model allowed for a physically-based extrapolation of the stage-discharge curve beyond the measured flow data.

Figure A.11 shows the stage-discharge data collected in each of the sub-basins for both summer and winter periods.

A.7.1 Extrapolation of Rating Curves using HEC-RAS

Flow measurement data did not encompass the maximum flow in the sub-basins as maximum flows were difficult to measure in-stream and timing a flow measurement to the peak of a hy-

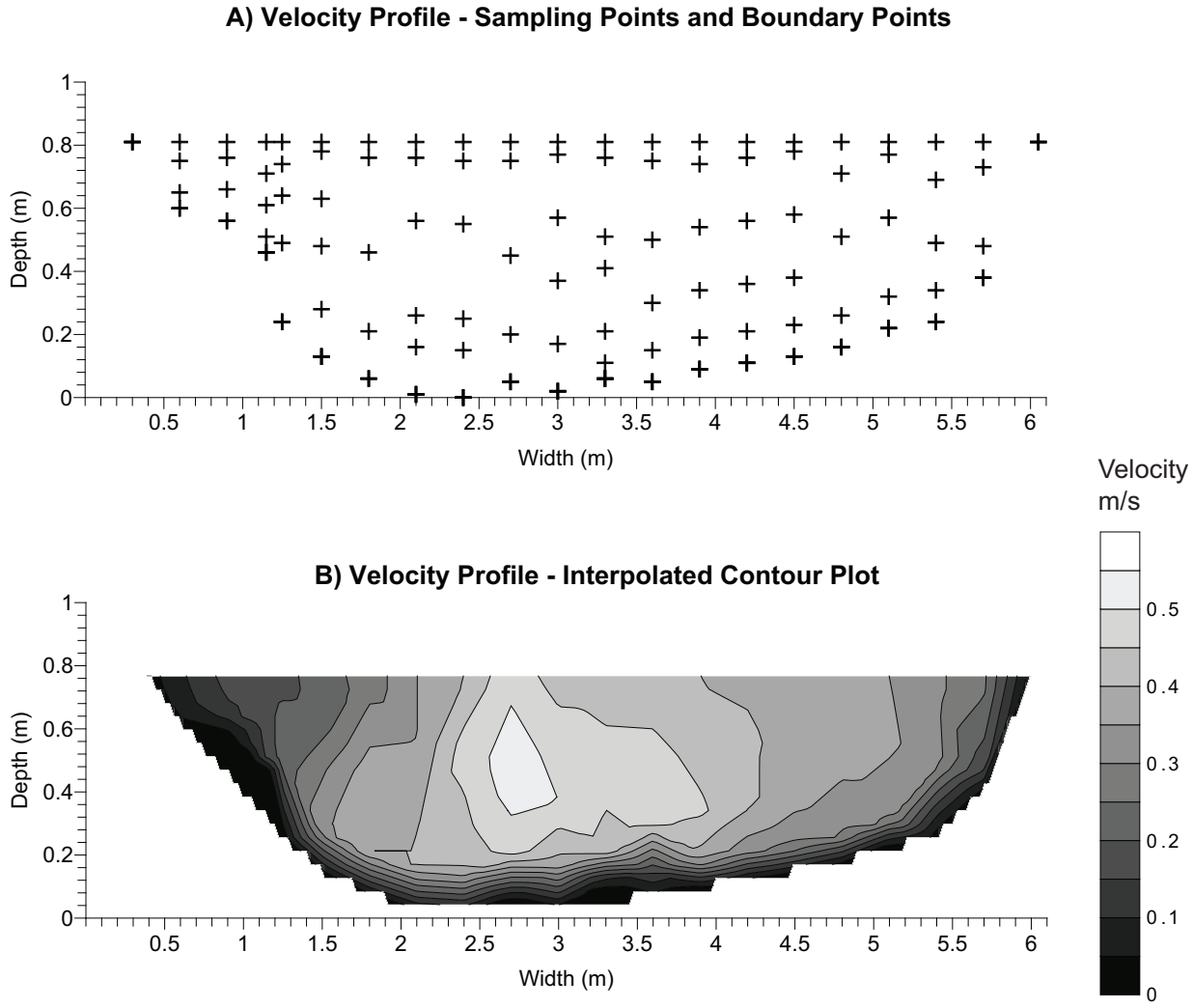

Figure A.8: Canagagigue Creek - West Sub-Basin, Velocity Profile (23-Mar-2007)

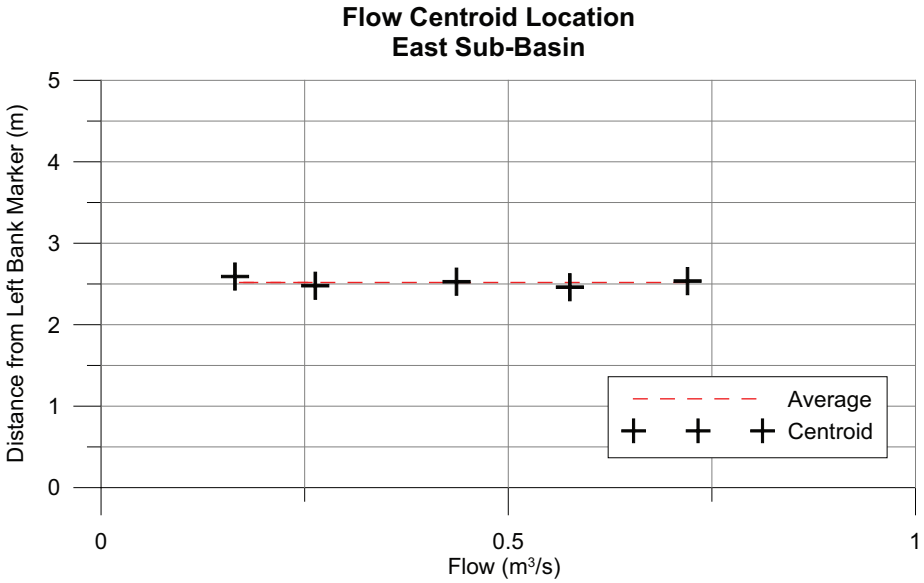

Figure A.9: Flow Centroid Calculation - East Sub-Basin

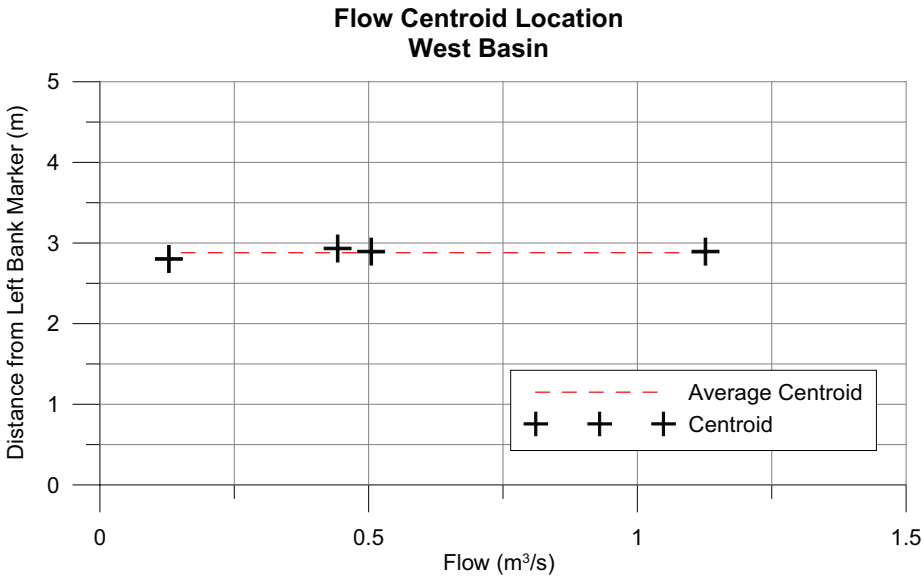

Figure A.10: Flow Centroid Calculation - West Sub-Basin

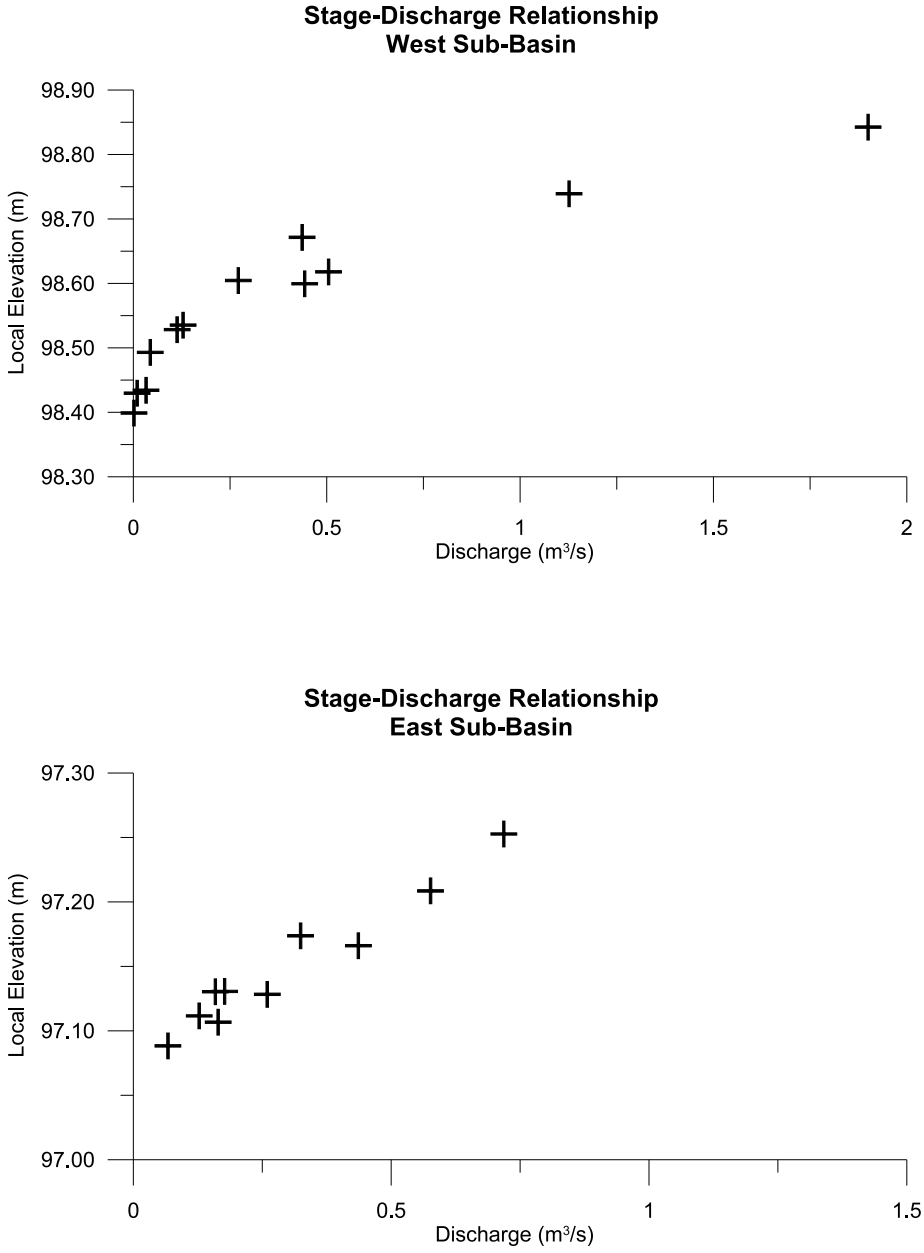

Figure A.11: Stage-Discharge Relationships

drograph was difficult. Consequently, a HEC-RAS hydraulic model was developed to allow for the generation of a rating curve that could extrapolate beyond the measured data. The topographic data of the area collected from the survey presented in Section A.3 were used to develop HEC-RAS model.

The HEC-RAS model was optimized to match the existing rating curves for both sub-basins through varying the roughness coefficient in each of the two sub-basins. The best fit results were used in the model to extrapolate the rating curve beyond the flow measurements collected to the peak values.

A.7.2 Estimation of Manning's n Values

The Manning's n values for the two channels were estimated using values from the literature. Chow (1959) outlined a number of factors that affect the Manning's n value for a channel including:

- Surface Roughness;
- Vegetation;
- Channel Irregularity;
- Channel Alignment;
- Silting and Scouring;
- Obstructions;
- Size and Shape of Channel; and
- Stage and Discharge.

For the small channels examined in this study many of the above are considered important in determining Manning's n roughness value. Of particular interest, especially in the west sub-basin channel, are Channel Irregularity, Obstructions, Channel Shape and Vegetation as these parameters appear to be significant. The west channel in particular exhibits a strong sinuous pool-riffle structure from the stage measurement point right to the confluence. There were large woody debris within the channel along it's length and the channel geometry changes very rapidly

through the pool riffle structures and around the channel debris. There are small islands forming in the west basin near the confluence, and during the summer vegetation grows and develops in the pools of the channel as the channel is ephemeral.

The east sub-basin channel is much more regular, with a relatively uniform cross section from the stage measurement station to the confluence, with much less sinuosity and less pronounced pools. The east basin flows all year and as such does not seem to promote the same degree of vegetation growth in the channel bottom.

Manning's n values were initially estimated using a number of methods:

1. Charts by site description (Chow, 1959);
2. The Cowan Procedure (Cowan, 1956); and
3. Comparison with photographic records of channels with known roughness (Barnes, 1987).

For Chow's procedure, the channel and floodplain descriptions are linked to ranges of Manning's n values. The west channel was identified as a Natural Minor Stream (top width < 100 ft) with "sluggish reaches, weedy, with deep pools" (D-1.7) for the winter and likely "Very weedy reaches, deep pools" (D-1.8) in the summer. The east channel was identified as a Natural Minor Stream "Clean, winding, some pools and shoals" (D-1.3) in the summer and "Clean, winding, some pools and shoals but some weeds and stones" (D-1.4) in the summer. The flood plain for both channels was best described as "Medium to Dense Brush" for both winter and summer (D-2.4 and D-2.5).

The Cowan Procedure is an empirical equation (Equation A.1 used to calculate Manning's n based on values for physical attributes in the channel that contribute to the overall roughness or energy loss.

$$n = (n_0 + n_1 + n_2 + n_3 + n_4)\, m_5 \tag{A.1}$$

where n is the calculated Manning's n coefficient, n_0 describes the material, n_1 accounts for material irregularity, n_2 accounts for cross-sectional variation, n_3 the effect of obstructions, n_4 the effect of vegetation, and m_5 the degree of meandering. The Cowan procedure was designed for small to medium channels and is not recommended to be used for channels with a hydraulic depth in excess of 4.57 m (Cowan, 1956). As the hydraulic depth of the two study channels never exceeded 1m this method was deemed appropriate for consideration in this study.

Manning's n values were also estimated using a photographic report by Barnes (1987). The east and west sub-basin morphology was compared to existing streams that had their roughness evaluated in the report. Several water courses were found to be similar to the east and west sub-basin creeks, and as such a number of possible values for Manning's n were collected.

The results of each of the procedures are presented in Table A.1.

Method	*West*		*East*	
	Summer	Winter	Summer	Winter
Chow (1959)	0.100	0.070	0.045	0.042
Cowan (1956)	0.290	0.192	0.068	0.058
Barnes (1987)	0.110, 0.125, 0.150		0.050, 0.060	

Table A.1: Manning's n Estimates

The results show a great degree of variability among the three approaches, particularly with regard to the west sub-basin and the use of the Cowan procedure. Of the approaches available it has been noted that the photographic method generally proves the most accurate (Haestad Methods Inc. et al., 2003), but the variability shows the degree of uncertainty in the estimates

Calibration of Manning's n Values in HEC-RAS Model

In order to generate a reliable rating curve the HEC-RAS model was run and calibrated to match the measured rating curves. In this way a more realistic stage-discharge rating curve could be extrapolated beyond the measured flow data. The estimated ranges of possible Manning's n values presented in Table A.1 were used as bounding conditions of expected values in the calibration of the model.

The HEC-RAS Model was calibrated by adjusting Manning's n for each basin. The objective function was the minimum of the root mean square (RMS) of the error between the calculated elevation based on a set flow and the measured elevation. Calibration runs were conducted for the winter rating curve, the summer rating curve, and the combined rating curve for both the west and east sub-basin channels. Figure A.12 and Figure A.13 show the optimization curves for each of the sub-basins for summer and winter data as well as the combined or total datasets (marked as "Total" in these figures). The minimum point of the RMS error in elevation on each curve is marked with a vertical solid line. It is noted however that for some of the calibration runs, the minima was very broad and a small change in the Manning's n value would have virtually no

effect on the RMS error, but may have a significant effect on the calculated depth. Of particular concern is the west basin, where a specific or exact value for the Manning's n value is shown to be difficult to determine. However, it is noted that the calibrated values do fall well within the range of expected values for these channels based on the three methods summarized in Table A.1. The selected Manning's n values based on the HEC-RAS model are shown in Table A.2.

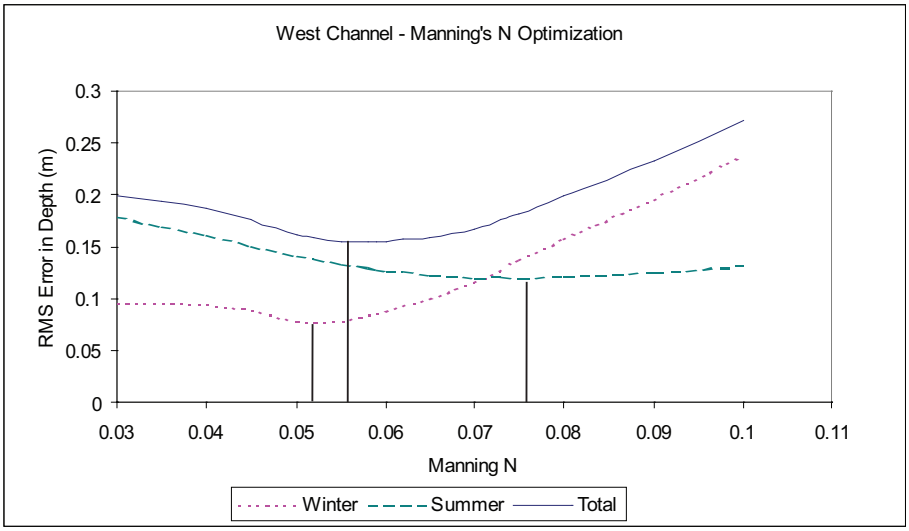

Figure A.12: HEC-RAS Manning's n Calibration - West Sub-Basin

Channel	**Season**	**Manning's n**
West	Winter	0.052
	Summer	0.075
	All Data	0.055
East	Winter	0.039
	Summer	0.050
	All Data	0.040

Table A.2: Calibrated Manning's n Values

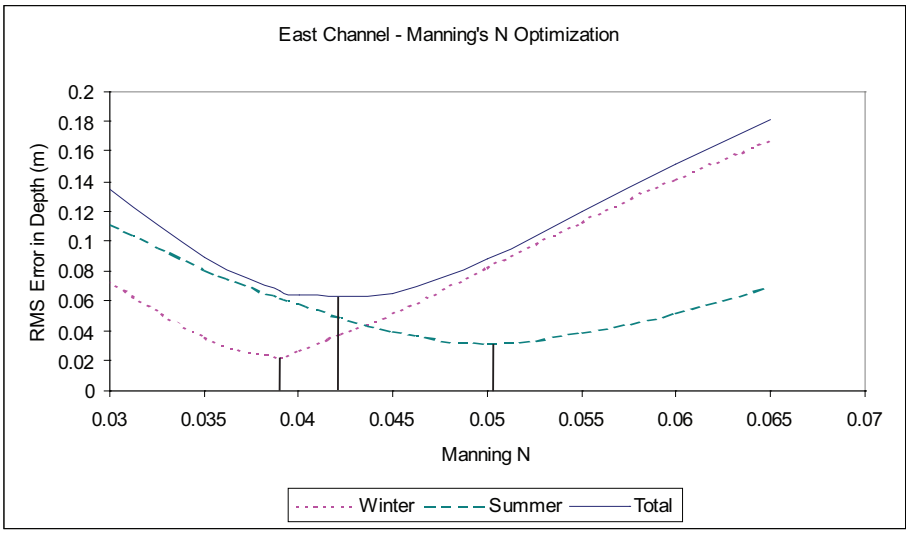

Figure A.13: HEC-RAS Manning's n Calibration - East Sub-Basin

Appendix B

Hydrological Data Collection and Analysis

B.1 Introduction

This appendix outlines the data collection, and when necessary validation, for incorporation into the WatFlood hydrologic model. This appendix includes information on the WatFlood model set-up, data quality assurance procedures, precipitation data collection, model calibration and performance, and the employed WatFlood parameter file.

B.2 WatFlood Model Set-up

The setting up of the WatFlood hydrologic model required the modification of drainage directions and drainage areas of the grid elements. This was done to comply with with the known and published drainage network, drainage directions and sub-basin delineations provided by the Grand River Conservation Authority.

Figure B.1 shows the WatFlood MAP file indicating the area distribution within the watershed model. The plotted model attribute, FRAC, indicates the percentage fraction of the standard grid area that applied to a particular grid, a valud of 100 representing the actual area of a full grid (in this case 1 km^2). The complete map file is presented in Figure B.7.2.

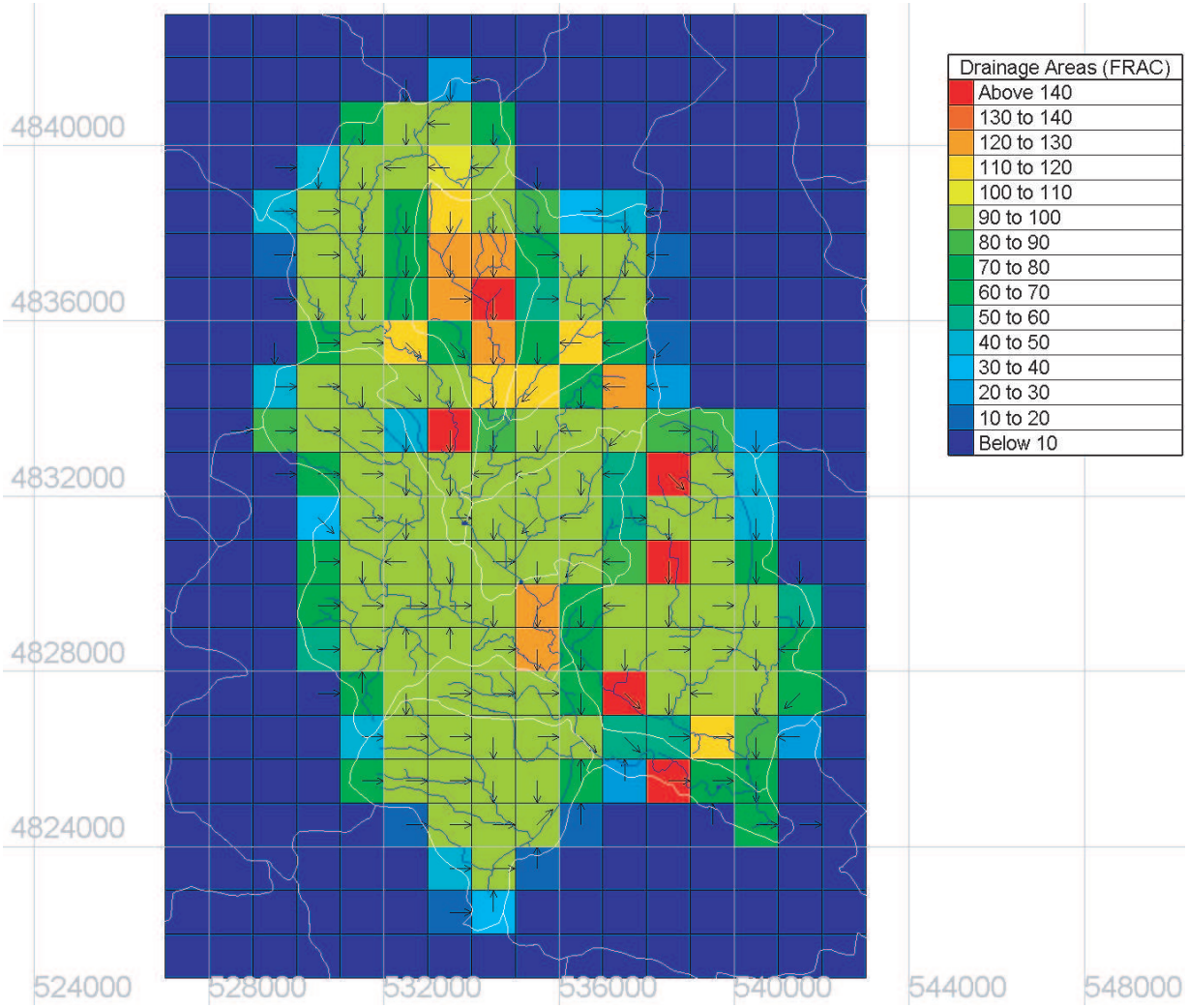

Figure B.1: Canagagigue Creek Grid Areas (FRAC)

Table B.2 tabulates the actual drainage areas provided by the sub-basin data set and those calculated by the WATFLOOD model.

			Sub-Basin Drainage Areas (sq. km)	
Streamflow Gauge	Northing	Easting	GRCA Delineated Sub-Basin	Watflood/EnSim Calculated Areas
East Study Basin	4833733	534872	11.50	11
West Study Basin	4833844	534743	10.40	11
Floridale	4831372	533820	53.14	54
Elmira	4825820	540311	31.55	28
Below Elmira	4825355	539629	116.12	117

Table B.1: Canagagigue Creek Sub-Basin Drainage Areas

B.3 Data Quality Assurance

The meteorological data provided by the GRCA and the Alma Research Station were considered provisional data, and were not screened for erroneous data. Quality assurance sweeps were conducted on the data after being submitted to the FSAM Database. These QA sweeps scanned the data for unrealisted values or sequences of values and flagged them as potentially requiring attention. These programmatic screenings included:

- probable maximum and minimum value violations;
- probable maximum accumulations over a period; and
- correlations of concurrent time-series with other similar gauges.

These checks were done withing the FSAM database using SQL queries to compare the data sets. If questionable data was identified it was flagged for manual inspection. Data items that could be marked as erroneous were noted as such in the database. The data items were not deleted, but rather marked as invalid and thereby automatically excluded from the model data generation routines.

B.4 Precipitation Data

Details of how the data from each of these sources was employed follows.

B.4.1 University of Waterloo Weather Station Precipitation

The Waterloo weather station provides 15 minute precipitation data using a number of precipitation measurement instruments. A combination of waterloo GeoNor and tipping bucket (Texas Electronics Model: TE525) rain gauge were used. The tipping bucket data was used for non-snowfall conditions. The GeoNor rain gauge records precipitation weight and was employed during snowfall events. The GeoNor records weight as a function of time recorded at 15 minute intervals. An anti-freeze liquid is added to the gauge to keep the stored water from freezing and evaporation from the gauge in minimized through the addition of a portion of buoyant oil. The data did show some slight drift in the available data, likely due to some amount of evaporation as during dry periods there was some mass loss observed. To compensate for drift the GeoNor data corrected to only use increases in mass recorded by the GeoNor gauge which correspond well with tipping bucket rain gauge events. Figure B.2 illustrates the relationship and shows the good agreement between the tipping bucket and GeoNor gauges from May to December 2005 with this correction (with the exception of August of that year when the Tipping Bucket gauge failed).

The University of Waterloo Weather Station (UW Weather Station) was located approximately 23 km from the study site and although the precipitation data from the station was included in meter logical input calculations, it played an insignificant role in that regard due to the large number of GRCA and Study Gauges that were much closer to the Canagagigue Creek. However, the UW Weather Station played an important role in independent quality assurance, as the data at that location were recorded independently and provided indications as to relative magnitude of events, timing of events and expected precipitation character (snow vs. rainfall).

B.4.2 Study Gauge Validation

The installed rainfall gauges (RG01 and RG02) were installed for periods of 2005, all of 2006 and periods of 2007. RG01 was moved in early 2005 from a location near the East Sub-basin stream flow gauge to a location south of the study basins for reasons of reduced canopy interference at the new location. The RG01 original location was re-tagged as “RG01_OLD” and the new

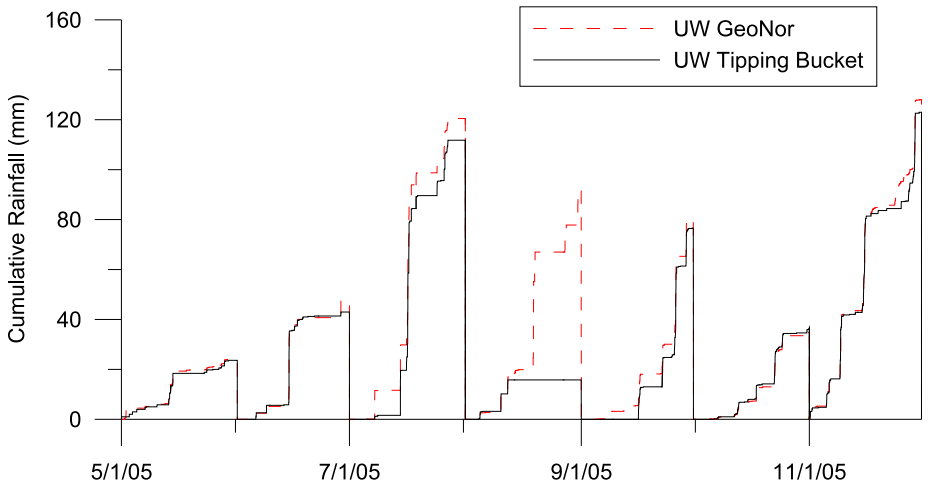

Figure B.2: UW Tipping Bucket and GeoNor Gauge Comparison

location for RG01 retained the "RG01" tag. To validate the performance of these additional rain gauges the monthly accumulated rainfall values were compared to the values of near-by GRCA rain gauges: Woolwich Dam, Conestogo, Arthur and Elmira. These four gauges are located to the approximate south, west, north and east of the study site respectively. The plot of the 2005 season is shown in Figure B.3, and both gauges show good agreement with the surrounding GRCA rain gauges.

B.4.3 Precipitation Quantity Assessment

The adjusted rainfall data are shown below in Figures B.4 to B.9 and show good general agreement when cumulative rainfall is compared as is expected with gauges in the same region.

To compare blocks of matched data that do not display normal distribution characteristics the nonparametric Friedman test is recommended (Helsel and Hirsch, 1991). Rainfall accumulations were compared for each station using the Friedman block test for each station for each of the 6 years of data. Comparisons showed that the for the 5 stations over the 6 years the medians of total rainfall were not distinct ($\alpha = 0.05$), implying that each of the stations produced on average the same amount of rainfall ($f = 4.8 < F(0.95, 4, 20) = 5.8$). This is an expected results if there are no systematic errors in the data, and similar rainfall totals can be expected across the region on average.

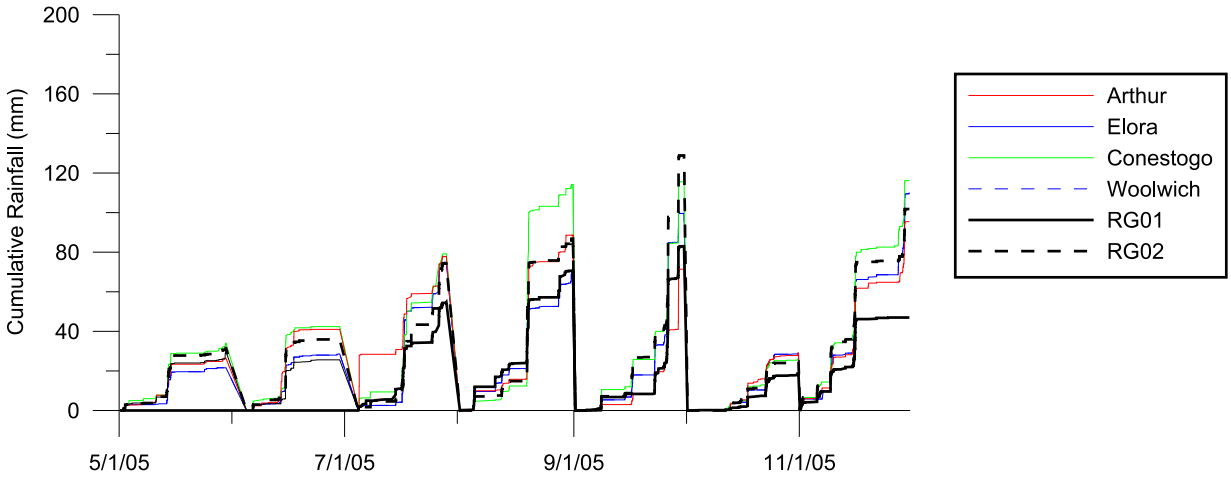

Figure B.3: Study Site Rain Gauge Validation - 2005

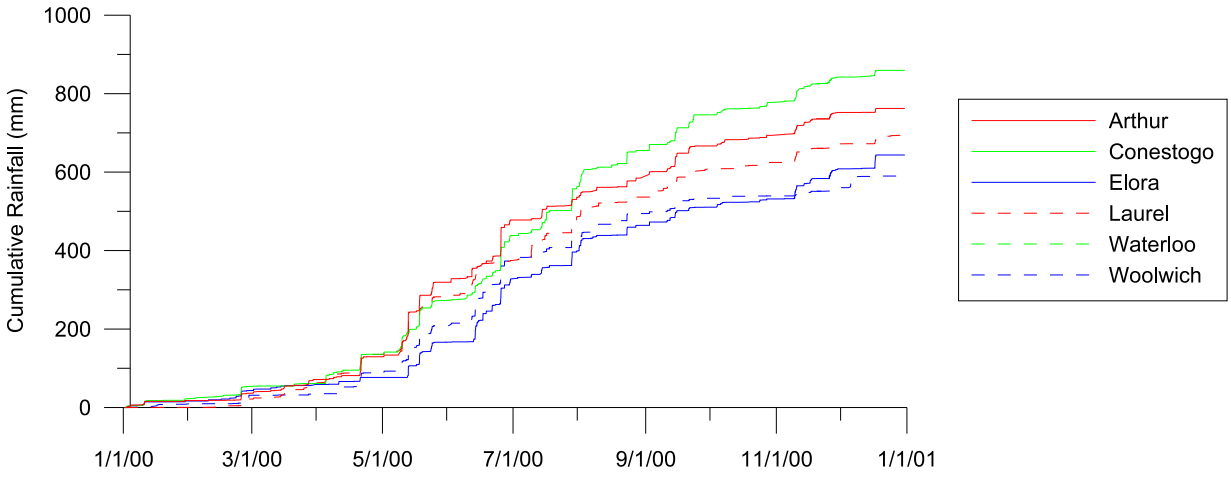

Figure B.4: GRCA Rainfall 2000

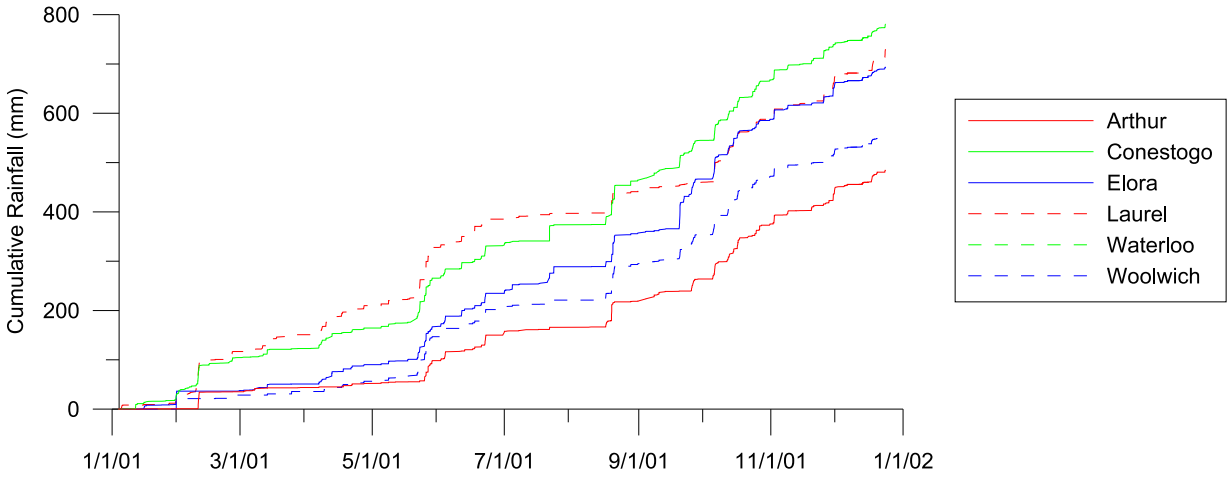

Figure B.5: GRCA Rainfall 2001

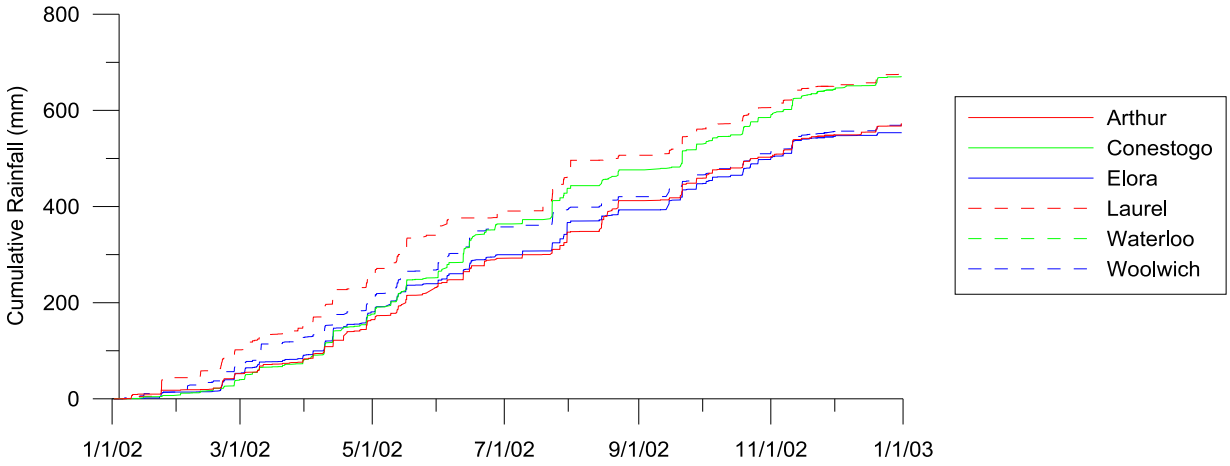

Figure B.6: GRCA Rainfall 2002

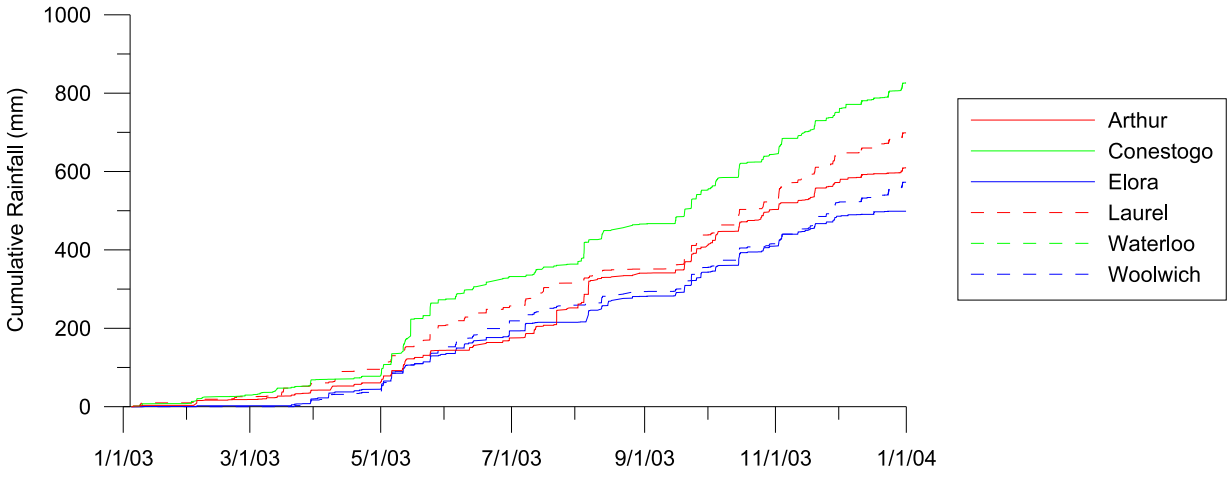

Figure B.7: GRCA Rainfall 2003

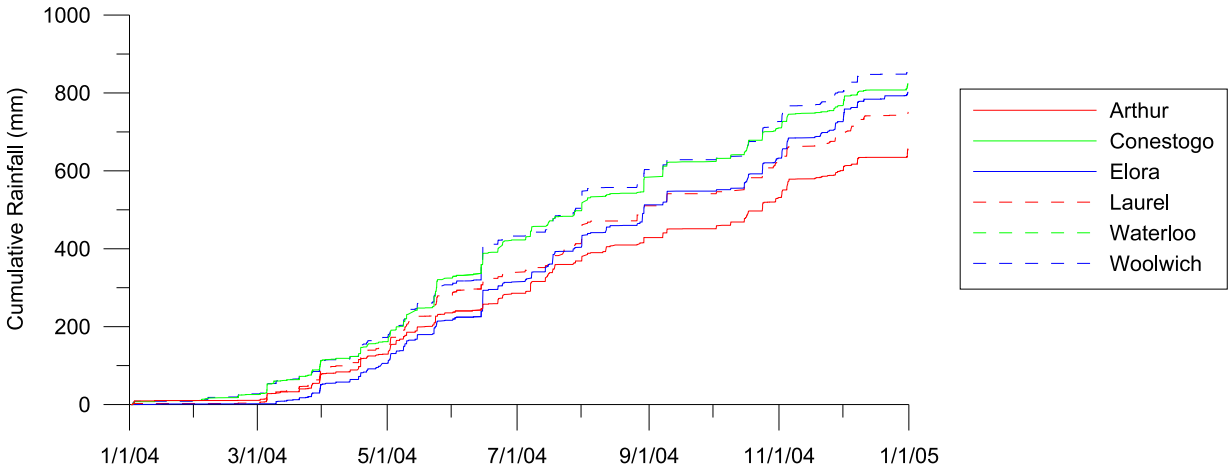

Figure B.8: GRCA Rainfall 2004

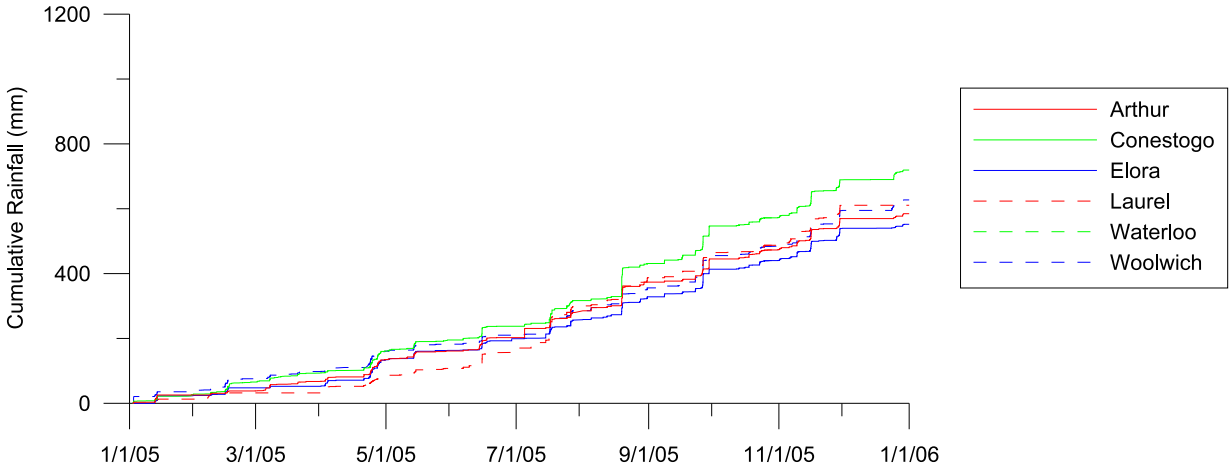

Figure B.9: GRCA Rainfall 2005

B.4.4 Rainfall Event Timing Assurance

It was necessary to assess the timing of the GRCA rain gauge data for accurate timing. The provided database has 1 hr data for each of the gauges to be be certain of the timing the precipitation graphs were compared with the UW Weather Station cumulative precipitation and the RADAR on a month-by-month basis. A time series of the King City RADAR precipitation was extracted at the location where the gauge being compared was located. Figure B.10 illustrates a typical month cumulative rainfall comparison. This figure illustrates a comparison of the Woolwich GRCA rain gauge, the UW Waterloo Weather station precipitation reading and the RADAR Rainfall estimate at the location of the Woolwich gauge. Although the rainfall intensities are quite different among the three measurements, the RADAR reading outlying significantly, the timing of the events is synchronous.

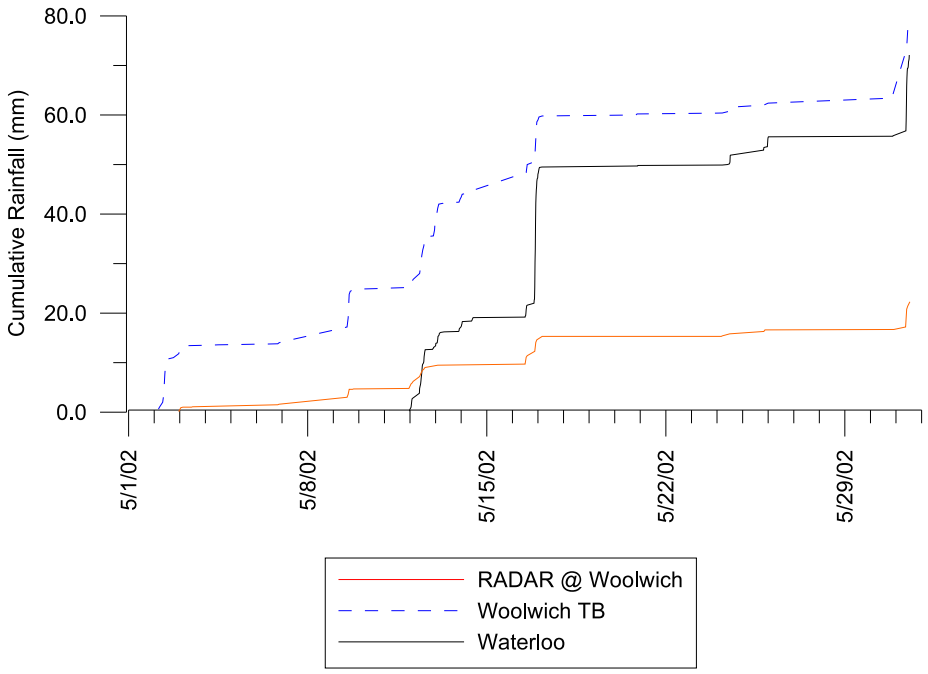

Figure B.10: Monthly Cumulative Precipitation Source Timing Comparison

B.4.5 King City RADAR Data

Radar data was obtained from the King City Radar Station (CWKR) as 5cm Doppler RADAR CAPPI 1 hour cumulative rainfall measurements.

RADAR data was employed in two capacities. It was used when the tipping bucket rain gauge data was unavailable due to faulty gauges or in winter months. Additionally, the RADAR data was used to independently assess the timing of the rainfall data provided by the GRCA for periods when the study site tipping bucket rain gauges were not available.

B.5 Streamflow and Dam Discharge Data

As outlined in Chapter 4 and Appendix A, streamflow data was collected as part of this study at the outlet of the two study sub-basins from spring 2005 to spring 2007. Other provisional flow data was acquired for the Canagagigue Creek from the GRCA from 2000 to 2007 inclusive. These data included discharge data from the Woolwich Dam, however records for discharge data from the Woolwich Dam was not available from 30 March 2005 onward.

B.6 Streamflow Modelling Results

The calibrated modelling results for the years of 2000 to 2005 are shown in Figures B.11 to B.16. Included in these plots are the measured streamflow hydrographs from the three employed GRCA gauges as well as the reservoir release flow rates at the Woolwich Dam. The reservoir release flow rates are displayed with the Elmira and the Below Elmira gauges to illustrate the portion of the hydrograph that is driven from the dam discharge.

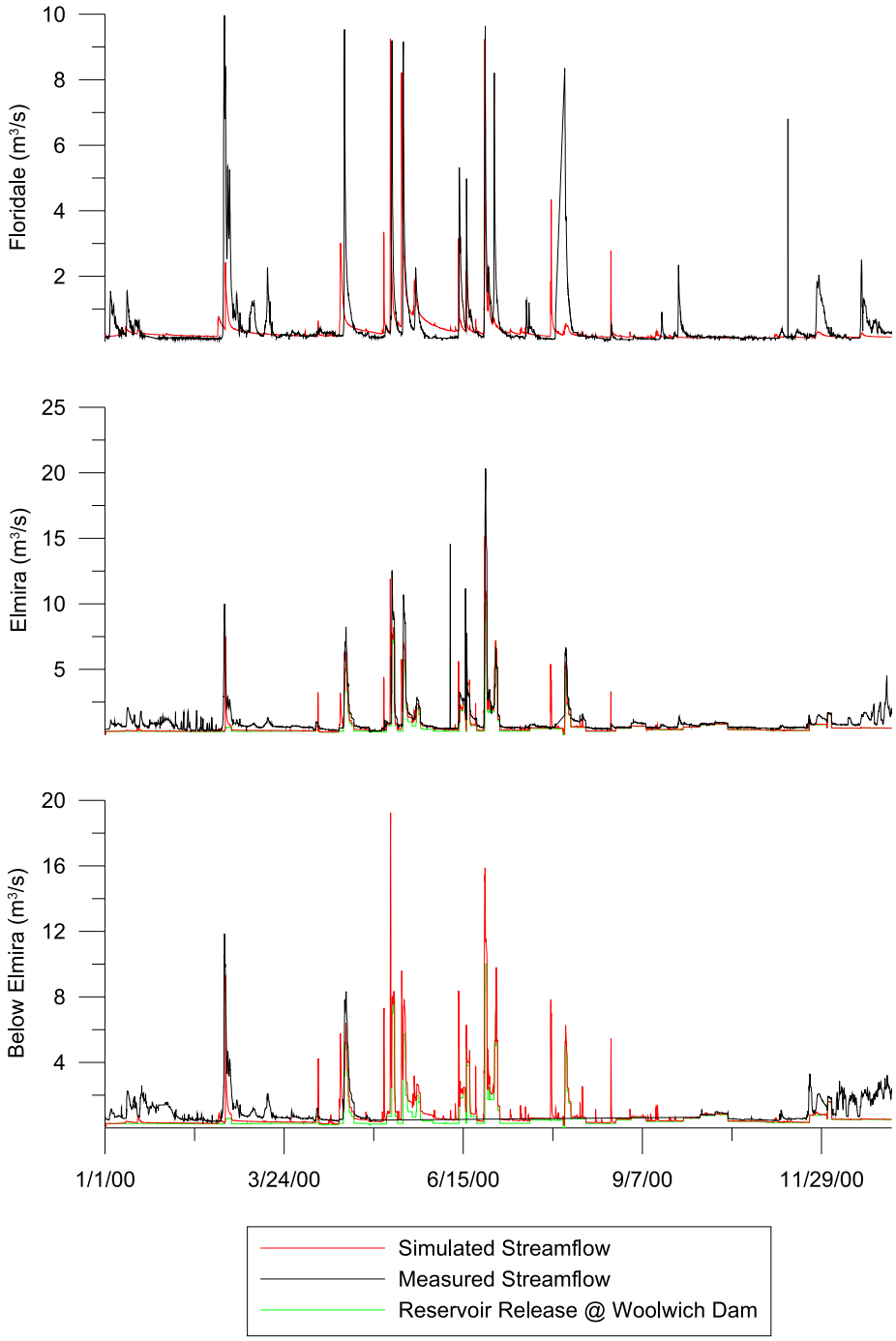

Figure B.11: Hydrologic Modeling - GRCA Stream Gauges - 2000

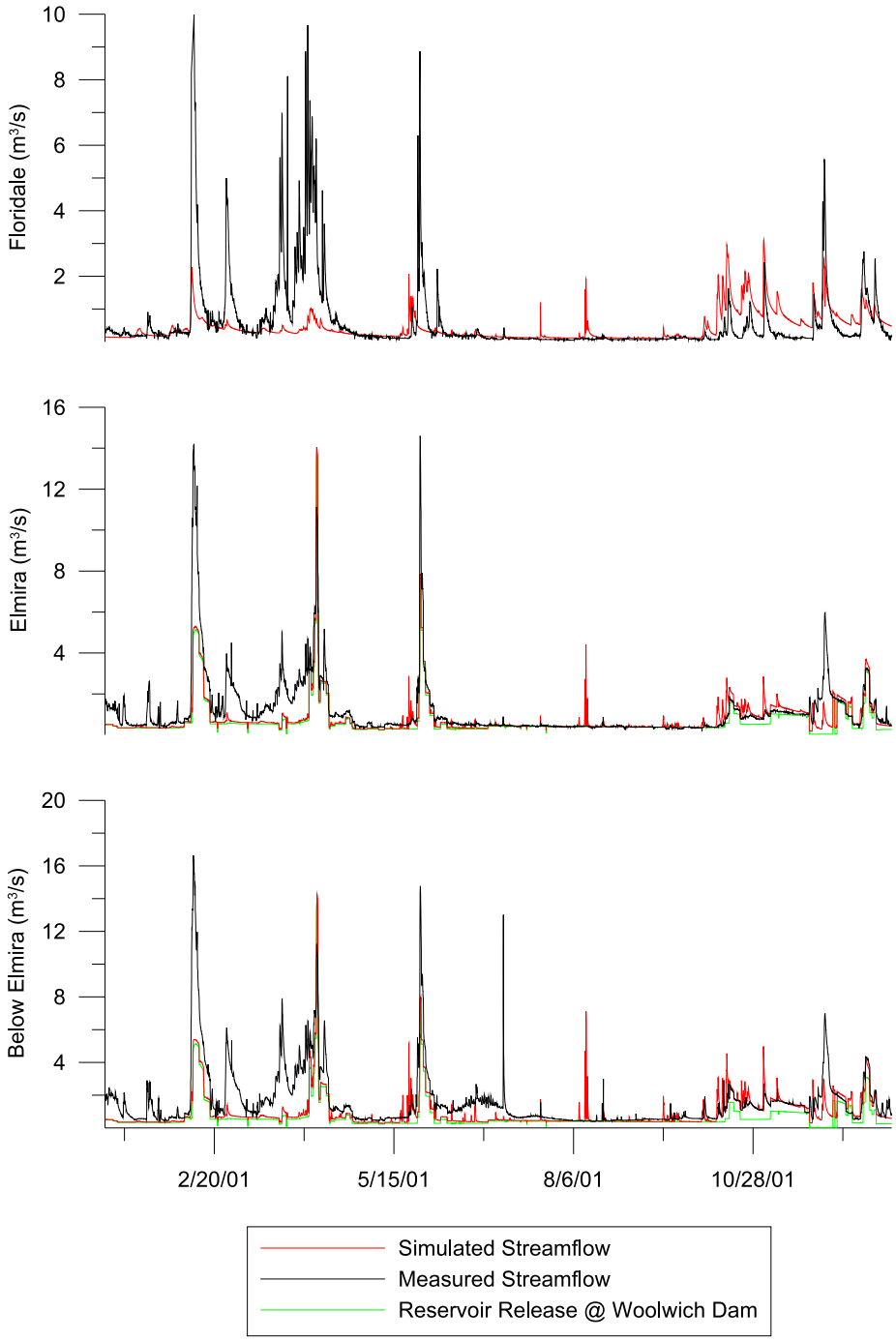

Figure B.12: Hydrologic Modeling - GRCA Stream Gauges - 2001

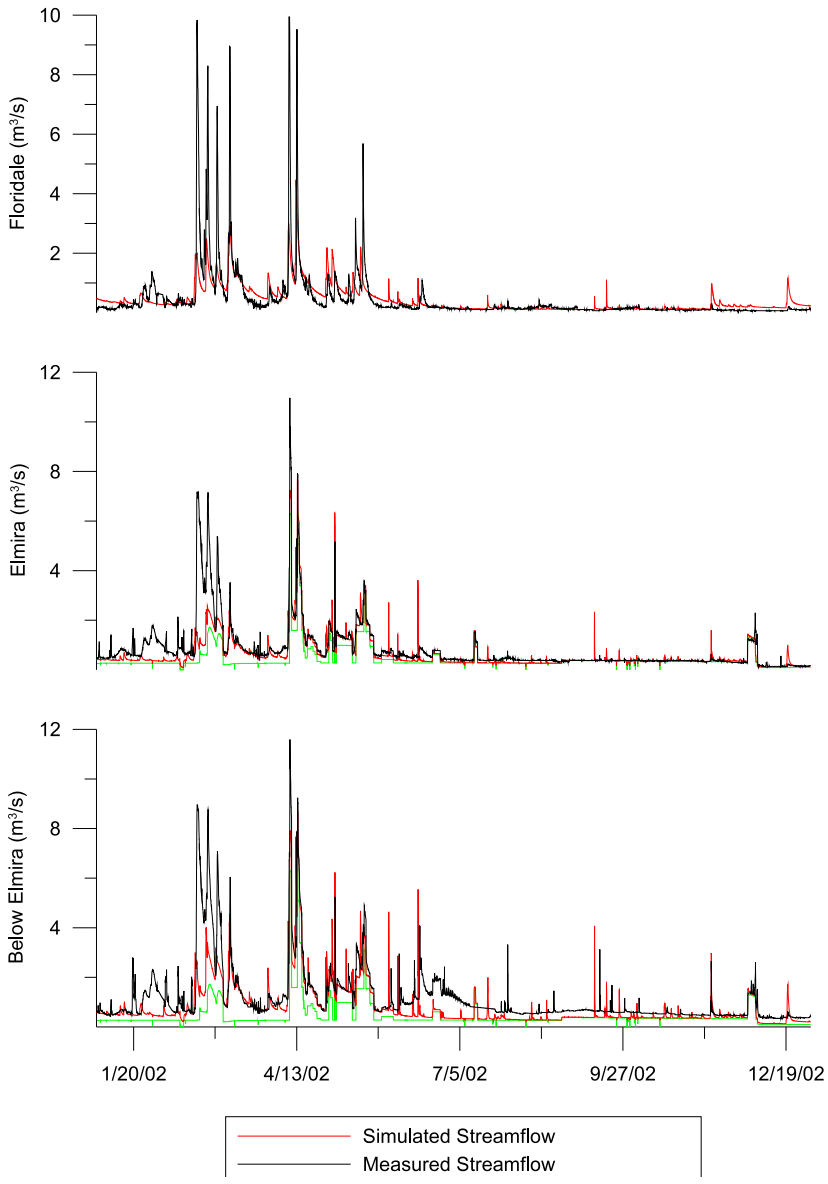

Figure B.13: Hydrologic Modeling - GRCA Stream Gauges - 2002

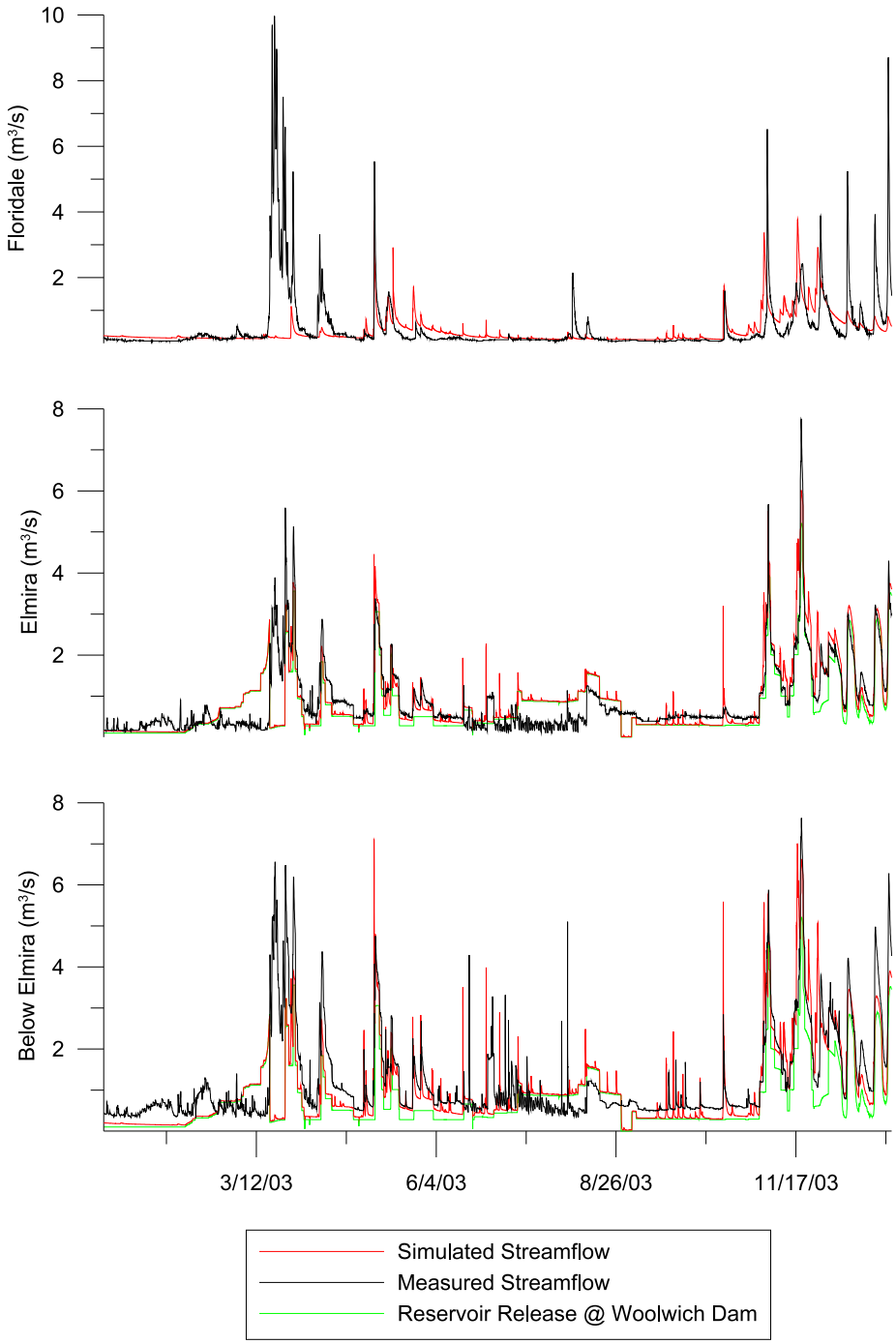

Figure B.14: Hydrologic Modeling - GRCA Stream Gauges - 2003

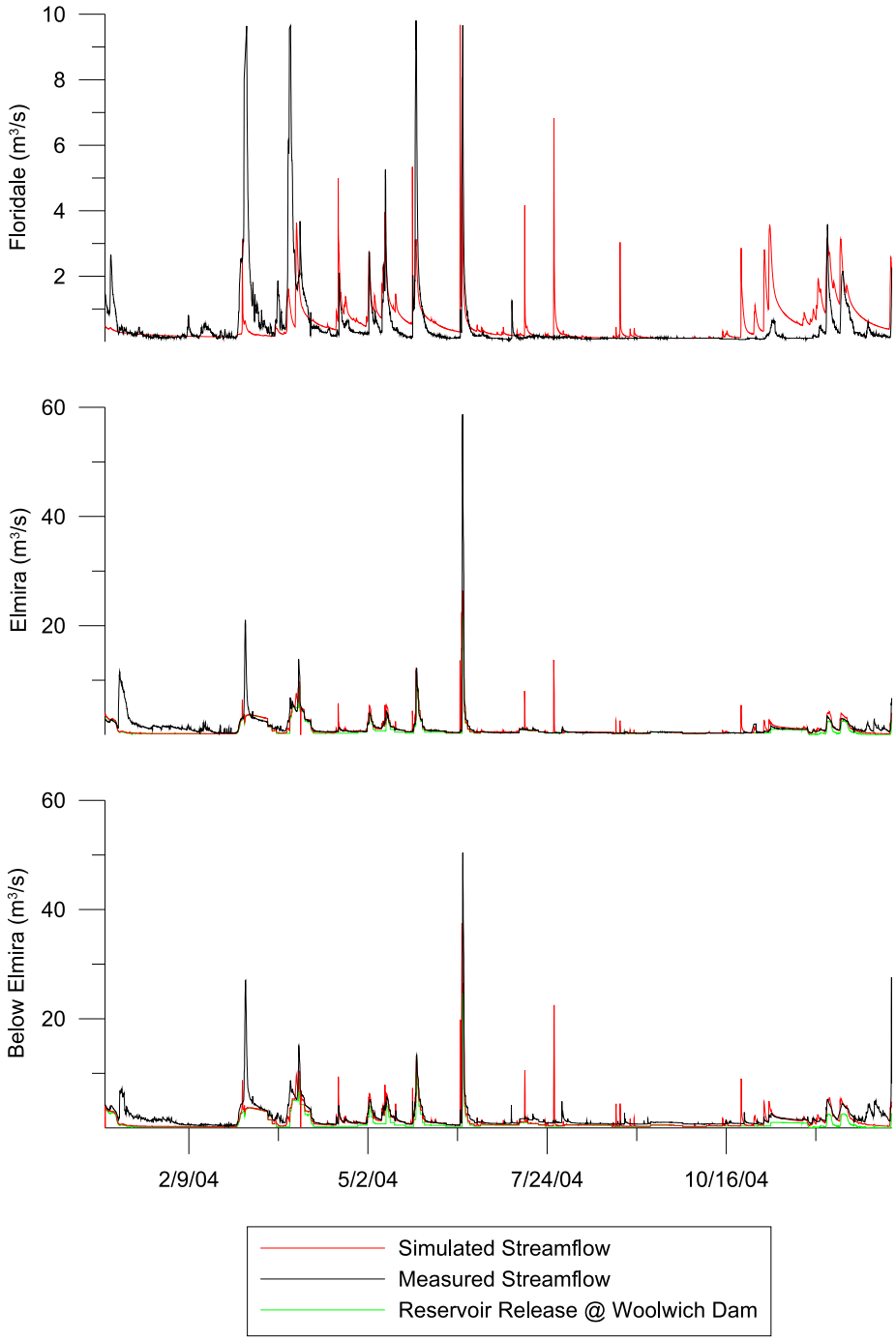

Figure B.15: Hydrologic Modeling - GRCA Stream Gauges - 2004

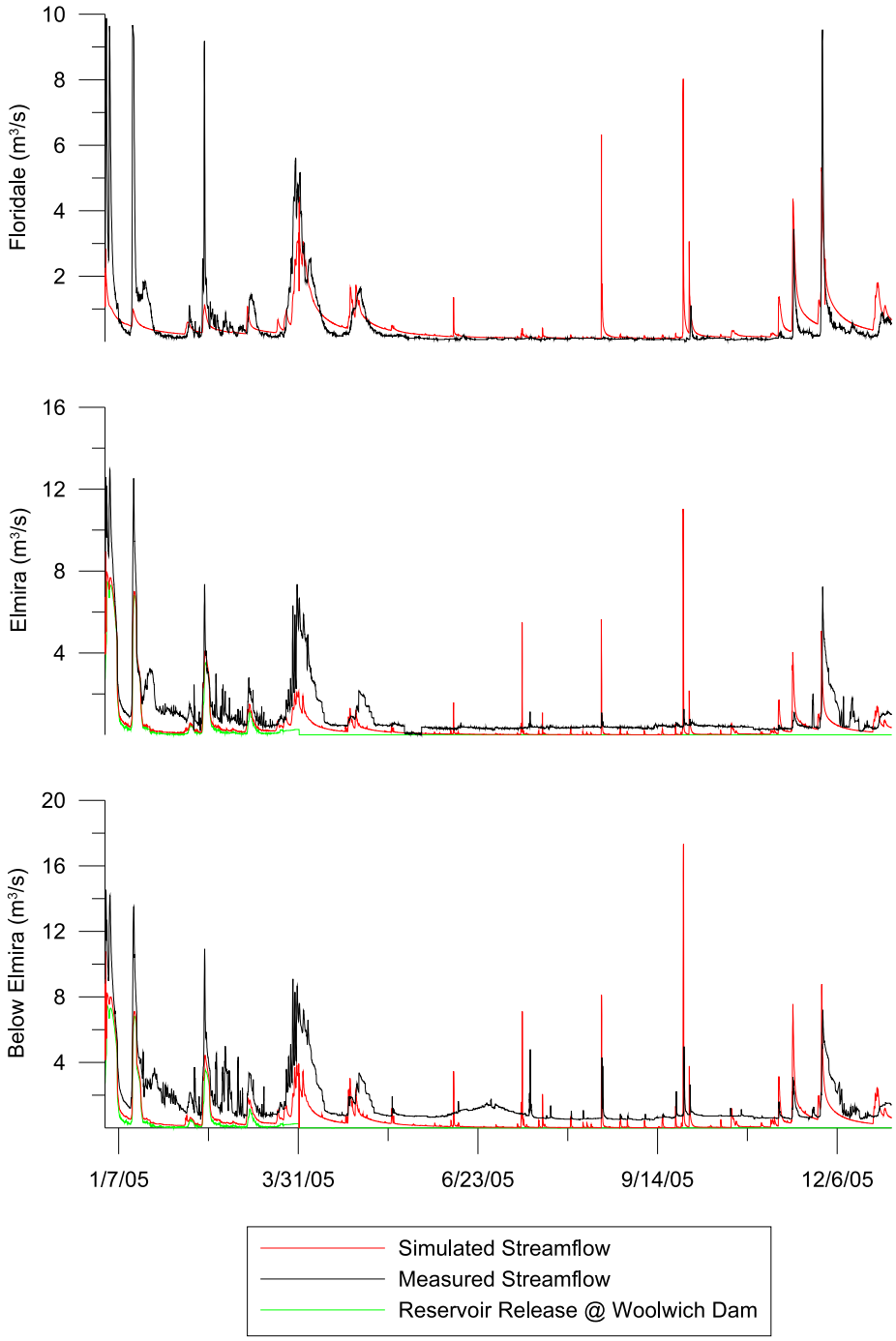

Figure B.16: Hydrologic Modeling - GRCA Stream Gauges - 2005

B.7 WatFlood Calibration and Results

Calibration was performed against the Floradale GRCA stream flow gauge. The stream flow gauges downstream of the Woolwich Dam were dominated by the reservoir discharge rates, which produced artificially positive results when the dam discharge data was available and artificially negative results when the dam discharge results were not available. The provisional nature and unreliable character of the dam discharge data allowed for the Elmira and Below Elmira gauges to be useful for qualitative assessment but were not useful for quantitative evaluation of the model performance.

Five calibration periods were chosen to capture a variety of flow events with good precipitation data and available streamflow data. A period of dryness was included to attempt to capture low flows, and several non-snowmelt event periods were chosen in the spring and fall. Table B.2 summarizes the calibration periods and the model calibrated performance for those periods including the Nash-Sutcliffe (N-S) and runoff volume difference (DV) results.

Calibration Period	Description	Hours	Start Date	End Date	Floridale N-S	Floradale DV (%)
Period 1	Low Flow	743	01 Oct 2001	01 Nov 2001	-21.089	-403.1
Period 2	Non S/M Spring Events	1462	01 Apr 2002	01 Jun 2002	0.569	4.4
Period 3	Non S/M Spring Events	311	01 May 2003	14 May 2003	0.706	0.7
Period 4	Fall Events	1150	14 Oct 2003	01 Dec 2003	0.349	-67.1
Period 5	Non S/M Spring Events	2183	01 Apr 2004	01 Jul 2004	0.473	-5.3

Table B.2: Calibration Results

Results in Table B.2 illustrate excellent calibration results for non-snowmelt (S/M) spring events. Period 1 exhibits very poor performance, but due to the low-flow conditions the DV and N-S parameters are elevated by minor variations. The low flow conditions were captured very well. Period 4 also exhibits relatively poor performance, but the performance of this period was balanced against the performance of the other periods. Additionally, Period 4 showed some unusual measured hydrograph responses perhaps indicative of erroneous data or rating curves making the N-S values, in particular, questionable in their value.

The statistical performance or validation of the model is shown in Figure B.17 below:

A graphical representation on the sub-basin performance are presented in Figures B.18 to B.20 as suggested by James and Burges (1982). These plots illustrate the accuracy of modelling of the East sub-basin over the West sub-basin. Figure B.20 shows poor performance primarily because it only includes the recession curve from the 2007 snow melt which was poorly modelled due to an underestimation of the quantity of snow for that year for both sub-watersheds..

	Nash-Sutcliffe			Runoff Volume Difference (%)		
Non-Snowmelt Period	Floradale	West	East	Floradale	West	East
2000	0.629	n/a	n/a	27.4	n/a	n/a
2001	-0.137	n/a	n/a	-16.3	n/a	n/a
2002	0.847	n/a	n/a	-1.6	n/a	n/a
2003	0.413	n/a	n/a	-34.3	n/a	n/a
2004	0.202	n/a	n/a	-32.8	n/a	n/a
2005	-0.023	0.202	0.043	-44.3	28.6	-9.0
2006	0.029	0.107	0.177	31.7	17.4	-14.1
2007	0.284	0.148	0.496	42.0	29.7	30.2

Figure B.17: Model Validation - Nash-Sutcliffe and Relative Volume Error

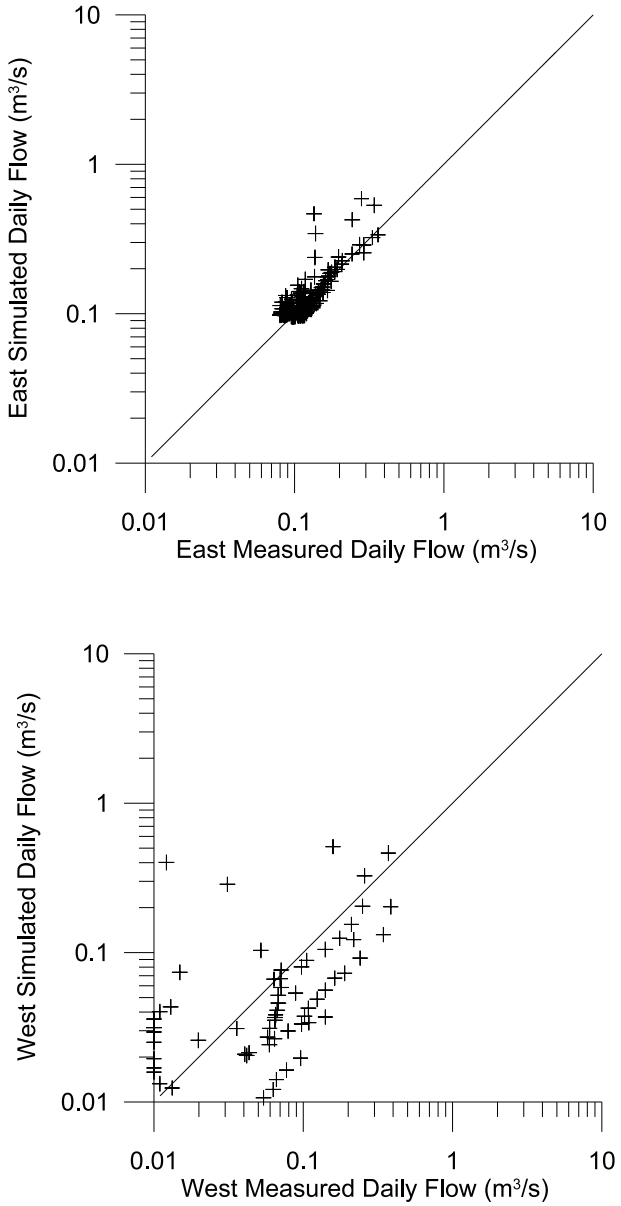

Figure B.18: Daily Runoff Comparison - 2005 (No Snow melt)

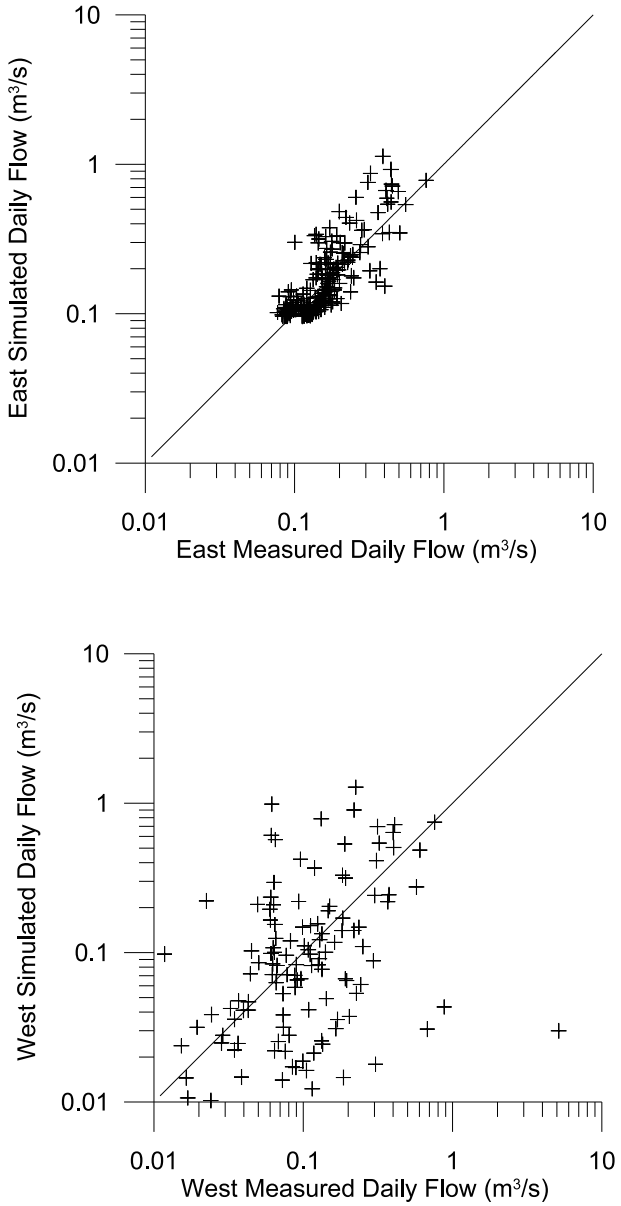

Figure B.19: Daily Runoff Comparison - 2006 (No Snow melt)

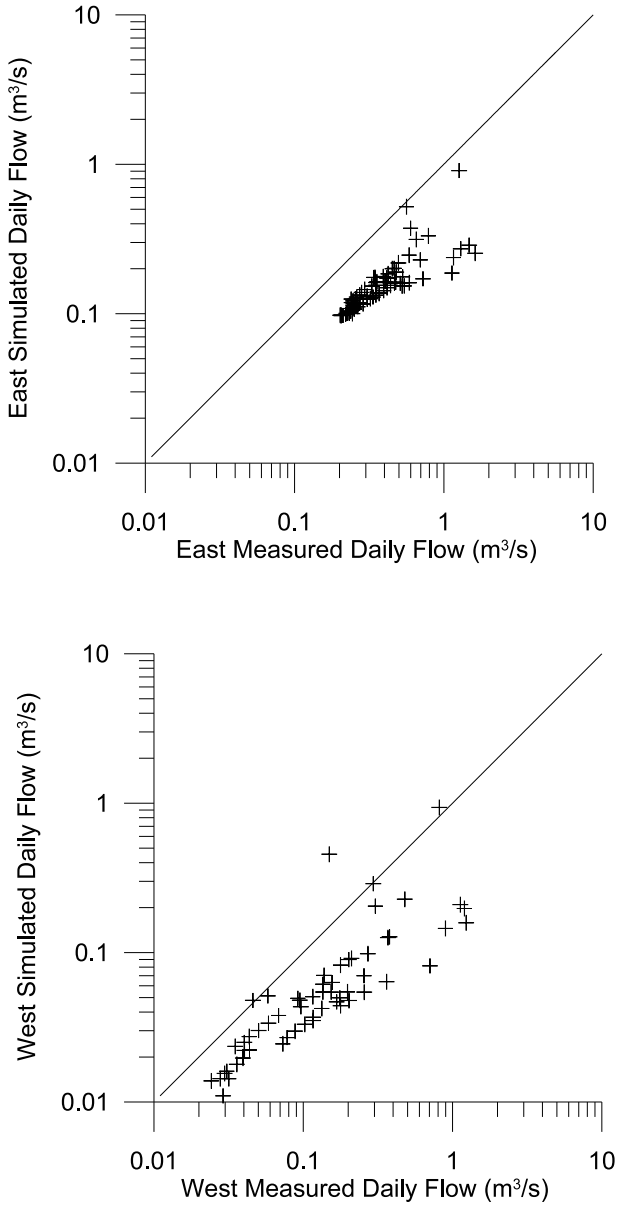

Figure B.20: Daily Runoff Comparison - 2007 (No Snow melt)

B.7.1 WatFlood Parameter File

```
# runtime    13:22:47
# rundate  2006-02-03
ver         9.4
iopt          1
itype         0
numa          0
nper          1
kc            5
maxn       2000
ddsfl         0
itrc          4
iiout         4
typeo         4
nbsn          3
a1        0.250
a2     -999.999
a3     -999.999
a4     -999.999
a5        0.985
a6      900.000
a7        0.500
a8        0.100
a9        0.330
a10       1.000
a11       0.010
a12       0.000
        Default      West      East
lzf   0.100E-03 0.100E-04 0.100E-04
pwr   0.288E+01 0.198E+01 0.162E+01
R1n   0.900E-01 0.900E-01 0.900E-01
R2n   0.201E-01 0.503E-01 0.402E-01
mndr  0.100E+01 0.100E+01 0.105E+01
aa2   0.200E+00 0.200E+01 0.200E+00
aa3   0.250E+01 0.800E+01 0.250E+01
aa4   0.550E+00 0.300E+00 0.550E+00
theta 0.330E+00 0.330E+00 0.338E+00
widep 0.200E+02 0.100E+02 0.120E+02
kcond 0.400E+00 0.400E+00 0.380E+00
pool  0.000E+00 0.100E+00 0.000E+00
     bare_soil forest    crops     wetland   water
ds     0.100E+01  0.100E-04  0.200E+01  0.100E+00  0.000E+00  0.100E+01
dsfs   0.100E+01  0.100E+02  0.200E+02  0.100E+00  0.000E+00  0.100E+01
Re     0.200E+01  0.200E+01  0.104E+01  0.100E+01  0.100E+00  0.100E+00
AK     0.201E-01  0.120E+02  0.100E+01  0.400E+03 -0.100E+01  0.110E+01
```

```
AKfs   0.200E+01  0.120E+01  0.100E+01  0.400E+03 -0.100E+01  0.110E+01
retn   0.750E+02  0.750E+02  0.100E+02  0.400E+00  0.100E+00  0.000E+00
ak2    0.132E+00  0.960E+00  0.132E+00  0.200E+00  0.100E-02  0.100E-09
ak2fs  0.660E-01  0.960E+00  0.330E-01  0.750E-10  0.100E-02  0.100E-09
R3     0.197E+02  0.848E+01  0.197E+02  0.898E-01  0.400E-01  0.000E+00
R3fs   0.100E+02  0.100E+02  0.200E+02  0.100E+00  0.400E-01  0.000E+00
r4     0.100E+01  0.100E+02  0.380E+00  0.100E+02  0.100E+02  0.000E+00
ch     0.100E+01  0.900E+00  0.700E+00  0.700E+00  0.600E+00  0.000E+00
MF     0.100E+00  0.160E+00  0.360E+00  0.120E+00  0.120E+00  0.150E+00
BASE   0.100E+01  0.322E+00 -0.800E+01  0.112E+02  0.000E+00  0.000E+00
NMF    0.100E+00  0.100E+00  0.100E+00  0.100E+00  0.100E+00  0.100E+00
UADJ   0.000E+00  0.000E+00  0.000E+00  0.000E+00  0.000E+00  0.000E+00
TIPM   0.100E+00  0.100E+00  0.100E+00  0.100E+00  0.100E+00  0.100E+00
RHO    0.333E+00  0.333E+00  0.333E+00  0.333E+00  0.333E+00  0.333E+00
WHCL   0.350E-01  0.350E-01  0.350E-01  0.350E-01  0.350E-01  0.350E-01
fmadj  0.000E+00  0.000E+00  0.000E+00  0.000E+00  0.000E+00  0.000E+00
fmlow     0.000
fmhgh     0.000
gladj     0.000
rlaps     0.000
elvrf     0.000
flgev      2.00 1 = pan; 2 = Hargreaves; 3 = Priestley-Taylor
albed      0.11
aw-a       0.18      0.11      0.11      0.11      0.11      0.11
fpet       1.00      3.00      4.96      2.00      0.50      0.50
ftal   0.100E+01  0.700E+00  0.900E+00  0.100E+01  0.000E+00  0.100E+01
flint  0.100E+01  0.100E+01  0.100E+01  0.100E+01  0.100E+01  0.100E+01
fcap   0.150E+00  0.150E+00  0.150E+00  0.150E+00  0.150E+00  0.150E+00
ffcap  0.100E+00  0.100E+00  0.100E+00  0.100E+00  0.100E+00  0.100E+00
spore  0.300E+00  0.300E+00  0.300E+00  0.300E+00  0.300E+00  0.300E+00
tempa  0.000E+00  0.000E+00  0.000E+00  0.000E+00  0.000E+00  0.000E+00
tempa  0.250E+03  0.000E+00  0.000E+00  0.000E+00  0.000E+00  0.000E+00
tempa  0.350E+03  0.000E+00  0.000E+00  0.000E+00  0.000E+00  0.000E+00
tton       200.
lat.        50.
mxmn  10.2 12.3 12.1 12.3 14.3 14.2 13.8 14.0 13.1 10.6  8.2  9.3
humid 59.5 60.5 62.5 55.5 50.0 54.5 59.0 58.5 63.5 58.0 64.5 62.5
pres  95.1 95.1 95.1 95.1 95.1 95.1 95.1 95.1 95.1 95.1 95.1 95.1
ti2    jan  feb  mar  apr  may  jun  jul  aug  sep  oct  nov  dec
h1    0.11 0.11 0.11 0.11 0.60 0.60 0.60 0.60 0.60 0.35 0.11 0.11
h2    1.20 1.20 1.20 1.20 1.60 1.90 1.90 1.90 1.90 1.20 1.20 1.20
h3    0.65 0.65 0.65 0.65 1.06 1.56 1.56 1.56 1.56 0.65 0.65 0.65
h4    0.65 0.65 0.65 0.65 0.85 1.00 1.00 1.00 1.00 0.65 0.65 0.65
h5    0.11 0.11 0.11 0.11 0.11 0.11 0.11 0.11 0.11 0.11 0.11 0.11
h6    0.01 0.01 0.01 0.01 0.01 0.01 0.01 0.01 0.01 0.01 0.01 0.01
```

B.7.2 WatFlood MAP File

```
#
:CoordSys           CARTESIAN
#
:xOrigin            527000.000000
:yOrigin            4821000.000000
#
:xCount             16
:yCount             22
:xDelta             1000.000000
:yDelta             1000.000000
#
:contourInterval    1.000000
:imperviousArea     0
:classCount         6
:elevConversion     1.000000
#---------------------------------------------------------------------
:endHeader
Channel Elevation (ELV)
0 0 0 0 0 0 0 0 0 0 0 0 0 0 0 0
0 0 0 0 0 449.987 450.2589 459.7505 0 0 0 0 0 0 0 0
0 0 0 0 439.7143 439.3989 446.7126 456.9253 0 0 0 0 0 0 0 0
0 0 443.5342 432.3142 432.4907 435.5879 435.983 449.5 451.5487 0 0 0 0 0 0 0
0 0 444.2039 431.4263 426.9317 430.406 429 445.733 438.776 424.391 407.868 415 0 0 0 0
0 0 427.7513 426.7671 420.1703 418 413.177 422.667 419.656 411.159 397.392 424.293 0 0 0 0
0 0 424 415.7209 410.7982 408.58 405.78 401.404 412.644 394.783 394.784 424.9998 0 0 0 0
0 0 410.946 409.3856 404.1123 397 402.233 395.885 388.846 390.84 408.95 416.296 0 0 0 0
0 0 405 402.486 400.3887 392.876 389.488 383.759 386.19 398.136 403.145 403.1464 0 0 0 0
0 406.8499 405.1402 397.7236 395.3988 390.289 380.615 381 385.4826 389.8754 403.144 404.0144 378.8936 366.7767 0 0
0 0 398.5236 394.3437 389.2024 382.0001 369.2115 373.814 382.1713 383.4299 392.173 388.229 365 362.2188 0 0
0 0 0 386.759 382 370.4435 362.3498 362.3488 364.882 373.1497 374.421 368.4925 364.9024 361 0 0
0 0 0 380.1984 364.2008 366.0106 365 362.348 362.347 368.16 371.282 365.624 365.8823 359.521 356.595 0
0 0 0 377 361.9391 360.7461 357.8787 356.722 354.149 362.922 369.8749 360.505 355.6302 353.8331 351.96 0
0 0 0 367 362.9204 360.7471 376.9427 353.7982 349.514 350.096 353.3828 357.243 354.544 345.7372 347.7139 0
0 0 0 370 367.8081 377.1946 373.5786 362.7948 347.7372 346.609 349.018 346.7248 347.7808 341.1941 344.8575 0
0 0 0 0 385.7544 375.7906 369.8058 365.3333 354.2298 341.486 340.119 340.019 337.834 335.5098 344.902 0
0 0 0 0 382.3734 372.8276 367.3079 361 357.8712 342 340.423 337.296 331.414 327.0765 0 0
0 0 0 0 0 369.2365 365.9149 353.0508 345.199 344.4005 0 0 0 321.8995 319.8669 316.893
0 0 0 0 0 0 359.7219 347.663 346.2336 0 0 0 0 0 0 0
0 0 0 0 0 0 355.741 348.9796 0 0 0 0 0 0 0 0
0 0 0 0 0 0 0 0 0 0 0 0 0 0 0 0
Drainage Area (FRAC)
0 0 0 0 0 0 0 0 0 0 0 0 0 0 0 0
0 0 0 0 0 1 28 8 0 0 0 0 0 0 0 0
0 0 0 0 70 93 100 70 0 0 0 0 0 0 0 0
```

0 0 1 45 100 100 110 91 6 0 0 0 0 0 0 0
0 0 43 100 100 75 115 100 85 37 49 9 0 0 0 0
0 0 14 100 100 75 125 130 70 100 100 18 0 0 0 0
0 0 5 95 100 70 130 140 60 100 97 4 0 0 0 0
0 0 1 66 100 115 70 125 75 115 70 12 0 0 0 0
0 0 46 100 100 100 95 120 115 70 130 26 0 0 0 0
0 3 83 100 100 50 160 90 100 100 100 83 89 24 0 0
0 0 5 62 100 100 100 100 100 100 60 140 100 50 0 0
0 0 0 33 100 100 100 100 100 100 60 100 100 50 0 0
0 0 0 61 100 100 100 100 100 100 90 150 99 75 1 0
0 0 0 72 100 100 100 100 130 70 100 100 100 100 54 0
0 0 0 58 100 100 100 100 125 75 100 100 100 100 67 0
0 0 0 3 76 100 100 100 100 65 175 100 100 100 63 0
0 0 0 0 47 100 100 100 100 100 60 60 120 85 28 0
0 0 0 0 63 100 100 100 100 62 27 140 78 71 0 0
0 0 0 0 0 19 92 100 94 15 0 0 0 64 9 0
0 0 0 0 0 0 43 96 19 0 0 0 0 0 0 0
0 0 0 0 0 0 18 40 0 0 0 0 0 0 0 0
0 0 0 0 0 0 0 0 0 0 0 0 0 0 0 0
Drainage direction (S)
0 0 0 0 0 0 0 0 0 0 0 0 0 0 0 0
0 0 0 0 0 4 4 6 0 0 0 0 0 0 0 0
0 0 0 0 4 4 6 4 0 0 0 0 0 0 0 0
0 0 2 4 4 6 6 6 4 0 0 0 0 0 0 0
0 0 2 2 4 4 4 4 4 2 4 6 0 0 0 0
0 0 2 2 4 4 4 4 2 4 4 6 0 0 0 0
0 0 2 4 4 4 2 4 2 4 6 6 0 0 0 0
0 0 4 2 2 3 3 4 4 6 6 5 0 0 0 0
0 0 2 2 4 3 4 4 5 4 6 6 0 0 0 0
0 2 2 2 2 4 4 4 4 6 5 2 4 4 0 0
0 0 2 2 2 4 4 6 6 4 6 3 2 4 0 0
0 0 0 3 2 4 2 4 5 6 2 4 2 4 0 0
0 0 0 2 4 6 4 2 4 5 6 4 2 4 4 0
0 0 0 2 2 2 2 4 4 4 6 4 2 4 4 0
0 0 0 2 2 8 8 2 4 3 4 2 2 4 6 0
0 0 0 2 8 4 2 2 2 4 3 4 6 4 5 0
0 0 0 0 2 2 2 4 2 3 3 2 2 4 6 0
0 0 0 0 2 2 2 4 4 8 8 2 2 4 0 0
0 0 0 0 0 2 2 2 1 8 0 0 0 2 2 0
0 0 0 0 0 0 2 2 8 0 0 0 0 0 0 0
0 0 0 0 0 0 2 8 0 0 0 0 0 0 0 0
0 0 0 0 0 0 0 0 0 0 0 0 0 0 0 0
River Class (IBN)
1 1 1 1 1 1 1 1 1 1 1 1 1 1 1 1
1 1 1 1 1 1 1 1 1 1 1 1 1 1 1 1
1 1 1 1 1 1 1 1 1 1 1 1 1 1 1 1

```
1 1 1 1 1 1 1 1 1 1 1 1 1 1 1 1
1 1 1 1 1 1 2 2 2 3 3 3 1 1 1 1
1 1 1 1 1 1 2 2 2 3 3 3 1 1 1 1
1 1 1 1 1 1 2 2 3 3 3 1 1 1 1 1
1 1 1 1 1 1 2 2 3 3 3 1 1 1 1 1
1 1 1 1 1 1 1 2 3 3 1 1 1 1 1 1
1 1 1 1 1 1 1 3 1 1 1 1 1 1 1 1
1 1 1 1 1 1 1 1 1 1 1 1 1 1 1 1
1 1 1 1 1 1 1 1 1 1 1 1 1 1 1 1
1 1 1 1 1 1 1 1 1 1 1 1 1 1 1 1
1 1 1 1 1 1 1 1 1 1 1 1 1 1 1 1
1 1 1 1 1 1 1 1 1 1 1 1 1 1 1 1
1 1 1 1 1 1 1 1 1 1 1 1 1 1 1 1
1 1 1 1 1 1 1 1 1 1 1 1 1 1 1 1
1 1 1 1 1 1 1 1 1 1 1 1 1 1 1 1
1 1 1 1 1 1 1 1 1 1 1 1 1 1 1 1
1 1 1 1 1 1 1 1 1 1 1 1 1 1 1 1
1 1 1 1 1 1 1 1 1 1 1 1 1 1 1 1
1 1 1 1 1 1 1 1 1 1 1 1 1 1 1 1
Contour Density (IROUGH)
1 1 1 1 1 1 1 1 1 1 1 1 1 1 1 1
1 1 1 1 1 35 35 48 1 1 1 1 1 1 1 1
1 1 1 1 24 30 32 28 1 1 1 1 1 1 1 1
1 1 27 34 26 31 33 28 26 1 1 1 1 1 1 1
1 1 31 32 32 30 35 45 32 34 41 83 1 1 1 1
1 1 29 28 29 33 39 40 35 33 54 69 1 1 1 1
1 1 28 28 31 25 26 47 49 63 63 66 1 1 1 1
1 1 33 25 29 46 31 37 27 31 25 30 1 1 1 1
1 1 19 24 27 28 41 33 28 17 35 60 1 1 1 1
1 26 25 30 25 23 38 38 30 38 49 72 41 50 1 1
1 1 27 30 28 33 60 50 42 29 44 62 47 31 1 1
1 1 1 27 26 47 51 59 44 48 33 19 16 16 1 1
1 1 1 20 38 40 41 17 23 18 18 10 12 11 41 1
1 1 1 29 36 40 38 37 45 17 17 10 10 12 42 1
1 1 1 40 32 40 41 47 53 32 21 5 15 19 19 1
1 1 1 41 39 35 29 34 32 35 29 20 12 27 18 1
1 1 1 1 40 26 24 20 40 42 22 34 39 41 49 1
1 1 1 1 33 28 34 33 24 25 27 26 45 69 1 1
1 1 1 1 1 24 22 35 29 23 1 1 0 62 35 0
1 1 1 1 1 1 39 35 18 1 1 1 1 1 1 1
1 1 1 1 1 1 49 30 1 1 1 1 1 1 1 1
1 1 1 1 1 1 1 1 1 1 1 1 1 1 1 1
Channel Density (ICHNL)
0 0 0 0 0 0 0 0 0 0 0 0 0 0 0 0
0 0 0 0 0 5 5 5 0 0 0 0 0 0 0 0
0 0 0 0 5 5 5 5 0 0 0 0 0 0 0 0
```

```
0 0 5 5 1 1 5 5 5 0 0 0 0 0 0 0
0 0 5 5 1 5 5 5 5 5 5 5 0 0 0 0
0 0 5 5 1 5 5 5 5 5 5 5 0 0 0 0
0 0 5 5 1 5 1 1 5 1 5 5 0 0 0 0
0 0 5 5 1 1 5 1 1 1 5 5 0 0 0 0
0 0 5 5 5 1 1 2 1 5 5 5 0 0 0 0
0 5 5 5 5 5 1 1 1 5 5 5 5 5 0 0
0 0 5 5 5 1 1 1 1 5 5 5 5 5 0 0
0 0 0 5 5 1 2 2 1 5 5 5 5 1 0 0
0 0 0 5 1 1 5 1 2 5 5 5 5 1 5 0
0 0 0 5 1 1 1 1 1 5 5 5 1 5 5 0
0 0 0 5 5 1 5 1 3 1 5 5 2 1 5 0
0 0 0 5 5 5 5 5 5 1 1 1 1 5 1 5 0
0 0 0 0 5 5 5 5 5 5 1 2 2 1 2 5 0
0 0 0 0 5 5 5 1 5 2 2 1 1 1 0 0
0 0 0 0 0 5 5 1 1 1 0 0 0 1 1 0
0 0 0 0 0 0 5 5 5 0 0 0 0 0 0 0
0 0 0 0 0 0 0 5 5 0 0 0 0 0 0 0
0 0 0 0 0 0 0 0 0 0 0 0 0 0 0 0
Reach Number (IREACH)
0 0 0 0 0 0 0 0 0 0 0 0 0 0 0 0
0 0 0 0 0 0 0 0 0 0 0 0 0 0 0 0
0 0 0 0 0 0 0 0 0 0 0 0 0 0 0 0
0 0 0 0 0 0 0 0 0 0 0 0 0 0 0 0
0 0 0 0 0 0 0 0 0 0 2 0 0 0 0 0
0 0 0 0 0 0 0 0 0 0 0 0 0 0 0 0
0 0 0 0 0 0 0 0 0 0 0 0 0 0 0 0
0 0 0 0 0 0 0 0 0 0 0 0 0 0 0 0
0 0 0 0 0 0 0 0 0 0 0 0 0 0 0 0
0 0 0 0 0 0 0 0 0 0 0 0 0 0 0 0
0 0 0 0 0 0 0 0 0 0 0 0 0 0 0 0
0 0 0 0 0 0 0 1 1 0 0 0 0 0 0 0
0 0 0 0 0 0 0 0 0 0 0 0 0 0 0 0
0 0 0 0 0 0 0 0 0 0 0 0 0 0 0 0
0 0 0 0 0 0 0 0 0 0 0 0 0 0 0 0
0 0 0 0 0 0 0 0 0 0 0 0 0 0 0 0
0 0 0 0 0 0 0 0 0 0 0 0 0 0 0 0
0 0 0 0 0 0 0 0 0 0 0 0 0 0 0 0
0 0 0 0 0 0 0 0 0 0 0 0 0 0 0 0
0 0 0 0 0 0 0 0 0 0 0 0 0 0 0 0
Impervious Area
0 0 0 0 0 0 0 0 0 0 0 0 0 0 0 0
0 0 0 0 0 0 0 0 0 0 0 0 0 0 0 0
0 0 0 0 0 0 0 0 0 0 0 0 0 0 0 0
```

```
0 0 0 0 0 0 0 0 0 0 0 0 0 0 0 0
0 0 0 0 0 0 0 0 0 0 0 0 0 0 0 0
0 0 0 0 0 0 0 0 0 0 0 0 0 0 0 0
0 0 0 0 0 0 0 0 0 0 0 0 0 0 0 0
0 0 0 0 0 0 0 0 0 0 0 0 0 0 0 0
0 0 0 0 0 0 0 0 0 0 0 0 0 0 0 0
0 0 0 0 0 0 0 0 0 0 0 0 0 0 0 0
0 0 0 0 0 0 0 0 0 0 0 0 0 0 0 0
0 0 0 0 0 0 0 0 0 0 0 0 0 0 0 0
0 0 0 0 0 0 0 0 0 0 0 0 0 0 0 0
0 0 0 0 0 0 0 0 0 0 0 0 0 0 0 0
0 0 0 0 0 0 0 0 0 0 0 0 0 0 0 0
0 0 0 0 0 0 0 0 0 0 0 0 0 0 0 0
0 0 0 0 0 0 0 0 0 0 0 0 0 0 0 0
0 0 0 0 0 0 0 0 0 0 0 0 0 0 0 0
0 0 0 0 0 0 0 0 0 0 0 0 0 0 0 0
0 0 0 0 0 0 0 0 0 0 0 0 0 0 0 0
0 0 0 0 0 0 0 0 0 0 0 0 0 0 0 0
0 0 0 0 0 0 0 0 0 0 0 0 0 0 0 0
class 2: forest
12 31 4 15 12 20 46 36 12 19 21 16 9 8 17 8
10 27 29 12 12 8 27 38 31 19 10 24 14 9 4 14
9 24 7 26 24 11 23 21 11 23 14 20 19 5 4 19
21 22 24 27 37 22 22 15 9 8 14 15 13 14 16 29
35 28 30 30 22 21 20 21 16 11 7 20 11 23 12 18
29 21 34 34 24 13 10 19 9 5 22 20 14 18 31 18
23 22 9 19 27 12 32 20 22 11 19 12 20 16 35 32
29 23 37 17 15 15 10 20 4 3 8 3 16 12 9 9
23 25 30 22 14 17 6 21 15 30 15 11 7 8 10 14
30 23 10 18 13 17 9 11 22 19 7 14 7 14 17 5
32 18 19 17 16 10 13 16 13 10 20 13 20 15 25 8
22 21 19 18 16 7 17 5 36 18 25 26 21 27 12 11
20 9 8 11 6 11 1 11 18 11 17 13 7 36 11 16
26 10 8 14 11 21 5 13 8 13 13 18 20 43 14 41
20 5 8 24 18 19 6 2 19 5 22 28 19 30 18 21
16 10 9 18 12 6 4 12 12 17 7 11 19 11 3 26
13 11 22 2 6 26 21 8 9 11 10 10 6 8 7 11
22 10 3 5 4 11 9 7 8 5 12 21 9 28 15 14
6 5 13 8 9 8 18 5 8 6 9 2 10 21 13 11
13 11 10 6 4 5 5 5 14 9 1 11 6 1 14 10
14 14 7 11 12 12 7 6 3 3 0 3 6 9 15 17
18 8 11 1 11 10 11 11 9 8 2 1 11 9 8 13
class 3: crops
54 39 92 81 86 75 52 55 68 66 71 78 90 89 81 88
85 63 70 87 84 90 69 59 55 75 86 74 83 86 95 81
86 73 91 71 75 85 70 75 82 72 83 77 73 94 95 78
```

```
73 58 72 71 59 75 69 69 78 86 84 81 81 77 81 67
46 61 62 68 72 74 76 71 71 87 80 72 88 72 68 81
66 76 58 61 75 84 87 77 86 92 63 74 85 76 58 79
74 76 89 72 58 85 65 79 75 75 67 79 79 82 56 64
56 73 58 82 82 82 87 77 79 82 86 74 81 85 88 87
75 69 58 72 84 82 93 77 62 59 80 80 91 90 86 84
69 68 89 80 84 81 90 75 76 75 90 78 92 82 77 80
56 80 69 79 76 89 83 75 83 87 53 52 73 80 73 86
72 76 78 75 76 84 76 91 59 72 53 62 74 53 81 86
74 87 86 84 91 84 96 43 54 87 78 78 91 48 86 67
60 82 90 82 78 78 93 65 85 83 86 79 77 42 80 47
78 89 90 72 76 78 87 96 74 81 76 69 77 63 81 64
80 84 87 81 85 86 90 86 55 74 84 85 76 87 80 65
81 77 74 90 90 70 68 66 67 74 87 89 87 85 79 82
75 79 88 92 94 82 89 85 83 92 84 68 83 65 71 74
88 85 82 87 87 91 78 89 88 93 86 96 86 70 75 81
80 82 82 85 94 94 92 94 79 90 98 87 93 96 80 82
81 82 85 65 79 80 88 92 94 96 93 95 92 77 74 72
81 84 85 73 85 84 84 88 88 84 96 97 84 78 84 83
class 4: wetlands
0 4 0 1 0 3 1 0 4 6 0 1 0 0 0 0
0 2 0 0 1 0 0 1 9 4 0 0 0 0 0 0
0 0 0 0 0 0 3 2 0 3 0 0 0 0 0 0
0 0 2 0 3 1 2 3 3 0 0 2 1 3 0 1
7 4 3 0 4 3 2 1 1 0 12 6 0 0 1 0
3 1 5 0 0 1 0 2 1 0 13 4 0 3 9 1
0 0 0 0 8 2 2 0 0 11 11 2 0 0 2 3
2 1 3 0 0 0 0 1 5 13 0 0 0 0 0 1
0 1 4 1 0 0 0 0 16 7 1 3 0 0 0 0
0 0 0 0 0 0 0 12 0 3 1 6 0 2 3 1
8 0 0 1 1 0 1 2 2 1 22 25 2 0 0 4
1 1 0 0 0 0 2 0 4 2 20 6 3 19 4 0
3 2 0 0 0 0 0 4 5 0 0 0 0 14 0 11
6 4 0 0 0 0 0 2 0 0 0 1 0 12 2 5
0 4 0 0 0 0 0 0 0 0 0 0 1 1 6 0 10
0 3 0 0 0 0 0 0 0 1 0 2 3 1 0 5
0 4 0 1 0 0 0 0 0 0 0 0 0 3 0 3
0 3 1 0 0 0 0 0 0 0 0 3 3 4 8 4
0 0 1 0 0 0 0 0 0 0 0 0 2 7 8 4
1 0 2 0 0 0 0 0 2 0 0 0 0 0 0 4
0 0 1 4 5 2 2 0 0 0 0 0 0 3 7 5
0 0 0 0 0 1 2 0 0 0 0 0 0 6 3 0
class 5: water
0 0 0 0 0 0 0 0 0 0 0 0 0 0 0 0
0 0 0 0 0 0 0 0 1 0 0 0 0 0 0 0
0 0 0 0 0 0 0 0 0 0 0 0 0 0 0 0
```

0 0 0 0 0 0 0 0 0 0 0 0 0 0 0 0 0 0
0 0 0 0 0 0 0 0 0 0 0 0 0 0 0 0 0 0
0 0 0 0 0 0 0 0 0 0 0 0 0 0 0 0 0 0
0 0 0 0 0 0 0 0 0 0 0 0 0 0 0 0 0 0
0 0 0 0 0 0 0 0 0 0 0 0 0 0 0 0 0 0
0 0 0 0 0 0 0 0 0 0 0 0 0 0 0 0 0 0
0 0 0 0 0 0 0 0 0 0 0 0 0 0 0 0 0 1
0 0 0 0 0 0 0 0 0 0 0 0 0 0 0 0 0 0
0 0 0 0 0 0 0 0 0 0 0 0 0 0 0 0 0 0
0 0 0 0 0 0 0 36 20 0 0 0 0 0 0 0 0 2
0 0 0 0 0 0 0 16 4 0 0 0 0 0 0 0 0 1
0 0 0 0 0 0 0 0 0 0 0 0 0 0 0 0 0 1
0 0 0 0 0 0 0 0 0 0 0 0 0 0 0 0 0 1
0 0 0 0 0 0 0 0 0 0 0 0 0 1 0 0 0
0 0 0 0 0 0 0 0 0 0 0 0 0 0 0 3 1
0 0 0 0 0 0 0 0 0 0 0 0 0 0 0 2 0
0 0 0 0 0 0 0 0 0 0 0 0 0 0 0 0 2
0 0 0 0 1 0 1 0 0 0 0 0 0 0 1 1
0 0 0 0 0 1 0 0 0 0 0 0 0 3 1 0
Impervious Area
32 24 2 1 0 0 0 6 14 7 6 3 0 2 0 2
4 5 0 0 1 0 1 0 1 0 2 0 1 2 0 3
4 1 0 0 0 1 3 1 4 1 0 0 5 0 0 1
4 18 0 0 0 1 4 11 7 5 0 0 3 2 0 0
10 5 3 1 0 0 0 5 11 1 0 0 0 3 17 0
0 0 0 3 0 0 1 0 2 1 0 0 0 1 0 0
0 0 1 7 6 0 0 0 0 1 1 6 0 0 4 0
11 1 0 0 2 2 1 0 11 0 4 21 1 1 0 0
0 4 6 3 0 0 0 0 5 1 2 3 0 0 2 0
0 7 0 0 0 0 0 0 0 1 0 0 0 0 1 10
2 0 10 2 5 0 1 6 0 0 2 8 3 3 0 0
2 0 1 5 7 8 2 2 0 5 0 5 0 0 1 0
1 0 4 4 1 3 1 4 0 0 4 8 1 0 0 2
6 2 0 2 10 0 0 0 0 2 0 0 0 2 1 4
0 0 0 2 5 1 5 0 4 13 0 0 0 0 0 1
2 0 3 0 1 6 5 1 31 5 8 0 1 0 15 1
4 7 3 6 2 3 9 25 22 12 1 0 3 1 12 1
1 6 6 2 0 6 0 6 8 1 3 6 3 2 1 5
4 8 1 3 2 0 2 5 2 0 3 1 0 0 0 2
4 6 4 7 1 0 1 0 4 0 0 0 0 1 3 0
3 3 5 17 1 3 0 0 1 0 6 0 0 9 1 2
0 7 2 25 3 2 1 0 1 6 1 0 3 2 2 2

Appendix C

Sampling Methods

C.1 Introduction

This appendix outlines sampling methods and performance not discussed in the main body of this document. The sections of this appendix include quality assurance and quality control, and calculated method detection limits for a number of analytical methods.

C.2 Quality Assurance / Quality Control Graphs

Quality Assurance / Quality Control (QA/QC) analytical laboratory samples were analyzed with the Ion Chromatograph and Spectrochromatographic analysis methods. The QA/QC samples were purchased (HACH Company) and diluted if necessary to a typical mid-range concentration for the detector. For the Ion Chromatographic techniques the autosamplers were loaded with QA/QC samples and a reagent blank for every 10 regular samples. For the run methods, two QA/QC samples were added for every 25 sample digestion, which would have contained up to 21 regular samples in total as well as 2 reagent blank samples. This was compliant with the 5% frequency generally employed in environmental sampling by the EPA and others (Zhang, 2007)

QA/QC Plots were generated to demonstrate the variability in measurement of repeated analysis of factory standards over a period and are shown for IC nitrate (Figure C.1), HACH

total phosphorus (Figure C.2, and HACH total nitrogen (Figure C.3).

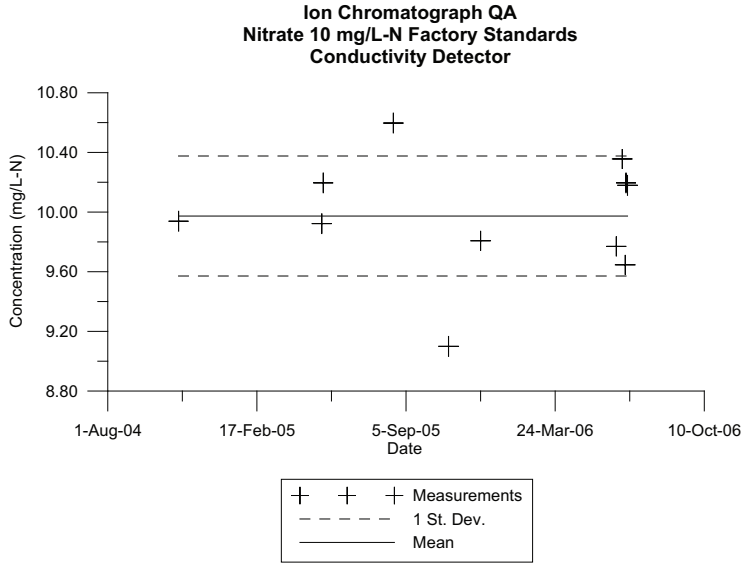

Figure C.1: Ion Chromatograph - Conductivity Detector - Nitrate QA

C.3 Method Detection Limits

The method detection limit for an analyste is defined by the US-EPA as follows (US-EPA, 2003):

> The method detection limit (MDL) is defined as the minimum concentration of a substance that can be measured and reported with 99% confidence that the analyte concentration is greater than zero and is determined from analysis of a sample in a given matrix containing the analyte.

The MDL method employed was that described by the US-EPA using reagent water US-EPA (2003). Data and results for the calculation of the method detection limits are described below.

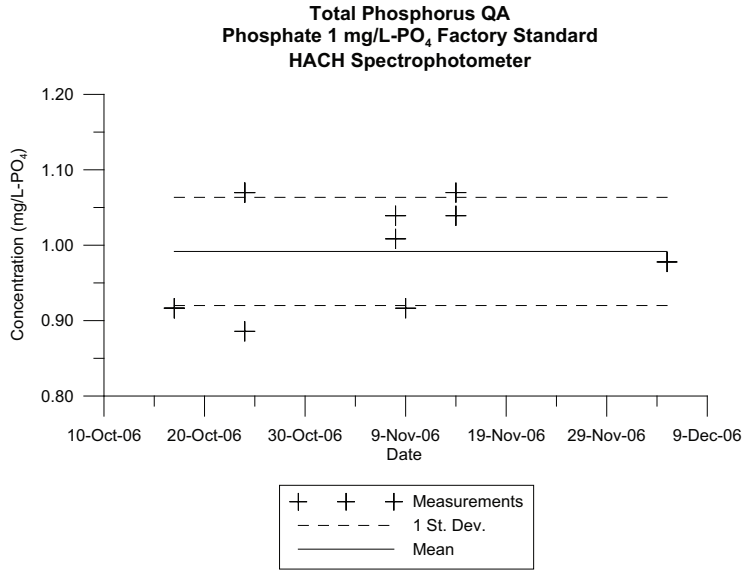

Figure C.2: HACH Spectrophotometer - Total Phosphorus QA

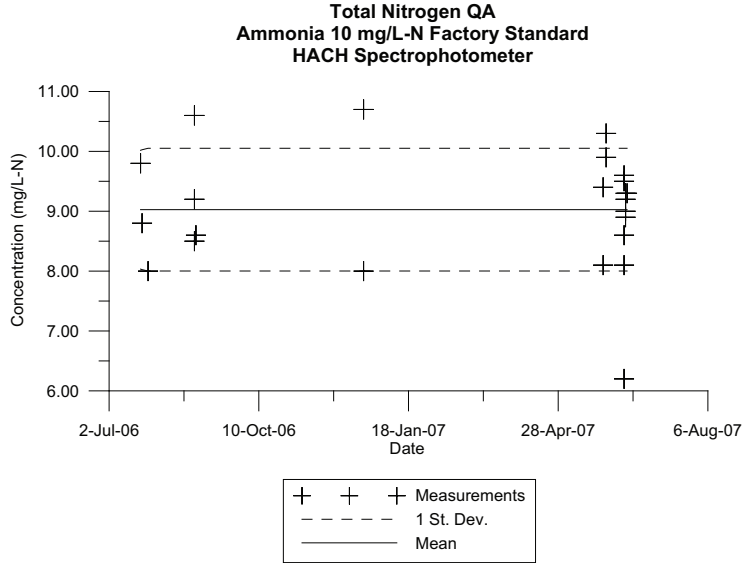

Figure C.3: HACH Spectrophotometer - Total Nitrogen QA

C.3.1 Total Phosphorus MDL

The Total Phosphorus (TP) Method Detection limit was calculated using a 0.05 mg/L-P standard that was determined to be approximately 3 times the standard deviation associated with repeated analysis of replicates. The MDL samples and calculations are outlined in Table C.1.

	Readings (mg/L-P)
1	0.04
2	0.06
3	0.11
4	0.03
5	0.07
6	0.05
7	0.04
8	0.04
9	0.02

Standard Deviation
0.027

Student's T-Statistic
2.896

MDL
0.077

Table C.1: Total Phosphorus - MDL

C.3.2 Total Nitrogen MDL

The Total Nitrogen (TN) Method Detection Limit was calculated using a 1 mg/L-N standard that was originally estimated to be approximately 3 times the standard deviation associated with a repeat analysis of blanks. The MDL samples are outlined in Table C.2.

	Readings (mg/L-N)
1	1.78
2	0.49
3	1.83
4	0.97
5	0.92
6	0.92
7	0.64
8	1.02
9	0.83

Standard Deviation
0.464

Student's T-Statistic
2.896

MDL
1.344

Table C.2: Total Nitrogen - MDL

C.3.3 Ion Chromatograph MDL

The MDL values for the anions and cations within a sample using the ion chromatograph method is outlined in Table C.3 and Table C.4 below. Low concentration standards of at least 3 standard deviations using reagent blank water were employed to determine the method detection limit. The UV detector does not exhibit any detectable signal noise with standard blanks using the method described in Chapter 6. A reagent concentration of of 0.5 mg/L -N was used.

		Chloride	*Nitrate - N*	*Sulphate*	*Nitrate - N (UV)*
Standard Concentration (mg/L)		0.50	0.25	1.00	0.5
Readings (mg/L)					
	1	0.47	0.23	0.97	0.53
	2	0.49	0.24	0.97	0.54
	3	0.50	0.23	0.97	0.53
	4	0.50	0.24	0.97	0.54
	5	0.50	0.21	1.02	0.49
	6	0.50	0.27	0.97	0.49
	7	0.51	0.26	1.02	0.49
	8	0.50	0.25	0.97	0.49
	9	0.51	0.23	0.99	0.52
	10	0.50	0.22	0.96	0.50
	11	0.46	0.21	0.99	0.52
	12	0.49	0.26	0.96	0.50
	13	0.46		0.99	
	14	0.49			
Standard Deviation (mg/L)		0.019	0.020	0.019	0.020
Student's T-Statistic (α=.99)		3.012	3.106	3.055	3.106
MDL (mg/L)		*0.056*	*0.063*	*0.057*	*0.061*

Table C.3: IC - Anion Method Deteciton Limits

		Sodium	***Potassium***	***Magnesium***	***Calcium***
Standard Concentration (mg/L)		0.50	0.25	0.50	0.50
Readings (mg/L)					
	1	0.44	0.22	0.50	0.42
	2	0.47	0.25	0.50	0.55
	3	0.45	0.23	0.51	0.53
	4	0.46	0.21	0.51	0.48
	5	0.45	0.20	0.50	0.53
	6	0.47	0.25	0.50	0.55
	7	0.45	0.25	0.49	0.53
	8	0.47	0.25	0.47	0.54
	9	0.45	0.25	0.52	0.52
	10	0.48	0.24	0.53	0.51
	11	0.44	0.25	0.53	0.52
	12	0.41		0.53	0.47
	13	0.40		0.53	0.53
	14			0.52	0.49
Standard Deviation (mg/L)		0.022	0.018	0.017	0.037
Student's T-Statistic (α=.99)		3.055	3.169	3.012	3.012
MDL (mg/L)		*0.068*	*0.058*	*0.052*	*0.112*

Table C.4: IC - Cation Method Deteciton Limits

Appendix D

Water Quality Model Development

D.1 Introduction

This section includes details regarding the development of the water quality sub-model within the WatFlood model, including unit test results of the water quality sub-model as well as employed parameter and input files used in the model simulations.

D.2 Contaminant Transport Model Development

D.2.1 Sub-Grid Storage Routing Algorithm

The sub-grid storage routing scheme uses a two-equation approach to the routing of contaminants through a WatFlood channel at a sub-grid level. Equations 7.10 and 7.11 are employed in an identical manner to the storage routing algorithm described in Section 7.2.2, except the modelled mass storage is performed on an element rather than a grid basis. When the sub-grid storage routing model operated with a single element per grid the model is identical to the current WatFlood contaminant transport routine.

Hydraulic Requirements

The storage routing contaminant transport model requires the following inputs from the WATFLOOD model: grid channel storage (S), grid inflow (Q_{in}), and grid outflow (Q_{out}) for each time step. The grid storage is averaged over the elements and the flow between elements is linearly interpolated over the length of the grid channel. For the sub-grid storage routing algorithm, the mass, not the concentration is stored as a state variable and concentrations are determined during post-processing by dividing by the storage volume in the element.

Boundary Conditions

The sub-grid storage routing algorithm is designed to be a mass-conservation algorithm. The only boundary condition that applies is that the mass that leaves an element should be added to the receiving grid based on (7.10), (7.11) and (7.12). This process applies equally between sub-grid elements and between grids.

Stability Analysis

The storage routing algorithm is often employed because it is generally immune to stability problems at extreme flows, and stability can be assured by ensuring that the time taken for a flood wave to move thorough a grid or reach does not exceed the time step (Courant et al., 1967; Dingman, 1994). As the storage routing model does not employ any explicit dispersion quantity, so no stability criteria associated with dispersion applies. WatFlood automatically adjusts the computational time step to ensure the effective Courant number is less than one over the domain, i.e. the flow volume leaving a grid channel in a time step is not in excess of the storage contained within the grid channel. When integrated with WatFlood the prescribed hydrologic routing time step is reduced by a factor of the number of elements per grid to ensure that stability of the routine is maintained.

Algorithm Limitations

The storage routing model for contaminants is limited in its ability to physically explain mixing and transport in rivers as the rate of transport is dependent on the grid size. This leads to contaminant breakthrough curves that are not explained by the dispersion within the stream, but rather the numerical dispersion inherent in the discretization of the watershed and channel reaches. This problem was illustrated in Figure 7.1, where the same conservative tracer is routed through a WATFLOOD channel at three different watershed grid discretization levels. With all other hydrologic conditions being equal the three different discretizations showed very different breakthrough profiles. If a model is to simulate event-based hydrologic phenomena then the storage-routing contaminant transport algorithm will be of limited utility.

D.2.2 QUICKEST Scheme

The Quadratic Upstream Interpolation for Convective Kinematics (QUICK) Scheme for advective and dispersive transport for steady flow and the modified scheme for unsteady flow using an "estimated streaming term" (QUICKEST) are commonly employed algorithms for one-dimensional finite-difference solutions of advective and dispersive transport. The scheme offers a an explicit mass-conservative solution with a high degree of accuracy (Leonard, 1979).

The QUICKEST algorithm finds its improved accuracy in the advective term through the estimation of the node boundary flux values by using a parabolic interpolation of the two adjacent node values as well as a third upstream node.

The QUICKEST scheme is a finite volume model that improves accuracy by using a cubic interpolation scheme to estimate the fluxes at the control volume boundaries. For reference, Figure D.1 illustrates the control volume and indexing sequence employed in the QUICKEST model code. In the following description of the algorithm the control volumes are indexed with a direct index number $i, i+1, i+2$ etc. and the interfaces or control volume adjoining faces are indexed with parentheses $(i), (i+1), (i+2)$, where a control volume will have the same index as its upstream interface. The arrows represent the flow

direction across the control volume elements.

To calculate the constituent concentration in control volume i at the subsequent time step (ϕ_i^{n+1}) a finite volume formulation uses the following mass balance equation for a uniform grid in one dimension with a uniform diffusion coefficient:

$$\frac{\phi_i^{n+1} - \phi_i^n}{\Delta t} = \frac{1}{\Delta x}\left[\left(u_{(i)}^n \phi_{(i)}^n - u_{(i+1)}^n \phi_{(i+1)}^n\right) - \left(D\left.\frac{\partial \phi}{\partial x}\right|_{(i)}^n - D\left.\frac{\partial \phi}{\partial x}\right|_{(i+1)}^n\right)\right] + S \qquad \text{(D.1)}$$

where $u_{(i)}^n$, $\phi_{(i)}^n$ and $\left.\frac{\partial \phi}{\partial x}\right|_{(i)}^n$ are the velocity, concentration and concentration gradient evaluated at the interface (i) at the current time step n and S is a prescribed source term. The equation is simplified through the introduction of the Courant number (C) and Péclet number (Pe) and dispersion parameter (α) which is the reciprocal of the Péclet number

$$C_{(i)} = \frac{u_{(i)}\Delta t}{\Delta x} \qquad \text{(D.2)}$$

$$Pe_{(i)} = \frac{1}{\alpha_{(i)}} = \frac{\left|u_{(i)}\right|\Delta x}{D} \qquad \text{(D.3)}$$

which, considering that no negative velocities are possible, simplifies (D.1) to

$$\phi_i^{n+1} = \phi_i^n + \left(C_{(i)}\phi_{(i)}^n - C_{(i+1)}\phi_{(i+1)}^n\right) - \left(\frac{\alpha_{(i)}}{C_{(i)}}\left.\frac{\partial \phi}{\partial x}\right|_{(i)}^n - \frac{\alpha_{(i+1)}}{C_{(i+1)}}\left.\frac{\partial \phi}{\partial x}\right|_{(i+1)}^n\right) + S\Delta t \qquad \text{(D.4)}$$

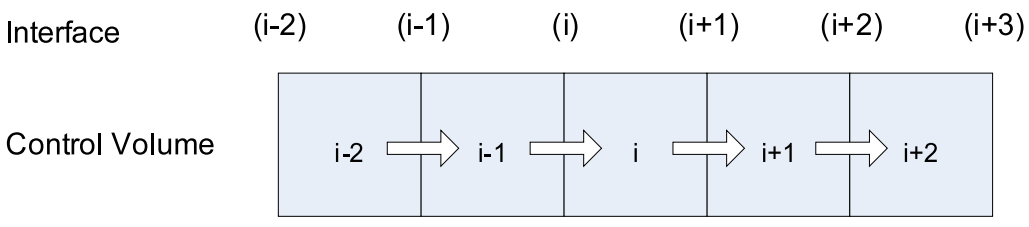

Figure D.1: QUICKEST Control Volume and Control Volume Interface Index Key

The QUICKEST model solves (D.4) for the values of the gradient and the concentrations at the interface by employing a quadratic upstream differencing scheme. The details are found in Leonard (1979) but the formulations for evaluating the concentrations and the gradients at the boundaries employed in this implementation which enforces a uniform grid are (D.5) and (D.6) respectively.

$$\phi^n_{(i)} = \frac{\phi^n_{i-1} + \phi^n_i}{2} - C_{(i+1)}\frac{\phi^n_i - \phi^n_{i-1}}{2} + \left(\alpha_{(i)} - \frac{1}{3}(1 - C^2_{(i)})\right)\frac{\phi^n_i - 2\phi^n_{i-1} + \phi^n_{i-2}}{2} \tag{D.5}$$

$$\left.\frac{\partial \phi}{\partial x}\right|^n_{(i)} = \frac{\phi^n_i - \phi^n_{i-1}}{\Delta x} - \left(\frac{C_{(i)}}{2}\right)\frac{\phi^n_i - 2\phi^n_{i-1} + \phi^n_{i-2}}{\Delta x} \tag{D.6}$$

It is seen from (D.5) and (D.6) that to calculate the concentration or gradient at a control volume interface using the quadratic upstream algorithm the concentrations for two control volumes immediately upstream are required as well as the concentration of the control volume directly downstream.

An important comparison between the storage routing algorithm and the QUICKEST algorithm is that QUICKEST employs concentration as the state variable whereas the storage routing algorithm uses mass as a state variable. In this implementation the mass stored in each element is calculated as a post-processing step using the calculated channel storage within the element by assuming uniform storage across the grid channel.

Hydraulic Requirements

The QUICKEST Algorithm requires a velocity at each element within the computational domain.

Velocities are acquired from the WATFLOOD model for each sub-grid element by linearly averaging the flow across the grid based on provided inflow and outflow values. The velocities are then determined by dividing the element flow by the active stream channel area.

Dispersion values are provided via a separate input parameter file for the watershed linked to a river class. The parameter is a dimensionless dispersion number in the form of

$$D_{par} = \frac{D}{du^*} \tag{D.7}$$

where D_{par} is the dimensionless dispersion coefficient stored in a parameter file, d is the river depth, and u^* is the shear velocity. The dispersion value D is calculated at each time step for each reach using the supplied d and u^* values provided by the hydrologic input.

Alternatively, if the dimensionless dispersion parameters are unavailable, the values for dispersion in a channel are calculated using the equation provided by Fischer (1979)

$$D = 0.011\frac{\bar{u}^2 w^2}{du^*} \tag{D.8}$$

where D is the longitudinal dispersion coefficient, $\bar{u}$ is the mean velocity, w is the channel width, d is the channel depth and u^* is the calculated shear velocity. As outlined by Rutherford (1994) the longitudinal dispersion coefficient is highly variable and can differ by several orders of magnitude in rivers with similar morphology and flow conditions. The precision of (D.8) can be misleading and the use of this approach is prescribed only in situations without other available mixing information.

Algorithm Stability

The QUICKEST Algorithm boasts a very large stability envelope, remaining stable for a wide range of Courant-Pecklet number combinations (Leonard, 1979). The reader is referred to Leonard (1979) and Abbott and Basco (1989) for a detailed von-Newmann stability analysis. However, it is important to know that for purely advective flow the scheme is stable for Courant numbers less than one, which was enforced in the WatFlood model.

Boundary Conditions

The QUICKEST scheme requires the establishment of a gradient and concentration value at the boundaries of each grid as a boundary condition. Due to the discontinuities in the

computational domain between grids, a zero-flux boundary condition is applied at each grid's upstream boundary. Mass from upstream grids are added to the receiving grids as a source term to the first receiving element. For the downstream boundary condition a zero gradient condition is established, indicating that advective processes determine the quantity of substance leaving a grid. This approach has been taken due to the inherent difficulties in determining the dispersion between adjacent reaches in a network structure and can be rationalized for highly advective flow conditions such as channel flow.

As the QUICKEST scheme requires known concentrations from two upstream control volumes to solve for a control volume interface concentration and gradient, the QUICKEST algorithm must be adjusted for the first two control volumes. For the upstream boundary condition the upstream flux term is set to zero

$$u^n_{(1)}\phi^n_{(1)} - D\left.\frac{\partial\phi}{\partial x}\right|^n_{(1)} = 0 \tag{D.9}$$

in which both $\phi^n_{(1)}$ and $\left.\frac{\partial\phi}{\partial x}\right|^n_{(1)}$ are set to zero to satisfy the condition. This is done directly in the algorithm for the upper boundary interface, replacing (D.5) and (D.6). For the second interface the calculation of the concentration and the gradient requires a lower order accuracy estimation due to the lack of available upstream elements. For reasons of stability the concentration at the boundary between the first and second grid is taken as the value of the first element (upstream differencing)

$$\phi^n_{(2)} = \phi^n_1 \tag{D.10}$$

which is a stable approach for the calculating the advective flux term at the expense of local accuracy (Chapra, 1997). The gradient at the boundary between the first and second element is taken as the centered difference between the adjacent nodes

$$\left.\frac{\partial\phi}{\partial x}\right|^n_{(2)} = \frac{\phi^n_2 - \phi^n_1}{\Delta x} \tag{D.11}$$

For the downstream boundary condition the boundary gradient is set to zero and the total flux leaving the last element is only a function of the concentration at the boundary

and the velocity at the boundary. The downstream boundary is not restricted from using the quadratic upwind scheme as there are an adequate number of upwind nodes provided there are 2 or more elements per grid. For this implementation the boundary condition at the last element is calculated using a ghost element as illustrated in Figure D.2. By employing the quadratic upwind approximation of the gradient at $(N+1)$ using (D.6) and setting the gradient equal to zero, the equivalent value for the concentration within the ghost element is

$$\phi^n_{N+1} = \phi^n_N \left(\frac{2\left(1 - C_{(N+1)}\right)}{2 - C_{(N+1)}} \right) + \phi^n_{N-1} \left(\frac{C_{(N+1)}}{2 - C_{(N+1)}} \right) \tag{D.12}$$

The total flux leaving a grid from the last element over a timestep Δt is approximated using

$$M^n_{out} = \phi^n_{(N+1)} u^n_{(N+1)} A^n_{(N+1)} \Delta t \tag{D.13}$$

where M^n_{out} is the estimate of the total mass leaving a grid over a time step, $A^n_{(N+1)}$ and $u^n_{(N+1)}$ are the area and velocity respectively as determined by the hydraulic model input data and Δt is the prescribed time step. The concentration at the downstream boundary $(\phi^n_{(N+1)})$ is determined using the standard QUICKEST interpolation described by (D.5). The total upstream mass exiting each upstream grid at time step n is added to the upstream receiving element of the next downstream grid at the start of the next time step $(n+1)$ as a source mass addition.

Hydraulic and Constituent Sources and Sinks

In the QUICKEST model the concentration is the state variable used in transport calculations. However, contaminant additions are added on a mass basis. Consequently at the end of every SOLROUTE time-step the concentrations are re-calculated considering changes in mass addition and changes in element storage using (7.12). With mass conserved, changes to the storage as indicated by the hydraulic input from WatFlood were converted to an equivalent change in concentration for the element. Mass additions due to upstream contribution or lateral input were considered equivalently with a supplied mass resulting

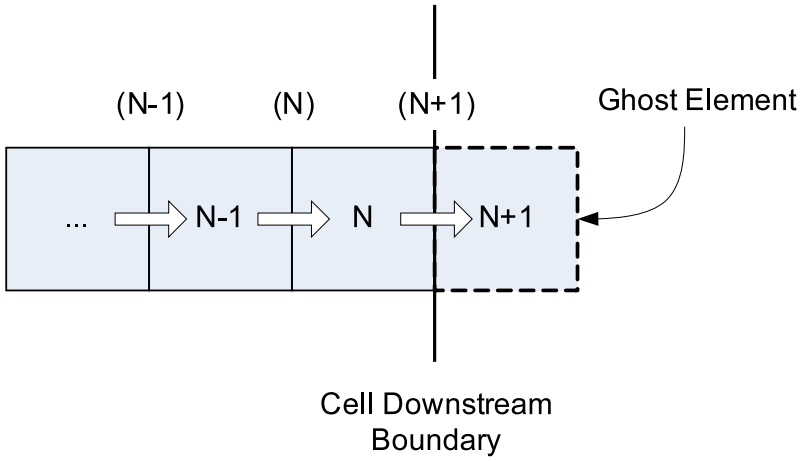

Figure D.2: QUICKEST Downstream Boundary Condition Schematic

in an updated concentration based on the storage in the receiving element.

Algorithm Limitations

The QUICKEST scheme is limited primarily by its stability envelope. Although the envelope provides some flexibility in terms of calculation time step, the variability of flow rates, dispersion rates and Courant and Péclet numbers with a WATFLOOD stream network made the maintenance of stability with this algorithm onerous. Additionally, this algorithm is characterized by "wiggles" or localized oscillations near steep gradients under highly advective conditions.

D.2.3 Holly-Preissmann / Crank-Nicholson Split-Operator Scheme

The Holly-Preissmann Scheme is fourth-order accurate pure advection algorithm that resists numerical dispersion by advecting polynomials of both the constituent profile and the derivatives of that profile using two computational points (Holly and Preissmann, 1977). The Holly-Preissmann advective scheme also shows a great degree of stability provided the upstream computational points can be accurately determined.

The Holly-Preissmann scheme has also been successfully combined with dispersion cal-

culations by Holly and Usseglio-Polatera (1984), whereby the Holly-Preissmann scheme was combined with an implicit Crank-Nicholson dispersion scheme to provide a split-operator advection-dispersion scheme, hereafter referred to the Holly-Preissman/Crank-Nicholson (HPCN) scheme.

Holly-Preissman Scheme Formulation

The Holly-Preissmann scheme is advective fourth-order accurate finite difference scheme presented originally by Holly and Preissmann (1977). It is an advective Lagrangian scheme that uses cubic polynomials to interpolate constituent values between nodes. To maintain the high accuracy of the advective scheme both the concentrations and the spatial gradients are advected with each time-step. For our one-dimensional case one begins with 1D advection dispersion equation

$$\frac{\partial \phi}{\partial t} + u\frac{\partial \phi}{\partial x} = D\frac{\partial^2 \phi}{\partial x^2} \tag{D.14}$$

where ϕ represents the constituent to be advected, u is the average velocity, D is the dispersion coefficient, x and t represent positions in the space and time domains respectively. Although the Holly-Preissmann scheme does not account for dispersion, it is required for the determination of the equation for the advection of the spatial gradients. This is accomplished by taking the first spatial derivative of (D.14).

$$\frac{\partial}{\partial x}\frac{\partial \phi}{\partial t} + \frac{\partial u}{\partial x}\frac{\partial \phi}{\partial x} + u\frac{\partial}{\partial x}\frac{\partial \phi}{\partial x} = \frac{\partial D}{\partial x}\frac{\partial^2 \phi}{\partial x^2} + D\frac{\partial}{\partial x}\frac{\partial^2 \phi}{\partial x^2} \tag{D.15}$$

The spatial gradients may be simplified using the following

$$\phi' = \frac{\partial \phi}{\partial x} \tag{D.16}$$

$$D' = \frac{\partial D}{\partial x} \tag{D.17}$$

$$u' = \frac{\partial u}{\partial x} \tag{D.18}$$

to provide equation (D.19)

$$\frac{\partial \phi'}{\partial t} + (u - D')\frac{\partial \phi'}{\partial x} = D\frac{\partial^2 \phi'}{\partial x^2} - u'\phi' \tag{D.19}$$

Equation (D.19) exhibits a similar form to (D.14) with the gradients advecting with a velocity adjusted by the dispersion coefficient gradient $(u - D')$. There is an additional term at the end of (D.19) which is the product of the velocity and concentration gradients $(-u'\phi')$ which acts as an additional source-like term.

The HPCN scheme uses a fitted cubic polynomial between two points within the computational domain to determine any concentration located between the two points.

$$\phi(C) = A_1 + A_2(C) + A_3(C)^2 + A_4(C)^3 \tag{D.20}$$

where C is the Courant number calculated for the element and A_1 to A_4 are fitted polynomial parameters. The local Courant number is calculated as previously defined in (D.2). The HPCN routine also applies a cubic polynomial to the concentration gradients $d\phi/dx$ or ϕ' to determine the concentration at any point between two computational points

$$\phi'(C) = B_1 + B_2(C) + B_3(C)^2 + B_4(C)^3 \tag{D.21}$$

where C is the Courant number calculated for the element and B_1 to B_4 are fitted polynomial parameters.

Algebraic manipulations outlined by Holly and Preissmann (1977) provide an update equation for the concentration at the next time step at location $i + 1$ based on a linear combination of concentrations and gradients at the i and $i + 1$ nodes based on (D.22) to (D.26).

$$\phi_{i+1}^{n+1} = \phi(C)^n = a_1\phi_i^n + a_2\phi_{i+1}^n + a_3\ \phi'^{\,n}_i + a_4\ \phi'^{\,n}_{i+1} \tag{D.22}$$

where

$$a_1 = (C)^2(3 - 2C) \tag{D.23}$$

$$a_2 = 1 - a_1 \tag{D.24}$$

$$a_3 = (C)^2(1 - C)(\Delta x) \tag{D.25}$$

$$a_4 = -C(1 - C)^2(\Delta x) \tag{D.26}$$

Constituent gradients are also advected in the Holly-Preissmann scheme and that is accomplished using equations (D.27) to (D.31).

$$\phi'^{n+1}_{i+1} = \phi x(C)^n = b_1\phi^n_i + b_2\phi^n_{i+1} + b_3\ \phi'^{n}_{i} + b_4\ \phi'^{n}_{i+1} \tag{D.27}$$

where

$$b_1 = 6C(C - 1)/(\Delta x) \tag{D.28}$$

$$b_2 = -b_1 \tag{D.29}$$

$$b_3 = C(3C - 2) \tag{D.30}$$

$$b_4 = (C - 1)(3C - 1) \tag{D.31}$$

Holly-Preissmann Boundary Conditions

Boundary conditions for the Holly-Preissmann scheme required special handling of the junctions between grids where several upstream grids may feed into a grid. Both the concentrations and the derivatives of concentrations are required at the upstream element. Concentrations at a grid's upstream element are determined as a flow weighted average of the upstream contributing concentrations.

$$\phi_1^{n+1} = \frac{\sum_j \left(\phi(C)_N^n|_j \, Q_j^n \right)}{\sum_j Q_j^n} \tag{D.32}$$

where ϕ_1^{n+1} is the concentration in the first node after the time step, and $\phi(C)_N^n$ is advected concentration as per (D.22) for the last or N$^{\text{th}}$ element in all j upstream contributing grids, and Q_j is the contributing flow rate for each of the upstream contributing grids. Grids with no upstream nodes are assumed to have no contributing upstream concentrations.

Advection of the gradients is performed in an identical manner taking the flow weighted average of the last element of all upstream grids.

$$\phi'^{\,n+1}_{\,1} = \frac{\sum_j \left(\phi' \, (C)_N^n|_j \, Q_j^n \right)}{\sum_j Q_j^n} \tag{D.33}$$

where $\phi' \, (C)_N^n$ is the advected upstream gradient as per (D.27) for the last or N$^{\text{th}}$ element in all j upstream contributing grids.

Crank-Nicholson Implicit Scheme Formulation

The Crank-Nicholson Implicit Scheme is employed to solve the diffusion equation over the elements within a grid. The Crank-Nicholson scheme operates on the diffusion equation in isolation:

$$\frac{\partial \phi}{\partial t} = D \frac{\partial^2 \phi}{\partial x^2} \tag{D.34}$$

where the (D.34) is disretized temporally using a forward-time approach and spatially using a centered space approach, but taking the average of the current and future solutions to the centered-space solution

$$\frac{\phi_i^{n+1} - \phi_i^n}{\Delta t} = \frac{D^{n+1}}{2} \frac{\phi_{i+1}^{n+1} - 2\phi_i^{n+1} + \phi_{i-1}^{n+1}}{\Delta x^2} + \frac{D^n}{2} \frac{\phi_{i+1}^n - 2\phi_i^n + \phi_{i-1}^n}{\Delta x^2} \tag{D.35}$$

Equation (D.35) can be simplified to separate the known current time step values with the unknown future time step values

$$\phi_i^{n+1} - \frac{D^{n+1}\Delta t}{2\Delta x^2}\left(\phi_{i+1}^{n+1} - 2\phi_i^{n+1} + \phi_{i-1}^{n+1}\right) = \phi_i^n + \frac{D^n\Delta t}{2\Delta x^2}\left(\phi_{i+1}^n - 2\phi_i^n + \phi_{i-1}^n\right) \tag{D.36}$$

which provides a tri-diagonal system of N equations where N is the number of elements within a grid. The tri-diagonal system of equations is solved using the Thompson algorithm described by Press et al. (1992).

The gradients must also be dispersed and are done so using an equation similar to (D.36) shown below in (D.37).

$$\phi'^{n+1}_i - \frac{D^{n+1}\Delta t}{2\Delta x^2}\left(\phi'^{n+1}_{i+1} - 2\,\phi'^{n+1}_i + \phi'^{n+1}_{i-1}\right) = \phi'^{n}_i + \frac{D^n\Delta t}{2\Delta x^2}\left(\phi'^{n}_{i+1} - 2\,\phi'^{n}_i + \phi'^{n}_{i-1}\right) \tag{D.37}$$

Crank-Nicholson Boundary Conditions

A flexible boundary condition specification was implemented for the Crank-Nicholson scheme. Equation D.38 parameterizes the boundary conditions for the upstream and downstream ghost nodes to force the required boundary conditions.

$$\phi_{BC} = \frac{\gamma\Delta x - \beta\phi}{\alpha\Delta x - \beta} \tag{D.38}$$

where ϕ_{BC} is the boundary condition (ghost node) value for the concentration, ϕ is the value of the node adjacent to the boundary, Δx is the distance between ϕ_{BC} and ϕ and α, β, and γ are constants passed to the algorithm to determine the character of the boundary conditions.

For this application of the SOLROUTE routine the boundary condition for the Crank-Nicholson was set to a zero-gradient at the grid boundaries for both the constituent concentrations and gradients ($\alpha = 0$, $\beta = 1$ and $\gamma = 0$) which is equivalent to the zero gradient considerations for the QUICKEST scheme described above. This can be justified if the transport processes are dominated by advective processes, which is true in most fluvial systems, and the sub-discretization of the channel reaches within the grid is of a fine enough resolution to capture the dispersive processes within each grid.

HPCN Initial Conditions

The concentrations are required as an initial condition and are provided as part of the initialization code within the SOLROUTE library, however the derivatives must also be known at each point within the computational domain. This was accomplished using a second order accurate finite difference approximation within the sub-grid domain and a first-order approximation at the grid boundaries as illustrated in (D.39) to (D.41) below.

$$\left.\frac{\partial \phi}{\partial x}\right|_i = \frac{\phi_{i-1} - \phi_{i+1}}{2\Delta x} \tag{D.39}$$

$$\left.\frac{\partial \phi}{\partial x}\right|_1 = \frac{\phi_1 - \phi_2}{\Delta x} \tag{D.40}$$

$$\left.\frac{\partial \phi}{\partial x}\right|_n = \frac{\phi_{n-1} - \phi_n}{\Delta x} \tag{D.41}$$

HPCN Stability

The Holly-Preissmann scheme is stable provided that the trajectory origin lies between the two computational elements in the above calculations. That is, the Courant number is less than or equal to one. The stability criteria of this algorithm is fortuitous with regards to WatFlood integration, as the routing model has an identical stability criterion, and the time steps in WatFlood are adjusted to maintain this stability criterion during normal hydraulic routing. The implicit Crank-Nicholson scheme is unconditionally stable so does not restrict the spatial or temporal discretization of the overall HPCN split operator scheme.

D.2.4 Contaminant Transport Model Performance Evaluation

Sub-Grid Solute Routing - Unit Test 1

The first routing unit test was a instantaneous point-loading advection-dispersion simulation within a single grid. Figure D.3 illustrates the differences between the three routing

algorithms with a modelled Courant number of 0.75, a Péclet number of 12.5, for 80 time steps of 15 seconds. The domain was 10km long with 50m grid sizes. These values were selected because they fit within the stability envelopes for all schemes. Figure D.3 shows that the storage routing was the least accurate with both the dispersion and timing of the constituent cloud very different from the analytical solution. The QUICKEST and HPCN routing routines were indistinguishable from the analytical solution on this figure. The storage routing model can expect to produce different contaminant concentration profiles based on the number of time steps taken

Mass conservation is of critical importance with the development of a water quality model. Figure D.4 illustrates the degree of mass conservation as a relative error over the computational domain for each of the routing schemes based on the parameters indicated above. The Storage routing scheme displayed an unacceptable degree of error in conservation of mass with over 10% error developing as the contaminant was routed downstream. The solute mass was shown to change continuously which is due to a regular reduction in modelled mass after a Gaussian-like profile develops. The QUICKEST model performed next best with a 0.002% approximate maximum error and the HPCN model showed an even greater degree of mass conservation accuracy with 0.0005% mass error, which approached the precision limit of the model state variables.

Figure D.5 illustrates the relative differences in the concentration profiles from the analytical solution in terms of relative error compared to the analytical peak concentration (C_{sp}) for the HPCN and QUICKEST algorithms. For the above test there was an error of approximately 2 % at the peak (overestimation) for the HPCN model and about 0.7 % relative error for the QUICKEST model (underestimation).

Sub-Grid Solute Routing - Unit Test 2

The second routing unit test was a instantaneous step-loading advection-dispersion simulation within a single grid. Figure D.6 illustrates the responses of the three routing algorithms with a modelled Courant number of 0.75, a Péclet number of infinity (Pe=∞ or no diffusion), for 80 time steps of 15 seconds. The domain was 10km long with 50m grid sizes. Figure D.6 shows that the storage routing again represented the least accurate

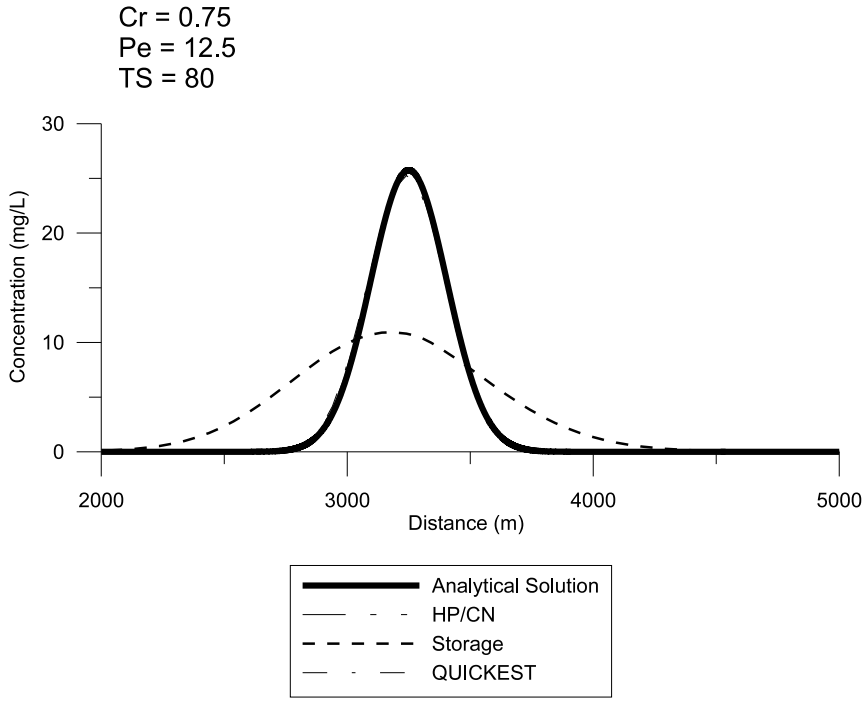

Figure D.3: Routing Profile Comparison - Point Constituent Addition of 200 at X=200m, Cr=0.75, Pe=12.5, Timestep = 15sec, Number of timesteps=80

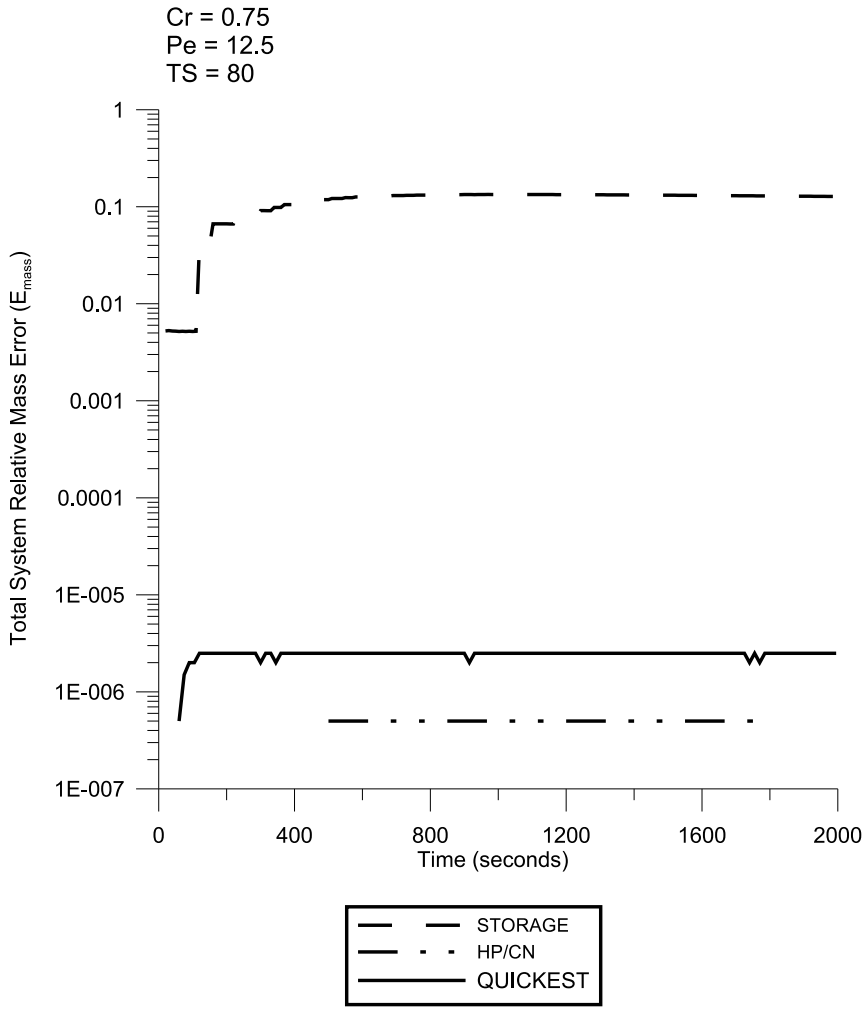

Figure D.4: Mass Conservation Comparison - Point Constituent Addition of 200 at X=200m, Cr=0.75, Pe=12.5, Timestep = 15sec

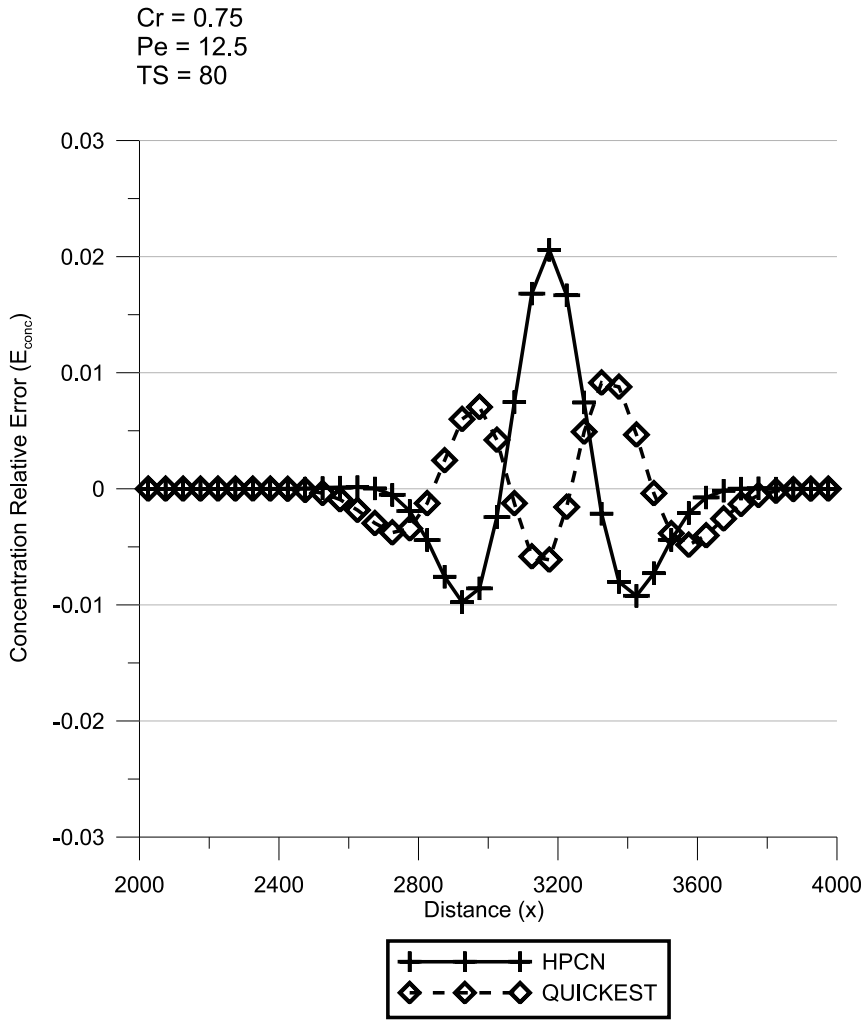

Figure D.5: Profile Error - HPCN and QUICKEST Routines - Point Constituent Addition of 200 at X=200m, Cr=0.75, Pe=12.5, Timestep = 15sec

scheme with both the dispersion and timing of the constituent cloud very different from the analytical solution with no clear ability to match the step loading, The QUICKEST and HPCN routing routines were much closer to the analytical solution both have predicted "wiggles" at the front and back of the step wave where the gradients are greatest.

Figure D.7 illustrates the degree of mass conservation as a relative error over the computational domain for each of the routing schemes based on the parameters indicated above. The Storage routing scheme again displayed the highest degree of error in conservation of mass with fluctuating error but with maximum error over 1% developing as the contaminant is routed downstream. The low error point in the storage routing mass conservation profile coincides with the point the error shifts from a positive error to a negative error. This explains the sharp point at approximately 700 seconds which appears because negative values cannot be shown on logarithmic plot. After this point the profile grows steadily in a similar manner to Figure D.3 and represents a steady reduction in modelled mass. The QUICKEST and HPCN models both performed similarly regarding mass conservation with a steady mass error near 0.02%.

A closer look at the error of the QUICKEST and HPCN routines as compared to the exact solution is shown in Figure D.8. This figure shows the step was modelled very well except for the sharp gradients which the two routines required several computation elements to resolve. The "wiggles" are characterised in Figure D.8 by the oscillations around the locations of the sharp fronts. The HPCN model showed better success in modelling the sharp advective fronts with a lower relative error than the QUICKEST model. Also the extent of the oscillations was reduced in the HPCN model with fewer neighbouring elements adversely affected by the sharp gradient.

Grid-to-Grid Solute Routing - Unit Test 1

The ability of the selected contaminant transport models to accurately transport contaminants from an upstream grid to a another downstream grid as illustrated in Figure 7.5 is of particular importance for the WatFlood model, with such a large number of junctions present. The Grid-to-Grid unit tests were designed to examine the effects of junctions on the advection-diffusion models. The first test involved the advection of a step curve without

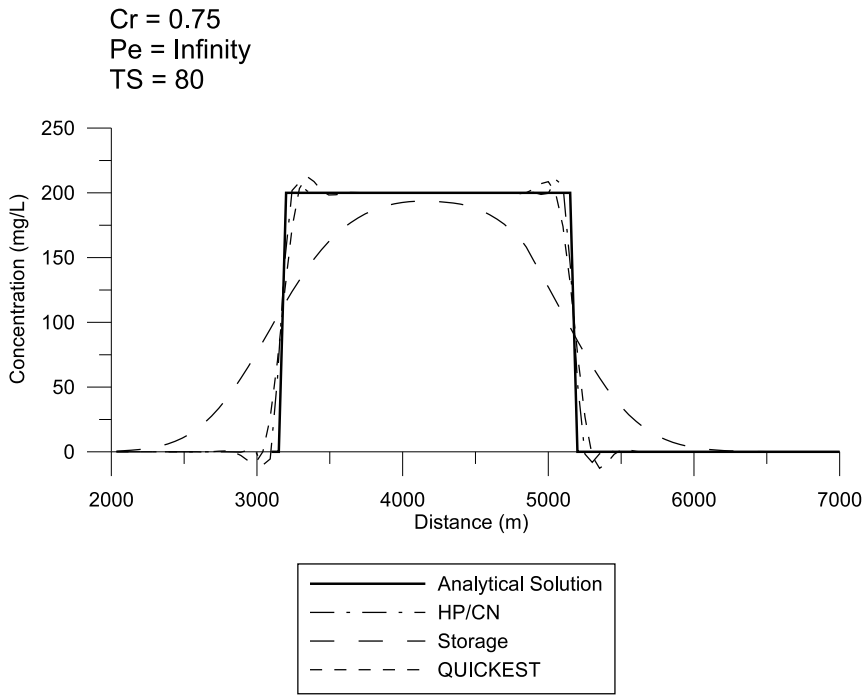

Figure D.6: Routing Profile Comparison - Step Constituent Addition of 200 from 125m - 2075m, Cr=0.75, Pe=∞, Timestep = 15sec

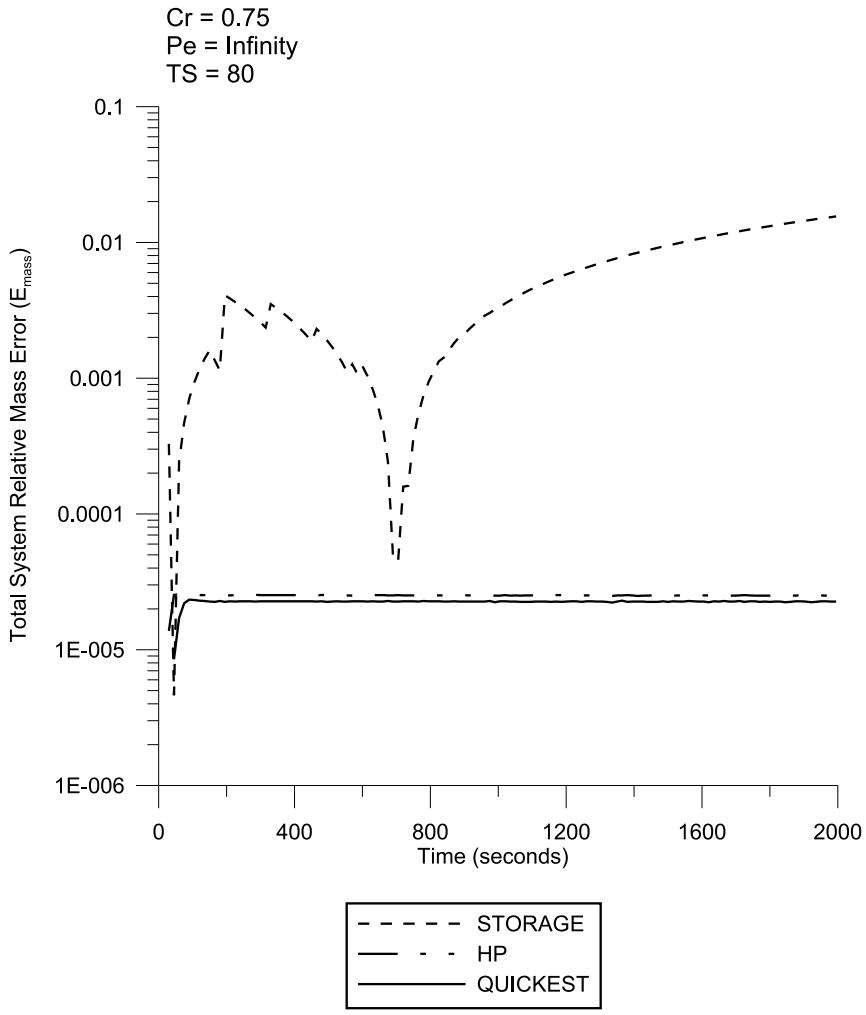

Figure D.7: Mass Conservation Comparison - Step Constituent Addition of 200 from 125m - 2075m, Cr=0.75, Pe=∞, Timestep = 15sec

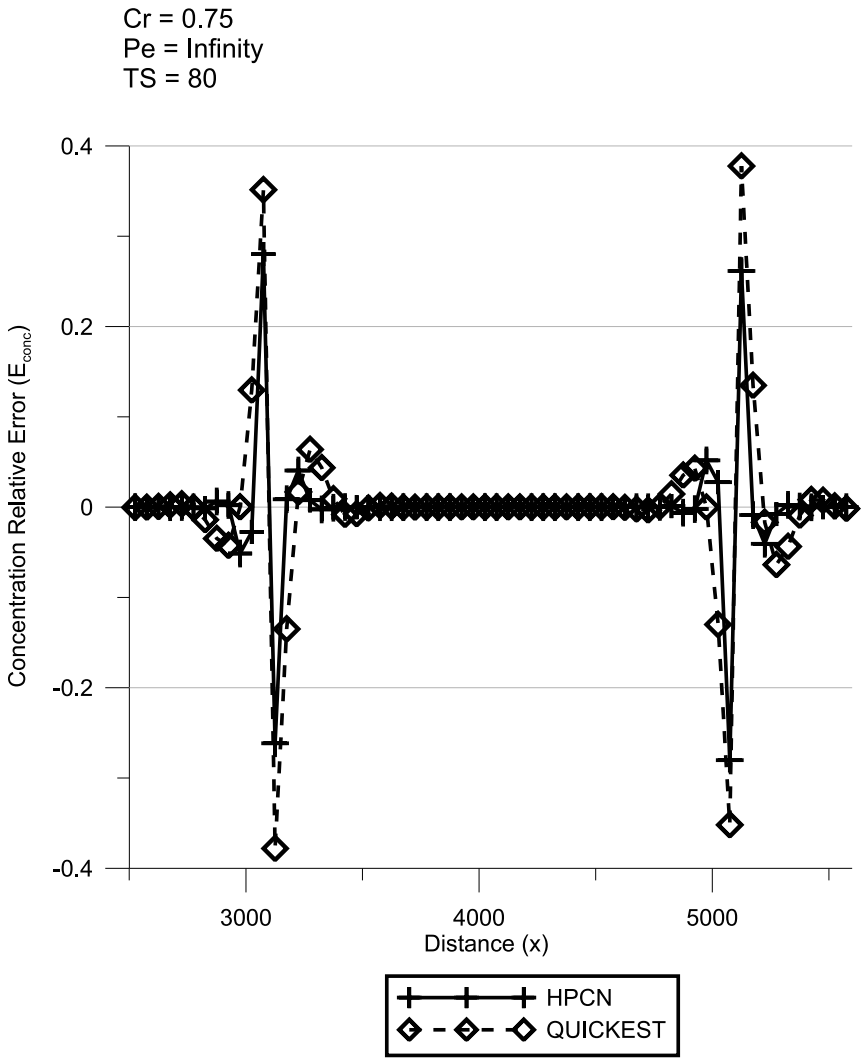

Figure D.8: Profile Error - HPCN and QUICKEST Routines - Step Constituent Addition of 200 from 125m - 2075m, Cr=0.75, Pe=∞, Timestep = 15sec

diffusion at a Courant number of one ($C = 1$). This condition provides a wiggle-free condition for both the QUICKEST and HPCN schemes within the grid solution domain. This unit test shows the impact of the interface formulations on the QUICKEST and HPCN schemes as they apply to pure advection. The profile progression from one grid to another for the three schemes is shown in Figure D.9 for three successive times with the plume wave moving from "Grid 1" to "Grid 2". The HPCN scheme showed complete preservation of the square wave, whereas the QUICKEST algorithm showed rounding at the sharp fronts due to the lower-order accuracy at the downstream edge of the grid interface. The storage routing algorithm showed a characteristic dispersion profile. A closer examination of the error in the profiles of the HPCN and QUICKEST scheme is shown in Figure D.10. The HPCN exhibits no error in the profile, whereas the QUICKEST showed a slightly earlier breakthrough with a general underestimation at the front and an overestimation at the back of the square wave following the steep gradients.

The mass conservation of the HPCN, QUICKEST and Storage routing schemes is shown in Figure D.11. The HPCN has no detectable error due to the exact profile conservation with a Courant number of unity. The QUICKEST scheme showed some error development as the sharp gradients moved across the grid boundary with a total mass error of approximately 0.0002 %. The Storage routing algorithm showed a similar error profile as shown previously. The grid boundary has no effect on the storage routing algorithm as the computation of the storage routing procedure does not change from the sub-grid test cases. The error for this algorithm remained close to 10 % with a steady loss of mass.

Grid-to-Grid Solute Routing - Unit Test 2

The second grid to grid unit test examined the effect of combined diffusion and advection across the grid boundaries. This is of particular importance considering the necessity to fix the grid boundaries to a zero gradient condition for both the HPCN and QUICKEST schemes. This test was identical to the advection-dispersion test conducted in the first sub-grid routing test (Sub-Grid Solute Routing - Unit Test 1), except the contaminant plume was permitted to cross the grid boundaries. The profile progression shown in Figure D.12 shows similar profile preservation across the boundary for both the HPCN and the

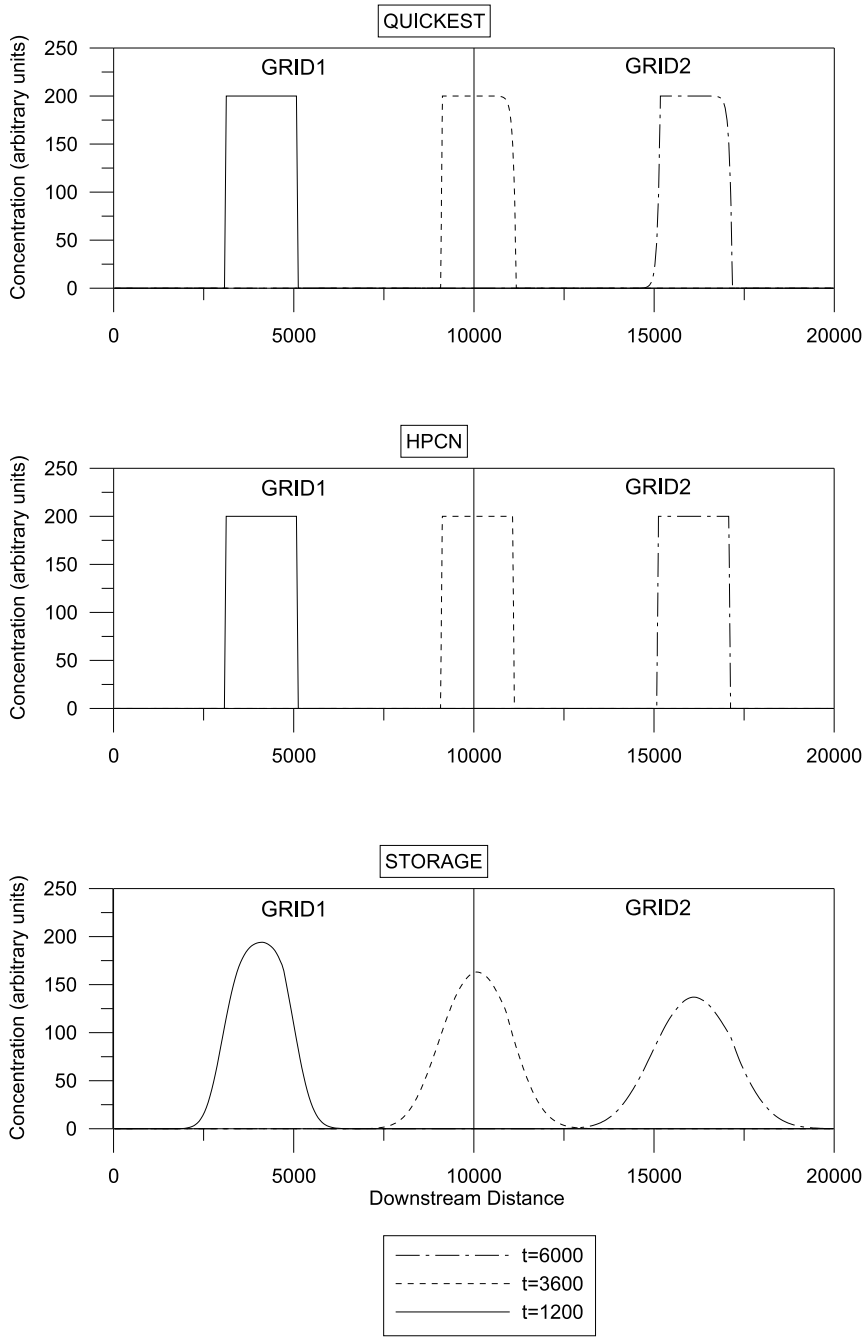

Figure D.9: Grid-to-Grid Profile Progression - Square Wave, C=1, α=0

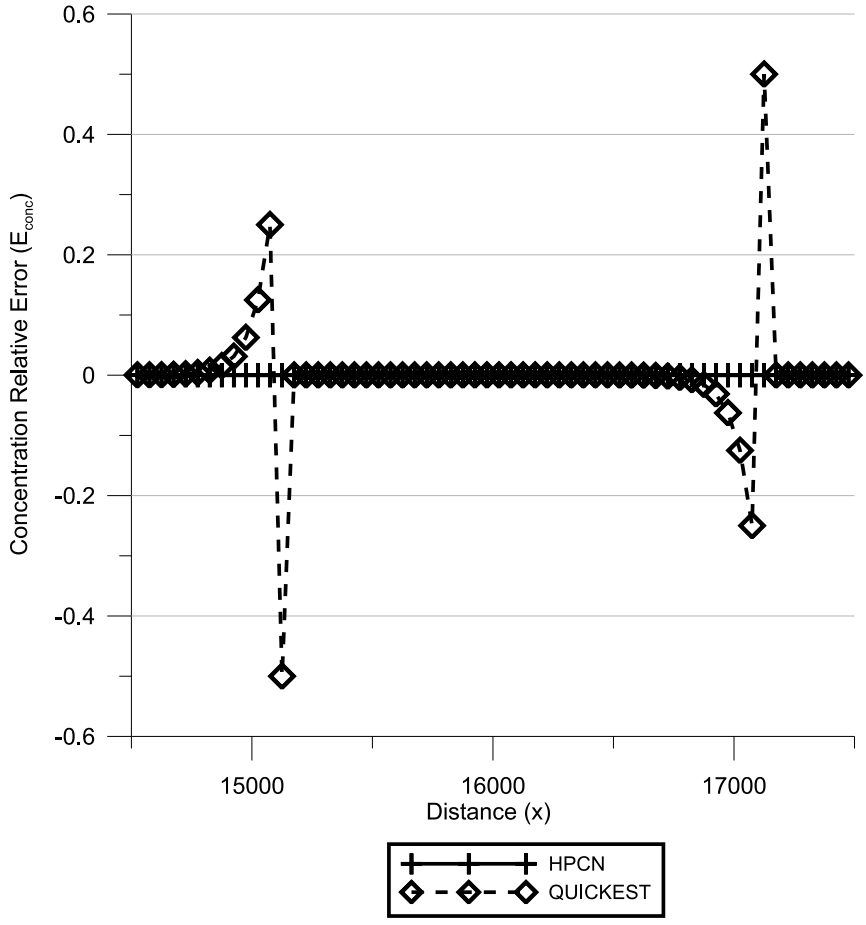

Figure D.10: Grid-to-Grid Profile Error Comparison - Square Wave, C=1, α=0, t=6000

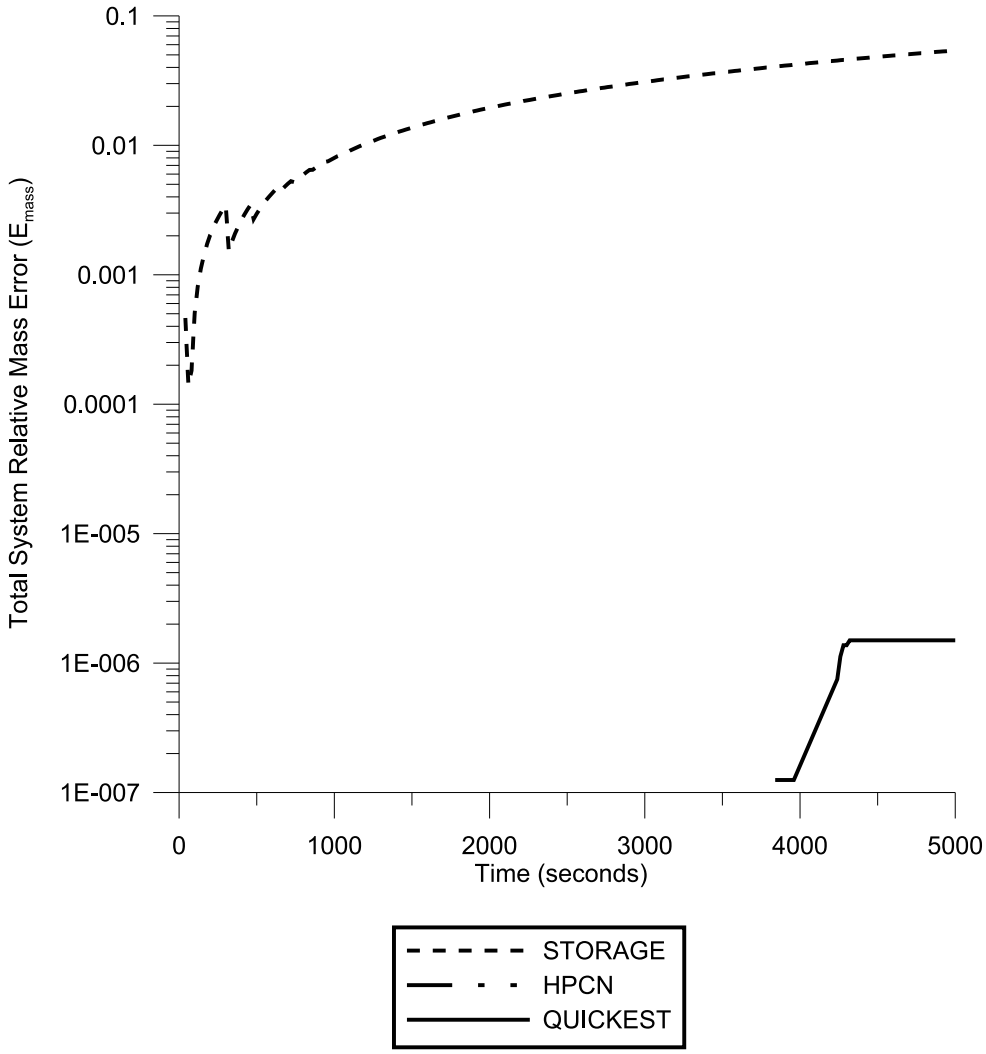

Figure D.11: Grid-to-Grid Mass Conservation - Square Wave, C=1, α=0

QUICKEST solution, with the Storage routing routine showing strong inaccuracies. A closer look at the grid boundary in Figure D.13 shows the HPCN routine over-estimated the peak and the QUICKEST routine under-estimated the peak at the boundary. The HPCN showed errors at the boundary due to the discontinuity in the advected profile caused by the application of Crank-Nicholson routine operating with a zero gradient boundary condition at the grid face. The QUICKEST scheme also showed some error here as expected, as the calculation of the advection at the boundary operated as a first-order upwind which dampened advection-dominated flows. A closer look at the error in the profile at the boundary in Figure D.14 shows the localization and extent of the error as the plume moves past the boundary. Of interest was the QUICKEST scheme error profile which was relatively balanced with positive and negative errors in the profile over the boundary. The HPCN scheme had predominantly positive, unbalanced errors.

The mass conservation analysis shown in Figure D.15 presents interesting findings when comparing the routines across the grid boundary. The HPCN and QUICKEST routines showed a good degree of accuracy for most of the simulation, and better than the storage routing in all cases. The QUICKEST scheme showed two sharp jumps in the total mass error, which occurred when the gradients were sharpest across the grid interface, which was expected considering the lower-order accuracy at the interface for this routine. The total error for the QUICKEST routine was about 0.01% for this simulation. However, the HPCN routine showed significant total mass error (close to 1%) as the plume moved across the face, after which the error decreased to a lower, more acceptable value (close to 0.001%). This error was alluded to when examining Figure D.14, above, where nearly all profile errors were positive as the plume moved across the gridface. This simulation shows the problem with using the Crank-Nicholson scheme with a concentration gradient boundary condition set to zero at the interface between the two grids, smoothing the profile and the gradients, and developing a discontinuity across the grid-face. The advection of this discontinuity then creates an error in mass calculations. As the profile is symmetric (or almost symmetric over time in which the plume is transported over the grid interface), most of the generated errors during the rising limb of the plume are "corrected" by balancing errors on the falling limb. Nevertheless, under different contaminant loading and hydraulic

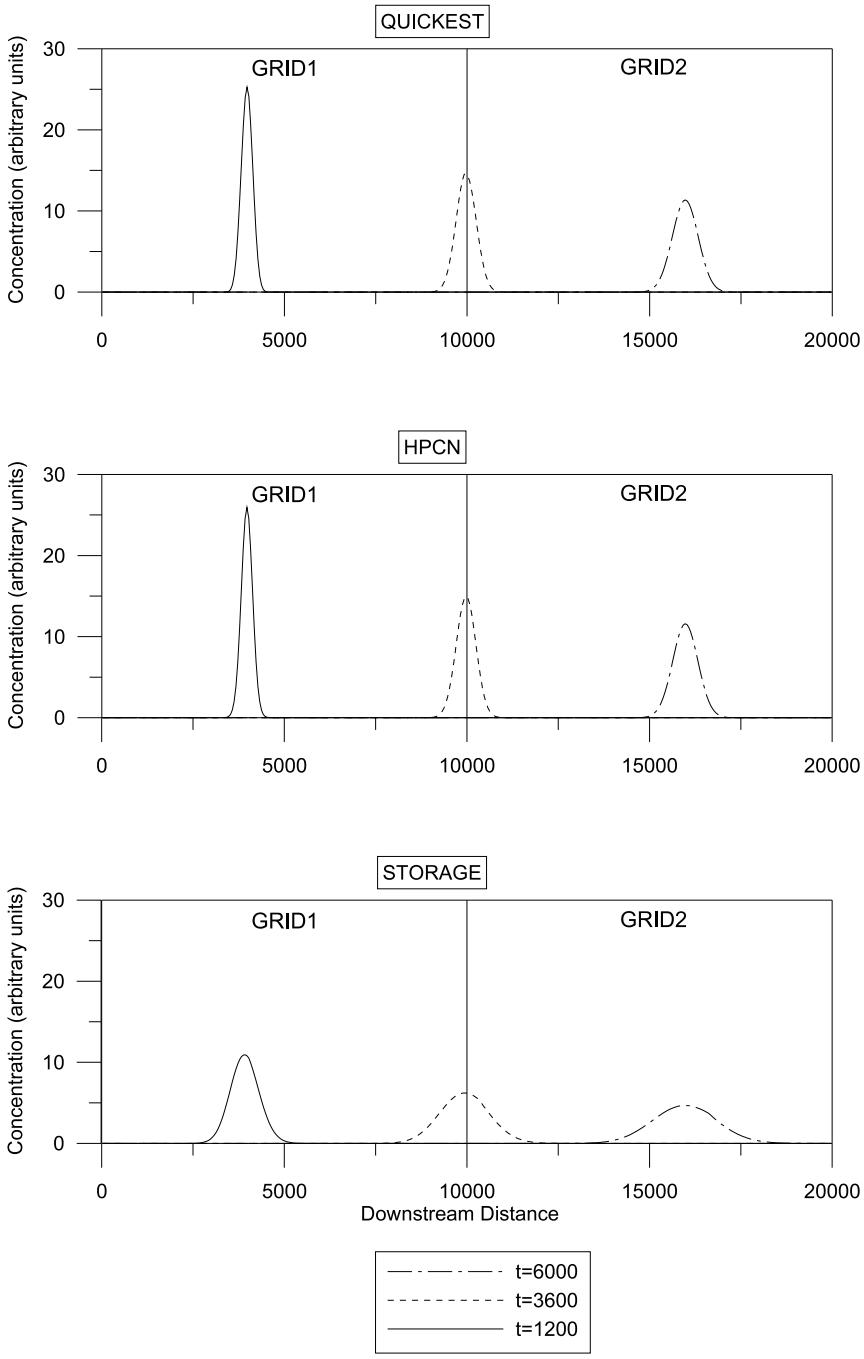

Figure D.12: Grid-to-Grid Profile Progression - Instantaneous Point Addition, C=0.75, Pe=12.5

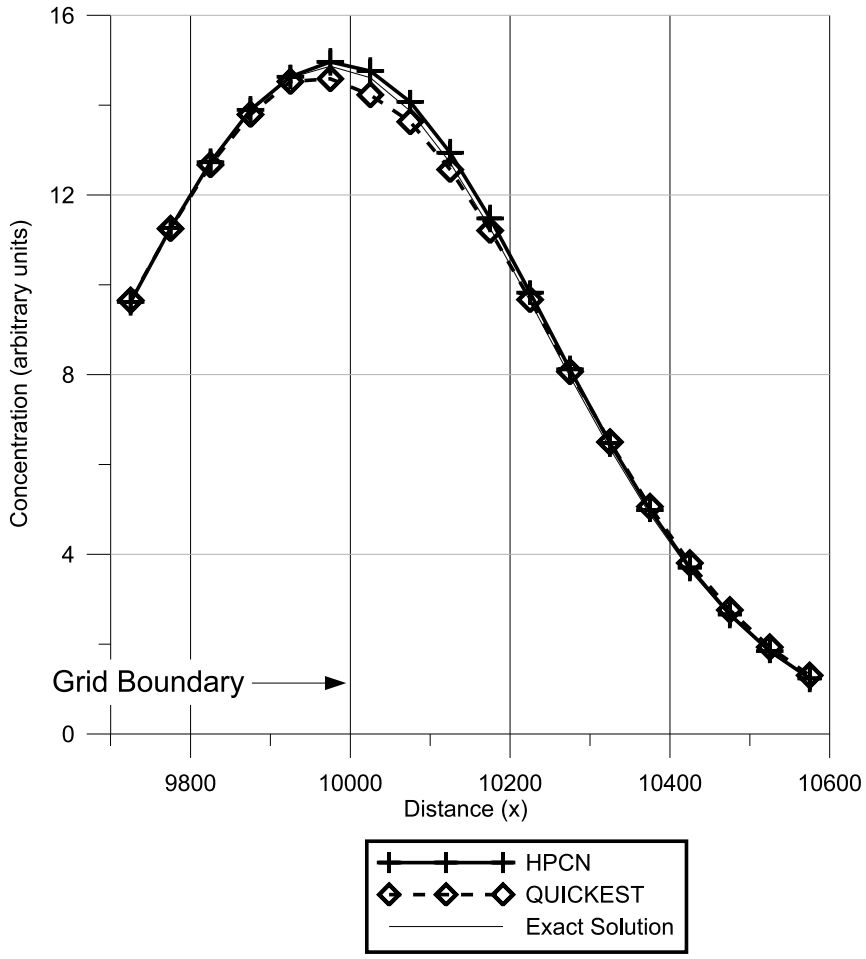

Figure D.13: Grid-to-Grid Profile at Grid Boundary - Instantaneous Point Addition, C=0.75, Pe=12.5, t=3600

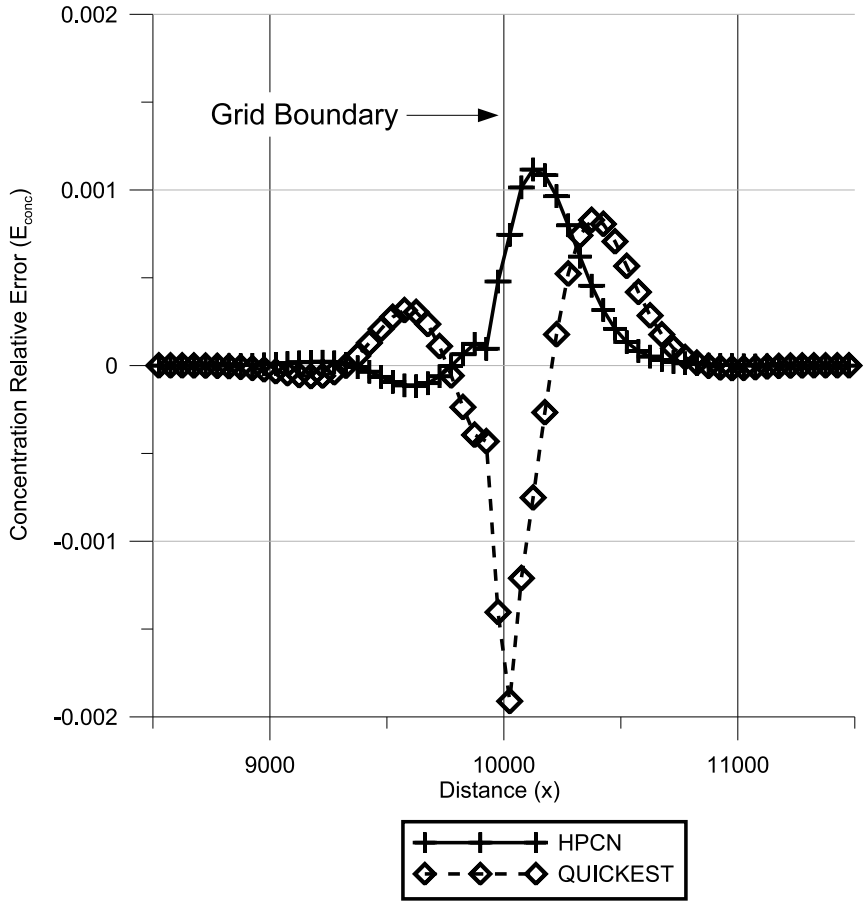

Figure D.14: Grid-to-Grid Profile Relative Error - Instantaneous Point Addition, C=0.75, Pe=12.5, t=3600

conditions mass errors in the HPCN routine could be expected to accumulate and persist.

D.3 In-Channel Sediment Transport Performance Evaluation

D.3.1 SOLROUTE Test Framework

The implemented suspended sediment resuspension and settling model outlined in (7.30) was compared to an analytical solution for the resuspension or settlement of the sediment. The analytical solution to (7.30) at a point along a stream corridor with an initial condition of $\phi_{sed}(x, t = 0) = 0$ produces (D.42) as a function of time, considering a uniform sediment concentration along the length of the channel

$$\phi_{sed}(t) = \phi_{sed\_max}\left(1 - e^{-(v_{sed\_res}t)/h}\right) \tag{D.42}$$

The results of the unit test for a number of time steps is shown in Figure D.16. The unit test results do validate the approach within the test framework as it can be seen that the numerical solution is almost indistinguishable from the analytical solution for the selected parameters and time steps. A closer look at the error within the concentration error profiles E_{conc} with the reference concentration being ϕ_{sed_max} (see Chapter 7, page 138 for definition) shows that the error does increase substantially with a larger time step but the solution does converge toward the exact solution with a more frequent time step. As expected with an Euler approach the routine will overstep during sharp gradients and this is observed in the error plots in Figure D.16.

Validating the sediment transport on a mass balance approach within the WatFlood model was not possible due to the lack of an analytical solution in that case.

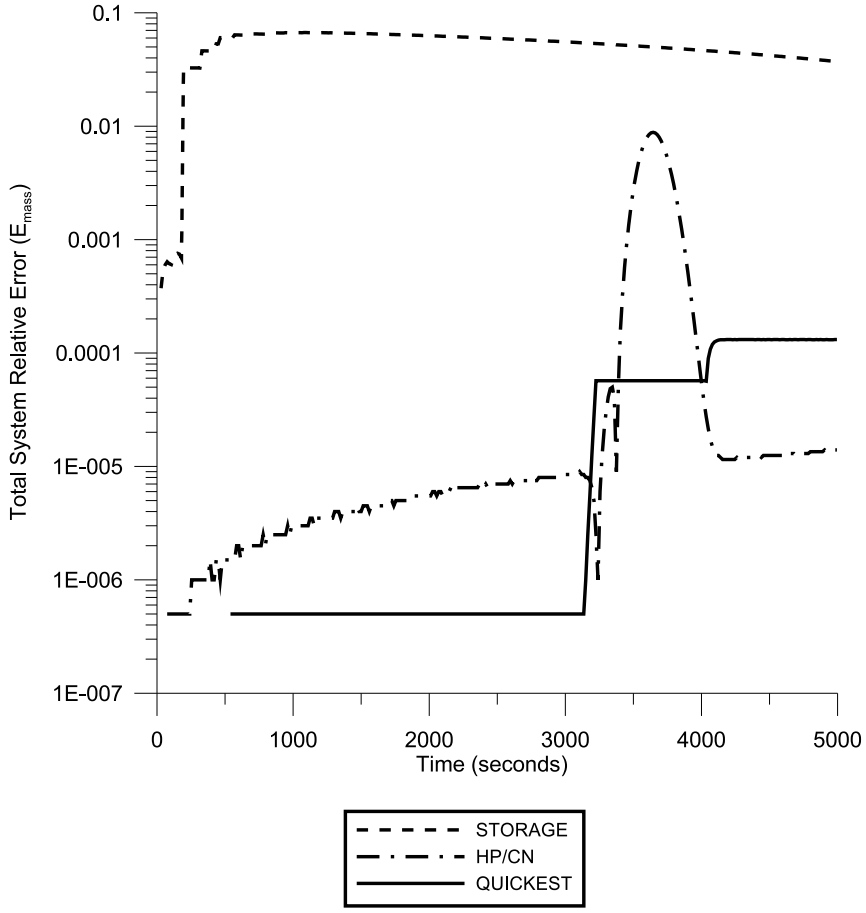

Figure D.15: Grid-to-Grid Mass Conservation - Instantaneous Point Addition, C=0.75, Pe=12.5

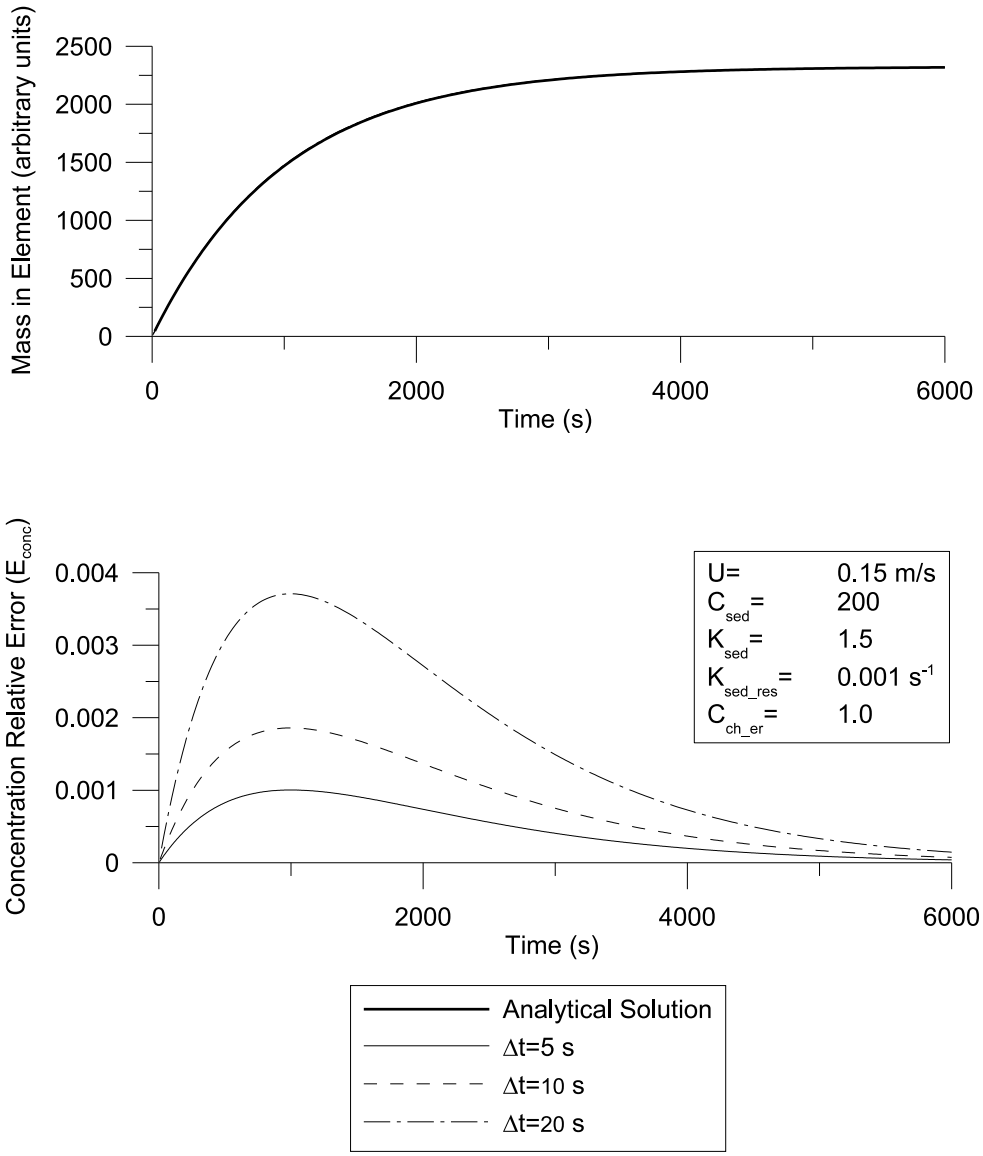

Figure D.16: Sediment Resuspension Test Case in SOLROUTE Framework - a) Resuspension Profile Comparison with Analytical Solution b) Relative Error by Time Step

D.4 In-Channel First-Order Decay Process Evaluation

SOLROUTE Test Framework

The first order decay routine was implemented in the test framework to validate the accuracy and correctness of the process as compared to analytical solutions. The results are presented in Figure D.17 for a point injection with advection, dispersion and decay across two grid cells. This test is identical to the one conducted in 7.2.9 for a point instantaneous constituent source over two grid cells, except with 1^{st}-order decay considered.

In Figure D.17a the decay of the point injection is clearly observed as the plume migrates along the channel and across the grids. Figure D.17b illustrates the close matching of the modelled solution with the analytical solutions at $t = 3600$ and Figure D.17c shows the small relative error in the solution at $t = 3600$.

The test framework also showed a good mass conservation when compared to the analytical solution for first order decay. Figure D.18 shows the total mass error of the simulation outlined above, both with and without the first order decay processes enabled. The QUICKEST mass conservation curve without decay is identical to the simulation presented in Figure D.15 on page 375. The addition of the decay processes to the QUICKEST model actually improves the accuracy when compared to the advection-dispersion model alone.

D.4.1 WatFlood Unit Test

In addition to a examination of the performance in a test framework, the decay equations were evaluated in the WatFlood model under a controlled test addition. The test was similar to the mass conservation test performed in the WatFlood model in Section 7.2.10, except with a known and constant decay coefficient.

A unit test was conducted in an identical way to Figure 7.9 with a point addition to the WatFlood Canagagigue Creek model but with a fixed decay rate of 0.0005 sec^{-1}. Comparison of the resulting constituent concentration profile has no analytical solution, but the total mass in the system should follow exactly the 1^{st}-order decay profile. The

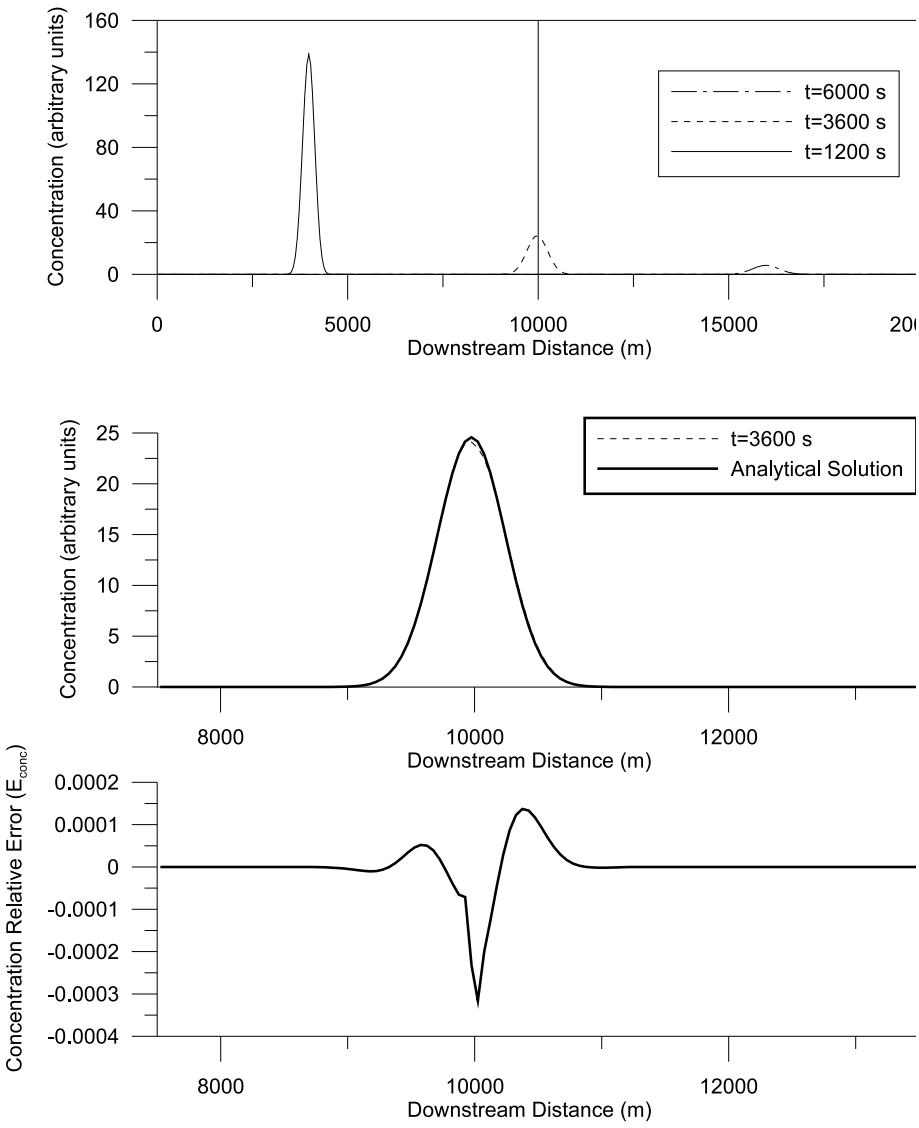

Figure D.17: First Order Decay - Test Framework - Point addition at x=1000 m, C=0.75, λ=0.0075, Pe=12.5 - a) Profiles at t=1200 s, t=3600 s and t=6000 s, b) comparison with analytical solution at t=3600 s c) Profile Error comparison at t=3600 s

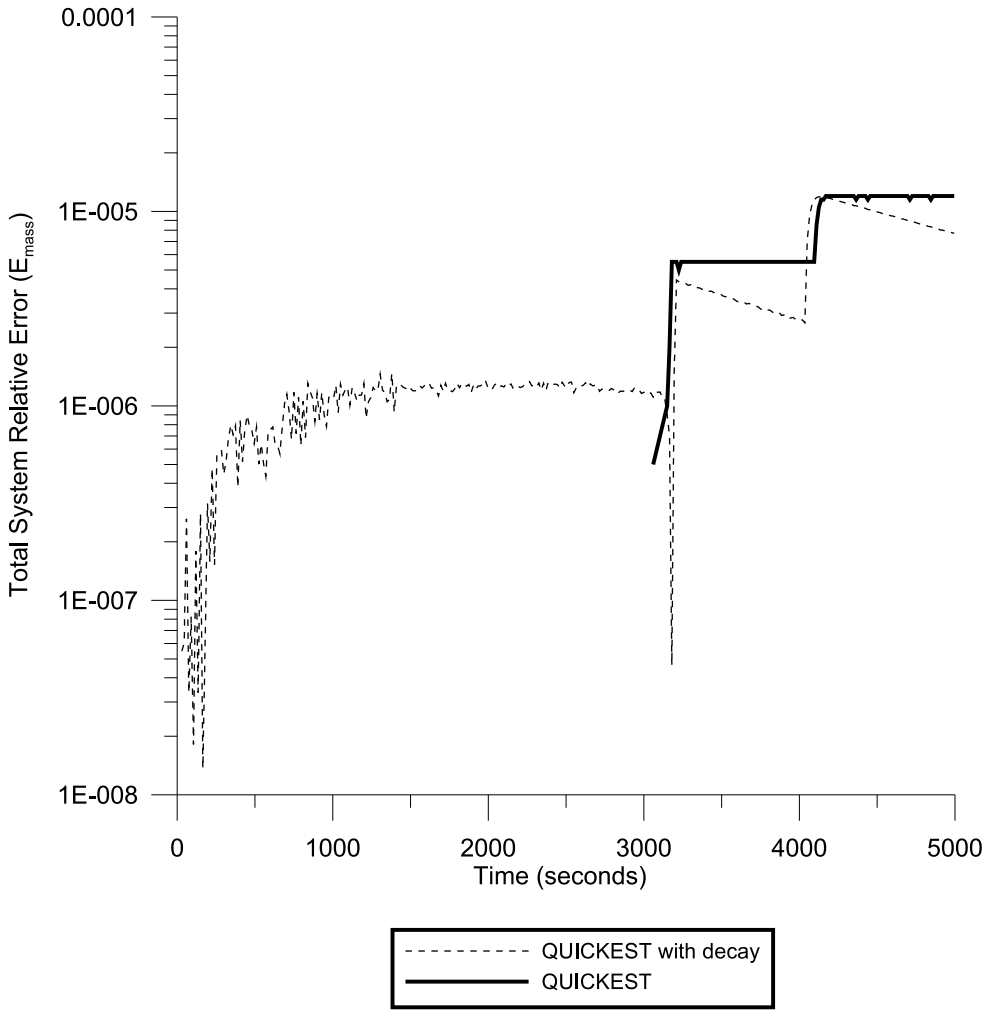

Figure D.18: Grid-to-Grid Mass Conservation - First Order Decay - Test Framework - Point addition at x=1000, C=0.75, Pe=12.5, λ=0.0075

WatFlood unit test results are shown in Figure D.19a which show the differences in the total mass in the system as compared to the analytical solution and Figure D.19b which shows the total error in the system as compared to the exact analytical solution. The legend identifies three QXX run types where XX is the number of sub-grid elements in the simulation. All sub-grid resolutions are indistinguishable from the analytical mass conservation solution in Figure D.19a and that the total mass error in the system never exceeds 0.1% for any of the sub-grid resolutions shown in Figure D.19b. The introduction of the decay process does not show any increase in the simulation error when compared with the QUICKEST simulation alone as illustrated in Section 7.2.10.

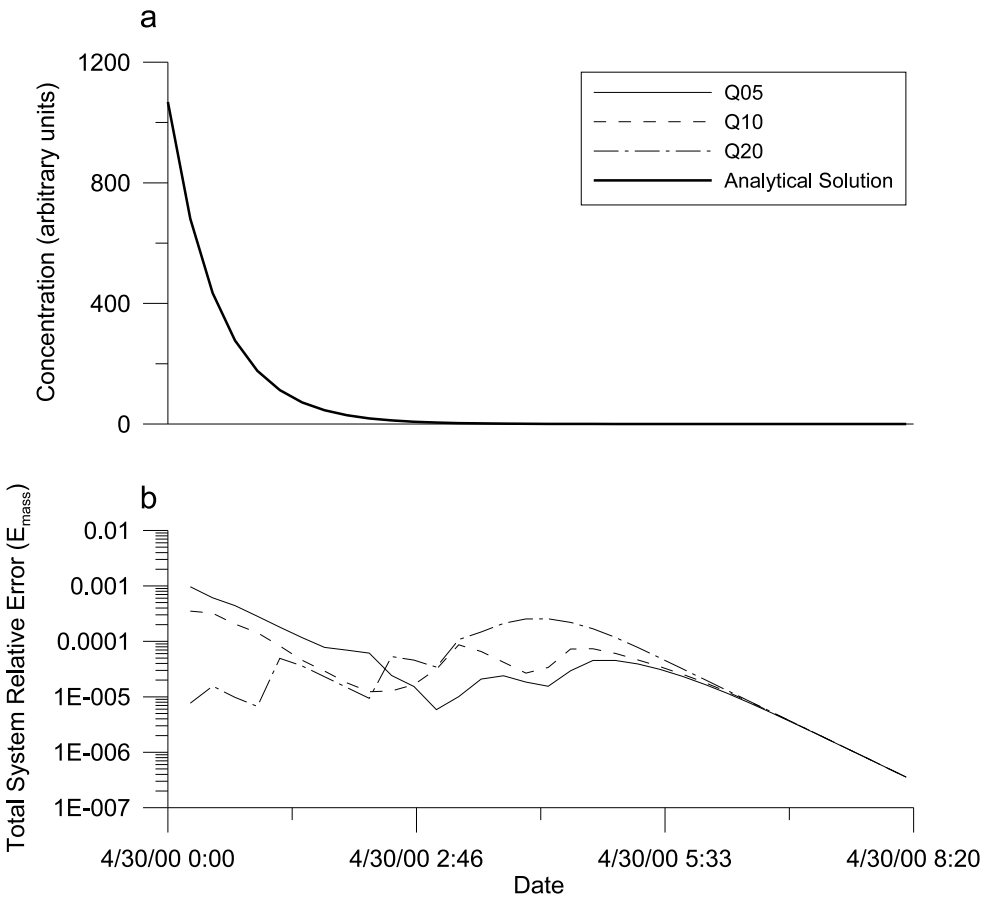

Figure D.19: QUICKEST Model in WatFlood with 1st-order decay (K=0.0005 sec^{-1} - Mass conservation with varied sub-grid element resolutions as compared to the analytical solution (a) and the total error in the system (b)

D.5 OMAFRA Fertilizer Loading Algorithm

The algorithm for loading organic and ammonia nitrogen to a GRU is illustrated in pseudocode in Figure D.20. This algorithm is interrogated hourly within the WATFLOOD model and is triggered on the first hour of a simulated day.

```
get date;
while is first day or last day of growing season do
    foreach GRU do
        if is first day of growing season then
            get ammonia and nitrate state variables ;
            get crop uptake rate : N_max ;
            get previous organic nitrogen applications ;
            calculate required nitrogen application: N_req ;
            get annual available manure nitrogen : N_man ;
            if N_req > N_man then
                apply 56% N_man ;
                apply N_req - N_man as ammonia;
            else
                apply 56% N_man ;
            end
        else
            apply 44% N_man ;
            apply calculated crop residual as organic nitrogen: N_resid ;
        end
    end
end
```

Figure D.20: Fertilizer Loading Algorithm

D.6 Water Quality Model Sensitivity

The sensitivity of the model was examined against the calibration objective function NOLS, and the total constituent loading over the study period. The adjusted parameters for the models are identified in Section 8.2 and Section 8.3. In addition the parameters adjusted in the WATFLOOD model are listed in Table D.1.

Parameter	Description	Units
	Channel	
lzf	Lower zone function factor	-
pwr	Lower zone function exponent	-
r1n	Overbank roughness (Manning's n)	-
r2n	Channel roughness (Manning's n)	-
mndr	Meander	-
aa2	Bankfull area - drainage area function coefficient	-
aa3	Bankfull area - drainage area function coefficient	-
aa4	Bankfull area - drainage area function coefficient	-
theta	Riparian wetland porosity	-
widep	Width - depth ratio	-
kcond	Riparian wetland conductivity	-
	Grouped Response Unit	
ds	Depression storage	mm
dsfs	Depression storage (snow)	mm
Re	Interflow recession constant	-
AK	Surface permiability	-
AKfs	Surface permiability (snow)	-
retn	Upper zone retention storage	mm
ak2	Drainage resistance parameter	-
ak2fs	Drainage resistance parameter (snow)	-
R3	Surface roughness	-
R3fs	Surface roughness (snow)	-
r4	Impervious area roughness	-
MF	Melt factor	mm/°C/hr
BASE	Base temperature for melt calculations	°C
NMF	Negative melt factor	-

Table D.1: WatFlood Hydrologic Parameter List

D.6.1 Sediment Model Sensitivity

The results from a 5% parameter perturbation sensitivity analysis outlined in Section 8.2.4 is presented here. Figure D.21 presents the absolute relative sensitivity of the model objective function values (NOLS and NASH) based on perturbations to sediment water quality model parameters. Figure D.22 presents the relative sensitivity of the model sediment loading estimates based on perturbatinos to sediment water quality model parameters. Figure D.23 presents the absolute relative sensitivity of the model objective function values (NOLS and NASH) based on perturbations to WatFlood hydrological model parameters. Figure D.24 presents the relative sensitivity of the model sediment loading estimates based on perturbatinos to WatFlood hydrological model parameters.

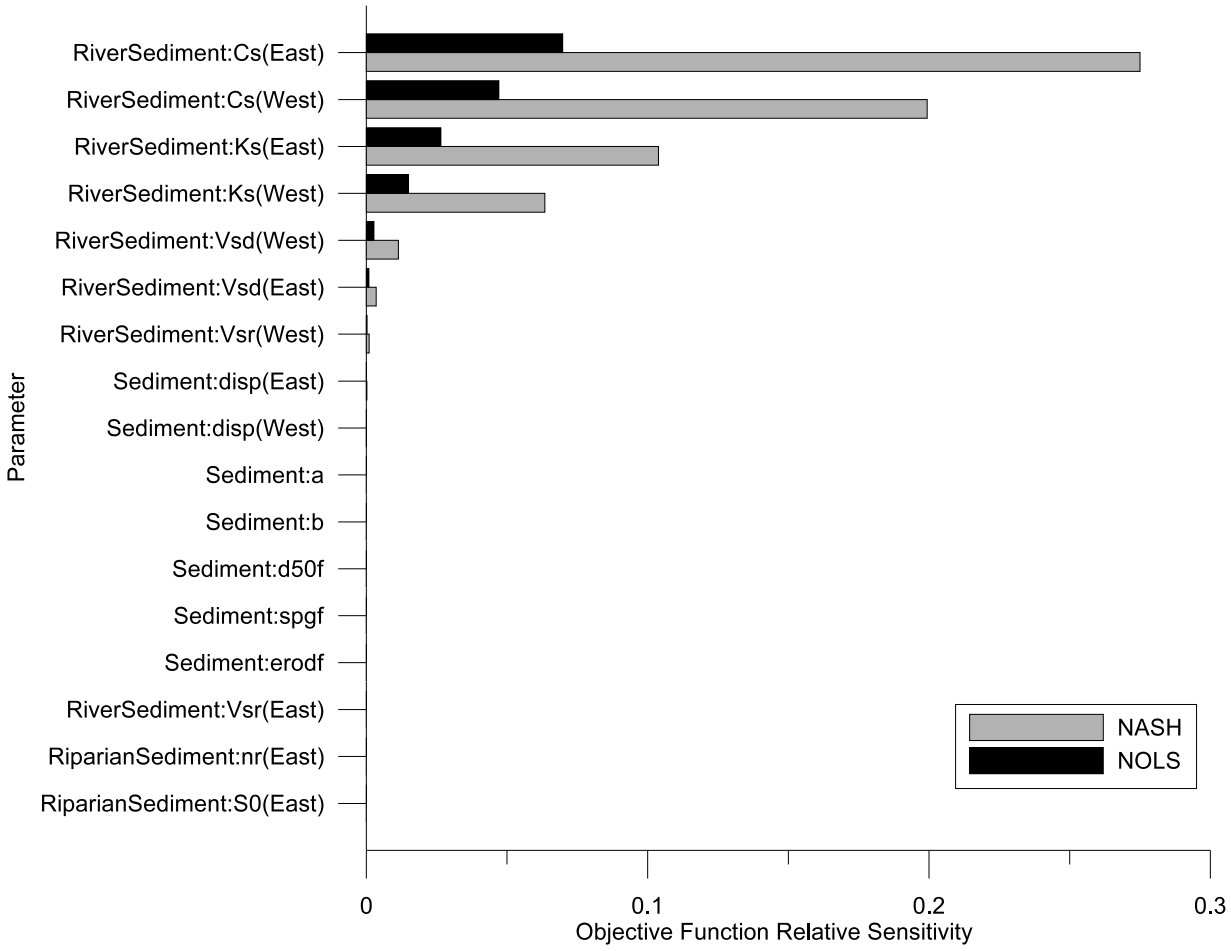

Figure D.21: Sediment Model Parameter Sensitivity - NOLS and NASH absolute sensitivity based on 5% parameter perturbation

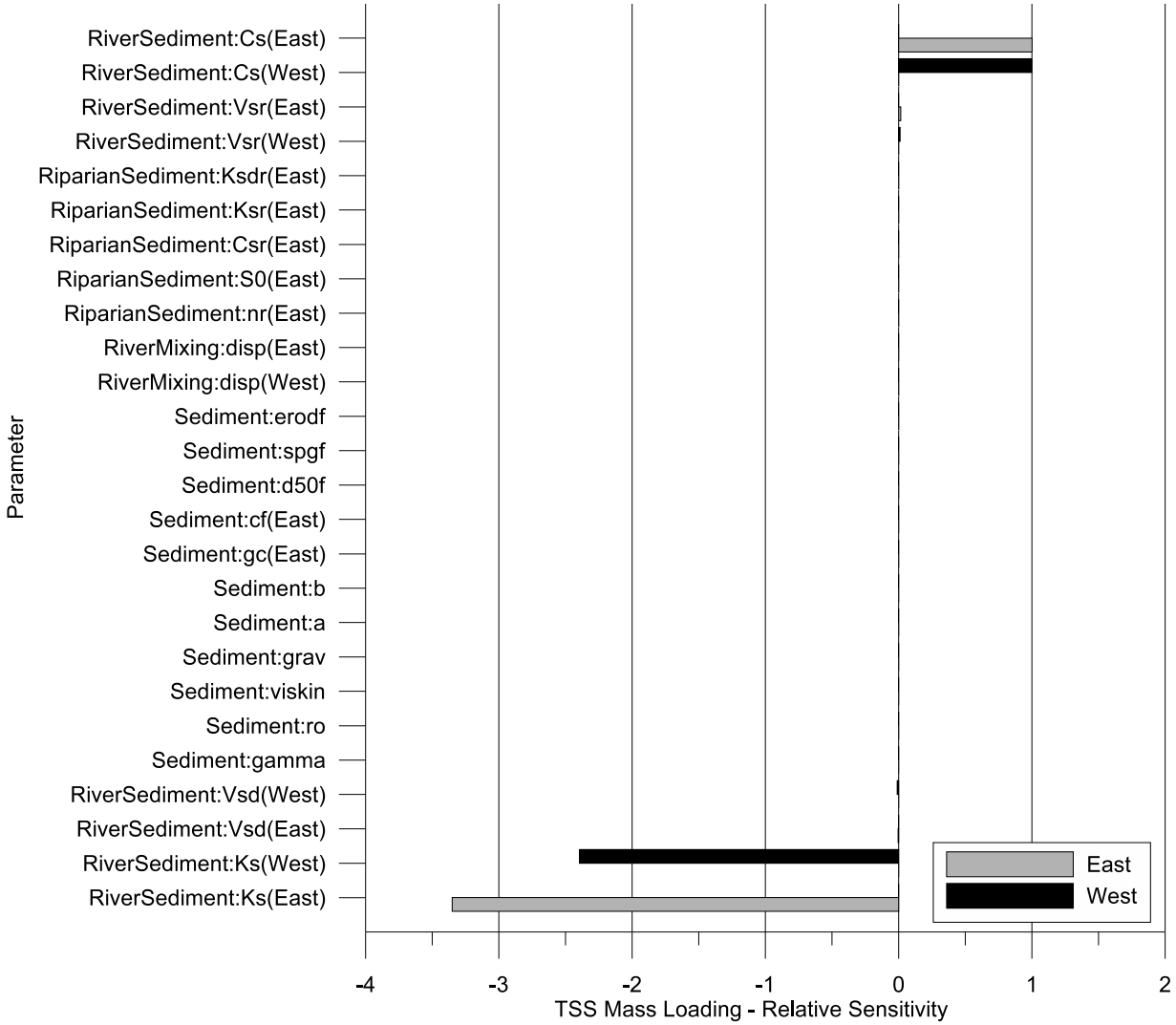

Figure D.22: Sediment Model Parameter Sensitivity - Total solids loading sensitivity by sub-basin based on 5% parameter perturbation

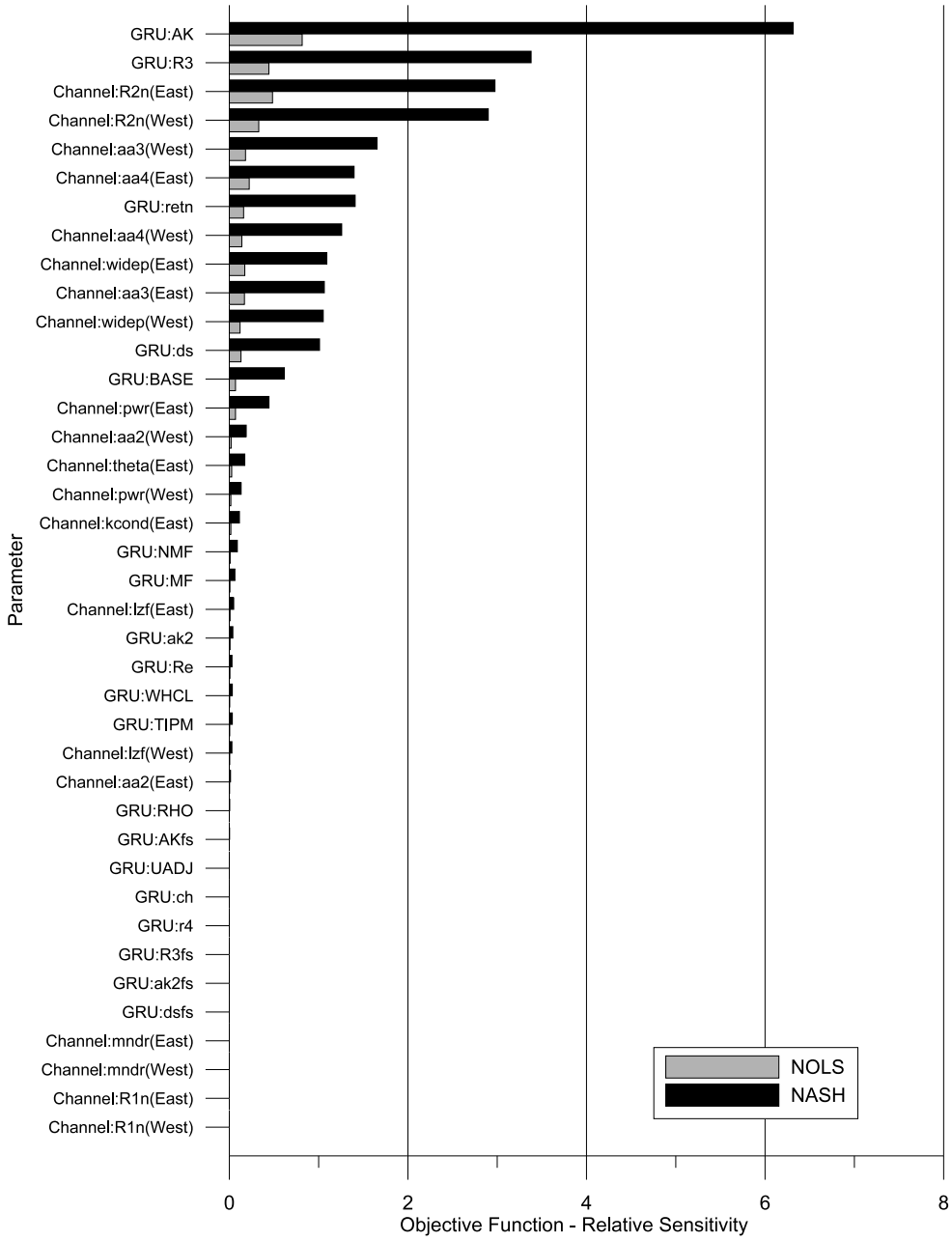

Figure D.23: Hydrologic Model Parameter Sensitivity - Sediment model NOLS and NASH absolute sensitivity based on 5% parameter perturbation

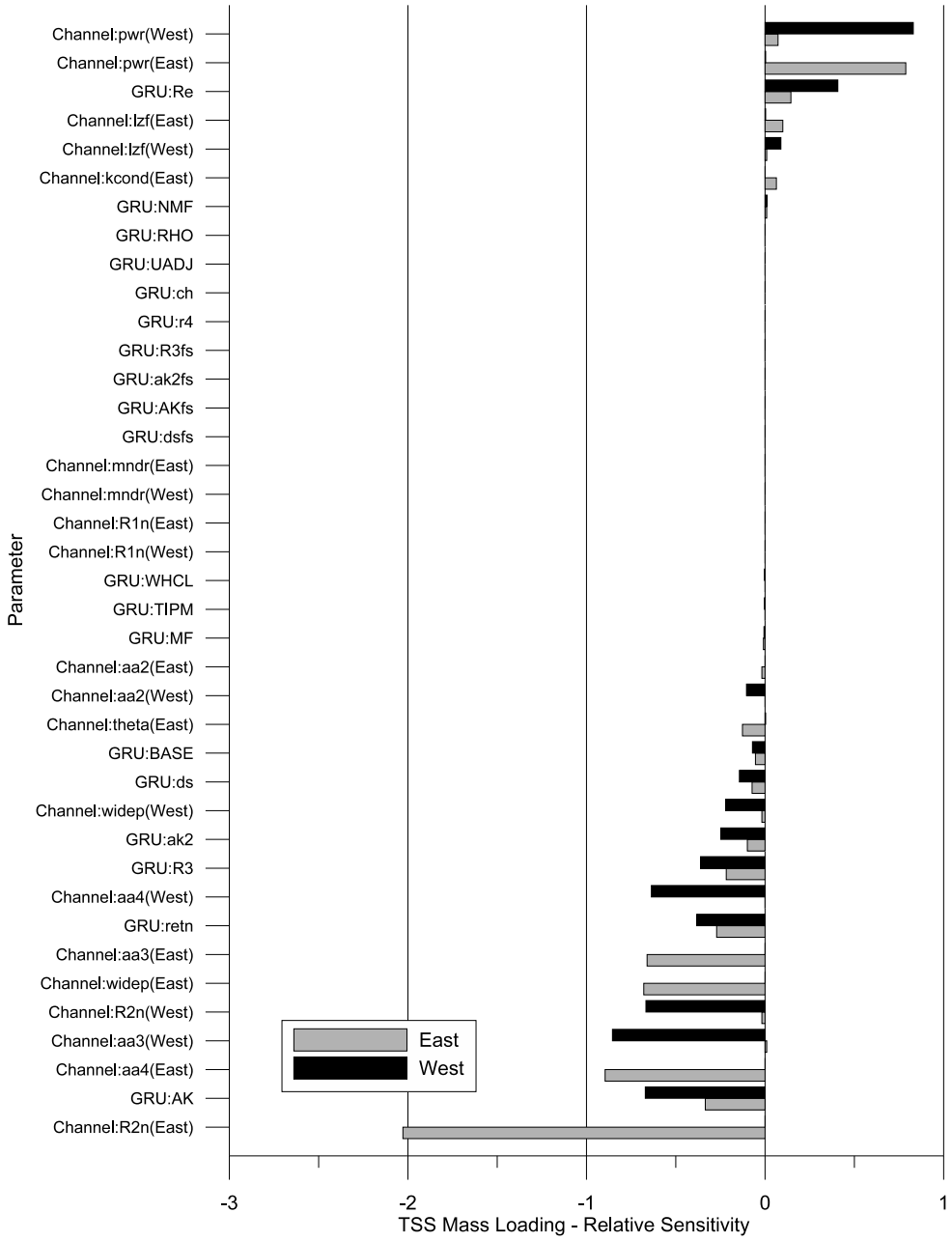

Figure D.24: Hydrologic Model Parameter Sensitivity - NOLS and NASH absolute sensitivity based on 5% parameter perturbation

D.6.2 Nitrate Model Sensitivity

The results from a 5% parameter perturbation sensitivity analysis outlined in Section 8.3.9 is presented here. Figure D.25 presents the absolute relative sensitivity of the model objective function values (NOLS and NASH) based on perturbations to nitrate water quality model parameters. Figure D.26 presents the relative sensitivity of the model nitrate loading estimates based on perturbatinos to nitrate water quality model parameters. Figure D.27 presents the absolute relative sensitivity of the model objective function values (NOLS and NASH) based on perturbations to WatFlood hydrological model parameters. Figure D.28 presents the relative sensitivity of the model nitrate loading estimates based on perturbatinos to WatFlood hydrological model parameters.

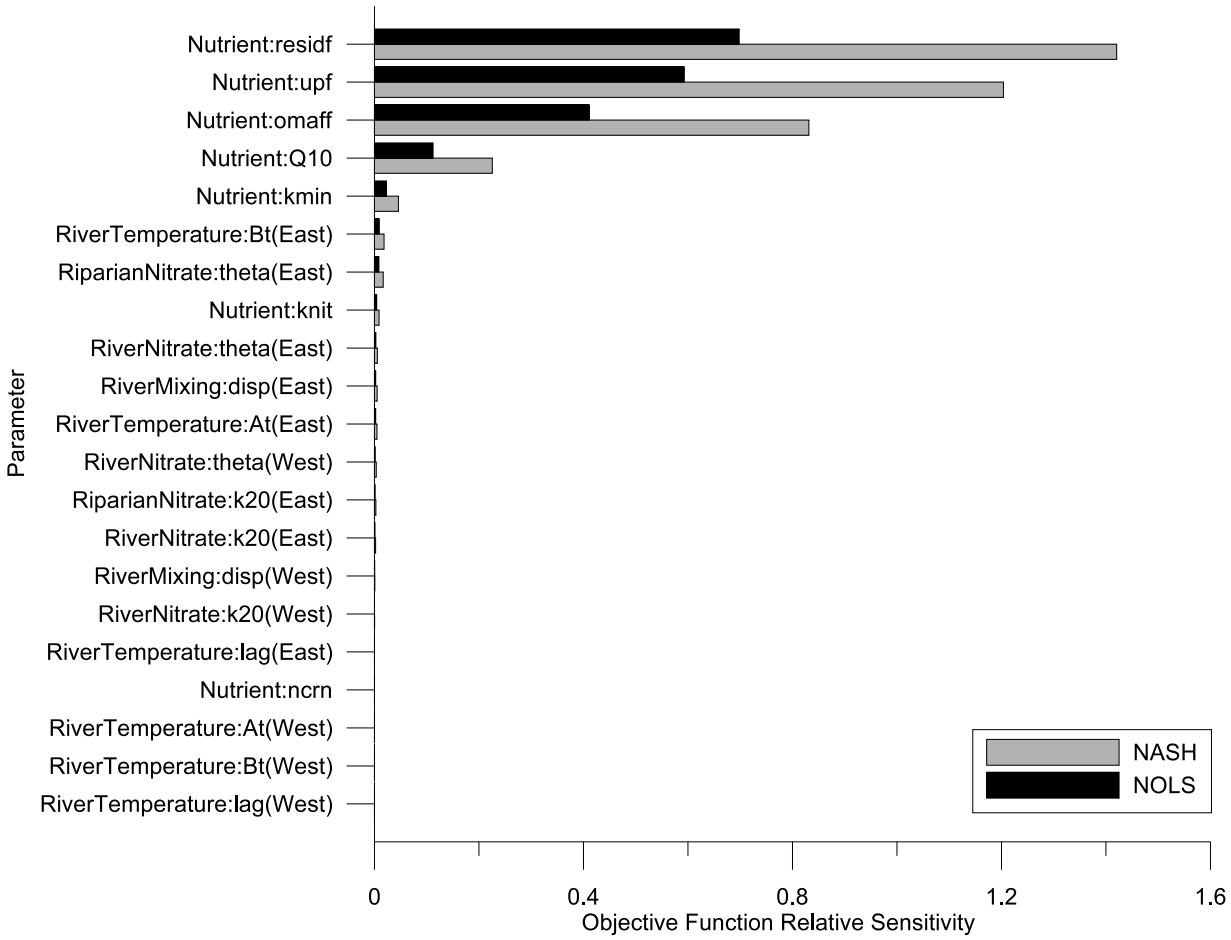

Figure D.25: Nitrate Model Sensitivity - Model performance absolute sensitivity by objective function based on 5% parameter perturbation

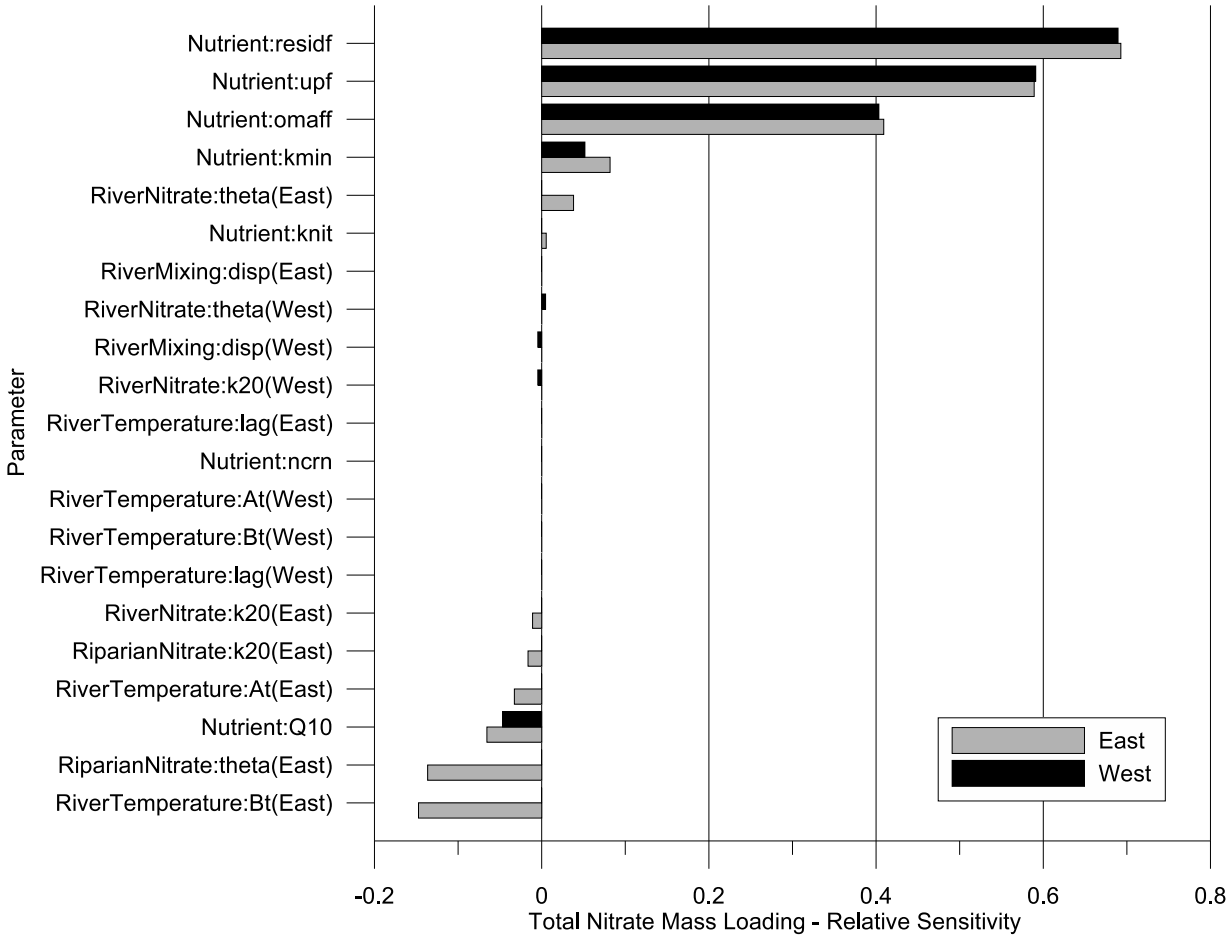

Figure D.26: Nitrate Model Sensitivity - Nitrate loading sensitivity by sub-basin based on 5% parameter perturbation (Jan 2005 – May 2007)

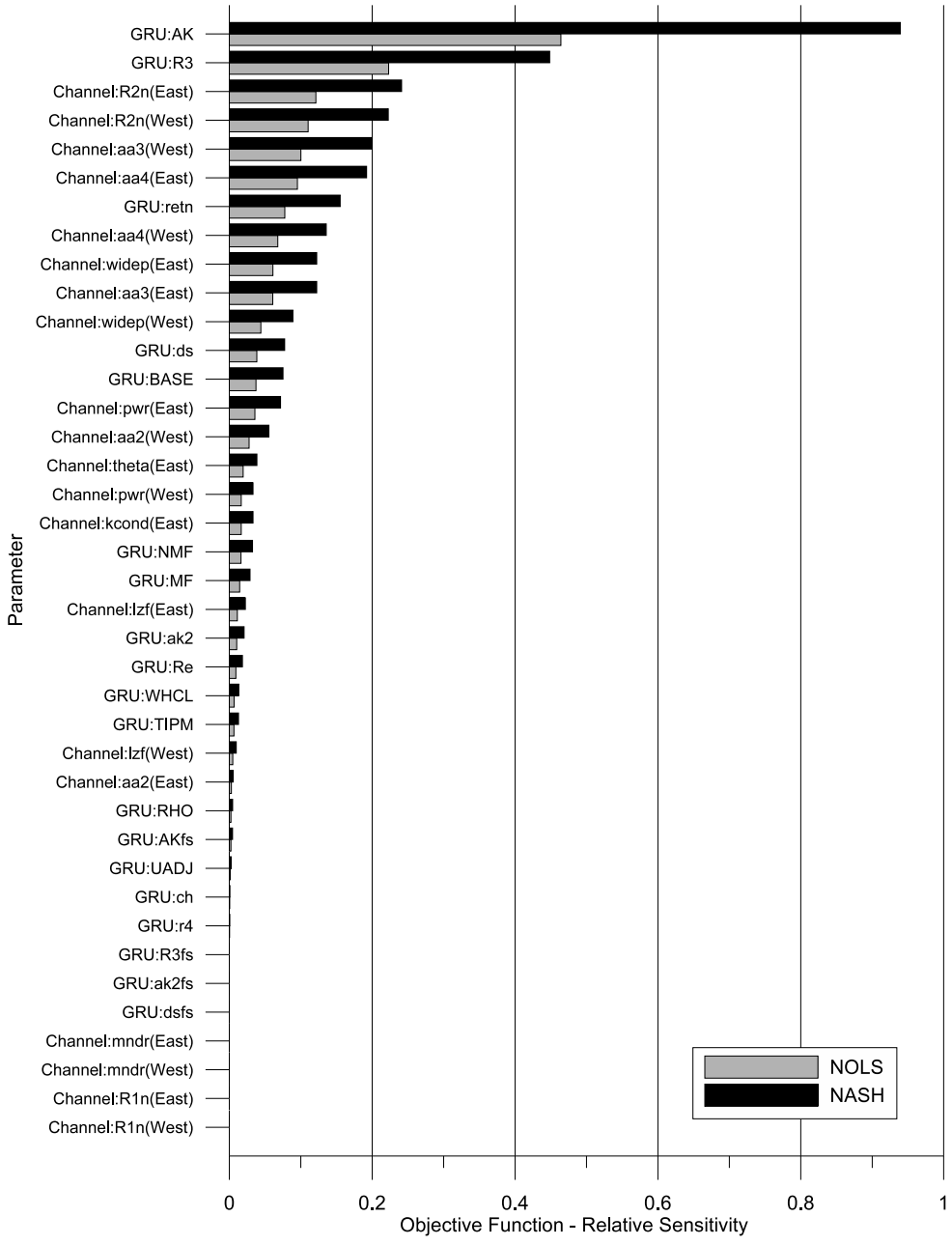

Figure D.27: Hydrologic Model Sensitivity - Model performance absolute sensitivity by nitrate objective function based on 5% parameter perturbation

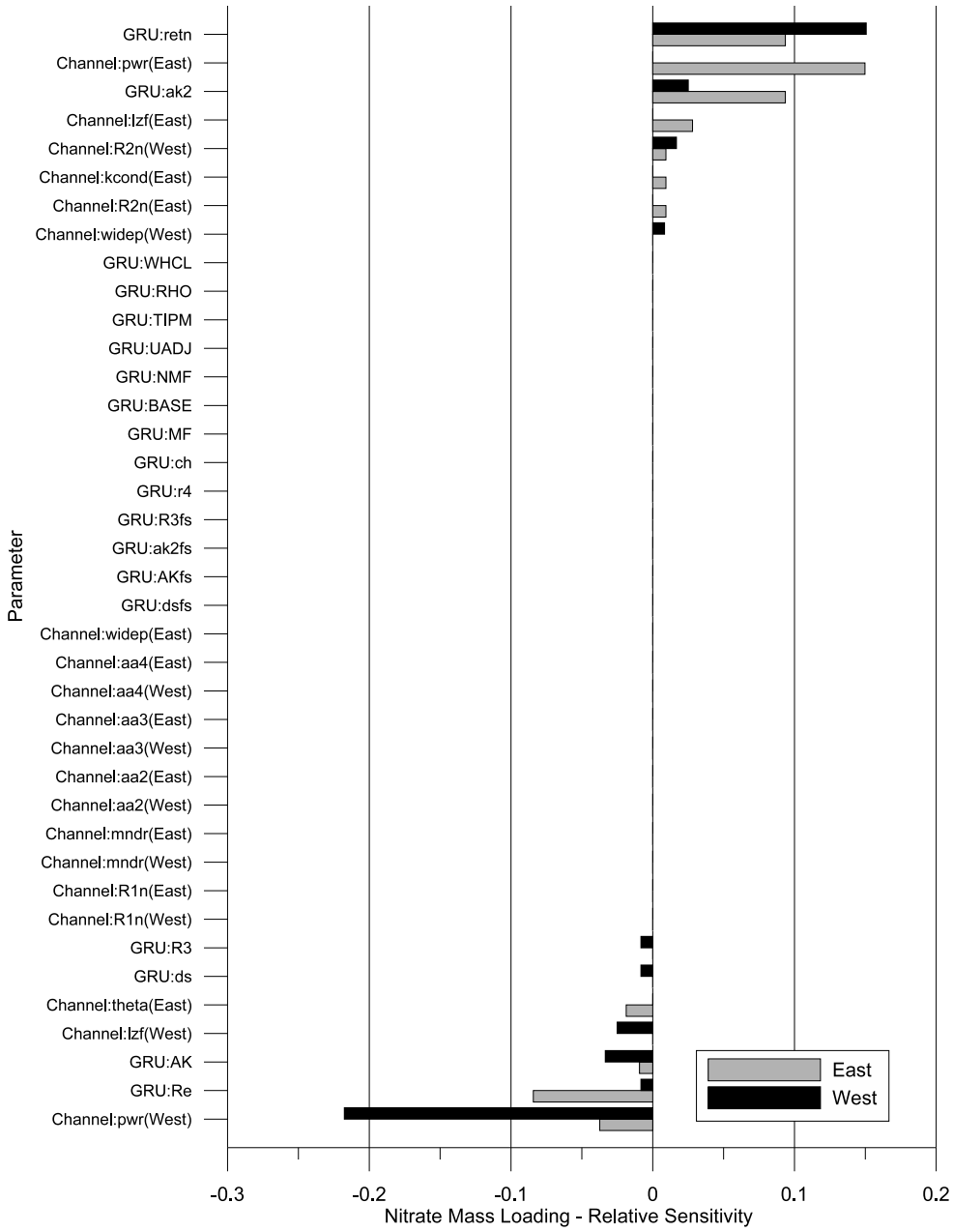

Figure D.28: Hydrologic Model Sensitivity - Nitrate loading sensitivity by sub-basin based on 5% parameter perturbation (Jan 2005 – May 2007)

D.7 Water Quality Parameter File (WQP)

```
# WATER QUALITY PARAMETER FILE
# SEDIMENT PARAMETERS
:gamma 9806
:ro      1000
:viskin   .000001
:grav    9.8066
:a       .00066
:b       1.61
:gc       0.10 0.10 0.80 0.50 0.60 0.00
:cf       0.90 0.90 0.40 0.60 0.50 0.00
# NUTRIENT PARAMETERS
:ncrn  0.00
:ndec 50
:pdec 50
:sdep 50
:nscn 0.0000
:ncpw 0
:nrec 0.050
:nlec 0.25
:pscn 0.0000
:pcpw 0
:prec 0.025
:plec 0.25
# RIVER MIXING PARAMETERS
:disp 300 300 300
# RIVER SEDIMENT PARAMETERS
:Cs 200 200  20000
:Ks 1.5 1.5 5.0
:Ksd 0.001 0.001 0.001
:Ksr 0.001 0.001 0.001
:Cer 1.00 1.00 1.00
# RIPARIAN SEDIMENT PARAMETERS
:nr 0.70 0.70  0.70
:S0 0.0001 0.0001 0.0001
:Csr 200 200 20000
:Ksr    1.5 1.5 5.0001
:Ksdr   0.001 0.001 0.001
```

D.8 Riparian Wetland Definition File (RIP)

```
# RIPARIAN DEFINITION FILE
```

```
# COVER RATIO
0 0 0 0 0 0 0 0 0 0 0 0 0 0 0 0
0 0 0 0 0 0 0 0 0 0 0 0 0 0 0 0
0 0 0 0 0 0 0 0 0 0 0 0 0 0 0 0
0 0 0 0 0 0 0 0 0 0 0 0 0 0 0 0
0 0 0 0 0 0 0 0 0 0 0.95 0 0 0 0 0
0 0 0 0 0 0 0 0 0 0 0.9 0 0 0 0 0
0 0 0 0 0 0 0 0 0 0 0.99 0 0 0 0 0
0 0 0 0 0 0 0 0 0.61 0.56 0 0 0 0 0 0
0 0 0 0 0 0 0 0 0.74 0 0.2 0 0 0 0 0
0 0 0 0 0 0 0 0 0.2 0 0.2 0.2 0 0 0 0 0
0 0 0 0 0 0 0 0 0.2 0.2 1 0.2 0 0 0 0 0
0 0 0 0 0 0 0 0 0 0.2 0.2 0.2 0 0 0.99 0 0
0 0 0 0 0 0 0 0 0 0 0 0 0 0 0.82 0 0
0 0 0 0 0 0 0 0 0 0 0 0 0 0 0.93 0 0
0 0 0 0 0 0 0 0 0 0 0 0 0 0 0.32 0 0
0 0 0 0 0 0 0 0 0 0 0 0 0 0 0.42 0 0
0 0 0 0 0 0 0 0 0 0 0 0 0 0 0 0
0 0 0 0 0 0 0 0 0 0 0 0 0 0 0 0
0 0 0 0 0 0 0 0 0 0 0 0 0 0 0 0
0 0 0 0 0 0 0 0 0 0 0 0 0 0 0 0
0 0 0 0 0 0 0 0 0 0 0 0 0 0 0 0
0 0 0 0 0 0 0 0 0 0 0 0 0 0 0 0
```

D.9 Sediment Definition File (SED)

```
 # Sediment Data
 # d50 [mm]
0 0 0 0 0 0 0 0 0 0 0 0 0 0 0 0
0 0 0 0 0 0.075 0.075 0.075 0 0 0 0 0 0 0 0
0 0 0 0 0.075 0.075 0.075 0.075 0 0 0 0 0 0 0 0
0 0 0.075 0.075 0.075 0.075 0.075 0.075 0.075 0 0.075 0 0 0 0 0
0 0 0.075 0.075 0.075 0.075 0.075 0.075 0.075 0.075 0.105 0.105 0 0 0 0
0 0 0.075 0.075 0.075 0.075 0.075 0.075 0.075 0.075 0.105 0.105 0 0 0 0
0 0 0.075 0.075 0.075 0.075 0.075 0.075 0.075 0.075 0.105 0.105 0 0 0 0
0 0 0.075 0.075 0.075 0.075 0.075 0.075 0.075 0.075 0.075 0.075 0 0 0 0
0 0 0.075 0.075 0.075 0.075 0.075 0.075 0.075 0.075 0.075 0.075 0 0 0 0
0 0.075 0.075 0.075 0.035 0.075 0.075 0.075 0.075 0.075 0.075 0.105 0.105 0.105 0 0
0 0 0.075 0.075 0.075 0.075 0.075 0.075 0.075 0.075 0.105 0.105 0.105 0.105 0 0
0 0 0 0.075 0.075 0.075 0.075 0.075 0.105 0.105 0.105 0.105 0.105 0.075 0 0
0 0 0 0.075 0.075 0.075 0.075 0.075 0.105 0.105 0.105 0.105 0.105 0.075 0.075 0
0 0 0 0.075 0.075 0.075 0.075 0.075 0.105 0.105 0.075 0.075 0.075 0.075 0.075 0
0 0 0 0.075 0.075 0.105 0.105 0.075 0.075 0.075 0.075 0.105 0.105 0.075 0.105 0
0 0 0 0.075 0.075 0.075 0.075 0.075 0.075 0.075 0.075 0.075 0.075 0.075 0.105 0
```

```
0 0 0 0 0.075 0.075 0.075 0.075 0.075 0.075 0.075 0.075 0.075 0.075 0.075 0
0 0 0 0 0.075 0.075 0.075 0.075 0.075 0.075 0.075 0.075 0.075 0.075 0 0
0 0 0 0 0 0.075 0.075 0.075 0.075 0.075 0 0 0.075 0.075 0.075 0.075
0 0 0 0 0 0 0.075 0.075 0.075 0 0 0 0 0 0 0
0 0 0 0 0 0 0.075 0.075 0 0 0 0 0 0 0 0
0 0 0 0 0 0 0 0 0 0 0 0 0 0 0 0
 # specific weight [-]
0 0 0 0 0 0 0 0 0 0 0 0 0 0 0 0
0 0 0 0 0 2.009 2.009 2.009 0 0 0 0 0 0 0 0
0 0 0 0 2.009 2.009 2.009 2.009 0 0 0 0 0 0 0 0
0 0 2.009 2.009 2.009 2.009 2.009 2.009 2.009 0 2.009 0 0 0 0 0
0 0 2.009 2.009 2.009 2.009 2.009 2.009 2.009 2.009 2.111 2.111 0 0 0 0
0 0 2.009 2.009 2.009 2.009 2.009 2.009 2.009 2.009 2.111 2.111 0 0 0 0
0 0 2.009 2.009 2.009 2.009 2.009 2.009 2.009 2.009 2.111 2.111 0 0 0 0
0 0 2.009 2.009 2.009 2.009 2.009 2.009 2.009 2.009 2.009 2.009 0 0 0 0
0 0 2.009 2.009 2.009 2.009 2.009 2.009 2.009 2.009 2.009 2.009 0 0 0 0
0 2.009 2.009 2.009 2.099 2.009 2.009 2.009 2.009 2.009 2.009 2.111 2.111 2.111 0 0
0 0 2.009 2.009 2.009 2.009 2.009 2.009 2.009 2.009 2.111 2.111 2.111 2.111 0 0
0 0 0 2.009 2.009 2.009 2.009 2.009 2.111 2.111 2.111 2.111 2.009 2.009 0 0
0 0 0 2.009 2.009 2.009 2.009 2.009 2.111 2.111 2.111 2.111 2.009 2.009 2.009 0
0 0 0 2.009 2.009 2.009 2.009 2.009 2.111 2.111 2.009 2.009 2.009 2.009 2.009 0
0 0 0 2.009 2.009 2.111 2.111 2.009 2.009 2.009 2.009 2.111 2.111 2.009 2.111 0
0 0 0 2.009 2.009 2.009 2.009 2.009 2.009 2.009 2.009 2.009 2.009 2.009 2.111 0
0 0 0 0 2.009 2.009 2.009 2.009 2.009 2.009 2.009 2.009 2.009 2.009 2.009 0
0 0 0 0 2.009 2.009 2.009 2.009 2.009 2.009 2.009 2.009 2.009 2.009 0 0
0 0 0 0 0 2.009 2.009 2.009 2.009 0 0 2.009 2.009 2.009 2
0 0 0 0 0 0 2.009 2.009 2.009 0 0 0 0 0 0 0
0 0 0 0 0 0 2.009 2.009 0 0 0 0 0 0 0 0
0 0 0 0 0 0 0 0 0 0 0 0 0 0 0 0
 # erodibility [g/J]
0 0 0 0 0 0 0 0 0 0 0 0 0 0 0 0
0 0 0 0 0 0.31 0.31 0.31 0 0 0 0 0 0 0 0
0 0 0 0 0.31 0.31 0.31 0.31 0 0 0 0 0 0 0 0
0 0 0.31 0.31 0.31 0.31 0.31 0.31 0.31 0 0.31 0 0 0 0 0
0 0 0.31 0.31 0.31 0.31 0.31 0.31 0.31 0.31 0.14 0.14 0 0 0 0
0 0 0.31 0.31 0.31 0.31 0.31 0.31 0.31 0.31 0.14 0.14 0 0 0 0
0 0 0.31 0.31 0.31 0.31 0.31 0.31 0.31 0.31 0.14 0.14 0 0 0 0
0 0 0.31 0.31 0.31 0.31 0.31 0.31 0.31 0.31 0.31 0.31 0 0 0 0
0 0 0.31 0.31 0.31 0.31 0.31 0.31 0.31 0.31 0.31 0.31 0 0 0 0
0 0.31 0.31 0.31 0.37 0.31 0.31 0.31 0.31 0.31 0.31 0.14 0.14 0.14 0 0
0 0 0.31 0.31 0.31 0.31 0.31 0.31 0.31 0.31 0.14 0.14 0.14 0.14 0 0
0 0 0 0.31 0.31 0.31 0.31 0.31 0.14 0.14 0.14 0.14 0.31 0.31 0 0
0 0 0 0.31 0.31 0.31 0.31 0.31 0.14 0.14 0.14 0.14 0.31 0.31 0.31 0
0 0 0 0.31 0.31 0.31 0.31 0.31 0.14 0.14 0.31 0.31 0.31 0.31 0.31 0
0 0 0 0.31 0.31 0.14 0.14 0.31 0.31 0.31 0.31 0.14 0.14 0.31 0.14 0
0 0 0 0.31 0.31 0.31 0.31 0.31 0.31 0.31 0.31 0.31 0.31 0.31 0.14 0
```

```
0 0 0 0 0.31 0.31 0.31 0.31 0.31 0.31 0.31 0.31 0.31 0.31 0.31 0
0 0 0 0 0.31 0.31 0.31 0.31 0.31 0.31 0.31 0.31 0.31 0.31 0 0
0 0 0 0 0 0.31 0.31 0.31 0.31 0.31 0 0 0.31 0.31 0.31 0.31
0 0 0 0 0 0 0.31 0.31 0.31 0 0 0 0 0 0 0
0 0 0 0 0 0 0.31 0.31 0 0 0 0 0 0 0 0
0 0 0 0 0 0 0 0 0 0 0 0 0 0 0 0
```